LITHOSTRATIGRAPHIC CORRELATION AT VARIOUS SPATIAL SCALES IN THE LIVERMORE BASIN AT THE LAWRENCE LIVERMORE NATIONAL LABORATORY, CALIFORNIA, U.S.A.

By

Leslie R. Mikesell

A DISSERTATION

Submitted to
Michigan State University
in partial fulfillment of the requirements
for the degree of

DOCTORATE OF PHILOSOPHY

Geological Sciences

2012

ABSTRACT

LITHOSTRATIGRAPHIC CORRELATION AT VARIOUS SPATIAL SCALES IN THE LIVERMORE BASIN AT THE LAWRENCE LIVERMORE NATIONAL LABORATORY, CALIFORNIA, U.S.A.

By

Leslie R. Mikesell

The stratigraphy of the tectonically active Livermore Basin, California is controlled by local tectonics which produce spatial scale variability within the stratigraphy. The sediments at the Lawrence Livermore National Laboratory (LLNL) form three stacked fluvial fan successions beneath the site. The sediment below 37 m was deposited by the Arroyo Seco, an intermittent stream. The sediment between 19 m depth and 37 m was deposited by the Arroyo Las Positas, another intermittent stream. The sediment above 19 m was deposited by the Arroyo Seco. These provenance study data, plus geomorphic evidence, including knowledge that the Arroyo Seco entered the basin through the Las Positas Fault uplift and an abandoned alluvial fan is present south of the uplift, suggests that the Arroyo Seco was captured and redirected into the basin.

With the assumption that large-scale units (approximately 20 m thick) existed beneath LLNL, facies correlations from 202 well cores taken from LLNL was attempted. The cores were described in detail, resulting in the recognition of seven facies, including a paleosol facies. Correlation attempts using the paleosols as marker units were unsuccessful at LLNL because neither the paleosols nor any of the other units were laterally continuous beyond 6 m to 9 m. Very few wells at LLNL are spaced this closely, and the remaining well spacing at LLNL exceeded the lateral spatial resolution required for correlatability. Since facies were not correlatable, major- and trace-element geochemical data were employed as a possible tool for correlating stratigraphic units. The elemental data, elemental ratios, and weathering indices were

plotted against depth and inspected for patterns that might point to a unique geochemical signature for one or more of the individual units. Geochemical plots did not result in identification of individual units that were correlatable between wells. Also, the plots did not indicate a difference in geochemistry between the three stack fluvial fan successions. Although the provenance study indicated a difference in the lithology of detritus, the detritus was isochemical because both local source areas had the same ancestral Sierran-Klamath arc source.

A new Index of Paleosol Development (IPD) was developed for this research to compare variability in the development of individual paleosols. The IPD allows for a quantitative assessment of the strength of paleosol developmental features. IPD values within a well core are used to calculate an average value for the entire core: the Core Index of Paleosol Development (CIPD). Well cores in the northwestern region of LLNL had the highest IPD and CIPD values, indicating strongly developed paleosols and/or comparatively more paleosols per core. The IPD and CIPD values in the central western region were lower, suggestive of weakly developed paleosols and/or few paleosols in that region. This variability in paleosol development across the study area reflects the relative surface stability on which the soils formed. The northwestern region of LLNL aligns with the northernmost anticline of the Springtown anticlines that plunge beneath the site. The syndepositional formation of this anticline provided a relatively stable surface allowing for more strongly developed soils, and thus, paleosols with higher IPD values. The central western region aligns with the plunging syncline of the Springtown anticline pair. The formation of the syncline provided a relatively less stable surface on which aggradation inhibited soil development via frequent burial. At LLNL, large scale features (e.g., stacked fan successions and the plunging Springtown anticlines) are correlatable, while smaller scale features (e.g., facies and sedimentary units thinner than the stacked fan successions) are not correlatable.

ACKNOWLEDGEMENTS

So many people contributed to my success and I am grateful for the opportunity to mention their names and give them recognition.

I owe a huge debt of gratitude to my guidance committee members, Dr. Kazuya Fujita, Dr. Randy Schaetzl, and Dr. Brian Hampton. I wish to thank them for being my allies in this endeavor. I cannot begin to express how instrumental my adviser, Dr. Michael Velbel, was in my success. He stepped in and made it possible for me to complete my degree. These four men have my respect for the rest of my life.

This material is based upon work supported by the National Science Foundation under Grant Nos. EAR-0617992 and EAR-0133666. Dr. Gary Weissmann was the P.I. on the NSF grants and I wish to thank him for providing funding for this research and sharing his knowledge with me.

I would like to thank those at the Lawrence Livermore National Laboratory Environmental Restoration Division who provided insight, knowledge, resources, and physical labor during my four summers on site. I'd like to especially thank Fred Hoffman, Charles Noyes, Zafer Demir, Dr. John Karachewski, Robert Bainer, Rick Blake, Linda Cohan, Ben Johnson, Paul Anderson, John Ulrech, and John Van Fossen.

I would like to thank students from Michigan State University who provided laboratory and field support, including Beth Apple, Rob Trahan, Sara Auer, Kent Dankenbring, Sarah Martell, Aimee Kniesel, Karen Strickling, Luke Zoet, Ginny Rust, Marylin Matice, as well as Jules Patry and Mike Luehmann for help with images. This dissertation also greatly benefited from discussions with faculty at MSU including Dr. Lina Patino and Dr. Tom Vogel.

In all truth, I would not have finished my degree without the unwavering support of my loving husband, Marc Mikesell. I cannot thank him enough for being completely unselfish on so many occasions and allowing me (and even prodding me) to fulfill my dream. He means more than the world to me.

My wonderful family also supported, encouraged, and believed in me throughout this whole process. I owe so much to Lowell and Betty Moore, Dawn and Scott Smithson, and Dan and Donna Mikesell.

I also appreciate my special friends who went above and beyond in their support of me during my studies. I wish to thank Nancy Rose, Donna Anderson, Anne Parton, Dee Ruther, Phyllis Wilson, Billie Gipe, Dr. Kevin Compton, Emily Compton, and Jackie and John Payne for encouraging me when I needed it.

"Who has measured the waters in the hollow of his hand, or with the breadth of his hand marked off the heavens? Who has held the dust of the earth in a basket, or weighed the mountains on the scales and the hills in a balance? Do you not know? Have you not heard? The Lord is the everlasting God, the Creator of the ends of the earth." Isaiah 40:12 and 28a.

TABLE OF CONTENTS

LIST OF TABLES

LIST OF FIGURES

KEY TO SYMBOLS OR ABBREVIATIONS

ϕ .... Phi (measure of grain size)

ALP .... Arroyo Las Positas

AS .... Arroyo Seco

CIPD .... Core Index of Paleosol Development

ERD .... Environmental Restoration Division

ETC .... East Traffic Circle

FA .... Franciscan Assemblage

GPS .... Global Positioning System

GVG .... Great Valley Group

IPD .... Index of Paleosol Development

LL .... Lower Livermore

LLNL .... Lawrence Livermore National Laboratory

LPF .... Las Positas Fault

Ma .... million years ago

PDI .... Profile Development Index

Psl .... paleosol

CHAPTER 1

Introduction

1. Introduction

Sedimentology and local tectonics affect the distribution of lithostratigraphic facies on alluvial fans (e.g., Koltermann and Goerelic, 1992; Holbrook and Schumm, 1999; Mather et al., 2000; Weissmann et al., 2002; Leleu et al., 2005). Viewing alluvial fan architecture and facies distributions at various spatial scales is important in understanding how the variability in spatial scale affects the distribution of oil and gas reserves (e.g., Jervey, 1988), groundwater resources (e.g., Larkin and Sharp, 1992; Fogg et al., 1999), as well as contaminant transport (e.g., Anderson, 1989; McNab et al., 2001). The Livermore Basin in California, specifically the Lawrence Livermore National Laboratory (LLNL) (Figure 1), provided an excellent location to study the lithostratigraphy of a tectonically active basin in order to better understand how various spatial scales affects distribution of lithostratigraphic facies.

The ability to correlate lithostratigraphic facies is a key component to understanding basin sedimentology and stratigraphy. Paleosols often serve as marker units and a starting point for facies correlation between wells (e.g., Shlemon, 1985; Weissmann et al., 2002). Weissmann et al. (2002) conducted a study of the large (3150 km^2) Kings River alluvial fan in California. They noted the mature paleosols were laterally continuous and served as marker units for stratigraphic correlations. The paleosols on the Kings River fan averaged 1.85 m in thickness and extended across an area greater than 100 km^2 (Weissmann et al., 2002). Shlemon (1985) noted that the clay-rich horizons of paleosols were traceable laterally for several kilometers along the California coast. The successful use of paleosols as marker units in other studies led to the expectation that paleosols would be useful in lithostratigraphic correlations at LLNL.

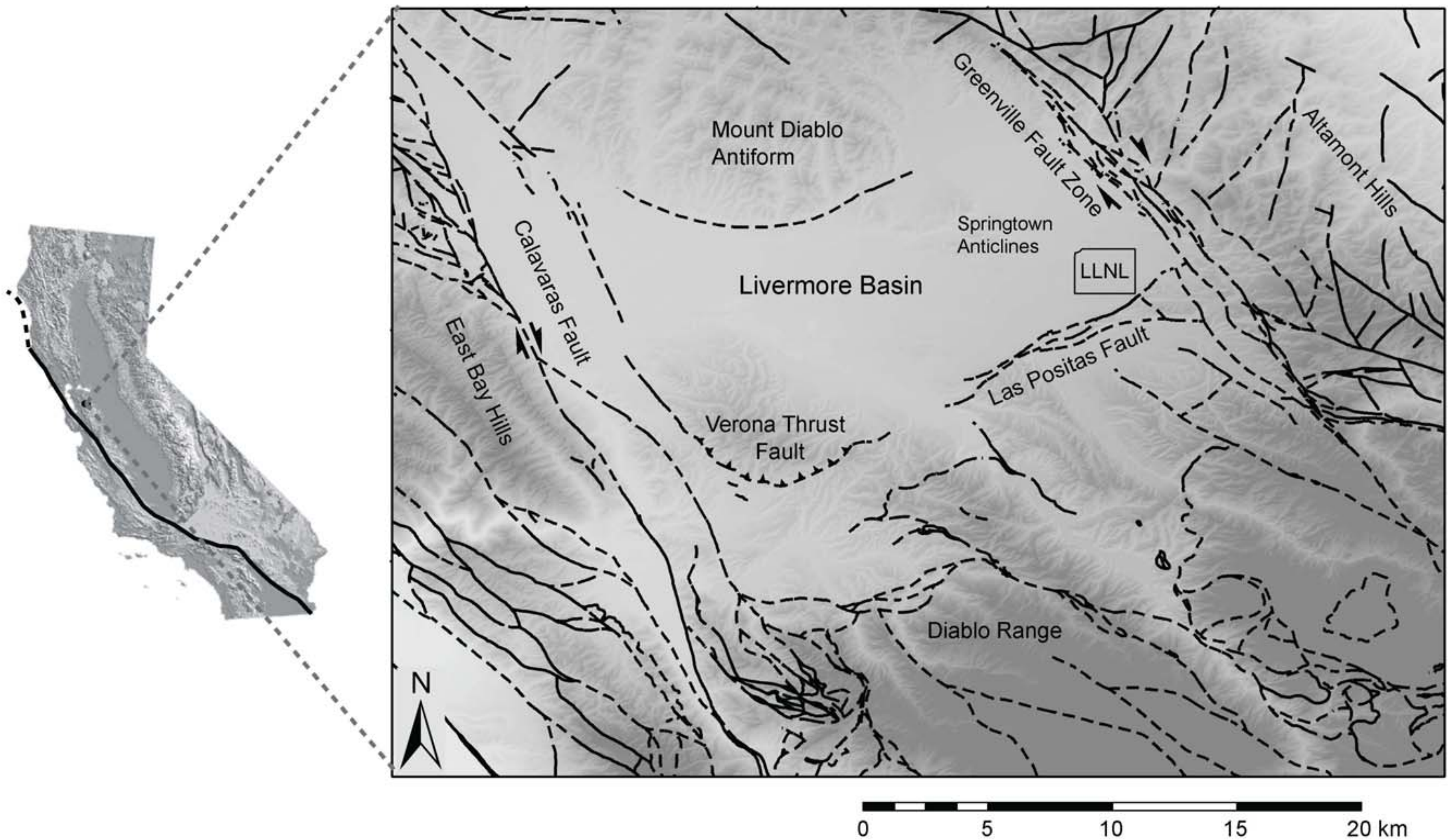

Figure 1. The Livermore Basin including the structural bounding features. The Lawrence Livermore National Laboratory is located in the southeastern section of the basin. The digital elevation model is from the Shuttle Radar Topographic Mission (SRTM) 1 arcsec coverage (modified from Mikesell et al., 2010). For interpretation of the references to color in this and all other figures, the reader is referred to the electronic version of this dissertation.

2. Purpose of Study

The purpose of this study is to examine the relationship between spatial scale and the correlatability of lithostratigraphy in a tectonically active basin. The stratigraphy and facies distribution of the fluvial fan system beneath the Lawrence Livermore National Laboratory (LLNL) in the Livermore Basin is controlled by the local tectonics. The goal of this study is to understand the LLNL lithostratigraphy at various scales.

3. Site Description

The Lawrence Livermore National Laboratory (LLNL) in Livermore, California is located about 65 km east of San Francisco at the southeastern corner of the Livermore Basin. LLNL is a Department of Energy research and development facility operated by the University of California. Prior to its current mission, the site was a U.S. Naval Air Base from 1942 through the 1946. Industrial chemicals associated with aircraft maintenance and cleaning were disposed of improperly during that time resulting in contaminated groundwater. Subsequent contamination has occurred due to leaking landfills, leaking gasoline storage tanks, and localized spills (Adams and Bainer, 1993; Aines et al., 1994). LLNL was established as a laboratory in 1952, then was added to the U.S. Environmental Protection Agency's National Priorities, or Superfund, list in 1987 (Adams and Bainer, 1993), since which time clean up has been ongoing.

The Environmental Restoration Division (ERD) of LLNL was charged with cleaning the contaminated groundwater plumes on site. In support of their efforts, ERD has drilled and collected cores from approximately 500 wells on site and maintains a core library of over 15 km of continuous well cores. In addition to the well cores, ERD collected complete geophysical data from these 500 wells and an additional 300 wells on site. The wells range in depth from 30 m to more than 90 m. Since the wells were drilled to support ERD's ongoing clean up, the core collection amounts (total meters per well) and locations (both vertical within each well, and placement laterally across the site) were dictated by their research and finances. The amount of core collected ranges from the complete well to approximately 10 m sections only in zones of interest to ERD researchers.

Gaining an understanding of LLNL's subsurface was a goal of ERD's research in support of their ground water remediation efforts. Based on hydraulic responses to pumping test, they were able to identify at least seven hydrofacies, or units with similar hydrogeologic properties (Ritzi et al., 1995; Klingbeil et al., 1999; Gaud et al., 2001), which they called Hydrostratigraphic Units (HSU) (Blake et al., 1995; Noyes et al., 200). Based on the success ERD experienced in mapping HSU boundaries, it was thought likely that the lithostratigraphy beneath LLNL would also be correlatable.

4. The Livermore Basin

The Livermore Basin is an east-west oriented topographical and structural depression that trends almost perpendicular to the strike of the Central California Coast Range within which it is located (Figure 1). The basin is approximately 26 km long east to west, and 11 km north to south. The land surface dips from the eastern side at 220 m in elevation down to 92 m in the southwest where the drainage leaves the basin (Thorpe et al., 1990). The Livermore Basin is located between the Mt. Diablo antiform in the north and the Diablo Range to the south. The eastern side is bordered by the Altamont Hills, which separates the Livermore Basin from the San Joaquin Valley. On the west it is bordered by the East Bay Hills, which separate the Livermore Basin from the San Francisco Basin.

4.1 Sedimentology and Stratigraphy

The Livermore Basin is a structural basin containing approximately 5 km of sediment (Meltzer, 1988). General thickening of sedimentary beds towards the center of the basin indicated syntectonic deposition (Carpenter et al., 1984). Bedrock beneath the Livermore Basin consists of the late Jurassic to Cretaceous Franciscan Assemblage and Great Valley Group formations, upon which lie Tertiary marine and non-marine sediments and Quaternary non-marine and terrestrial sediments (Barlock, 1989; Graymer et al., 1996) (Table 1).

The Livermore Basin is being filled by sediment derived from the surrounding elevated terrain. The southeastern portion of the basin is being filled with sediment derived from the Altamont Hills, which consists of the Great Valley Group and the Franciscan Assemblage. The Great Valley Group is Cretaceous in age and consists of massive bedded arkosic to lithic arenites and graywackes deposited in a forearc basin. The late Jurassic- to Cretaceous-aged Franciscan Assemblage rocks were an accretionary prism and were brought to the top of the North American Plate as a result of tectonics. In this region, the Franciscan Assemblage consists of graywacke, chert and metamorphosed facies including schist. The two complexes of rock are juxtaposed with the Franciscan Assemblage placed tectonically over the Great Valley Group. The boundary of these two complexes is located at the southeast edge of the Livermore Basin.

Two intermittent streams enter the southeastern region of the basin and cross LLNL. The Arroyo Seco flows to the northwest over the southwestern portion of the site. However, a 1940 aerial photograph shows a north-south oriented Arroyo Seco channel across what is now LLNL.

Table 1. Generalized stratigraphy of the southern Livermore Basin with sediment descriptions (Huey, 1948; Page, 1981; Sweeny and Springer, 1981; Carpenter et al., 1984; Ollenburger, 1986)

Age	Formation	Description
Quaternary Late Pleistocene to Holocene	Alluvium, Fluvial, Fan, Floodplain and Terrace deposits	Conglomerate, sand, silt, and clay deposits. Massive to bedded. Gray to brown or tan. Poorly- to well-sorted. Some units contain fossils, carbonate nodules, iron staining, or mottles. 90-150 m
Pleistocene	Upper Livermore Formation	Non-marine gravels consisting of predominantly lithic sandstones comprised of >35% sandstone clasts, >49% graywacke clasts, <30% fine-grained vein quartz clasts, and minor metamorphic clasts and volcanic clasts. Bedded in thick horizontal, clast-supported units with planar and trough cross-bedding. Finer-grained facies include lacustrine and fluvial.
Tertiary Late Pliocene	Lower Livermore Formation	Non-marine gravel consisting of abundant lithic sandstone comprised of >30% sandstone clasts, <30% graywacke clasts, 20 - 45% fine-grained vein quartz clasts, and few volcanic clasts. Bedded in thick horizontal, clast-supported units with planar and trough cross-bedding. Total Livermore Fm ~1220 m.
Pliocene to Miocene	Green Valley and Tassajara Fms. (includes Tuff)	Non-marine sandstone, siltstone, and conglomerate. Tuff is 5 m thick and is a marker bed for stratigraphic correlation.
Late Miocene	Neroly Sandstone	Marine sandstone with abundant volcanic rocks. Brown and massive.
	Cierbo Sandstone	Marine sandstone with fossils. Light gray and massive. Conglomerate near base of unit.
Middle Eocene	Tesla Fm.	White quartz to buff-colored sands interbedded with dark carbonaceous shales, lignite seams, and white to blue clays
Late Jurassic to Cretaceous	Great Valley Group, Panoche Formation: unnamed sandstone	Massive to bedded sandstone, coarse- to fine-grained, biotite- and quartz-bearing lithic wacke and siltstone. Lenses of cobble conglomerate and minor amounts of mudstone.
	Great Valley Group, Panoche Formation: unnamed siltstone	Siltstone interbedded with minor sandstone, shale, and clay.
	Great Valley Group, Panoche Formation: unnamed mudstone	Massive to bedded gray mudstone and fine-grained siltstone. Includes minor amounts of biotite- and quartz-bearing lithic wacke.
	Coast Range Thrust Fault	
	Coast Range ophiolite	Massive basalt, diabase, gabbro, and serpentinite.
	Franciscan Assemblage	Graywacke interbedded with siltstone, shale, chert, greenstone, and metamorphic rocks.

The Arroyo Las Positas once flowed west from the Altamont Hills across LLNL, but in 1965 the stream was confined to drainage ditches and redirected north then west around the site as part of an erosion-control project (Carpenter et al., 1984). Together, the two streams deposited at least 60 m of Quaternary-aged basin fill locally. The approximate 2.6 km^2 LLNL site is located on the 7 km^2 fluvial fan deposited by the Arroyo Seco and the Arroyo Las Positas. The term fluvial fan is used to indicate fan-shaped deposits that are dominated by fluvial processes in order to distinguish them from alluvial fans which are dominated by debris-flow or sheet-flood (Weissmann et al., 2005).

To better understand the dynamics of the fluvial fan system at LLNL, well cores from ERD's core library were examined. In support of this research, 202 well cores amounting to 6.7 km of continuous core were described in detail. Well cores were viewed and described from key locations across the site to ensure the densest description coverage of the site as allowed by time and resources. The detailed observations resulted in seven facies being described: 1) clast-supported gravel, 2) matrix-supported gravel, 3) sand, 4) silty sand, 5) silty sand with clay lamellae, 6) paleosol, and in accordance with local nomenclature, 7) the "Lower Livermore" (LL) unit.

4.2 Tectonics and Structure

The Livermore Basin is bounded on all sides by tectonic features. Two dextral, N30W-trending (Graymer et al., 1996) strike-slip faults, which are splays of the left-stepping San Andreas Fault system, bound the Livermore Basin on the east and the west (Unruh and Sawyer, 1997). On the basin's west boundary, at the base of the East Bay Hills, is the Calaveras Fault. On the east, at the base of the Altamont Hills, is the Greenville Fault. The Greenville Fault exhibits numerous splays and en-echelon segments with the presently active trace being the easternmost (Carpenter et al., 1984). Both of the bounding faults are semi-active and have ruptured historically (Carpenter et al., 1984).

The Livermore Basin is bordered on the north by the asymmetric, doubly-plunging Mt. Diablo anticline (Unruh and Sawyer, 1995; 1997). This fault-propagation fold was a result of the contractional deformational zone (Unruh and Sawyer, 1997) that uplifted the region approximately 4 Ma (Andersen et al., 1995).

The east-northeast-trending, sinistral Las Positas Fault zone (Herd, 1977) forms part of the southern border of the Livermore Basin (Unruh and Sawyer, 1997). The Las Positas Fault zone is bounded by northern and southern branches, both of which have nearly vertical dip and terminate at the Greenville Fault, and is extensively described in Carpenter et al. (1984). Carpenter and Clark (1982) report slickensides in young (< 80 Ka) deposits along the northern branch near the Arroyo Seco that plunge 19°, indicating dominantly strike-slip motion. They also report that geologic contacts, however, are generally offset with the north side down. Carpenter et al. (1984), however, report slickensides with a 9° plunge but with the northwest side-up. The block between the north and south branches is topographically (~50 m) and stratigraphically (~60 m) elevated, and is shown in some interpretation as forming a horst (Carpenter et al., 1984; Hedegaard et al., 1993). The southern branch, however, has also been mapped as a thrust (Carpenter et al., 1984) and is said to be undergoing neotectonic uplift (Shlemon and Qualheim, 1993). One possible interpretation for the conflicting observations is that the block between the fault branches originated as a horst during the development of the Livermore basin but is now being reactivated as a pop-up or flower structure as the basin contracts in its current stress field (Unruh and Lettis, 1998). I refer to this structure as a horst in

Chapter 3, with the understanding that its present kinematic nature may be different. With the uncertainty as to the origin and present kinematic nature of this structure, I will refer to it as the Las Positas Fault uplift (Crane, 2003). The vertical uplift rate over the past million years is about 0.06 mm/yr with a total (mainly sinistral) displacement rate of 0.3 mm/yr (Carpenter and Clark, 1982; Carpenter et al., 1984). The extent of the Las Positas fault zone to the west is debated (Carpenter et al., 1984). The fault has been active throughout the Holocene and parts of it may have undergone displacement during the January, 1981, Greenville fault earthquake (Carpenter et al., 1984).

The Livermore Basin is bordered to the southwest by low hills that are underlain by the Verona Thrust Fault. The Verona Fault, along with the Las Positas Fault to its east, separates the Livermore Basin from the Northern Diablo Range to the south.

The Livermore Basin is a transtensional basin currently in its contractional phase (Unruh and Sawyer, 1997). The basin has been experiencing compressional deformation since the Mendocino Triple Junction passed Livermore's latitude at approximately 10 Ma (Springer, 1983; Andersen et al., 1995). The triple junction migration effectively terminated subduction after the Farallon Plate subducted and initiated transform shear on the western margin of North America (Dickinson and Snyder, 1979).

Based on focal mechanism analyses, the seismogenic deformation field exhibits subhorizontal northeast-southwest shortening and northwest-southeast extension within the basin (Unruh and Sawyer, 1997). The orientation of principle strain axes indicates a clockwise rotation of the basin block relative to the San Andreas Fault to the west (Carpenter et al., 1984; Unruh and Sawyer, 1997). The tectonic block south of the Livermore Basin is also experiencing clockwise rotation and is the cause of the thrusting in the Verona Thrust Fault (Carpenter et al., 1984). The strike-slip faults that border the east and west sides of the Livermore Basin are consistent with this regional deformation (Unruh and Sawyer, 1997), while internal deformation accommodates local strain (Carpenter et al., 1984; Unruh and Sawyer, 1997).

The Springtown anticlines are an anticline-syncline-anticline complex that is an expression of intra-basin deformation (Unruh and Sawyer, 1997). These structural features are most likely due to the compression of the basin, with the primary compression forces being normal to the trend of the anticline pair, and are presumed to be the result of back-thrusting above secondary faults beneath the Livermore Basin (Unruh and Sawyer, 1997). The anticlines plunge to the southeast and below LLNL (Sawyer, 1999). Although the anticlines form low hills approximately 3 km northwest of LLNL, there is no surface topographical evidence of the anticlines at LLNL.

Two lines of evidence indicate the Springtown anticlines have been deforming throughout the Quaternary (Unruh and Sawyer, 1997). First, a series of three older Quaternary stream terraces cross the axis of the easternmost anticline. The terraces diverge from one another and the active stream channel where the stream crosses the anticline axis, then converge downstream of the anticline. Downcutting of the stream during uplift of the anticline resulted in stair-step terraces. Secondly, the longitudinal profile of the stream is convex and mimics the anticline axes. The stream is underlain by poorly consolidated valley fill along its entire reach; therefore, the convexity of the profile was not associated with change in underlying material, but rather is a result of tectonic deformation. Based on their observations, Unruh and Sawyer (1997) concluded that the Springtown anticline uplift rate was 0.1 to 0.3 mm/yr through the Quaternary and they were synchronous with the stream terraces' formation and channel profile adjustment.

5. Present-Day Strain Field

The current strain in the Livermore valley was determined through analysis of public domain GPS data. Data from fourteen GPS stations in and around the Livermore Basin were chosen. These sites are part of the larger Bay Area Regional Deformation (BARD) GPS network dataset (BARD, 2008). BARD is a project involving a consortium of institutions including: the University of California at Berkley, University of California at Davis, Stanford University, U.S. Geological Society, and Trimble Navigation. The project was designed to monitor crustal deformation along the Pacific-North America plate boundary, specifically in the San Francisco Bay area. Dr. David Hindle of the GZG, Structural Geology and Geodynamics, Göttingen, Germany, calculated the strain rates by decomposing the region into triangles with the GPS stations located at the vertices (Hindle and Mackey, 2011). The triangles were rotated flat to calculate strain. The strain tensors were then rotated to common axes, summed and averaged. The tensors were then set relative to a common north-south reference line, and were oriented with respect to stable North America (Hindle and Mackey, 2011). The results of this analysis indicate a present-day northeast-southwest compression with minimal northwest-southeast extension resulting in a clockwise rotation of the basin (Figure 2). The direction of this strain regime is perpendicular to the strike of the Springtown anticlines suggesting their continued deformation and growth at the present. These results agree with the focal mechanism analyses and indicate the current strain regime is consistent with the earlier Quaternary strain in the basin as inferred from Unruh and Sawyer (1997).

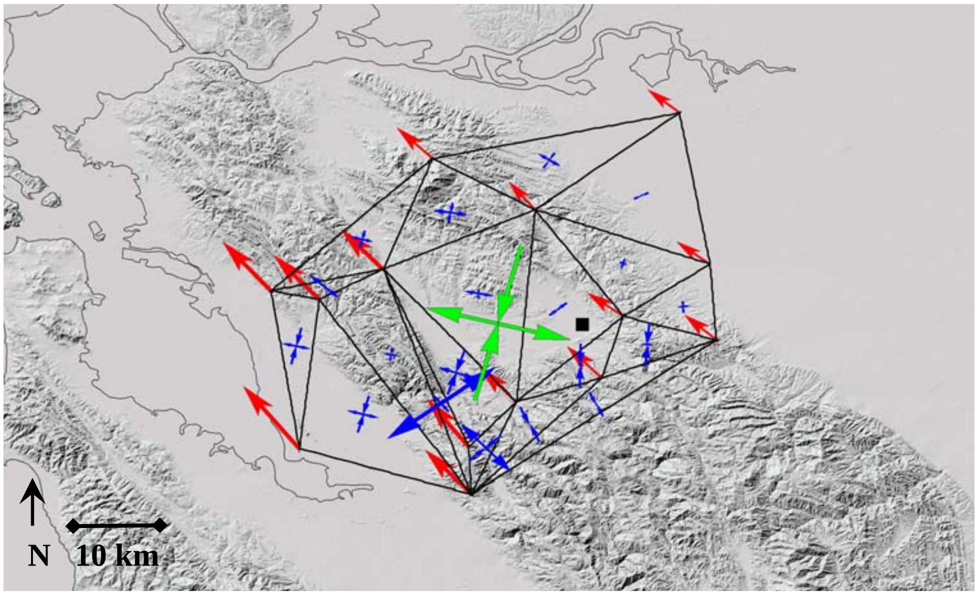

Figure 2. Surface displacement and inferred strain field calculated from BARD GPS data by Dr. David Hindle, GZG, Structural Geology and Geodynamics, Gottingen, Germany. LLNL location is indicated by the black box. Blue arrows indicate direction and magnitude of strain calculated within each triangle. Red arrows indicate overall direction and magnitude of movement at each GPS data collection site with respect to a stable North America. Green arrows indicate overall direction and magnitude of ground movement and inferred strain for the Livermore Basin. Strain field image is placed on a 1 arcsec seamless digital elevation model from the USGS.

6. Research Topic

The unconsolidated sediment beneath LLNL exhibits rapid lateral and vertical facies changes. In addition to the two intermittent streams influencing facies distribution, the stratigraphic character at the LLNL site may be strongly influenced by underlying structures and varying subsidence rates caused by the development of these structures. Due to the complexity of the site, there are multiple research topics related to lithostratigraphy and spatial scale variability addressed in this study. They are:

1) Paleosols are generally laterally extensive stratigraphic units and frequently serve as correlatable marker units when correlating stratigraphic sections (e.g., Shlemon, 1985; Weissmann et al., 2002). However, the paleosols at LLNL do not appear to be laterally

continuous across the site. Rust (2006) conducted a study on the eastern side of LLNL in which she attempted to correlate units using stratigraphic columns from 51 wells. She concluded the maximum well spacing for good correlation was 9 m. In order to understand the geology of LLNL, stratigraphic column correlation will be attempted in a region of LLNL where the well spacing is 6 m to 20 m. It is expected that due to highly variable sedimentology created by the two intermittent streams, and tectonic overprinting, the attempted stratigraphic correlations will result in poor correlation and uncertainty as to the accuracy of the resulting correlations.

2) The paleo-Arroyo Seco, which once flowed northwest into the Livermore Basin, shifted to the south, possibly due to faulting and the uplift of the Las Positas Fault uplift, and was then captured by a headward eroding stream and subsequently followed a new flow path into the basin. While the paleo-Arroyo Seco was blocked from the valley, the paleo-Arroyo Las Positas, a westwardly flowing stream, was the primary source for sediment in the basin. These streams drained different portions of the Altamont Hills with different lithologies. It is expected that a provenance study of the fluvial fan sediments will result in being able to distinguish the different stream deposits. The lithologically distinct deposits will indicate periods of time during which the paleo-Arroyo Seco was either present or absent in the basin.

3) The Springtown anticlines are a pair of low-amplitude, southeast-plunging Quaternary folds (Unruh and Sawyer, 1995, 1997; Sawyer, 1999) that plunge beneath LLNL and produce variable subsidence rates locally. Although there is no surficial expression of the folds at LLNL, the structural features beneath the site may be observable by the differences in stratigraphy above the anticlines as compared to the stratigraphy above the syncline. A comparison will be made of facies distributions and paleosol development from well cores above the anticlines to well cores above the syncline. A new index of paleosol development will be used to numerically assess the

amount of paleosol material and strength of paleosol development within each well core for purposes of comparing one well to another. It is expected that resulting data will show different regions of paleosol development, and that the different regions will be correlatable with the mapped off-site Springtown anticlines.

BIBLIOGRAPHY

Chapter 1

Bibliography

Adams, M.L., Bainer, R.W., 1993. Use of three-dimensional, high-resolution seismic technology to optimize the location of remedial systems. Livermore, California, Lawrence Livermore National Laboratory (UCRL-JC-111786), 11 pp.

Aines, R., Newmark, R., Ziagos, J., Copeland, A., Udell, K., 1994. Cleaning up underground contaminants. Energy and Technology Review (LLNL UCRL-52000-94-5), 11-21.

Andersen, D. W., Isaacson, K. A., Barlock, V. E., 1995. Neogene evolution of the Livermore basin within the California Coast Ranges. In: Fritsche, A.E. (Ed.), Cenozoic Paleogeography of the Western United States – II. SEPM Pacific Section, Book 75, pp. 151-161.

Anderson, M., 1989. Hydrogeologic facies models to delineate large-scale spatial trends in glacial and glaciofluvial sediments. Geological Society of America Bulletin 101, 501-511.

Bay Area Regional Deformation (BARD), 2008. http://www.seismo.berkeley.edu/ (last accessed April 2008)

Barlock, V. E., 1989. Sedimentology of the Livermore gravels (Miocene-Pleistocene), southern Livermore Valley, California. United States Geological Survey, Open-File Report 89-131.

Carpenter, D. W., and Clark, R. J., 1982. Geologic studies for seismic hazard assessment, Las Positas fault zone: California Division of Mines and Geology, Special Publication 62, p. 147-154.

Carpenter, D. W., Sweeney, J. J., Kasameyer, P. W., Burkhard, N. R., Knauss, K. G., Shlemon, R. J., 1984. Geology of the Lawrence Livermore National Laboratory site and adjacent areas. Livermore, California, Lawrence Livermore National Laboratory (UCRL-53316), 188 pp.

Crane, R., 2003. Geology of Central California – Mount Diablo-Diablo Range Intersection - The Altamont Hills (Field Guide). Northern California Geological Society, Alameda, 28 pp.

Dickinson, W.R., Snyder, W.S., 1979. Geometry of triple junctions related to San Andreas transform. Journal of Geophysical Research 84, 561-572.

Fogg, G.E., LaBolle, E.M., Weissmann, G.S., 1999. Groundwater vulnerability assessment; hydrogeologic perspective and example from Salinas Valley, California. Geophysical Monograph 108, 45-61.

Graymer, R. W., Jones, D. L., Barbb, E. E., 1996. Preliminary geologic map emphasizing bedrock formations in Alameda County, California: Derived from the digital database. United States Geological Survey, Open-File Report 96-252.

Hedegaard, R. F., Barber, K., and Wagoner, J. L., 1993. Use of gravel provenance to define stratigraphic units in the Sandia windgap trench, Livermore, California (abstract): Geological Society of America, Abstracts with Programs, v. 25(5), p. 50.

Hindle, D., Mackey, K., 2011. Earthquake recurrence and magnitude and seismic deformation of the northwestern Okhotsk plate, northeast Russia. Journal of Geophysical Research 116, B02301.

Holbrook, J., Schumm, S.A., 1999. Geomorphic and sedimentary response of rivers to tectonic deformation: A brief review and critique of a tool for recognizing subtle epeirogenic deformation in modern and ancient settings. Tectonophysics 305, 287-306.

Huey, A.S., 1948. Geology of the Tesla Quadrangle, California. California Division of Mines Bulletin 140, 52.

Jervey, M.T., 1988. Quantitative geological modeling of siliciclastic rock sequences and their seismic expression. In: Wilgus, C.K., Hastings, B.S., Ross, C.A., Posamentier, H., Van Wagoner, J., Kendall, Christopher G.S.C. (Eds.), Society of Economic Paleontologists and Mineralogists Special Publication 42. Society for Sedimentary Geology, Tulsa, Oklahoma, p. 47-69

Koltermann, C.E., Gorelick, S.M., 1992. Paleoclimatic signature in terrestrial flood deposits. Science 256, 1775-1782.

Larkin, R.G., Sharp, J.M., 1992. On the relationship between river-basin geomorphology, aquifer hydraulics, and ground-water flow direction in alluvial aquifers. Geological Society of America Bulletin 104, 1608-1620.

Leleu, S., Ghienne, J.F., Manatschal, G., 2005. Upper Cretaceous-Paleocene basin-margin alluvial fan documenting interaction between tectonic and environmental process (Provence, SE France). In: Harvey, A.M., Mather A.E., Stokes, M. (Eds.), Alluvial Fans: Geomorphology, Sedimentology, Dynamics. Geological Society of America Special Publication 251, 217-239.

Mather, A.E., Harvey, A.M., Stokes, M., 2000. Quantifying long-term catchment changes of alluvial fan systems. Geological Society of America Bulletin 112 (12), 1825-1833.

McNab, W.W., Karachewski, J.A., Weissmann, G.S., 2001. Field measurements of electro-osmotic transport of ground water contaminants in a lithologically heterogeneous alluvial-fan setting. Livermore, California, Lawrence Livermore National Laboratory (UCRL-ID-144879), 45 pp.

Meltzer, A.S., 1988. Crustal structure and tectonic evolution: Central California: unpublished Ph.D. dissertation, Rice University, 284 pp.

Mikesell, L.R., Weissmann, G.S., Karachewski, J.A., 2010. Stream capture and piracy recorded by provenance in fluvial fan strata. In: Wilford, D., Giles, P., Nichols, G. (Eds.), Alluvial Fan Research and Management: From Reconstructing Past Environments to Identifying contemporary hazards, 115 (3-4). Geomorphology, Exeter, UK, p. 267-277.

Ollenburger, R.D., 1986. Source and stratigraphy of the Livermore Gravels, Alameda County, California. unpublished MS Thesis, California State University, California, 218 pp.

Page, B.M., 1981. The southern Coast Ranges. In: Ernst, W.G., (Eds.), The Geotectonic Development of California. Prentice-Hall, Englewood Cliffs, New Jersey, p. 329-417.

Rust, G.L., 2006. Geologically-based modeling of complex groundwater flow patterns at Lawrence Livermore National Laboratory: A combined application of geostatistical methods and multiple geologic scenarios for capturing subsurface realities. unpublished MS Thesis, University of New Mexico, New Mexico, 216 pp.

Sawyer, T. L., 1999. Assessment of contractional deformation rates of the Mt. Diablo fold and thrust belt, eastern San Francisco Bay region, northern California: Final technical report. United States Geological Survey, Department of the Interior, National Earthquake Hazards Reduction Program, Award Number 98-HQ-GR-1006, 38 pp.

Shlemon, R.J., 1985. Application of soil-stratigraphic techniques to engineering geology. Bulletin of the Association of Engineering Geologists 22 (2), 129-142.

Shlemon, R. J., and Qualheim, B., J., 1993. The Sandia National Laboratory and adjacent windgaps, southeastern Livermore Valley, Alameda County, California (abstract): Geological Society of America, Abstracts with Programs, v. 25(5), p. 146.

Soil Survey Staff, 1966. Soil Survey Alameda Area, California. US Department of Agriculture Soil conservation Service, Series 1961, No. 41, 95 pp.

Springer, J. E., 1983. Structural analysis of the southeastern Livermore Basin, California. Livermore, California, Lawrence Livermore National Laboratory (UCID-19805).

Sweeny, J.J., Springer, J.E., 1981. Geology of the southern Livermore Valley, Alameda County, California. Lawrence Livermore National Laboratory (UCRL-53220).

Thorpe, R. K., Isherwood, W. S., Dresn, M. D., Webster-Scholten, C. P., 1990. Remedial investigations report for the LLNL Livermore Site. Livermore, California, Lawrence Livermore National Laboratory (UCAR-10299).

Unruh, J.R., Sawyer, T.L., 1995. Late Cenozoic growth of the Mt. Diablo fold and thrust belt, central Contra Costa County, California and implications for transpressional deformation of the northern Diablo Range. Pacific Section Convention, American Association of Petroleum Geologists and Society of Economic Paleontologists and Mineralogists, 47 pp.

Unruh, J. R., Sawyer, T. L., 1997. Assessment of blind seismogenic sources, Livermore valley, eastern San Francisco Bay region: Final technical report. United States Geological Survey, Department of the Interior, National Earthquake Hazards Reduction Program, Award Number 1434-95-G-2611, 88 pp.

Weissmann, G.S., Mount, J.F., Fogg, G.E., 2002. Glacially driven cycles in accumulation space and sequence stratigraphy of a stream-dominated alluvial fan, San Joaquin Valley, California, USA. Journal of Sedimentary Research 72, 270-281.

Weissmann, G. S., Bennett, G. L., Lansdale, A. L., 2005. Factors controlling sequence development on Quaternary fluvial fans, San Joaquin Basin, California, USA. In: Harvey, A. M., Mather, A. E., Stokes, M. (Eds.), Alluvial Fans: Geomorphology, Sedimentology, Dynamics. Geological Society, London, Special Publications 251, 169–186.

CHAPTER 2

Sedimentology and Stratigraphy

at Lawrence Livermore National Laboratory

1. Introduction

Understanding the stratigraphy at Lawrence Livermore National Laboratory (LLNL) was a goal of this study. The stratigraphy of LLNL was assessed using the data and well cores already collected by LLNL personnel. The Environmental Restoration Division (ERD) of LLNL maintains a core library of over 12 km of continuous well cores from approximately 500 wells, as well as complete geophysical data from these wells and an additional 300 wells on site. The wells range in depth from 30 m to more than 90 m. The wells were drilled by LLNL to support their ongoing research, so the core collection amounts (total meters per well) and locations (both vertical within each well, and laterally across the site) were dictated by their research and finances. The amount of core collected ranges from the complete well to approximately 10 m in zones of interest to LLNL researchers.

In support of this research, 202 well cores were described in detail amounting to 6.7 km of continuous core. Well cores were viewed and described from key locations across the site to ensure the densest description coverage of the site as allowed by time and resources (Figure 3).

2. Core Description Methods

Students from Michigan State University who described core for this study were trained and supervised by me to ensure continuity of work. The well cores were treated and viewed in the same manner by all workers.

The well cores were recovered as either three-inch or five-inch diameter cores by LLNL personnel. These cores were placed in labeled cardboard boxes and allowed to dry in the sun then stacked for storage. For description, the cores were broken in half lengthwise with a chisel and hammer to produce a fresh surface for inspection. Each box of core was first surveyed

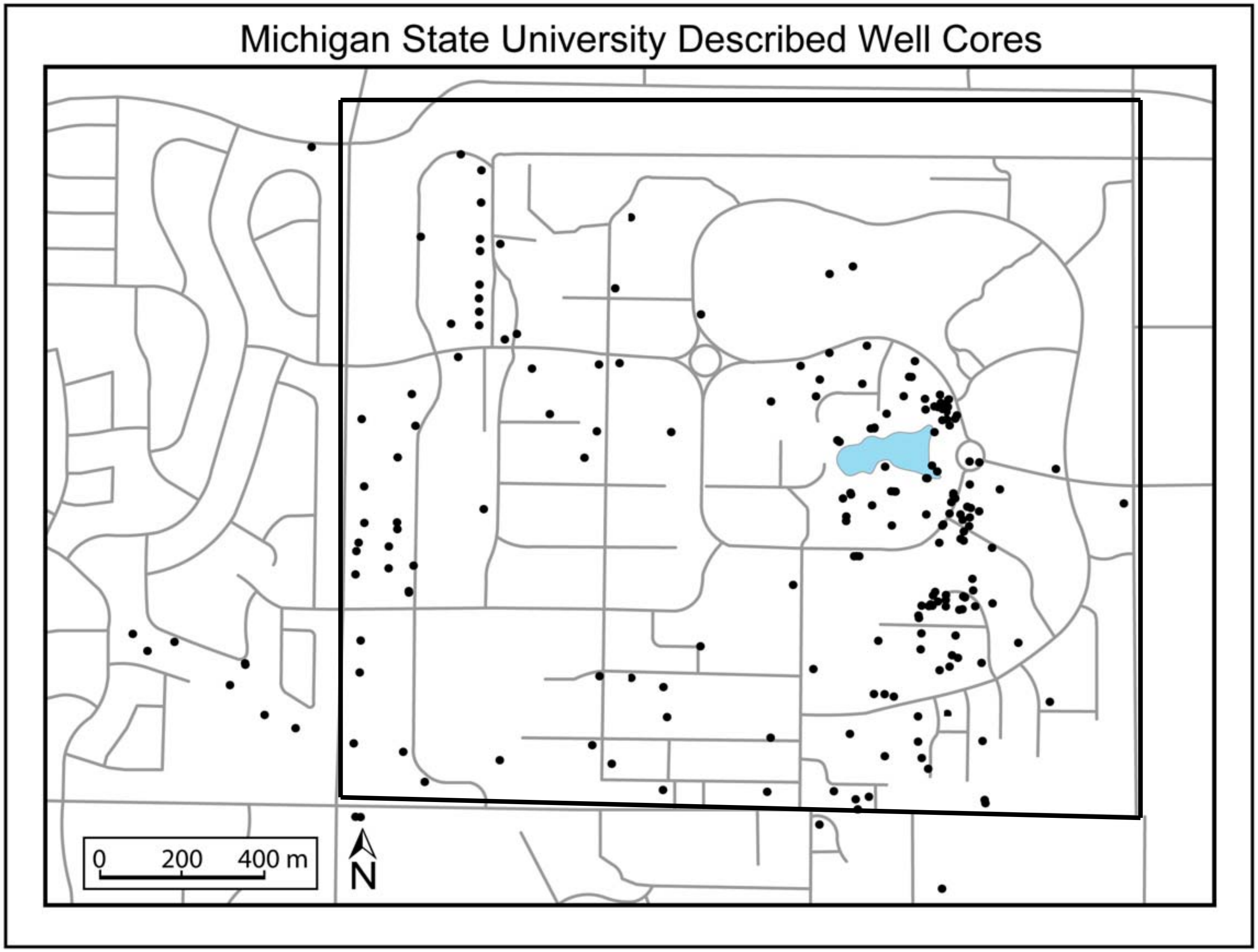

Figure 3. Location of the 202 LLNL well cores that were described by Michigan State University students. The black box outlines the extent of LLNL and corresponds to the LLNL indicator box in Figure 1, Chapter 1.

for different units, then the depth of the unit boundaries were recorded on a standard form (Figures 22a and 22b, Appendix A) used by those describing the core. After each unit boundary was identified, the description of each unit was recorded on the form. The features measured and observed are presented in Table 2. Grain size range was recorded, along with general sorting and roundness. The color of the sedimentary unit was recorded according to the Munsell Soil Color Charts (Munsell Color, 1998). Then other features were noted such as manganese oxide concentrations, root traces, soil structural units or peds, burrows, clay films or argillans, clay-rich lamellae, mottles, and carbonate accumulation. These features were described with qualitative modifiers such as few, some, or many. The argillans were described on a continuum from thin, through moderate, to very thick. The carbonate accumulation was described as Stages based on diffuse, filaments, filling root traces, nodules, or cemented core. These detailed descriptions were then used to differentiate seven different facies within the well cores.

Table 2. Measurement and determination of features in core descriptions at LLNL

Feature	**Feature Value**	**Measurement or Determination**	**Reference**
Grain Size		Determinations were made with a hand lens and a chart for reference.	Wentworth, 1922
	Silt	0.0039 mm - 0.0625 mm	
	Very Fine Sand	0.0625 mm - 0.125 mm	
	Fine Sand	0.125 mm - 0.25 mm	
	Medium Sand	0.25 mm - 0.5 mm	
	Coarse Sand	0.5 mm - 1.0 mm	
	Very Coarse Sand	1.0 mm - 2.0 mm	
	Granule	2.0 mm - 4.0 mm	
	Pebble	4.0 mm - 32 mm	
	Cobble	32 mm - 256 mm	
Color		Colors were matched to Munsell Charts	Munsell, 1998
Burrows		Noted if present	
Lamellae		Noted if present	
Mottles		Noted if present and record colors	Munsell, 1998

Table 2 (continued). Measurement and determination of features in core descriptions at LLNL

Feature	**Feature Value**	**Measurement or Determination**	**Reference**
Sorting	 Very Poorly Poorly Moderately Well Well Very Well	Determinations were made with a hand lens and a chart for reference.	Harrell, 1984
Roundness	 Very Angular Angular Subangular Subrounded Rounded Well Rounded	Determinations were made with a hand lens and a chart for reference.	Powers, 1953
Argillans	 Thin Thin to Moderate Moderate Moderate to Thick Thick Very Thick	No measurements were taken of argillan thicknesses. Determinations were made by students who were trained by me to observe the different classifications. The students were also spot-checked by me to ensure consistency in descriptions.	
Carbonate Accumulation	 Stage I Stage I+ Stage II Stage II+ Stage III	Stage determination was made based on following observations: Diffuse to few thin filaments Many filaments Many filaments and small nodules Large nodules and filled root traces Core-diameter nodules or cemented	Gile et al., 1966
Soil Structure	 Massive Prismatic Subangular Blocky	Determinations were made by students.	Soil Survey Staff, 1975
Manganese Concentrations	 Small Large Root-filling Ped-coating	Determination was made based on following observations: Up to approximately 1 mm Approximately 1 mm to 3 mm Within root traces Surface of ped covered	

3. Facies Descriptions

The descriptions allowed the well cores to be divided into seven facies: 1) clast-supported gravel, 2) matrix-supported gravel, 3) sand, 4) silty sand, 5) silty sand with clay lamellae, 6) paleosol, and the finer-grained facies of the Upper Livermore Formation locally (Wigginton and Carey, 1982), in accordance with local nomenclature, 7) the "Lower Livermore" (Table 3). Together, these facies and facies associations represent a typical fluvial fan system (Chapter 3 in Reading, 1996).

Table 3. Facies described in LLNL well cores with interpreted depositional environments

Facies	Description	Interpretation
Paleosol	Moderate- to well-sorted, silt- to medium-grained sand, exhibiting pedogenic characteristics (e.g., root traces, burrows, argillans, carbonate accumulations, peds, manganese oxide concentrations)	Paleo-soils that were at one time the active soil on the landscape and have subsequently been buried
Silty sand	Poorly-sorted, silt- to fine-grained sand, angular to subangular grains, massive, no discernable structural soil units	Floodplain deposits
Silty sand with clay lamellae	Silty sand facies interbedded with darker, clay-rich lamellae	Crevasse splay and floodplain deposits
Sand	Well- to moderately well-sorted, medium- to coarse-grained sand, subangular to subrounded grains, units were often friable	Sand bar and point bar deposits
Clast-Supported Gravel	Very poorly-sorted, sand to coarse gravel, angular to rounded, clast-supported with fine-grained matrix	Channel deposits
Matrix-supported gravel	Very poorly-sorted, angular to rounded, matrix-supported with clay-rich matrix	Apex of fan, result of mass movement or hyperconcentrated flow
"Lower Livermore" (local nomenclature)	Below the fluvial fan and the lower boundary of fan system, clay-rich aquitard with dense bluish-green to blue-black clay beds, often exhibited very thick carbonate accumulations	Playa lake with reducing conditions resulting in the bluish color due to reduced iron

3.1 Clast-Supported Gravel Facies

The clast-supported gravel facies were the coarsest units with larger pebbles up to 5 cm in diameter (Figure 4). These units were moderately- to very poorly- sorted and the clasts were angular to rounded. The clast-supported gravel facies were not clean gravels in that they contained a finer-grained matrix as well as reddish clay coatings on many pebbles. Manganese oxide was common on the matrix and larger clasts.

Figure 4. Example of clast-supported gravel facies from LLNL. The orange material is a plastic place marker inserted by the driller. Core box is 0.6 m wide. Depth increases from upper left to lower right.

3.2 Matrix-Supported Gravel Facies

The matrix-supported gravel facies were similar to the clast-supported gravel units with up to 5 cm clasts except they were clay-rich and matrix-supported (Figure 5). The matrix incorporated fine-grained sand, but was dominated by clay. This facies was very poorly-sorted and the clasts were very angular to subrounded. These units also exhibited manganese oxide concentrations on the matrix.

Figure 5. Example of matrix-supported gravel facies from LLNL. The portion of core box shown is 0.3 m wide. Depth increases from upper left to lower right.

3.3 Sand Facies

The sand facies contained medium- to coarse-grained sand with very few finer grains and no silt or clay (Figure 6). These units were often friable. They were well- to moderately well-sorted and the grains were subrounded to subangular. These units were occasionally interbedded with layers of coarse to very coarse sand. Some units showed signs of cross-stratification.

Figure 6. Example of sand facies from LLNL. The upper row shows friable sand that is held together by driller's mud. The lower row shows bedded sand with possible cross-stratification. The portion of core box shown is 0.3 m wide. Depth increases from upper left to lower right.

3.4 Silty Sand Facies

The silty sand facies were units of finer-grained sands with a high silt content (Figures 7 and 8). These units were generally poorly-sorted and the grains were subangular to angular. They were massive with no discernable structures. The silty sand units typically contained root traces, manganese oxide concentrations and frequently very thin to thin argillans.

Figure 7. Example of silty sand facies from LLNL. Black marks on the core are manganese oxide concentrations. The core box is 0.6 m wide. Depth increases from upper left to lower right.

Figure 8. Example of silty sand facies from LLNL. This photograph was taken with a flash allowing the manganese oxide concentrations to be more visibly distinct. The core box is 0.6 m wide. Depth increases from left to right.

3.5 Silty Sand with Clay Lamellae Facies

The silty sand with clay lamellae facies contained layers of the silty sand facies from 1 cm to 6 cm thick interbedded with 1 mm to 3 mm layers of silty clay (Figures 9 and 10). The silty sand and the silty clay layers were distinguished visually by their different colors with the silty clay layers being darker than the silty sand.

Figure 9. Example of silty sand with clay lamellae facies from LLNL. The silty clay lamellae can be seen as the darker stripes within the core. The core box is 0.6 m wide. Depth increases from left to right.

Figure 10. Close up of an example of silty sand with clay lamellae facies from LLNL. The silty clay lamellae can be seen as the darker stripes within the core. Tape-measure is for scale. Depth increases from left to right.

3.6 Paleosol Facies

The paleosol facies exhibited several pedogenic features to various degrees (Figure 11). In general, the paleosols were developed in silt- to medium-grained sediment that was moderately- to well-sorted. Most of the units had soil structural units or peds that were either blocky or prismatic. The paleosols had thin to very thick argillans causing the units to be darker and redder in color than the other sedimentary units in the well cores. They also had secondary carbonate accumulation in various forms from thin filaments to coating ped faces (Figure 12). These facies also showed evidence of biota as seen by root traces or burrows (Figure 13). The root traces were occasionally drab-haloed and were filled with clay or carbonate (Figure 14). Manganese oxide was common on the ped faces (Figure 15).

Figure 11. Example of paleosol facies from LLNL. The paleosol starts in the second row and continues into the third row. The reddish clay of the paleosol is distinct from the silty sand facies in the first and fourth rows. Secondary carbonate is also visible filling root traces within the paleosol. The core box is 0.6 m wide. Depth increases from upper left to lower right.

Figure 12. Example of Stage III, ped-coating carbonate accumulation within a paleosol facies from LLNL. The carbonate is the white material seen on the core face. The portion of core box shown is 0.3 m wide. Depth increases from upper left to lower right.

Figure 13. Close up of an example of a burrow within a paleosol facies from LLNL. The burrow is filled with clay. Tape-measure is for scale. Depth increases from left to right.

Figure 14. Close up of an example of a root trace within a paleosol facies from LLNL. The root trace is filled with clay and has a lighter-colored drab halo surrounding it. Manganese oxide can also be seen as small concentrations on the left side of the photograph and as filling root traces on the right side. Tape-measure is for scale. Depth increases from left to right.

Figure 15. Example of ped-coating manganese oxide concentration within a paleosol facies from LLNL. The manganese oxide is the black material seen on the core face. The portion of core box shown is 0.3 m wide. Depth increases from left to right.

3.7 "Lower Livermore" Facies

The "Lower Livermore" (LL) facies, as known by local nomenclature, was below the fluvial fan and was the lower boundary of the fluvial fan system (Figure 16). LL was a bluish-green to blue-black unit below the tan to brown fluvial fan deposits (Figure 17). LL also contained thick, very dense, black clay beds and often exhibited thick carbonate accumulation (Figure 18). Occasional small, cubic-shaped voids were observed in the core that were the result of the dissolution of soluble salts. Present, but rare, were slickensides in the upper part of LL (Figure 19).

Figure 16. Example of "Lower Livermore" facies from LLNL. This is an example of the bluish-green colored sediment. The white material in the top row is paper towel used by the driller as a space marker. The core box is 0.6 m wide. Depth increases from upper left to lower right.

Figure 17. Example of “Lower Livermore” facies from LLNL. This photograph shows the tan to brown fluvial fan sediments in the top two rows and the LL bluish-green sediments in the lower three rows. The core box is 0.6 m wide. Depth increases from upper left to lower right.

Figure 18. Example of “Lower Livermore” facies from LLNL. This is an example of the bluish-black colored sediment with carbonate. The carbonate is the white material on the dark LL clay-rich sediment. The core box is 0.6 m wide. Depth increases from upper left to lower right.

Figure 19. Close up of an example of a slickenside within the “Lower Livermore” facies from LLNL. This slickenside was recovered from an approximate depth of 83 m. Ruler is for scale.

4. Facies Interpretations

The depositional environment for each facies was interpreted based on facies characteristics (Table 3) (Chapter 3 in Reading, 1996).

4.1 Clast-Supported Gravel Facies

The clast-supported gravel facies was interpreted as channel deposits (Weissmann, 2001; Trahan, 2003). The fine-grained sediment included with the pebble-sized clasts indicates streams with periods of lower flow velocity allowing the fine sediment to settle out of suspension along with the pebbles.

4.2 Matrix-Supported Gravel Facies

The matrix-supported gravel facies was interpreted as hyperconcentrated debris flow deposits which are characterized by poorly sorted sediment that lacks sedimentary structure. These facies were only found in the southeastern and central eastern portion of LLNL. This location is near the apices of the fluvial fans and where mass movement could produce hyperconcentrated flow of sediment and debris flow.

4.3 Sand Facies

The sand facies was interpreted to be the deposits of sand bars and point bars along the edge of the main channel and between anastomosing channels where the water has lower velocity than the center of the channel allowing the sand-size clasts to settle. These regions are characterized by cross-stratification, which were seen in the LLNL well cores.

4.4 Silty Sand Facies

The silty sand facies was interpreted to be floodplain deposits which occur when the stream overtops its banks and deposits fine-grain sediment adjacent to the stream.

4.5 Silty Sand with Clay Lamellae Facies

The silty sand with clay lamellae facies was interpreted to be crevasse splay deposits and floodplain deposits. Floodwaters containing both fine-grain and silt-sized sediments occasionally breach the stream’s natural levees. When this occurs, the coarser sediment settles out of suspension first leaving the silt and clay particles to settle on top the coarser sediment forming the thin silty clay lamellae.

4.6 Paleosol Facies

The paleosol facies were pedogenically altered sedimentary units. These units were once the active soil on the geomorphic surface and then were buried by the sedimentation processes of the fluvial fan. These facies have been determined to be paleosols based on evidence of soil development (Retallack, 1988; Wright, 1990; Alonso-Zarza et al., 1999).

4.6.1 Evidence for Paleosol Classification

In order to determine whether a stratigraphic unit is a paleosol and not simply a sedimentary unit, it is best to describe it as one would a modern soil using standard pedologic techniques (Schaetzl and Anderson, 2005). The stratigraphic units at LLNL that were classified as paleosols were identified using soil characteristics (e.g., root traces, burrows, soil structural units, clay argillans, carbonate accumulation, and manganese oxide accumulation) because these features indicate the unit was once the active soil on the landscape and has subsequently been buried.

Retallack (1988) lists three main features of paleosols that are useful in distinguishing them from the unaltered sediment, or parent material. First, Retallack (1988) cites biota activity such as root traces as evidence that a particular unit was a soil because by most definitions a soil sustains plant life. Along with root traces, Retallack (1988) also mentions burrows because burrowing animals reside in the soil.

Second, Retallack (1988) lists soil horizons as evidence that a unit was once a soil. Horizonation, or the conditions and processes that organize the profile into horizons by means of additions, removals, transfers, and transformation of material (Schaetzl and Anderson, 2005) is indicative of a soil. However, Retallack (1988) cautions that that the nature of paleosol horizons varies considerably.   The paleosols described from LLNL cores do not have distinct horizons or a developed profile, and most likely were soils that fit into what Reading (1996) describes as 'alluvial soils' or 'accumulative hydromorphic soils'. These immature soils are found on most vegetated floodplains. Due to the continual sedimentation they usually lack clearly developed profiles; however, these units are still classified as soils (Reading, 1996).

The third and final feature from Retallack's (1988) list is soil structural units. Soil structural units, or peds which are aggregates of soil material, form at the expense of the parent material's original sedimentary structures (e.g., bedding, crystal structure, and schistosity) (Retallack, 1988). The wetting and drying cycles, bioturbation, illuviation of clay into the solum, and other soil-forming processes create peds. Peds are a result of pedogenic processes and therefore indicative of a soil.

Clay on ped faces is indicative of soil development (Schaetzl and Anderson, 2005). This clay can be from illuvial clay (clay that has washed down into the soil), or by clay that is formed *in situ* (Schaetzl and Anderson, 2005). Clay-rich horizons in soils are so common that soil taxonomies recognize them in nomenclature with the horizon suffix of 't', from the German word *ton* for potter's clay (Soil Survey Staff, 1999).

Another feature used to identify paleosols at LLNL was the presence of secondary carbonate accumulations. These accumulations are a result of surface water passing through the soil and leaving precipitated calcium carbonate. Such accumulation of calcium carbonate is widespread in many semi-arid and arid environments (Wright, 1990; Alonso-Zarza et al., 1999).

The final feature used in identifying paleosols at LLNL was manganese oxide concentrations. The presence of manganese oxide concentrations indicates a soil environment of alternating periods of wetting and drying resulting in alternating periods of reducing and oxidizing conditions (Schaetzl and Anderson, 2005). During the wet periods, the manganese is reduced and mobile allowing movement with groundwater along flow pathways. During dry periods, the manganese oxidizes and is immobile forming dark-colored concentrations and nodules (Schaetzl and Anderson, 2005). Although this feature many be present in non-soil sediment, the manganese oxide concentrations were notably larger and more abundant in the paleosol units at LLNL.

4.7 “Lower Livermore” Facies

The “Lower Livermore” facies was interpreted as a playa lake environment. Evidence of soluble salts remained in the form of cubic-shaped voids. In this semi-arid Mediterranean climate, these salts likely formed upon evaporation during the drier season. The bluish and black color of the sediment was produced due to the reducing redox (i.e. reducing or oxidation) state during the formation of this unit. The very thick, dense clay is indicative of a lake system. Due to the thick clay, this unit serves as an aquitard locally. LL is the lower boundary of the fluvial fan system and likely correlative with the finer-grained facies of the Upper Livermore Formation (Wigginton and Carey, 1982) (Table 1, Chapter 1).

5. Stratigraphic Columns

Facies data from the described LLNL well cores were entered into LogPlot, a graphics computer program (RockWare, 2002). Using LogPlot, stratigraphic columns were generated that were used for this study (Appendix B, Figures 23 – 224).

6. Stratigraphic Correlation at LLNL

6.1 Paleosols as Stratigraphic Markers

Soils are the result of a dynamic interaction of forces and conditions acting upon a parent material changing it into a complex system with distinct horizons in a process known as pedogenesis. Schaetzl and Anderson (2005) provide a partial list of soil-forming conditions and environmental factors which interact affecting and altering a parent material to create a soil. Their list includes: original parent material, burial, climate changes, additions of organic matter, biomechanical mixing, water table effects, microclimate associated with topography, and input of eolian dust. Soils form in all climatic regimes with different climate-dependent horizon characteristics [e.g., tropical (e.g., Chorover et al., 2004; Jiang et al., 2011), Mediterranean-like, semi-arid (e.g., Badía et al., 2009; Sauer, 2010)], and are therefore present on most geomorphic surfaces.

A paleosol, or buried soil, indicates a time when that stratigraphic unit was the land surface and soil was forming (Shlemon, 1985). These stratigraphic units are potentially useful in facies correlation because soils develop across a majority, if not all, of a geomorphic surface (Shlemon, 1985; Harden et al., 1991; Schaetzl and Anderson, 2005) starting at the onset of surface stability (Harden et al., 1991), and are generally laterally continuous making a buried soil potentially ideal as a correlation tool (Shlemon, 1985). Many researchers have used the continuity of paleosols as a starting point to understanding the stratigraphy in their study sites (e.g., Shlemon, 1985; Weissmann et al., 2002). Shlemon (1985) reported that the remnant argillic, or clay-rich, horizons of paleosols along the California coast were laterally traceable for several kilometers. Mature soils formed on the Kings River alluvial fan in the Great Valley of California during interglacial periods when the fan surface was stable, thus marking the unconformity between the two depositional sequences (Weissmann et al., 2002). These paleosol facies were correlatable across the entire 3150 km^2 fan (Weissmann et al., 2002).

6.2 Paleosol Unit Correlation at LLNL

Understanding and mapping the stratigraphy at LLNL was one of the goals of this study. The correlation of stratigraphic units primarily focused on the paleosol units.

6.2.1 Correlation of Facies Pilot Project at LLNL

Weissmann (2001) conducted a detailed hydrostratigraphic analysis of the aquifer beneath the LLNL Helipad Site examining 15 wells with a spacing of 6 m to 8 m from which he produced stratigraphic columns and generated 15 cross sections. Weissmann (2001) stated that within the approximately 1,600 m^2 Helipad Site (Figure 20) only the paleosols could be correlated with any certainty, and it appeared that the paleosols were the stratigraphic units which marked sequence boundaries within the alluvial fan deposits beneath LLNL. It was concluded that further work was needed to understand the sequence stratigraphy at the site, and the study area needed to be expanded to help provide evidence that the paleosols were laterally extensive units (Weissmann, 2001).

6.2.2 Helipad Site Correlation of Facies at LLNL

Trahan (2003) conducted a hydrologic study at the LLNL Helipad Site and immediately surrounding area (Figure 20) in order to model pumping tests within a heterogeneous alluvial aquifer. To support these models, 32 wells were characterized and 14 cross sections were generated. Trahan (2003), like Weissmann (2001), stated the paleosols were laterally extensive

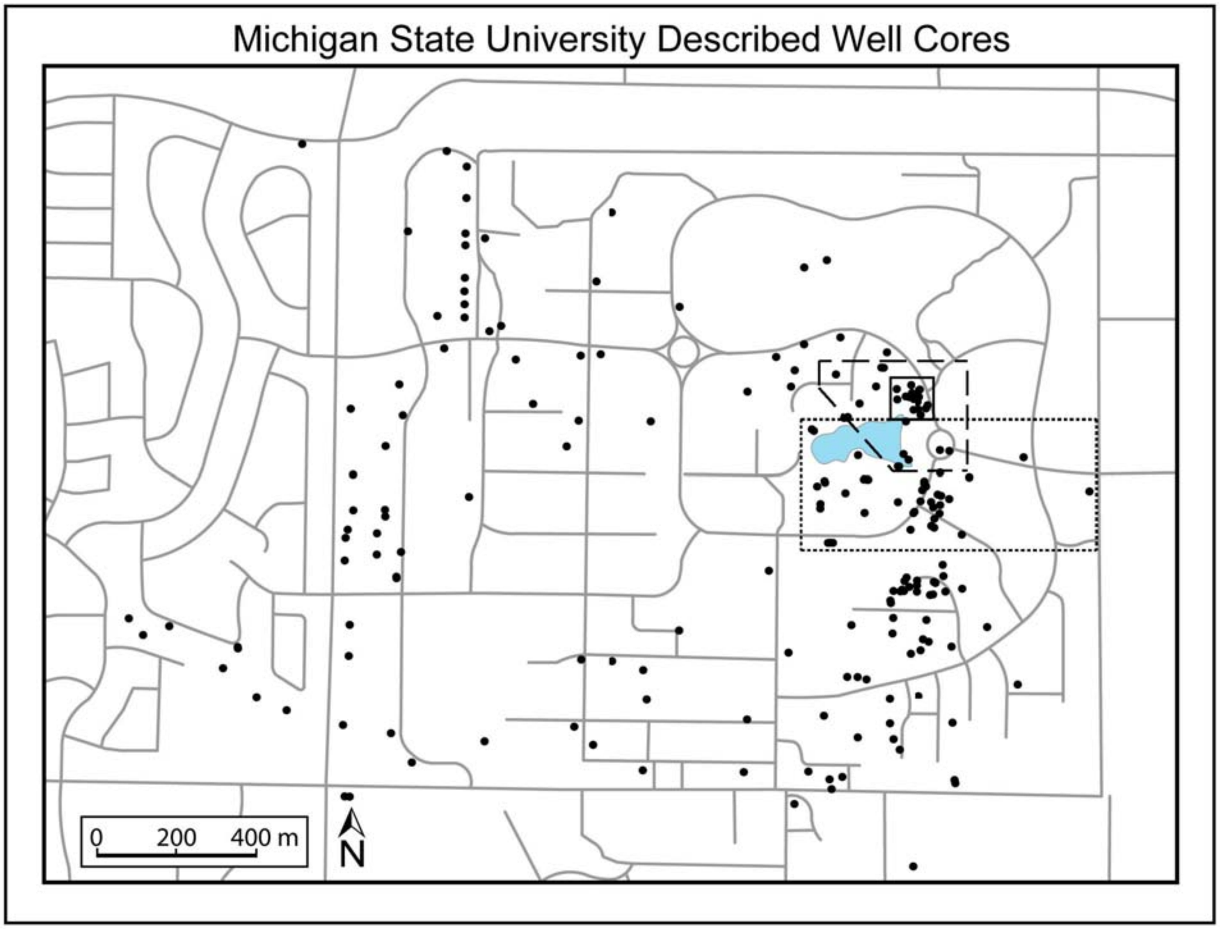

Figure 20. Map of studies conducted at LLNL. Weissmann (2001) study area at the Helipad Site is indicated by the solid line. Trahan (2003) study area at the Helipad Site and immediately surrounding area is indicated by the large-dashed line. Rust (2006) study area at the East Traffic Circle is indicated by the dotted line.

across the entire Helipad Site and could be correlated between most wells with some certainty. In well cores where expected paleosols were missing, a unit of gravel or sand was present in their place. The placement of these gravel units could indicate that during or after the time of soil-formation the geomorphic surface was locally eroded by a stream which in turn left stream bed deposits in place of the paleosol (Weissmann, 2001; Trahan, 2003). The successful paleosol correlations at this location provided the basis for the expectations of the present study that paleosol correlation would be possible throughout the larger LLNL site.

6.2.3 East Traffic Circle Correlation of Facies at LLNL

Based on the successful correlation of units at the Helipad Site, Rust (2006) conducted a study at the LLNL East Traffic Circle (ETC) which is located south of the Helipad Site (Figure 20). Fifty-one wells from within the 12,100 m^2 site were examined for this study. The primary goal of the study was to develop a geologically-based conceptual model to increase the knowledge of the hydrological system beneath LLNL. To produce the model Rust (2006) attempted to correlate the strata beginning with correlating the paleosols in the 51 wells. Rust (2006) found 3 m to be the maximum lateral extent of good correlation within that site and noted that correlations became less certain at 9 m well spacing.

During the correlation exercise, it was noticed that the Lower Livermore (LL) unit was vertically offset by 5 – 15 m between wells. LL is an aquitard locally and marks the lower depth boundary for the studies of the fluvial fans at LLNL. The depositional environment of LL has been interpreted as being a lake or playa due in part to the presence of voids left by the dissolution of soluble salts, very thick clay units, and an overall bluish color indicating a reducing redox state. This interpretation suggests one continuous geomorphic surface and therefore lateral continuity of LL. Based on that premise, Rust (2006) hypothesized faulting was the cause for both the offset in LL and the lack of lateral continuity in the paleosols.

By shifting the stratigraphic columns and generating cross sections in which the LL was aligned, Rust (2006) noted that the paleosols became observably more continuous. Extent of lateral continuity was based on the ability to visually follow paleosol units in cross-sections from well to well at roughly the same depth. After shifting the stratigraphic columns to align LL in all wells, the paleosols were traceable in more wells than they were prior to shifting. Rust (2006) went on to cite an unpublished seismic survey conducted in 1996 which revealed a high number of normal faults throughout her study area, yet revealed no faulting within the Helipad Site where stratigraphic correlation was successful (Weissmann, 2001; Trahan, 2003). The conclusions from Rust's (2006) study state that the paleosols were not laterally continuous at ETC and were not useful as stratigraphic markers because: 1) the scale of sedimentological variability is below the resolution of the available data, 2) paleosols are not appropriate markers for correlations in this region possibly due to erosion by stream channel avulsion and meandering on the fan surface, or 3) faulting which significantly disrupted the stratigraphy. The difficulty of correlating the ETC facies is due to the complex depositional environment and the tectonic overprinting which has resulted in highly variable facies geometries (Rust, 2006). Based on these conclusions, Rust (2006) suggests that paleosols are not suitable as stratigraphic markers in correlation attempts for LLNL regions larger than 1,600 m^2 or which have experience faulting.

6.2.4 Correlation of Facies at Helipad Site Based on Realignment of LL

The correlation method Rust (2006) used of realigning stratigraphic columns was based on vertically shifting adjacent columns so that the top of LL was aligned. After LL was aligned, the columns were inspected for other correlatable units above the LL. This technique was considered for correlating other stratigraphic columns at LLNL. Since Rust (2006) concluded that a distance of 3 m to 9 m between wells was the maximum lateral extent for good correlation, only closely spaced wells were considered for this exercise. Within LLNL, the wells at the Helipad Site are the most closely spaced (Figure 20).

Five wells from the Helipad Site were chosen to apply Rust's (2006) realignment technique (Figure 21). W-1553 (Figure 191) intercepts LL at a depth of 41 m. The wells closest to W-1553 to the north and east (W-1650 (Figure 197) at a distance of 10 m from

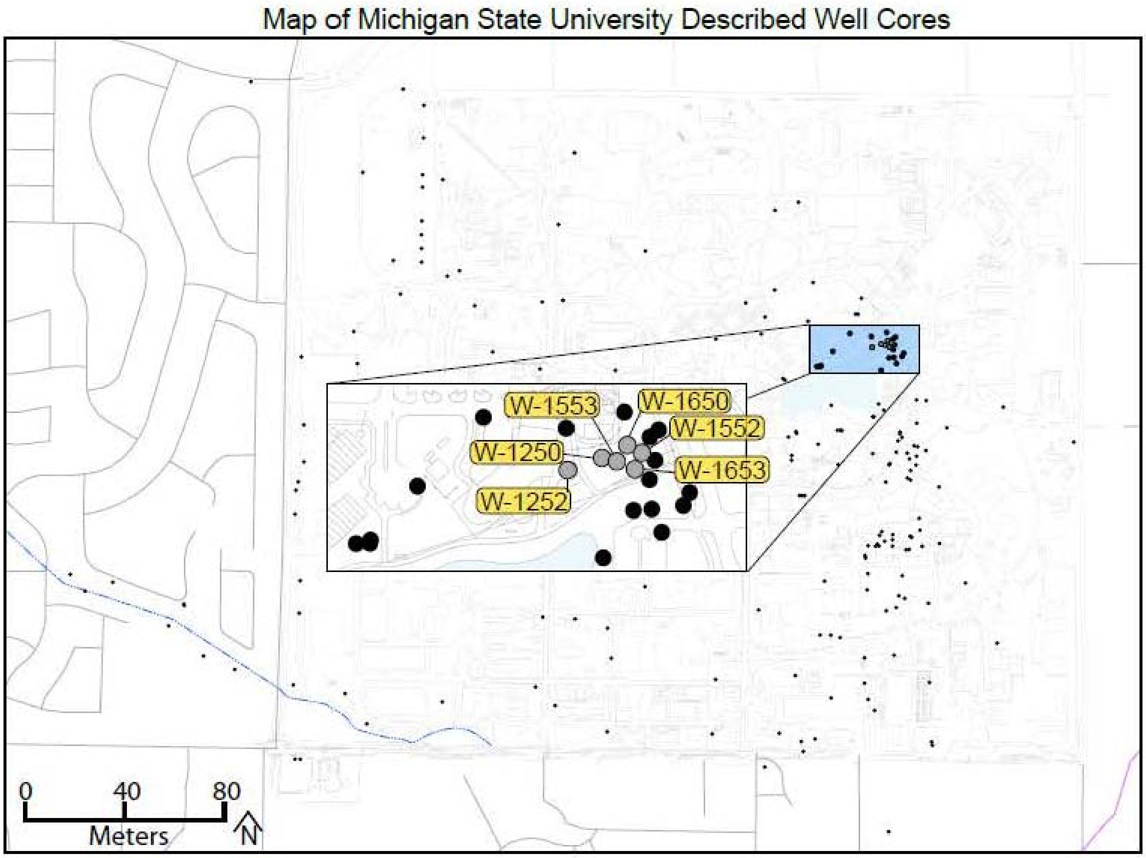

Figure 21. Closely spaced Helipad Site wells that were used for stratigraphic correlation using Rust's (2006) method of aligning LL. The scale bar indicates distances within the enlarged box.

W-1553, W-1552 (Figure 190) at a distance of 18 m from W-1553, and W-1653 (Figure 198) at a distance of 10 m from W-1553) do not intercept LL. The well closest to W-1553 to the west is W-1250 (Figure 139) at a lateral distance of 8 m. W-1250 intercepts LL at a depth of 55.5 m, or 14.5 m deeper than does W-1553. With the surface of the stratigraphic columns aligned between these two wells, four units appeared to correlate. After shifting the stratigraphic columns 14.5 m so that LL was aligned, four different units appeared to correlate. Within 41 m of described well core, the number of correlatable units did not change after applying Rust's (2006) technique. The next closest well to W-1250 that intercepts LL is W-1252 (Figure 141) at a lateral distance of 26 m. Even though the distance exceeds Rust's (2006) recommended 3 m to 9 m, W-1252 was chosen for this exercise because it did intercept LL. LL is deeper in W-1250 with a vertical offset of 4.5 m. Again the stratigraphic columns from these two well were visually inspected and three units were correlatable when the surface was aligned. After shifting the columns by 4.5 m to align LL, three different units appeared to correlate. After applying Rust's (2006) technique of shifting the columns and aligning LL, the correlatability of units between these two wells did not improve. Even with closely spaced wells, Rust's (2006) technique did not improve correlatability between wells at the Helipad Site.

Unlike at ETC, the correlatability of the stratigraphic columns of the closely spaced Helipad Site wells did not improve after aligning LL. This result may be due to the faults noted in Rust's (2006) study area for which compensation was made by realigning the columns. Since there were no faults noted within the Helipad Site (Rust, 2006), the offset of LL in that area may be due to other factors that cannot be corrected by simple realignment of the stratigraphic columns.

6.2.5 Correlation of Facies Site-Wide at LLNL

The correlation method Rust (2006) used of realigning stratigraphic columns was not attempted for the entire LLNL site. This exercise was not possible for correlation site-wide because only approximately 35 percent of the wells intercept LL and most of the wells west of ETC do not intercept LL. The subsidence is higher basinward and thus LL is deeper to the west. Without the benefit of deep wells which could intercept LL, realignment of stratigraphic columns based on this method was not possible. Rust (2006) also concluded that correlation at LLNL requires a 3 m to 9 m maximum well spacing for acceptable correlation. The wells outside of the Helipad Site and ETC have a well spacing far in excess of 9 m making facies correlation difficult even if alignment of LL were possible between the wells.

7. Conclusion

The well cores described at LLNL indicate the stratigraphy of a fluvial fan environment with all regions of the geomorphic landscape represented. The clast-supported gravels indicate the stream channels and the sand facies were deposited as bars along the channels. The silty sand facies indicate the floodplain environment, and crevasse splays were indicated by silty sand with clay lamellae. Matrix-supported gravel units were found near the apices of the fans and indicate hyperconcentrated flow of sediment onto the fan surface. The paleosol facies indicate regions of the fan that were stable for long enough periods of time for soil to develop. The whole fluvial fan system is underlain by the "Lower Livermore" facies that is clay-rich and a local aquitard.

Correlating units between wells at LLNL is difficult due to several factors. The sedimentary deposits of the streams in this fluvial fan system are limited to less than several meters in lateral extent. The lateral continuity of the sedimentary deposits is further disturbed by faulting in the area. As noted by Rust (2006), several small faults disturb the lateral continuity in some areas of LLNL making unit correlation difficult, if not impossible at the scale at which the wells are spaced. Even though the well spacing in areas of LLNL (e.g., Helipad Site and ETC) is relatively close (i.e., 10 m to 30 m) this spacing exceeds the apparent optimal distance for strong correlation of units within LLNL well cores. This work supports the conclusion of Rust (2006) that a well spacing of approximately 3 m would be needed for correlatability of LLNL well cores.

APPENDIX A

Blank Core Description Form

Well Name: Location:

Date: Described by:

		Sedimentary and Biogenic Texture and Structures												Graphic Grain Size										Sorting				
				Sand												Sand												
Core #	Depth (__)	Clay/Shale	Silt	V. Fine	Fine	Medium	Coarse	V. Coarse	Gravel	Pebbles	Cobbles	Basic Rock	Type	Clay/Shale	Silt	V. Fine	Fine	Medium	Coarse	V. Coarse	Granule	Pebbles	Cobbles	V. Poorly	Poorly	Moderately	Well	V. Well

Figure 22a. Blank core description form used in describing LLNL core. The form presented here has been modified to meet Michigan State University Graduate School's formatting requirements; the font size here is larger than on the original one-page form.

Page: of

Roundness						Color	Comments
V. Angular	Angular	Subangular	Subrounded	Rounded	Well Rounded		

Figure 22b. Continuation of the blank core description form used in describing LLNL core. The form presented here has been modified and the font size here is larger than on the original one-page form.

APPENDIX B

Lawrence Livermore National Laboratory

Stratigraphic Columns

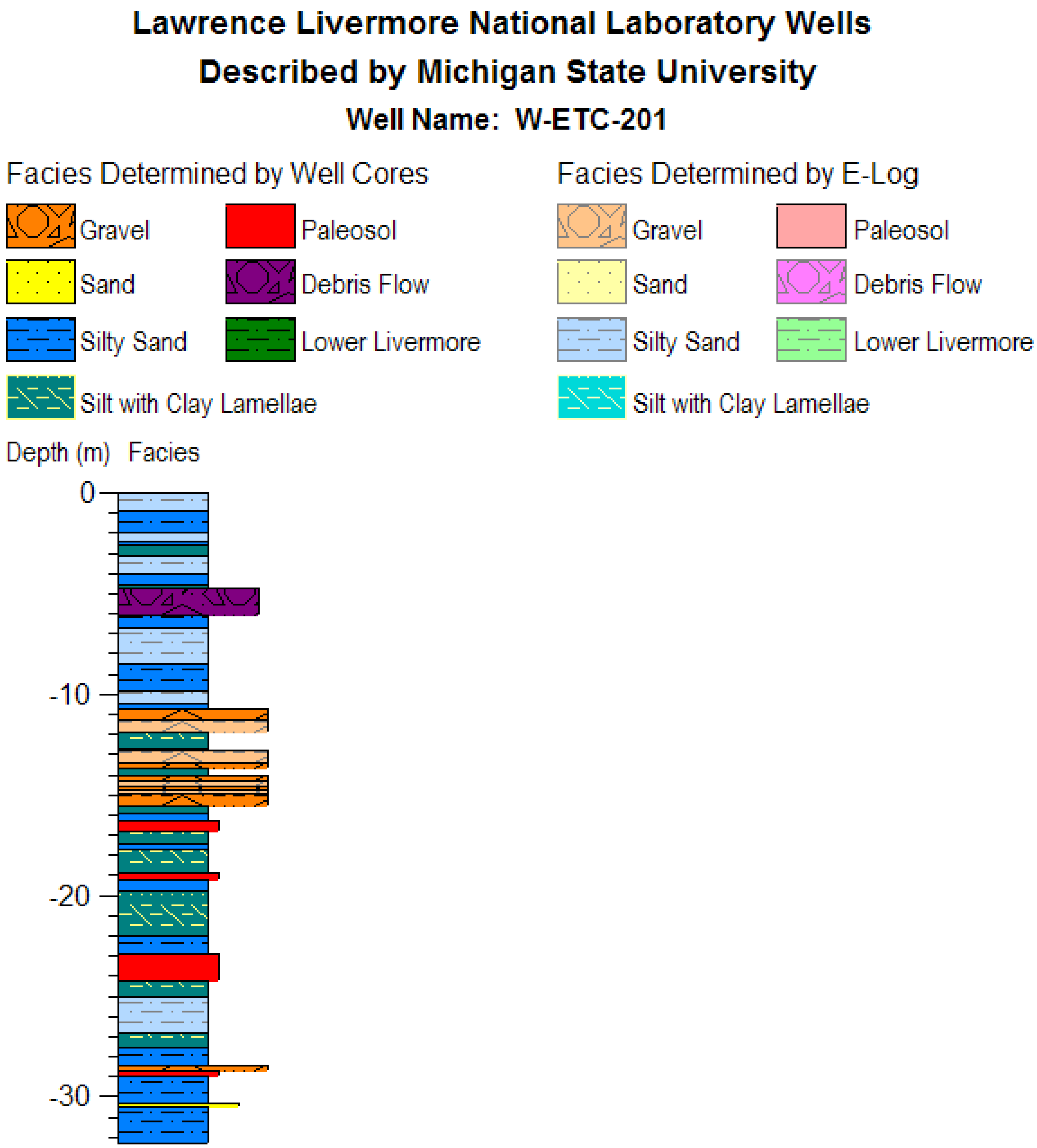

Figure 23. W-ETC-201 stratigraphic column.

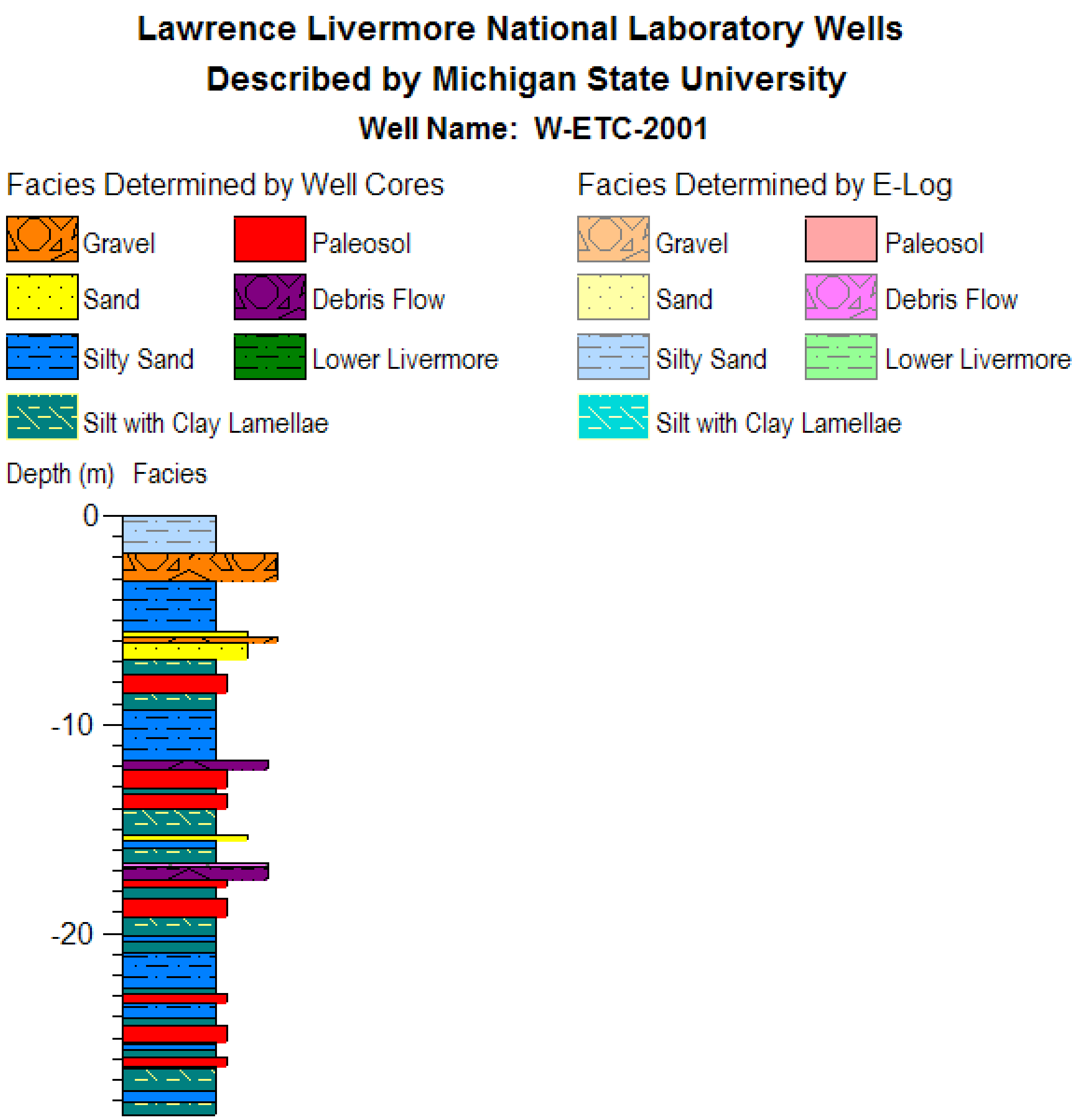

Figure 24. W-ETC-2001 stratigraphic column.

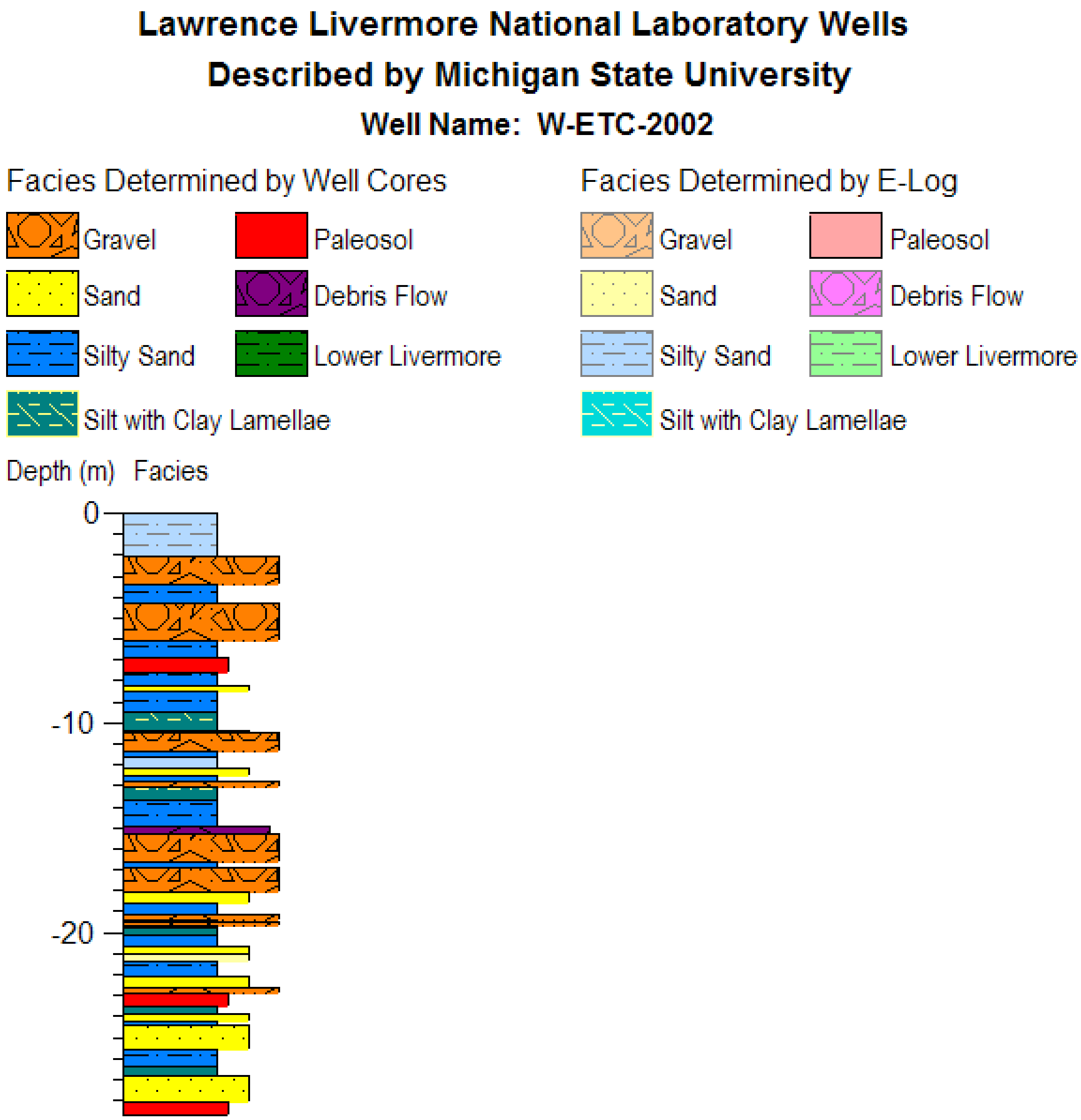

Figure 25. W-ETC-2002 stratigraphic column.

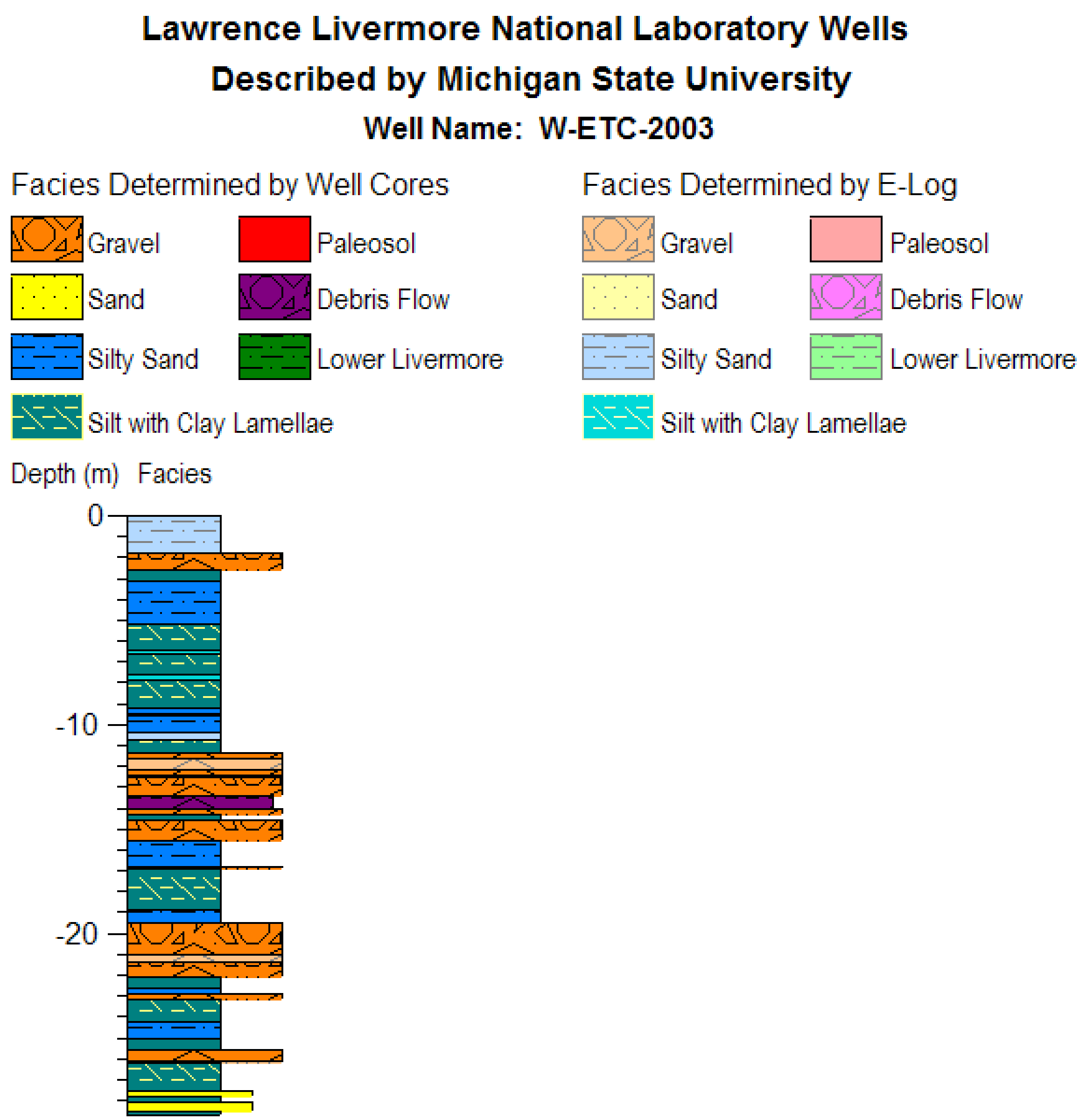

Figure 26. W-ETC-2003 stratigraphic column.

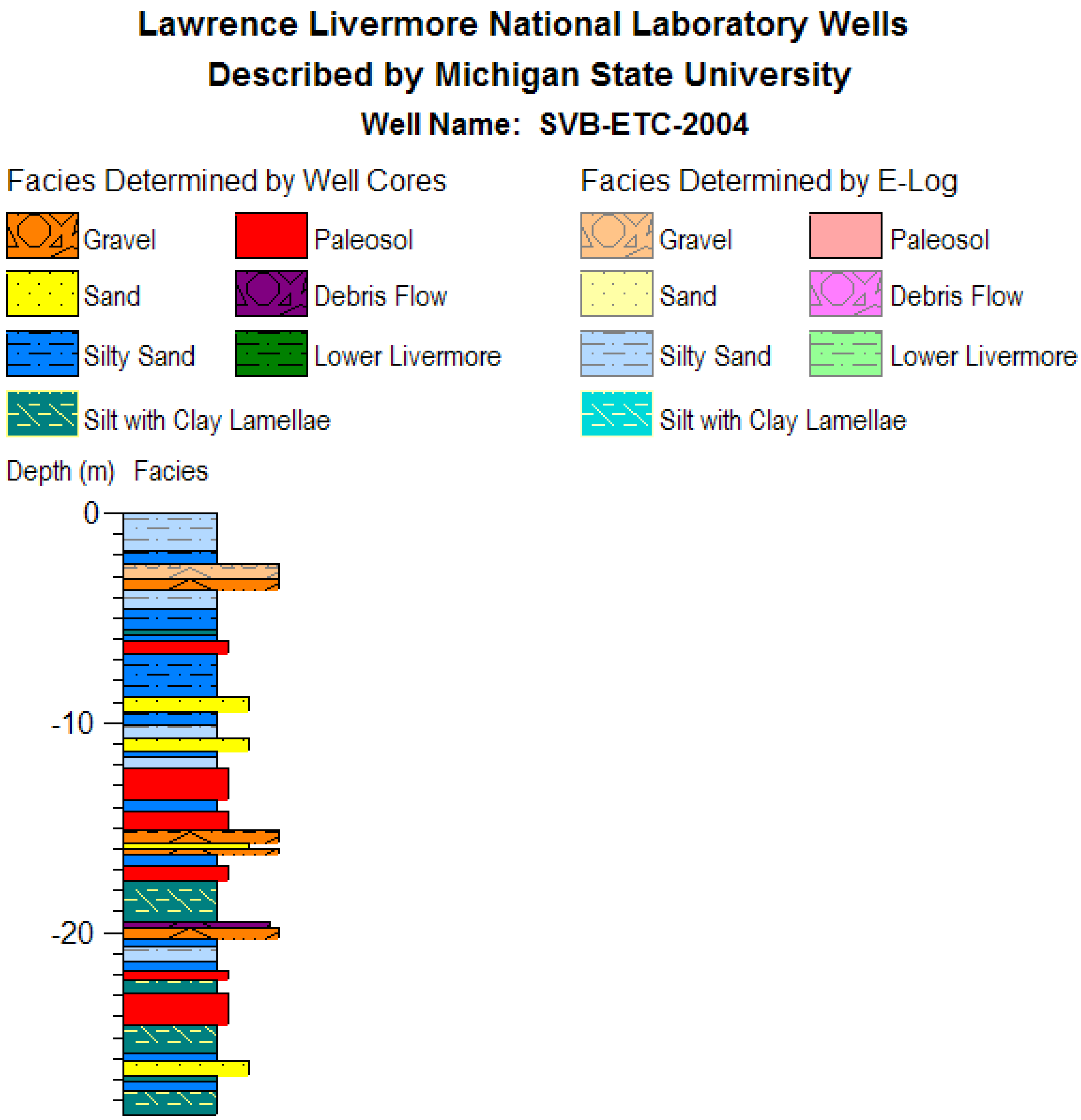

Figure 27. SVB-ETC-2004 stratigraphic column.

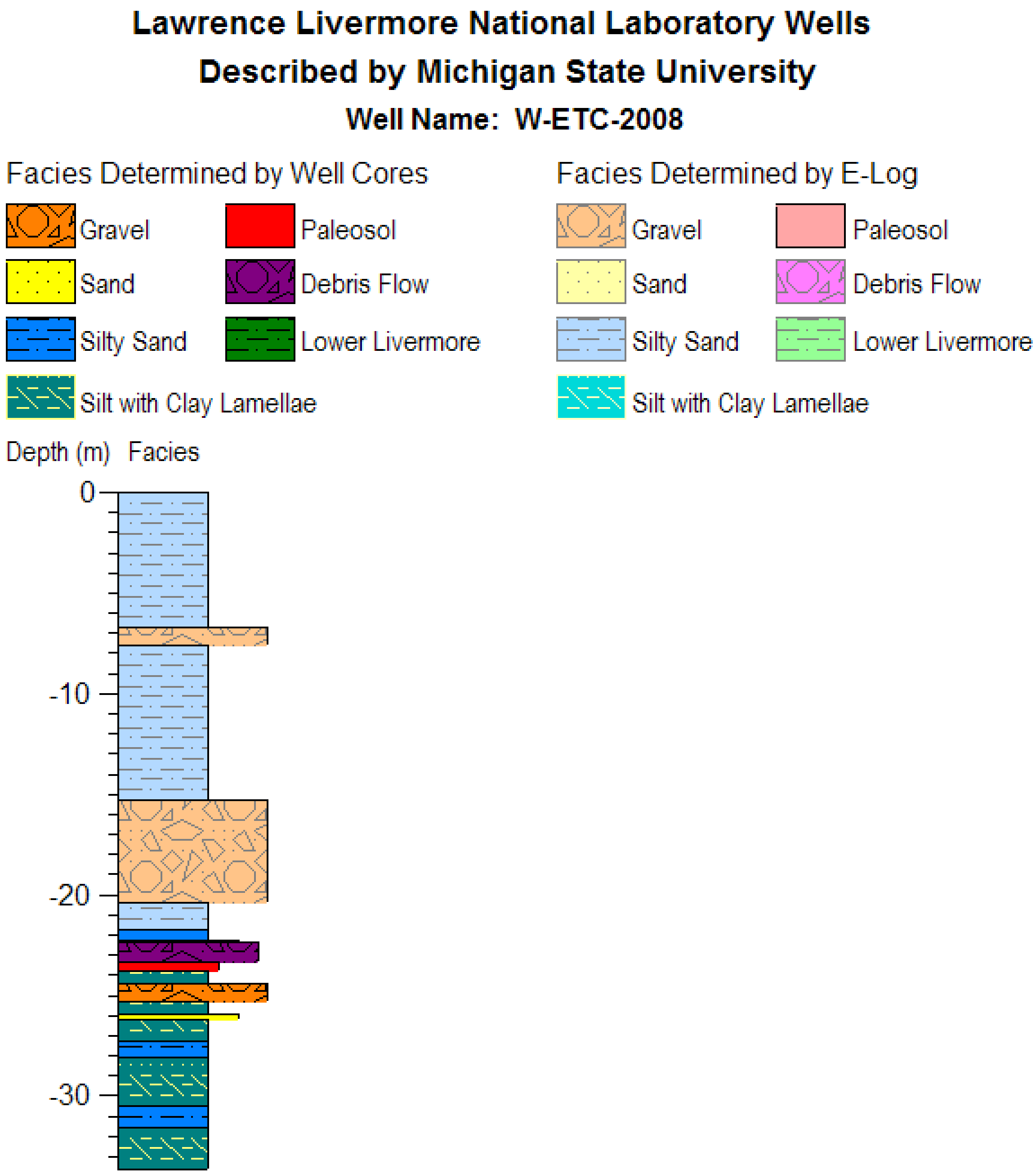

Figure 28. W-ETC-2008 stratigraphic column.

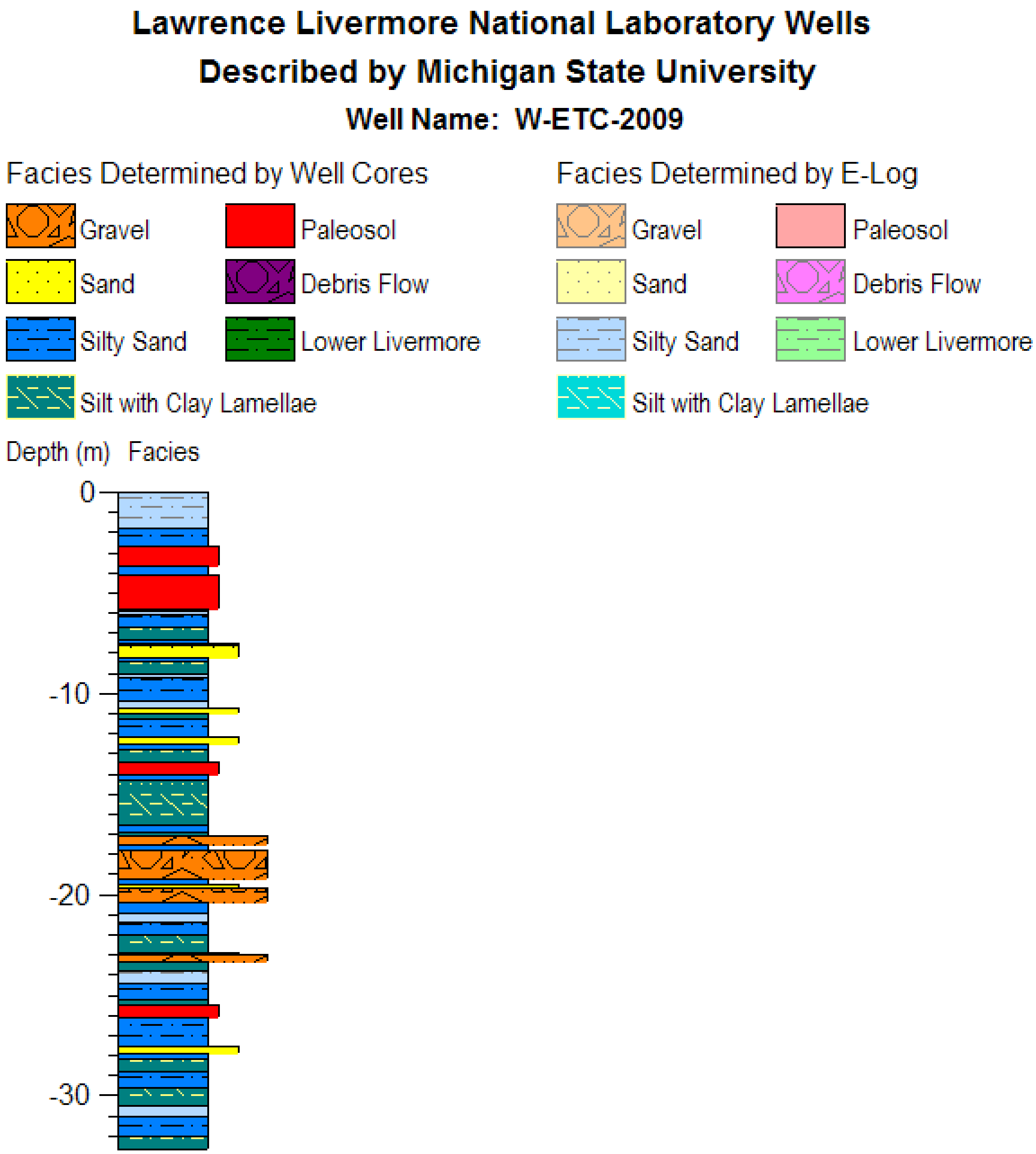

Figure 29. W-ETC-2009 stratigraphic column.

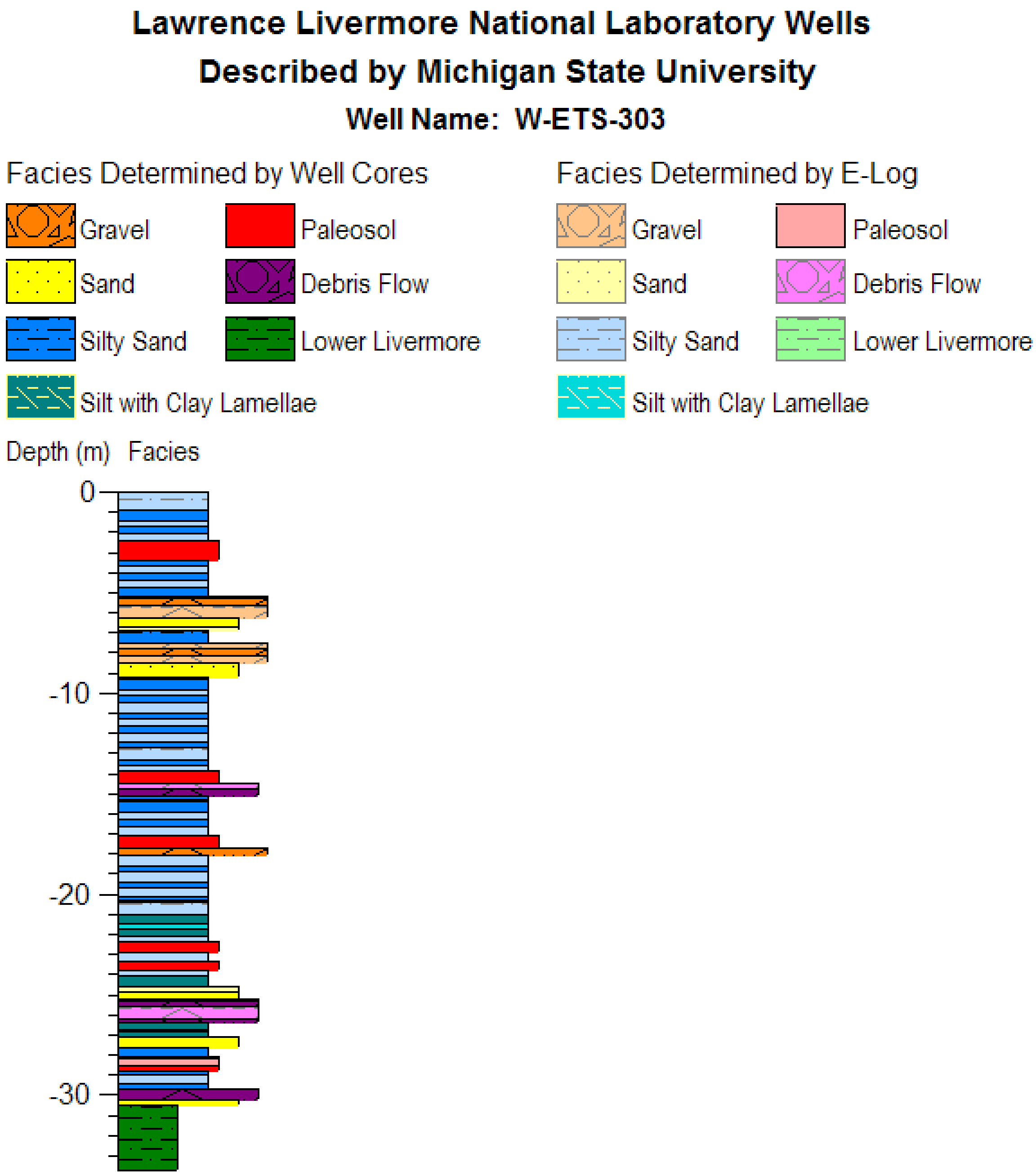

Figure 30. W-ETS-303 stratigraphic column.

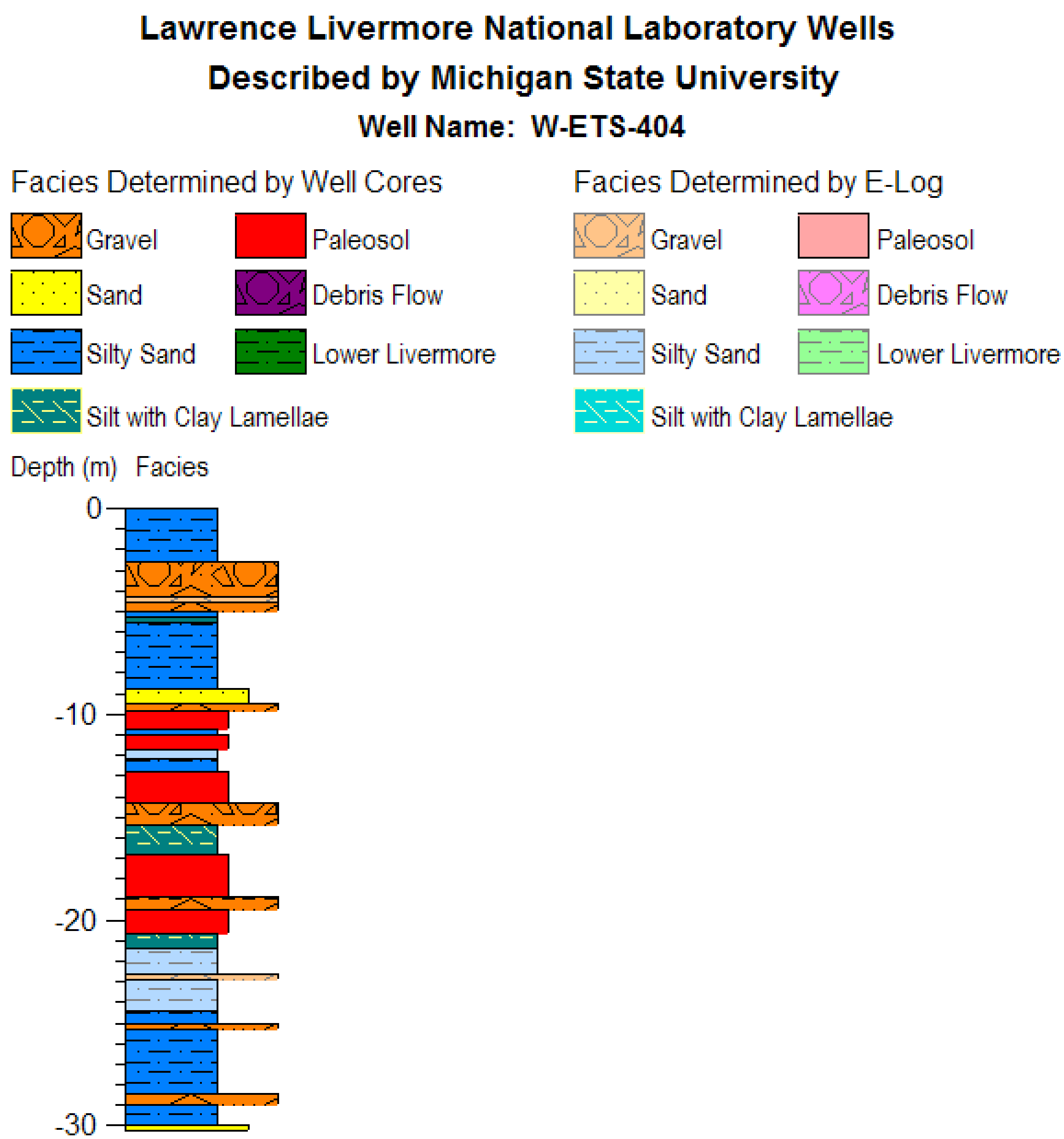

Figure 31. W-ETS-404 stratigraphic column.

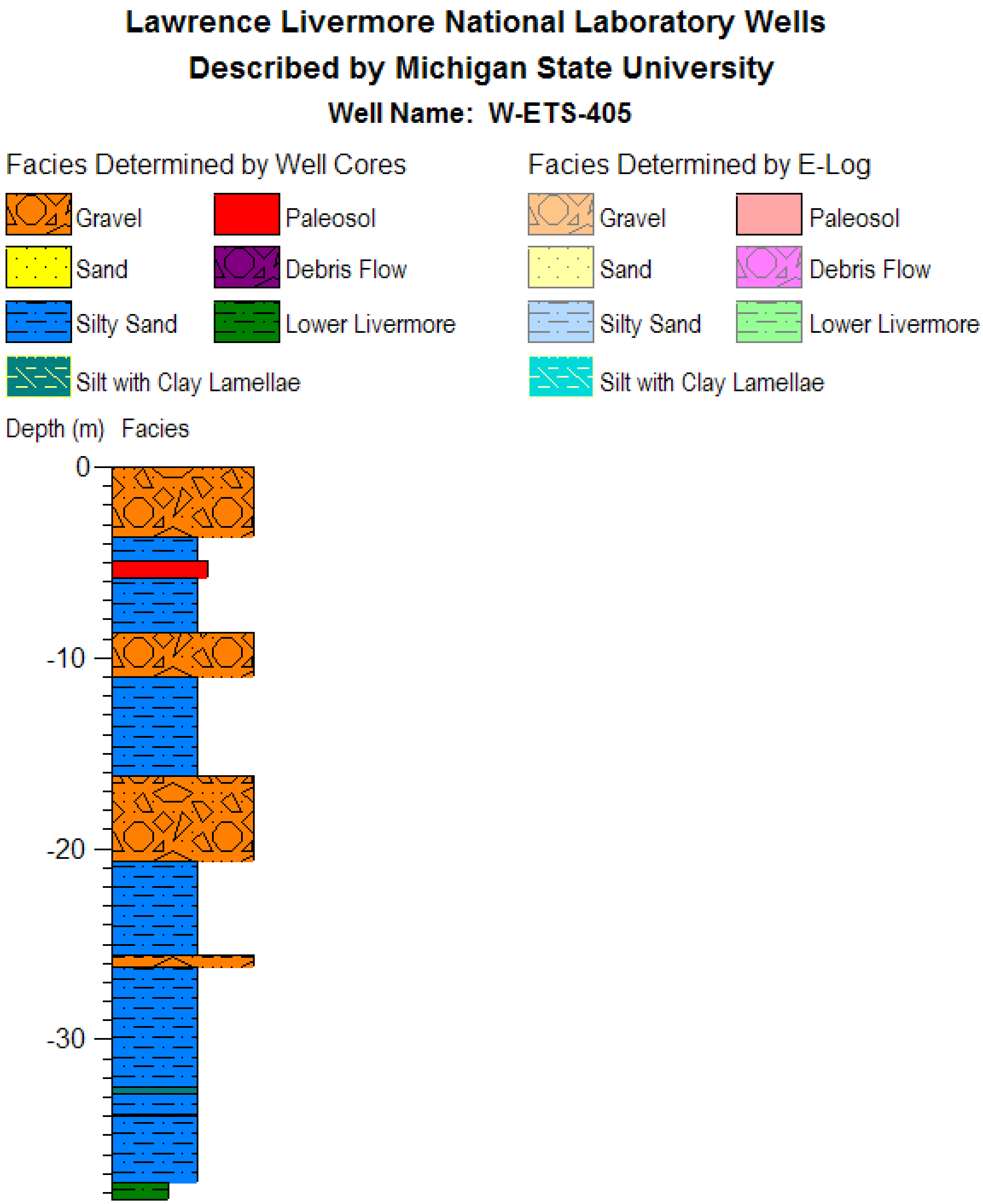

Figure 32. W-ETS-405 stratigraphic column.

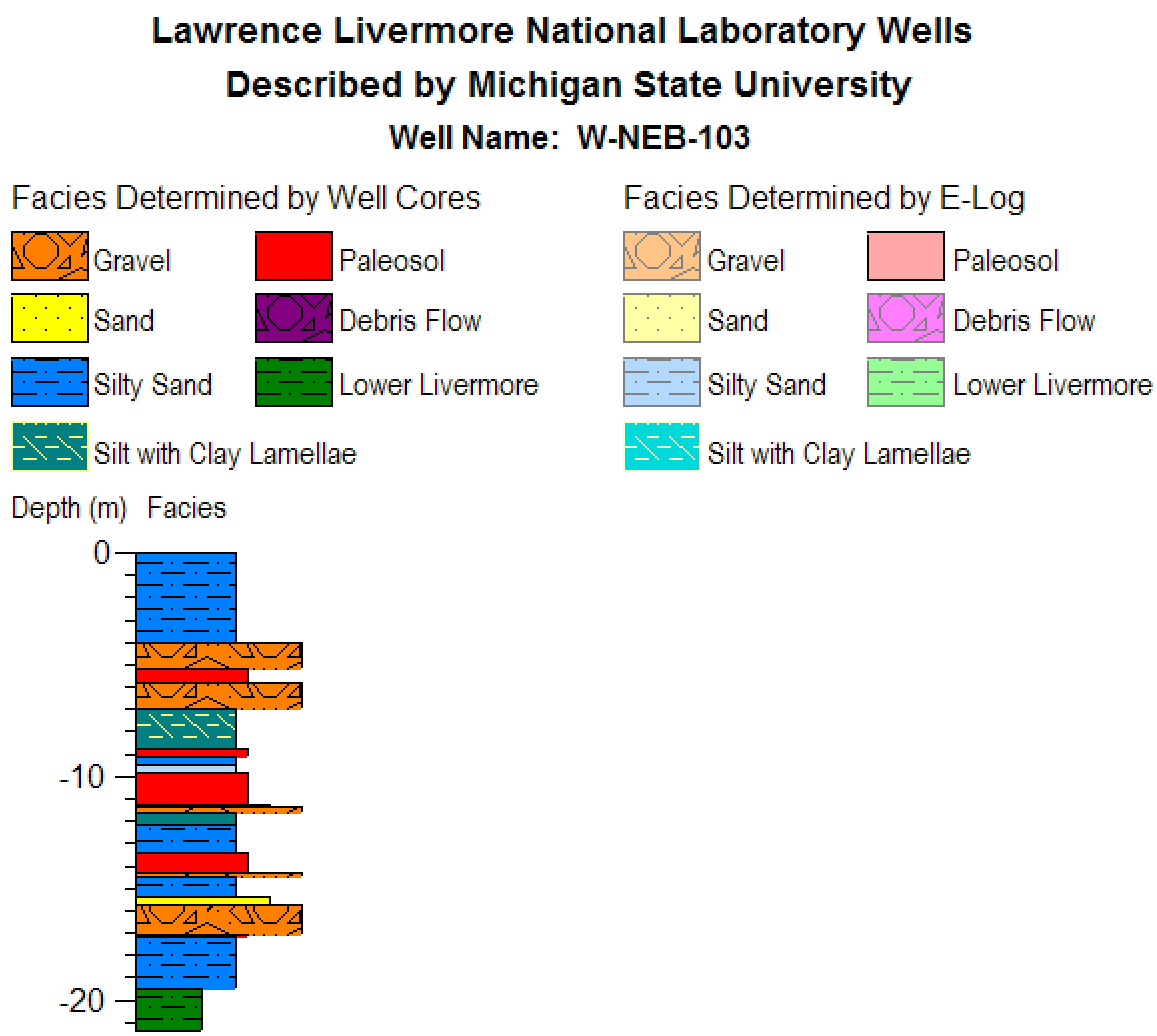

Figure 33. W-NEB-103 stratigraphic column.

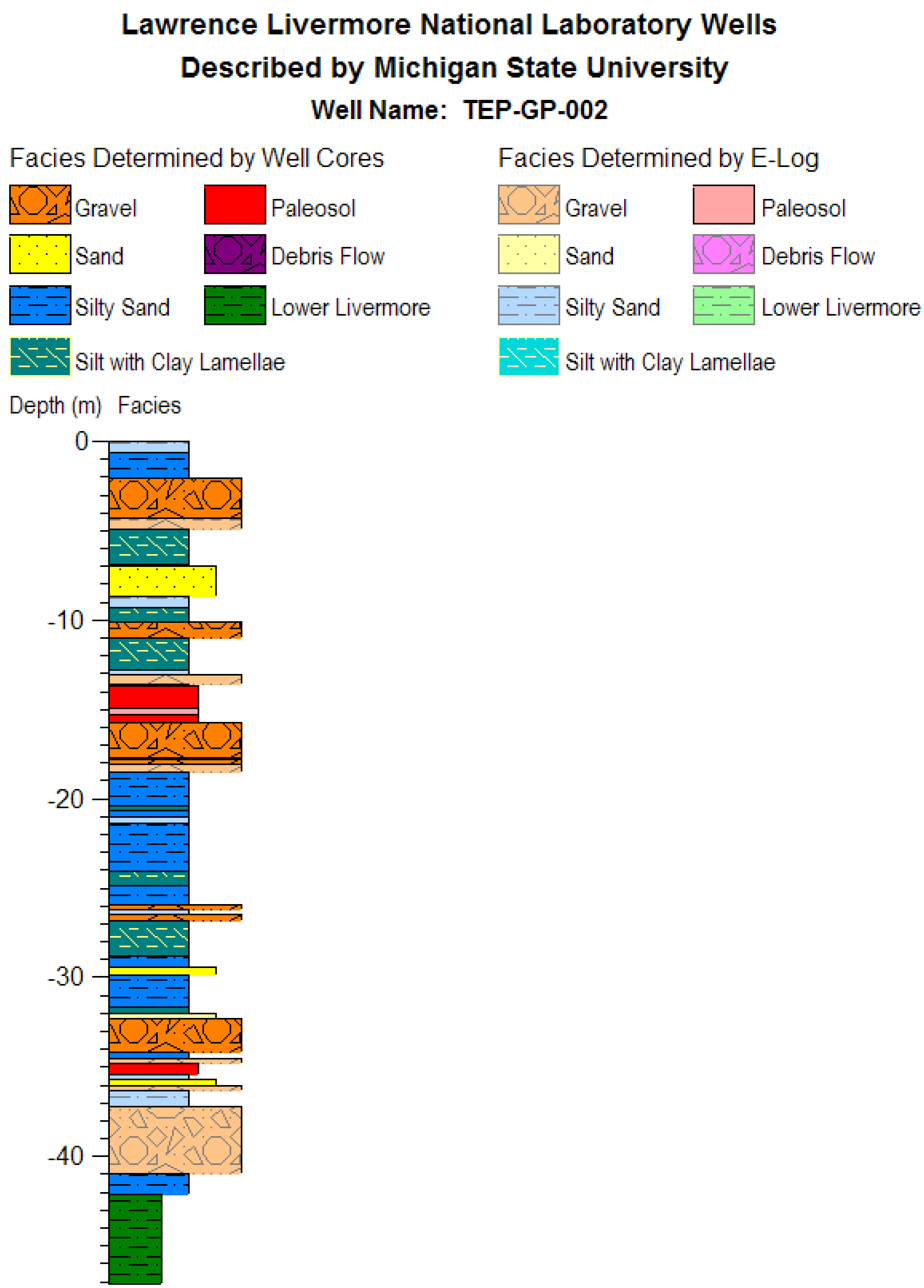

Figure 34. TEP-GP-002 stratigraphic column.

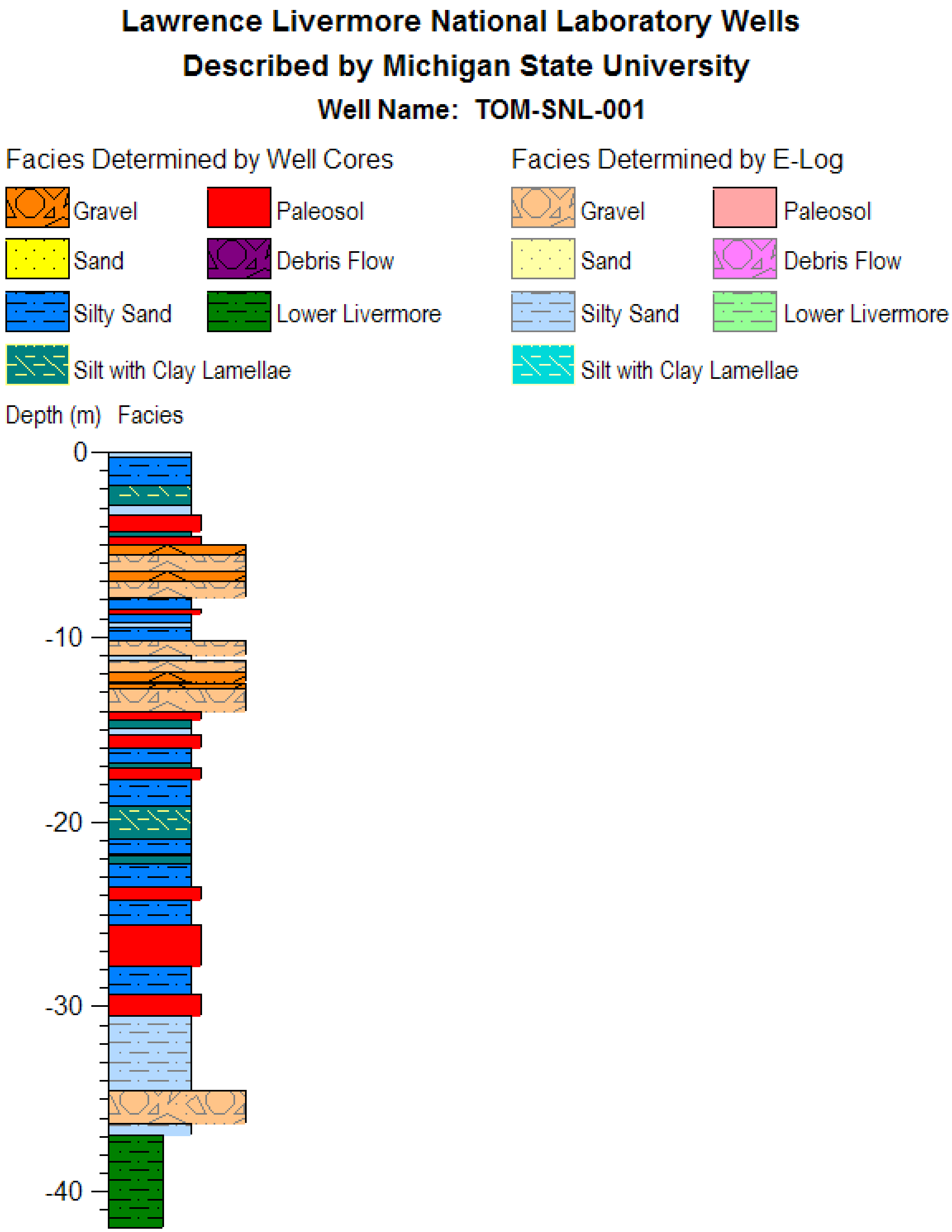

Figure 35. TOM-SNL-001 stratigraphic column.

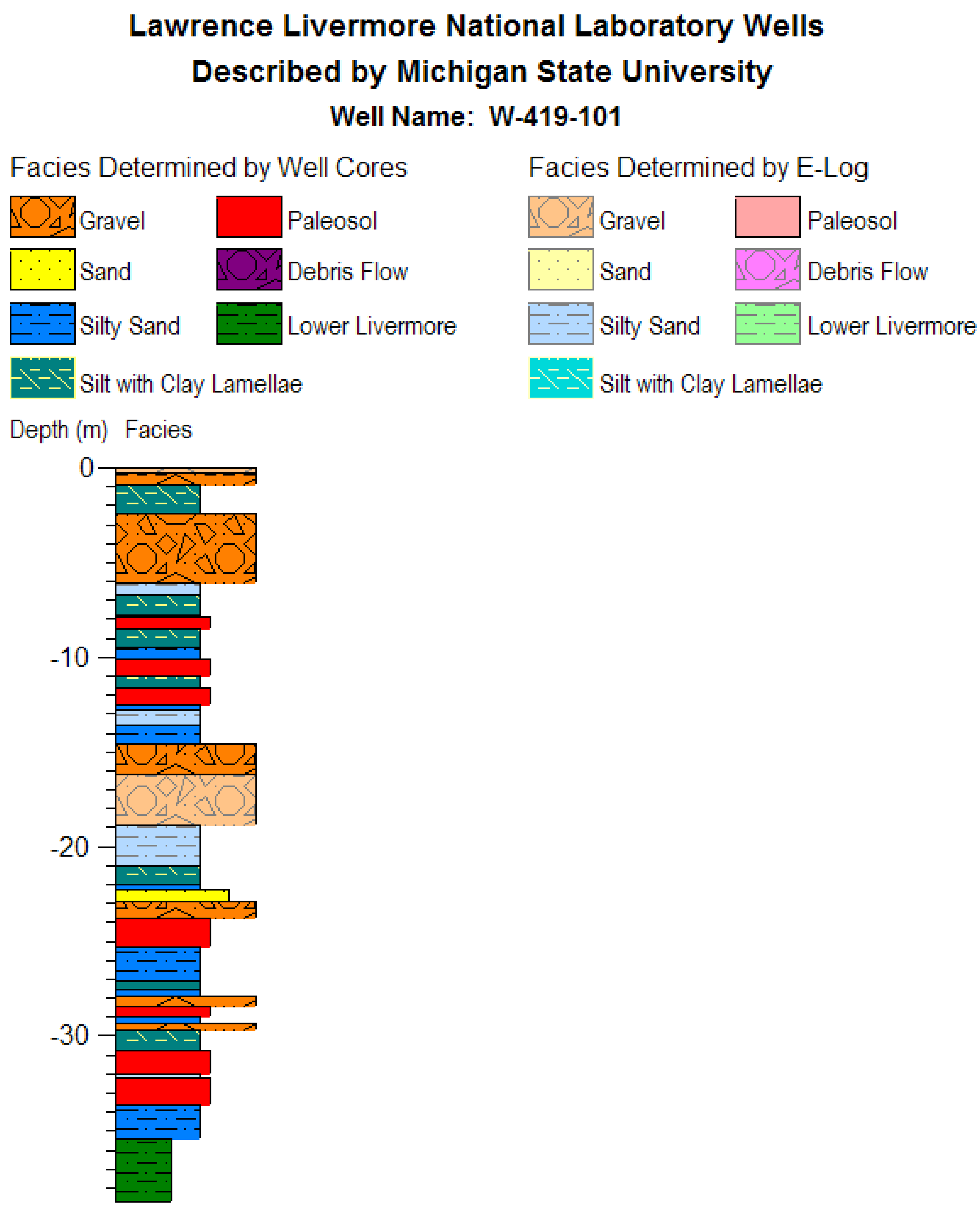

Figure 36. W-419-101 stratigraphic column.

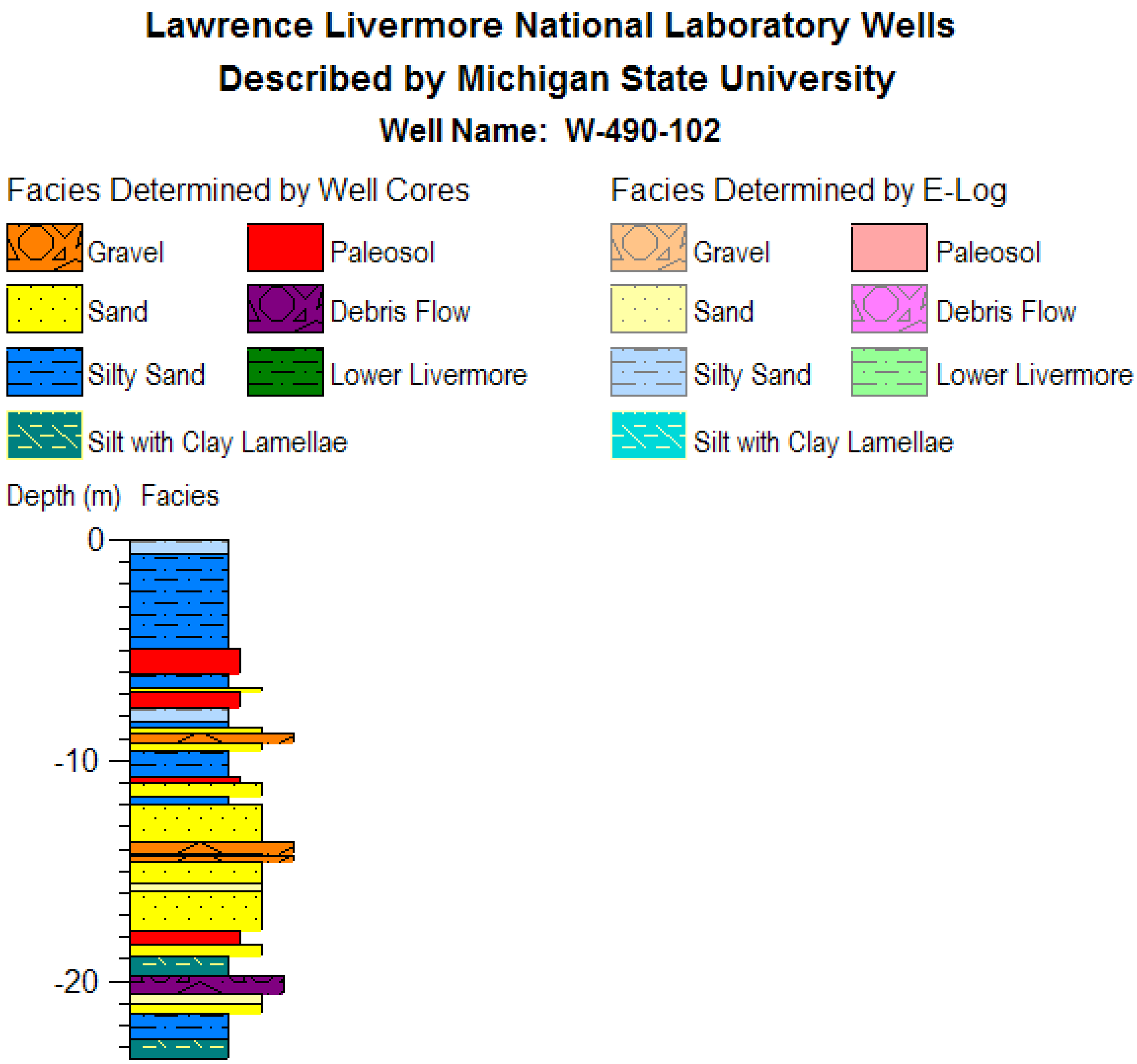

Figure 37. W-490-102 stratigraphic column.

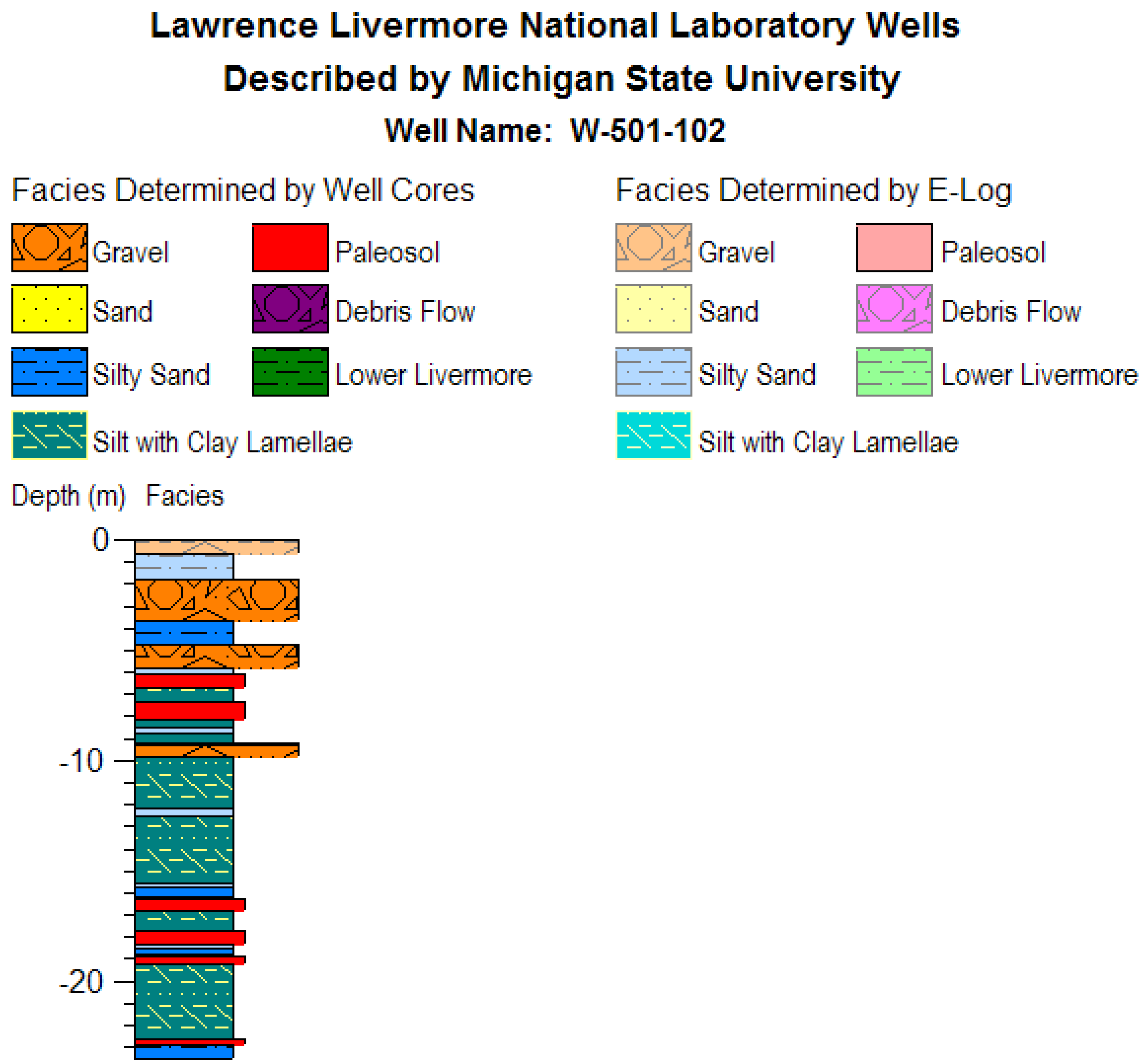

Figure 38. W-501-102 stratigraphic column.

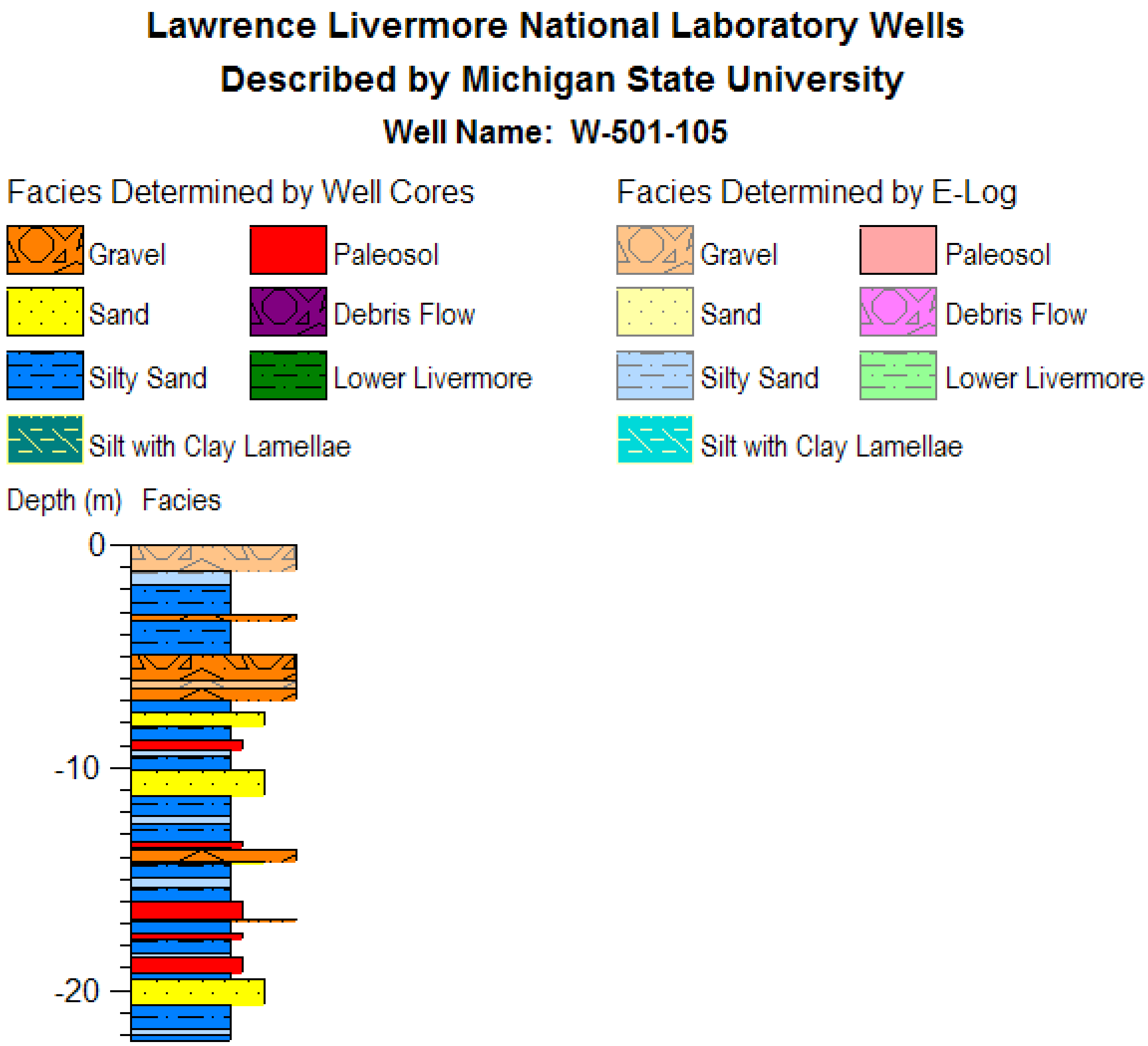

Figure 39. W-501-105 stratigraphic column.

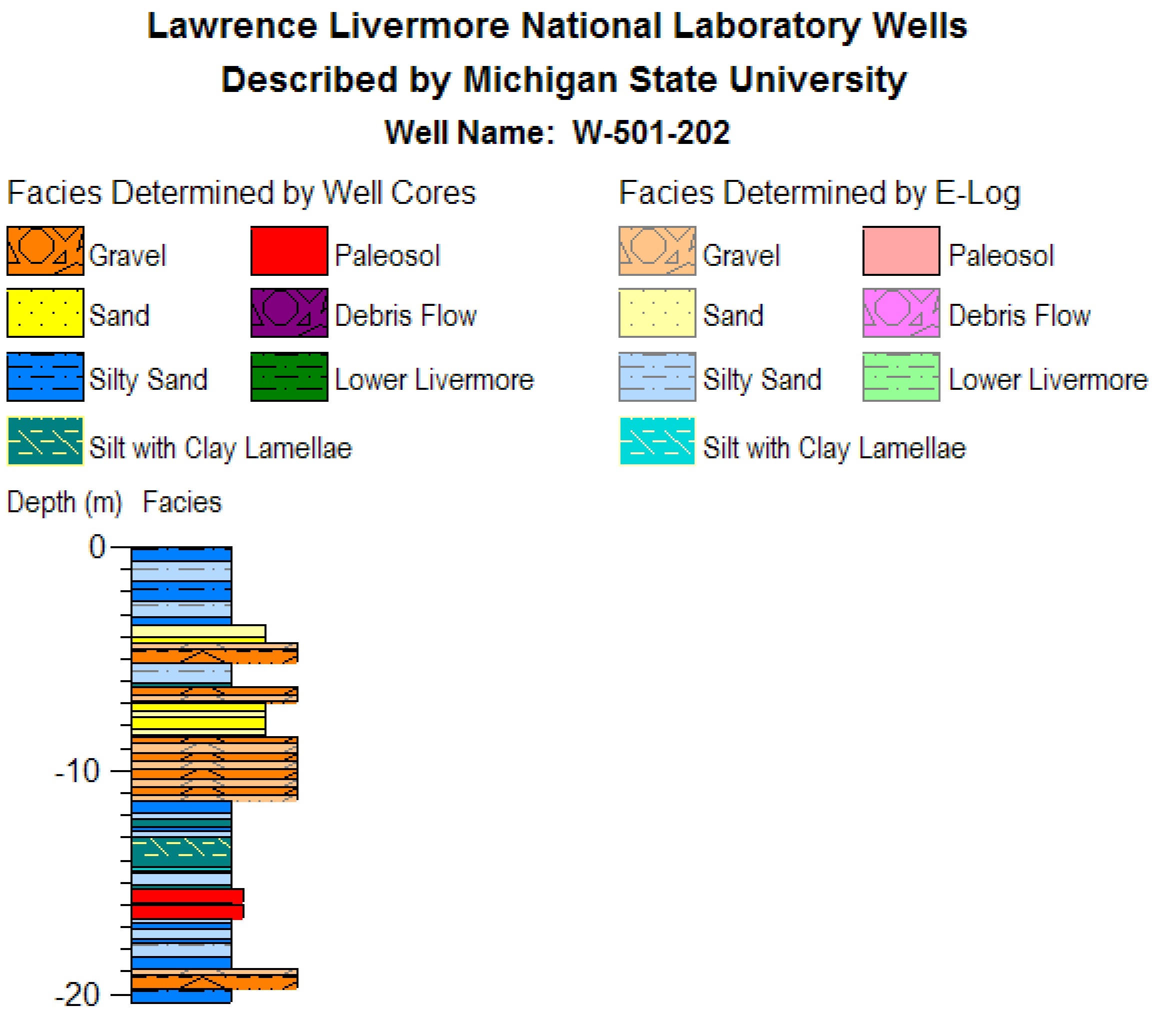

Figure 40. W-501-202 stratigraphic column.

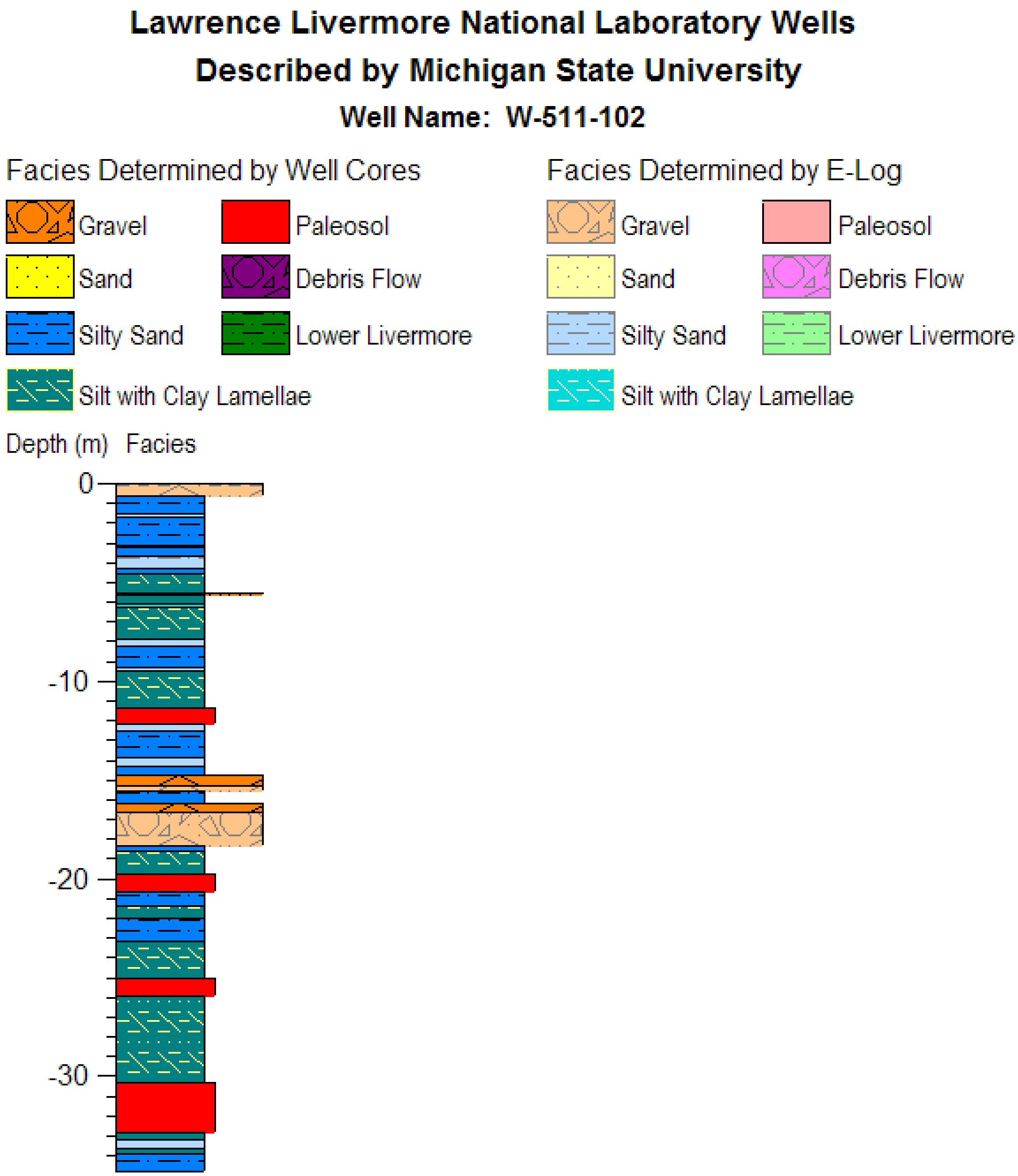

Figure 41. W-511-102 stratigraphic column.

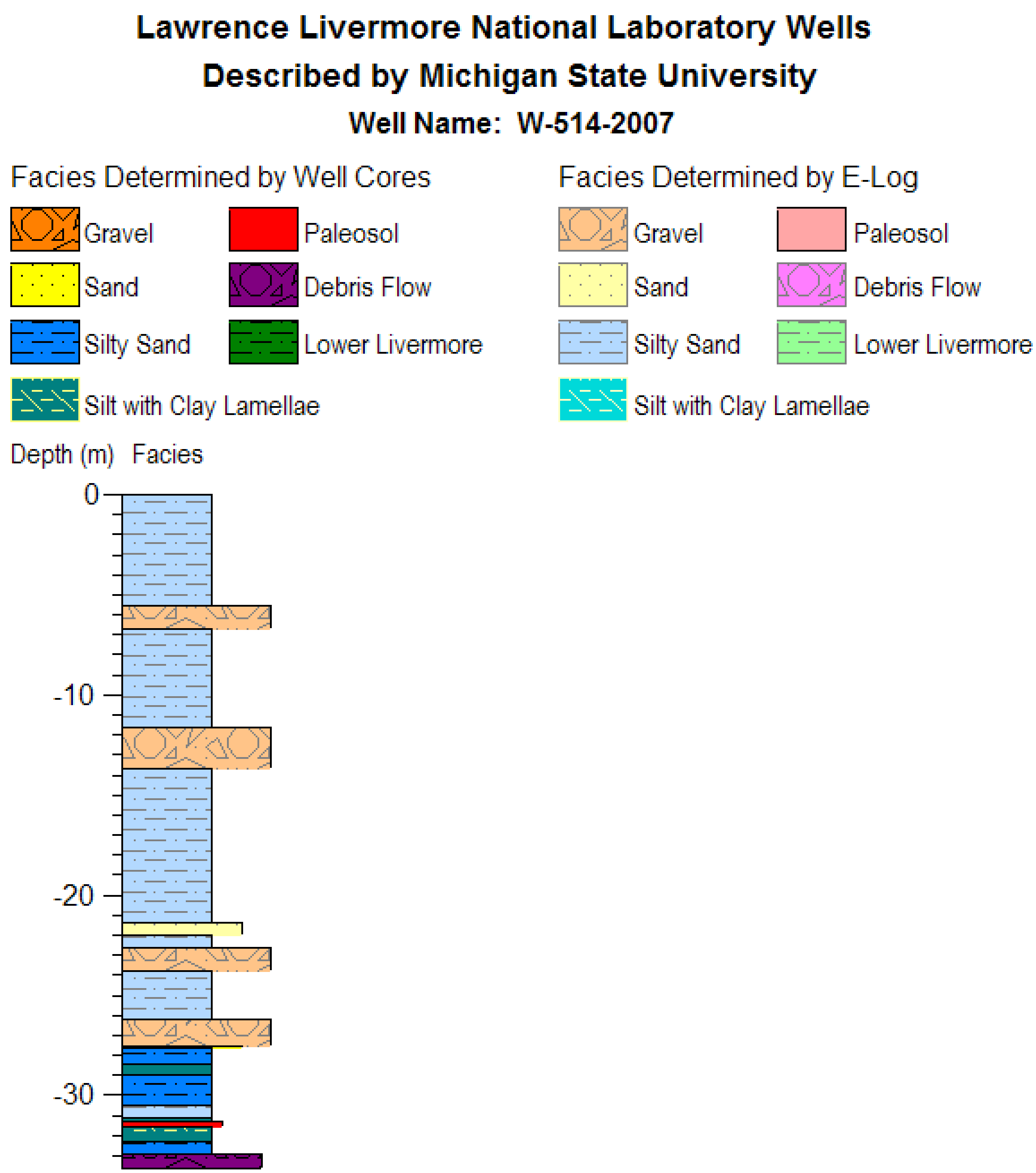

Figure 42. W-514-2007 stratigraphic column.

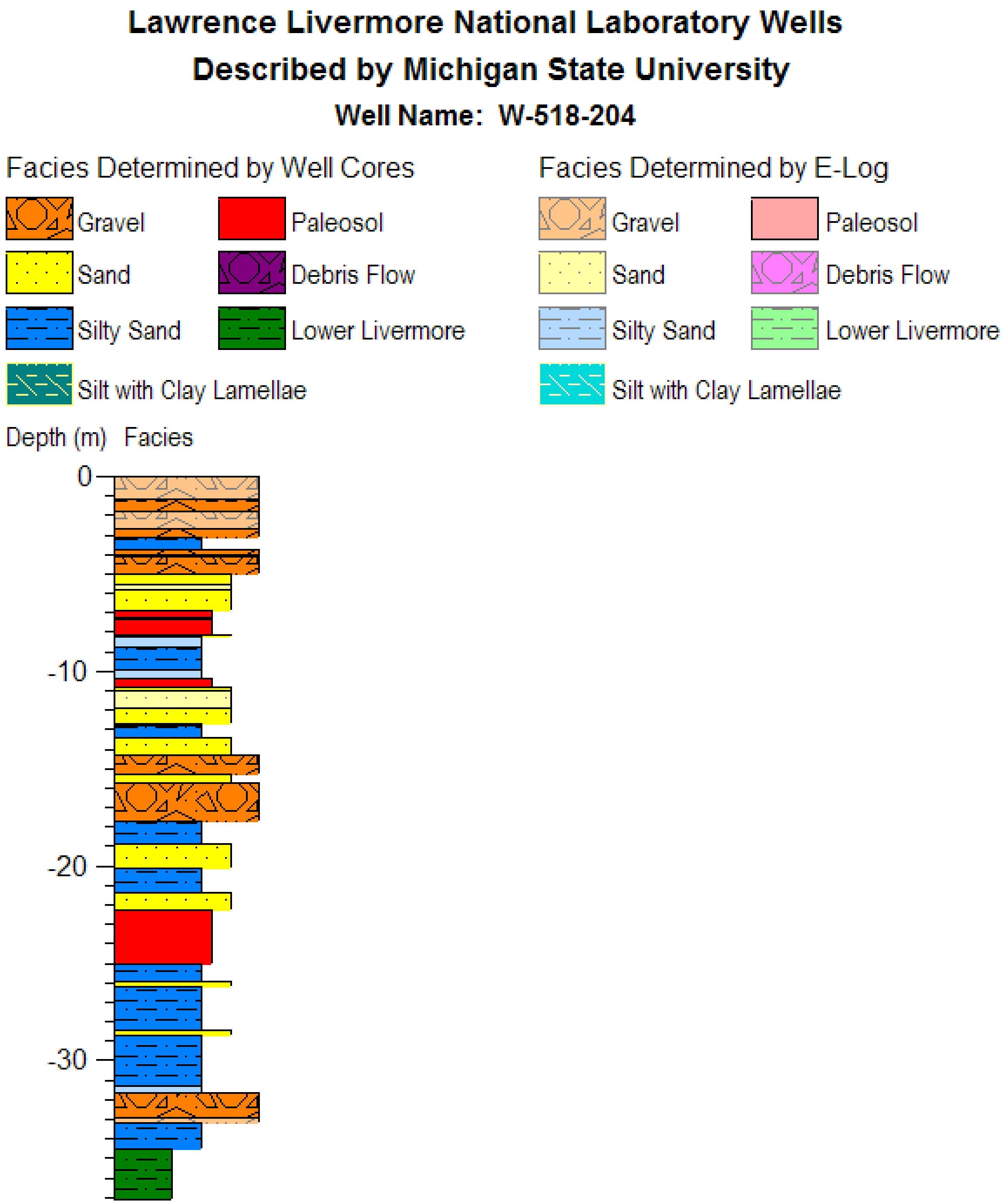

Figure 43. W-518-204 stratigraphic column.

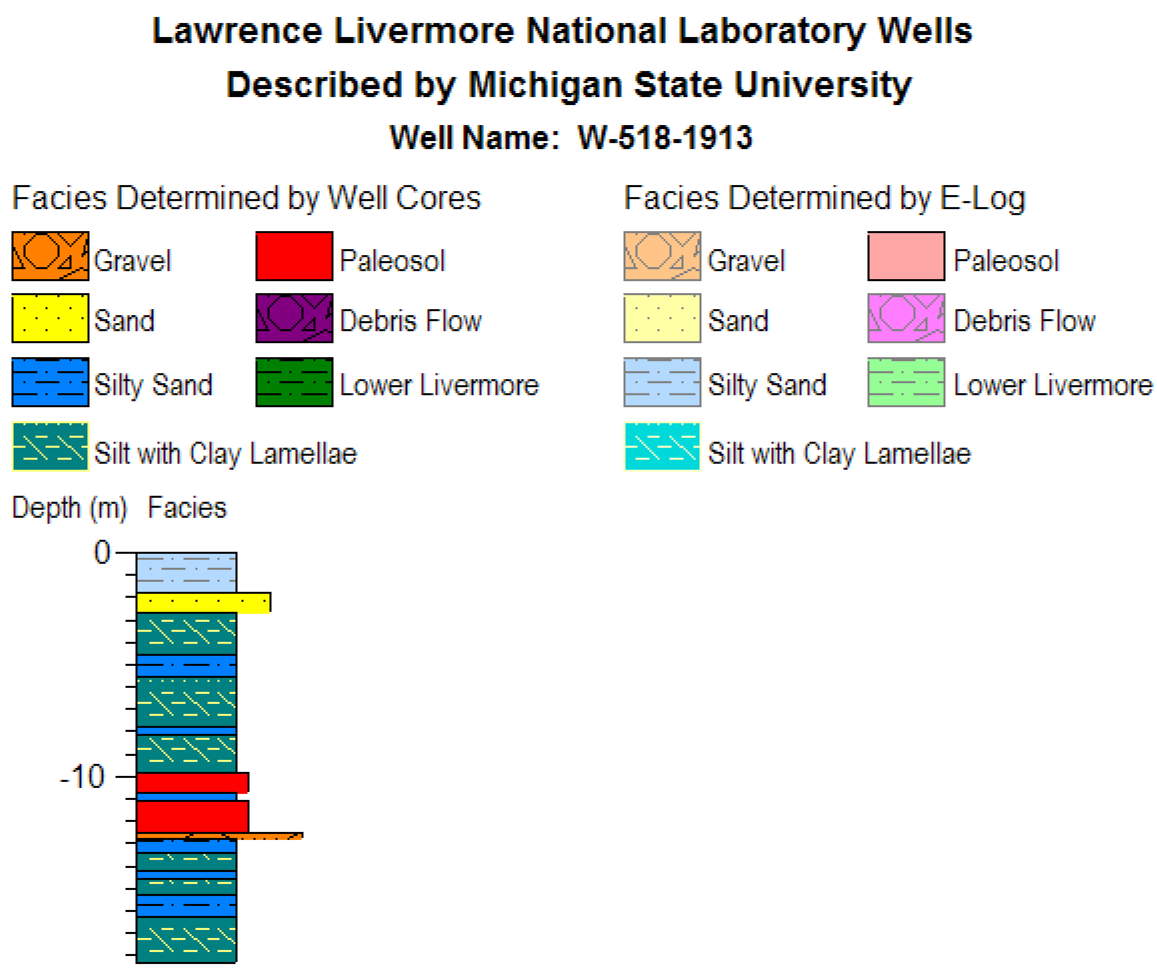

Figure 44. W-518-1913 stratigraphic column.

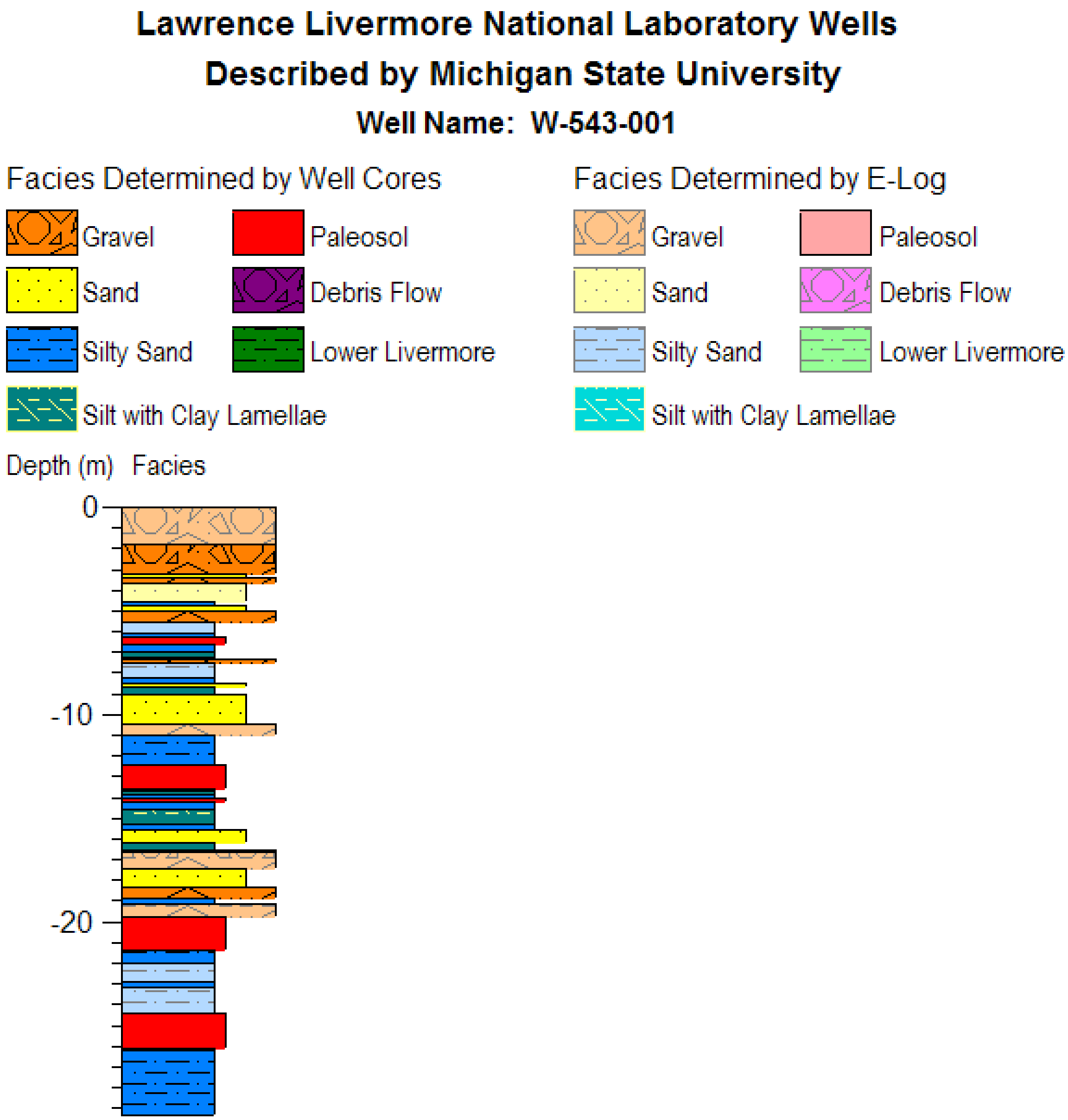

Figure 45. W-543-001 stratigraphic column.

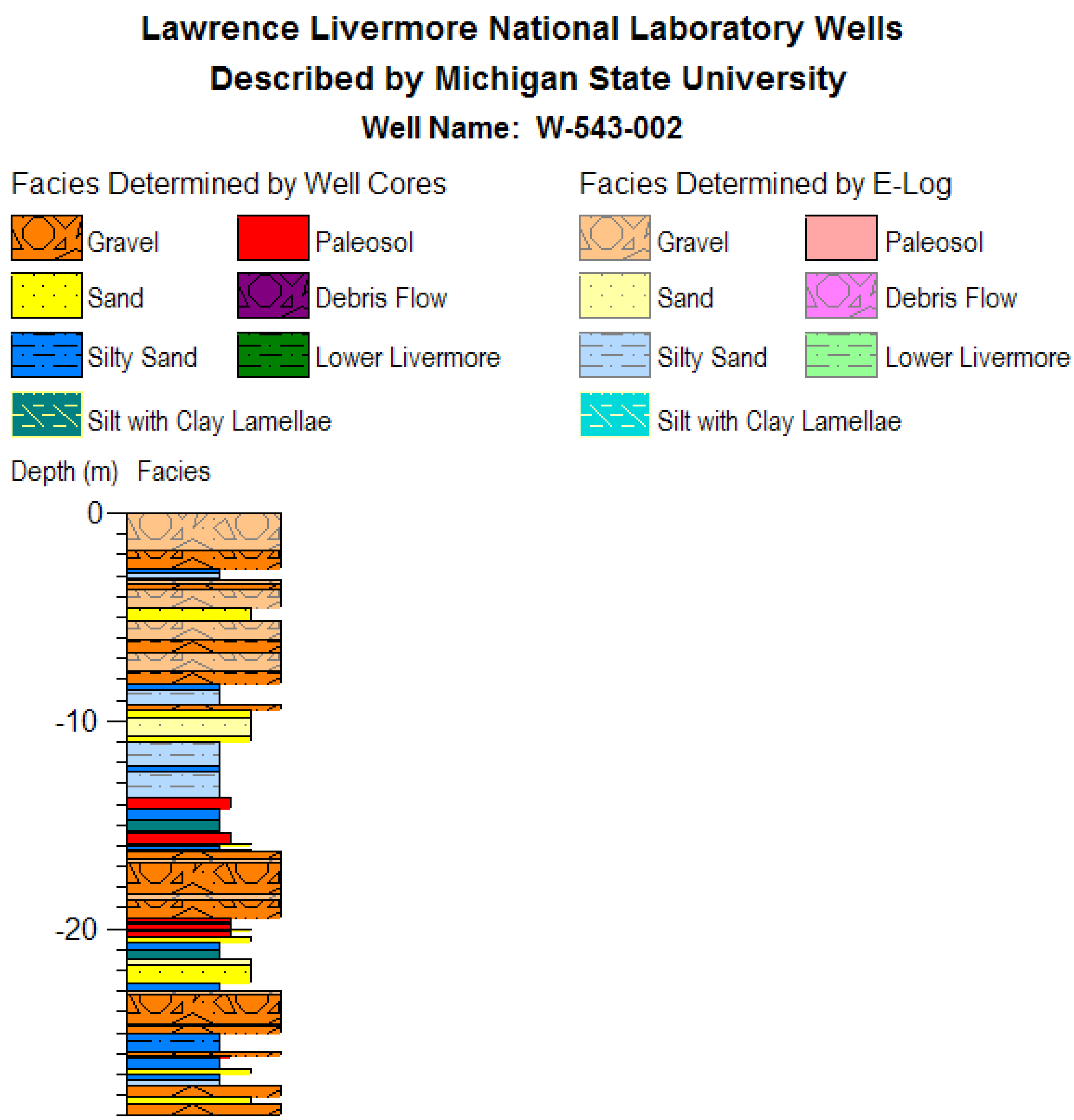

Figure 46. W-543-002 stratigraphic column.

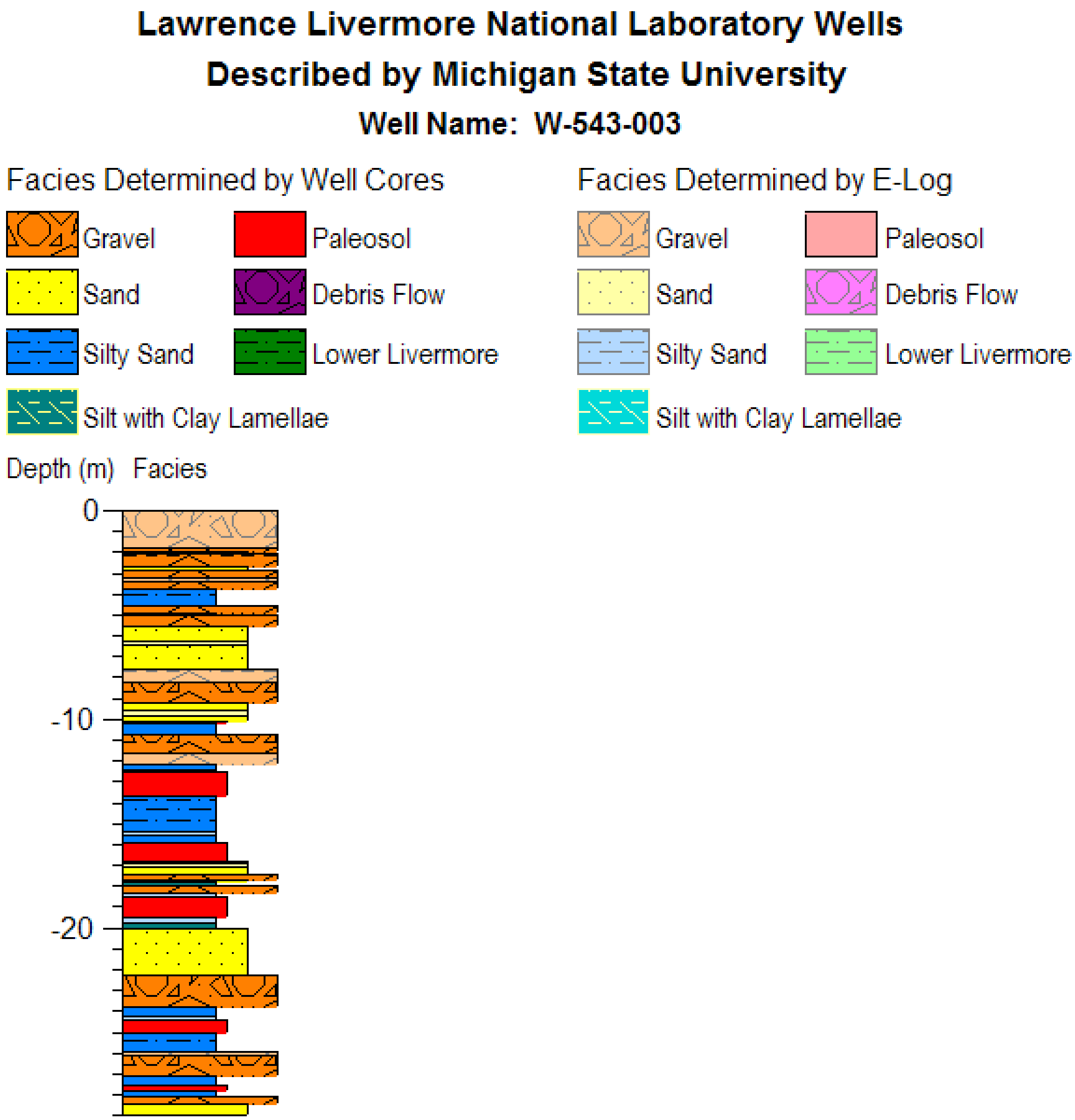

Figure 47. W-543-003 stratigraphic column.

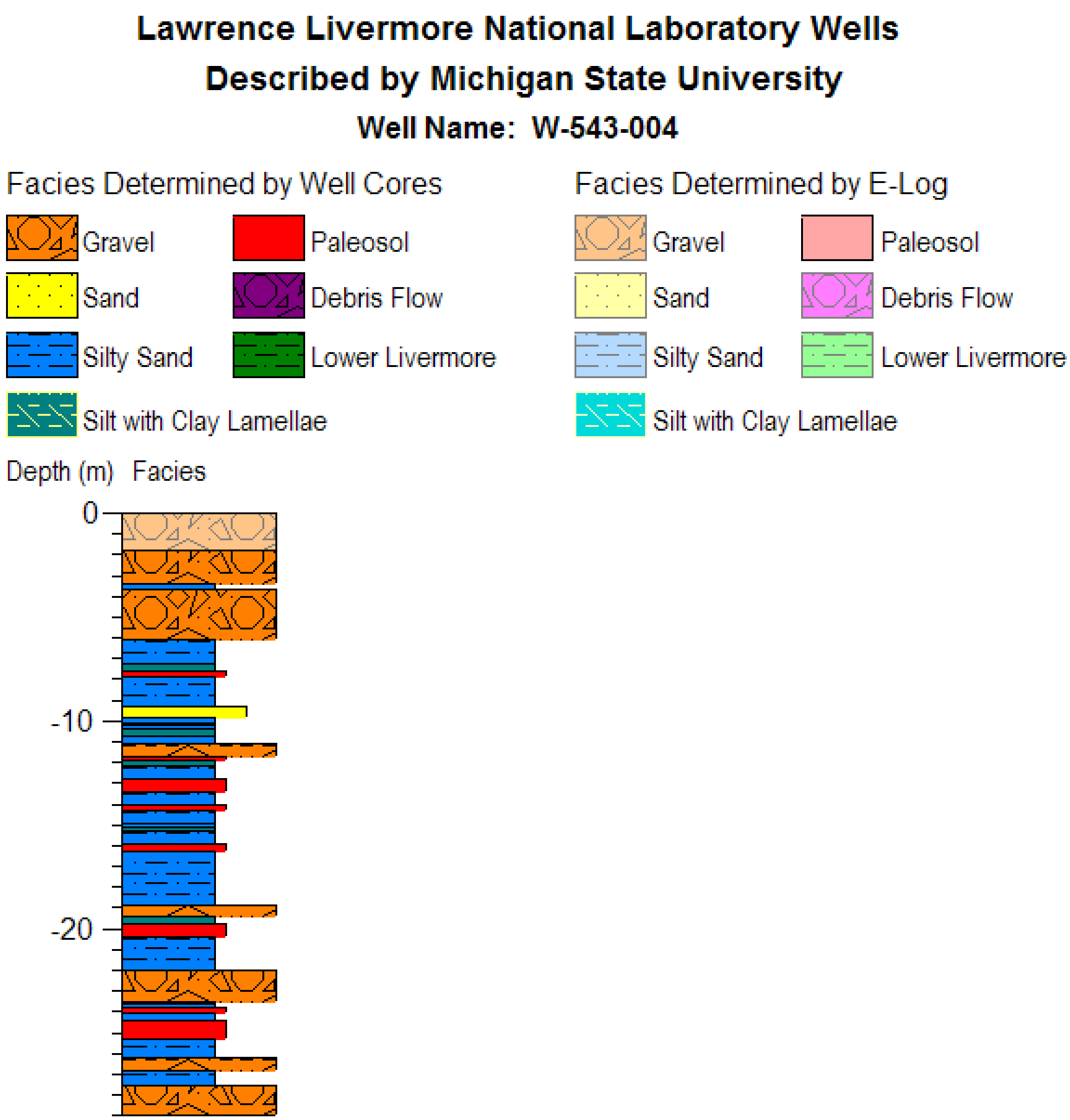

Figure 48. W-543-004 stratigraphic column.

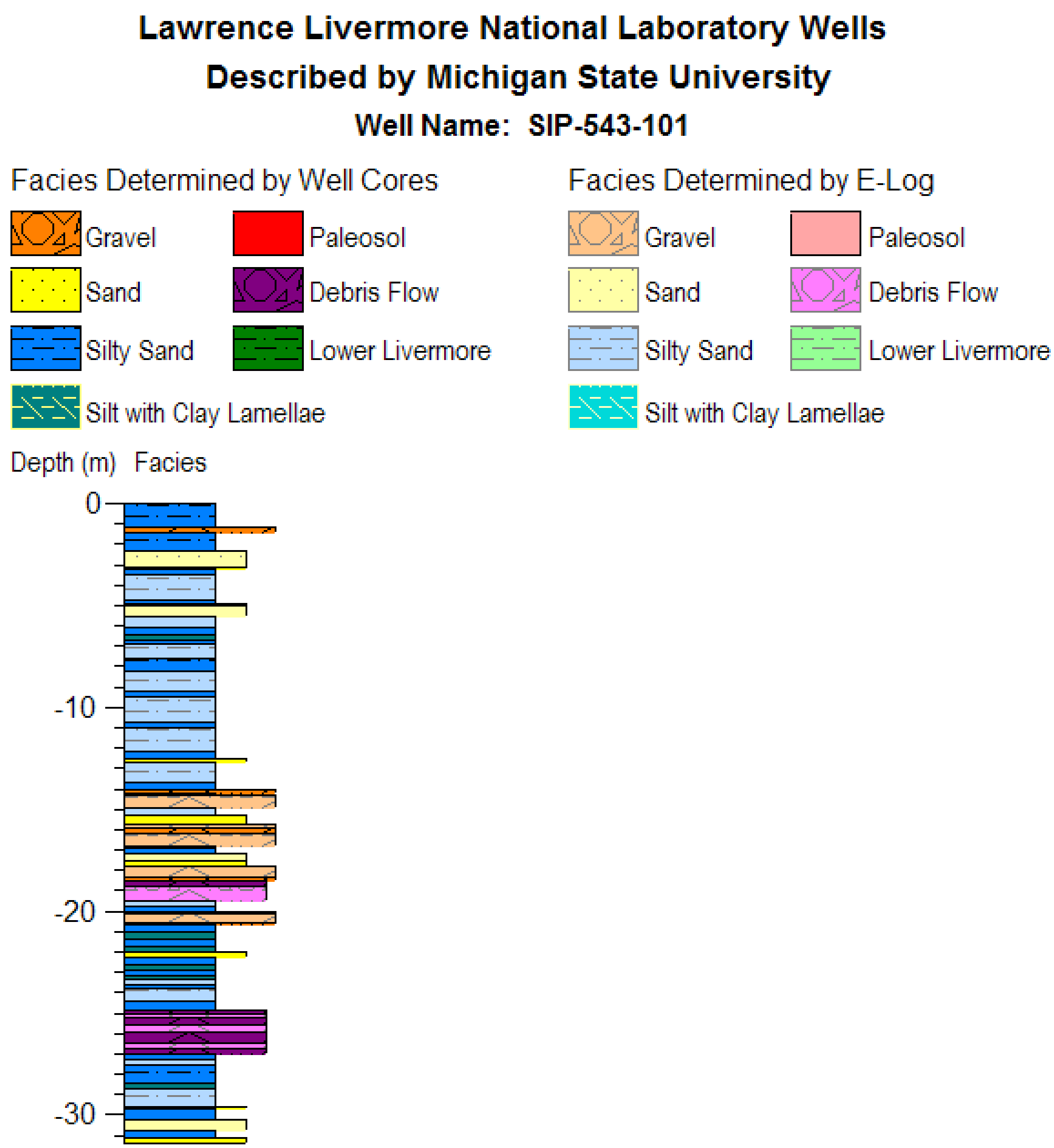

Figure 49. SIP-543-101 stratigraphic column.

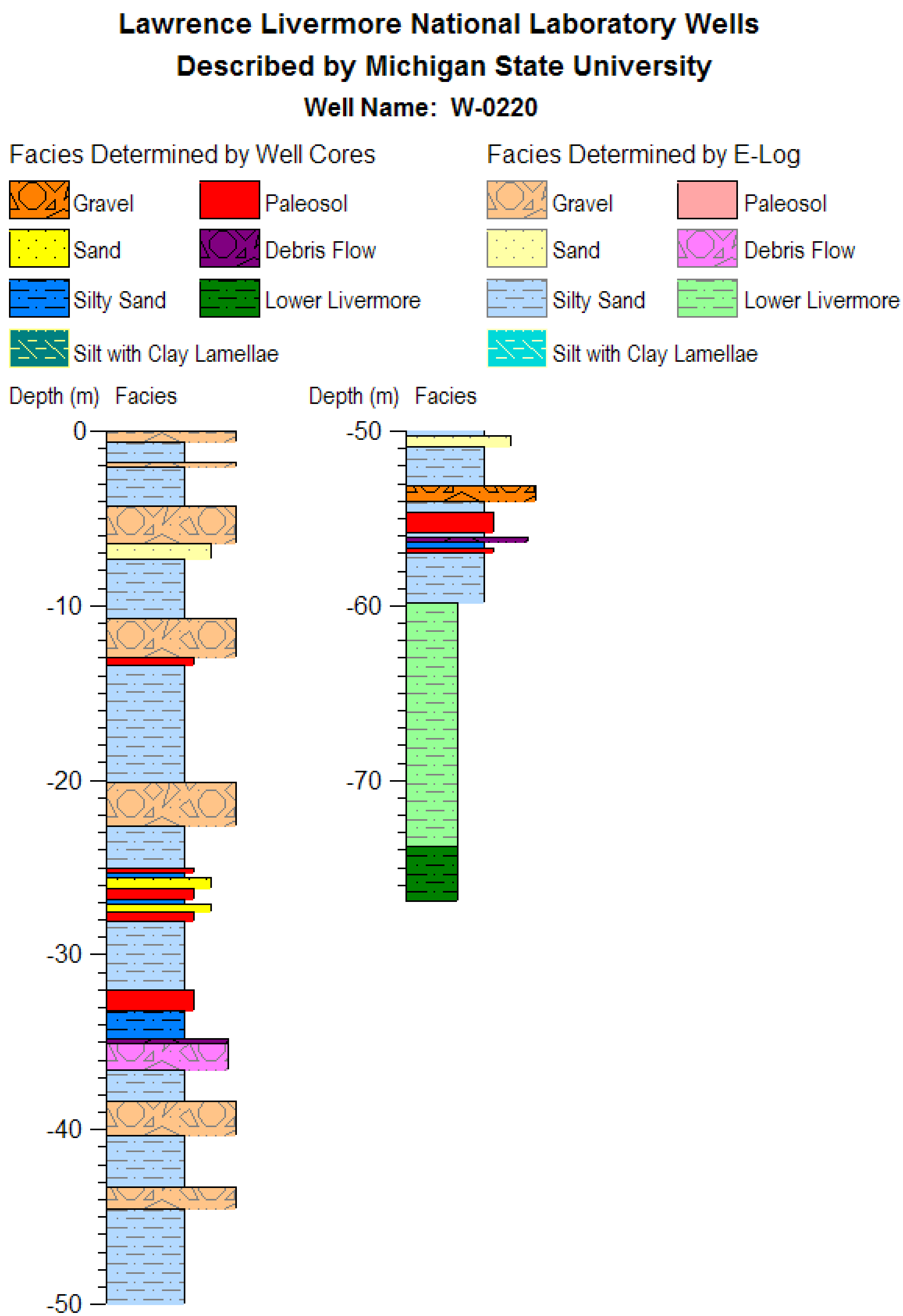

Figure 50. W-0220 stratigraphic column.

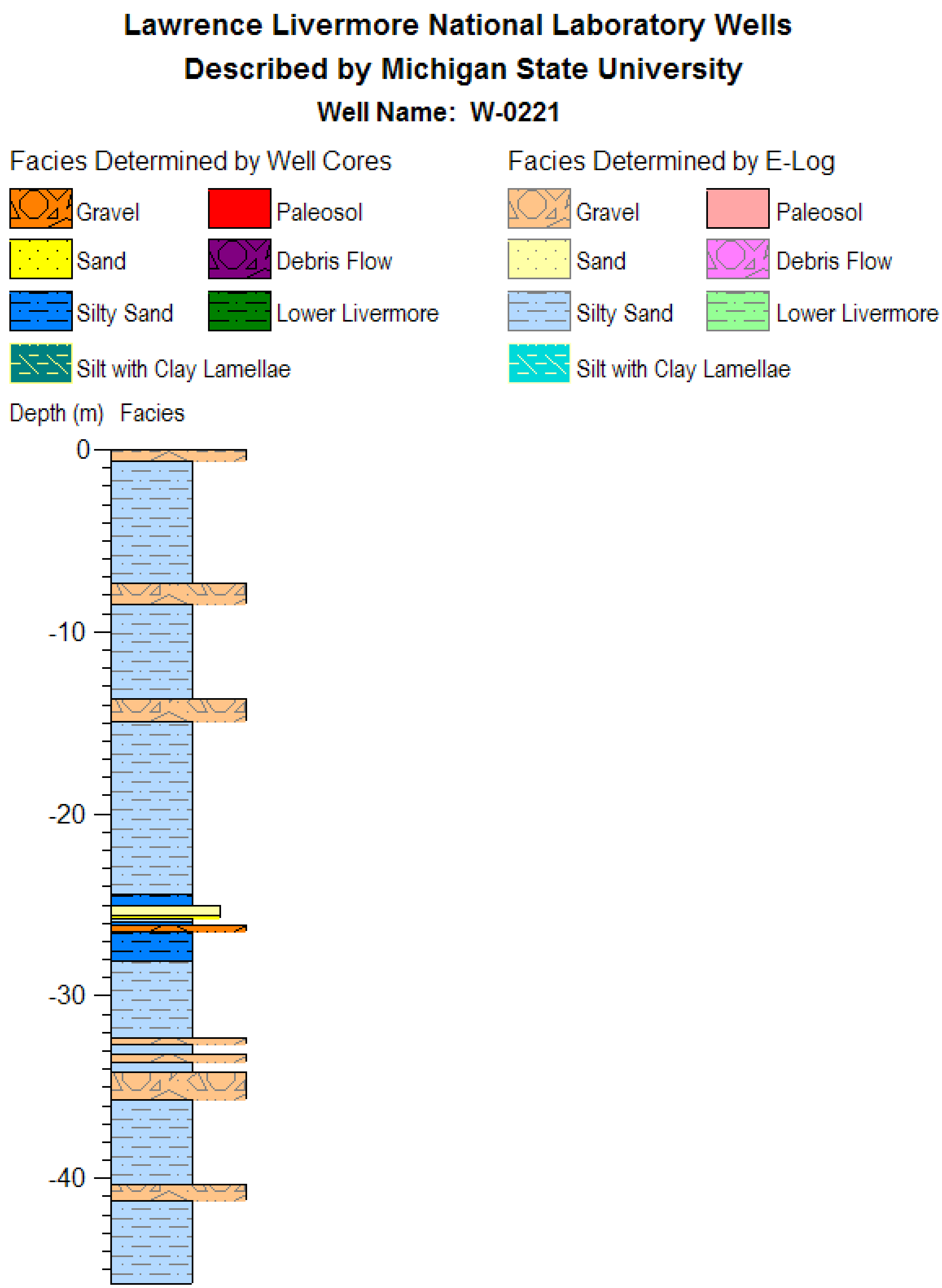

Figure 51. W-0221 stratigraphic column.

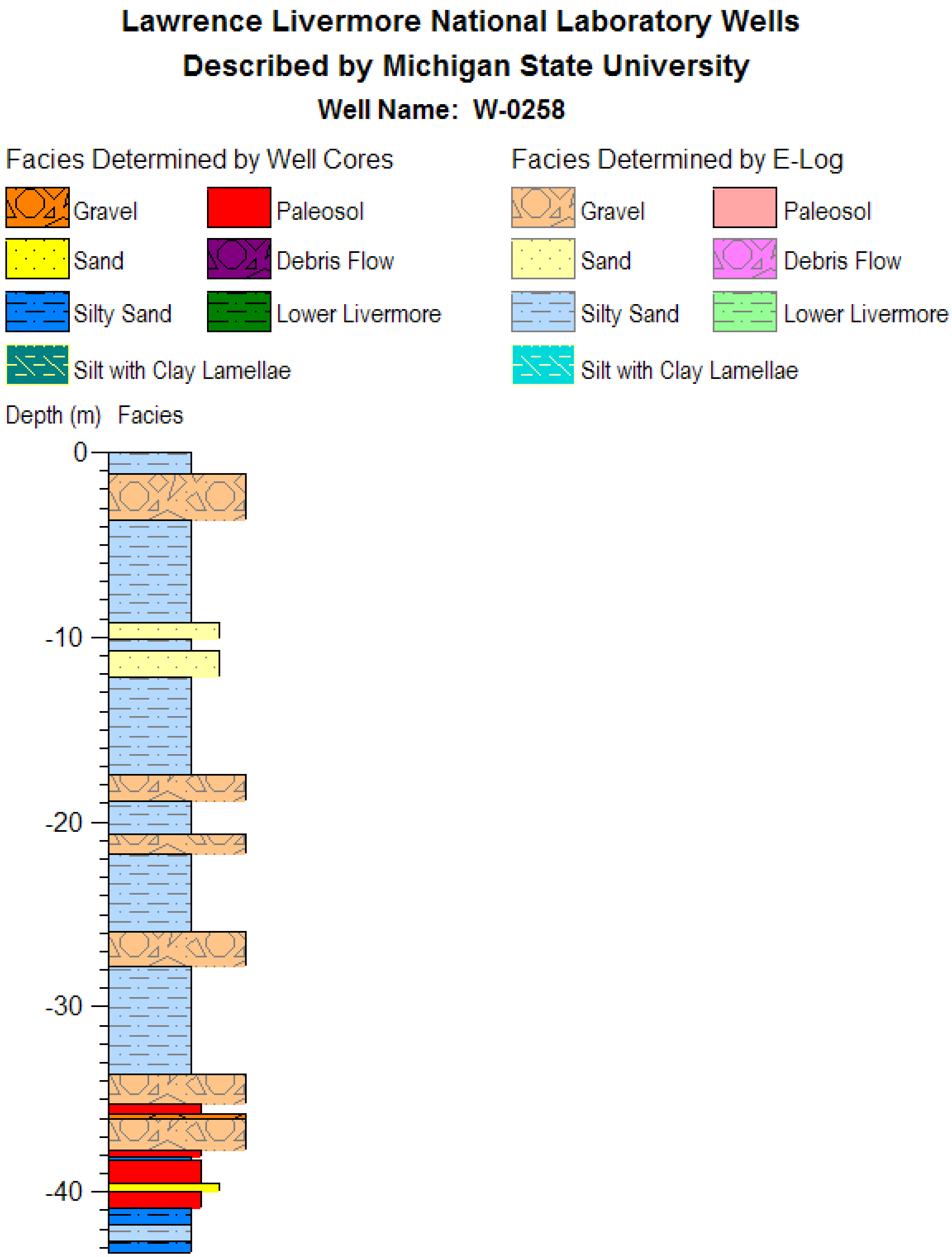

Figure 52. W-0258 stratigraphic column.

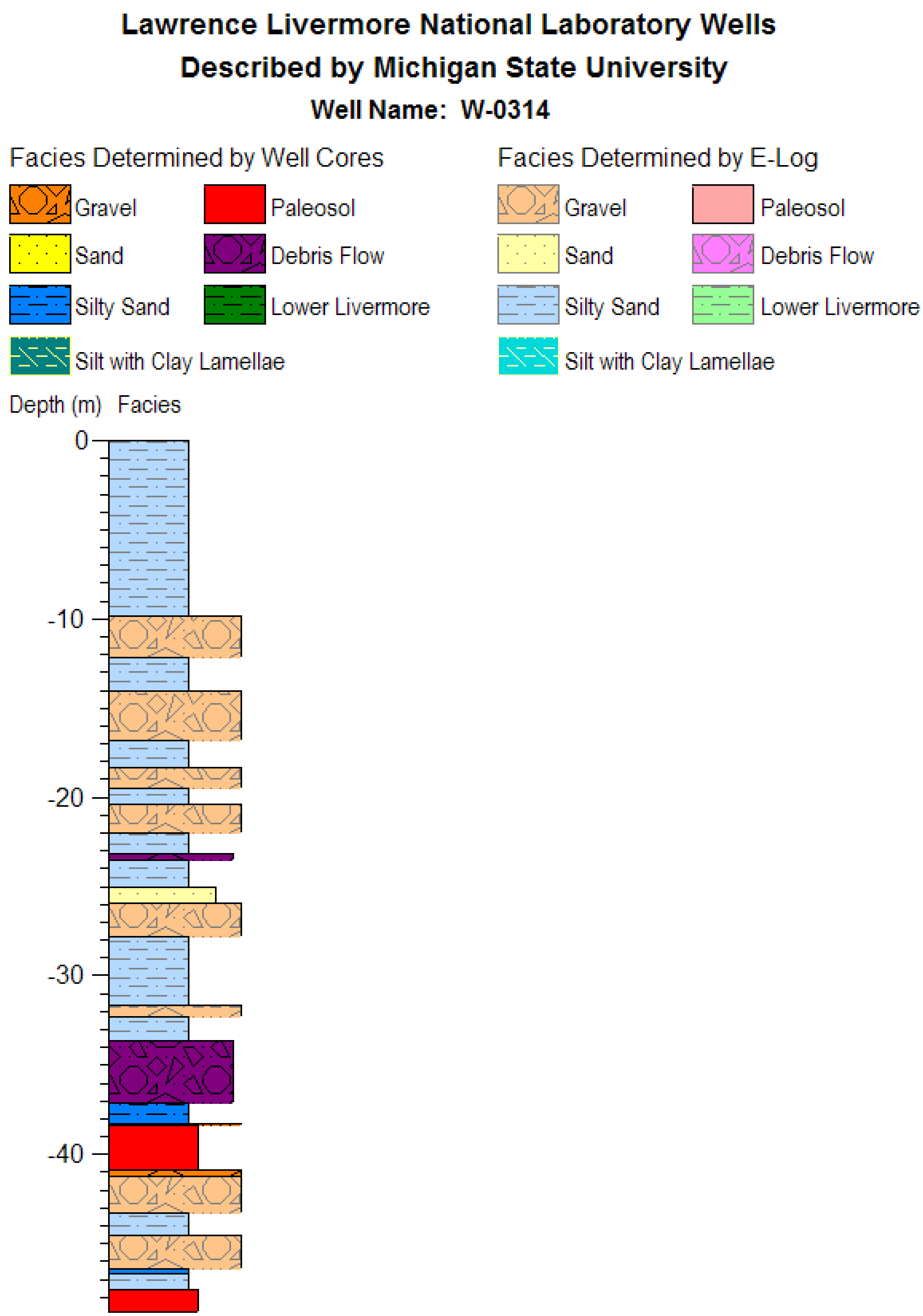

Figure 53. W-0314 stratigraphic column.

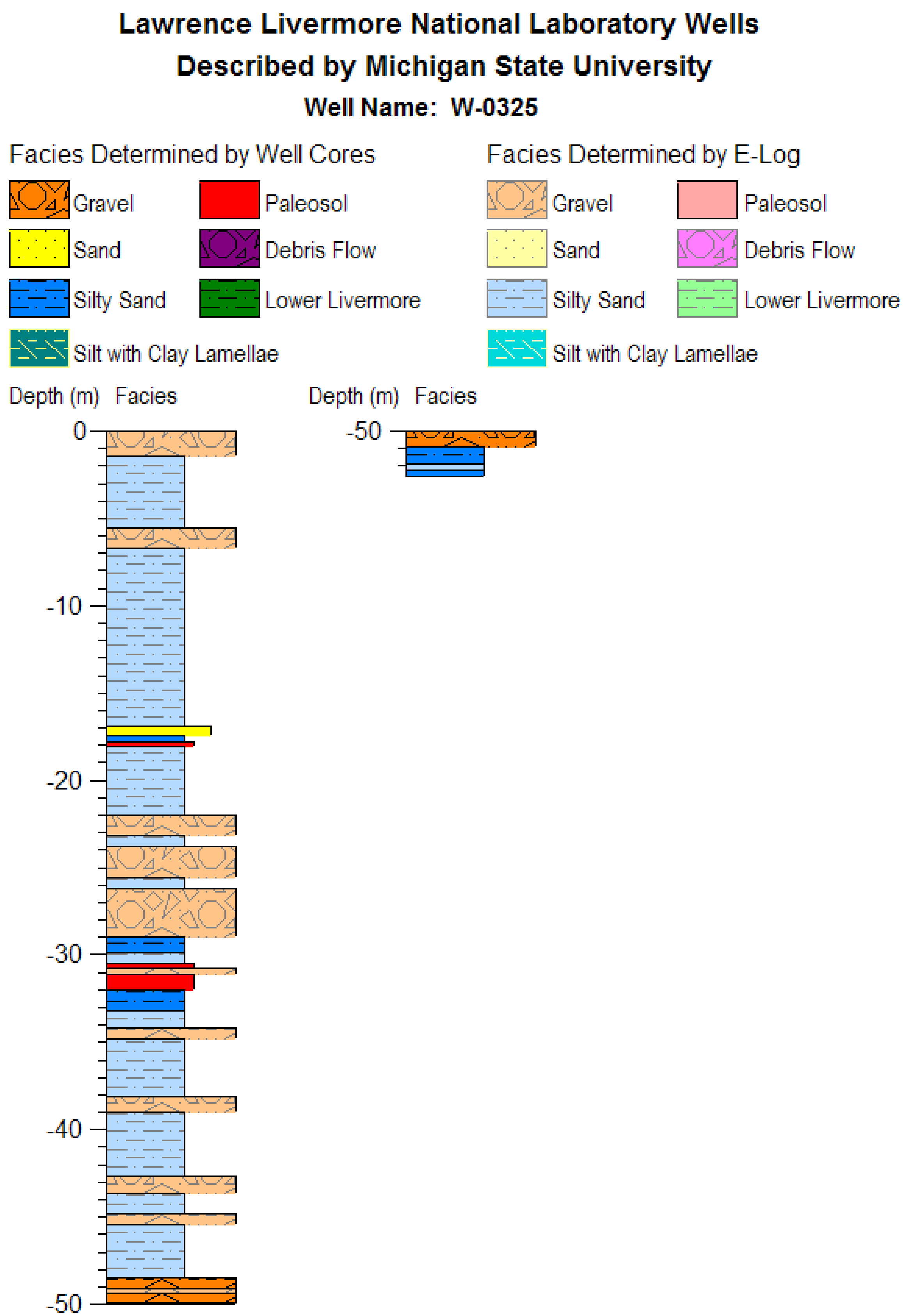

Figure 54. W-0325 stratigraphic column.

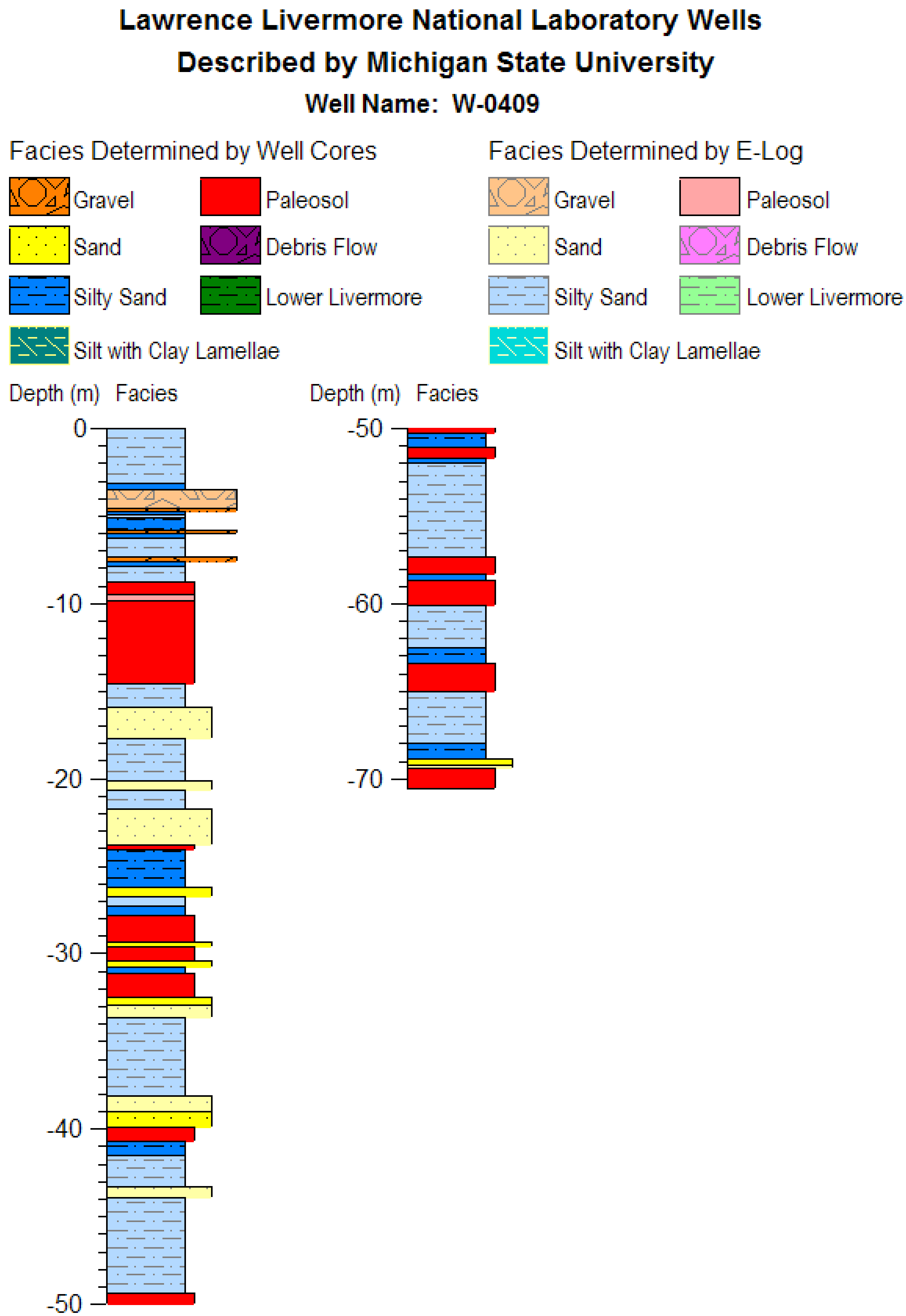

Figure 55. W-0409 stratigraphic column.

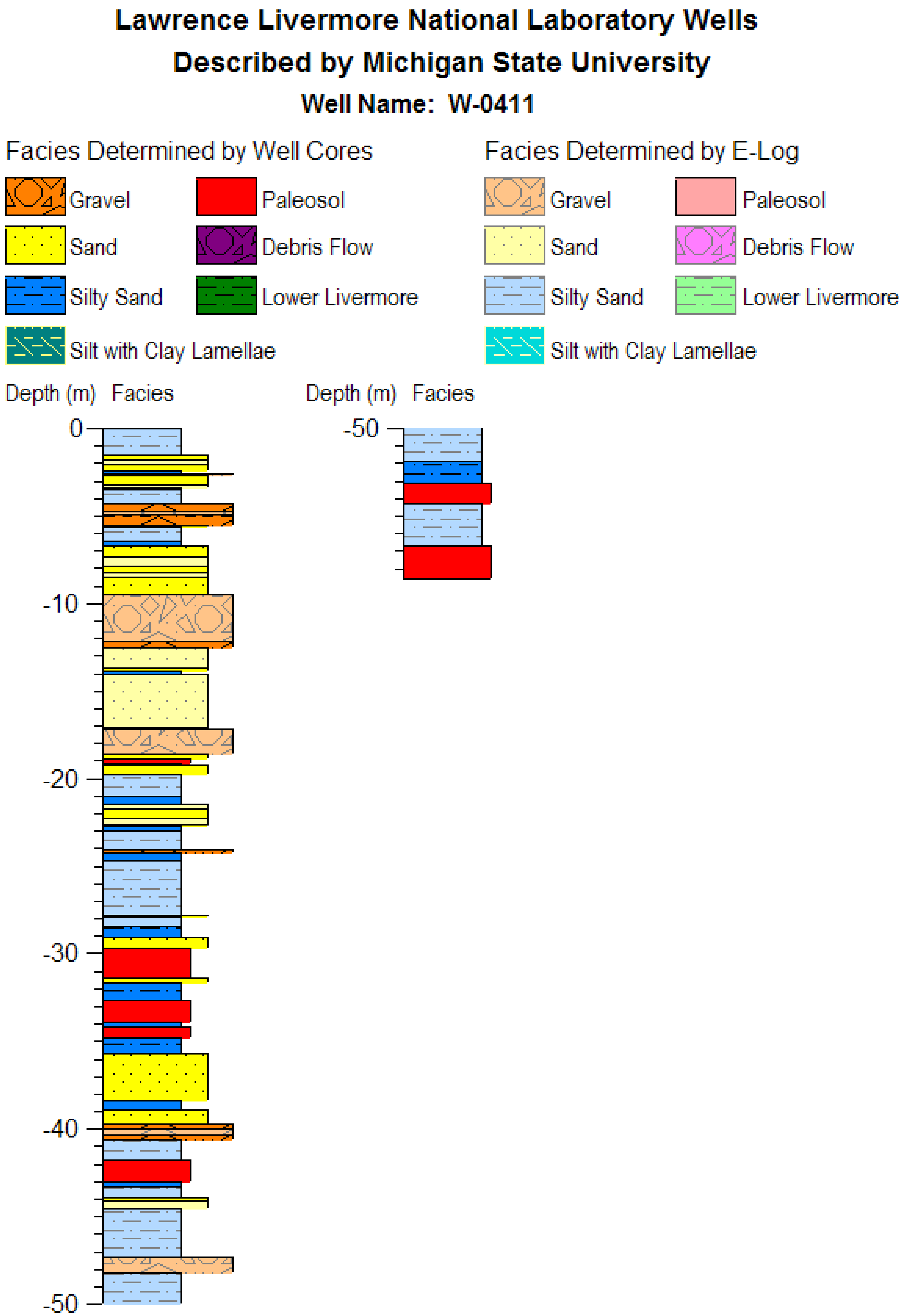

Figure 56. W-0411 stratigraphic column.

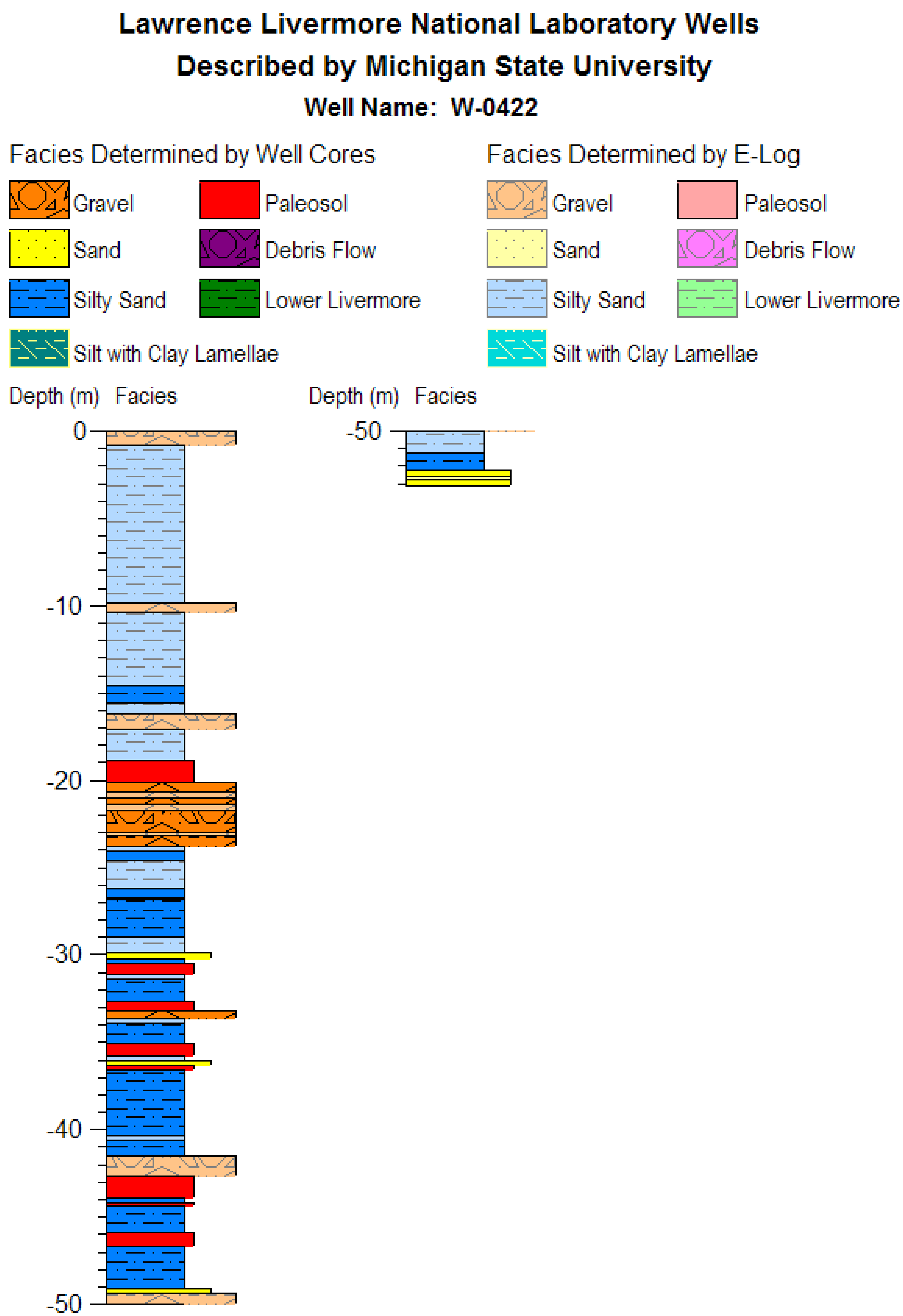

Figure 57. W-0422 stratigraphic column.

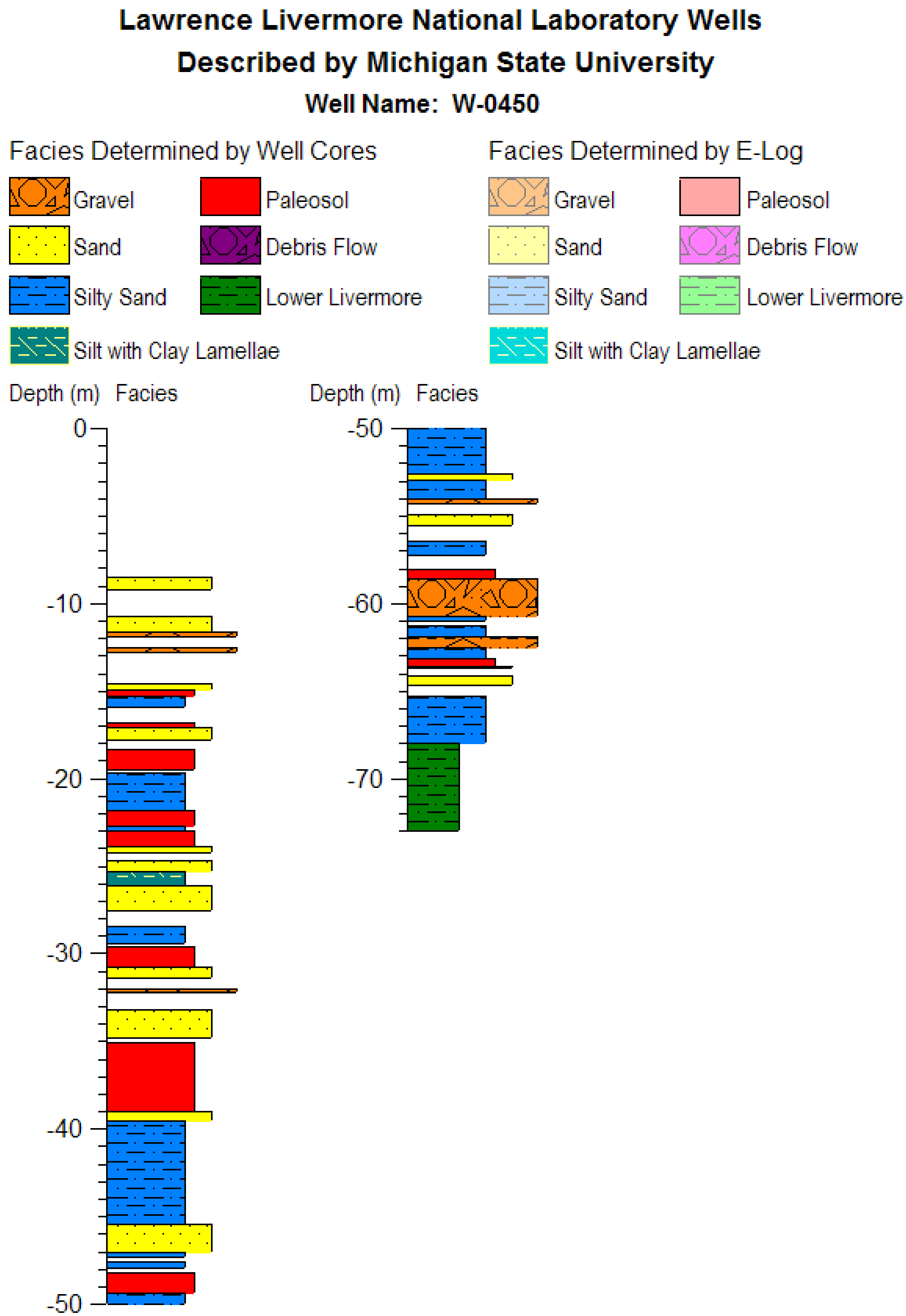

Figure 58. W-0450 stratigraphic column.

Figure 59. W-0452 stratigraphic column.

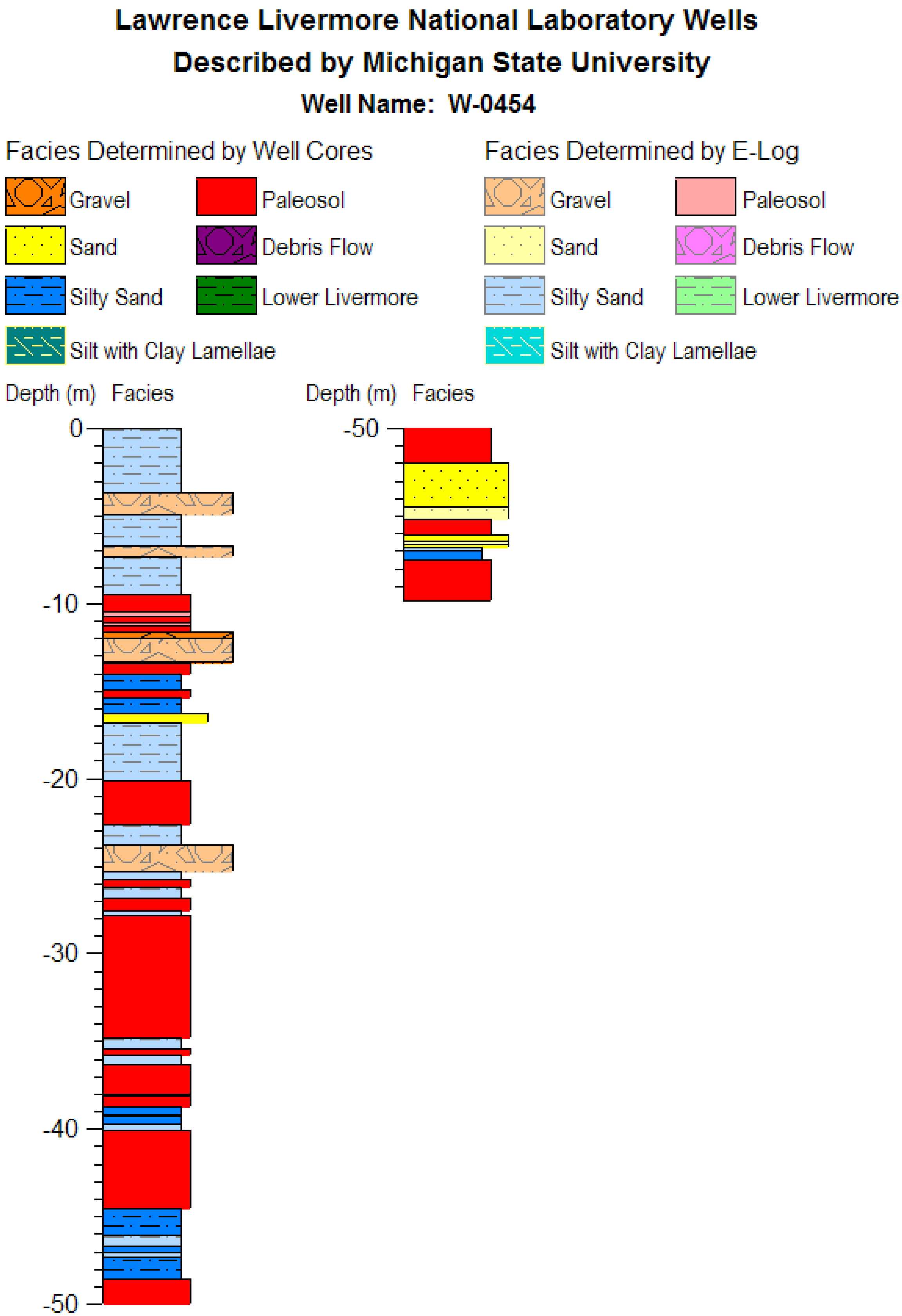

Figure 60. W-0454 stratigraphic column.

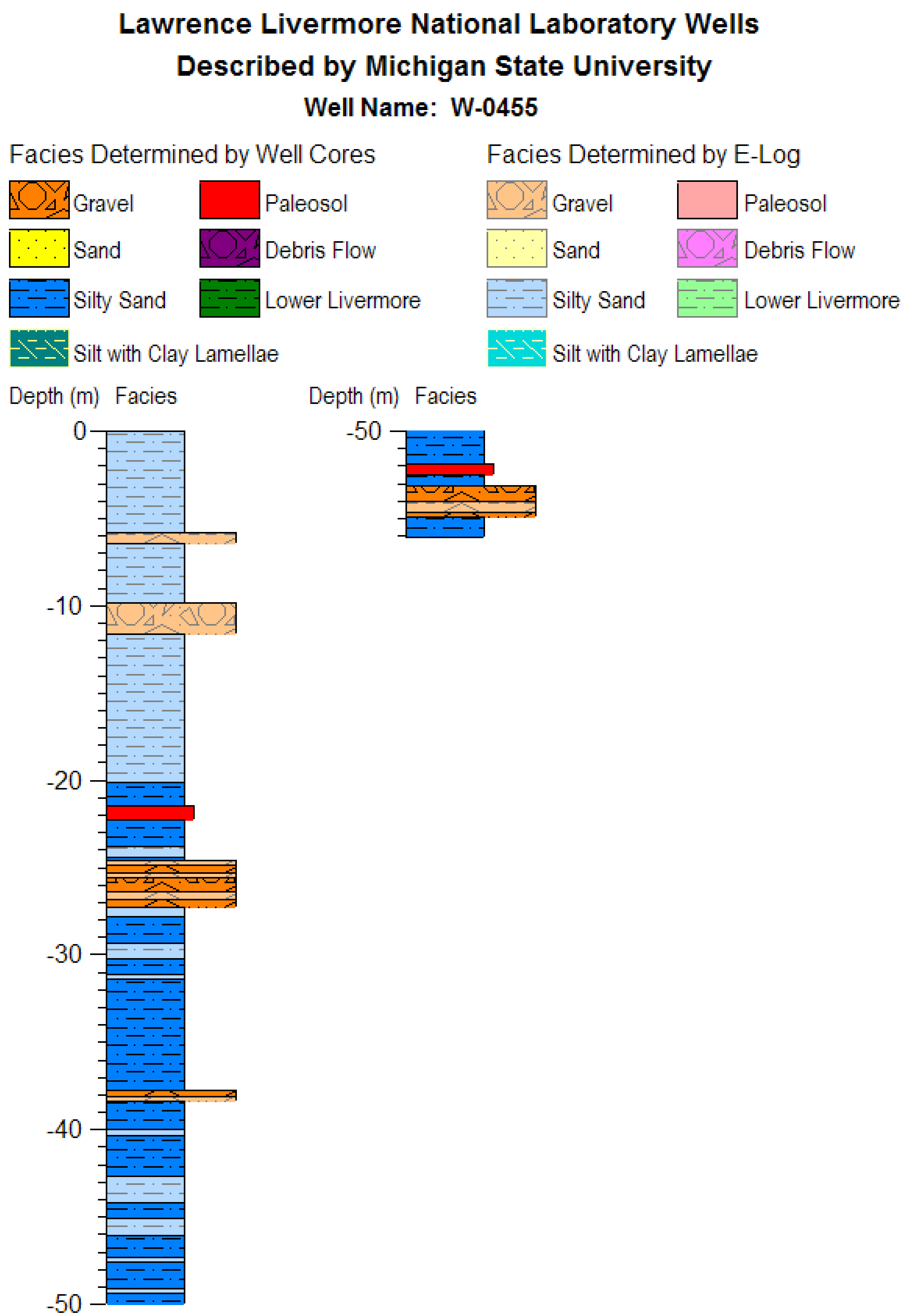

Figure 61. W-0455 stratigraphic column.

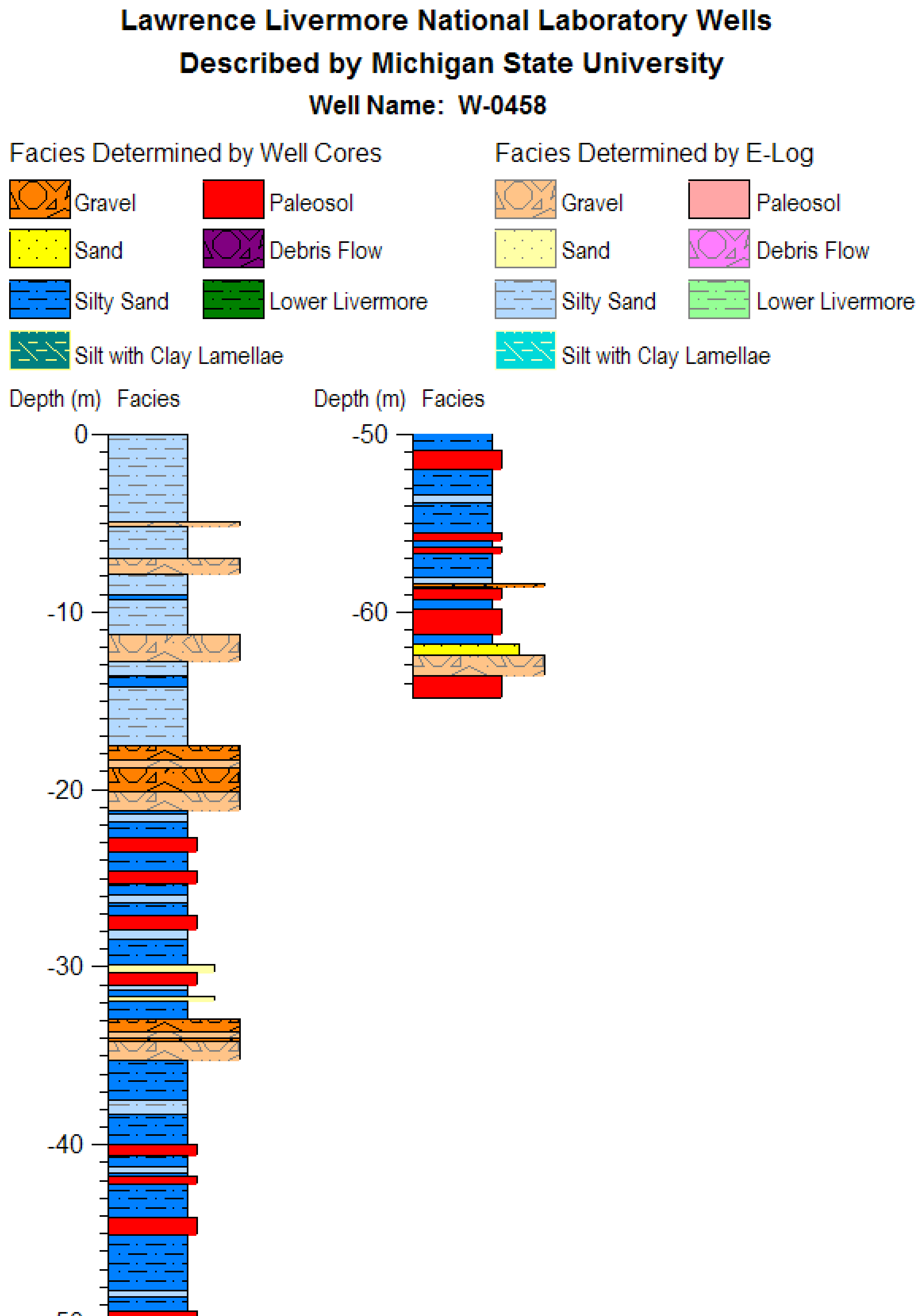

Figure 62. W-0458 stratigraphic column.

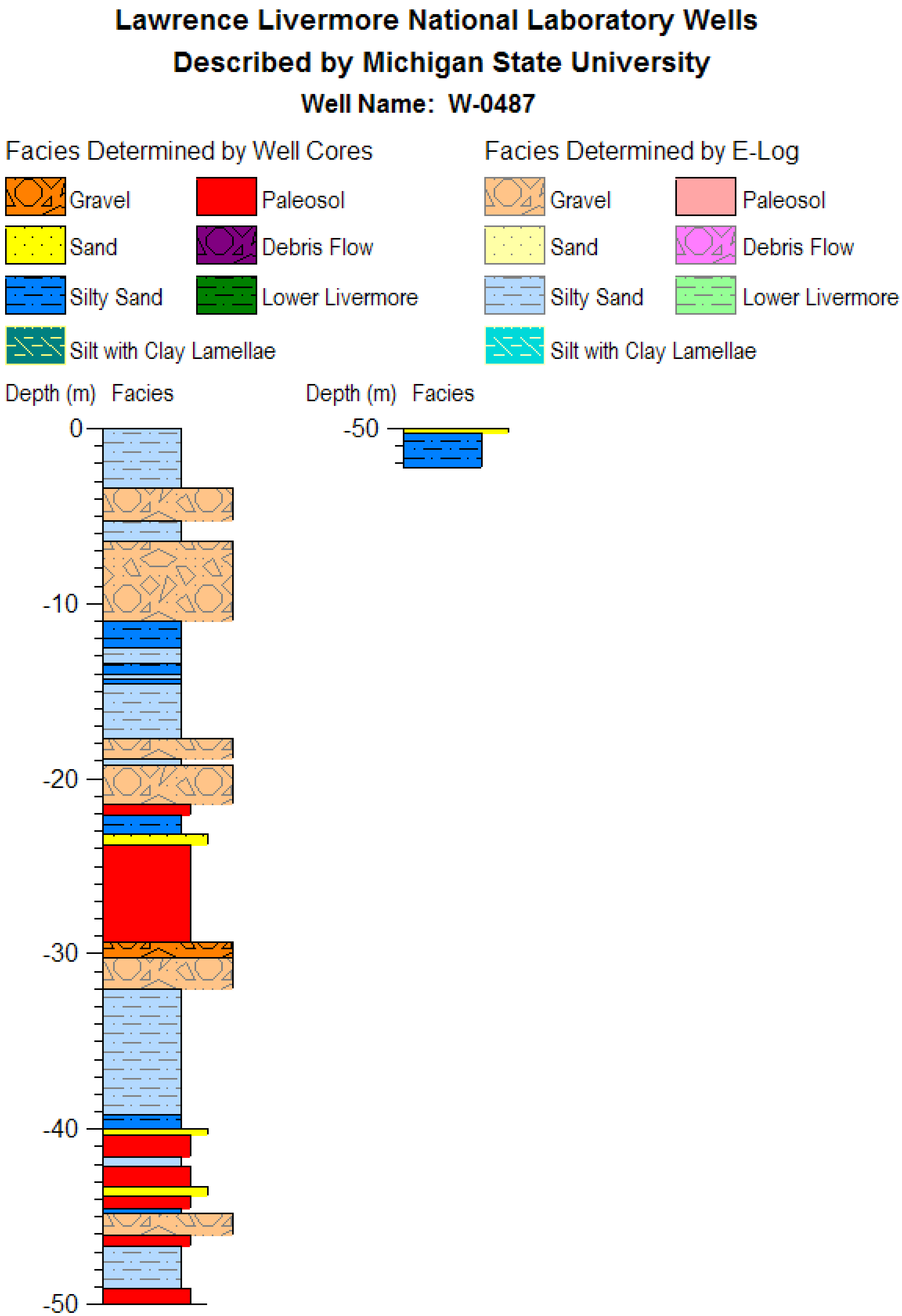

Figure 63. W-0487 stratigraphic column.

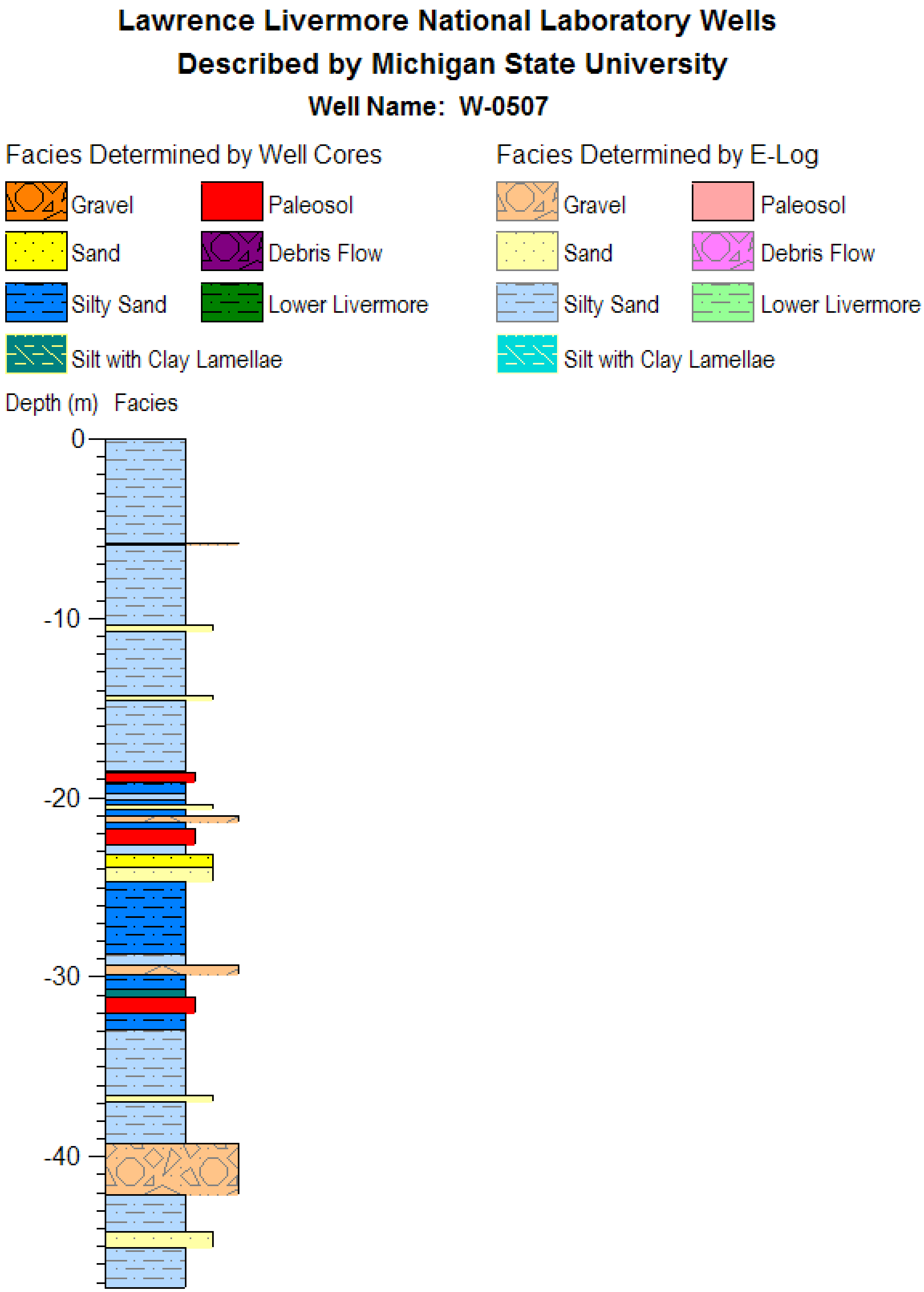

Figure 64. W-0507 stratigraphic column.

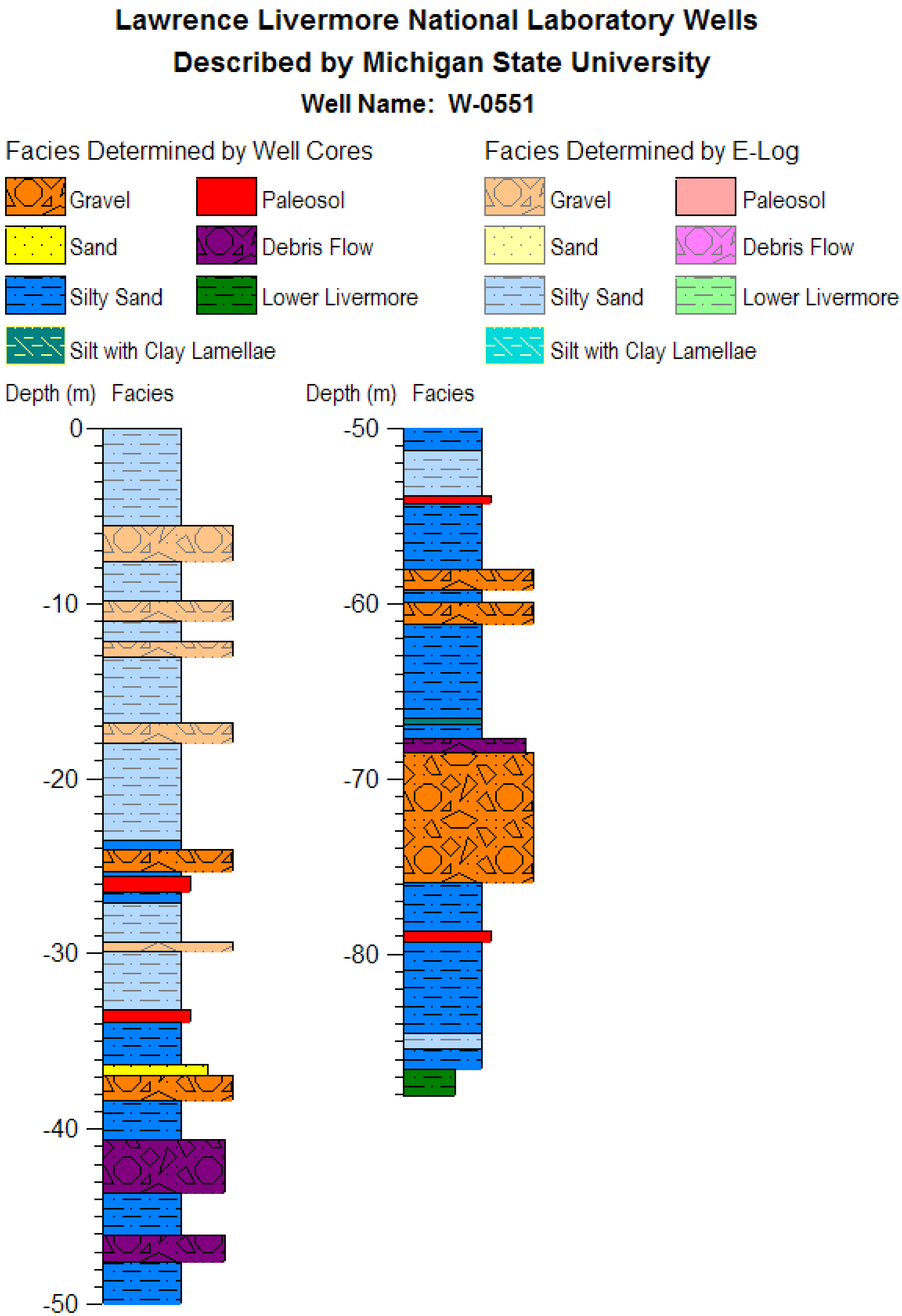

Figure 65. W-0551 stratigraphic column.

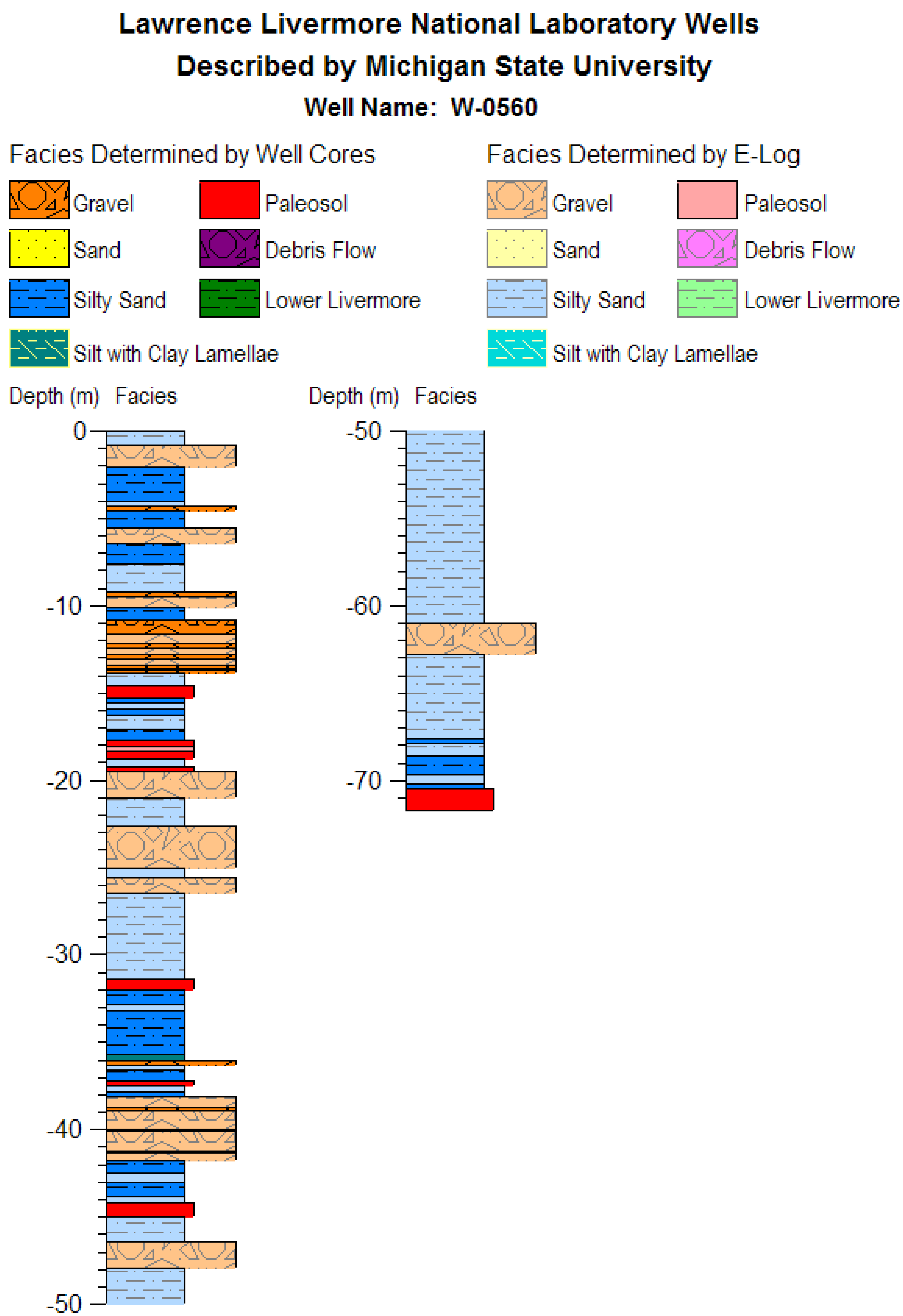

Figure 66. W-0560 stratigraphic column.

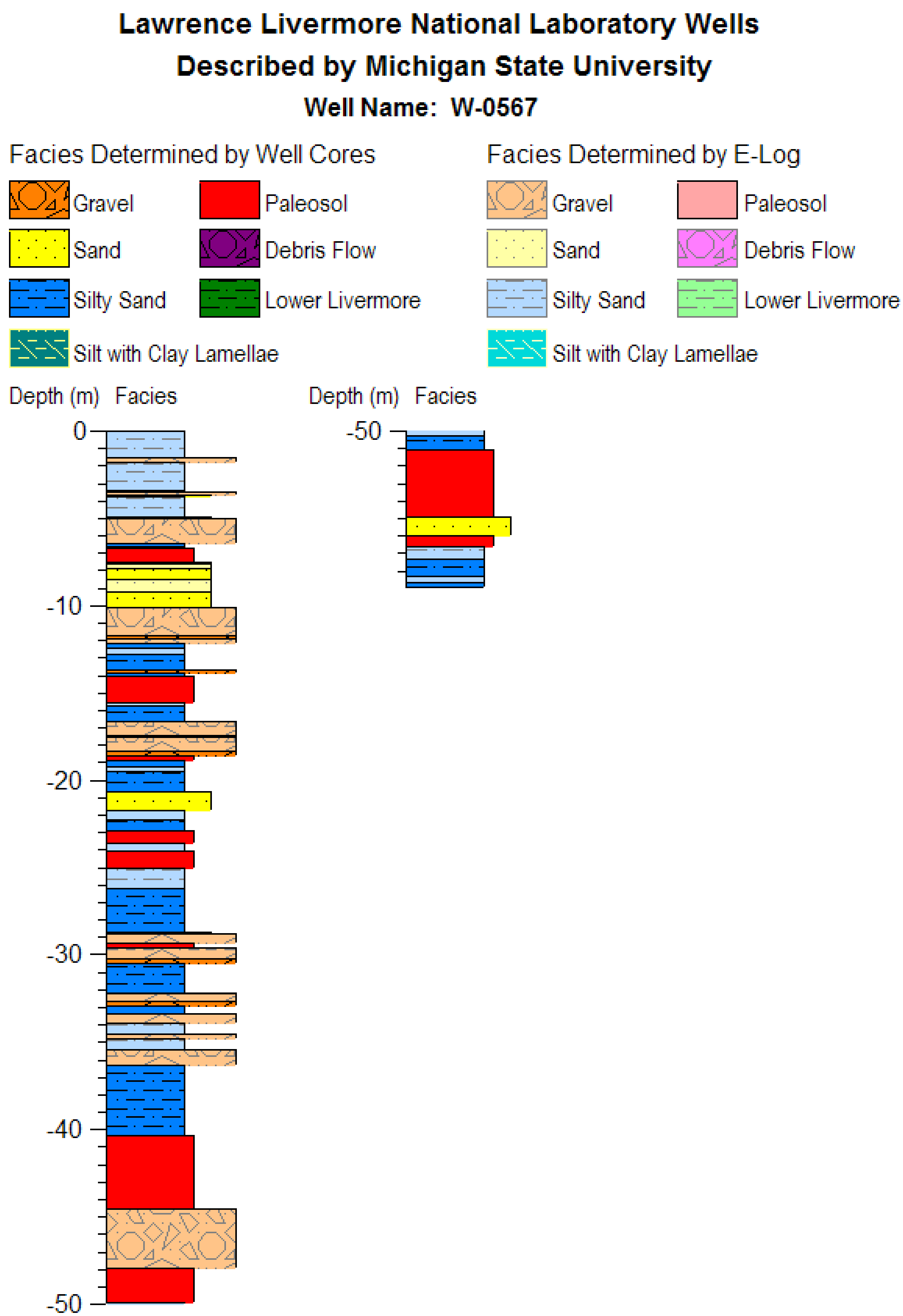

Figure 67. W-0567 stratigraphic column.

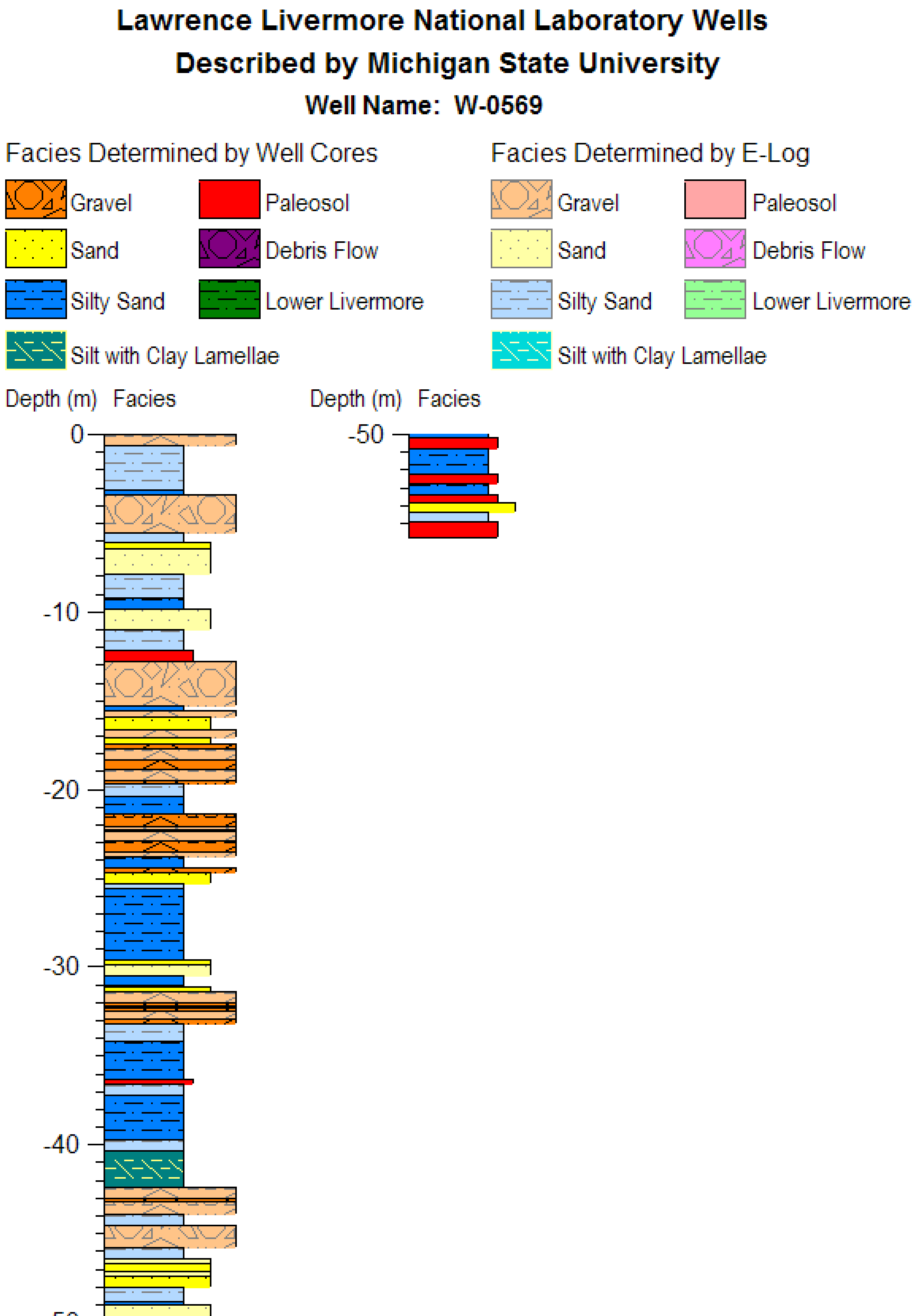

Figure 68. W-0569 stratigraphic column.

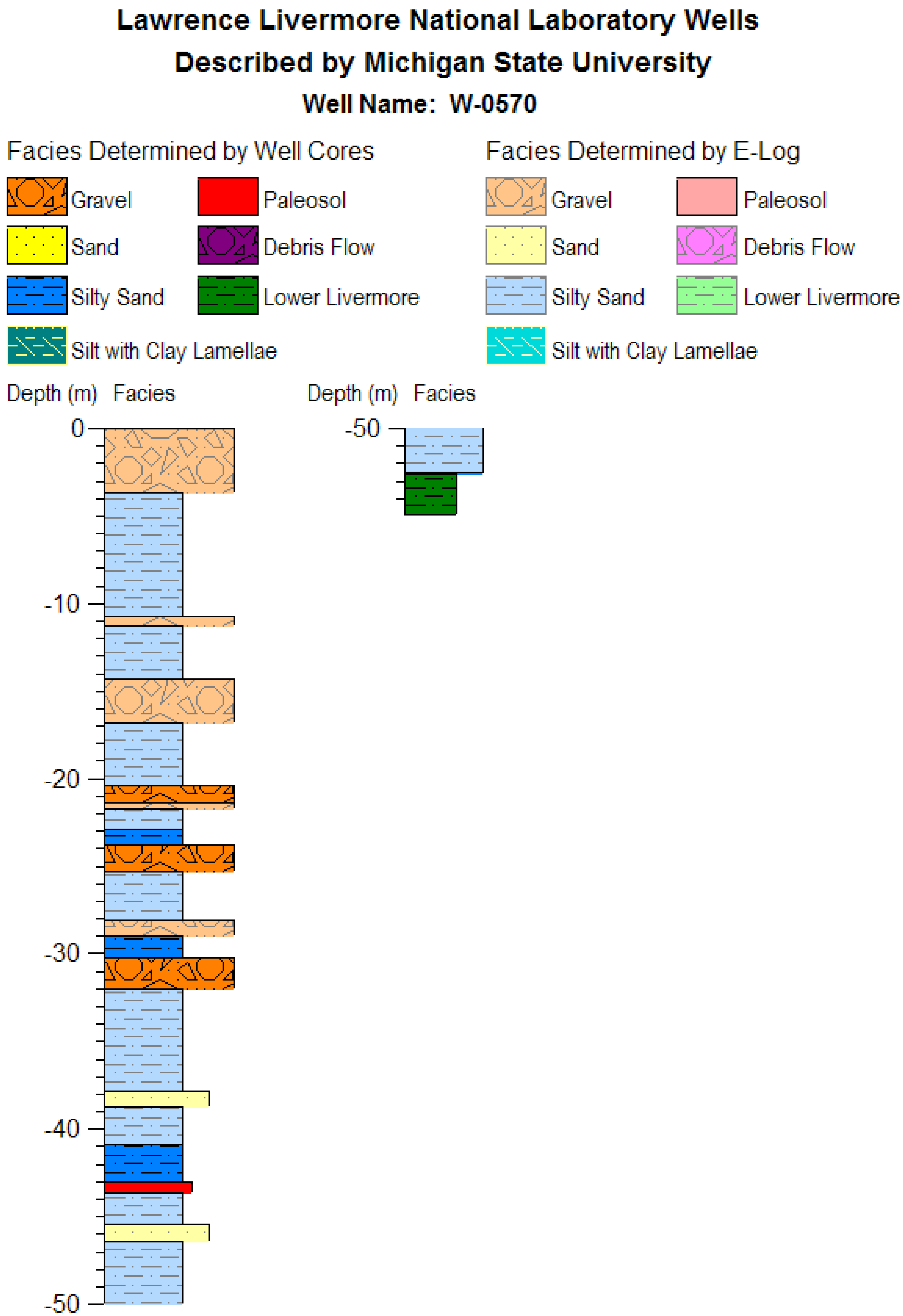

Figure 69. W-0570 stratigraphic column.

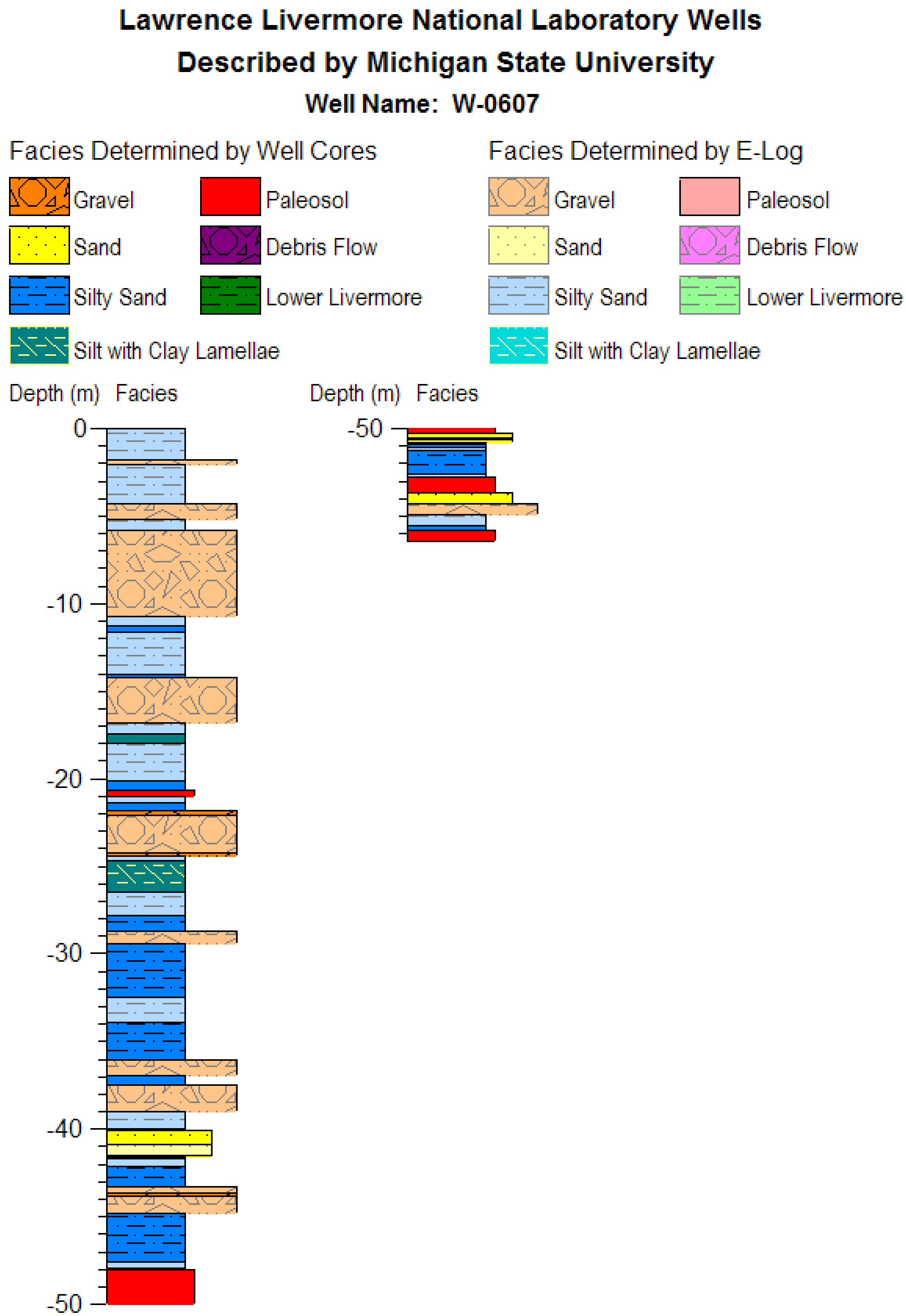

Figure 70. W-0607 stratigraphic column.

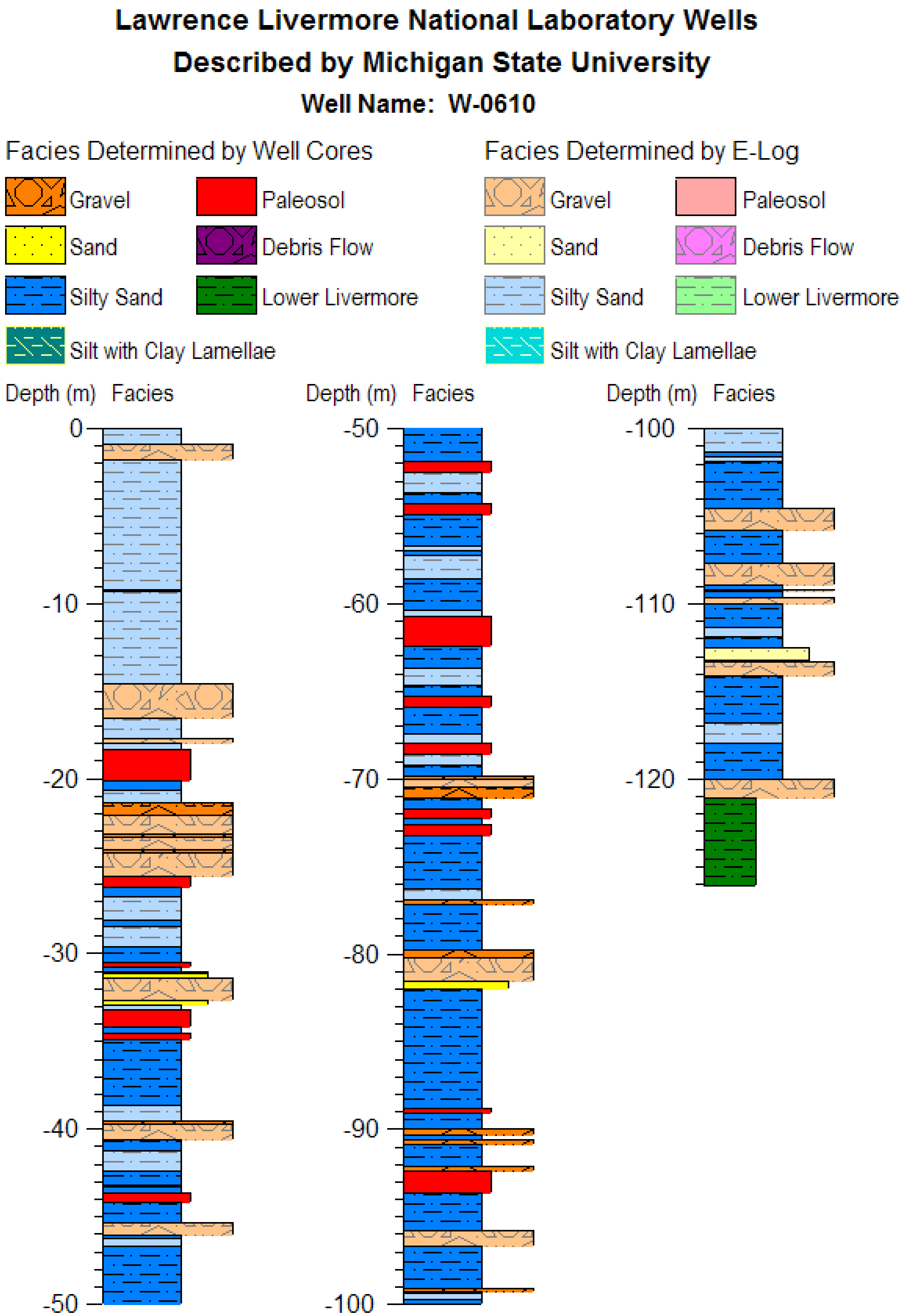

Figure 71. W-0610 stratigraphic column.

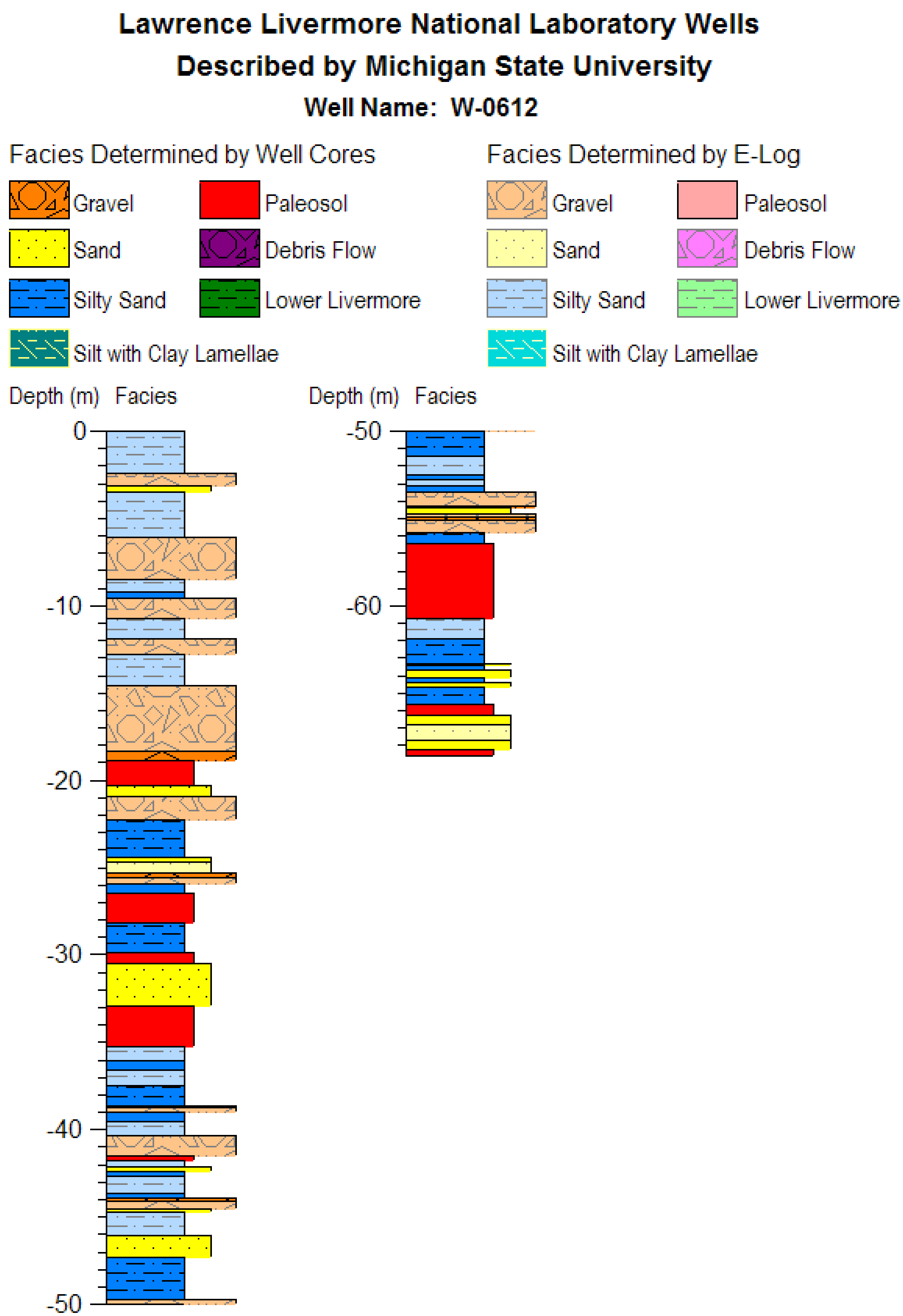

Figure 72. W-0612 stratigraphic column.

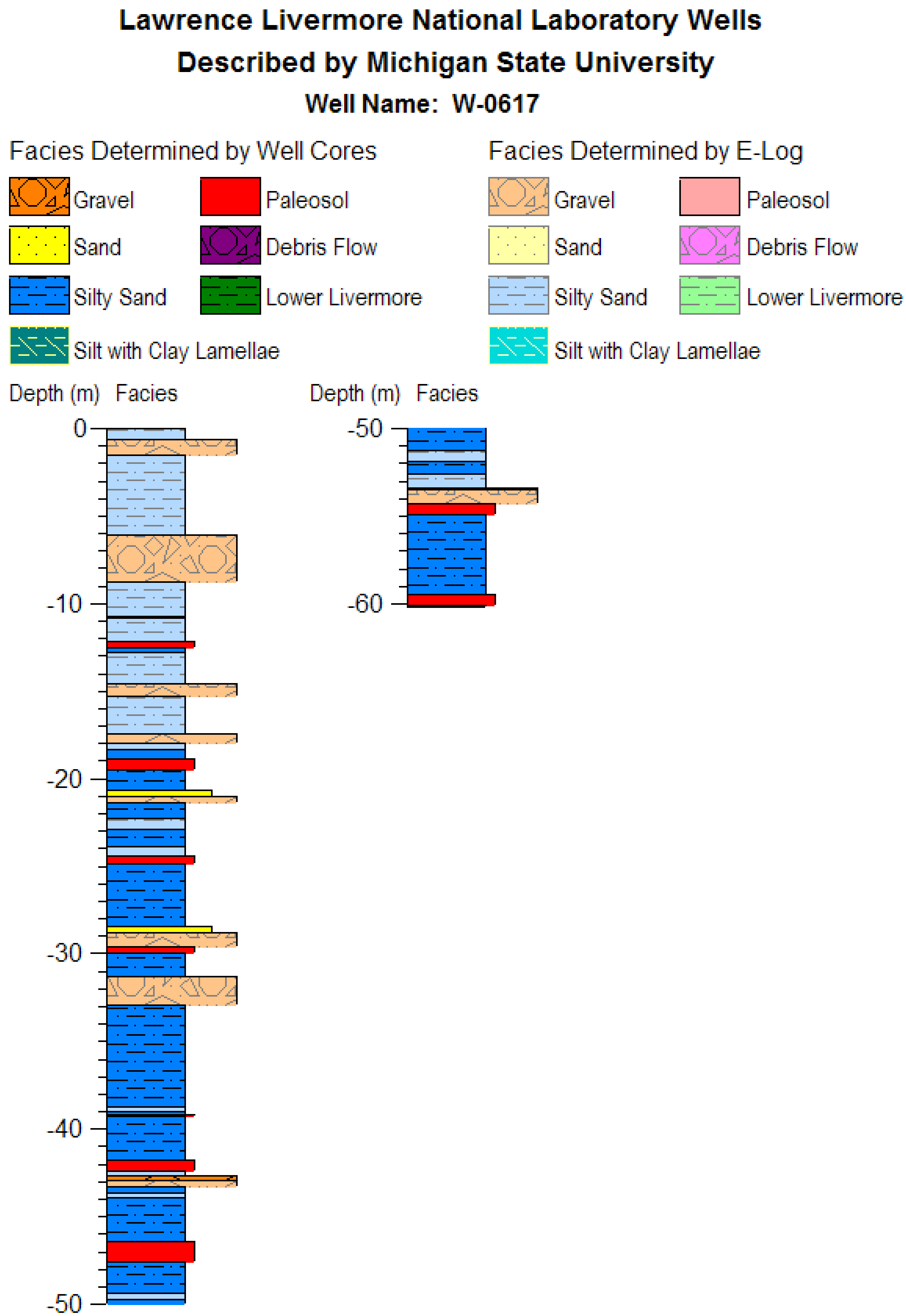

Figure 73. W-0617 stratigraphic column.

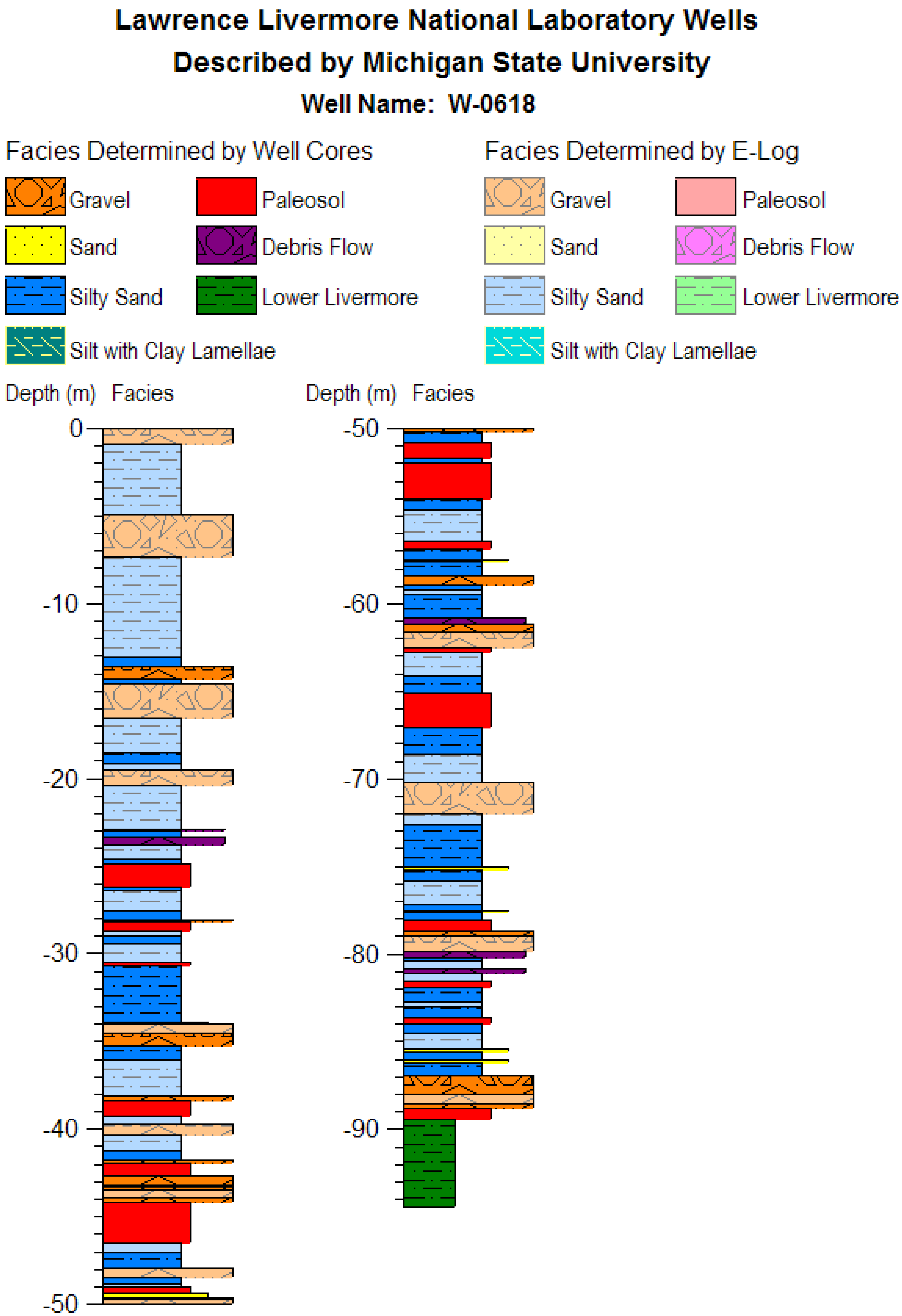

Figure 74. W-0618 stratigraphic column.

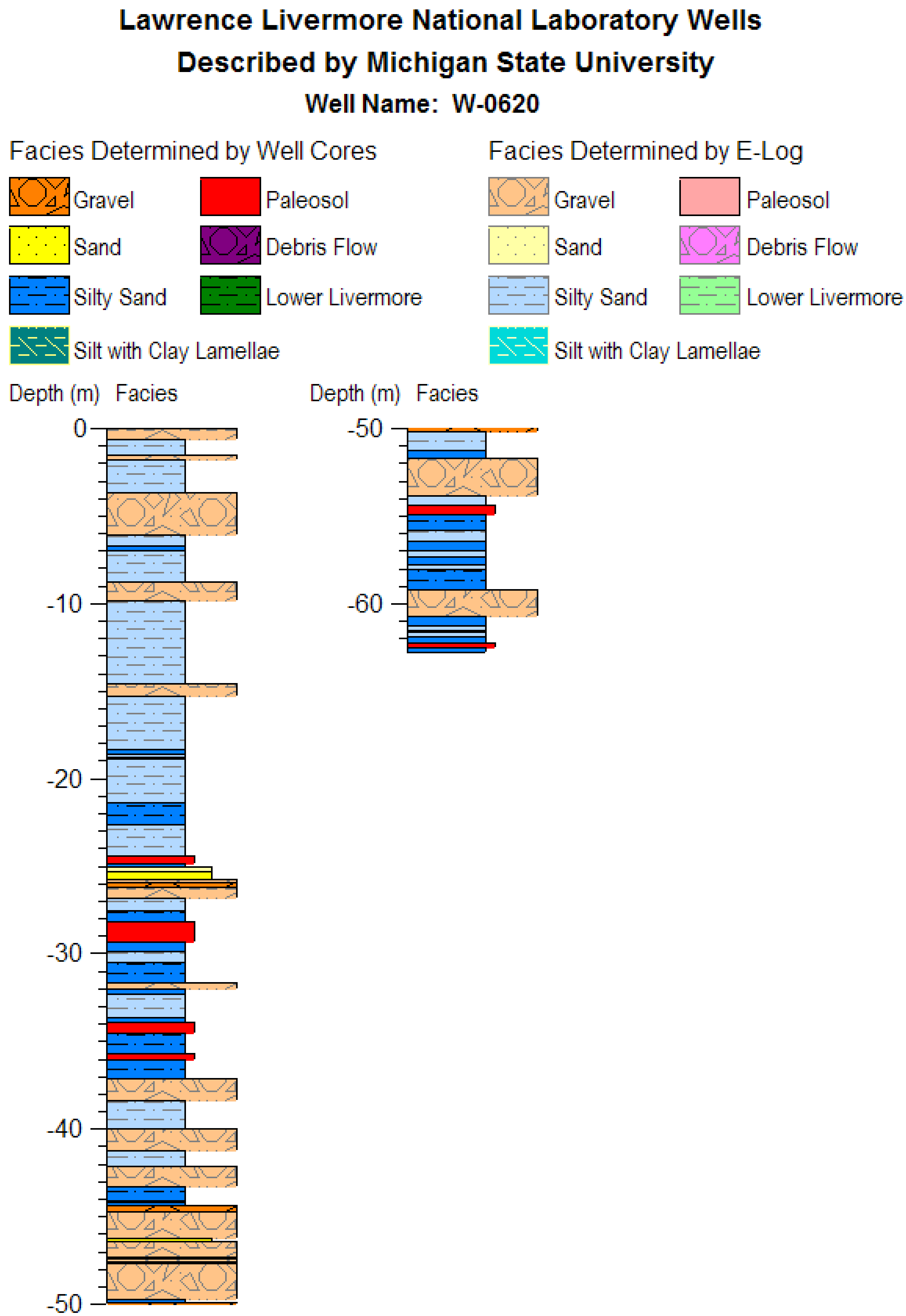

Figure 75. W-0620 stratigraphic column.

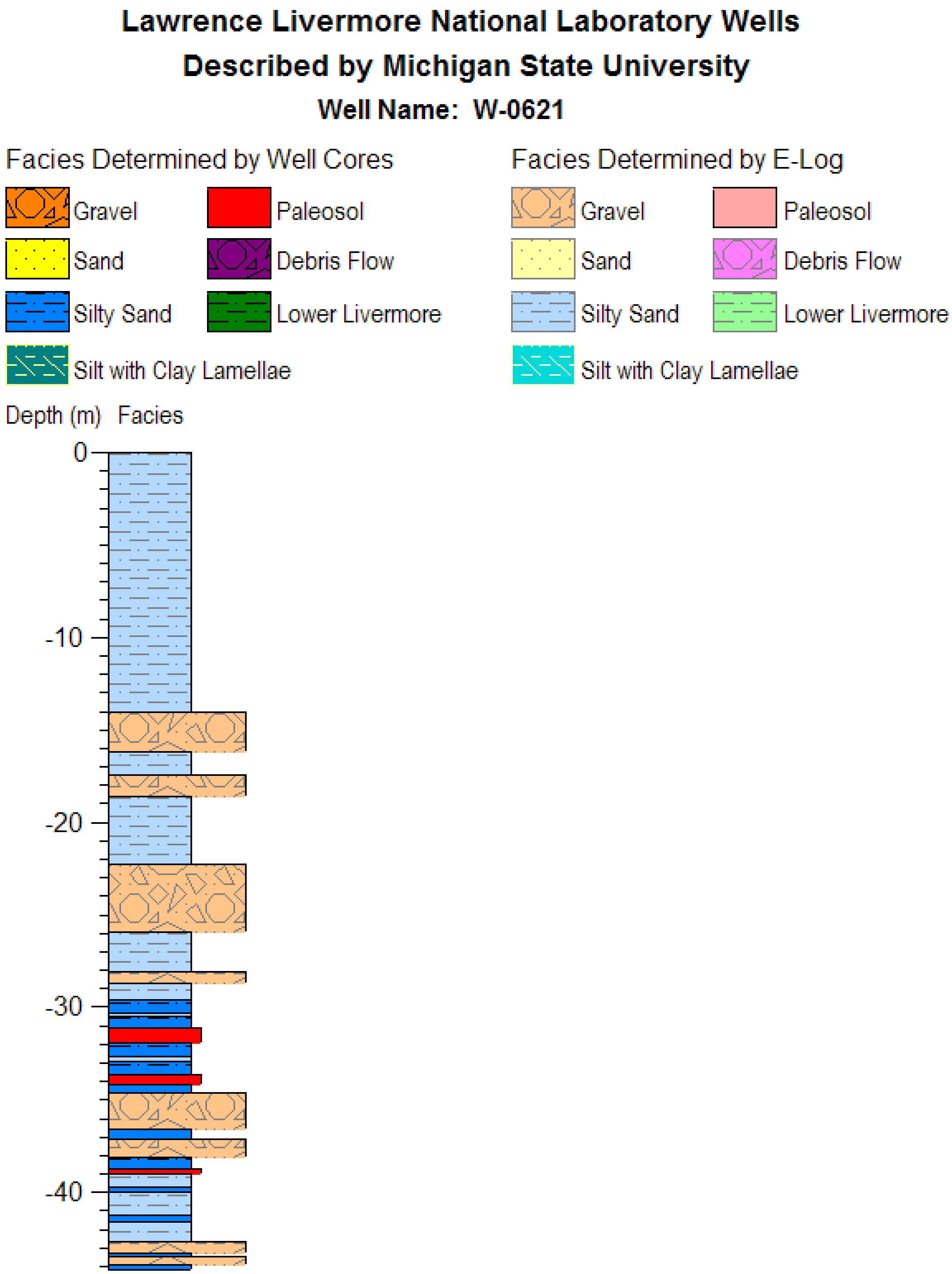

Figure 76. W-0621 stratigraphic column.

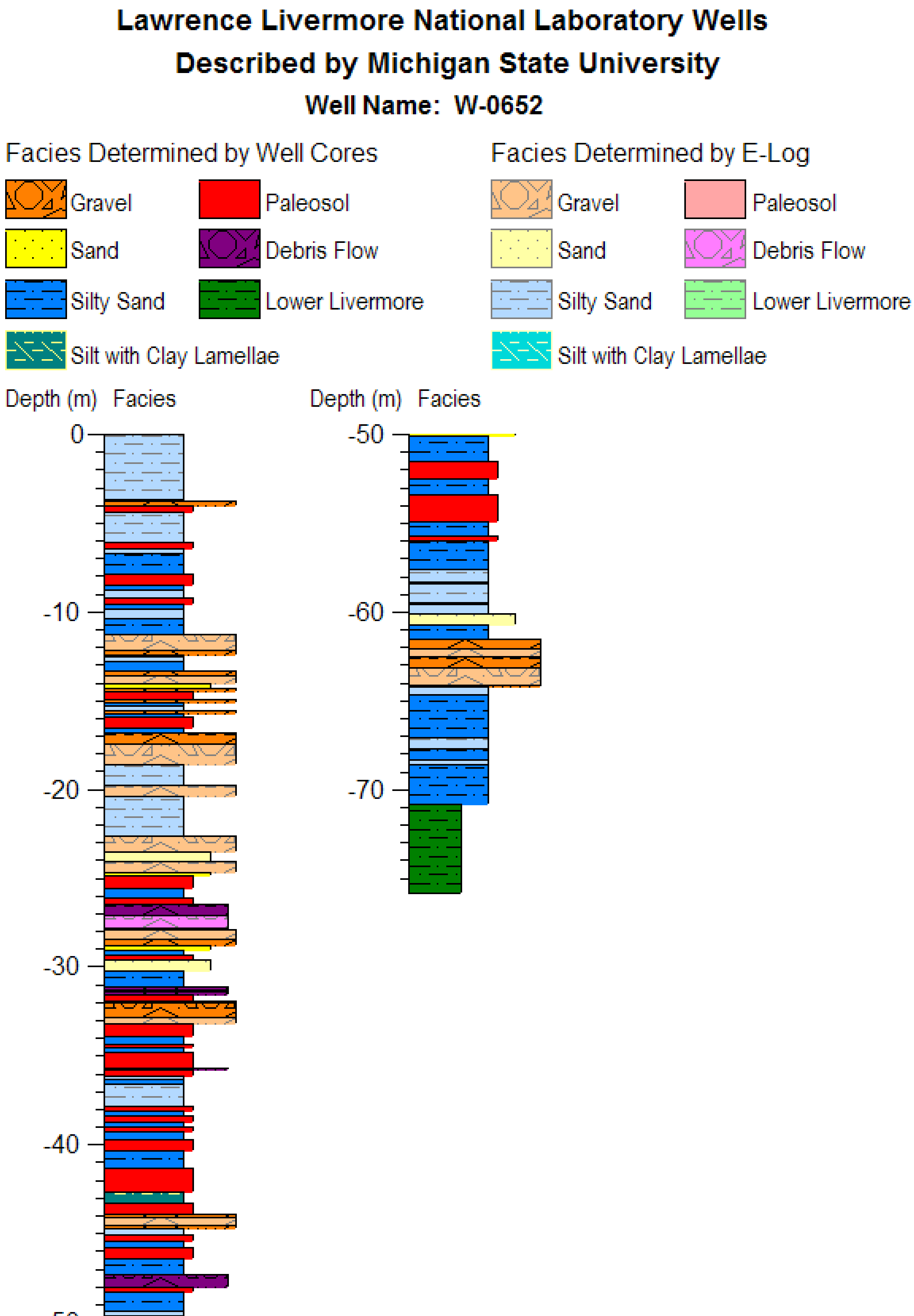

Figure 77. W-0652 stratigraphic column.

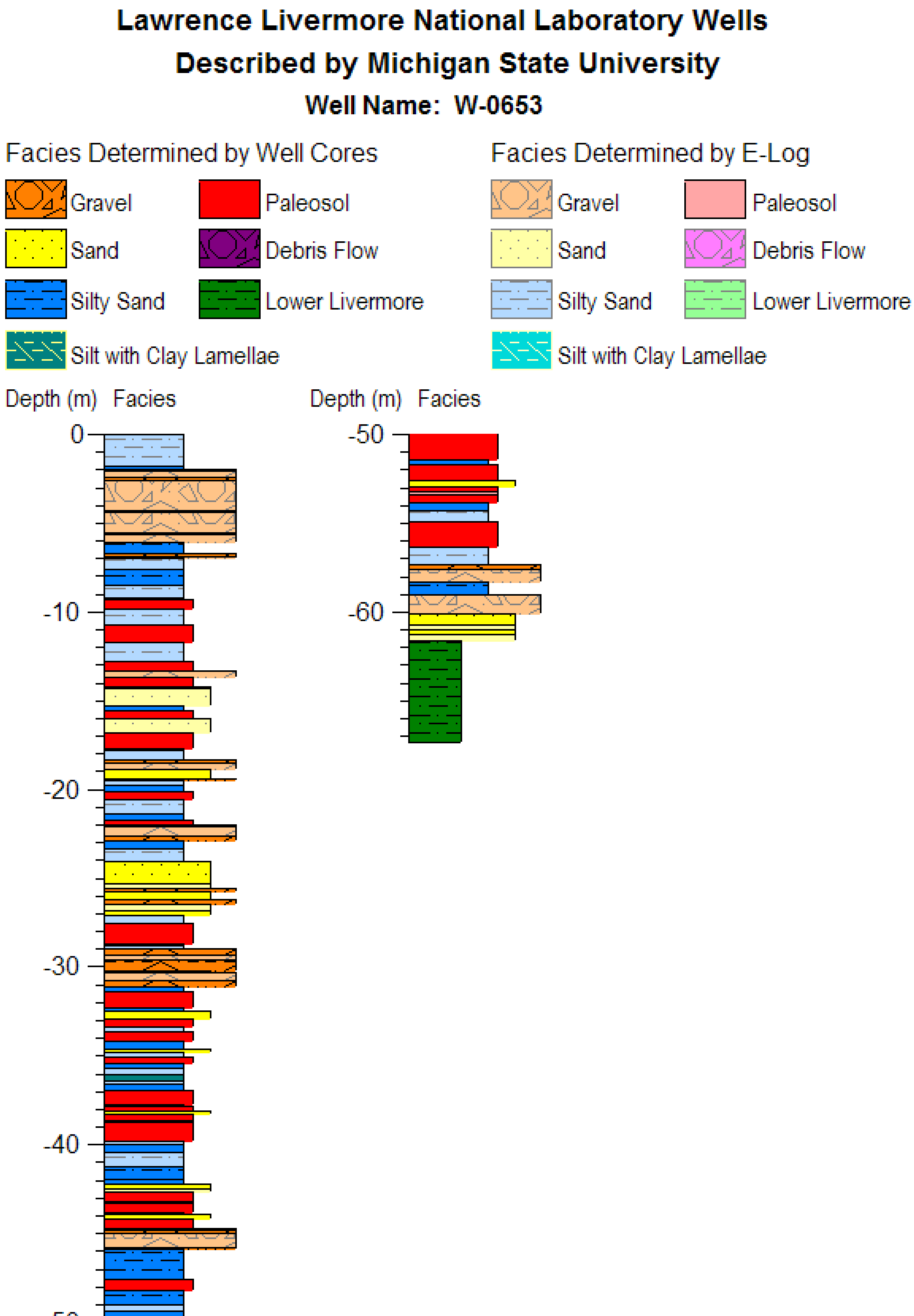

Figure 78. W-0653 stratigraphic column.

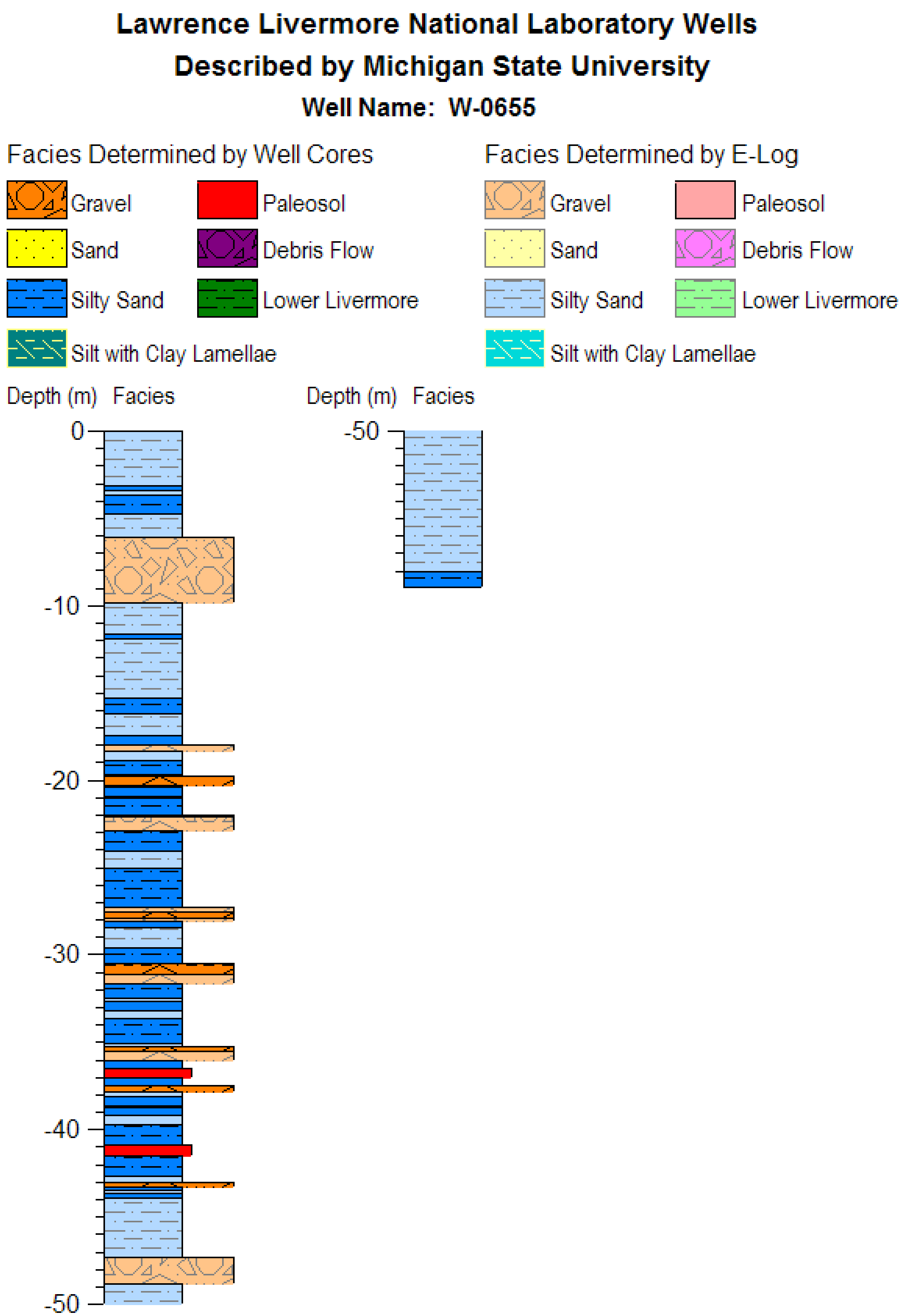

Figure 79. W-0655 stratigraphic column.

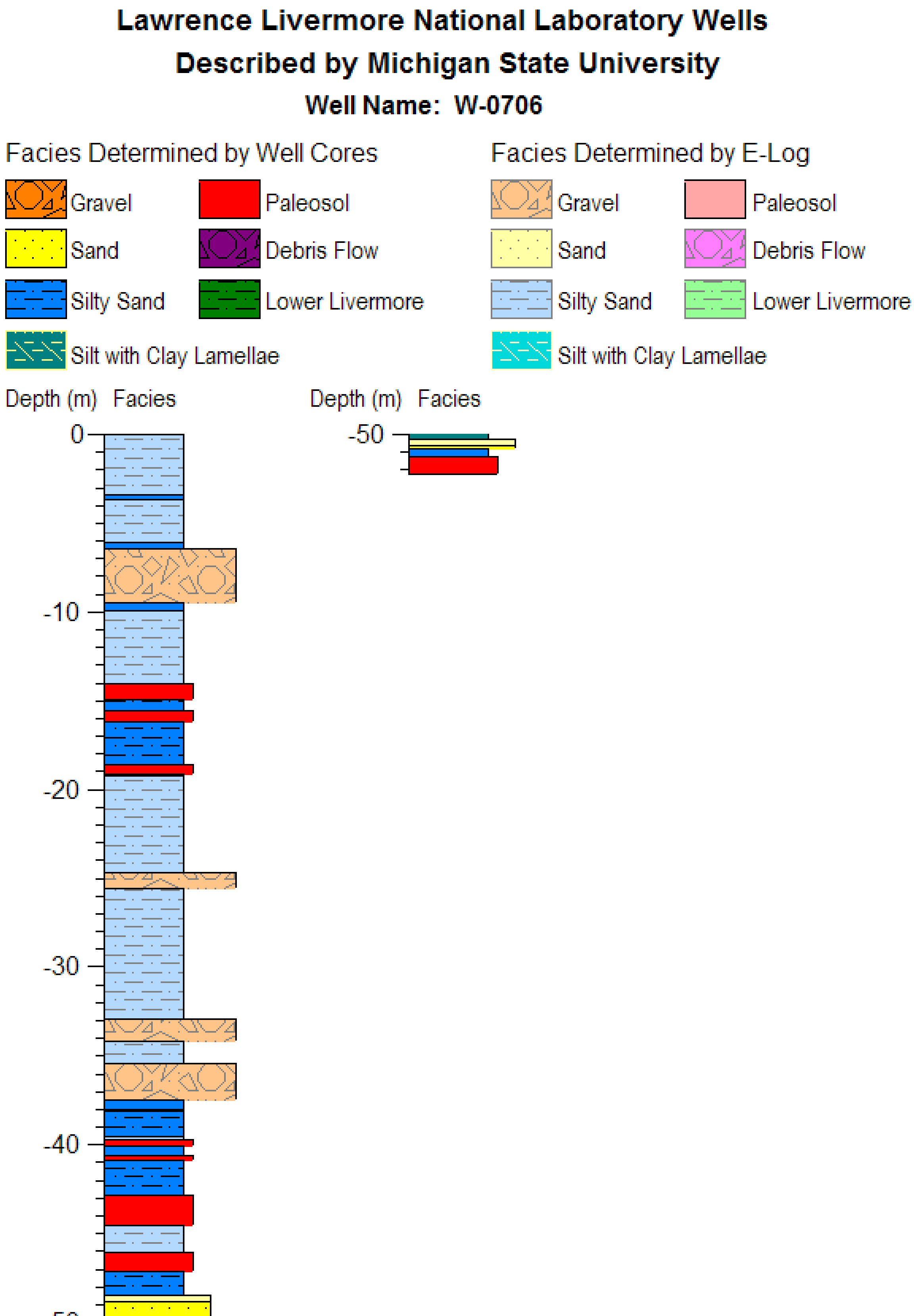

Figure 80. W-0706 stratigraphic column.

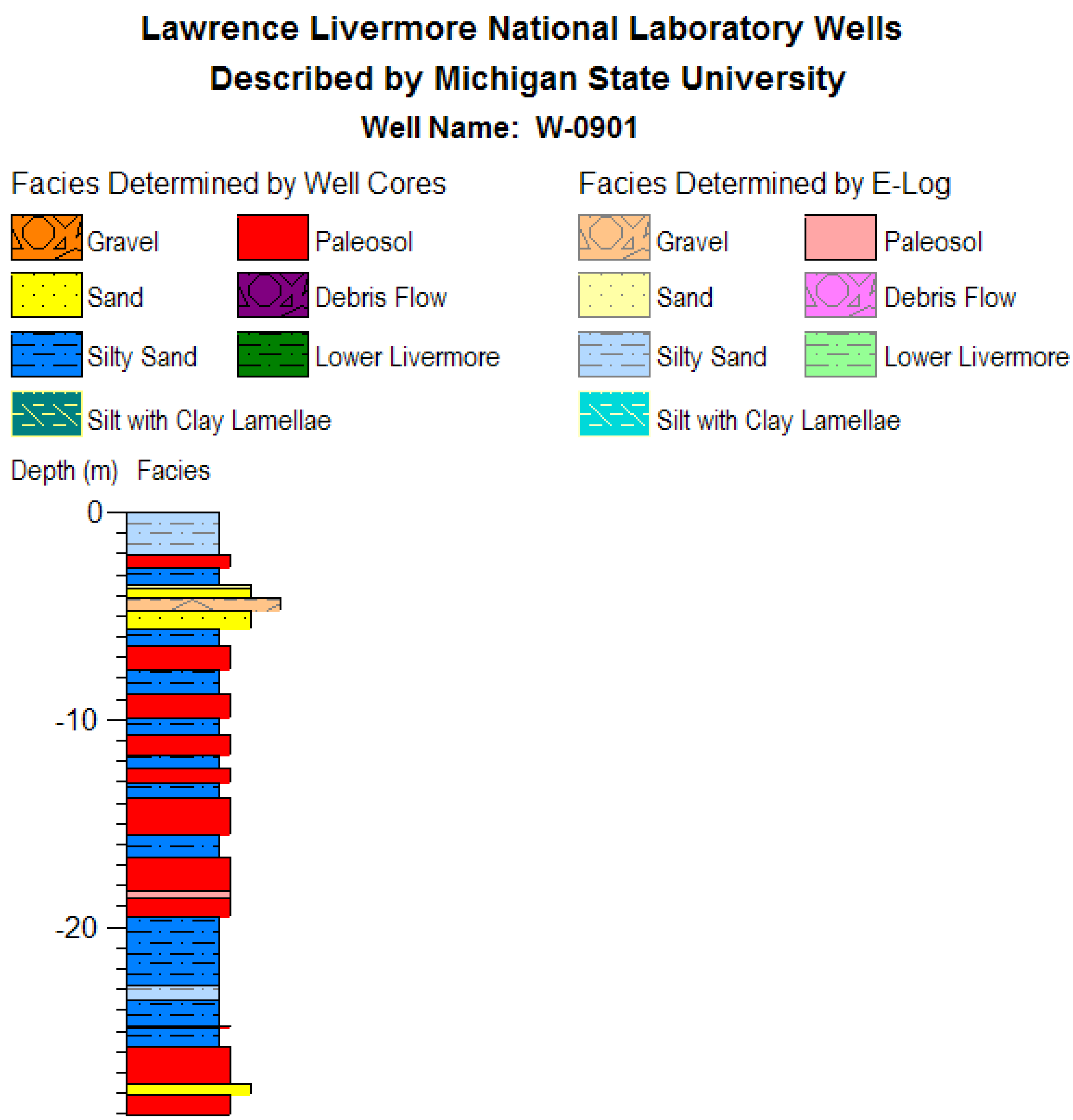

Figure 81. W-0901 stratigraphic column.

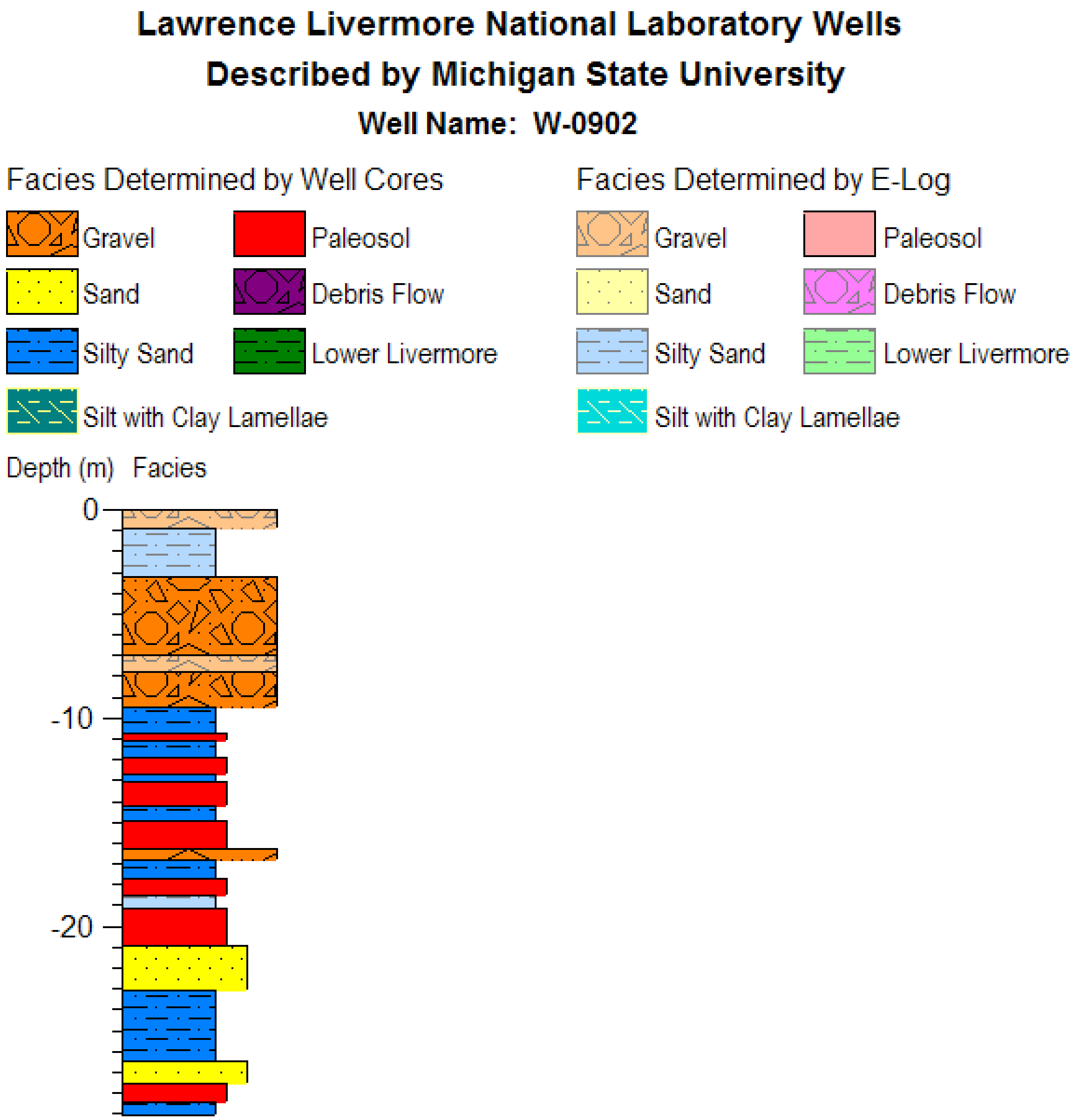

Figure 82. W-0902 stratigraphic column.

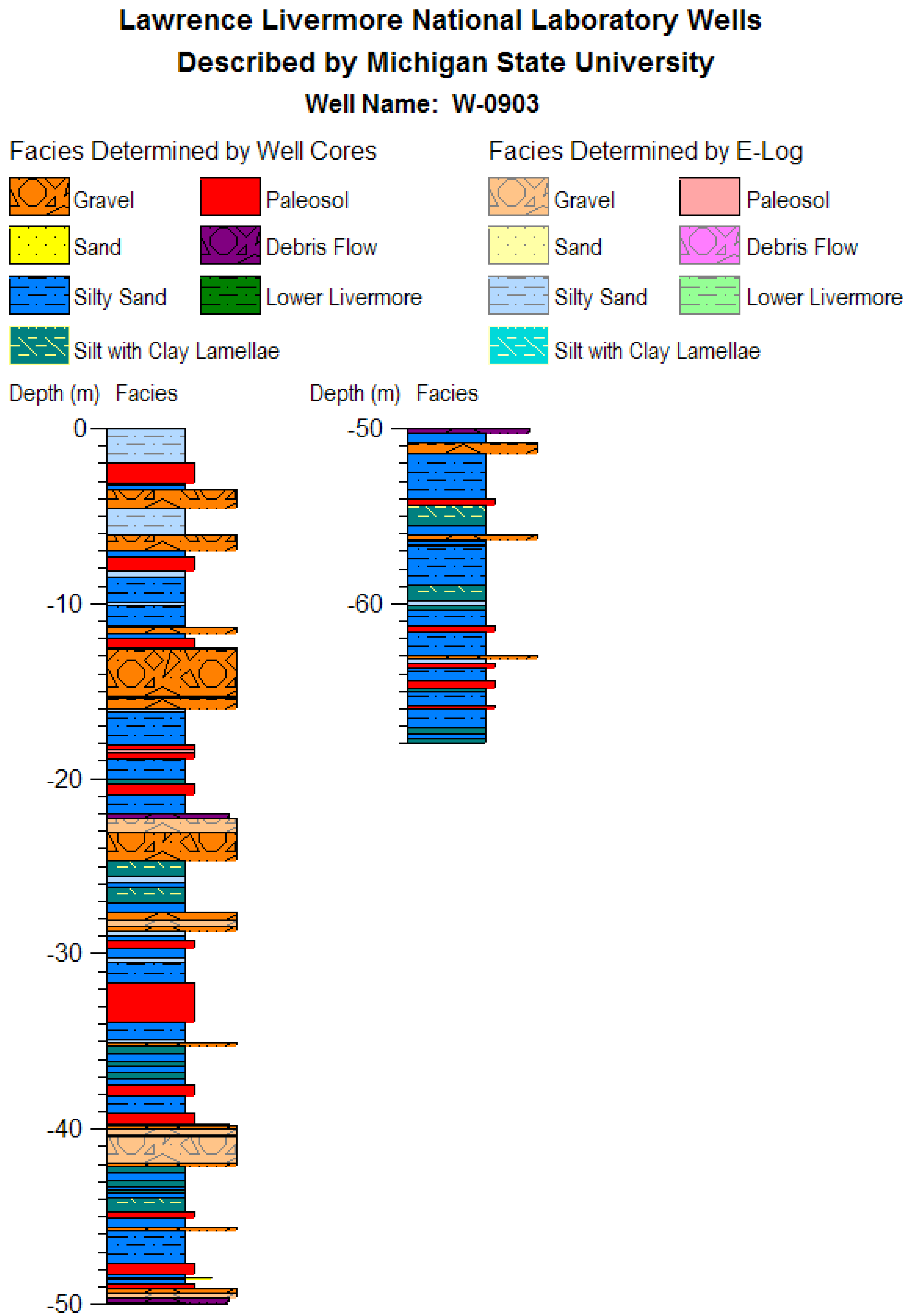

Figure 83. W-0903 stratigraphic column.

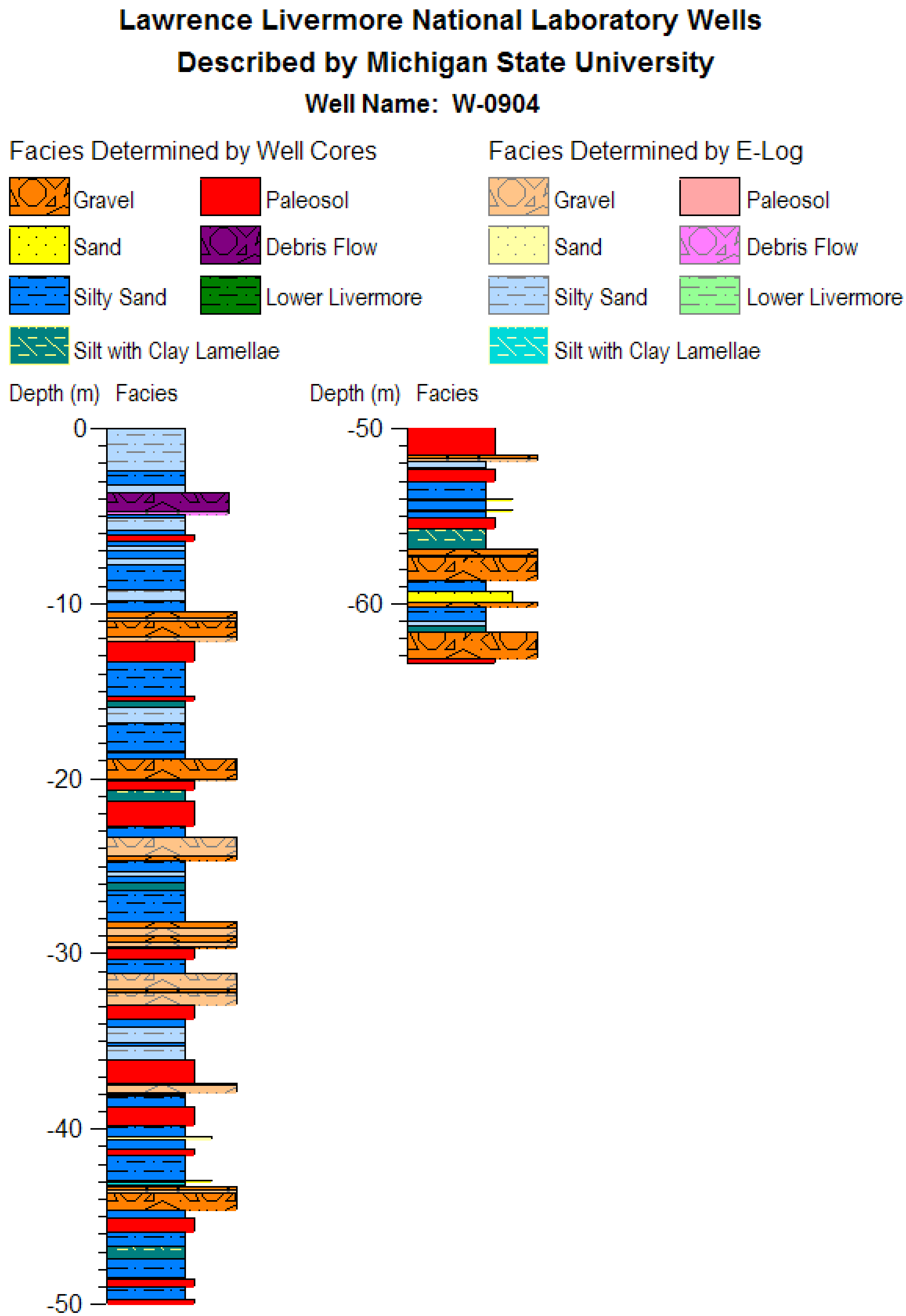

Figure 84. W-0904 stratigraphic column.

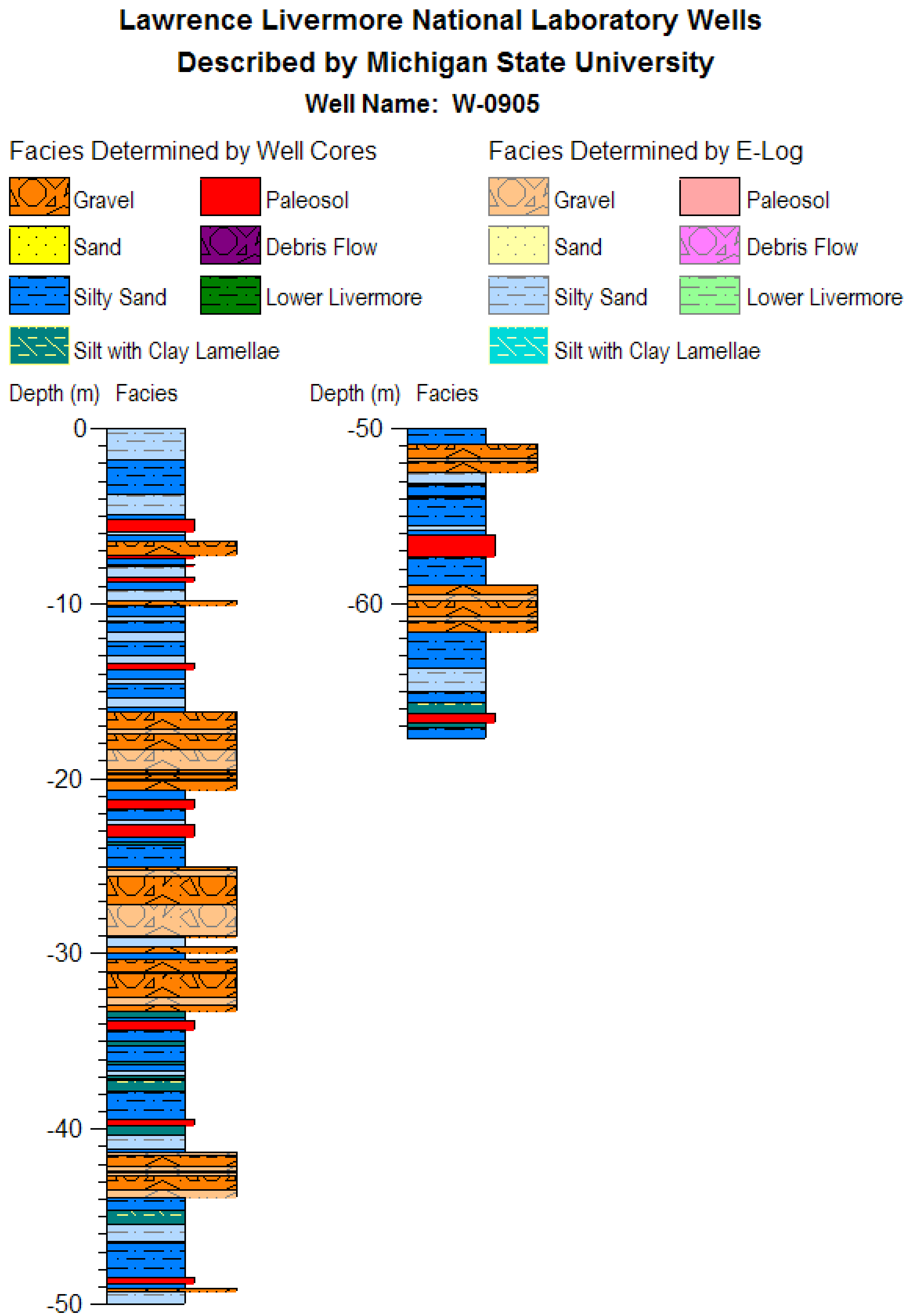

Figure 85. W-0905 stratigraphic column.

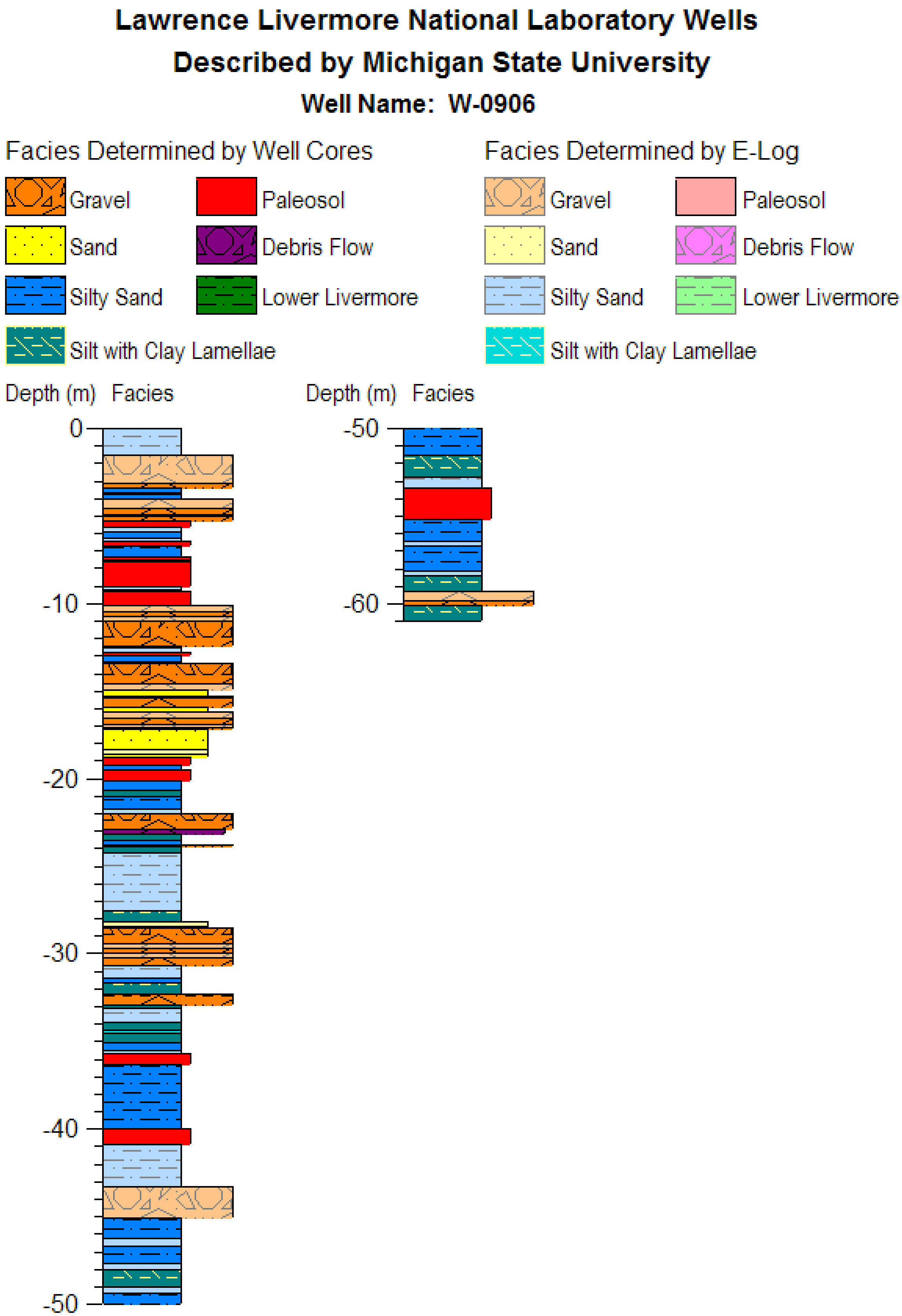

Figure 86. W-0906 stratigraphic column.

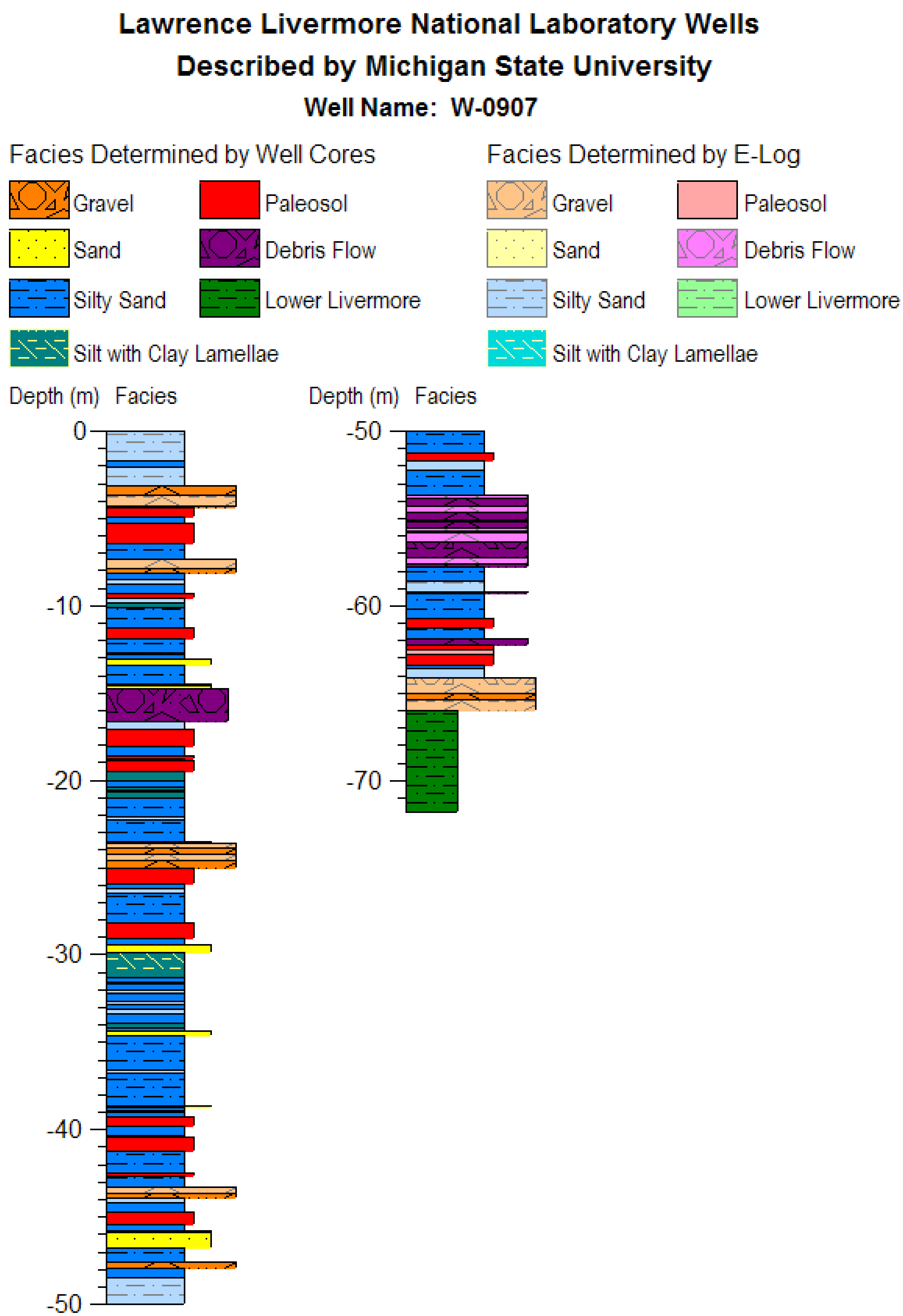

Figure 87. W-0907 stratigraphic column.

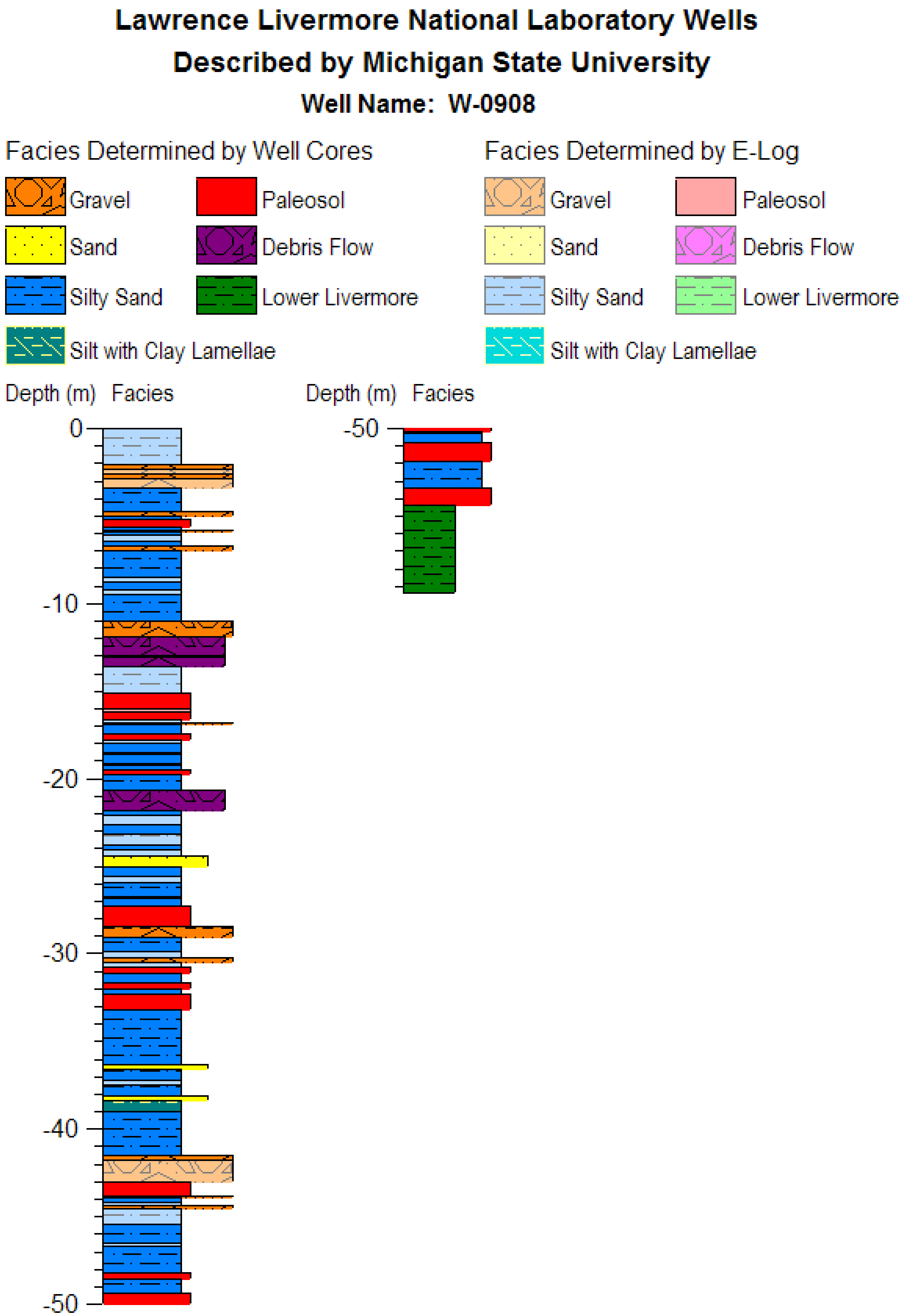

Figure 88. W-0908 stratigraphic column.

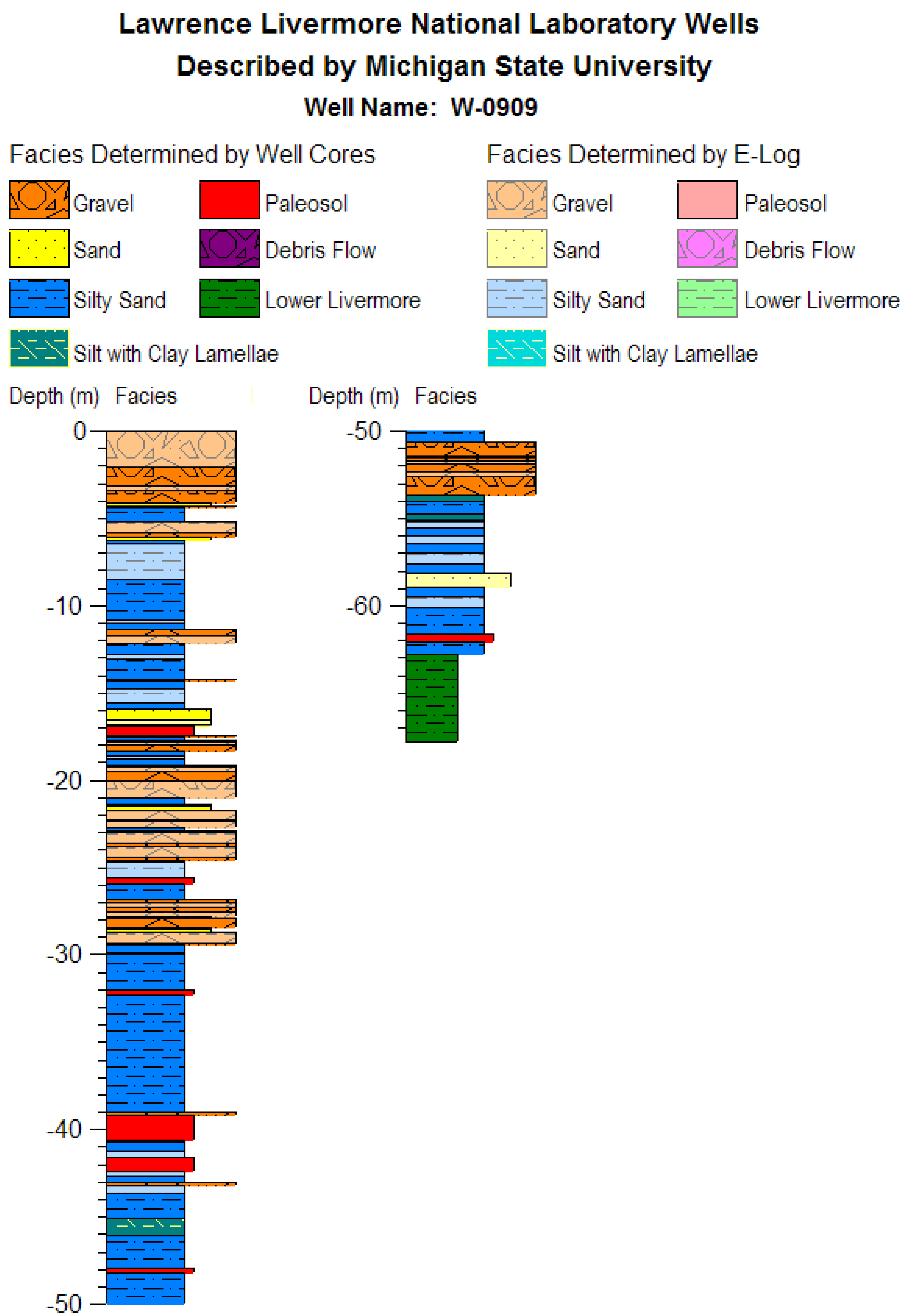

Figure 89. W-0909 stratigraphic column.

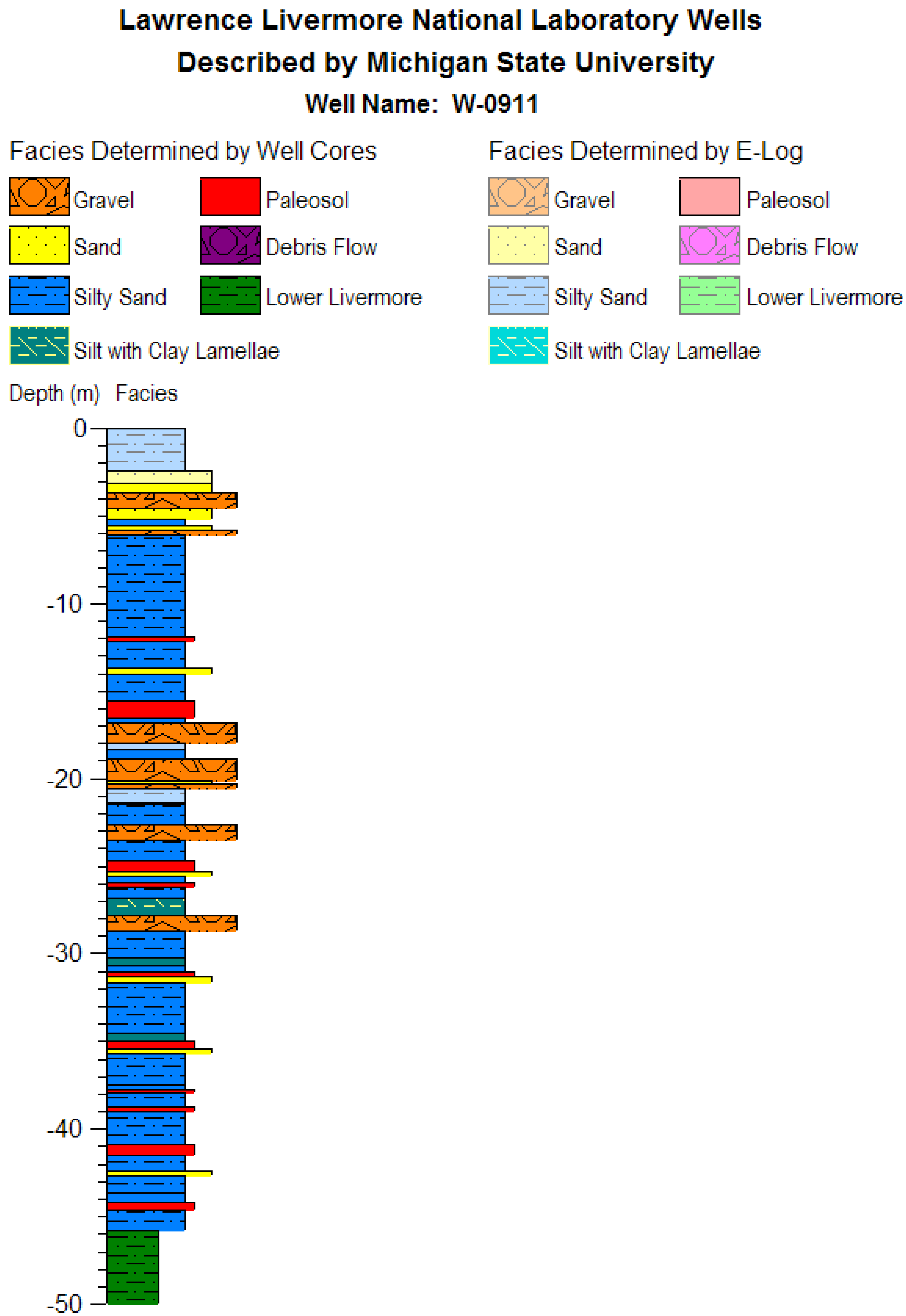

Figure 90. W-0911 stratigraphic column.

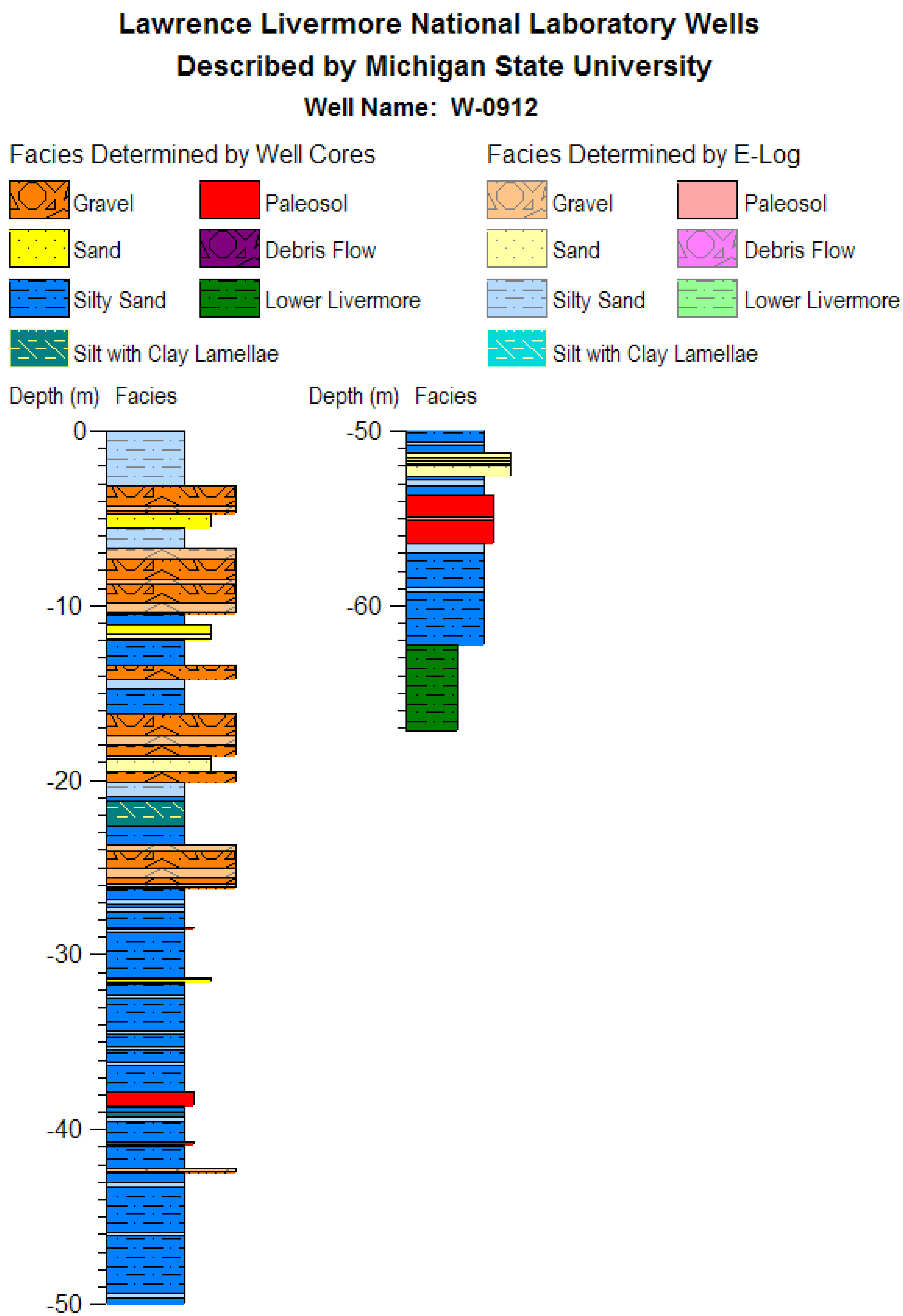

Figure 91. W-0912 stratigraphic column.

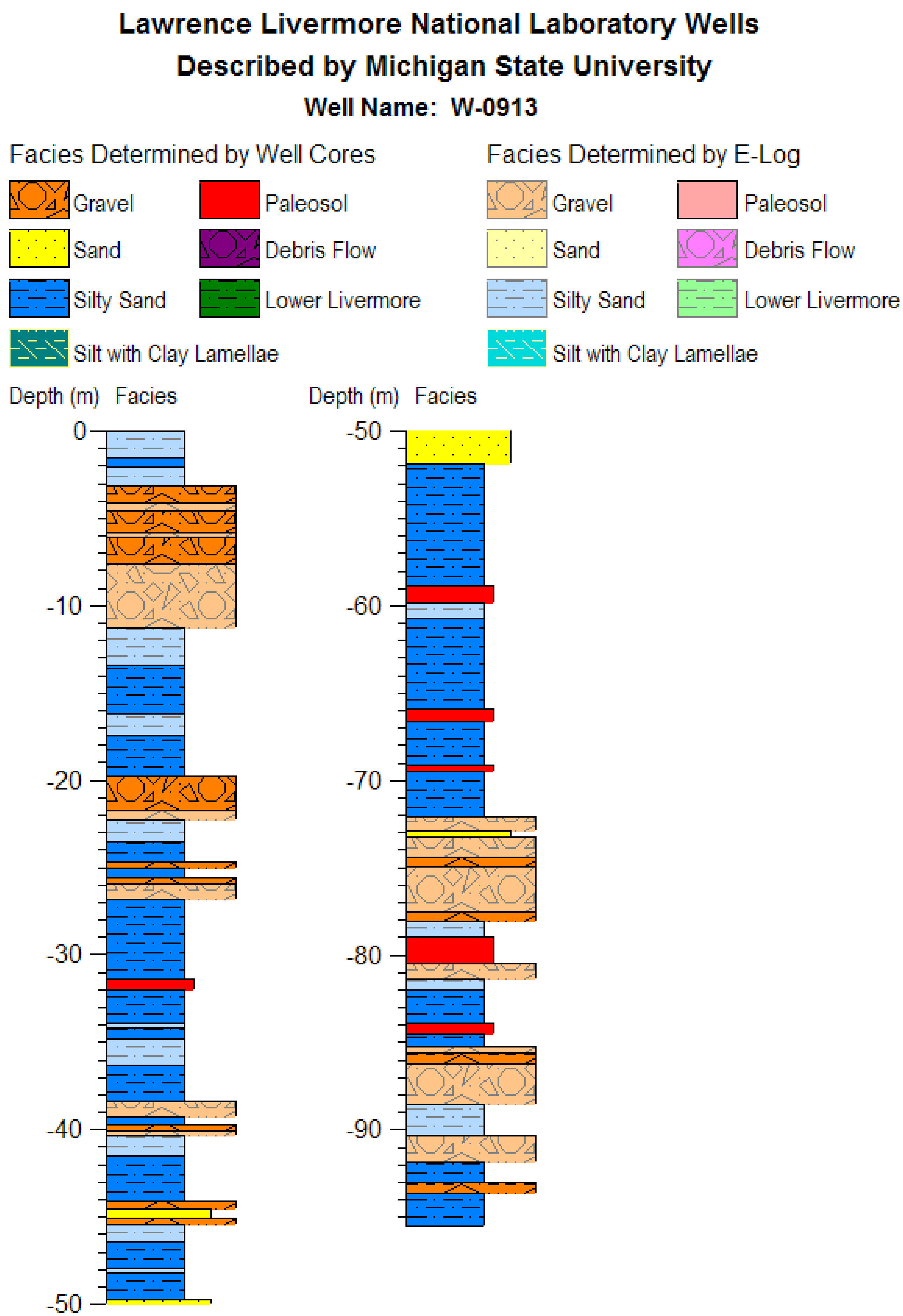

Figure 92. W-0913 stratigraphic column.

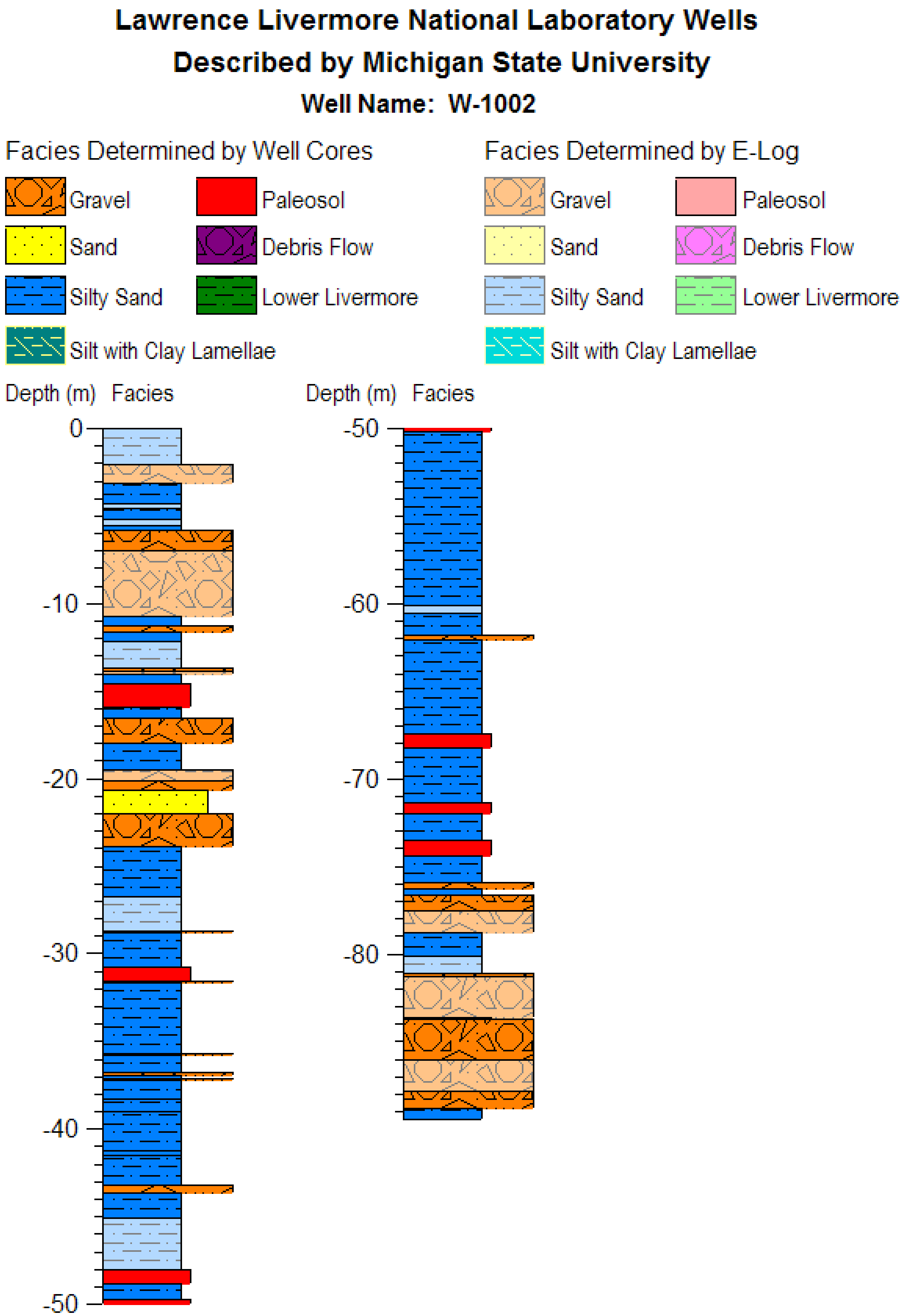

Figure 93. W-1002 stratigraphic column.

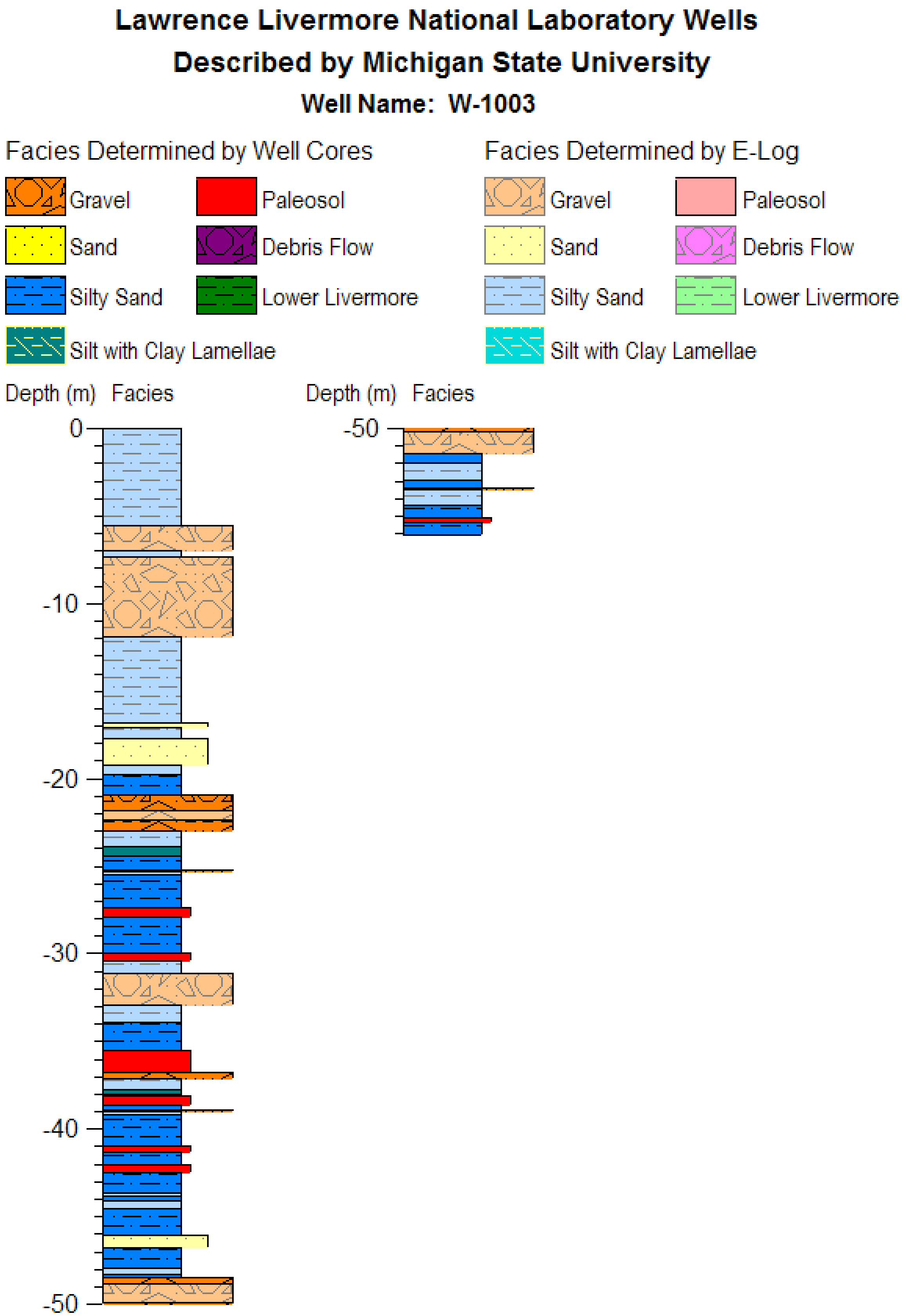

Figure 94. W-1003 stratigraphic column.

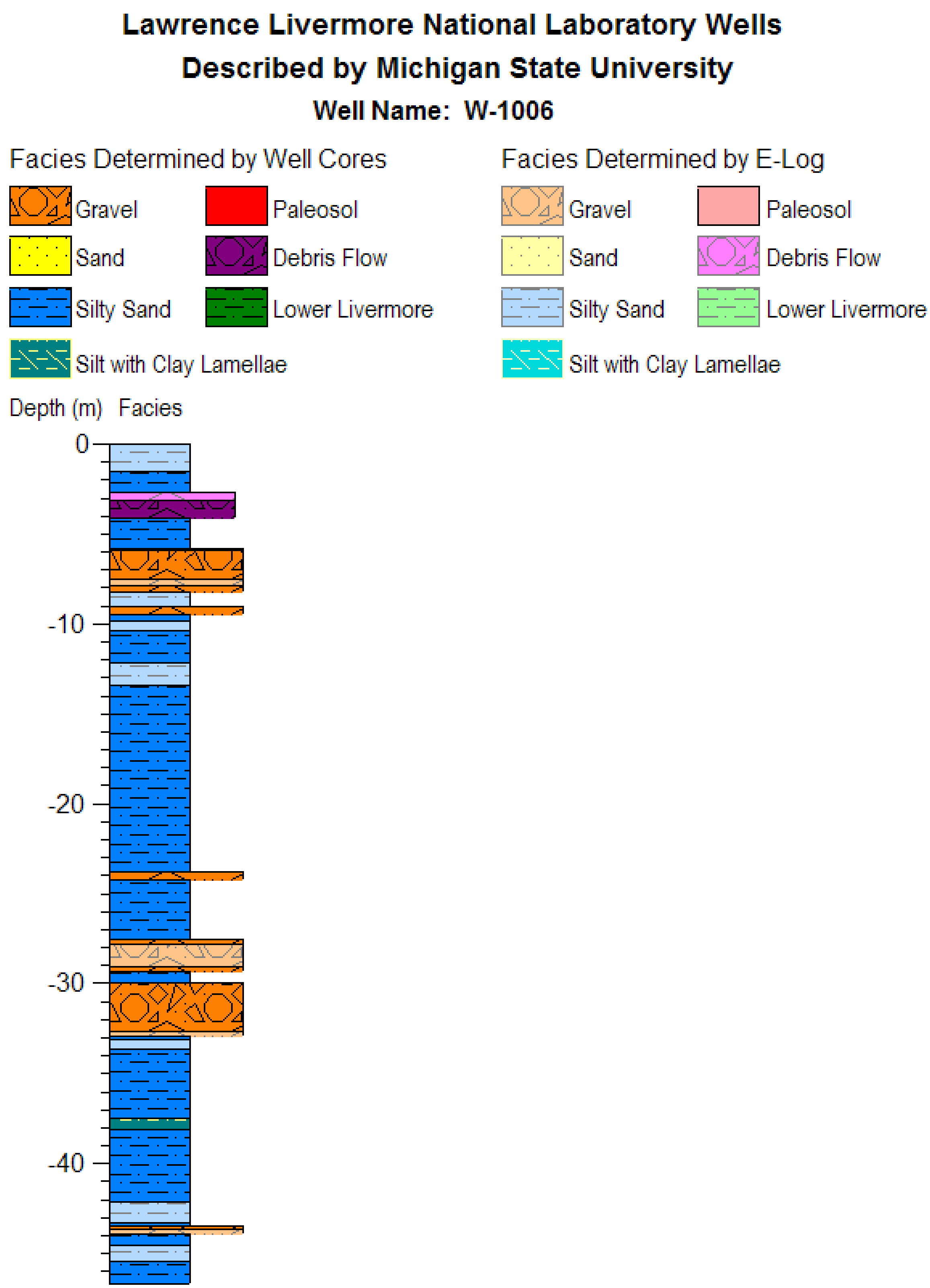

Figure 95. W-1006 stratigraphic column.

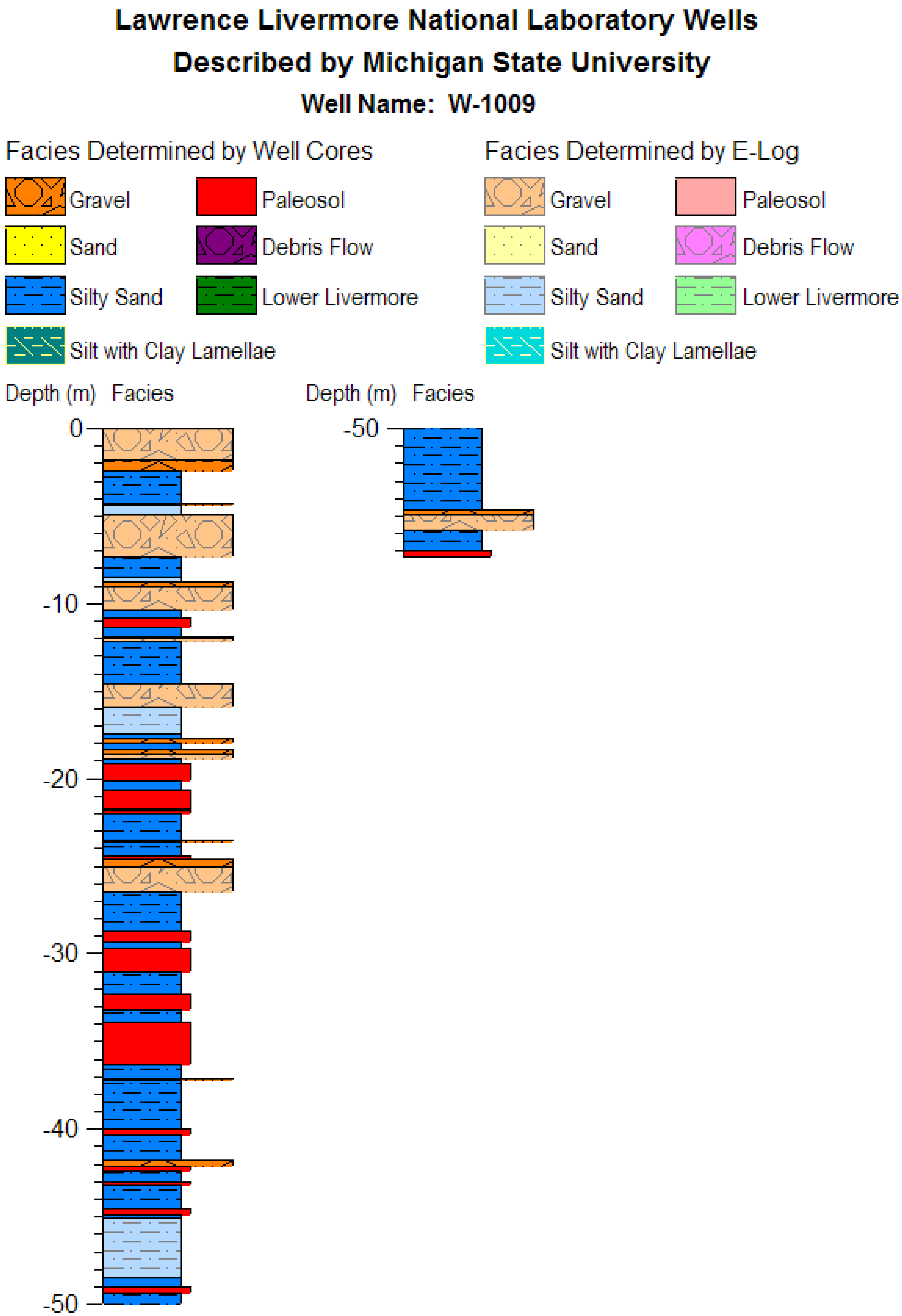

Figure 96. W-1009 stratigraphic column.

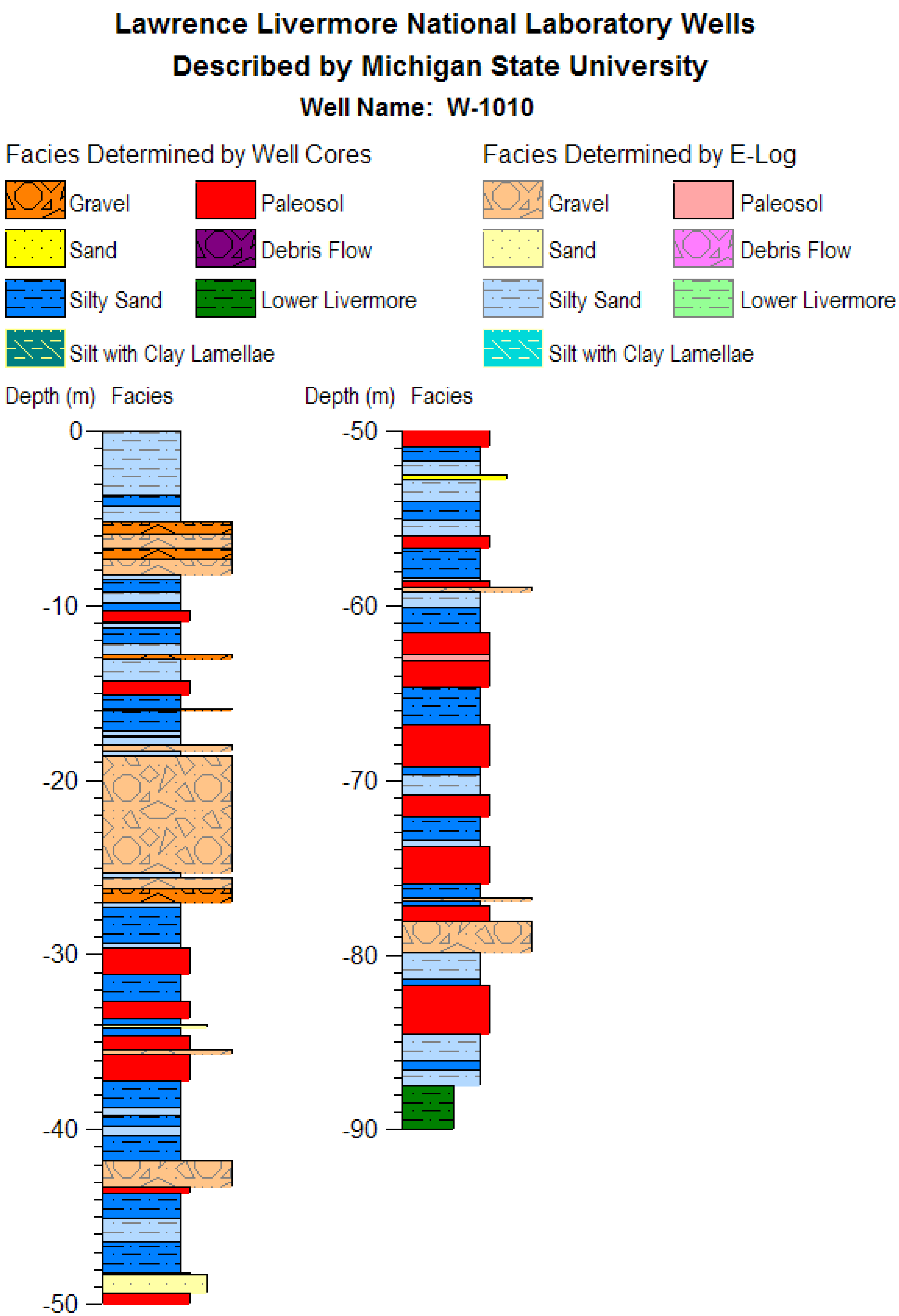

Figure 97. W-1010 stratigraphic column.

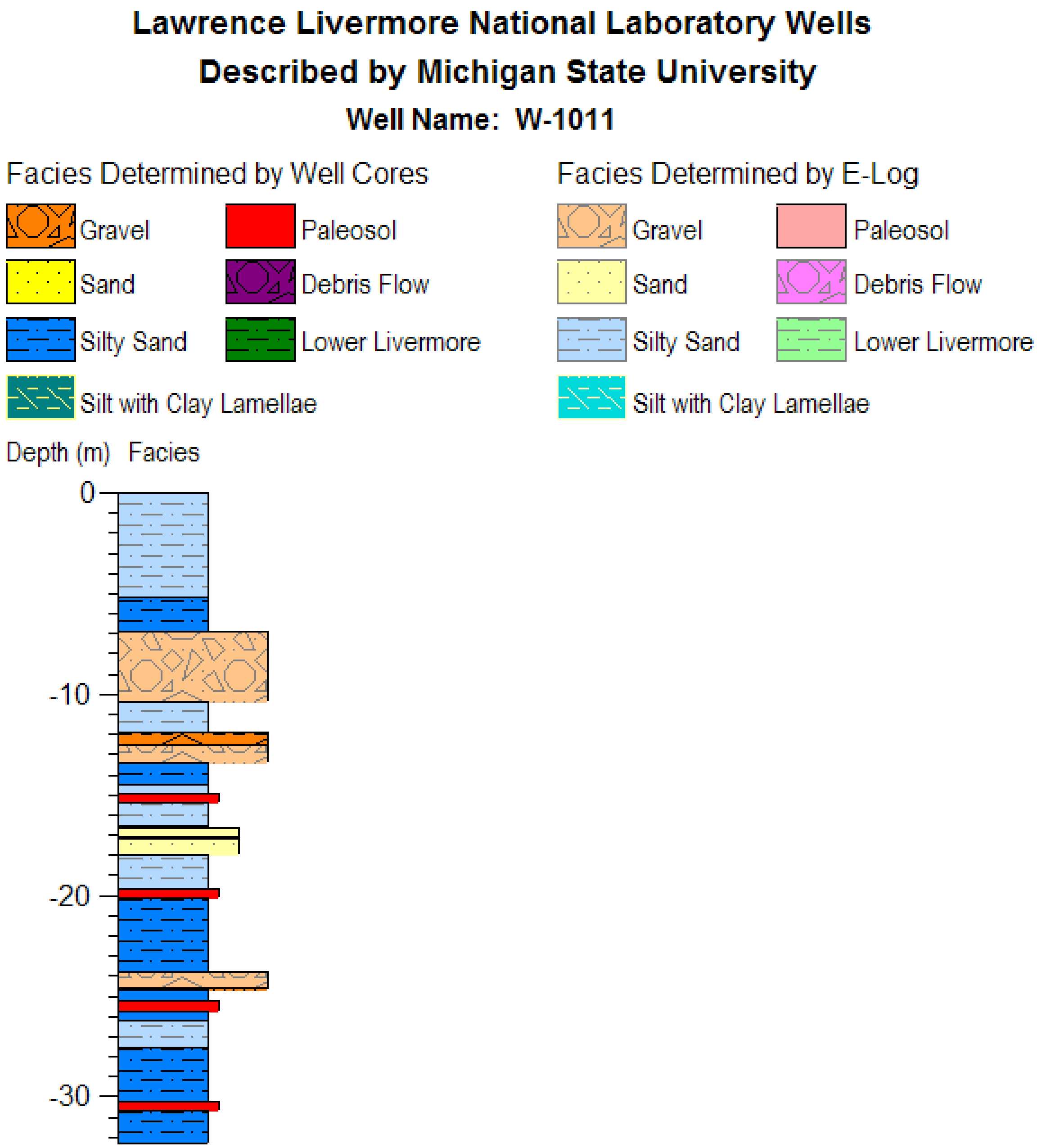

Figure 98. W-1011 stratigraphic column.

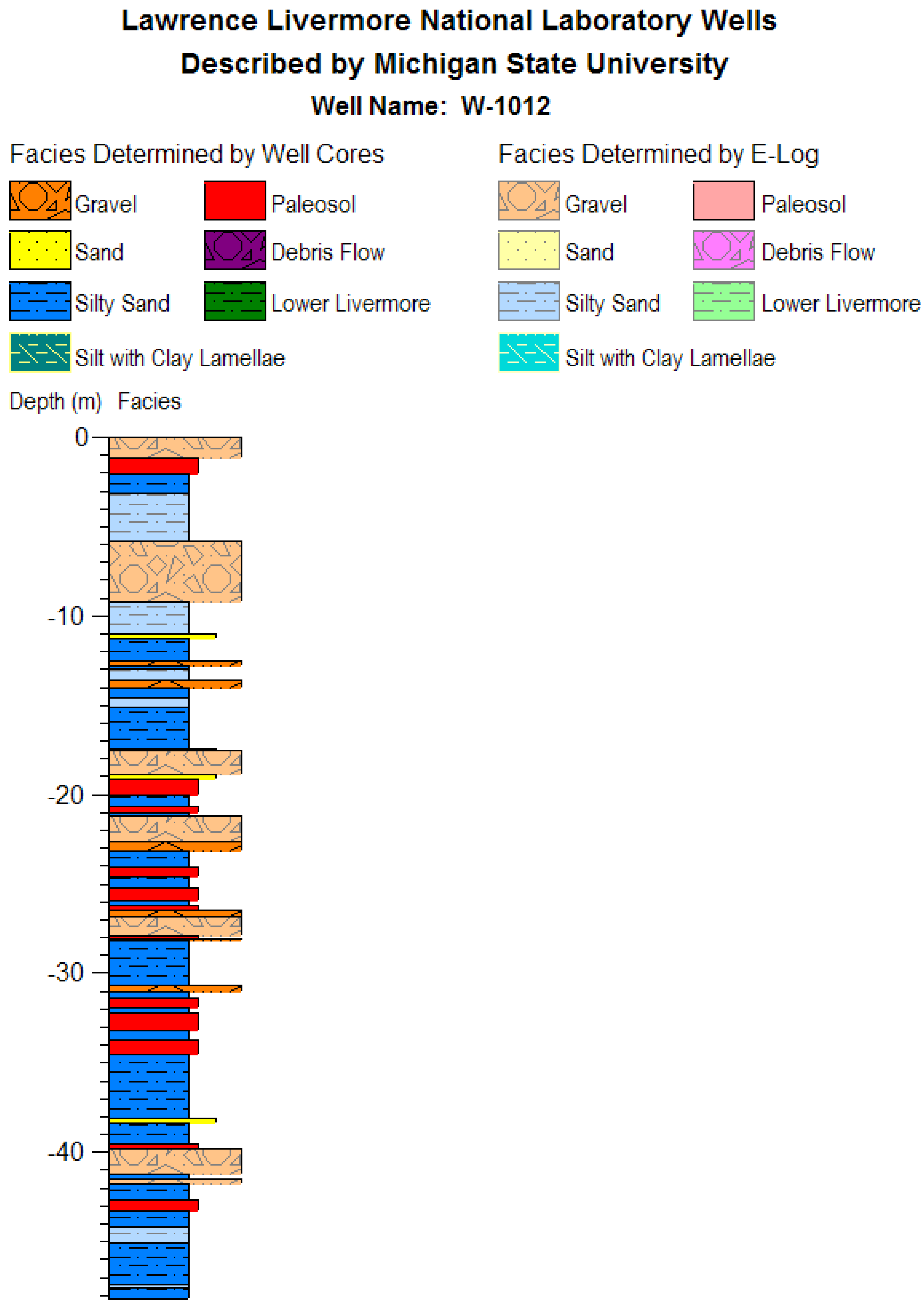

Figure 99. W-1012 stratigraphic column.

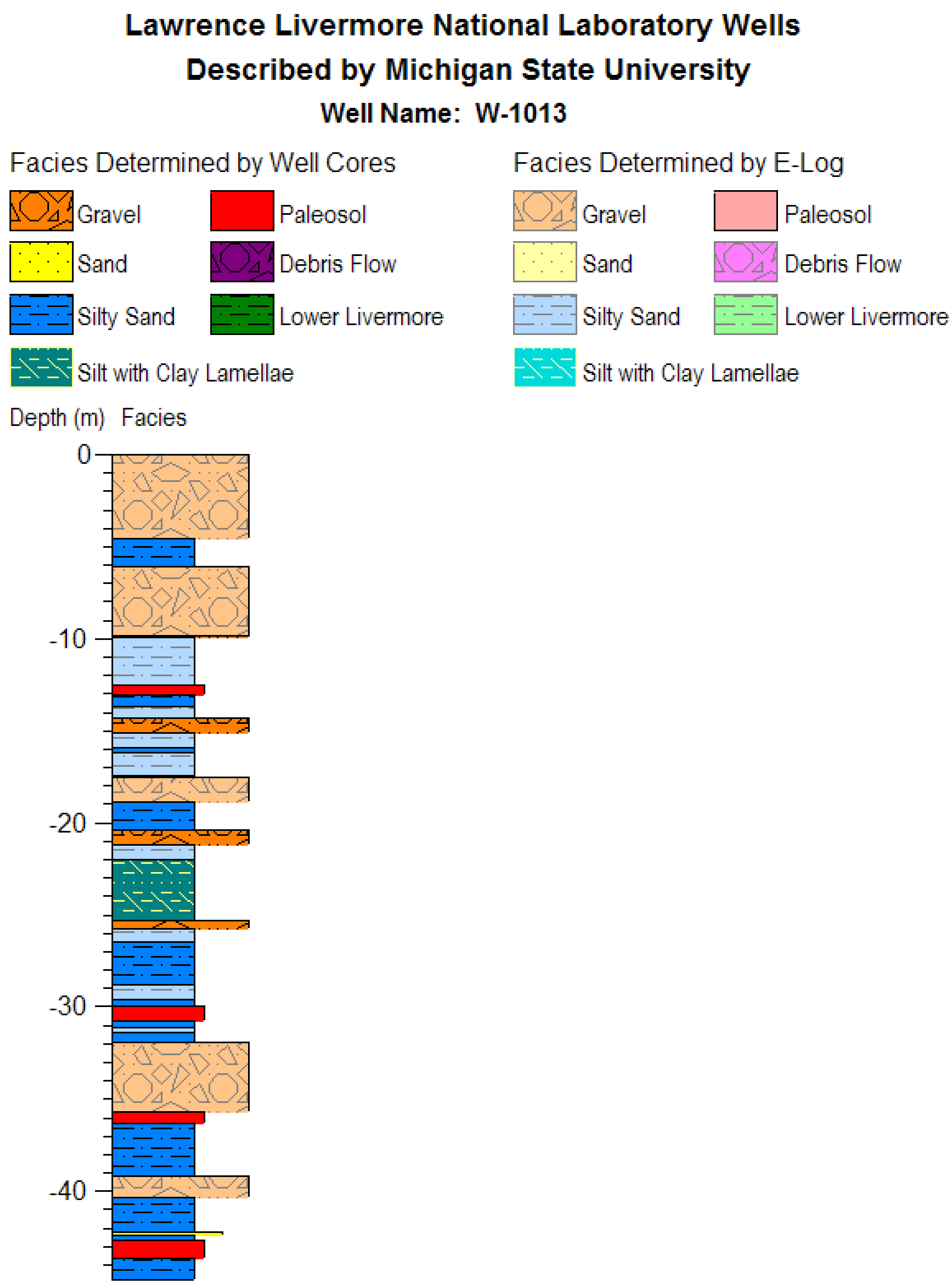

Figure 100. W-1013 stratigraphic column.

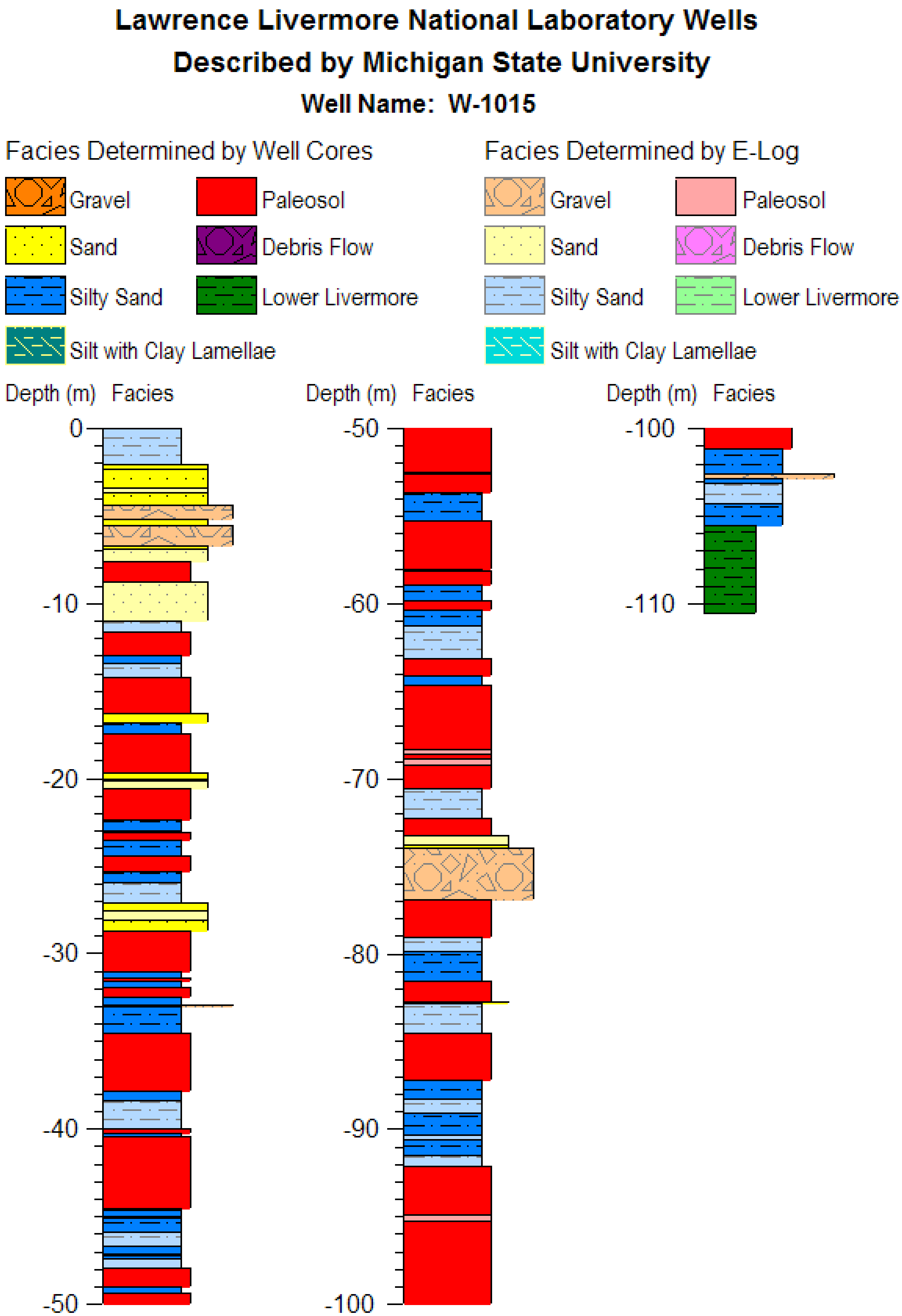

Figure 101. W-1015 stratigraphic column.

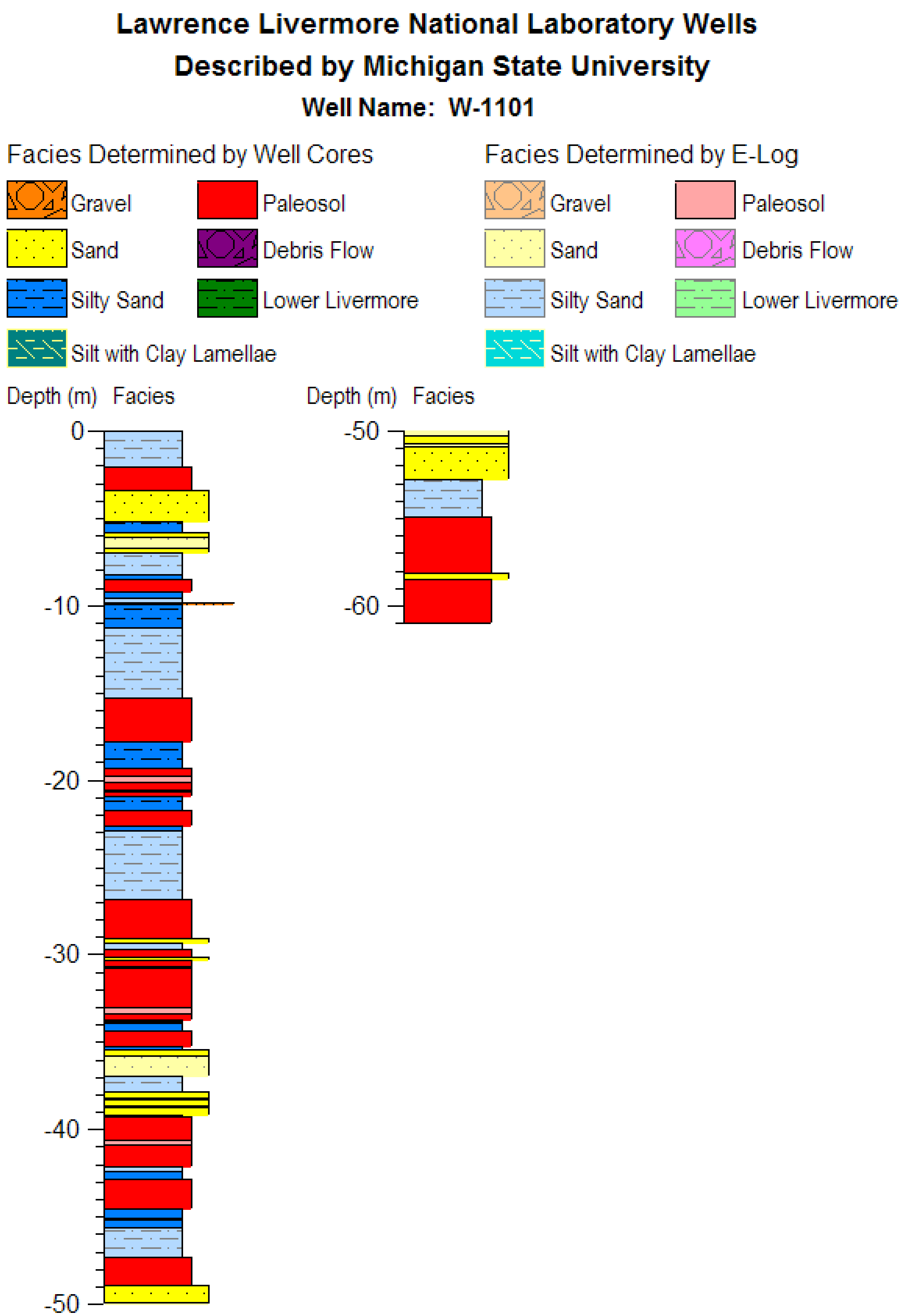

Figure 102. W-1101 stratigraphic column.

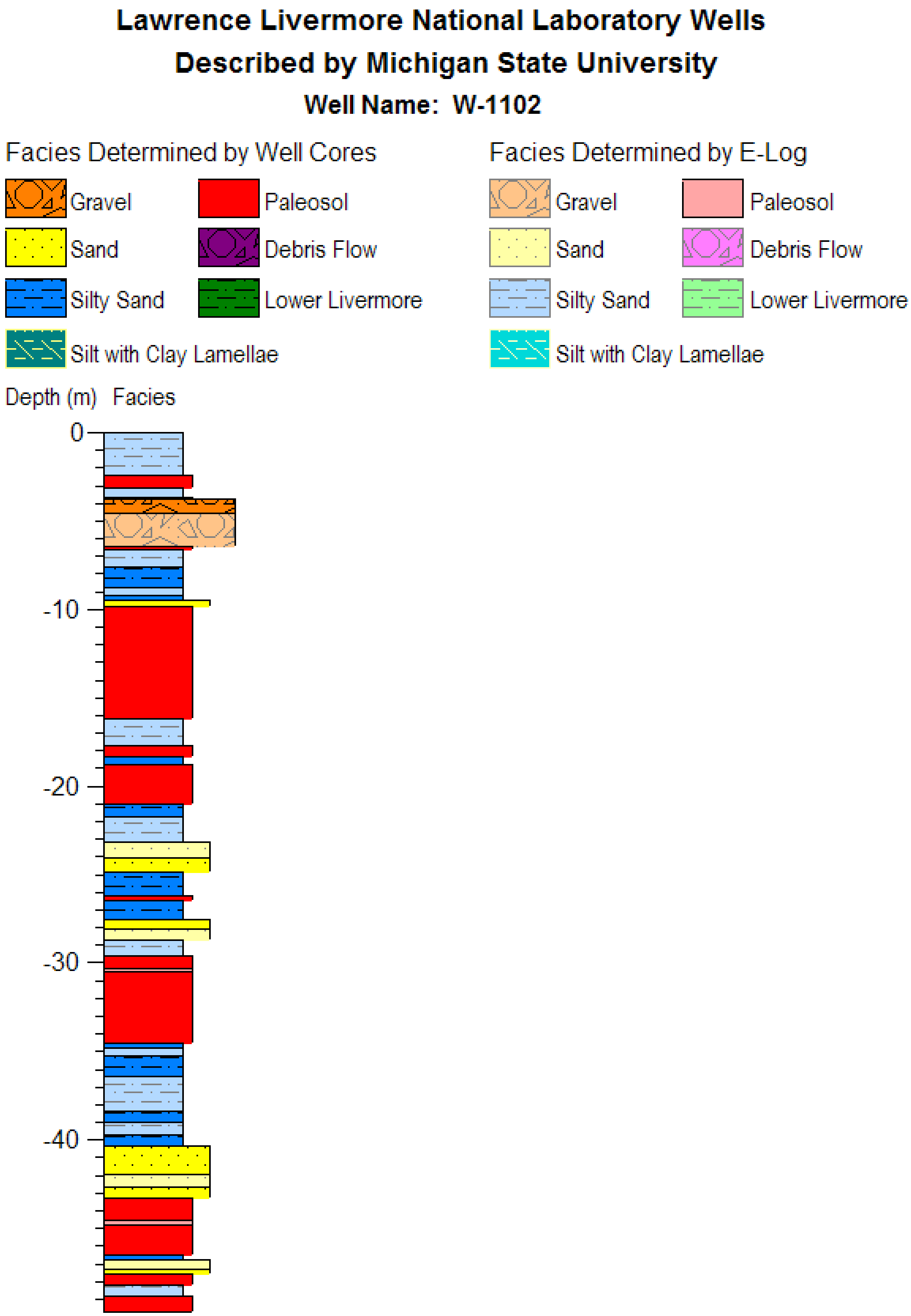

Figure 103. W-1102 stratigraphic column.

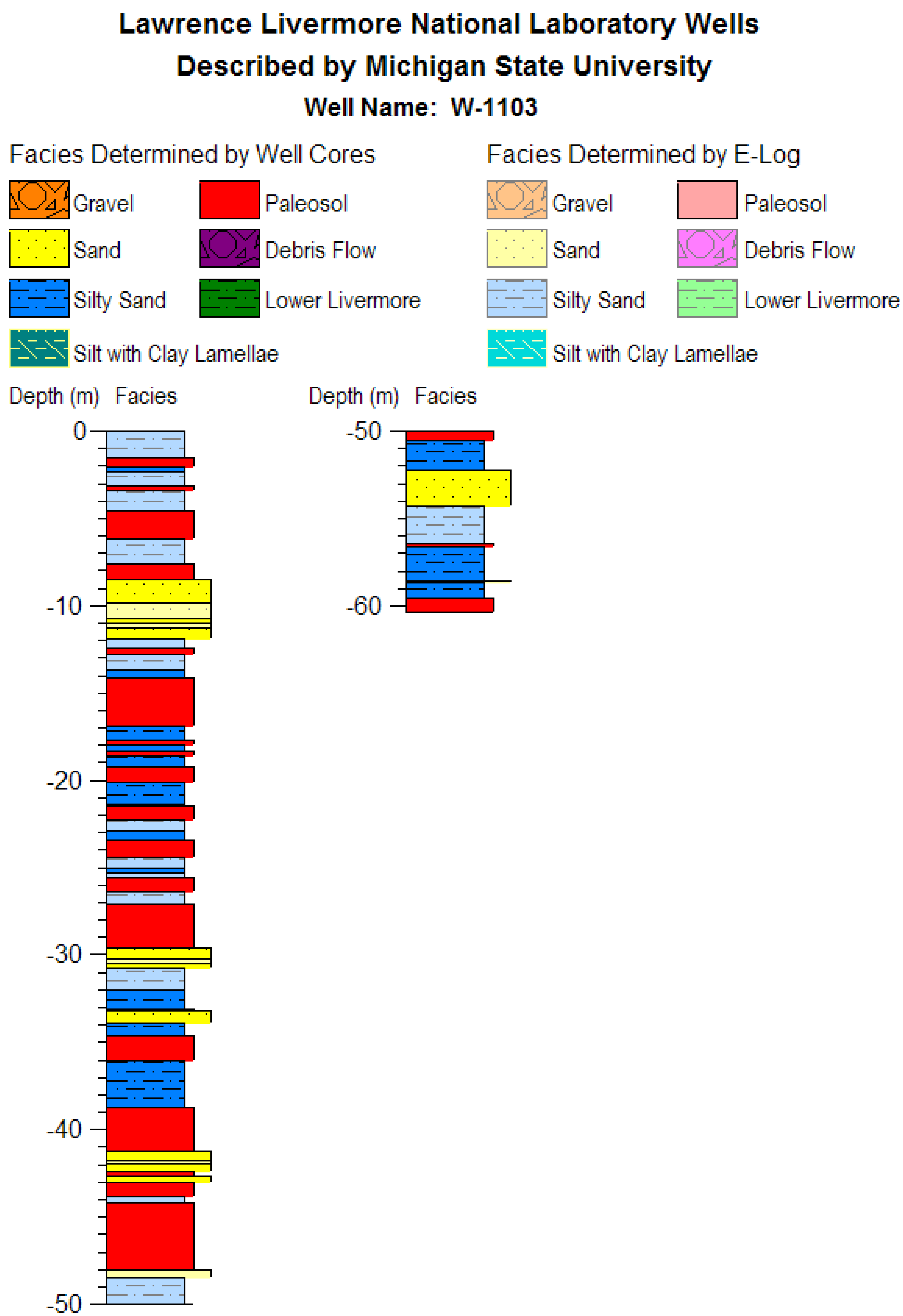

Figure 104. W-1103 stratigraphic column.

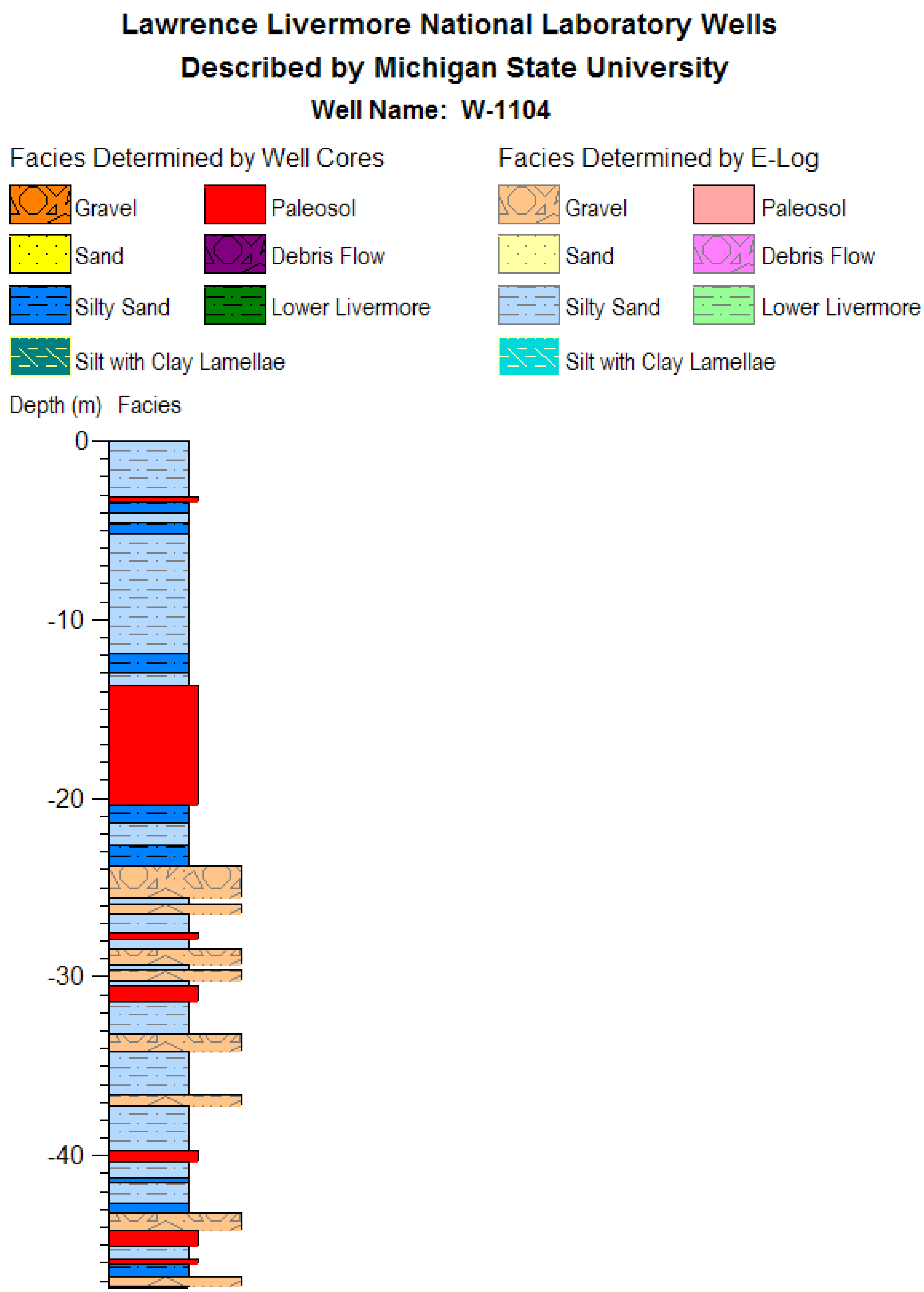

Figure 105. W-1104 stratigraphic column.

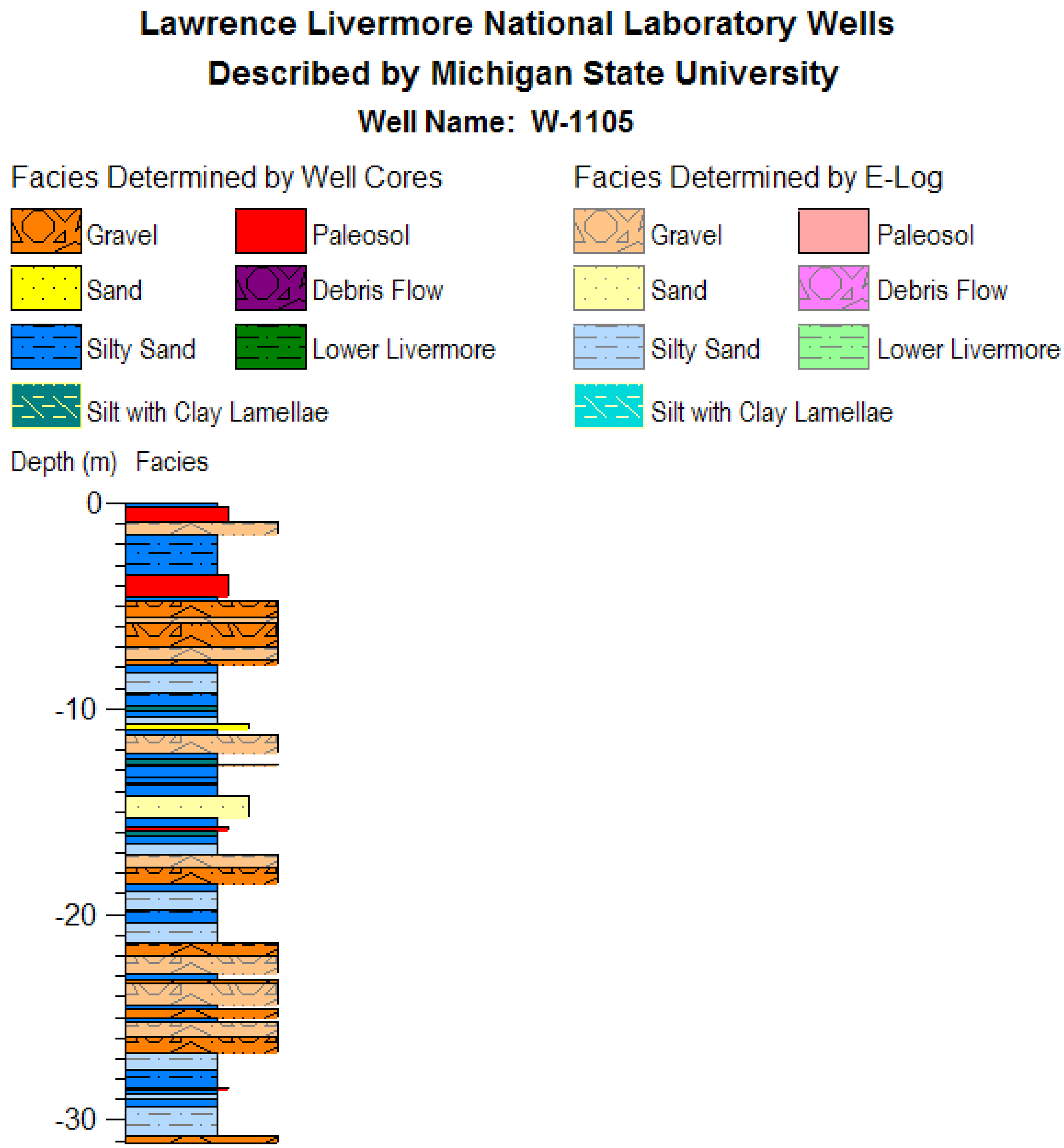

Figure 106. W-1105 stratigraphic column.

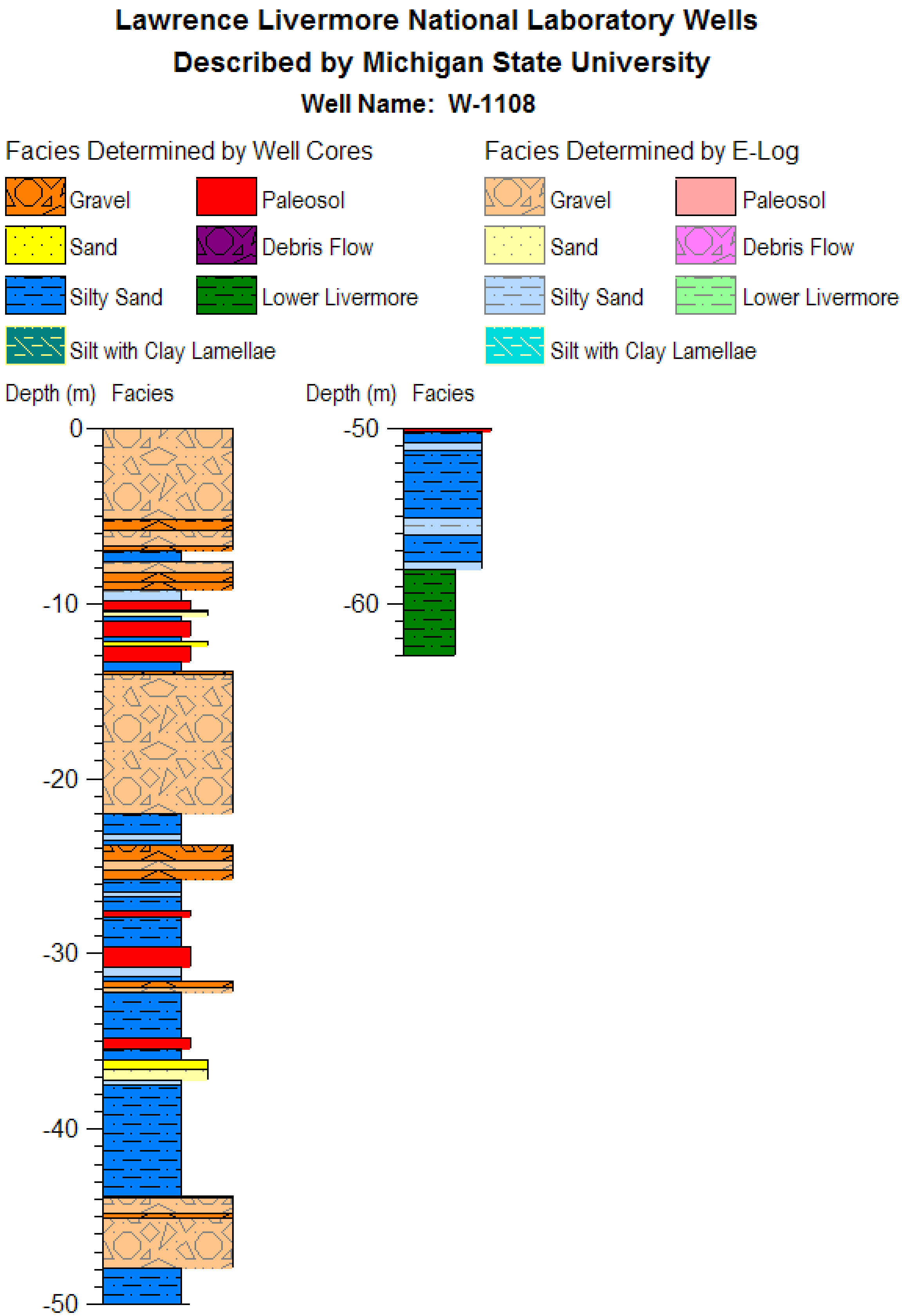

Figure 107. W-1108 stratigraphic column.

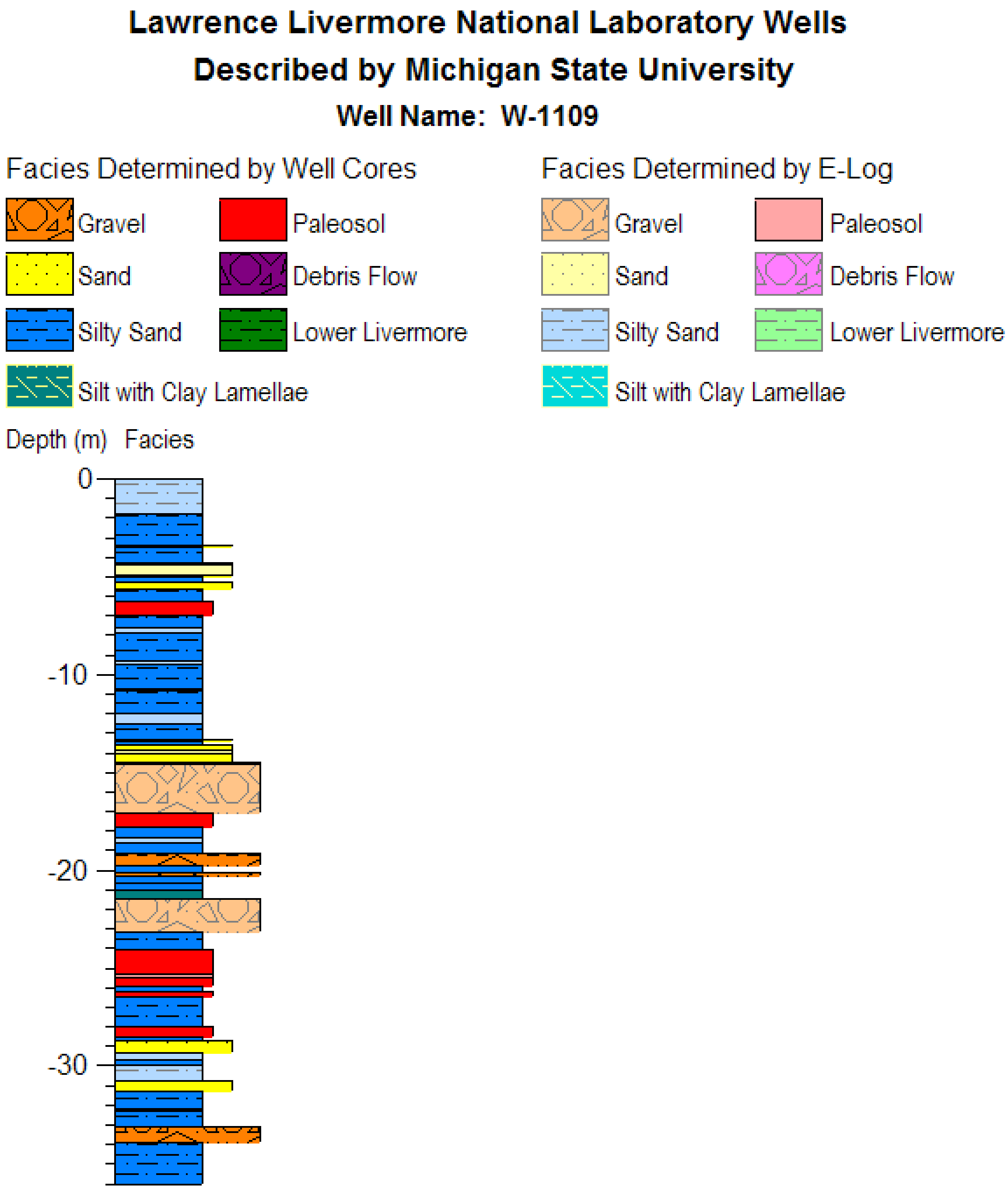

Figure 108. W-1109 stratigraphic column.

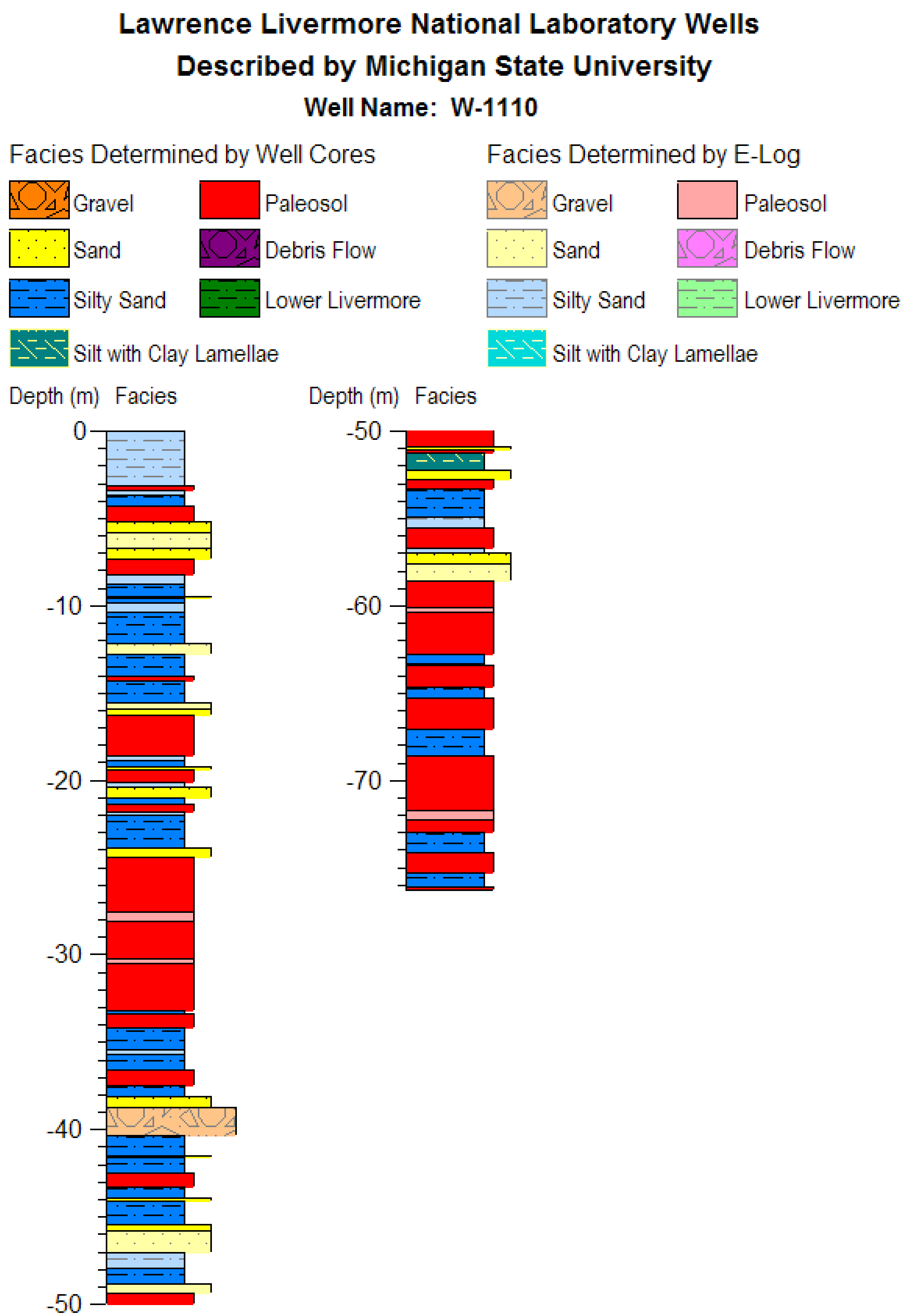

Figure 109. W-1110 stratigraphic column.

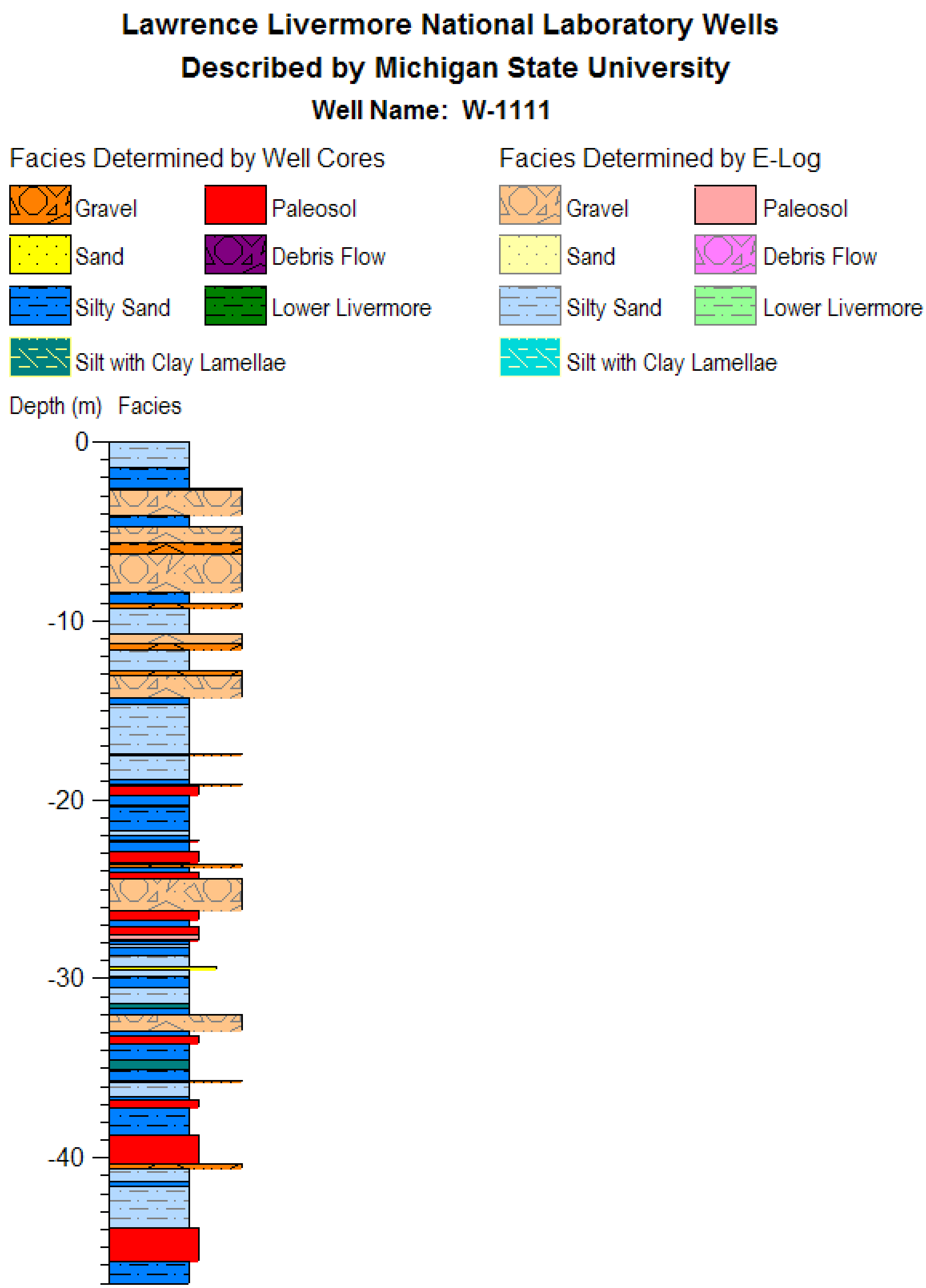

Figure 110. W-1111 stratigraphic column.

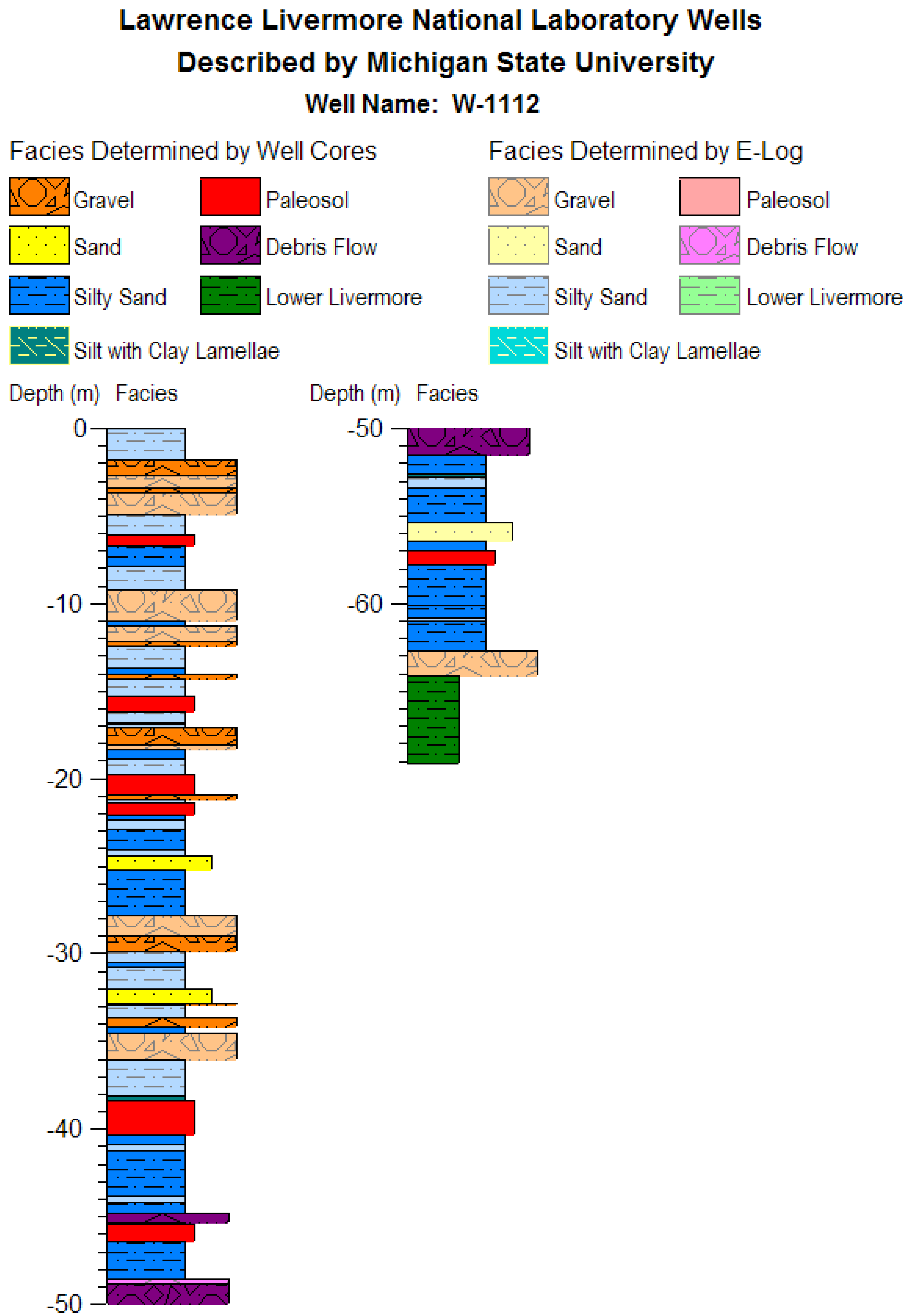

Figure 111. W-1112 stratigraphic column.

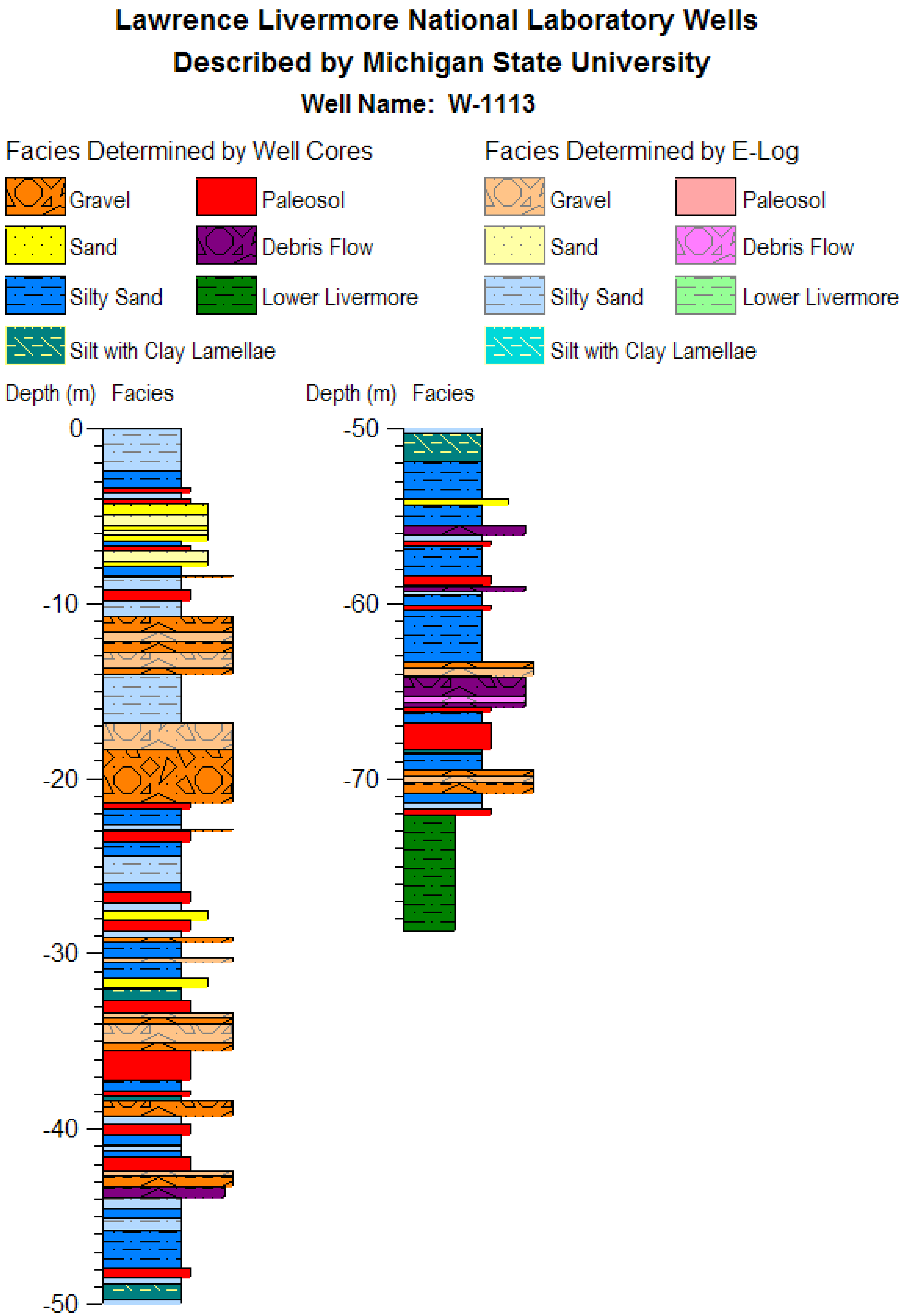

Figure 112. W-1113 stratigraphic column.

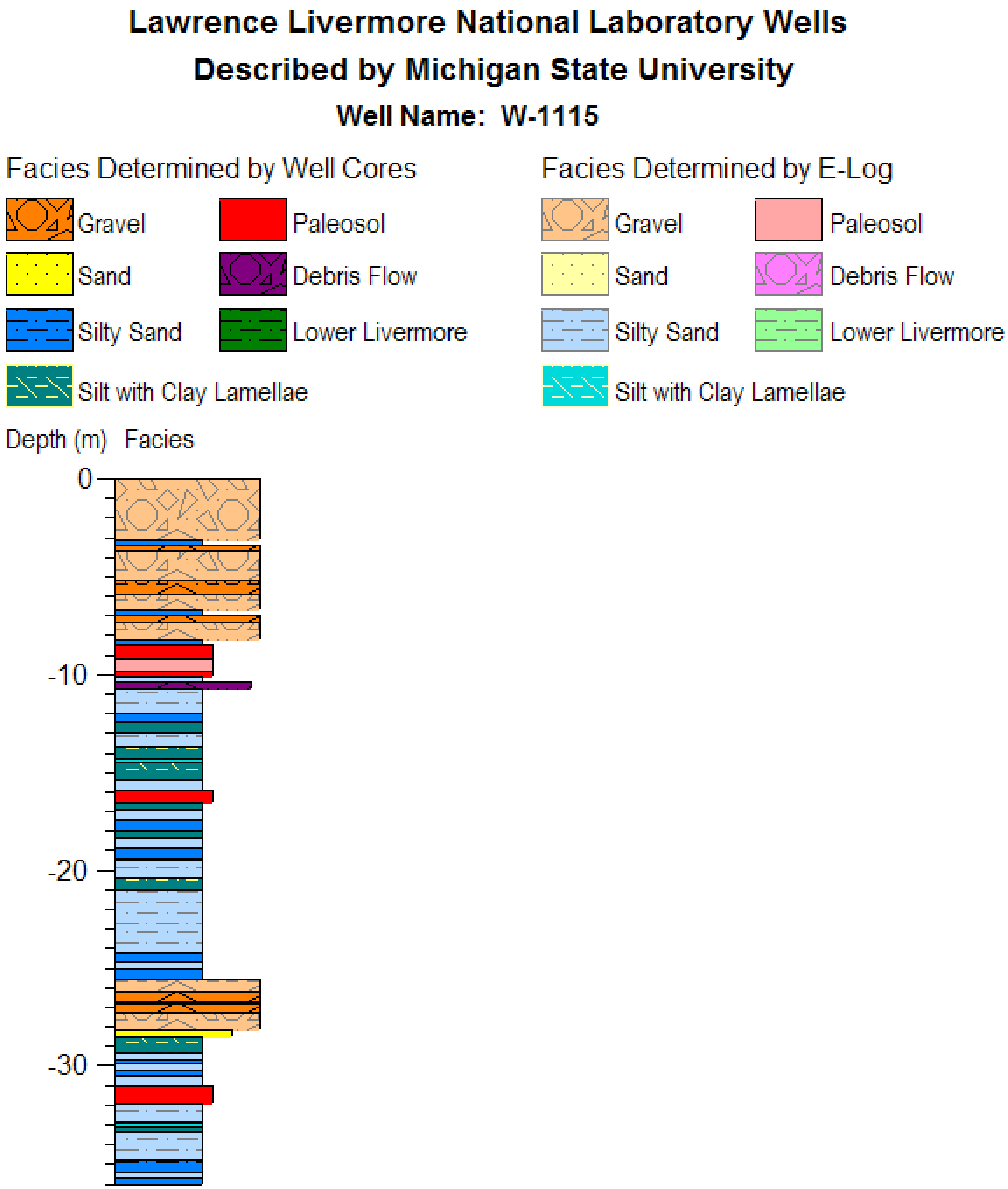

Figure 113. W-1115 stratigraphic column.

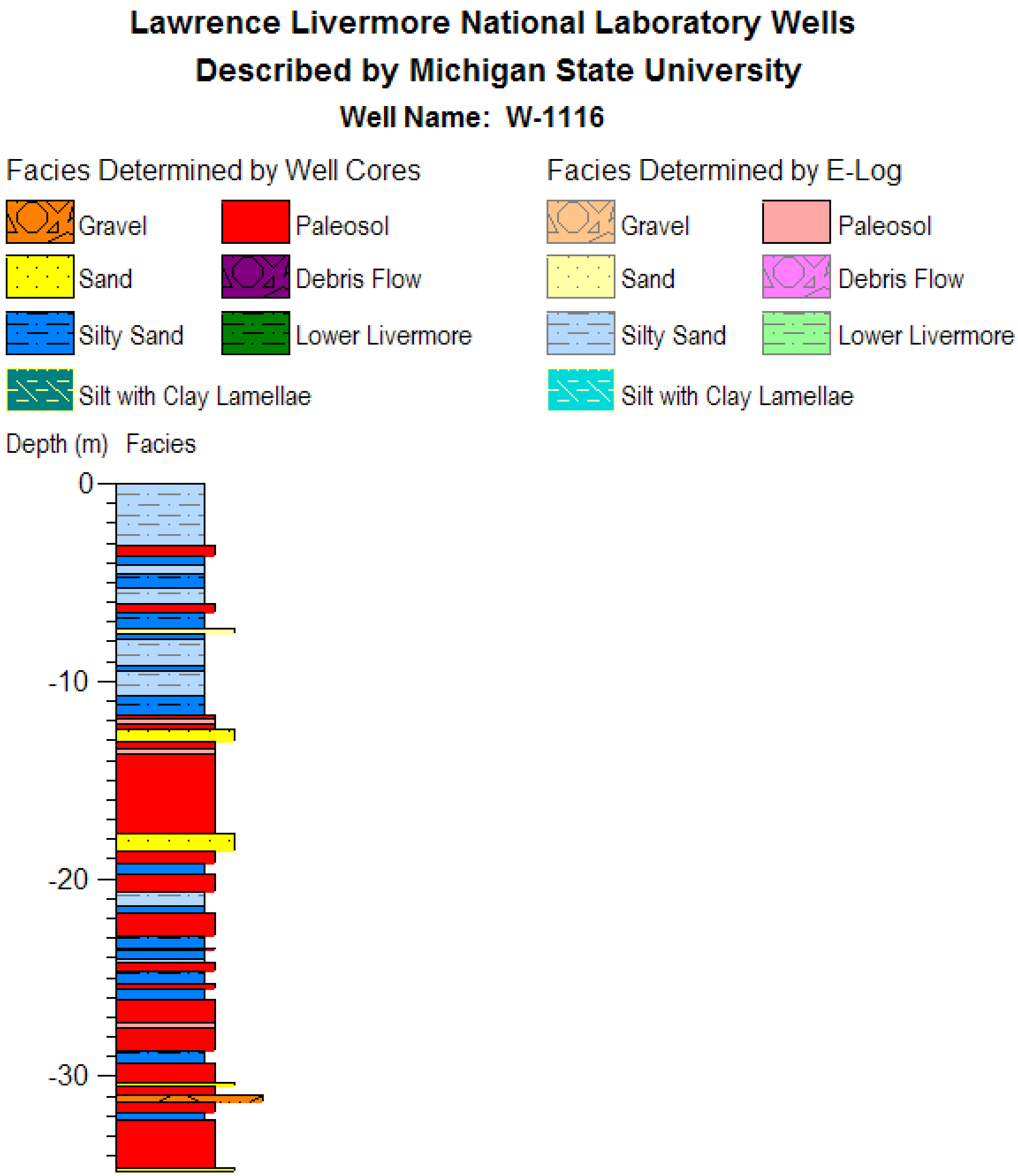

Figure 114. W-1116 stratigraphic column.

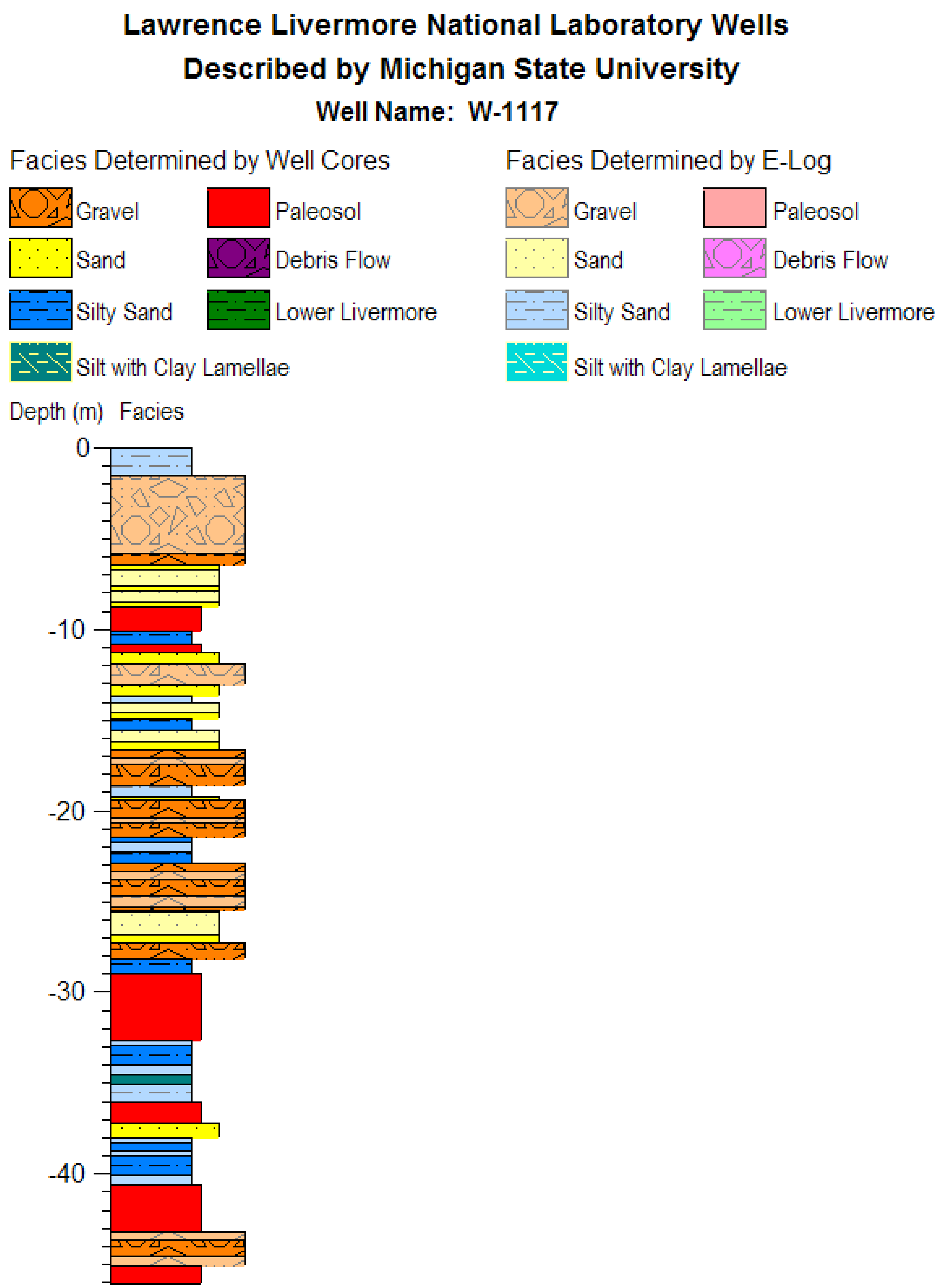

Figure 115. W-1117 stratigraphic column.

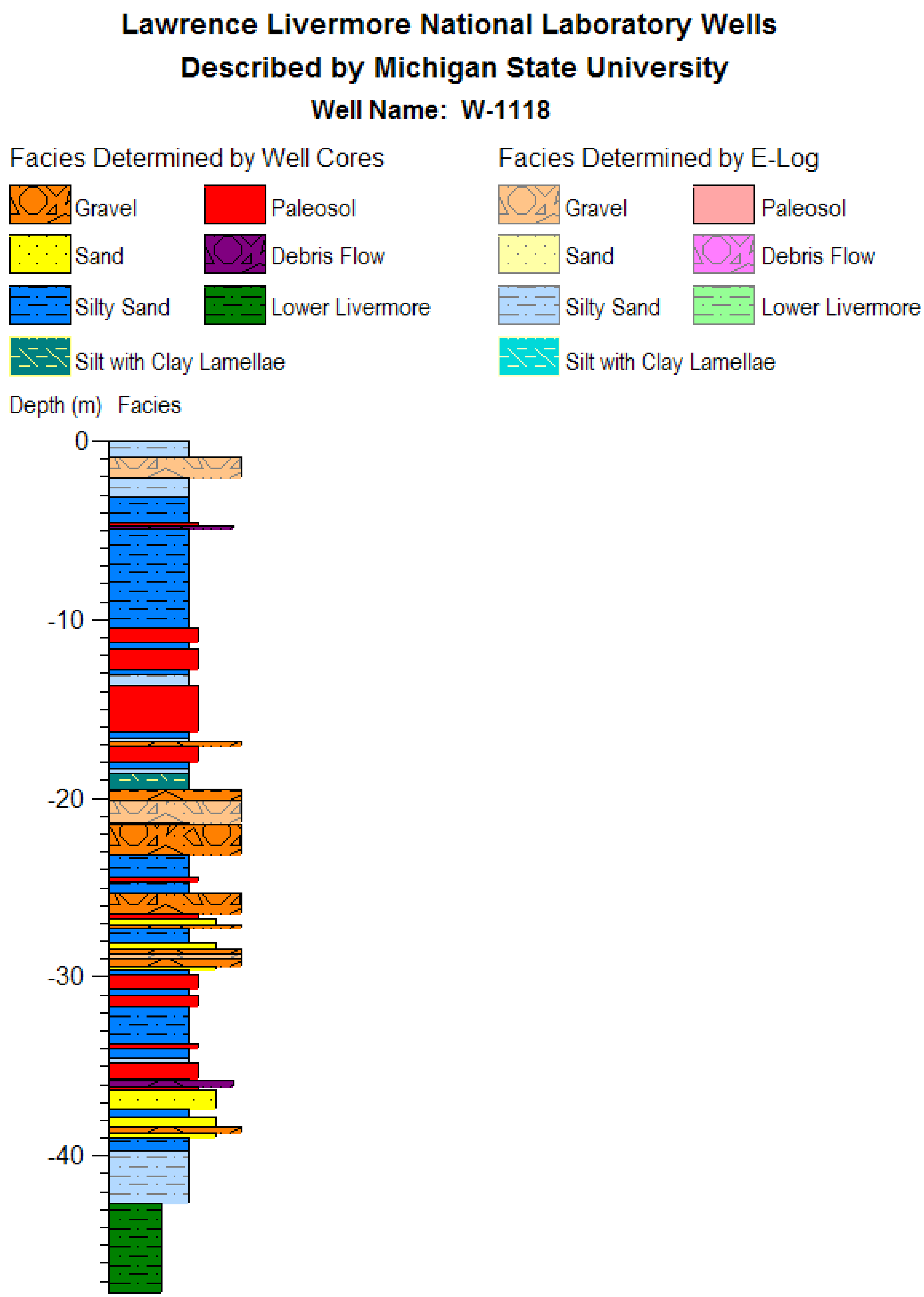

Figure 116. W-1118 stratigraphic column.

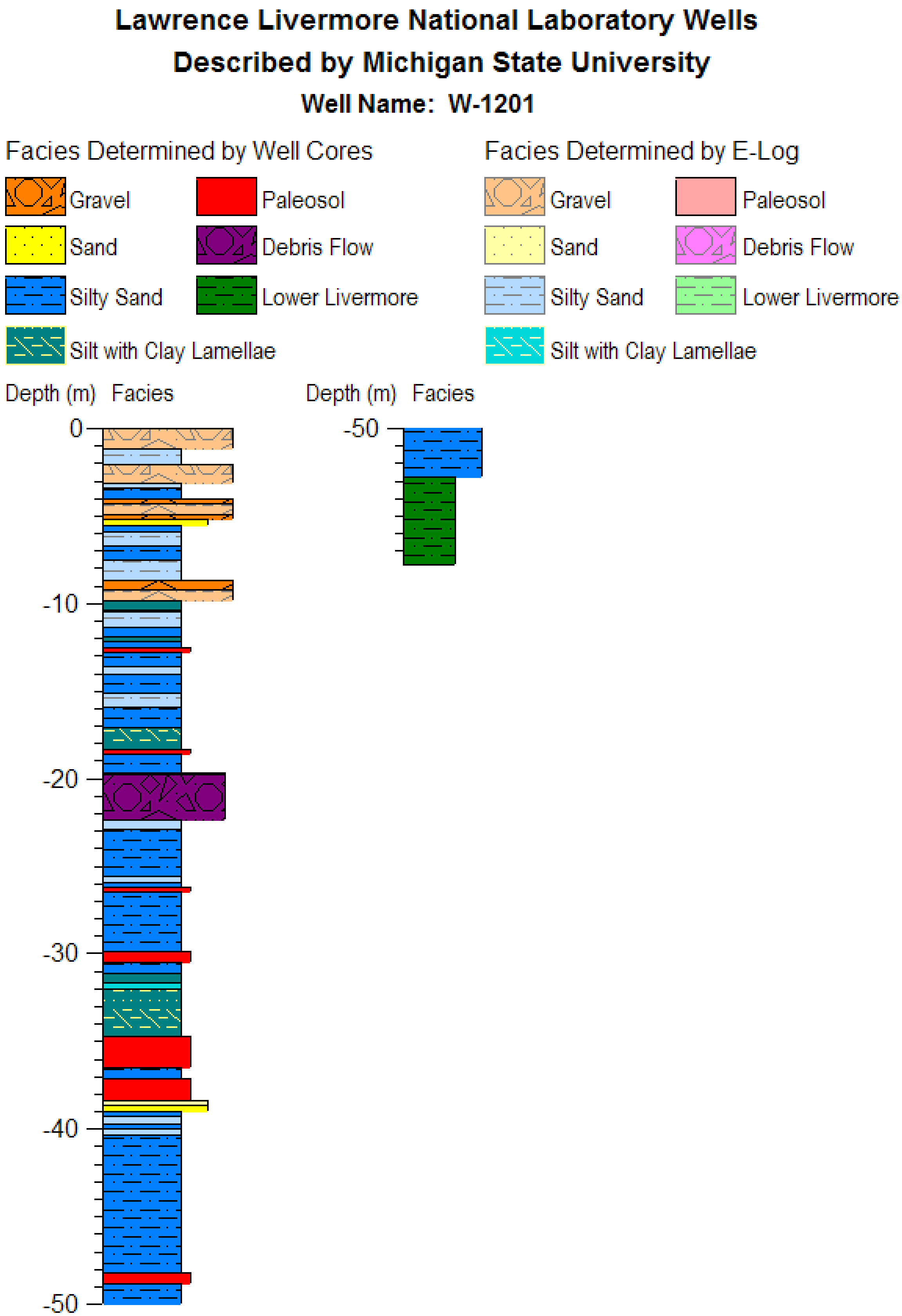

Figure 117. W-1201 stratigraphic column.

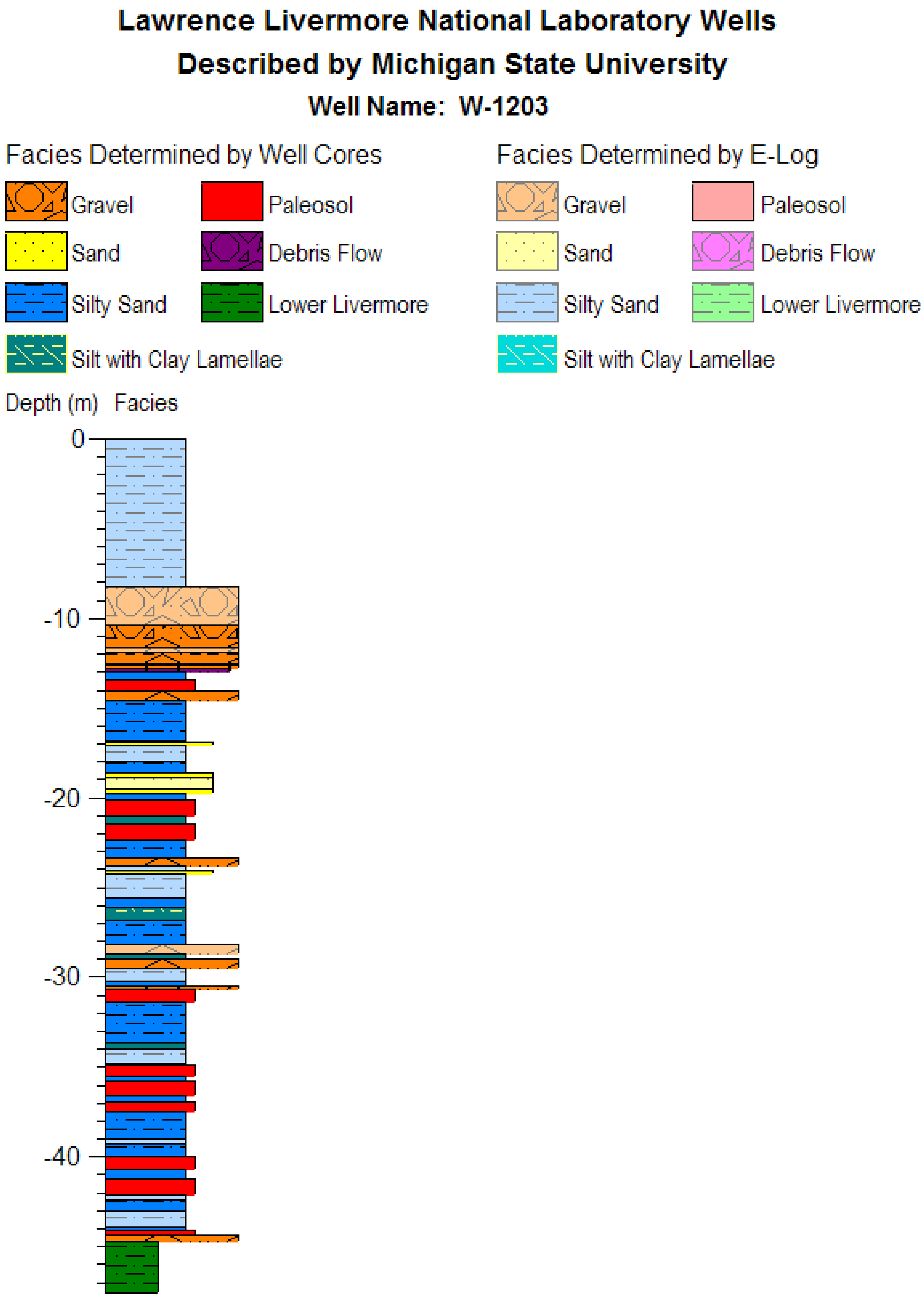

Figure 118. W-1203 stratigraphic column.

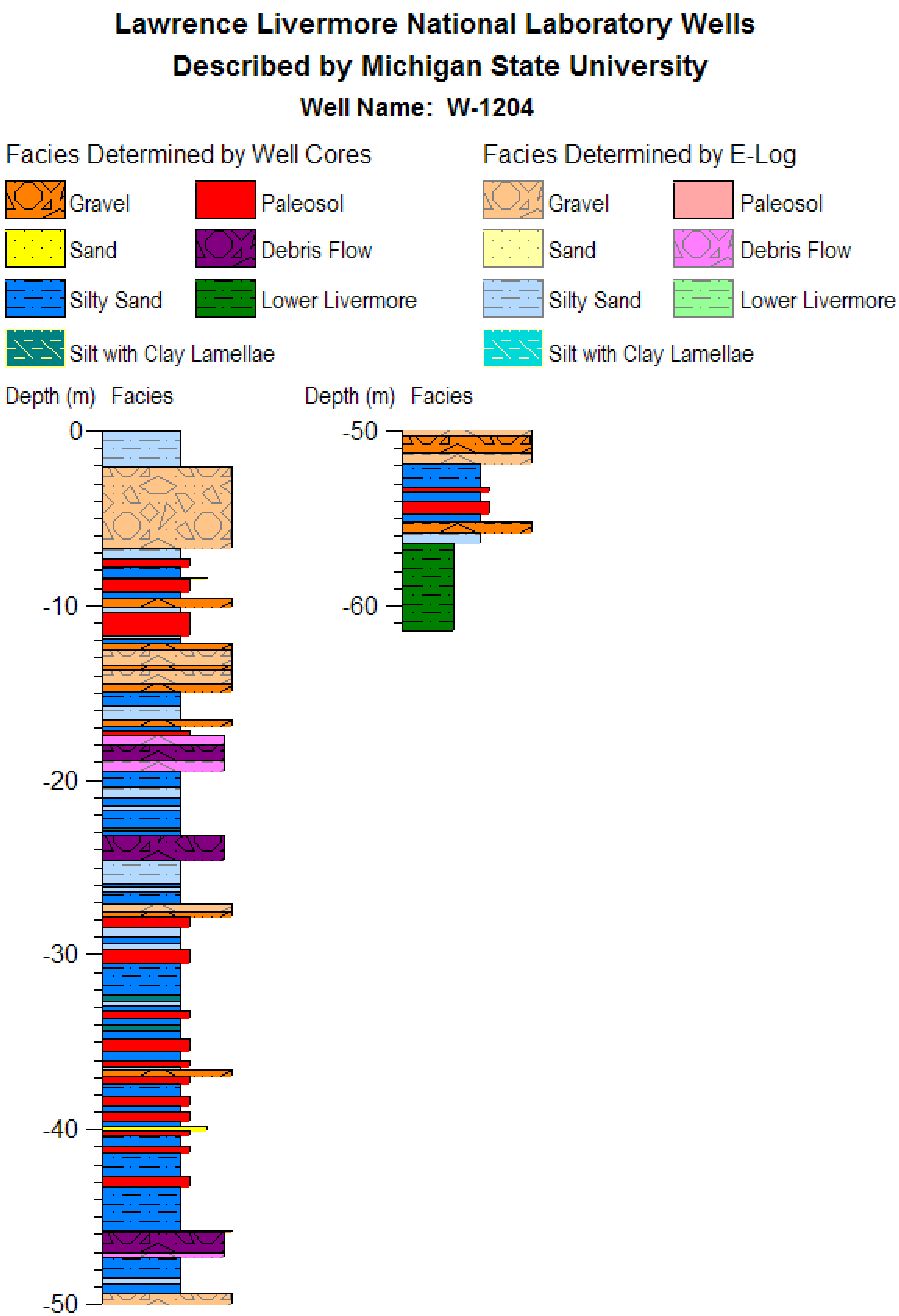

Figure 119. W-1204 stratigraphic column.

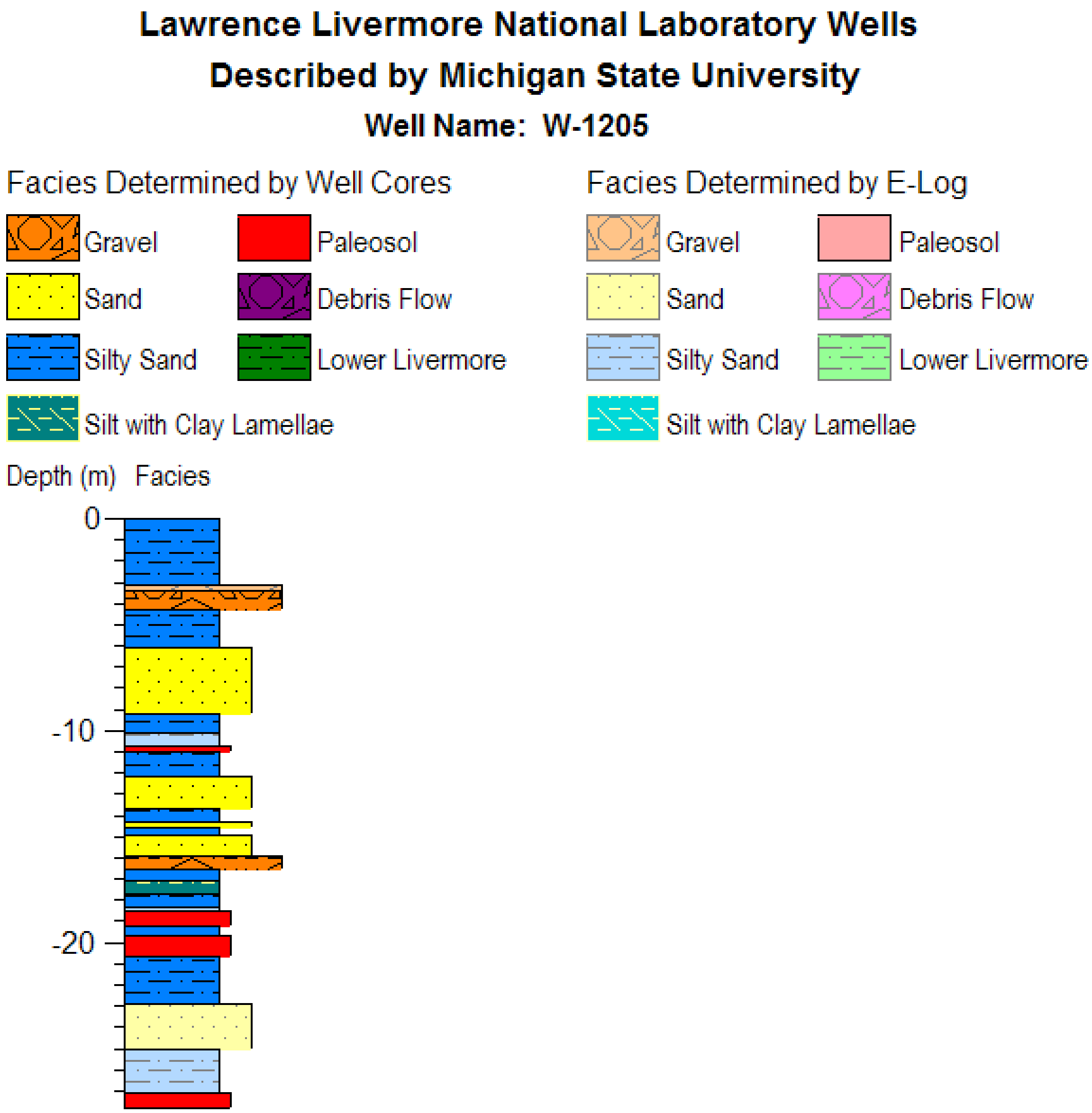

Figure 120. W-1205 stratigraphic column.

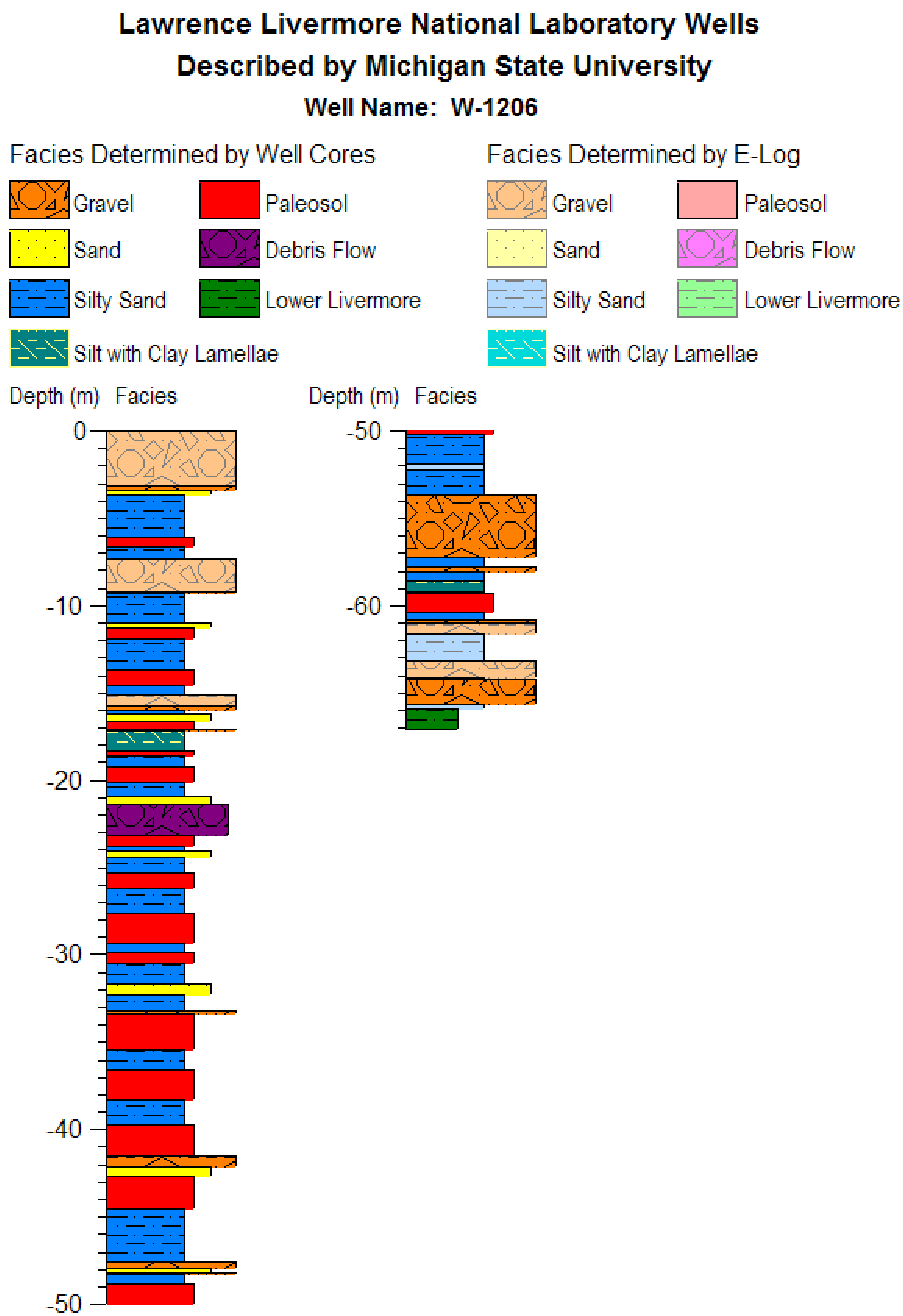

Figure 121. W-1206 stratigraphic column.

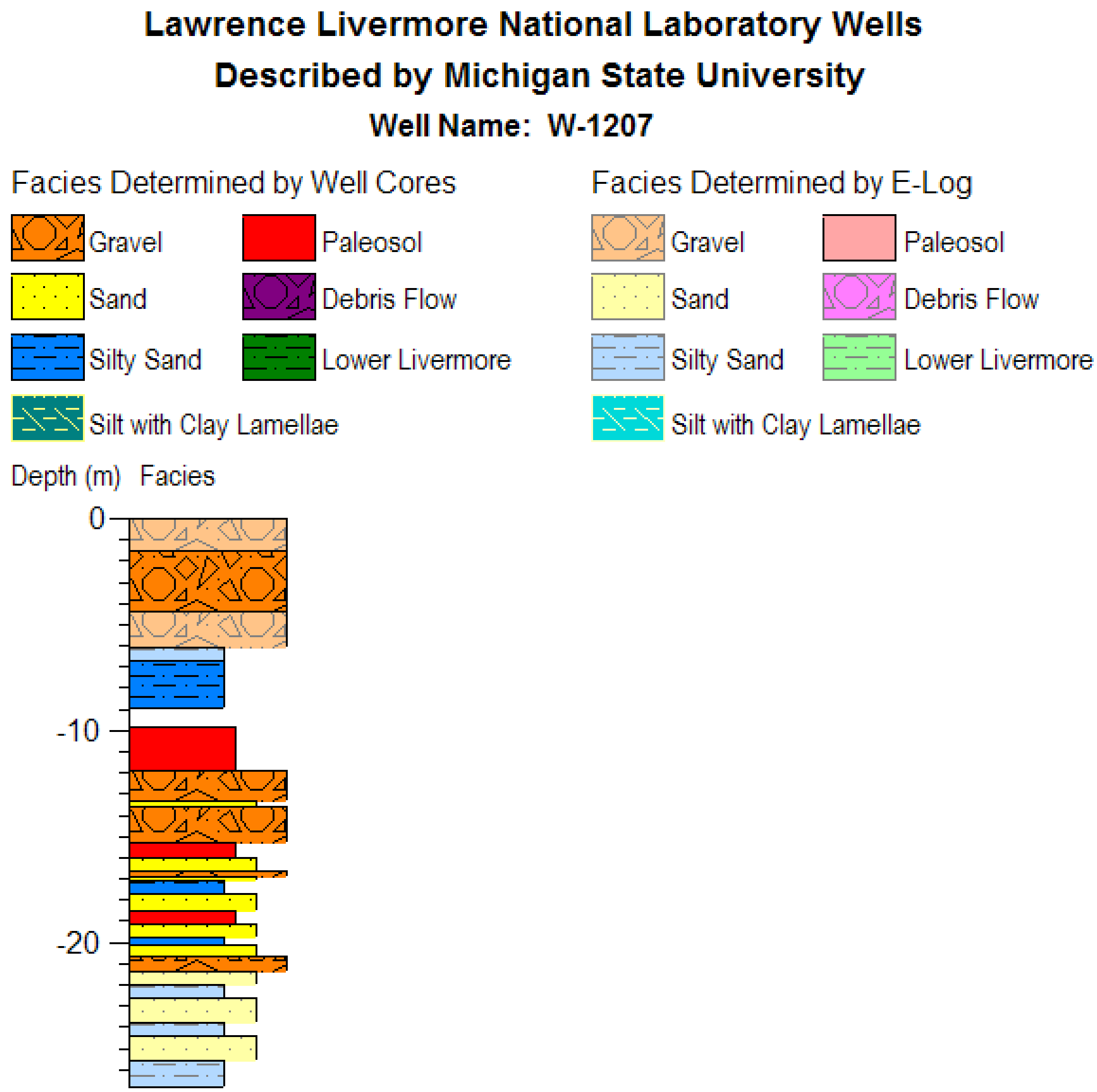

Figure 122. W-1207 stratigraphic column.

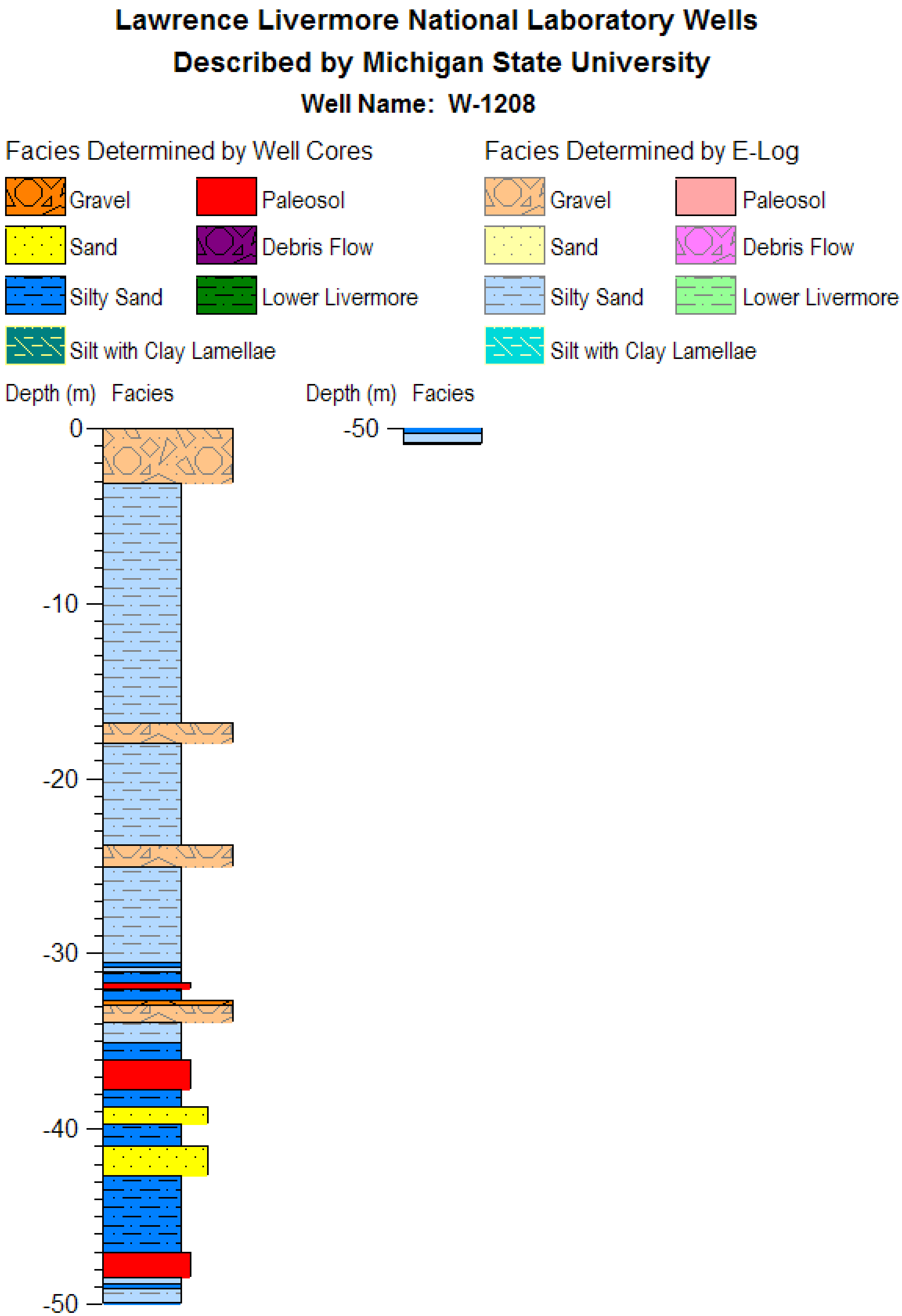

Figure 123. W-1208 stratigraphic column.

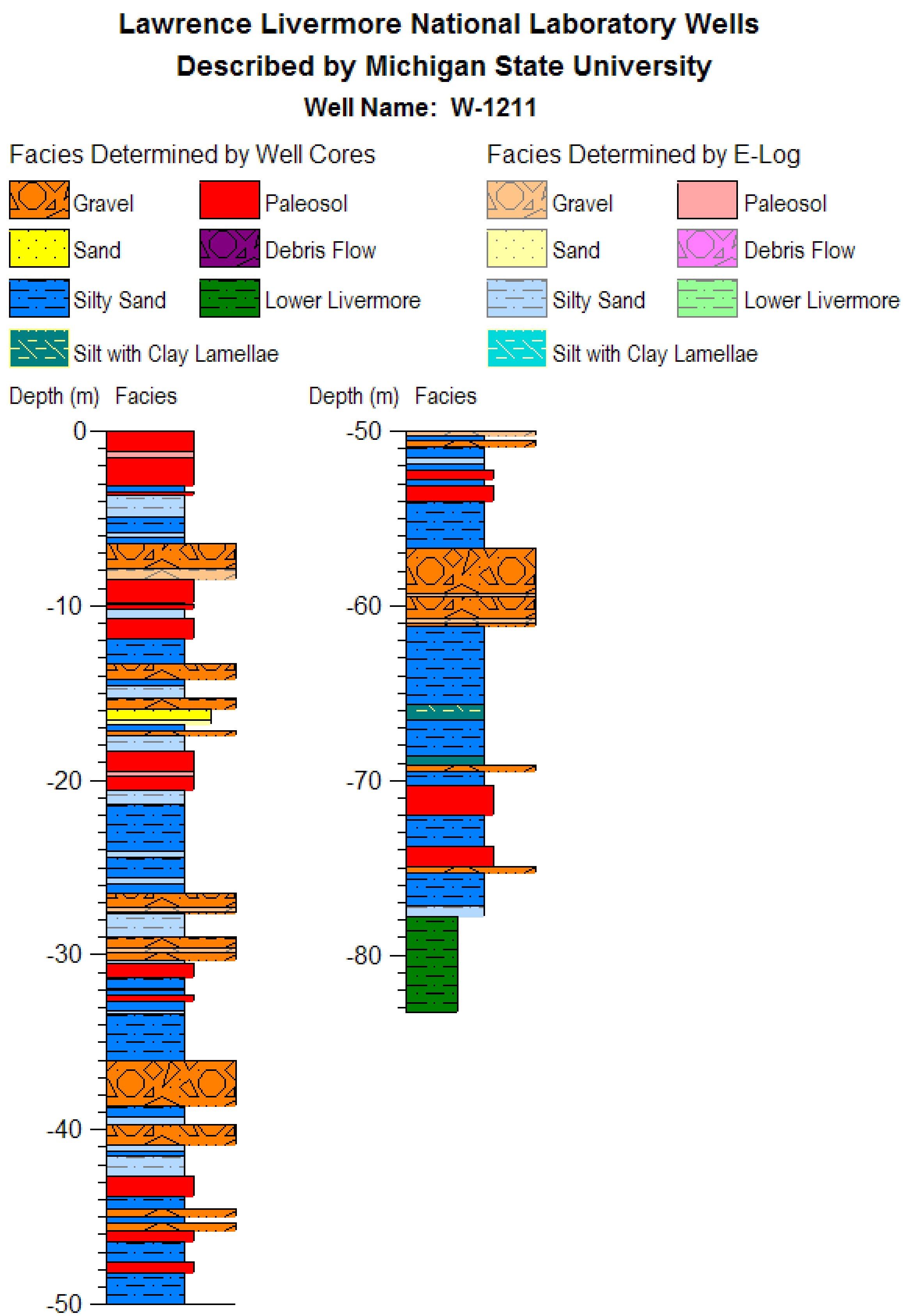

Figure 124. W-1211 stratigraphic column.

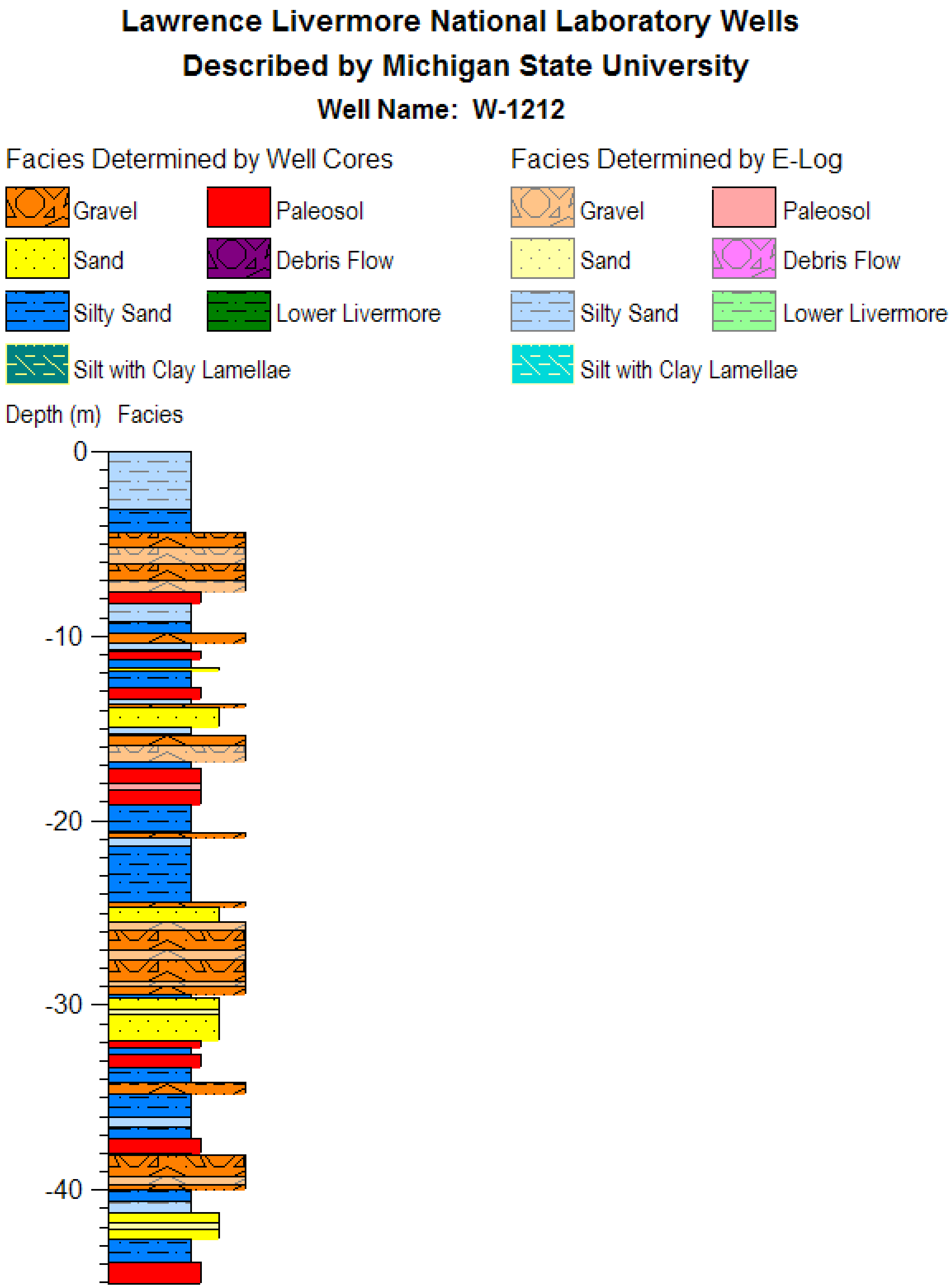

Figure 125. W-1212 stratigraphic column.

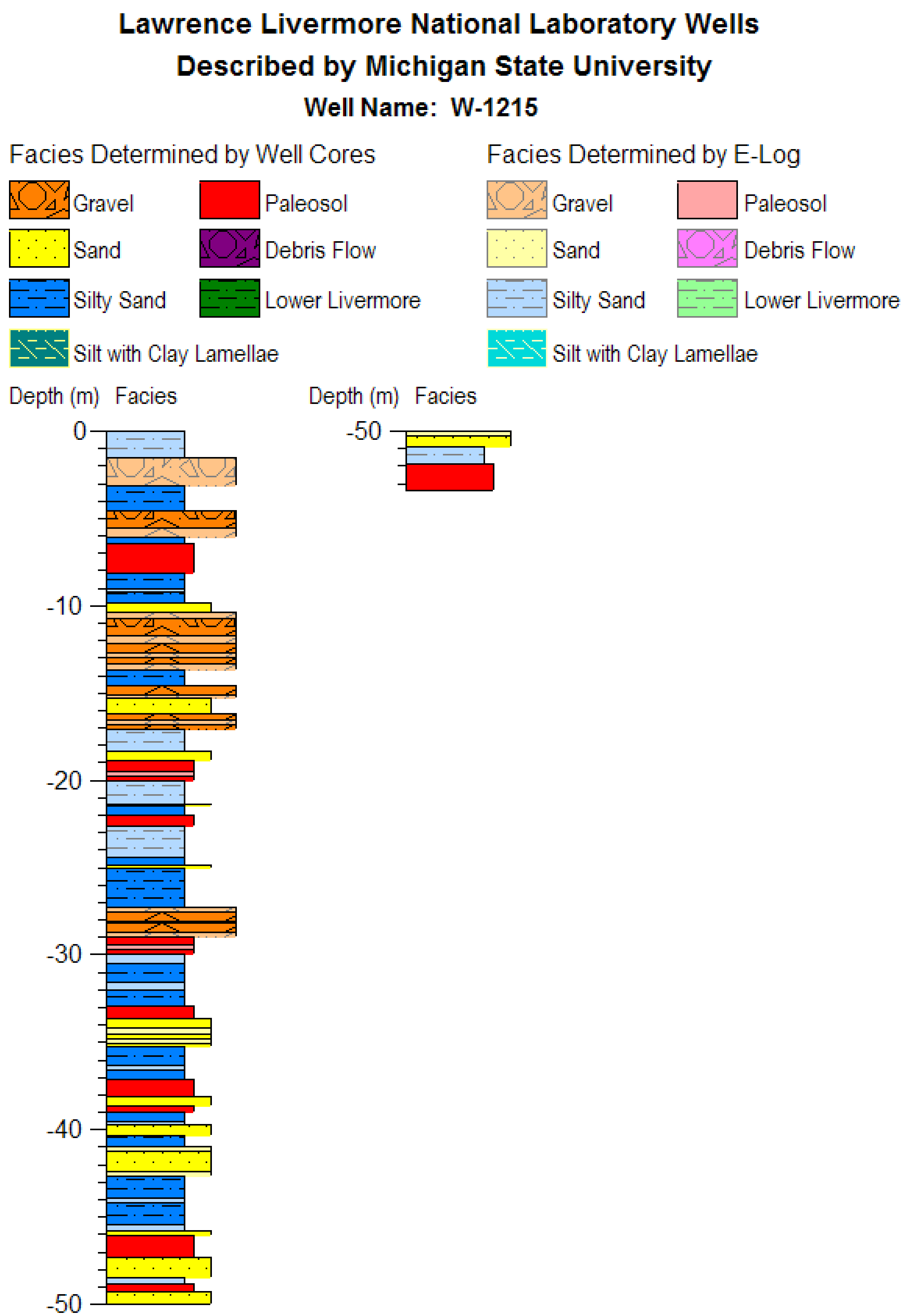

Figure 126. W-1215 stratigraphic column.

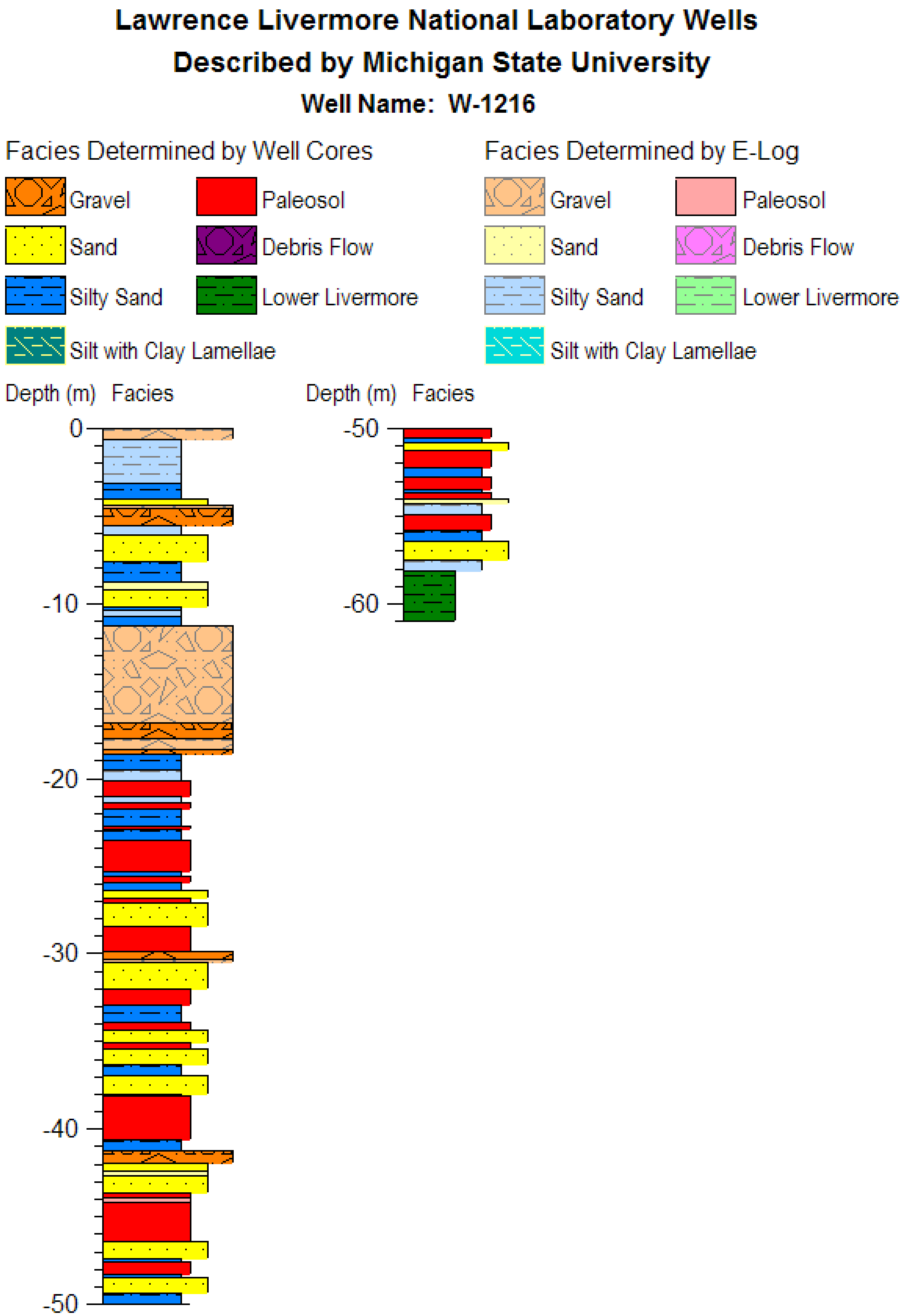

Figure 127. W-1216 stratigraphic column.

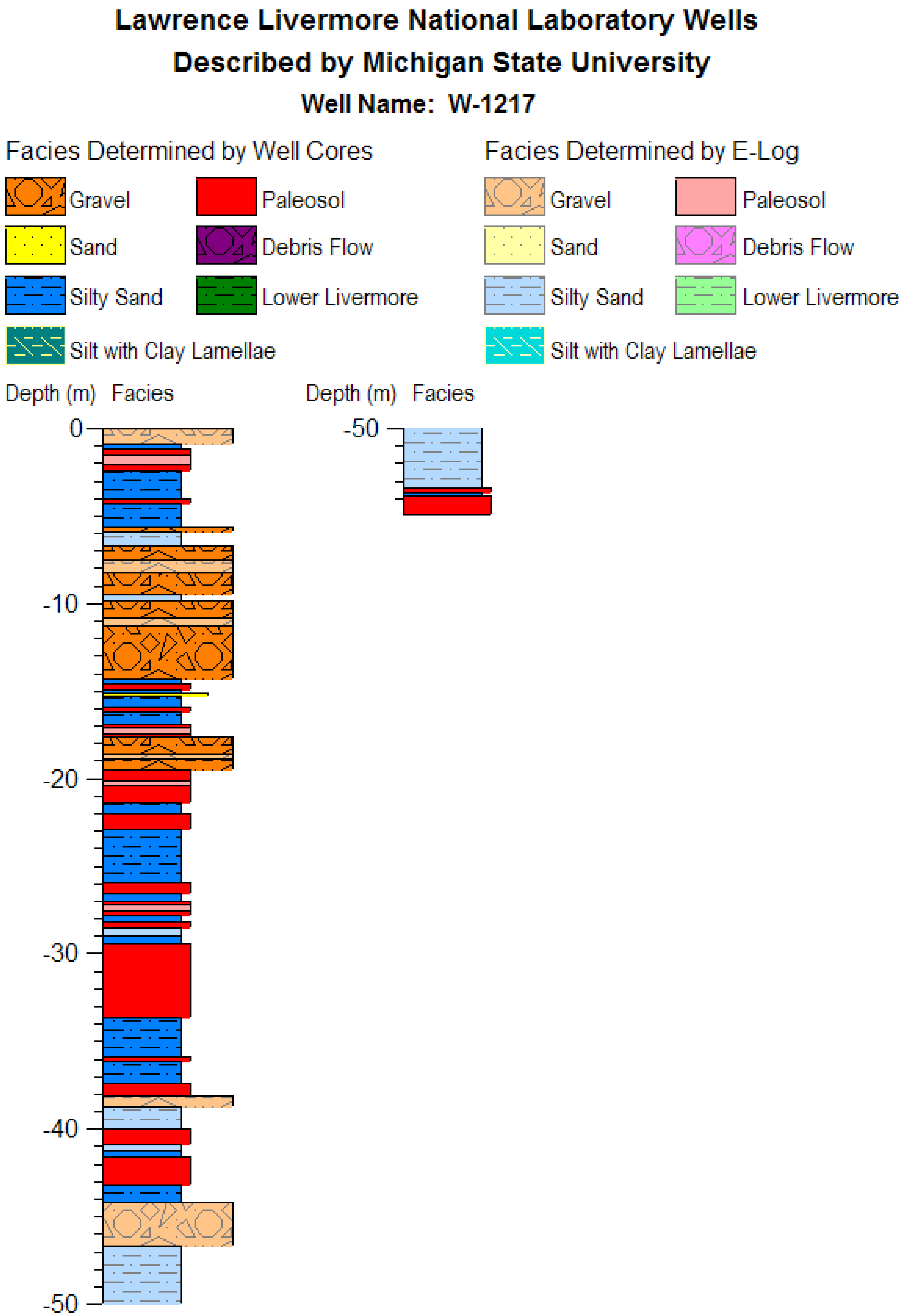

Figure 128. W-1217 stratigraphic column.

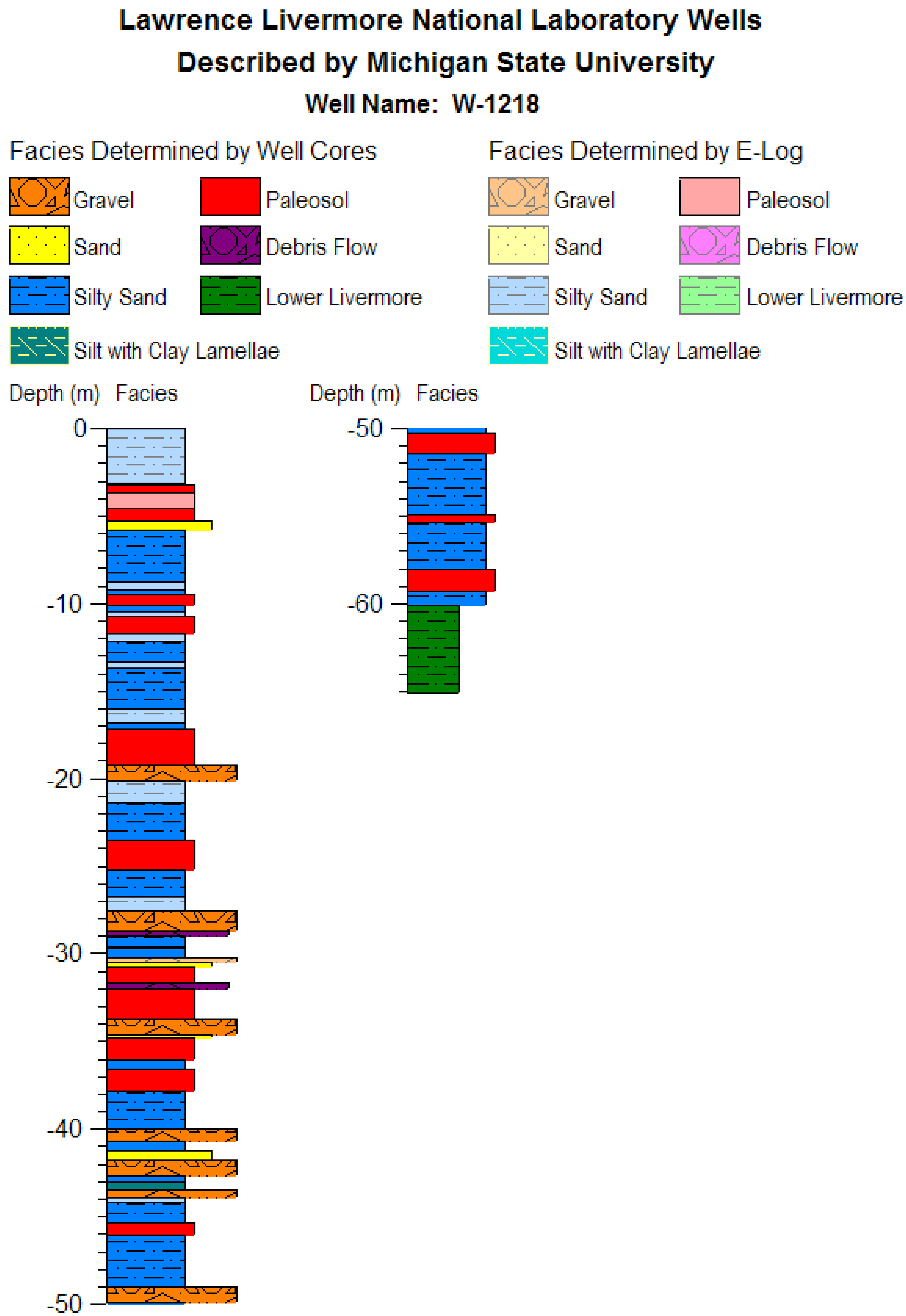

Figure 129. W-1218 stratigraphic column.

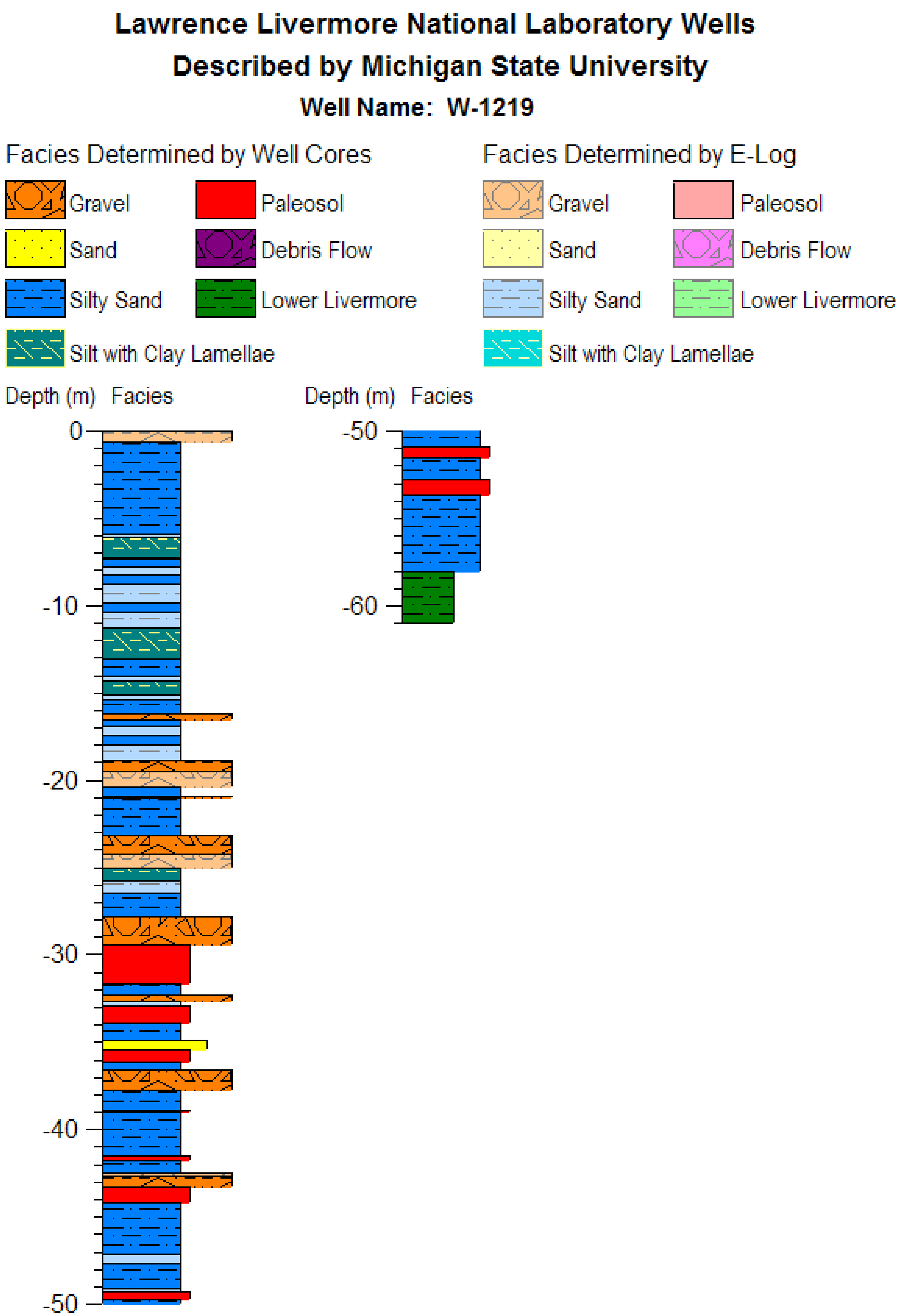

Figure 130. W-1219 stratigraphic column.

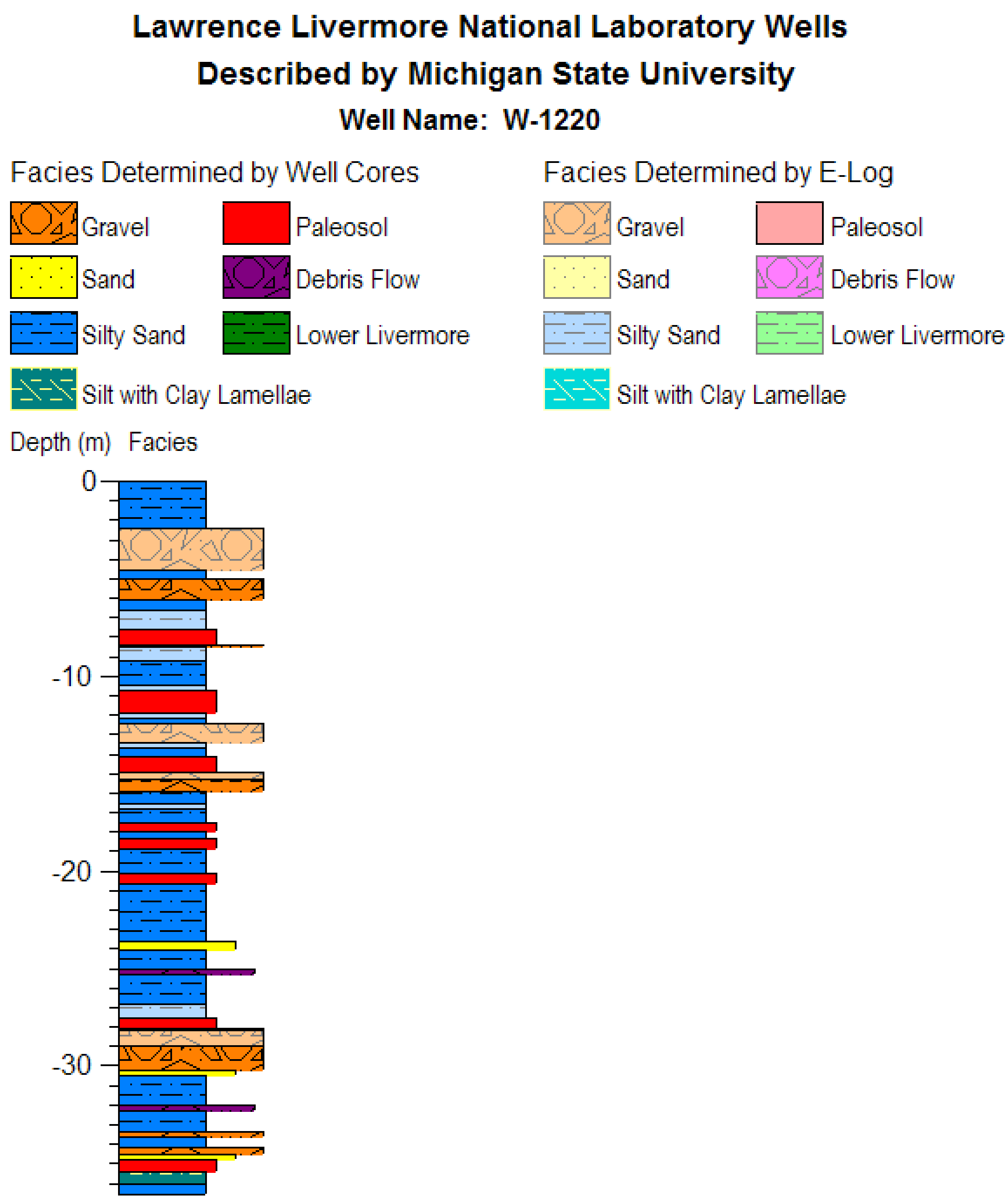

Figure 131. W-1220 stratigraphic column.

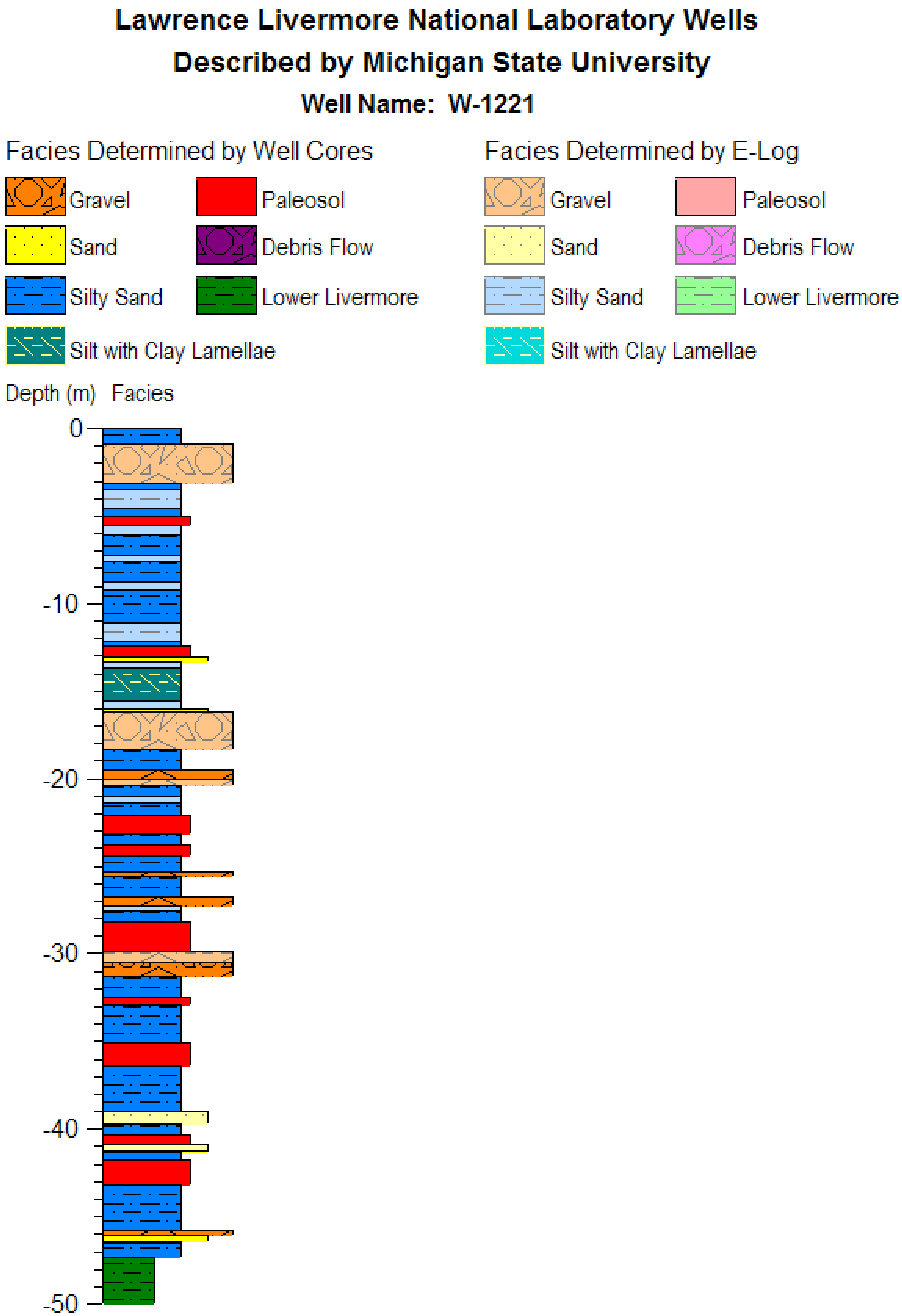

Figure 132. W-1221 stratigraphic column.

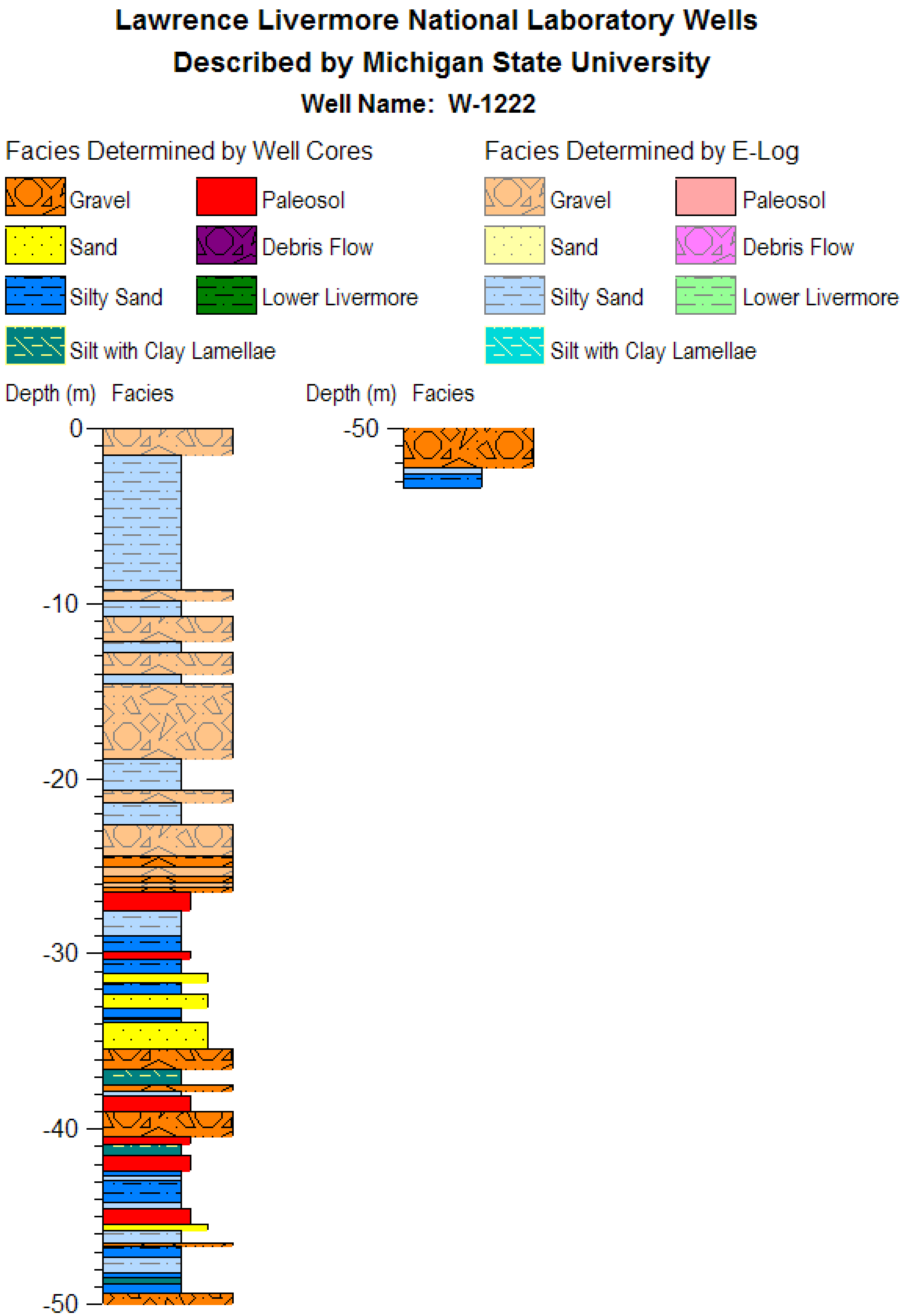

Figure 133. W-1222 stratigraphic column.

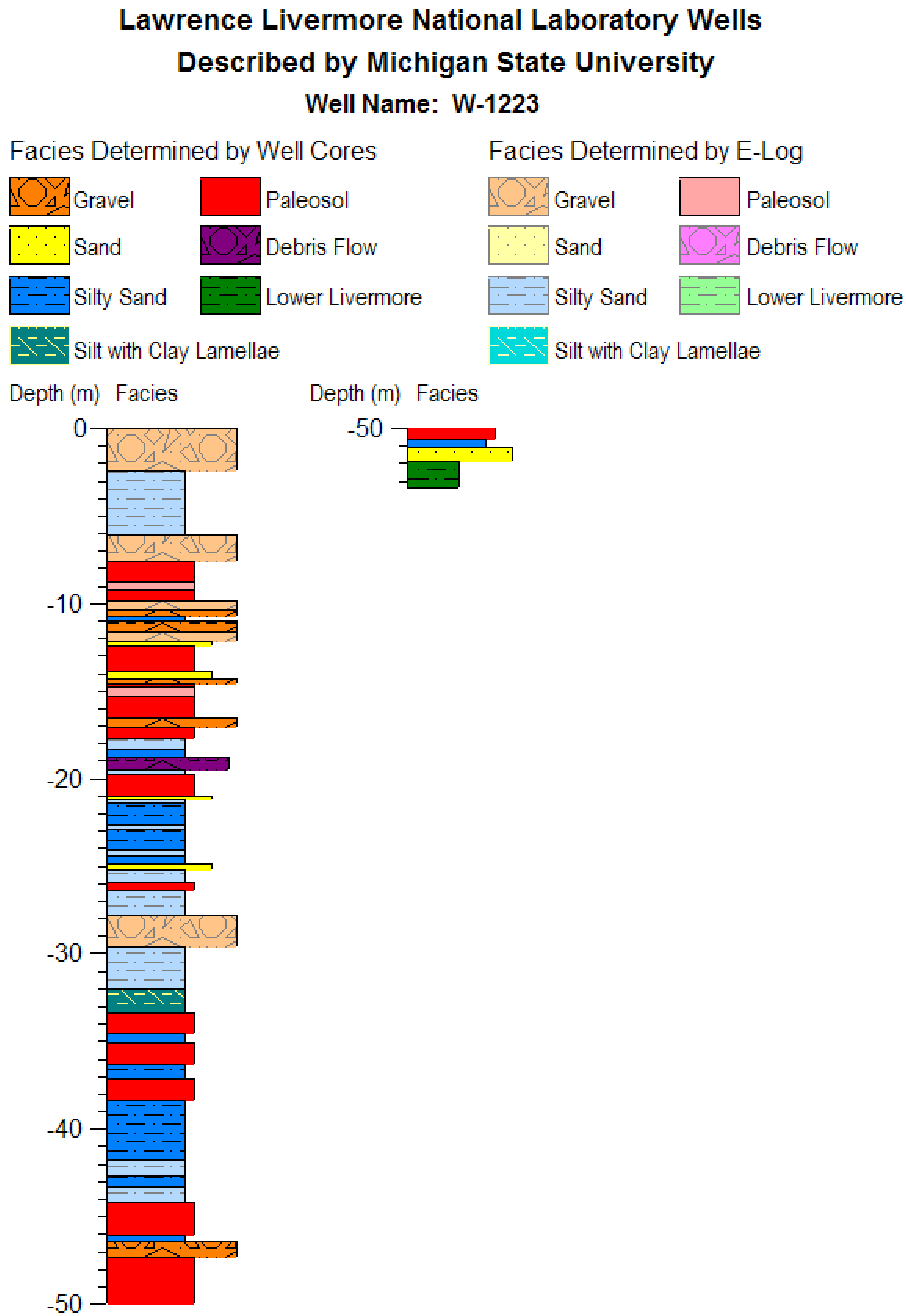

Figure 134. W-1223 stratigraphic column.

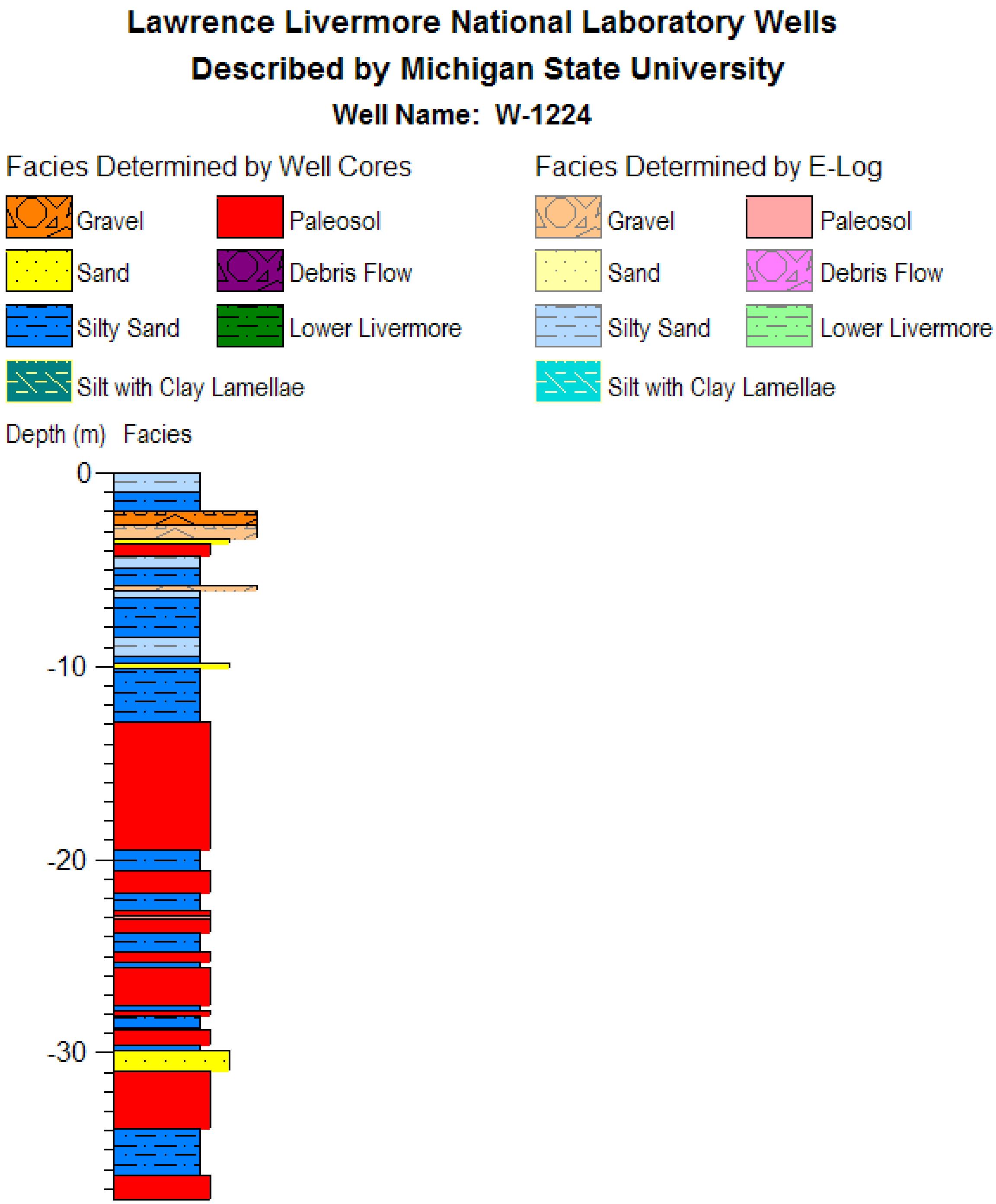

Figure 135. W-1224 stratigraphic column.

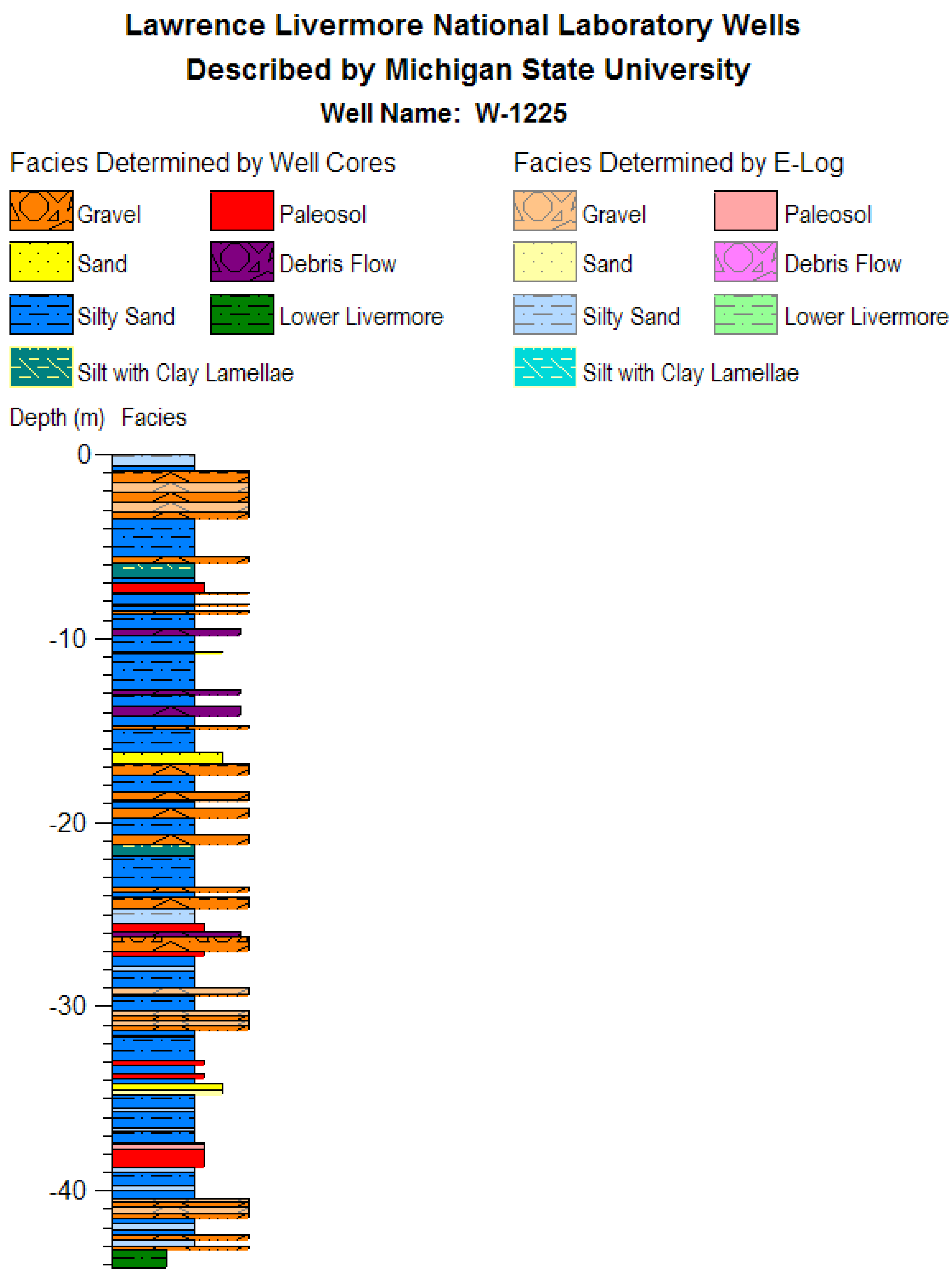

Figure 136. W-1225 stratigraphic column.

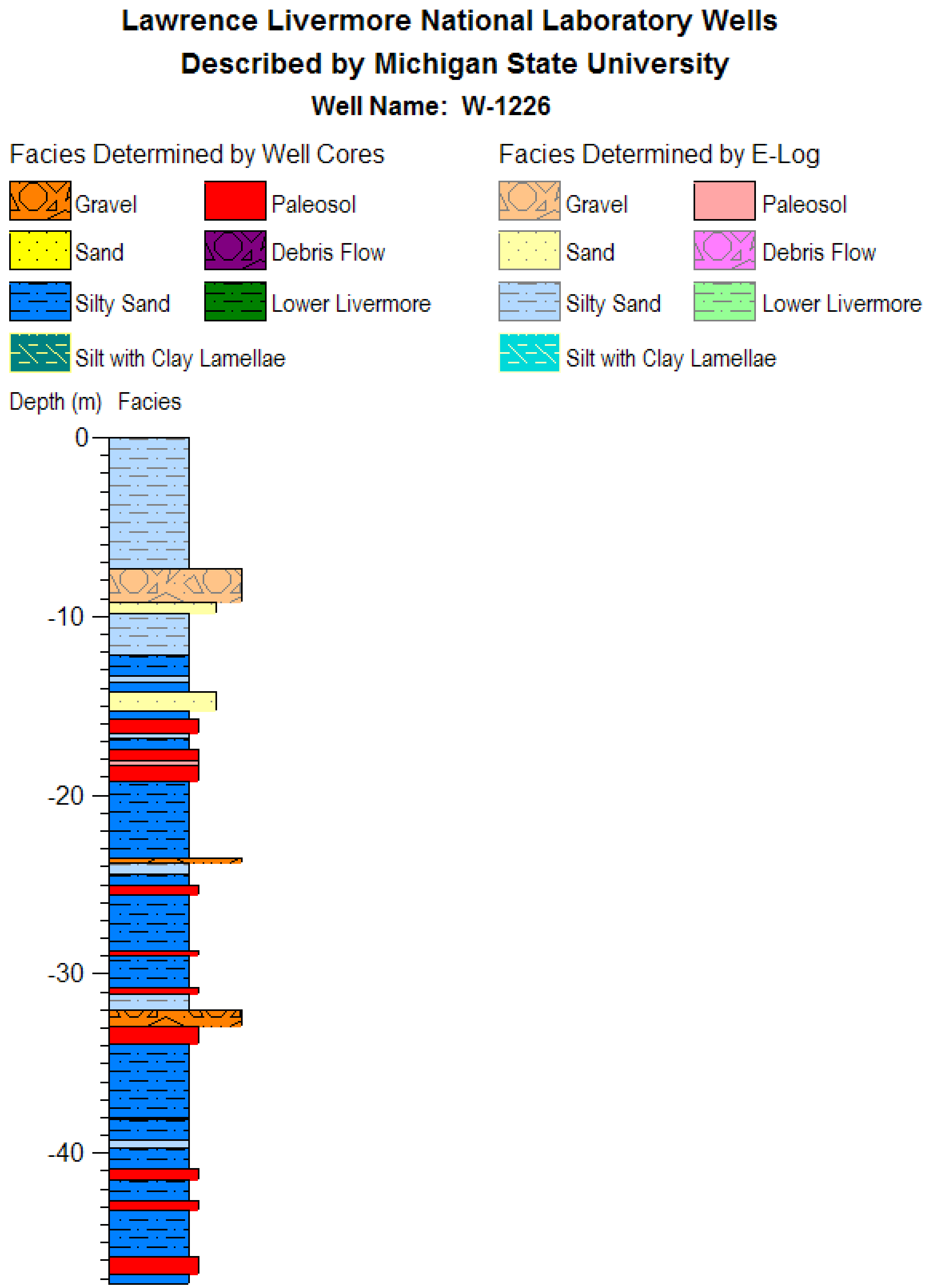

Figure 137. W-1226 stratigraphic column.

Figure 138. W-1227 stratigraphic column.

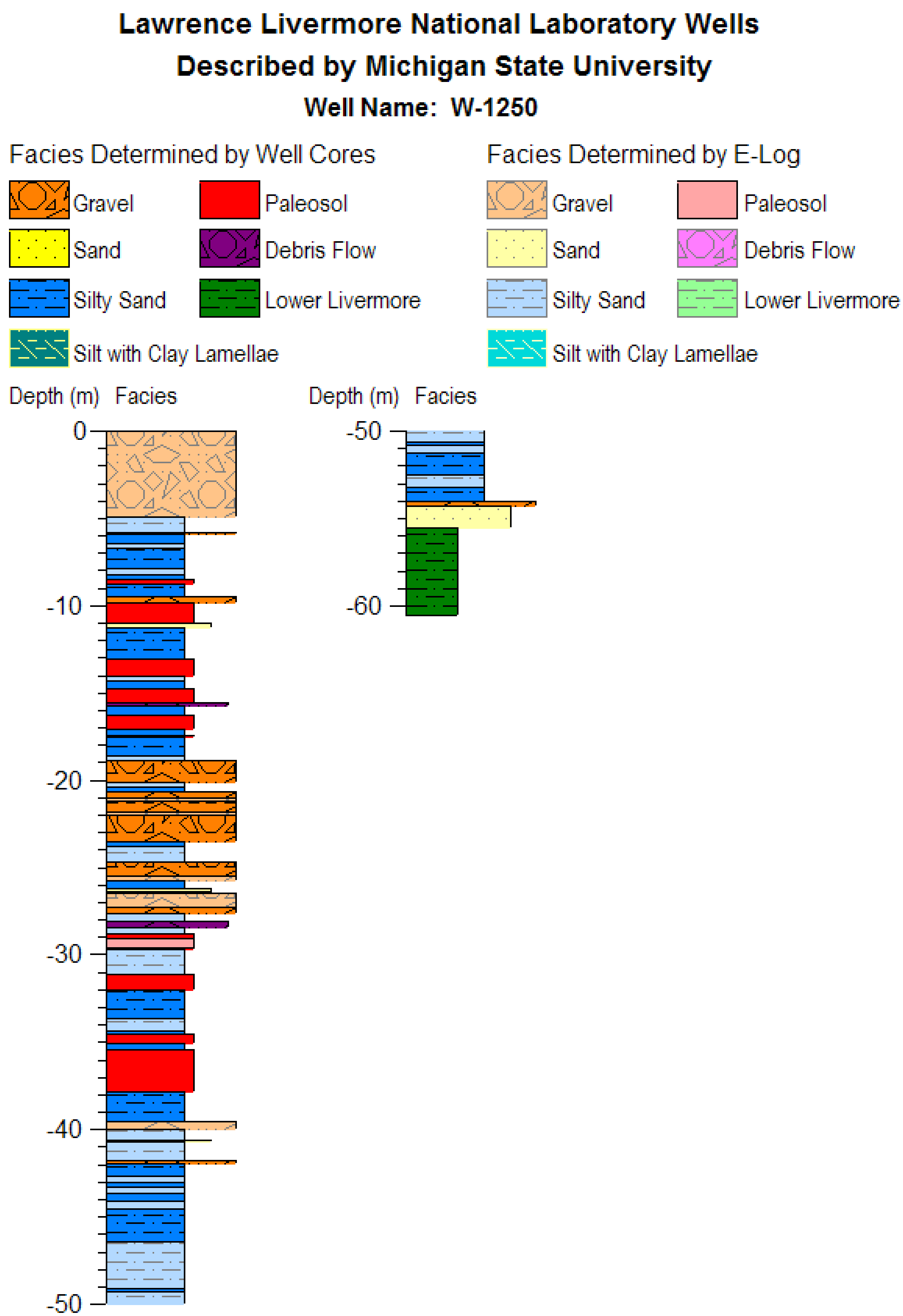

Figure 139. W-1250 stratigraphic column.

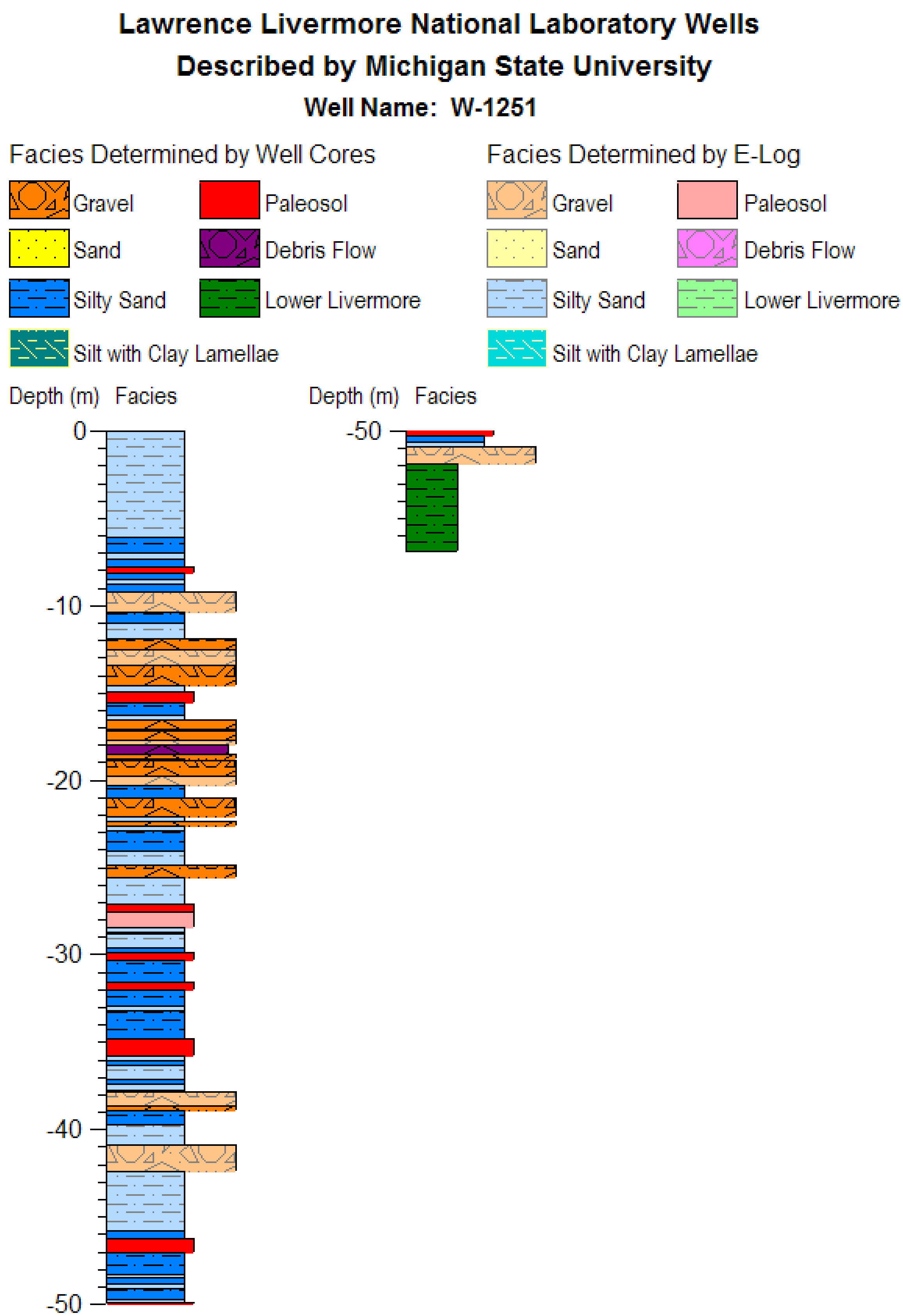

Figure 140. W-1251 stratigraphic column.

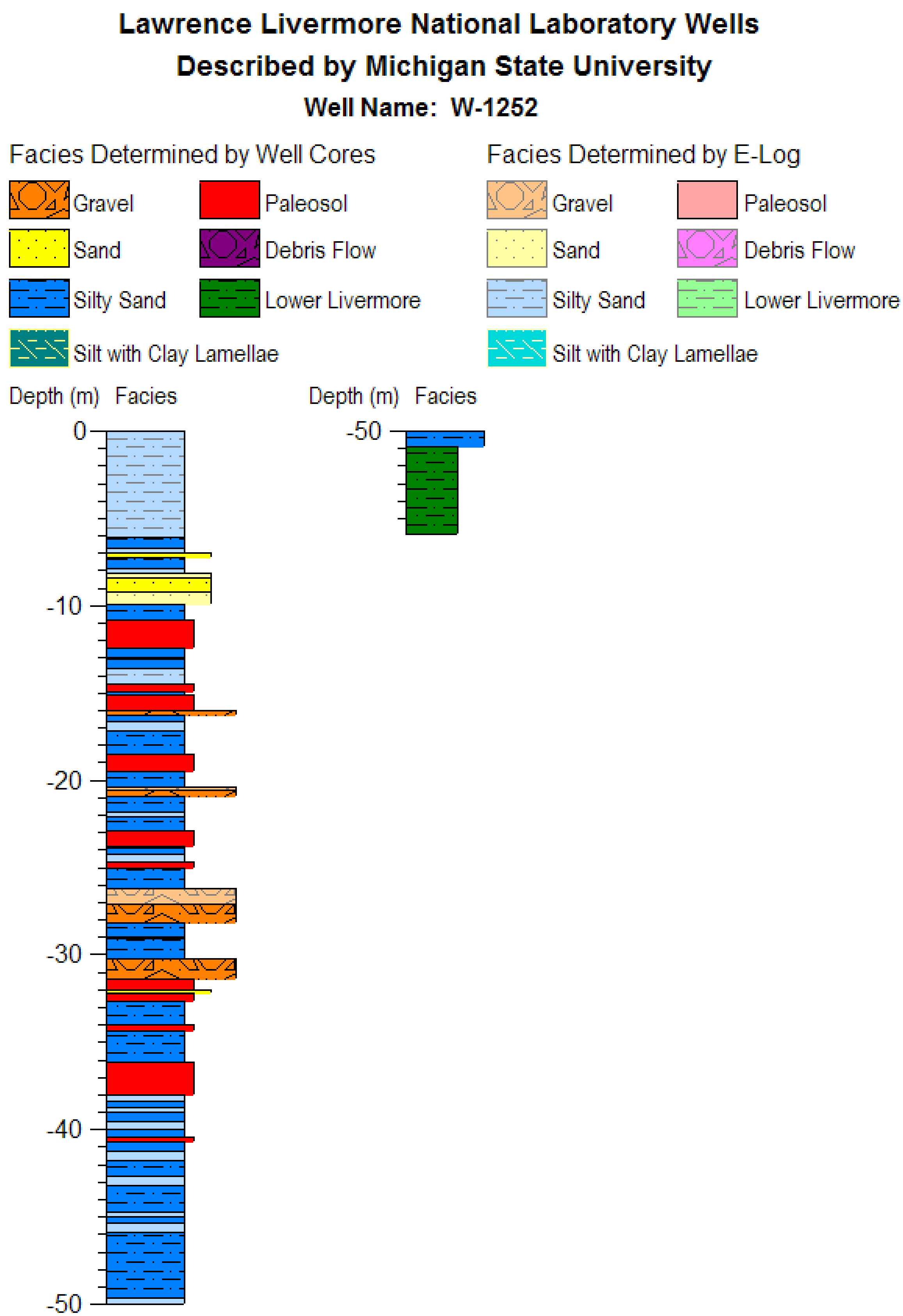

Figure 141. W-1252 stratigraphic column.

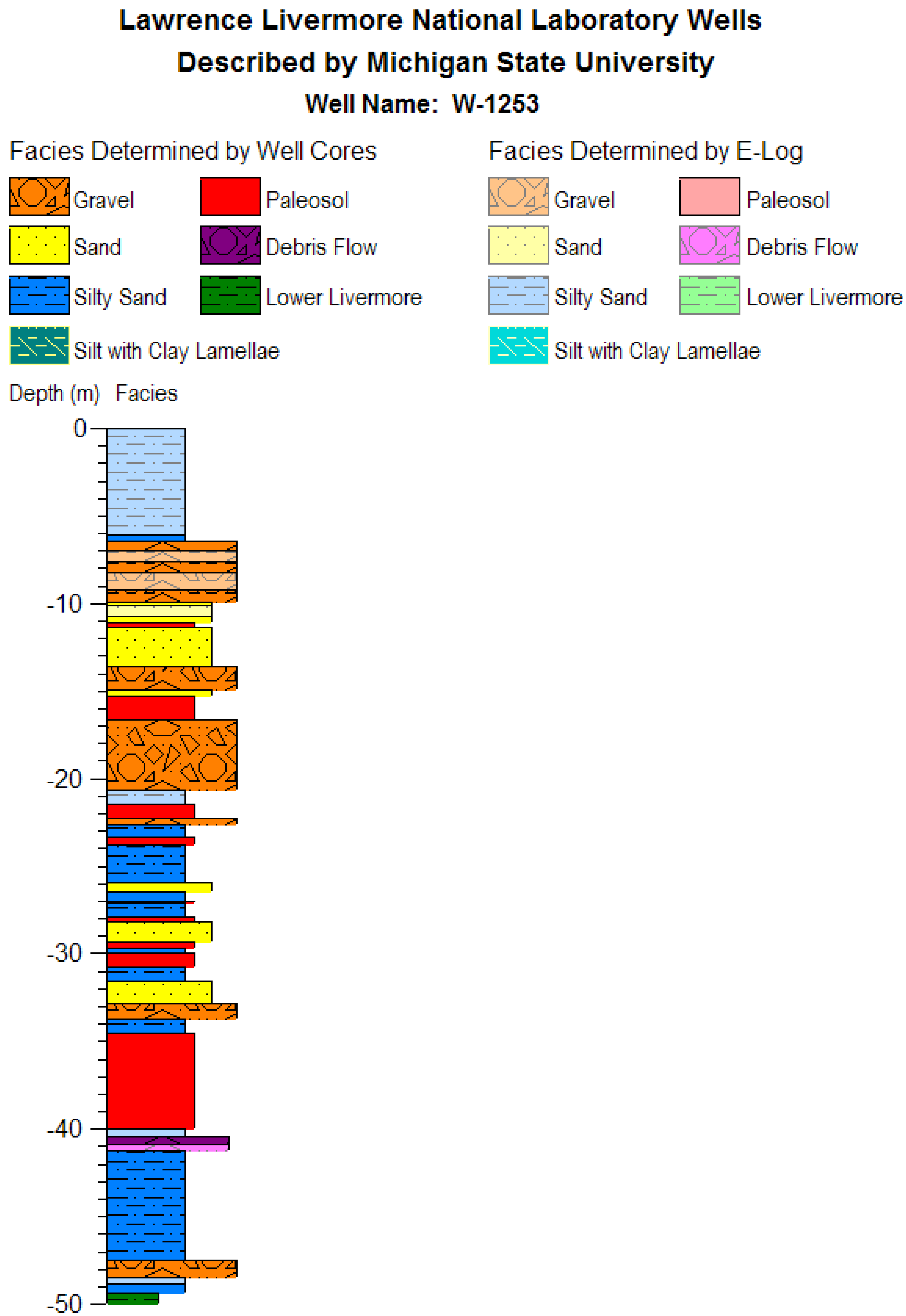

Figure 142. W-1253 stratigraphic column.

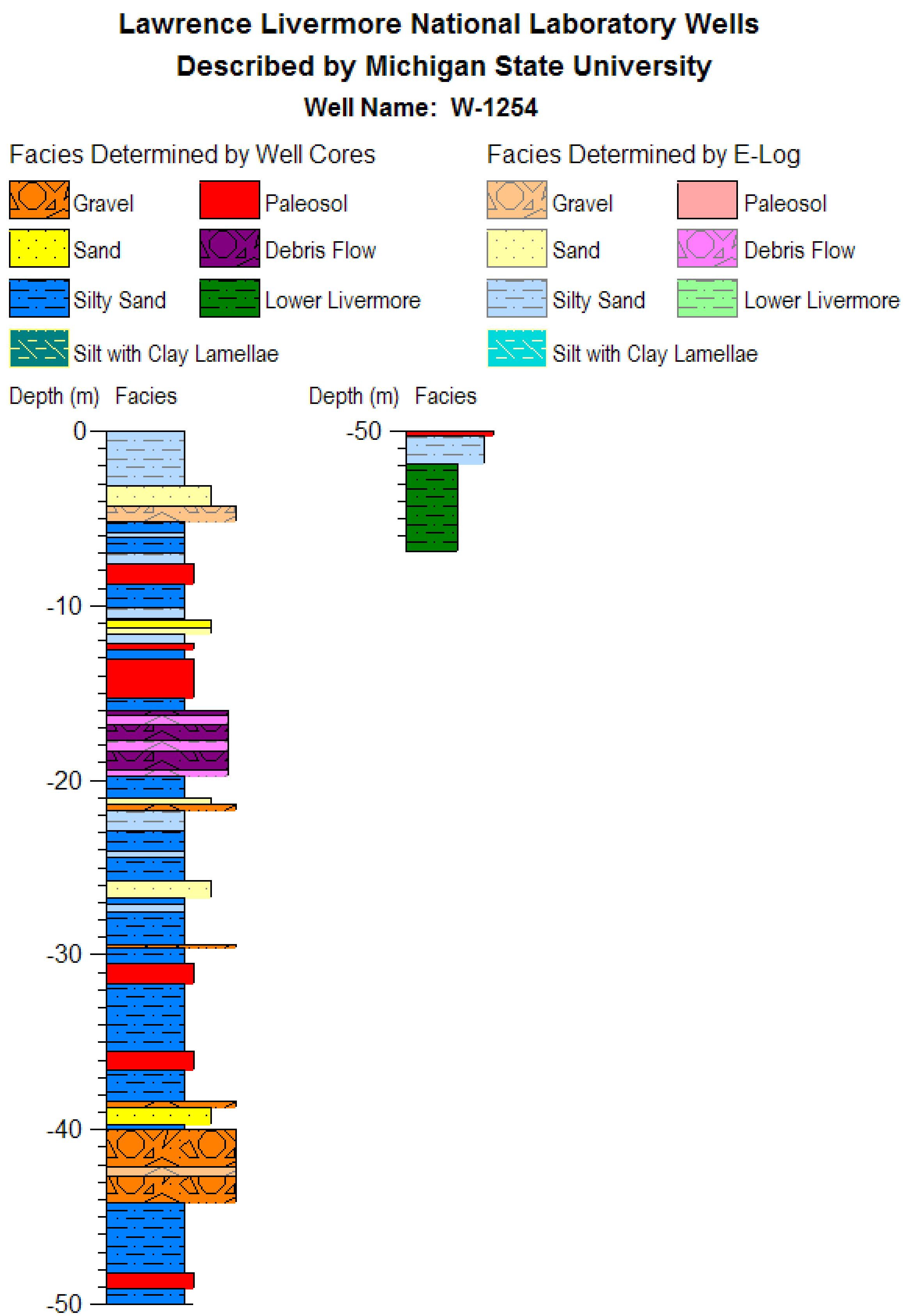

Figure 143. W-1254 stratigraphic column.

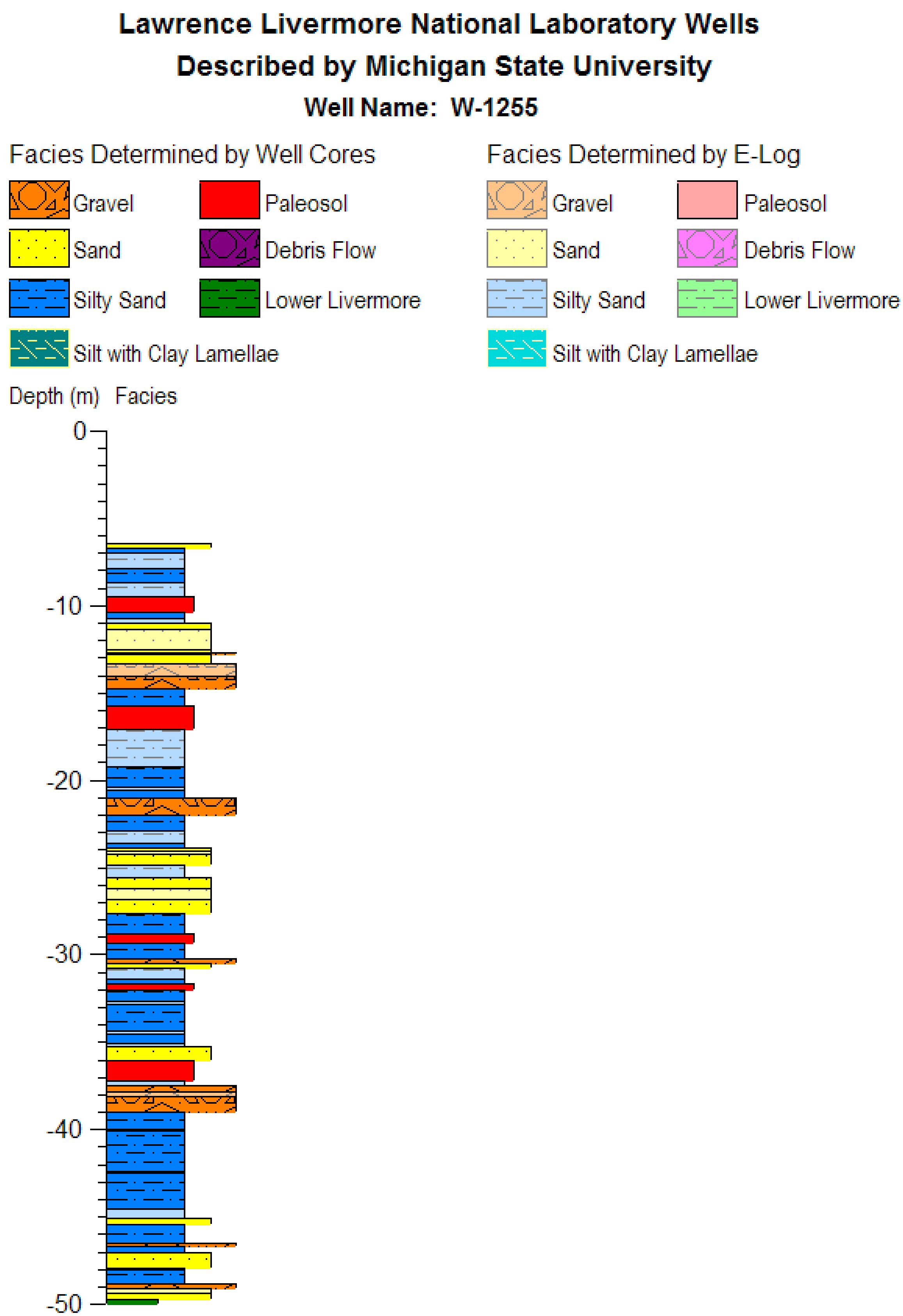

Figure 144. W-1255 stratigraphic column.

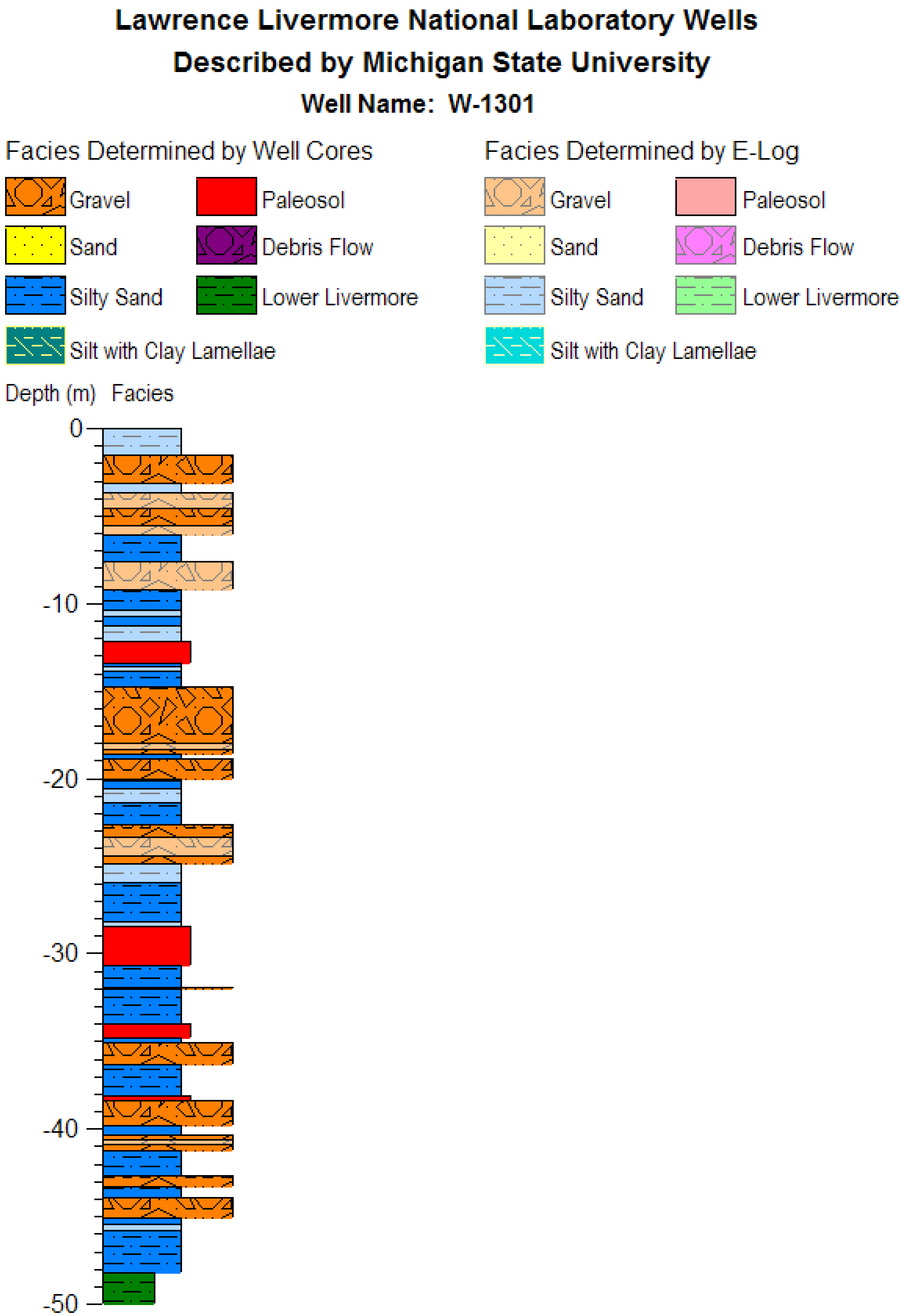

Figure 145. W-1301 stratigraphic column.

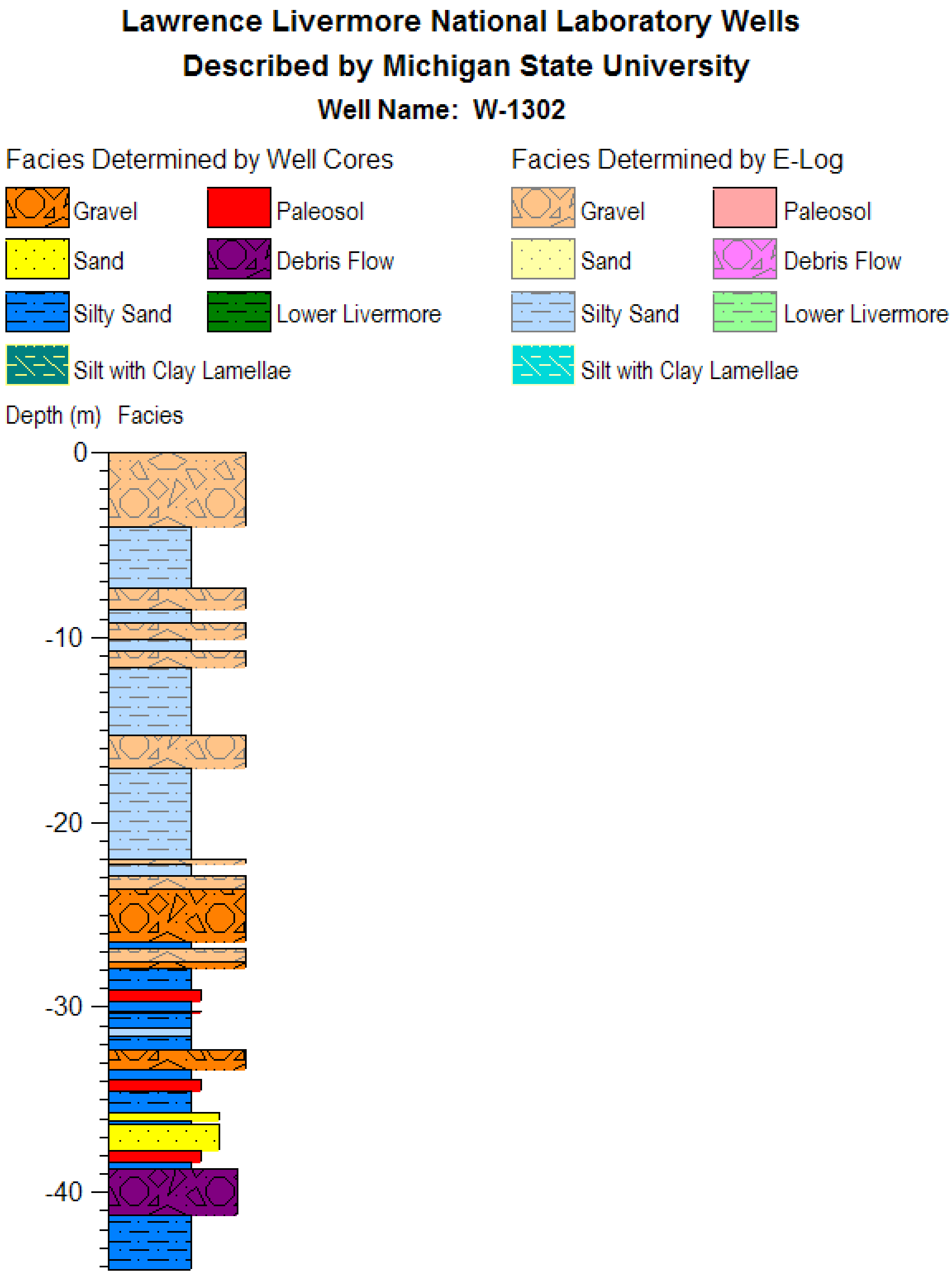

Figure 146. W-1302 stratigraphic column.

Figure 147. W-1303 stratigraphic column.

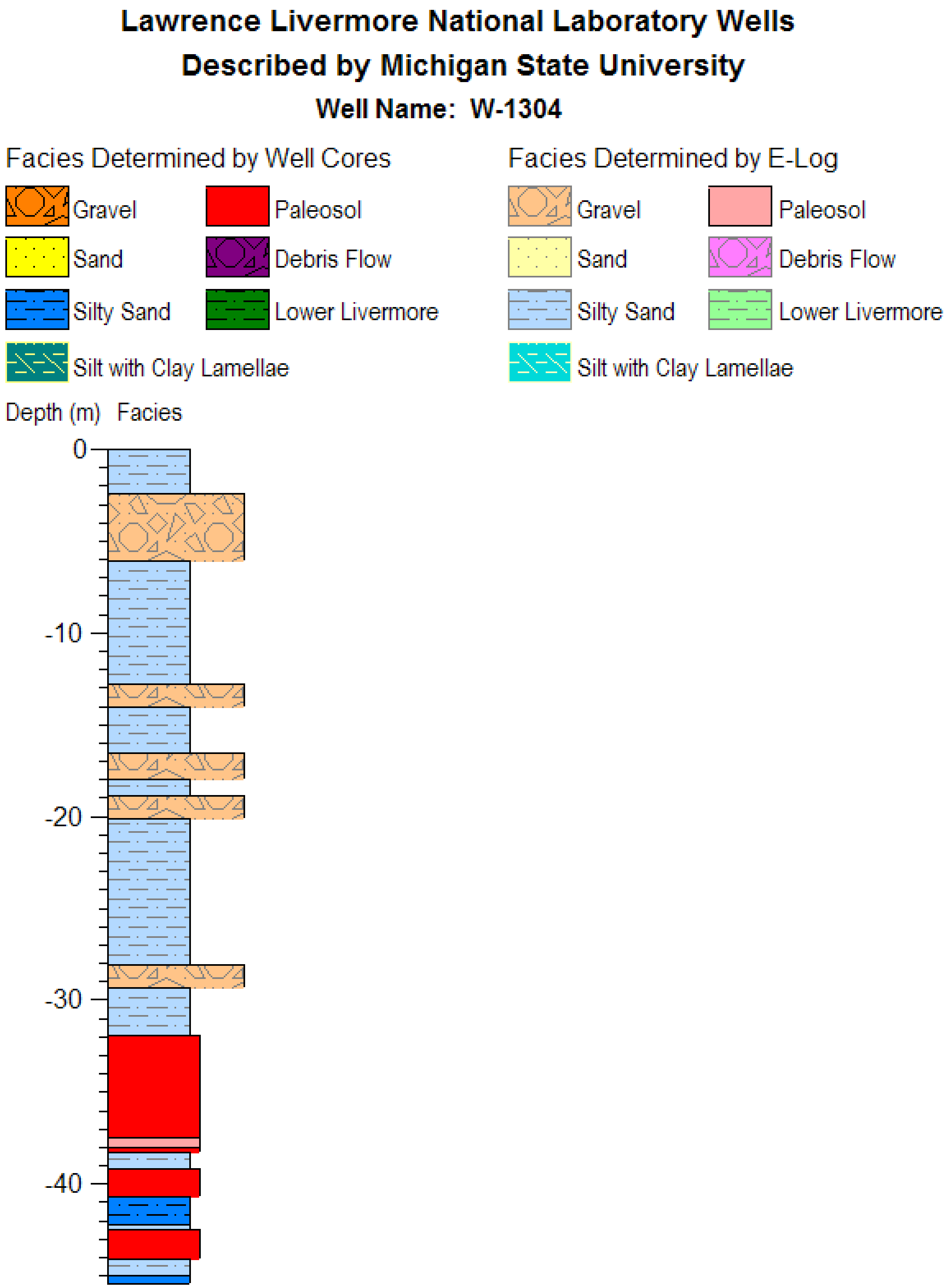

Figure 148. W-1304 stratigraphic column.

Figure 149. W-1306 stratigraphic column.

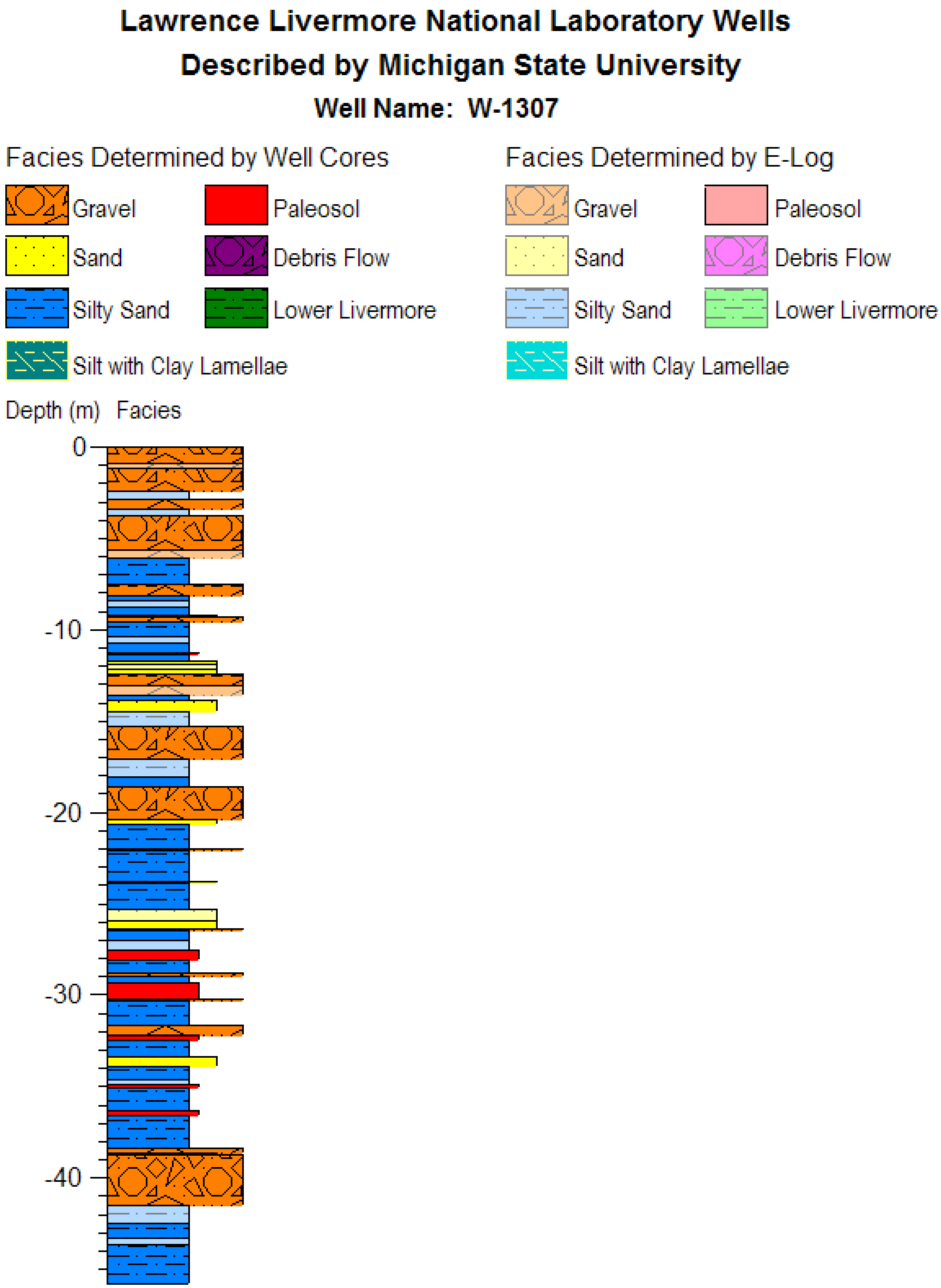

Figure 150. W-1307 stratigraphic column.

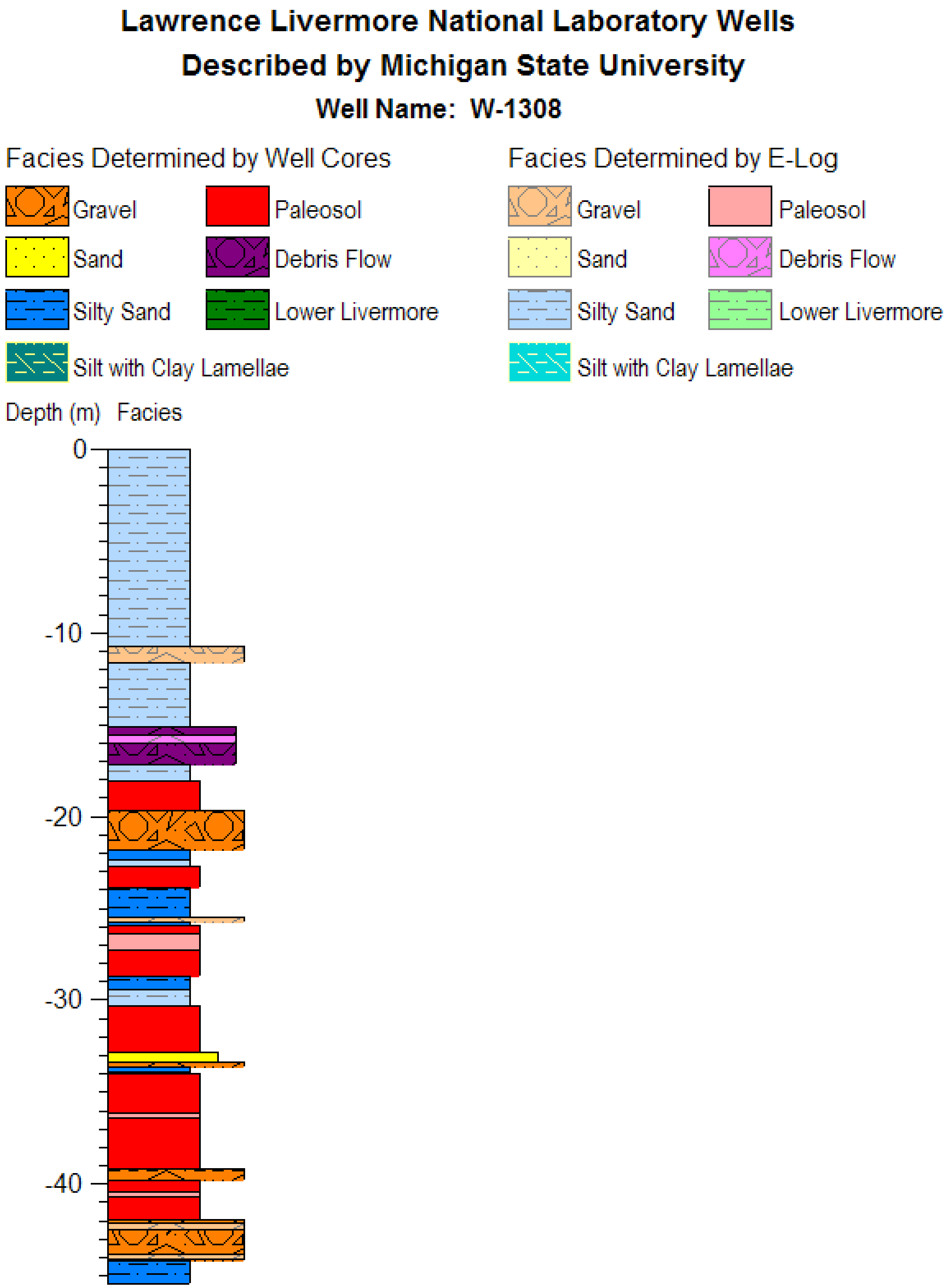

Figure 151. W-1308 stratigraphic column.

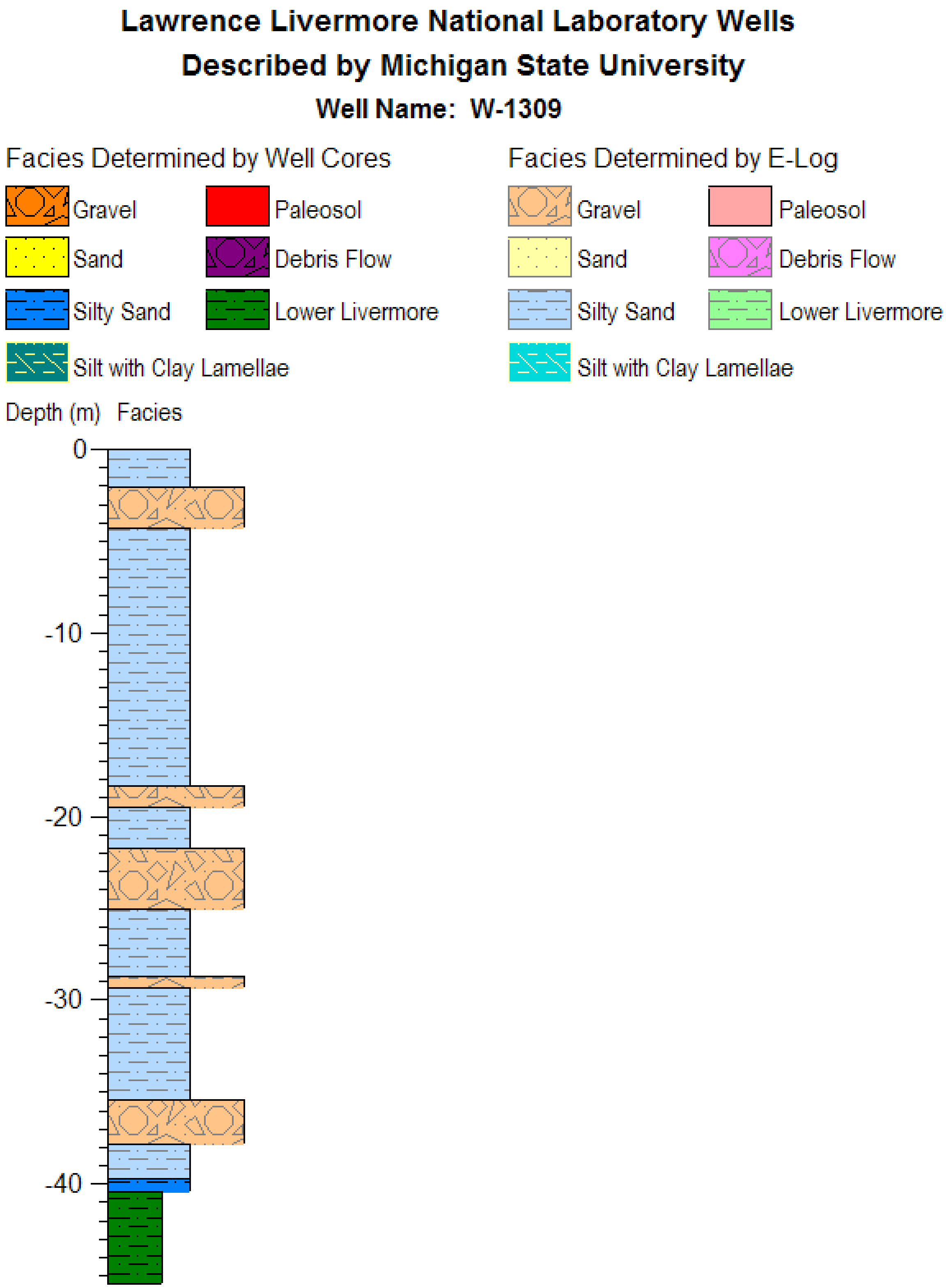

Figure 152. W-1309 stratigraphic column.

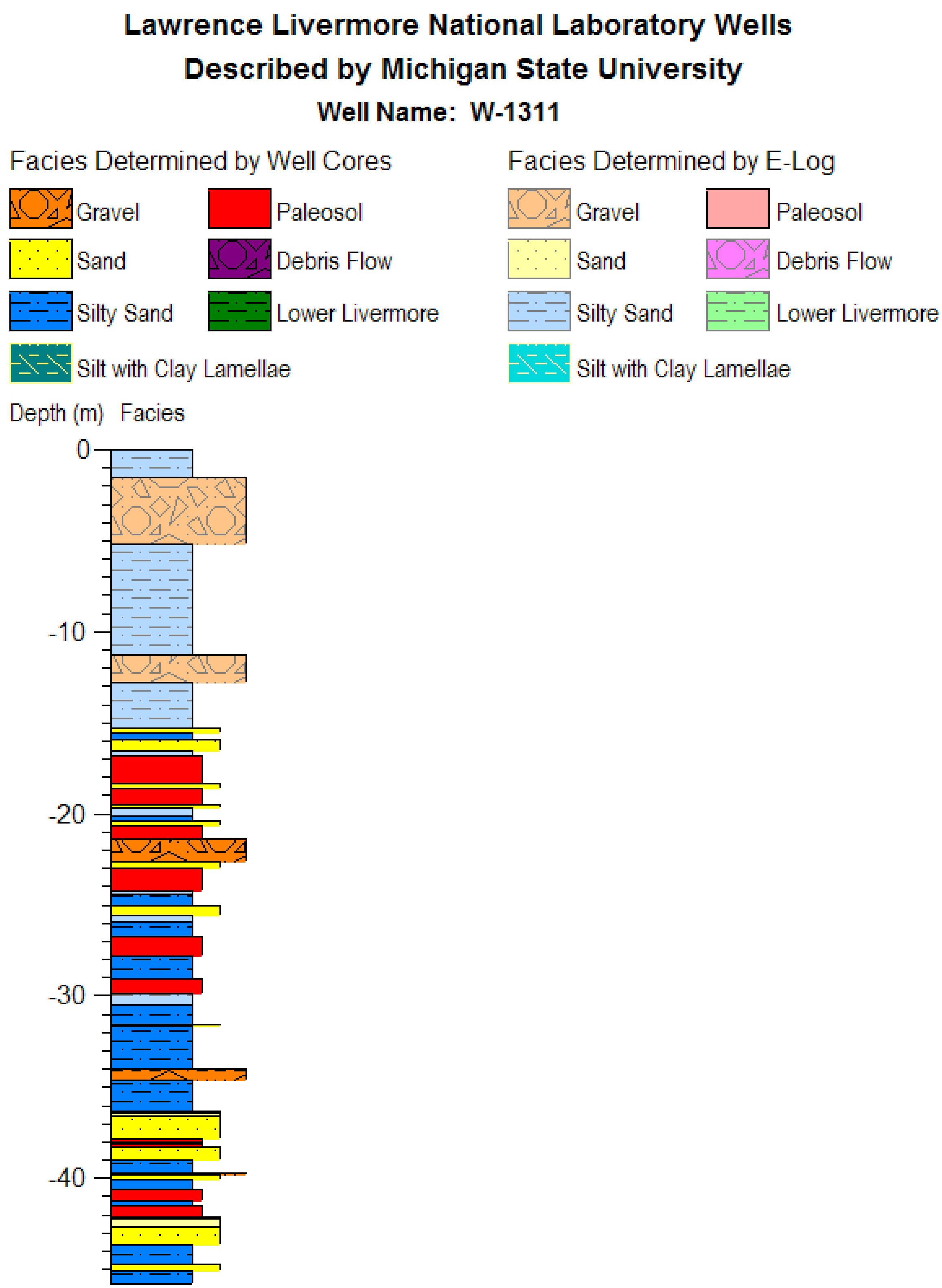

Figure 153. W-1311 stratigraphic column.

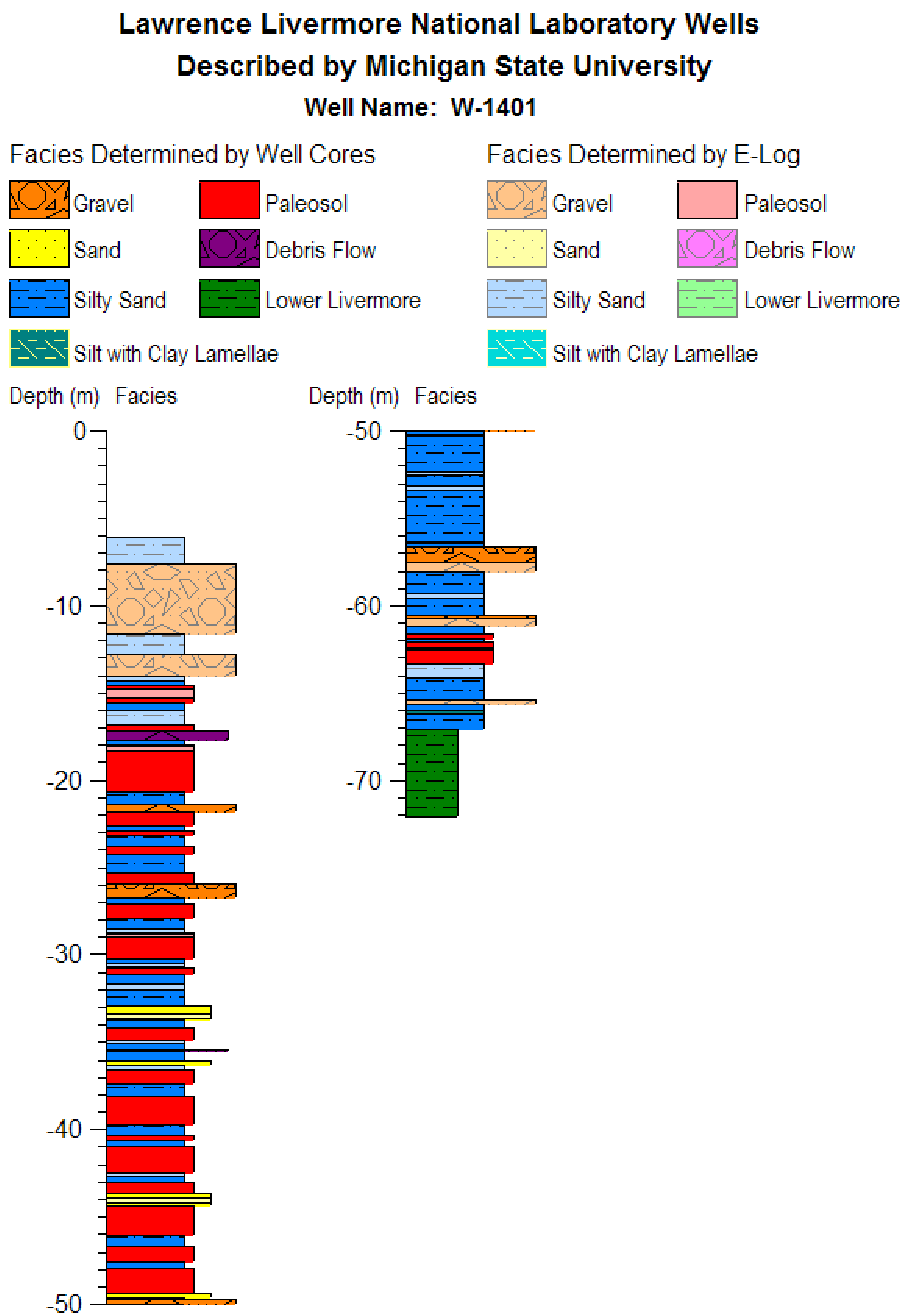

Figure 154. W-1401 stratigraphic column.

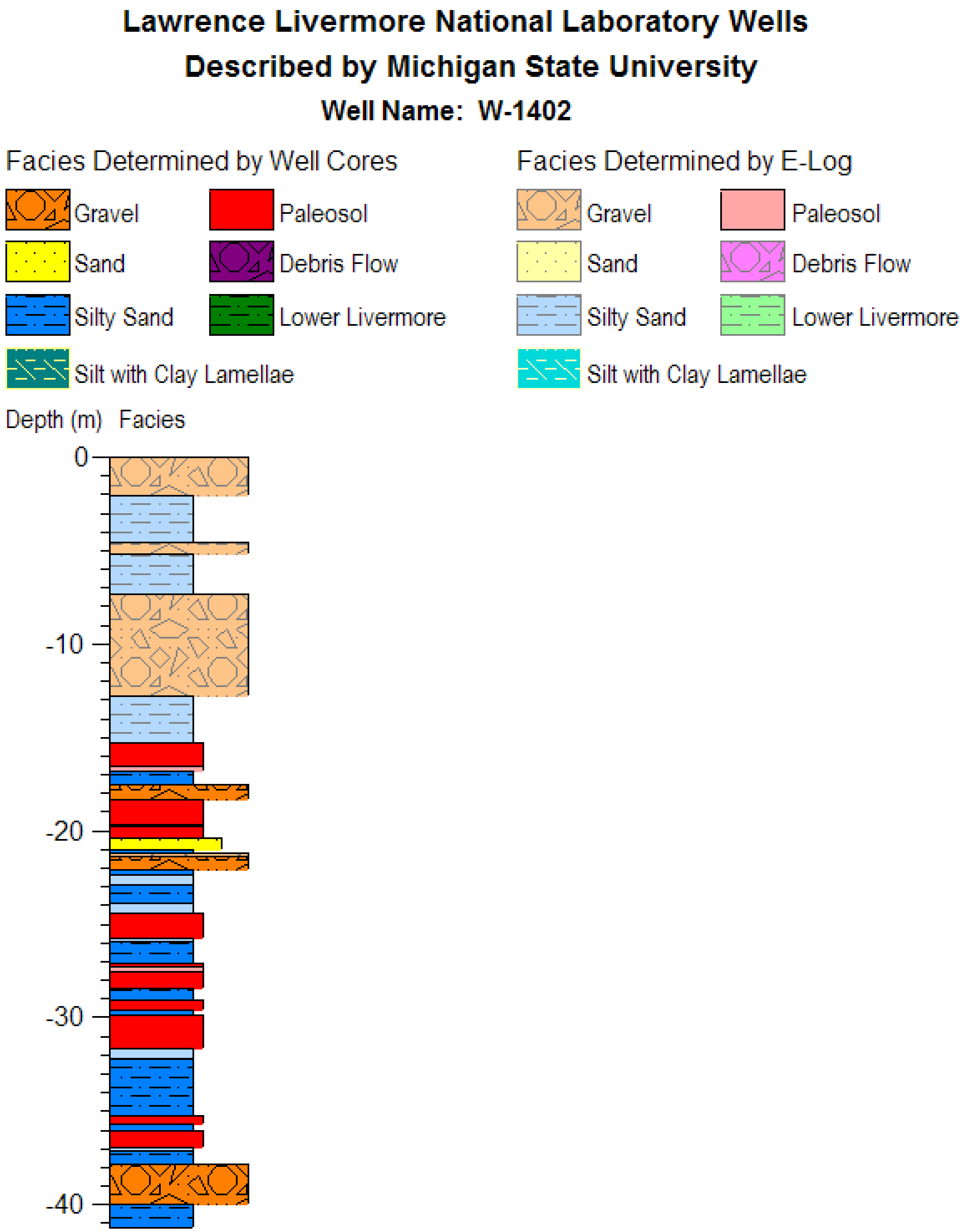

Figure 155. W-1402 stratigraphic column.

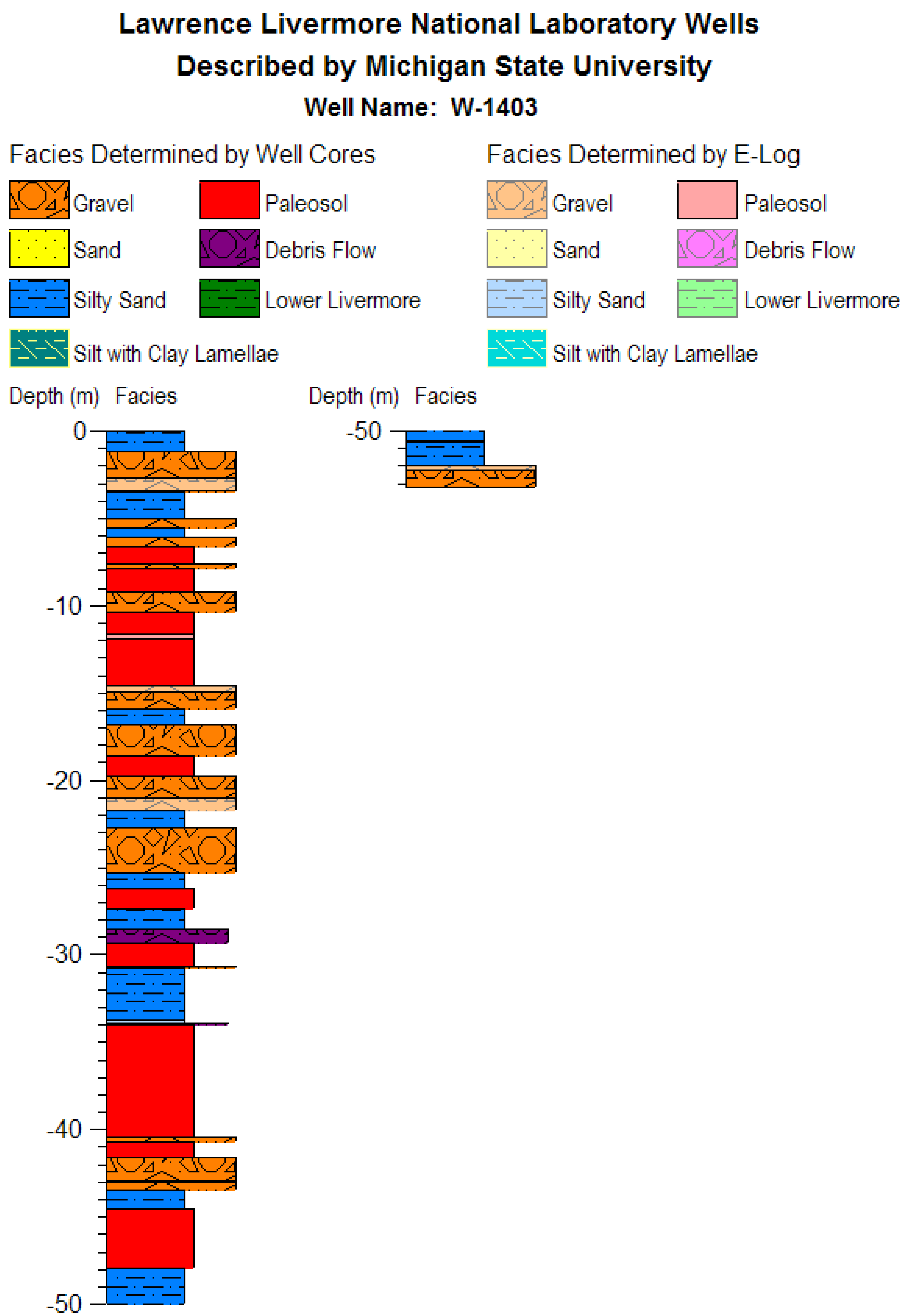

Figure 156. W-1403 stratigraphic column.

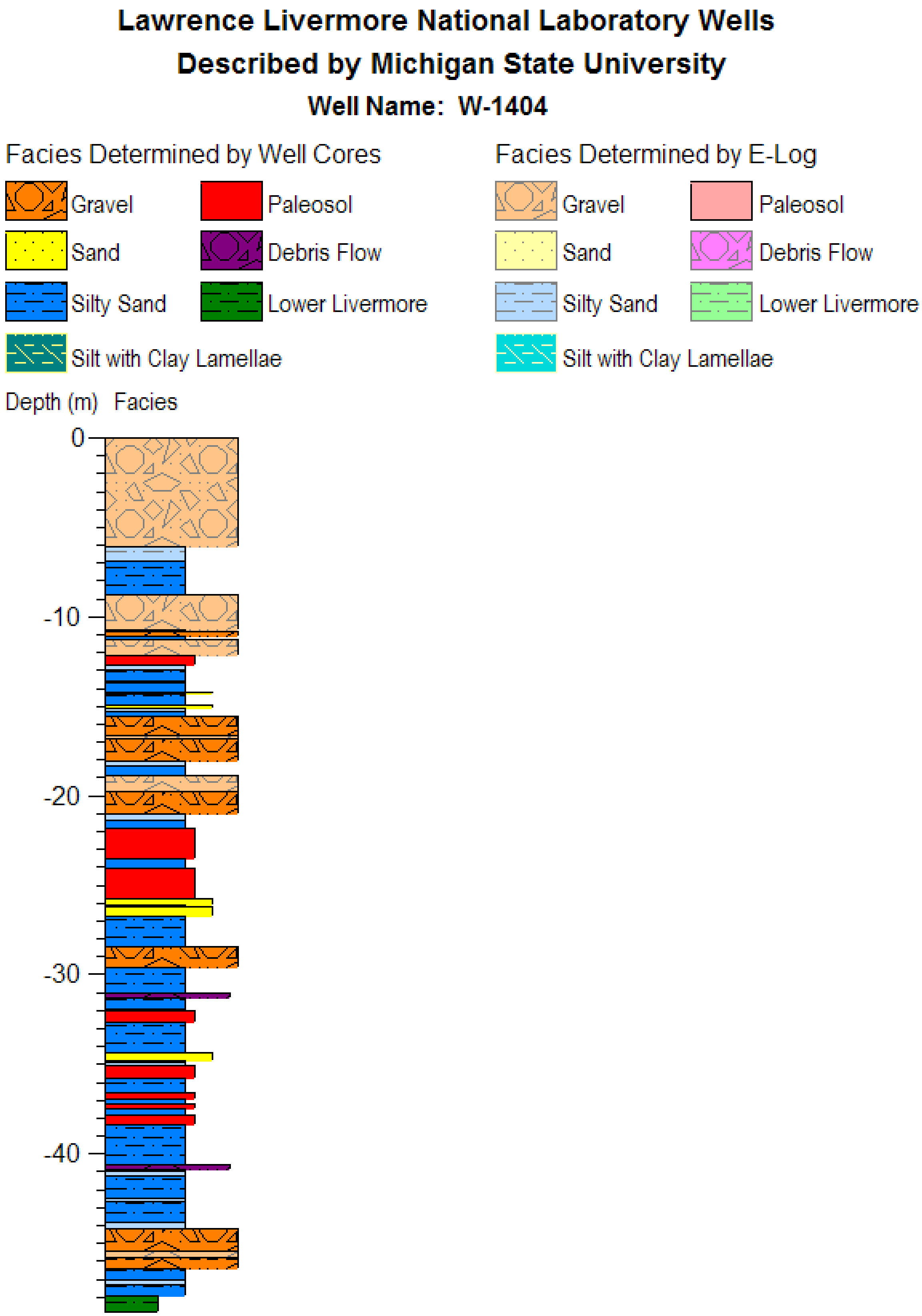

Figure 157. W-1404 stratigraphic column.

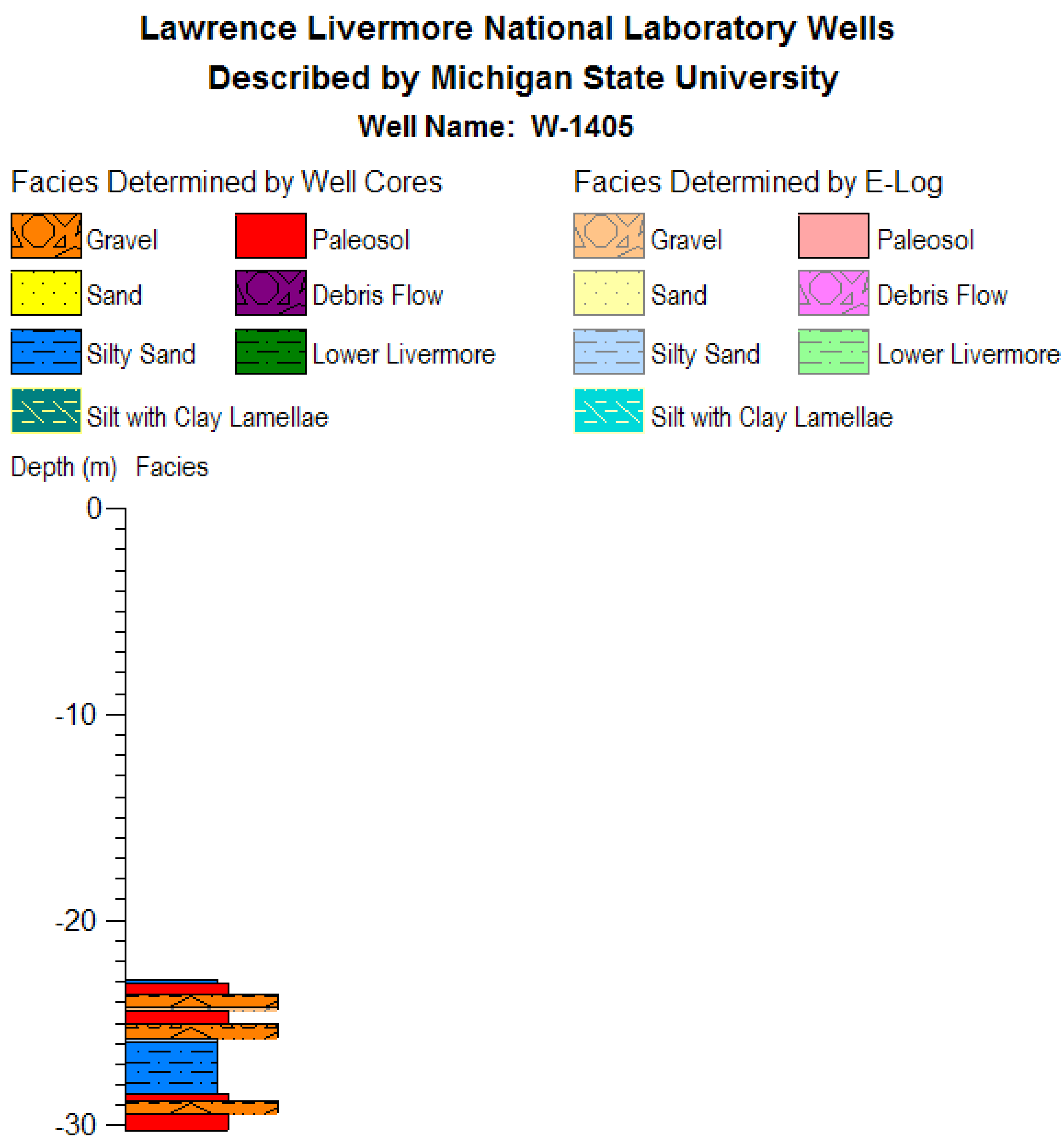

Figure 158. W-1405 stratigraphic column.

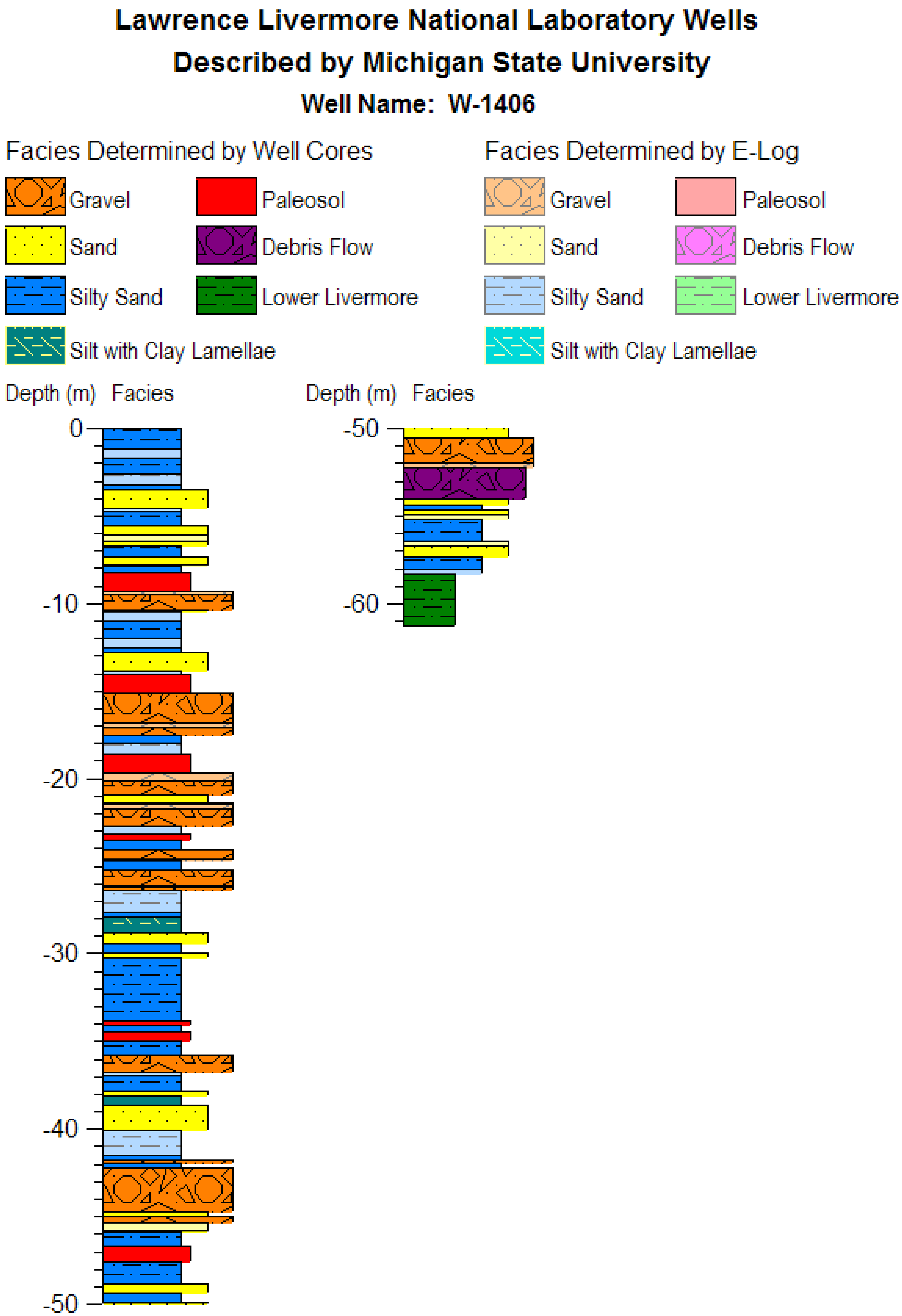

Figure 159. W-1406 stratigraphic column.

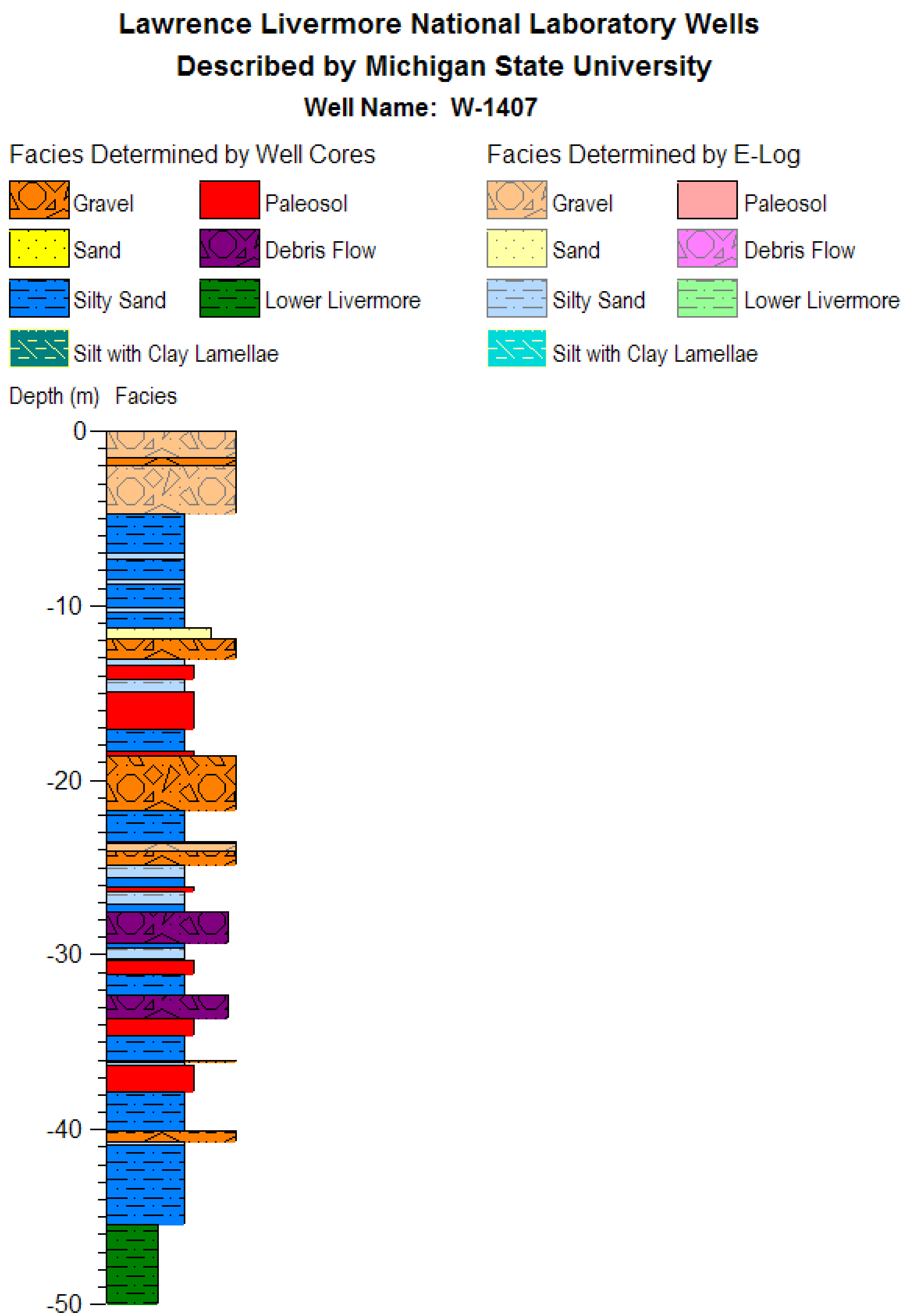

Figure 160. W-1407 stratigraphic column.

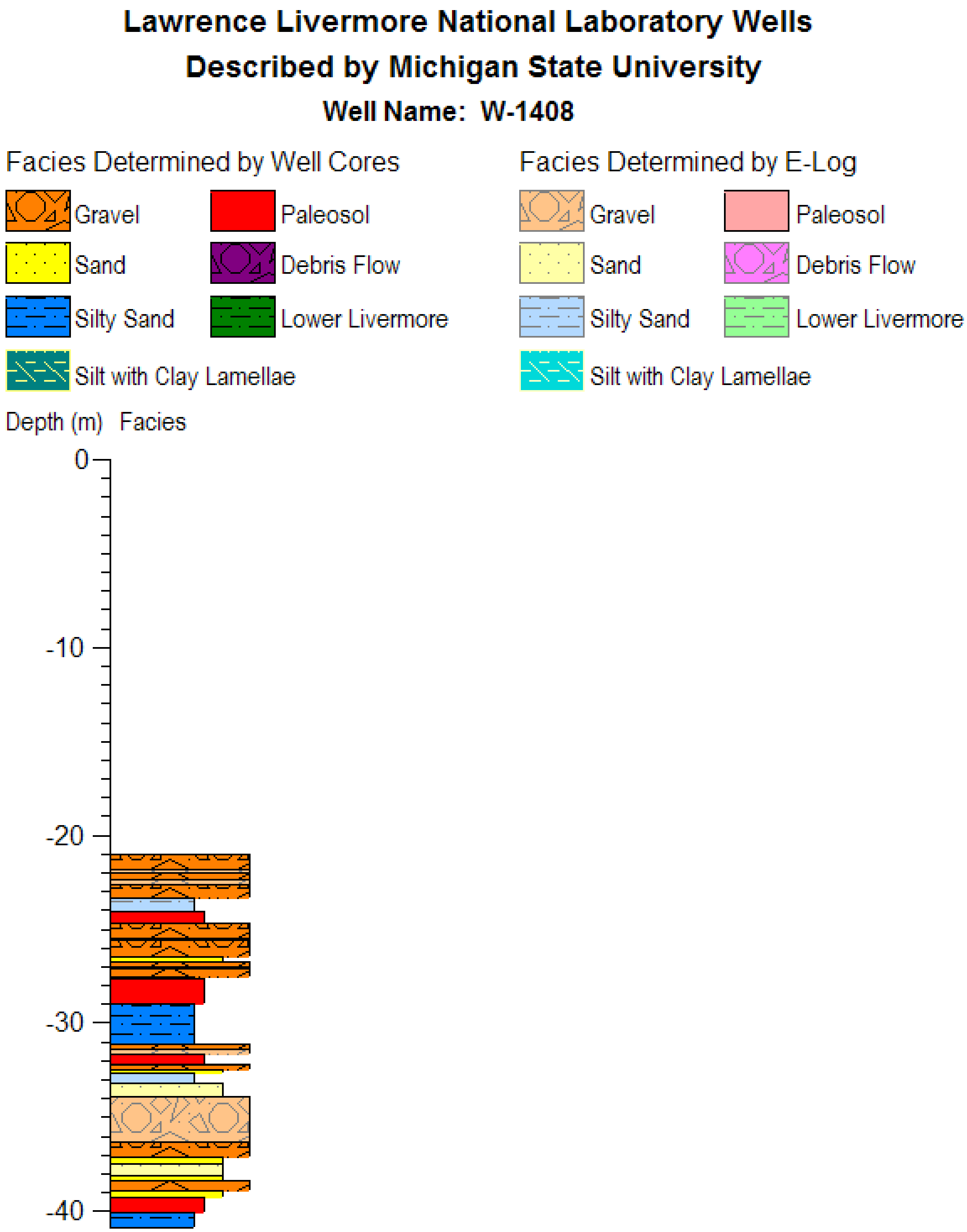

Figure 161. W-1408 stratigraphic column.

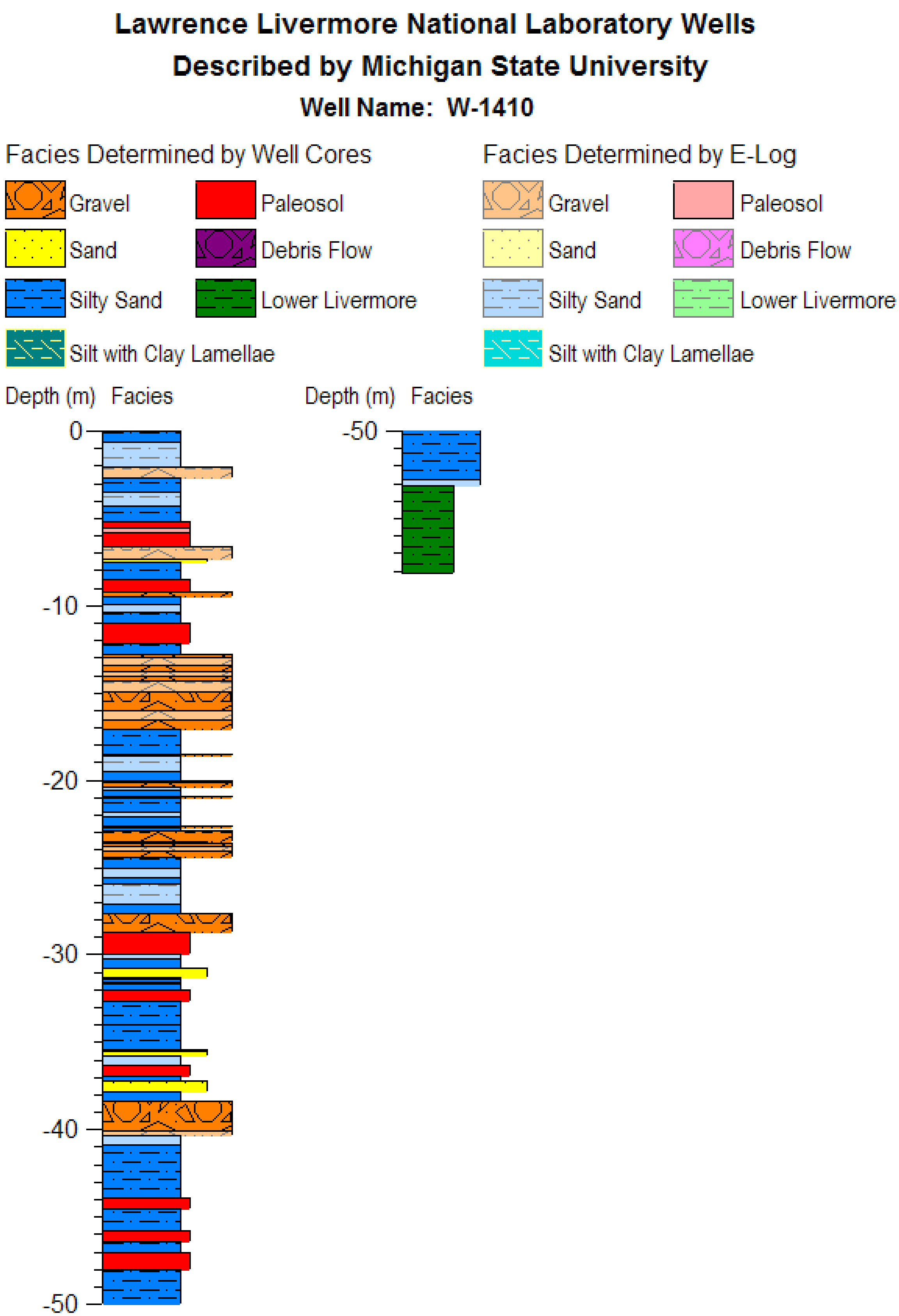

Figure 162. W-1410 stratigraphic column.

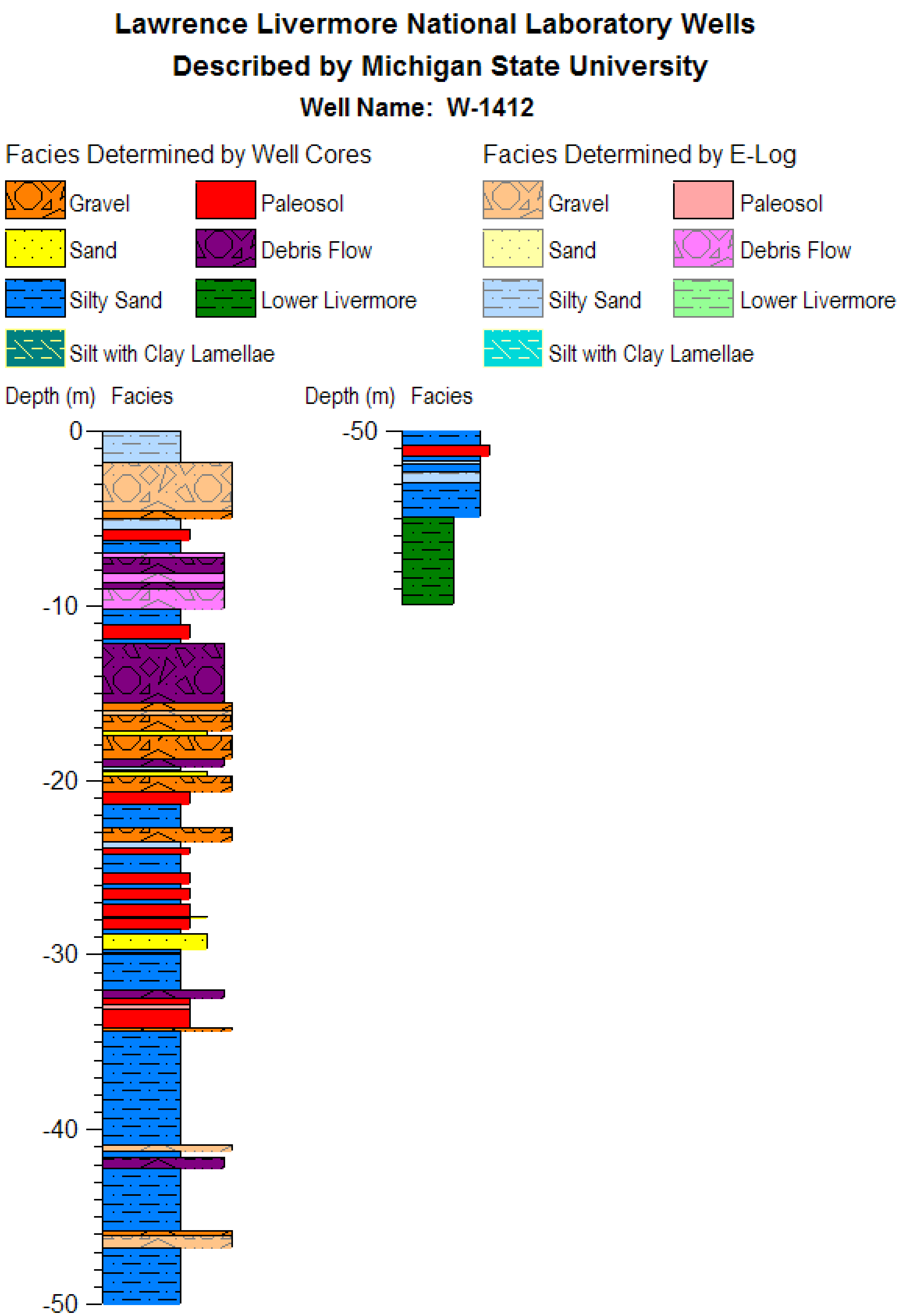

Figure 163. W-1412 stratigraphic column.

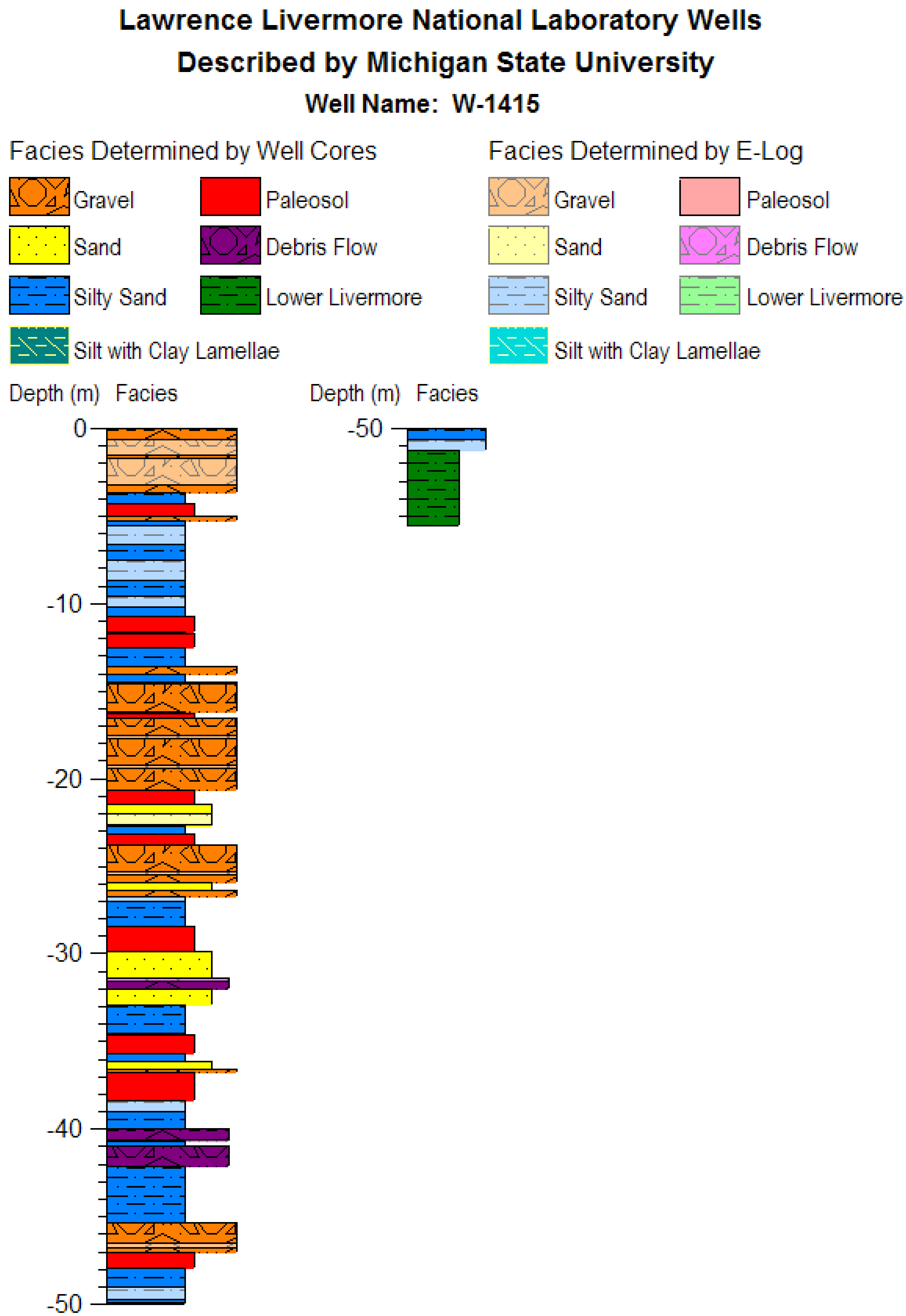

Figure 164. W-1415 stratigraphic column.

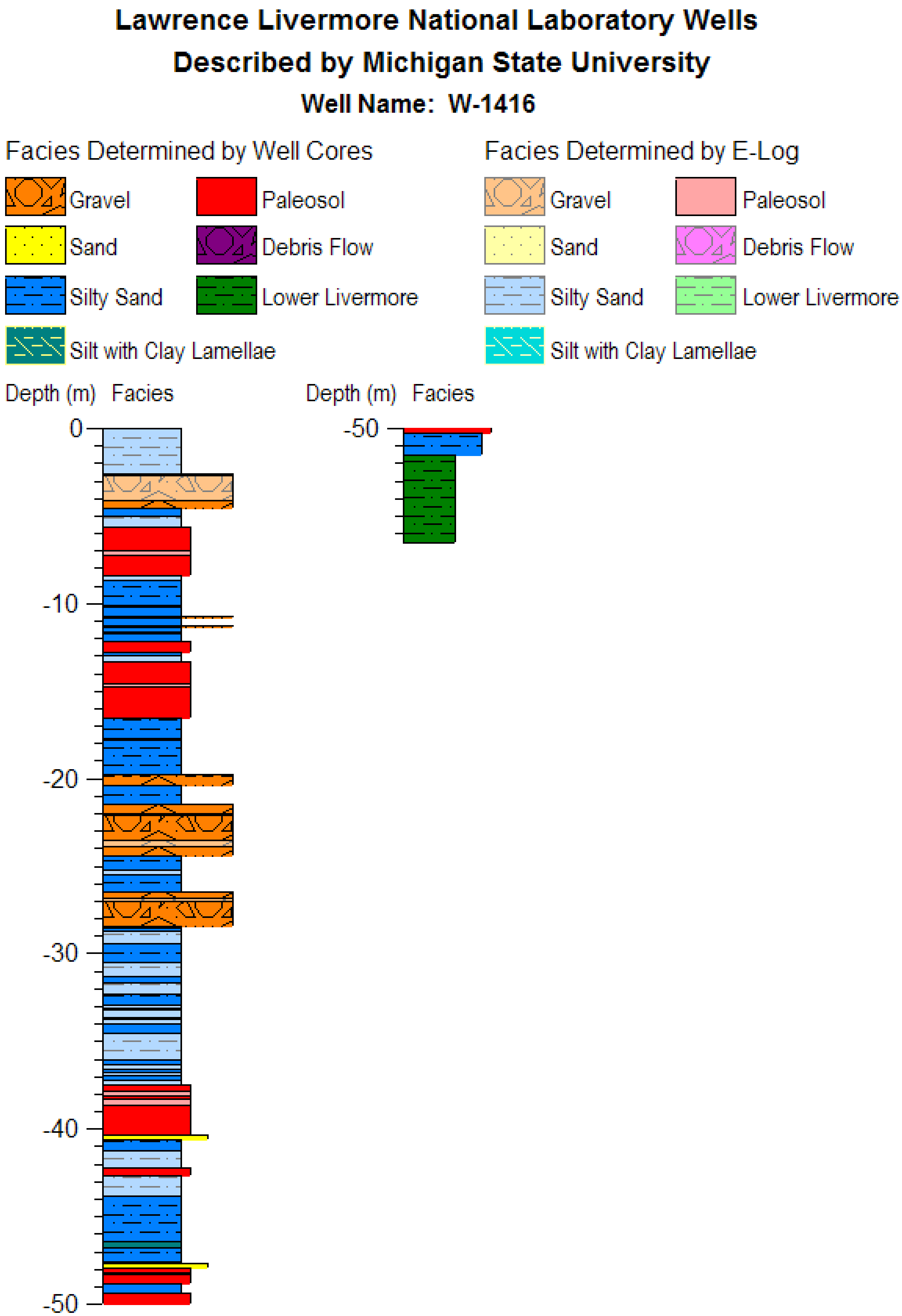

Figure 165. W-1416 stratigraphic column.

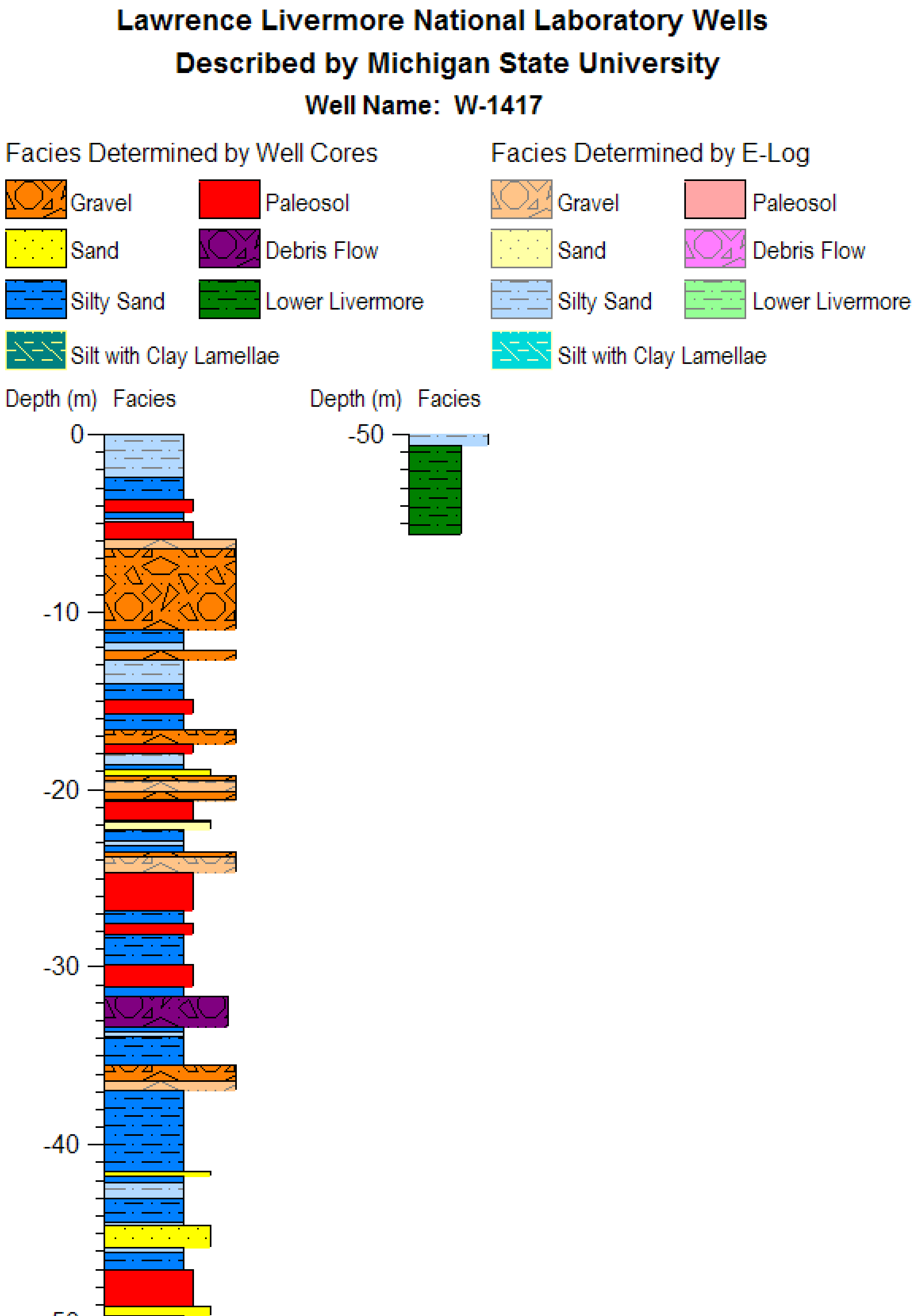

Figure 166. W-1417 stratigraphic column.

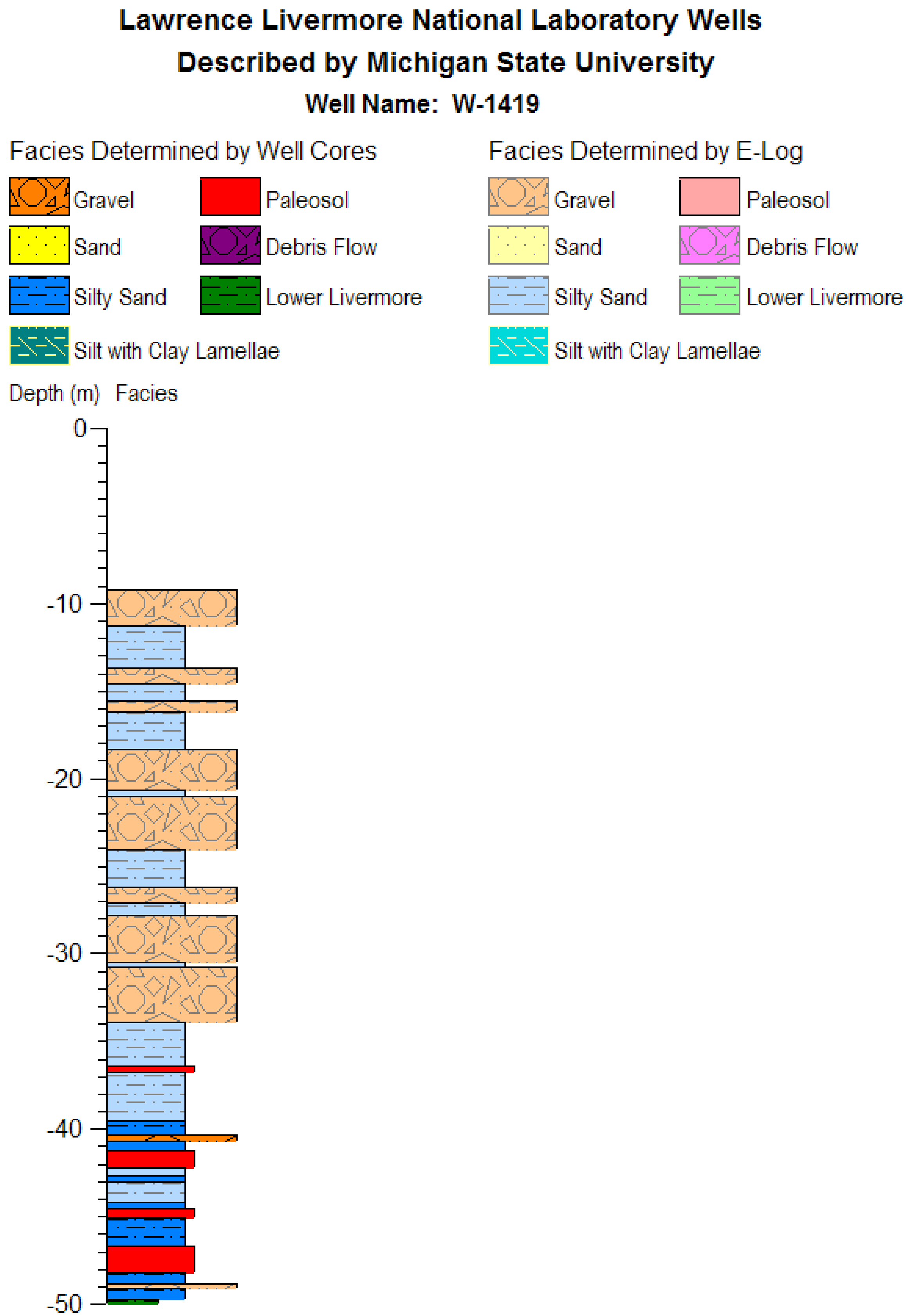

Figure 167. W-1419 stratigraphic column.

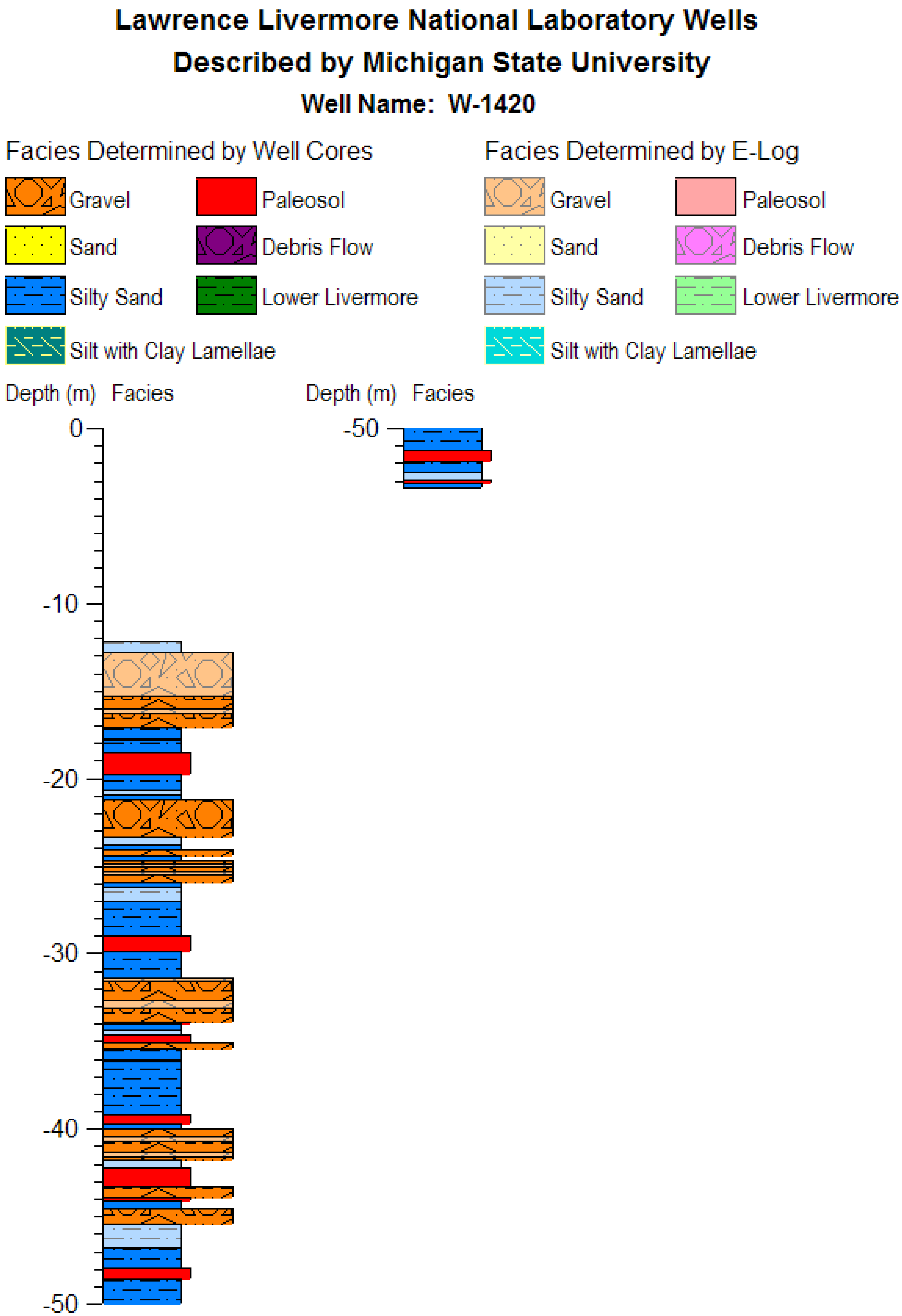

Figure 168. W-1420 stratigraphic column.

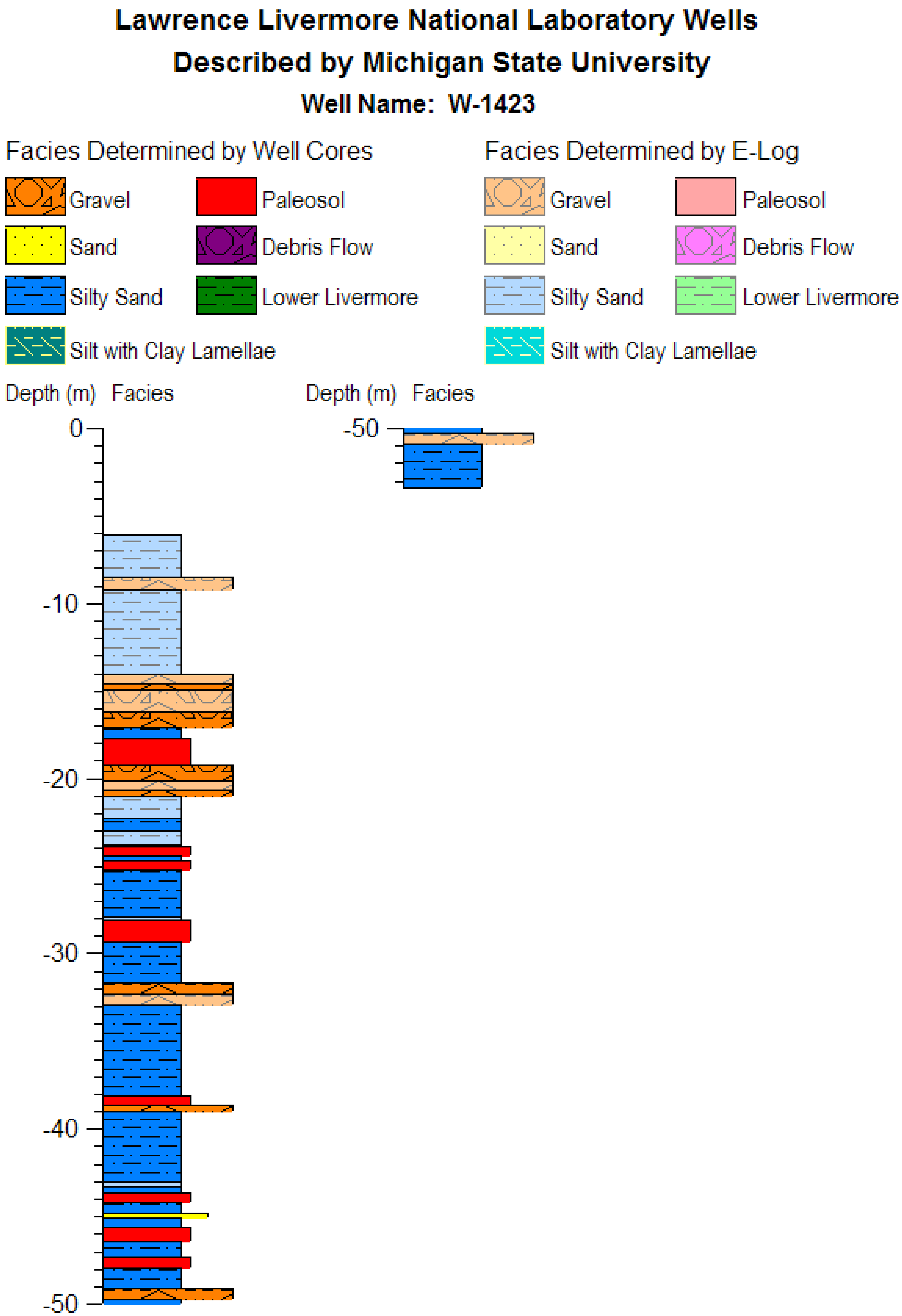

Figure 169. W-1423 stratigraphic column.

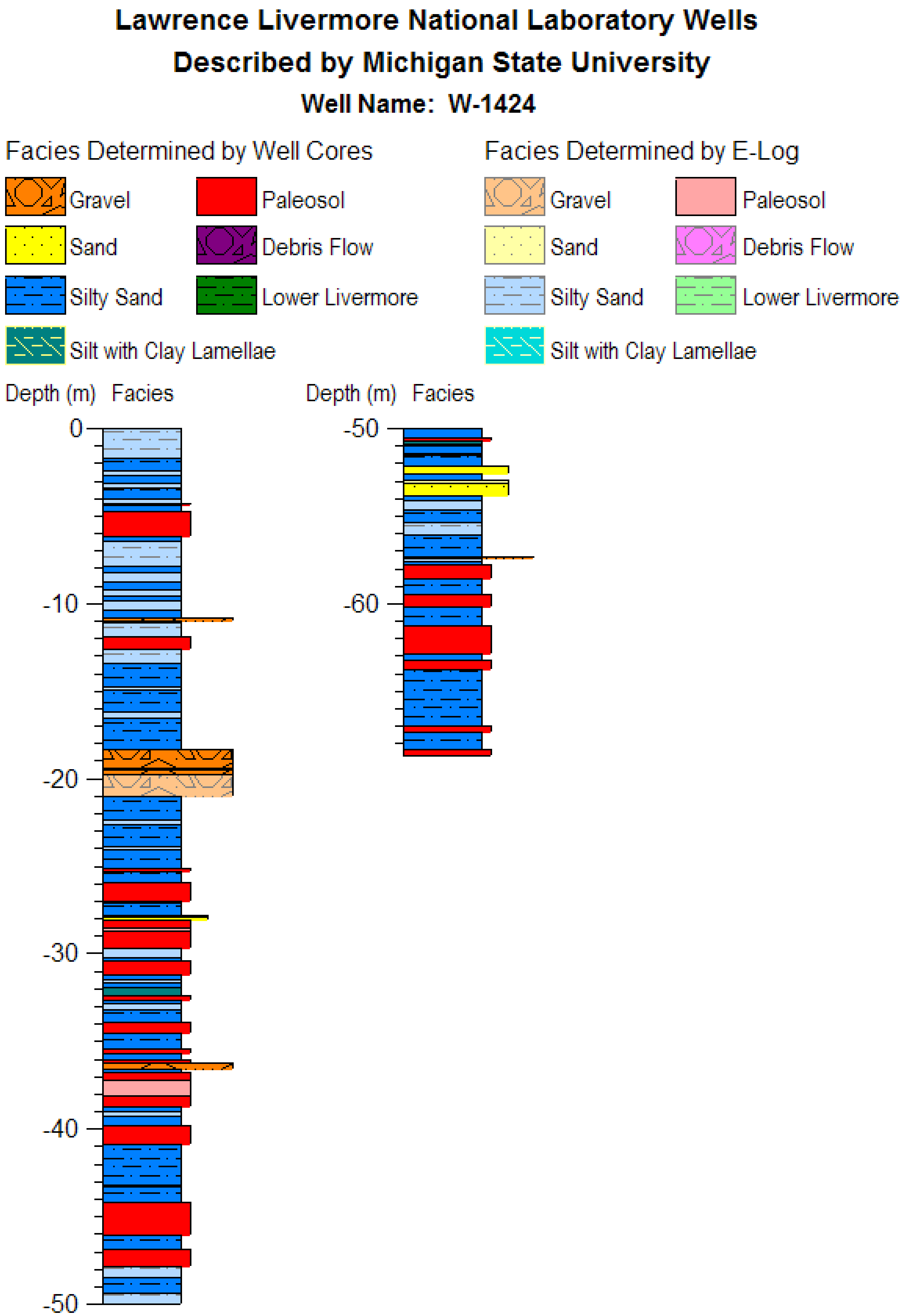

Figure 170. W-1424 stratigraphic column.

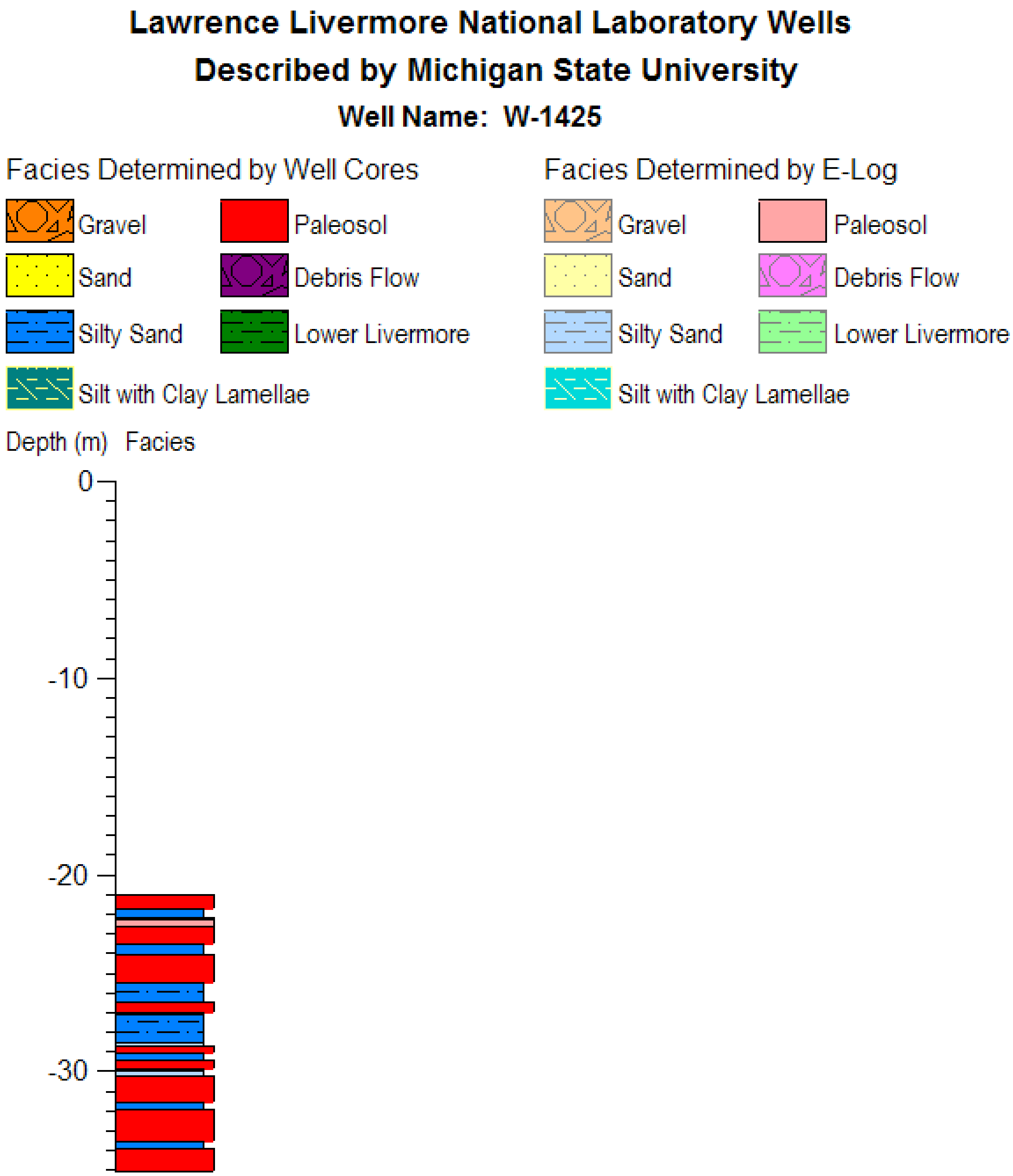

Figure 171. W-1425 stratigraphic column.

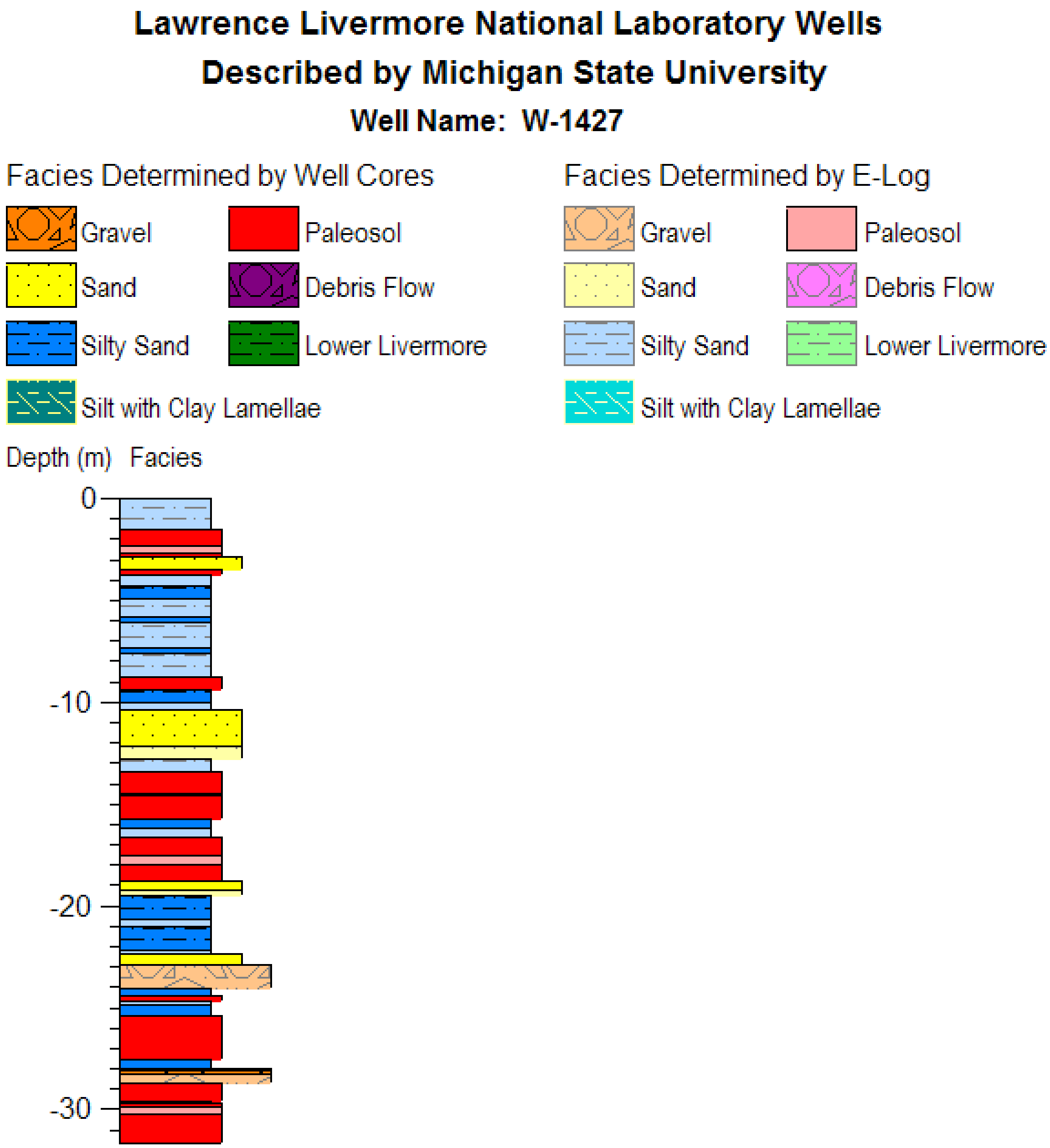

Figure 172. W-1427 stratigraphic column.

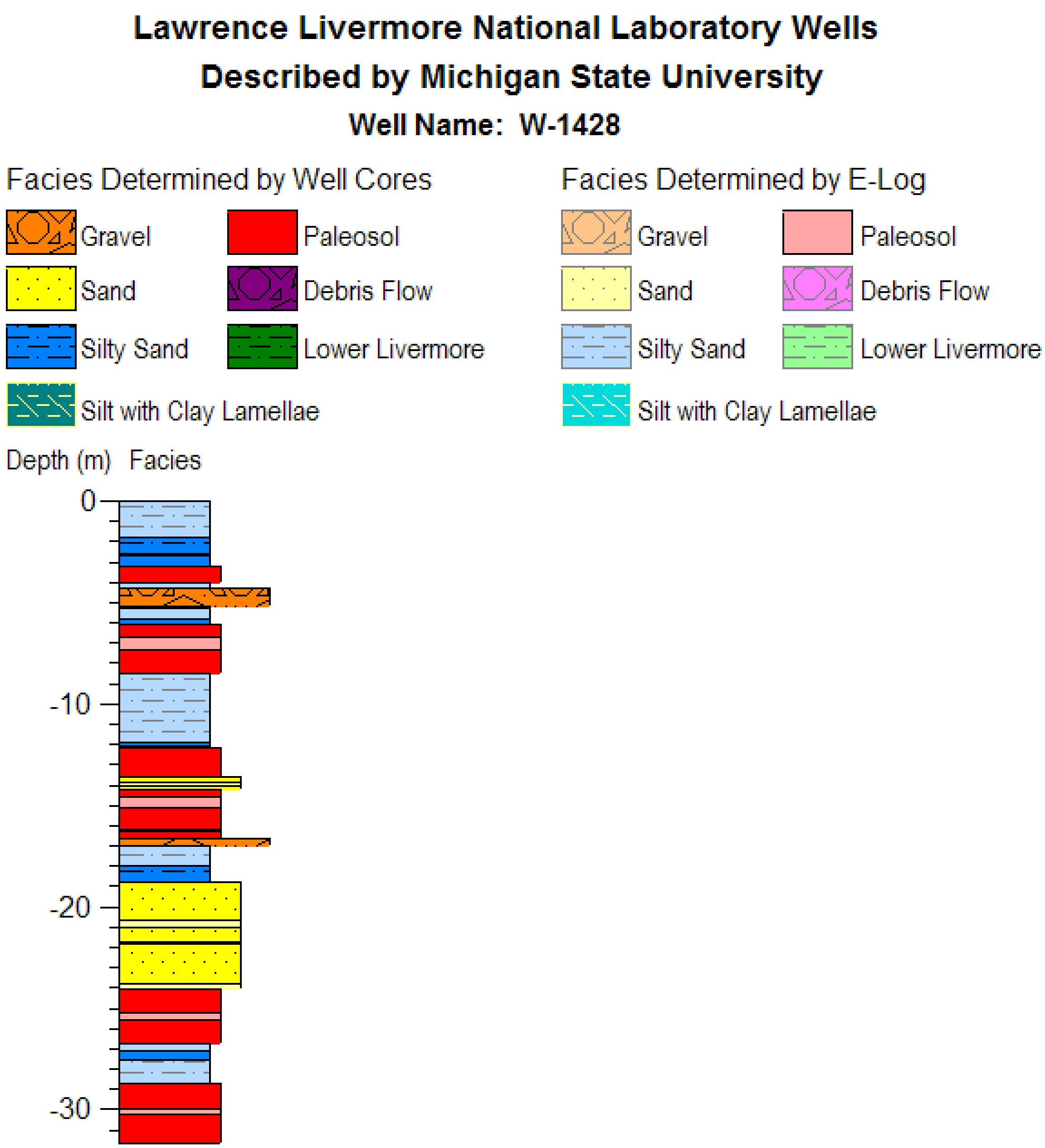

Figure 173. W-1428 stratigraphic column.

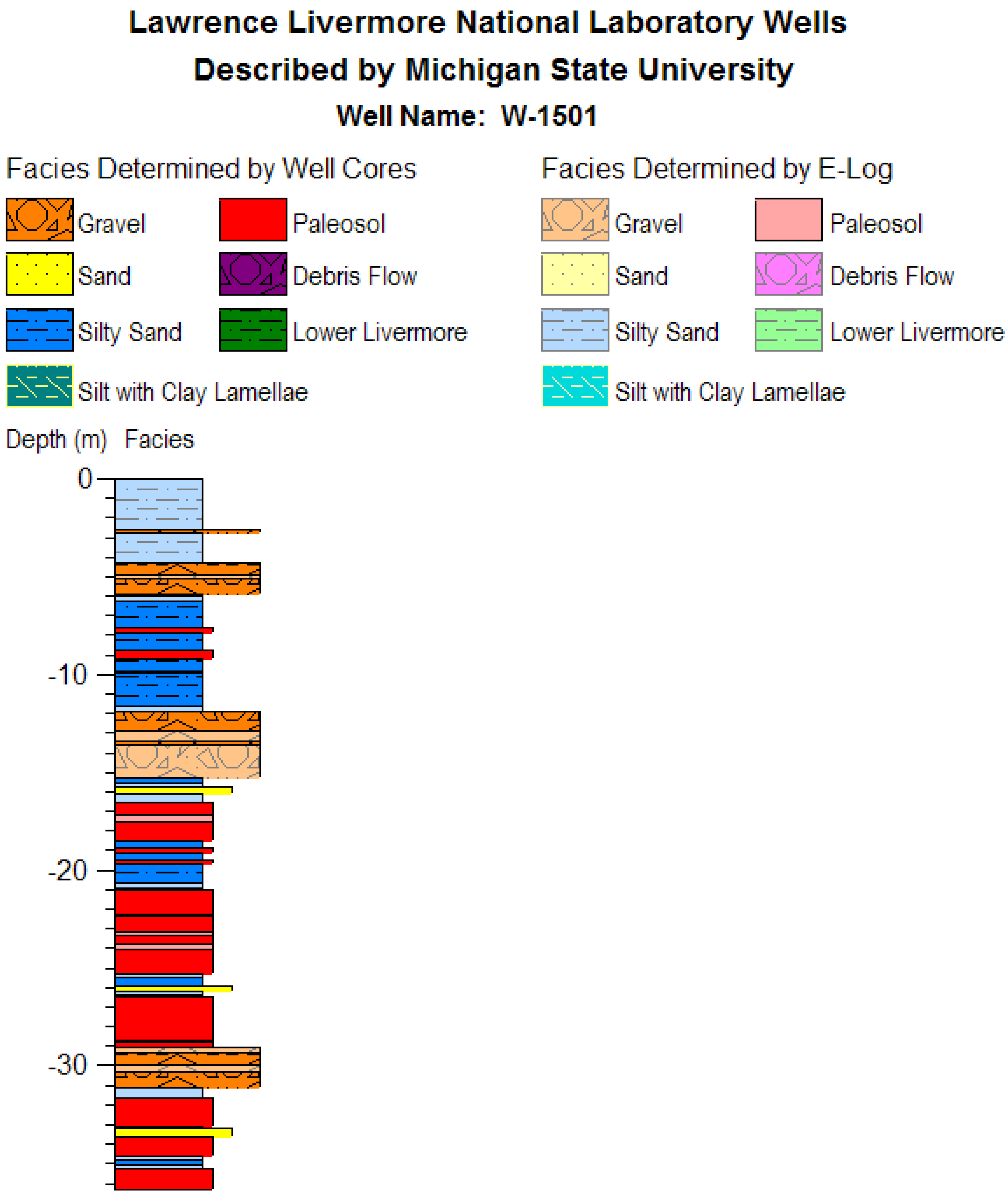

Figure 174. W-1501 stratigraphic column.

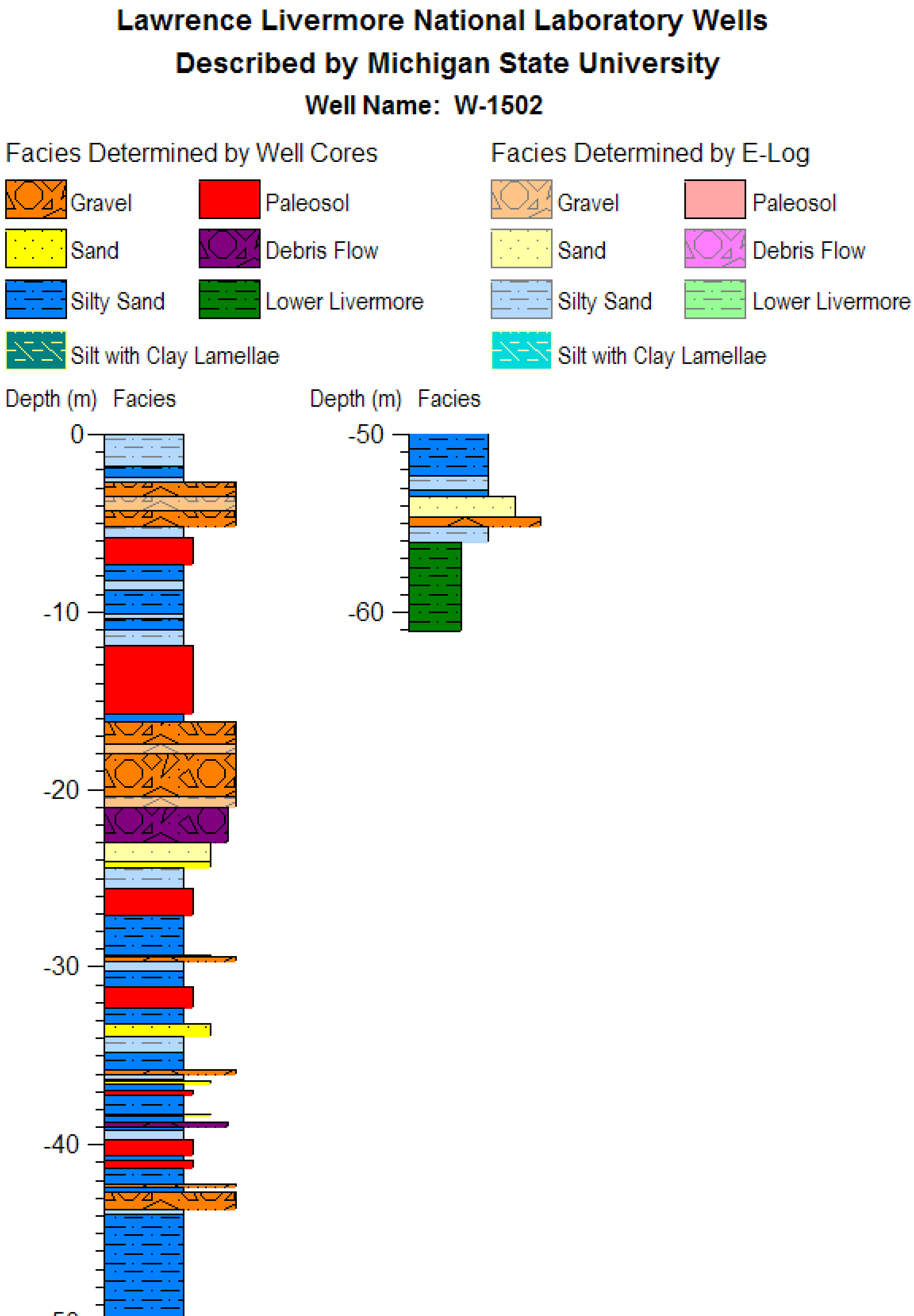

Figure 175. W-1502 stratigraphic column.

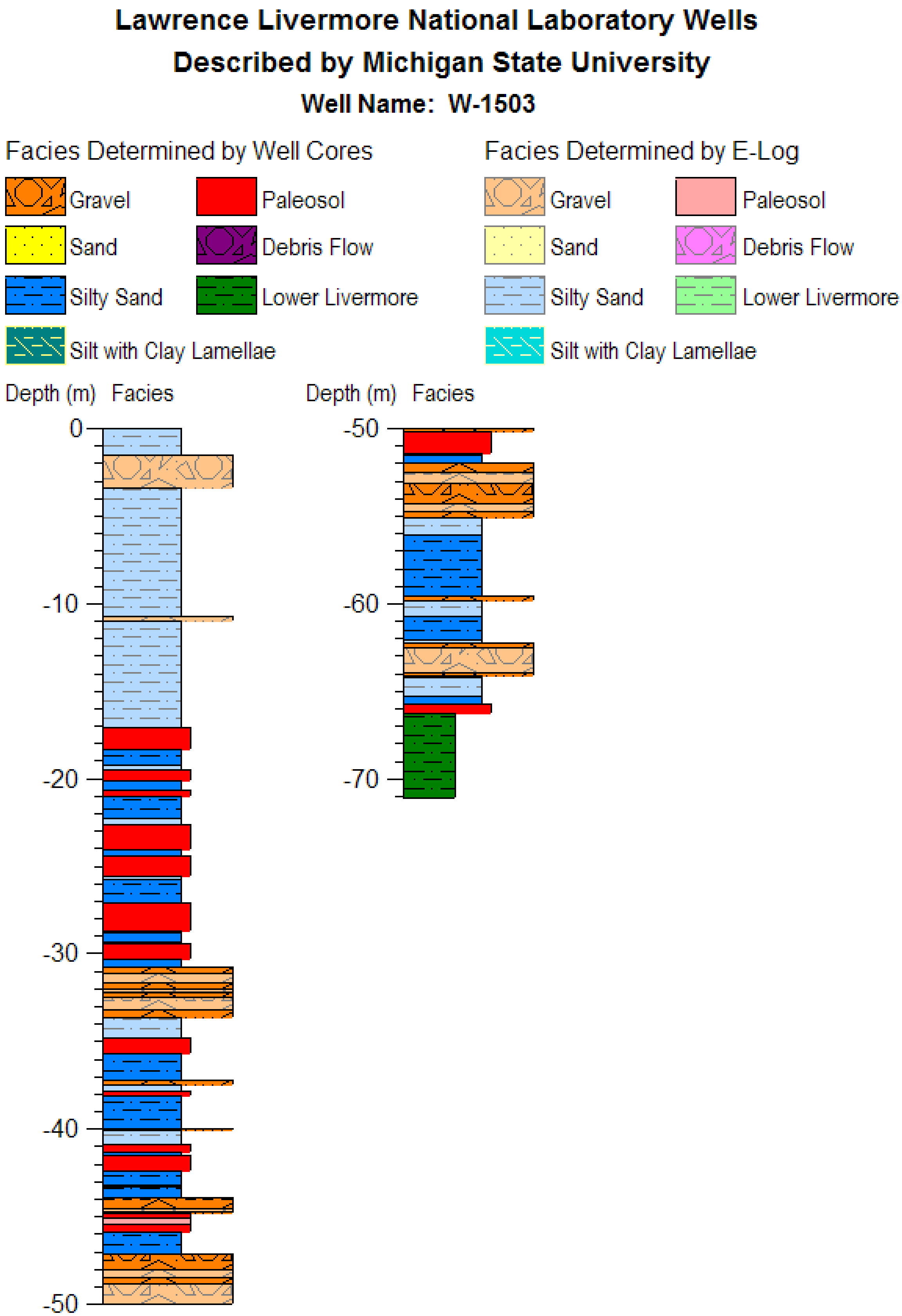

Figure 176. W-1503 stratigraphic column.

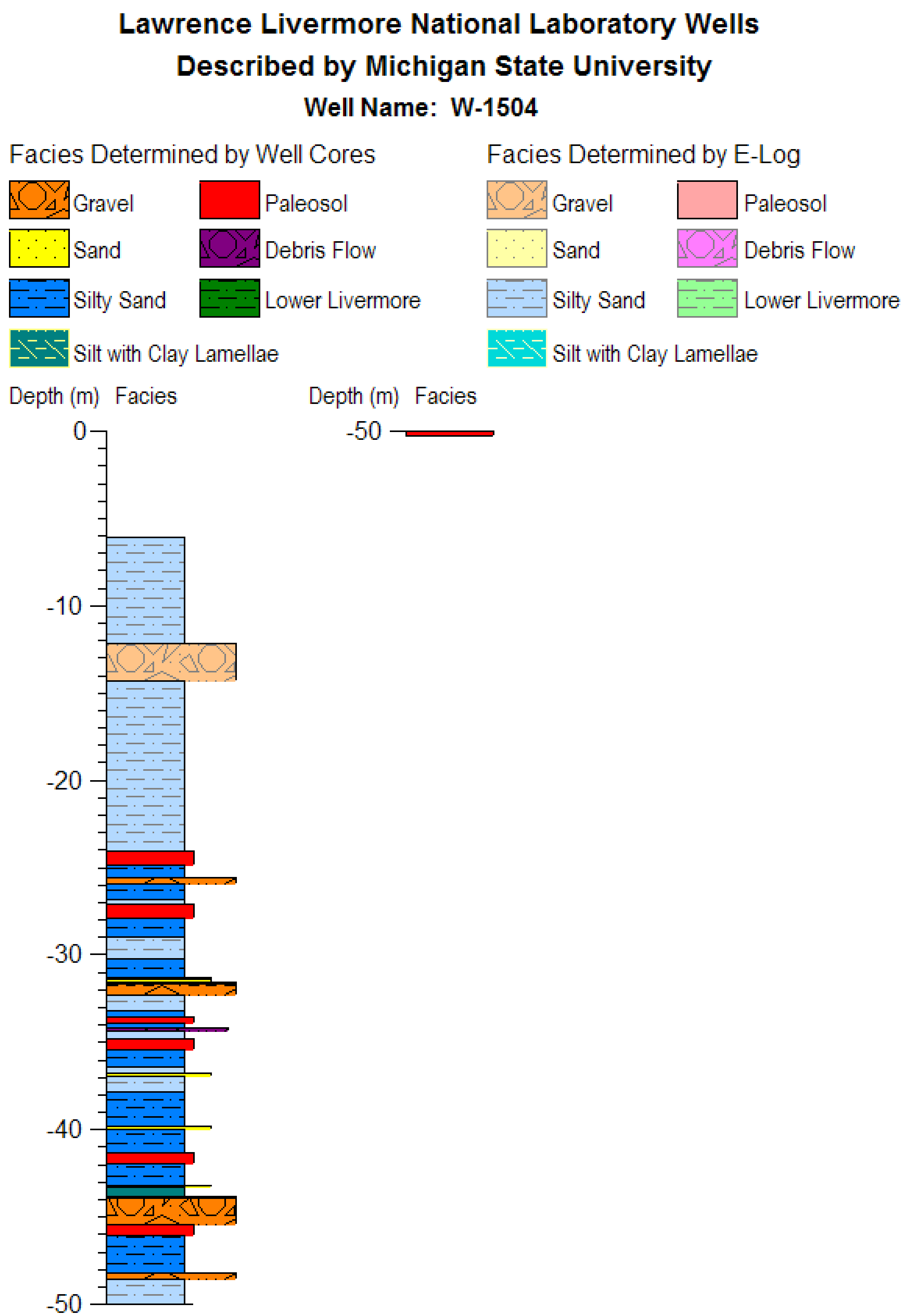

Figure 177. W-1504 stratigraphic column.

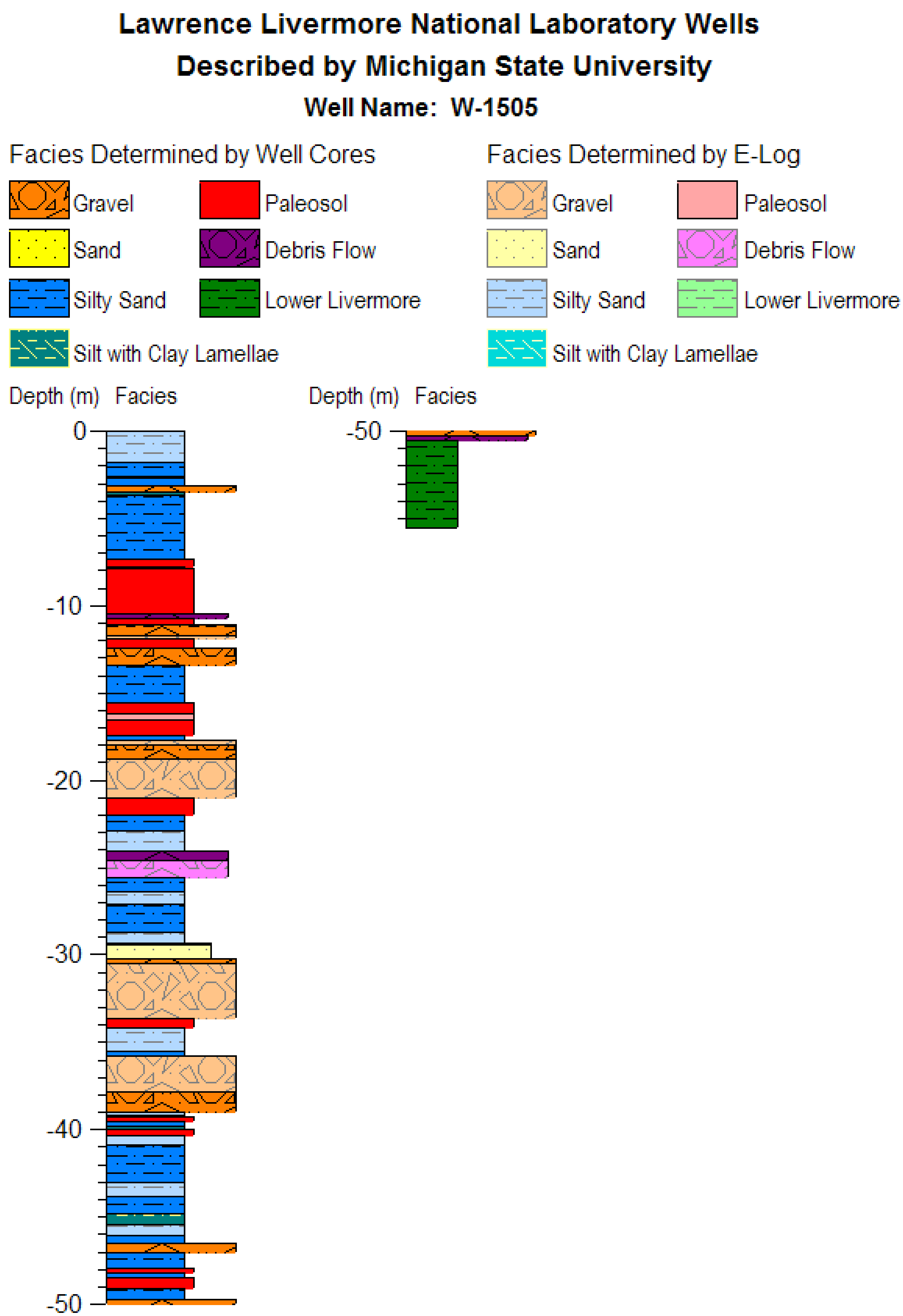

Figure 178. W-1505 stratigraphic column.

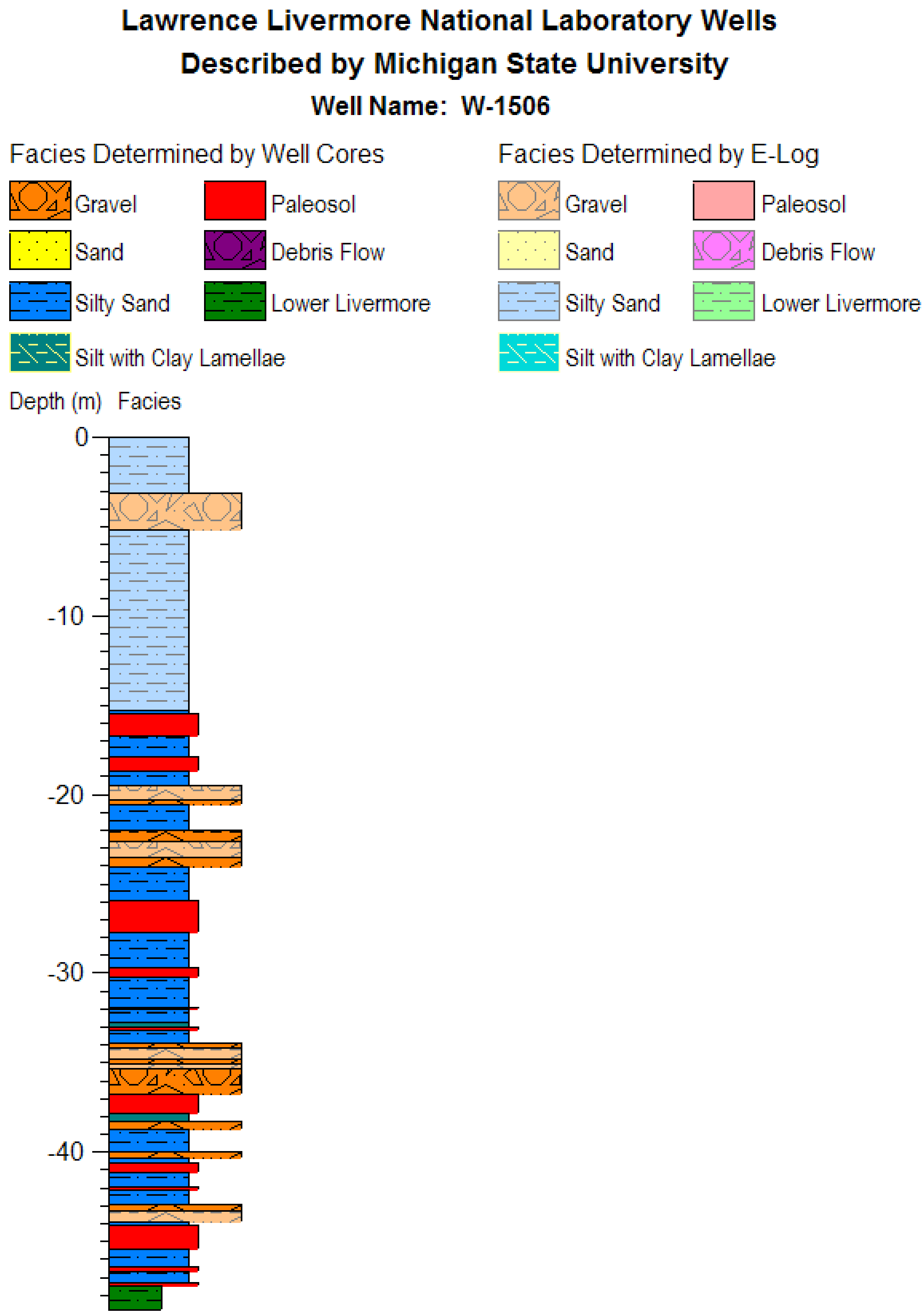

Figure 179. W-1506 stratigraphic column.

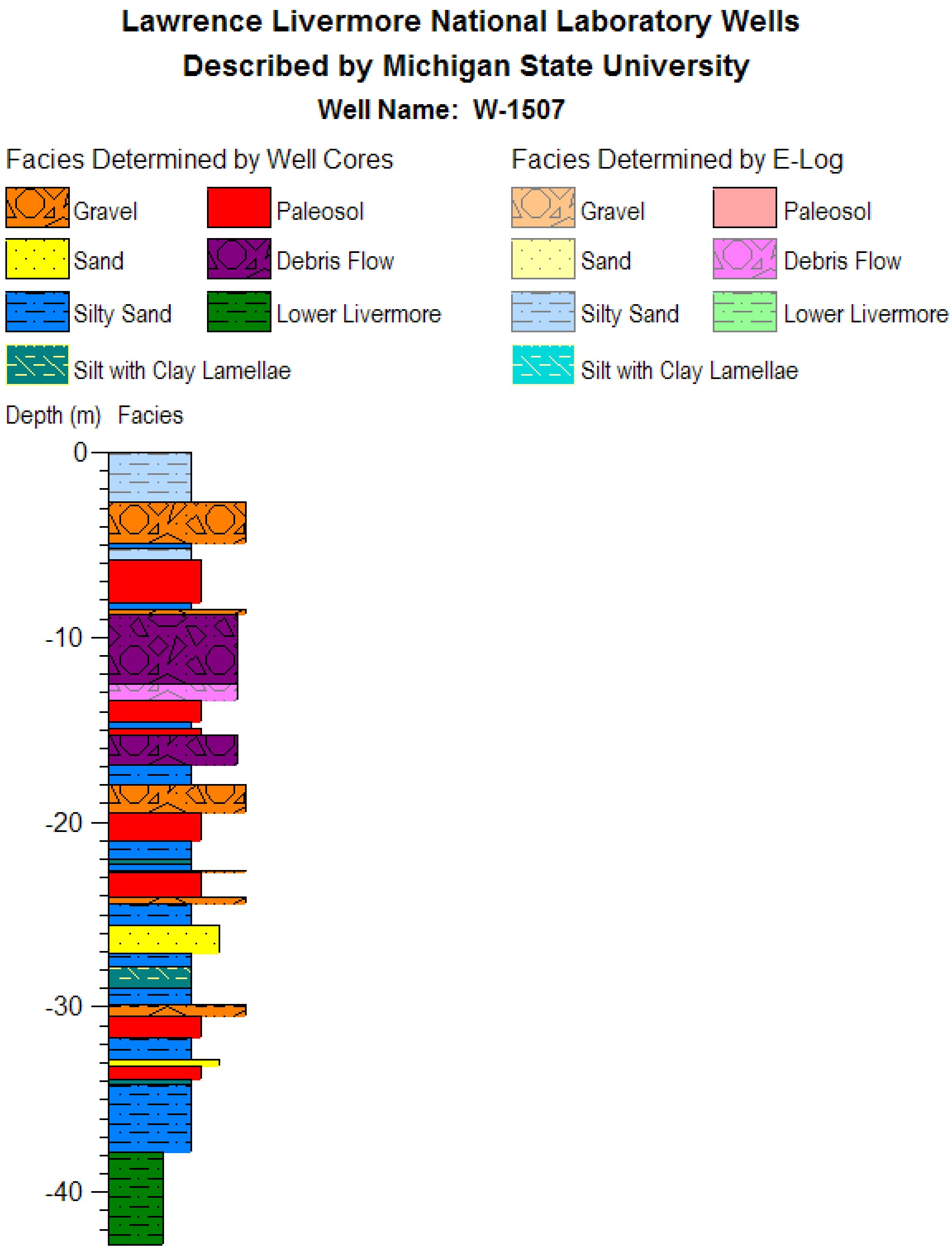

Figure 180. W-1507 stratigraphic column.

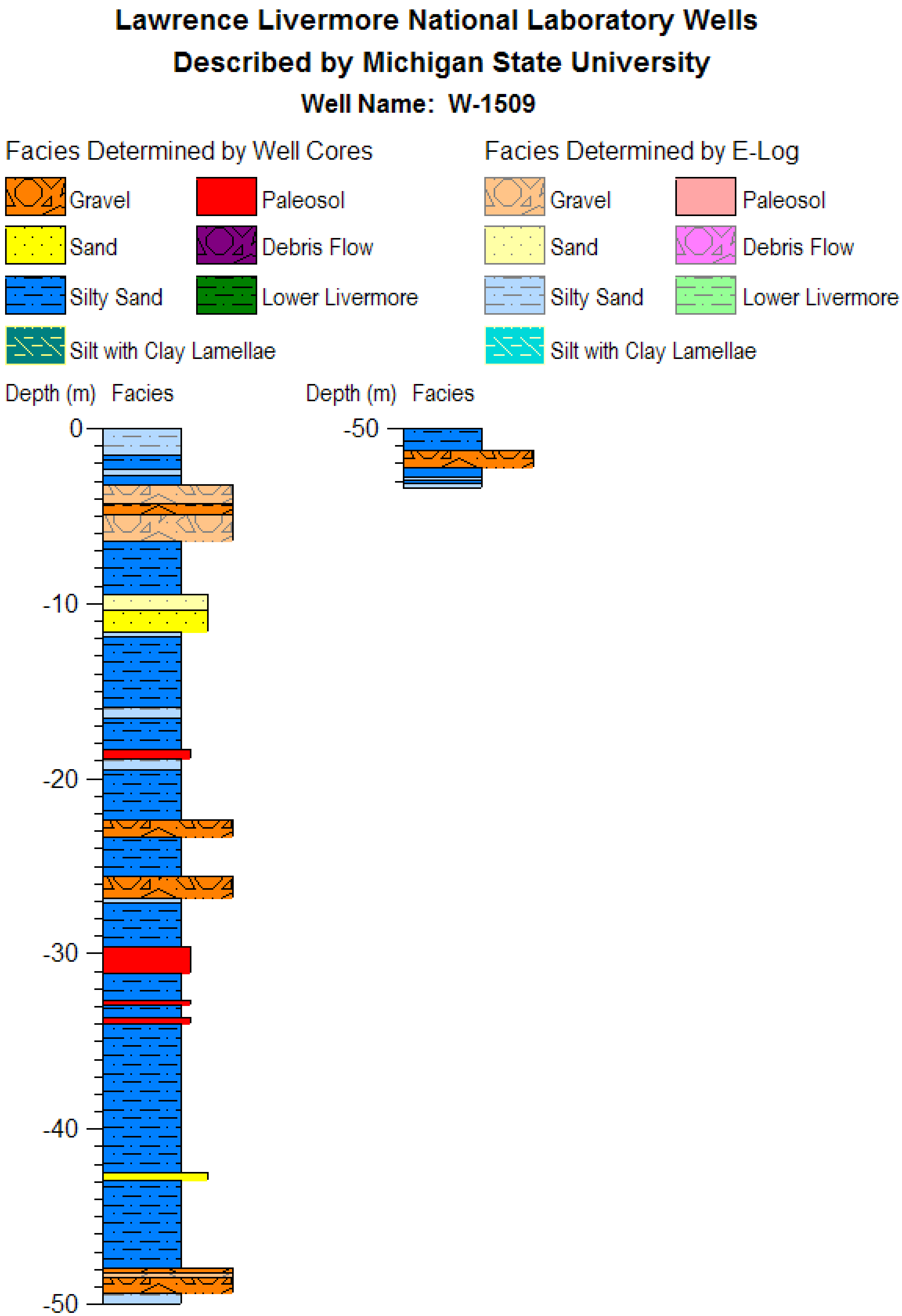

Figure 181. W-1509 stratigraphic column.

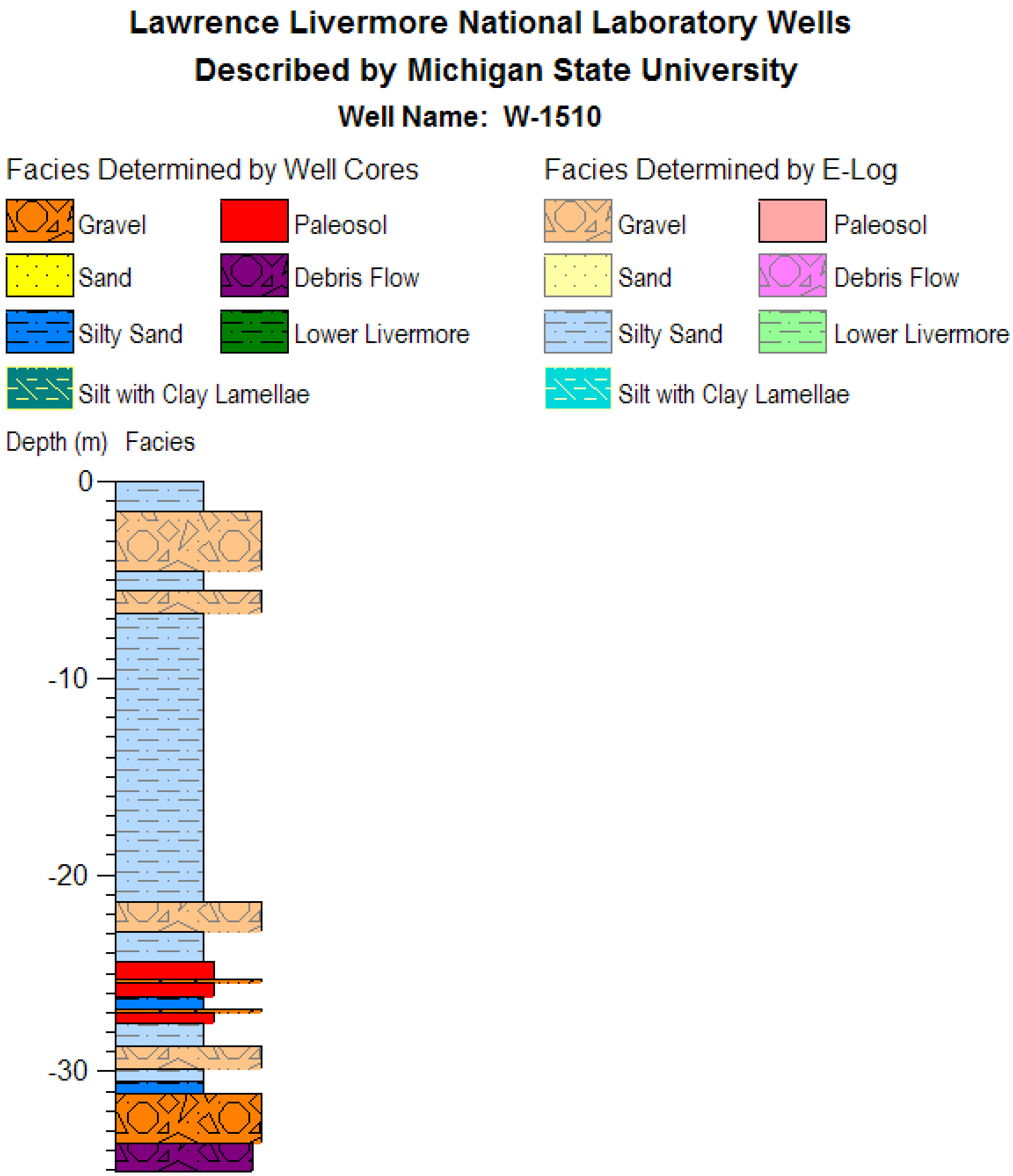

Figure 182. W-1510 stratigraphic column.

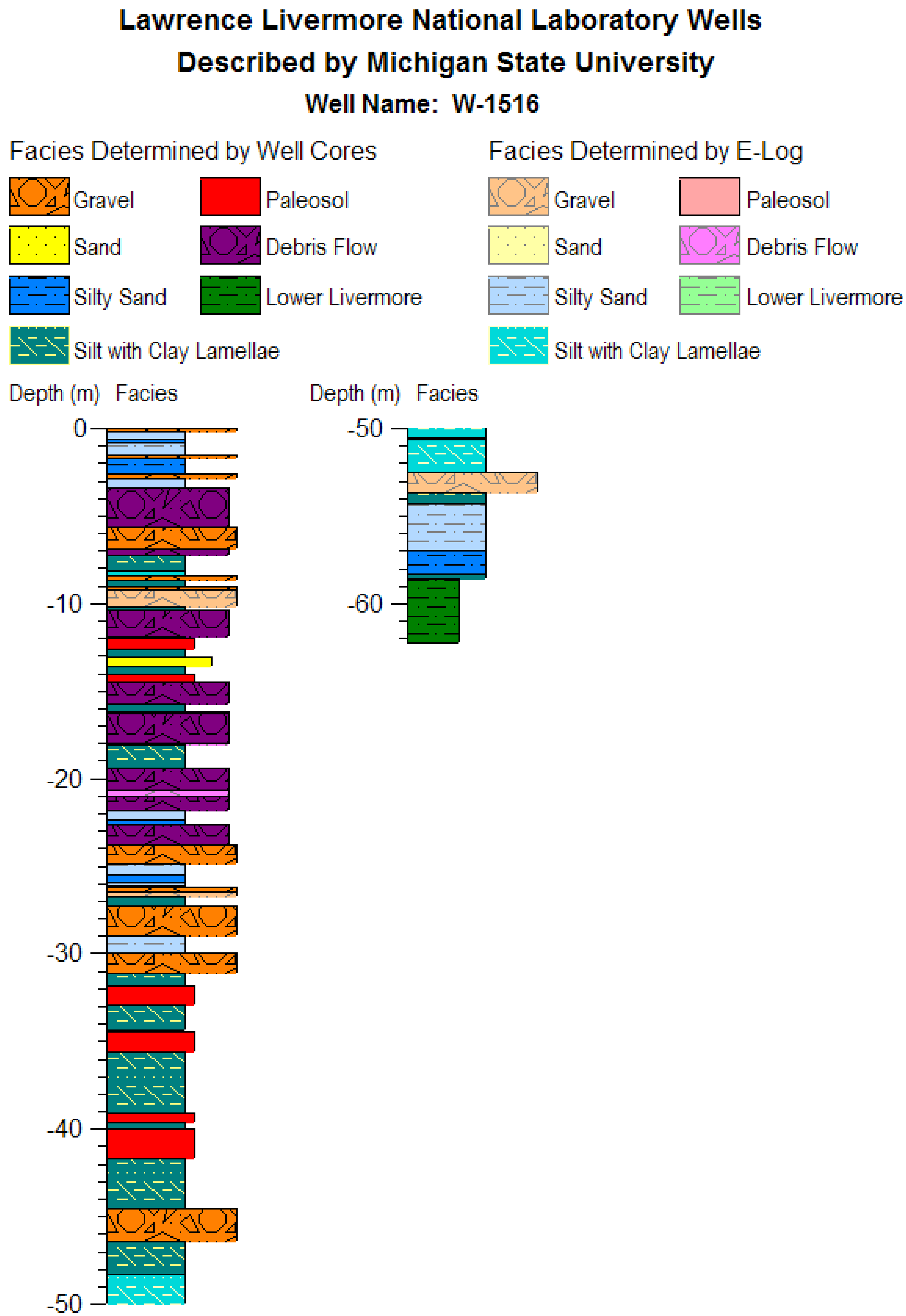

Figure 183. W-1516 stratigraphic column.

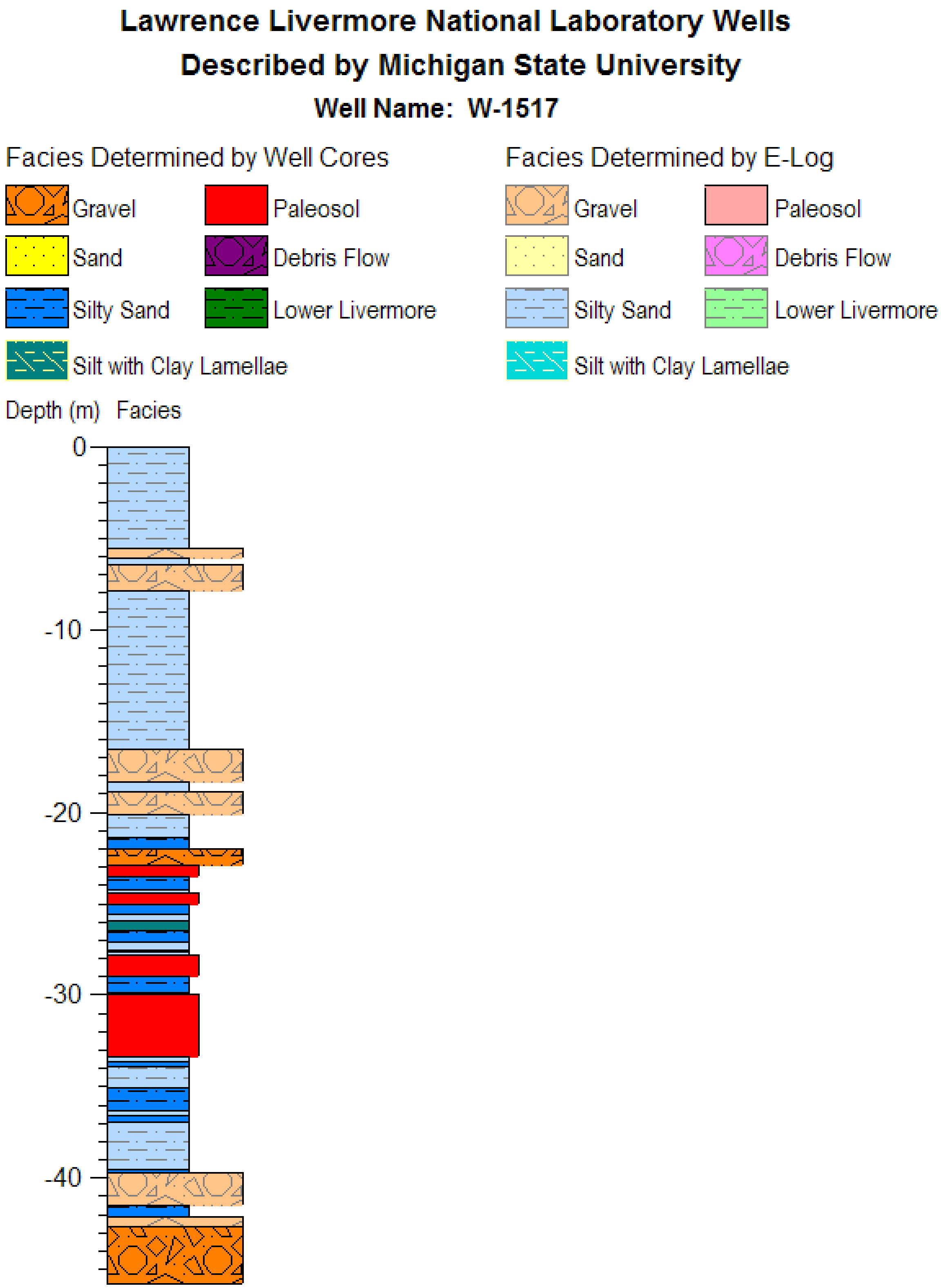

Figure 184. W-1517 stratigraphic column.

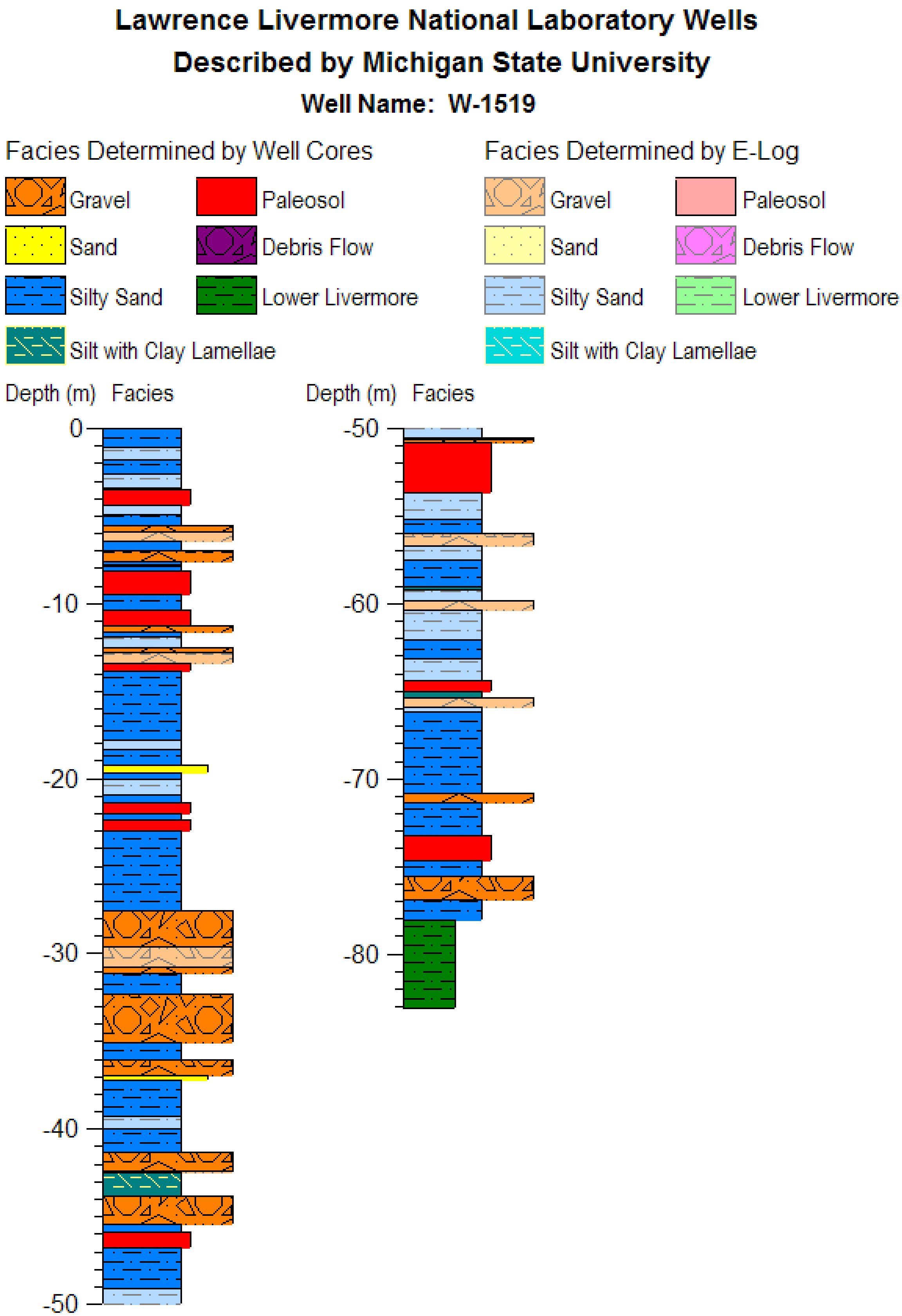

Figure 185. W-1519 stratigraphic column.

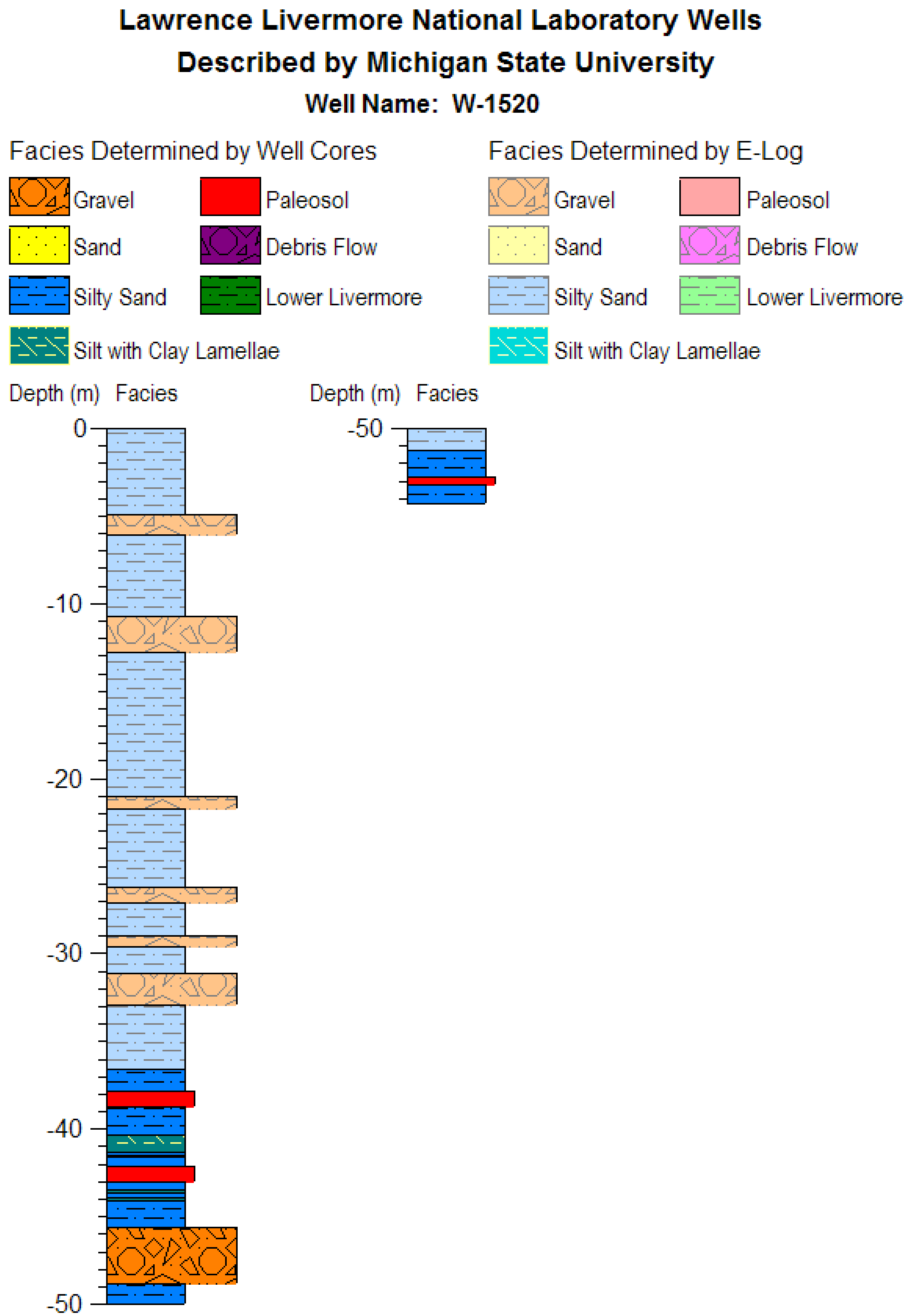

Figure 186. W-1520 stratigraphic column.

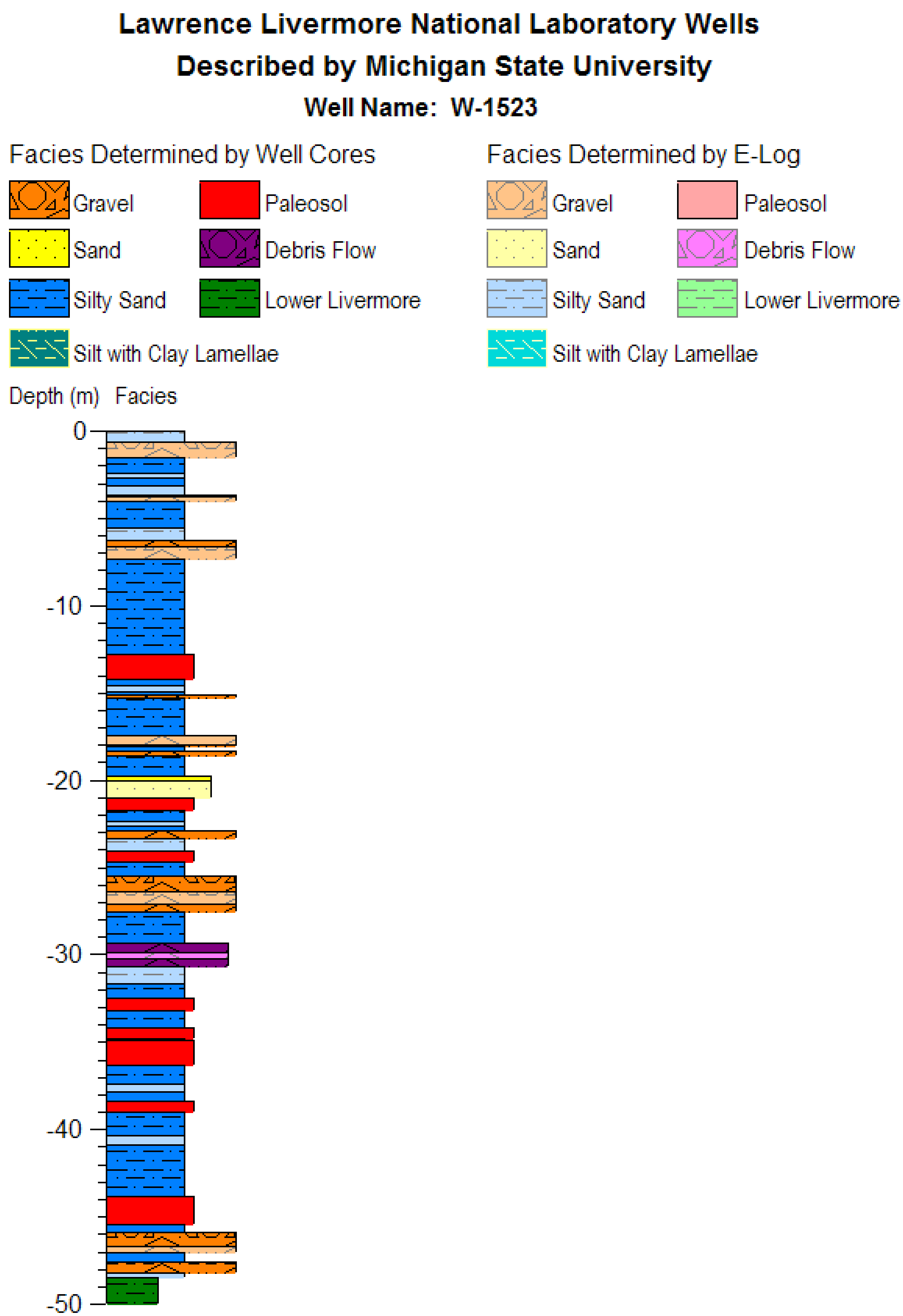

Figure 187. W-1523 stratigraphic column.

Figure 188. W-1550 stratigraphic column.

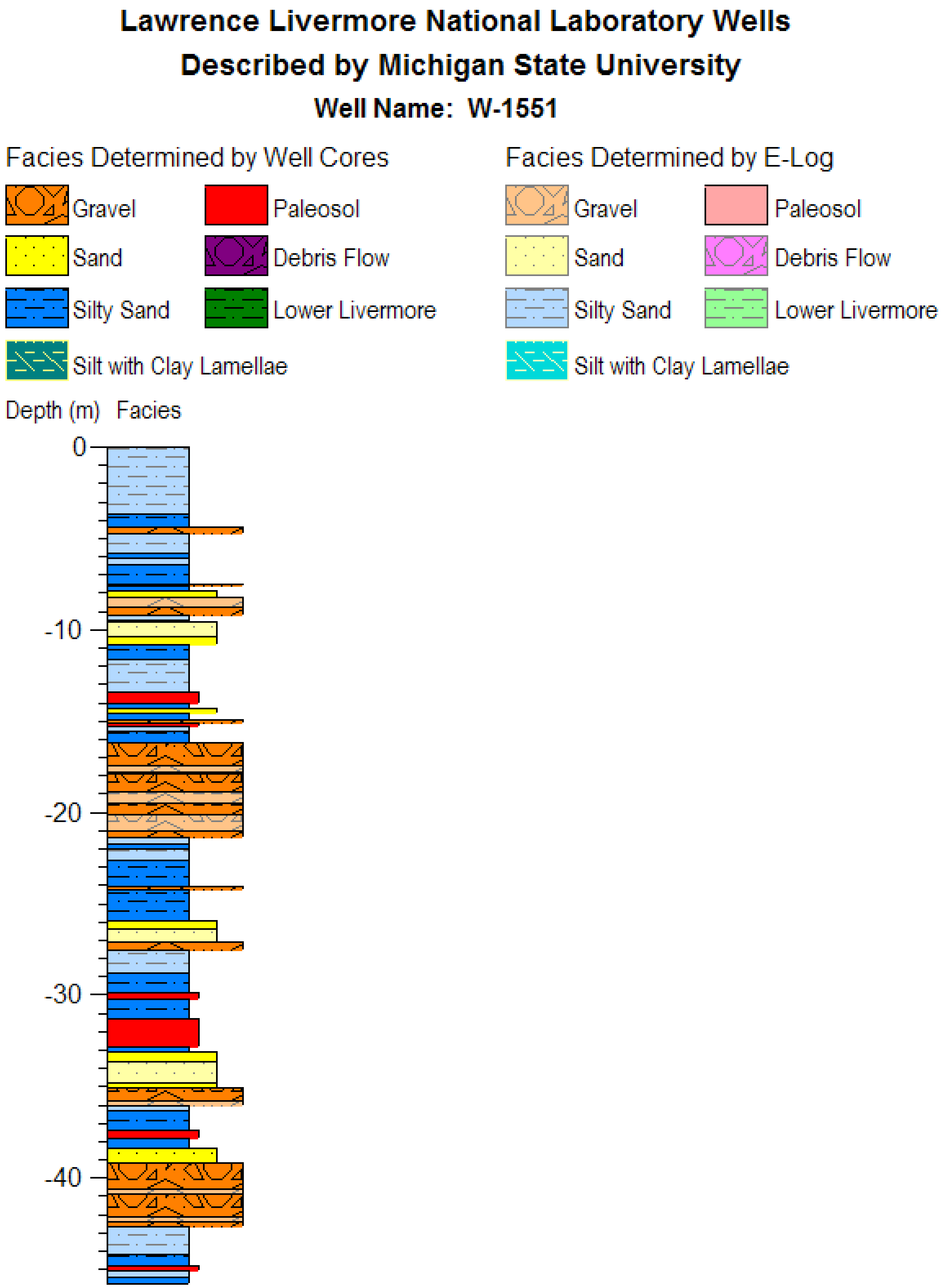

Figure 189. W-1551 stratigraphic column.

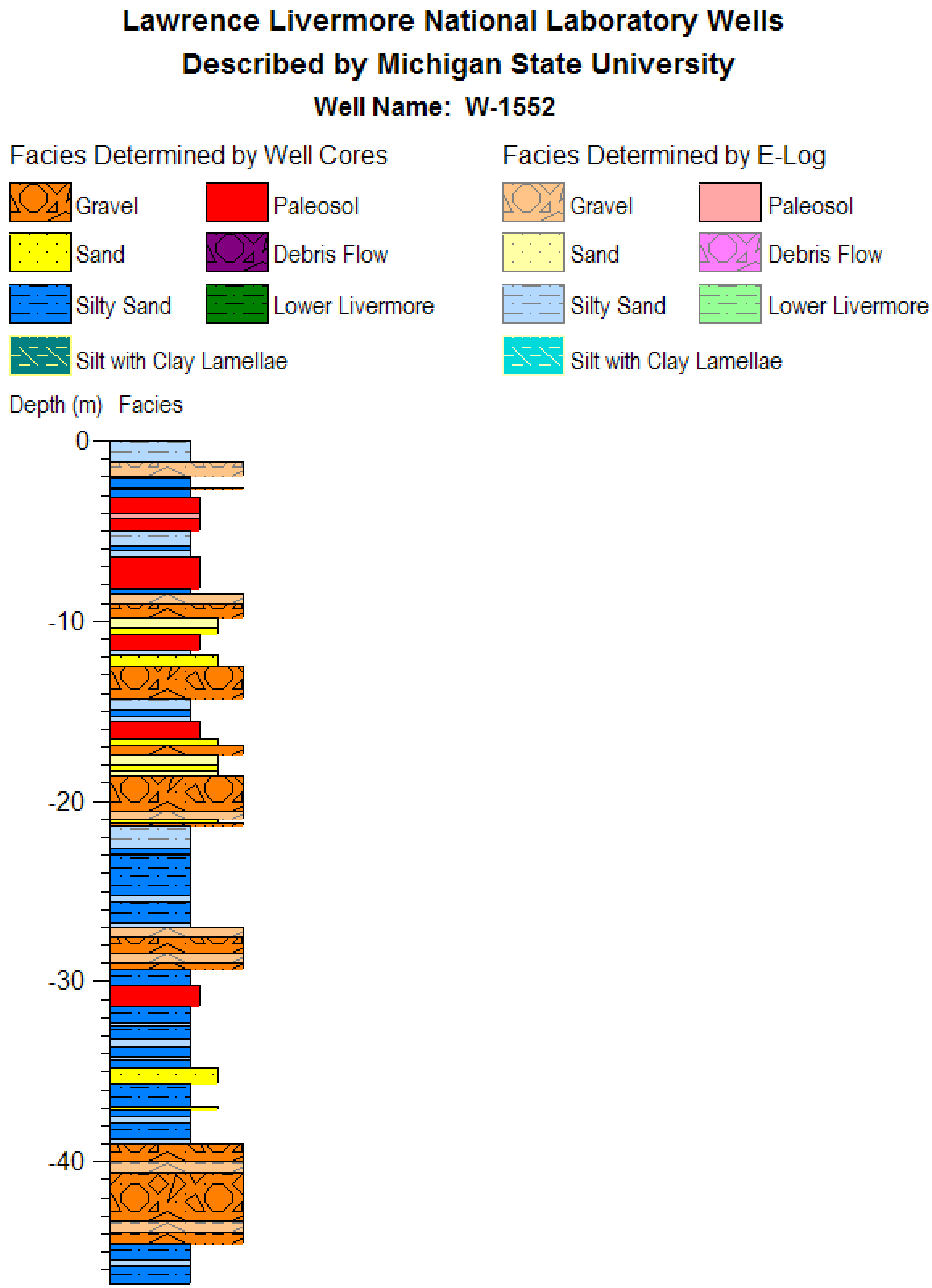

Figure 190. W-1552 stratigraphic column.

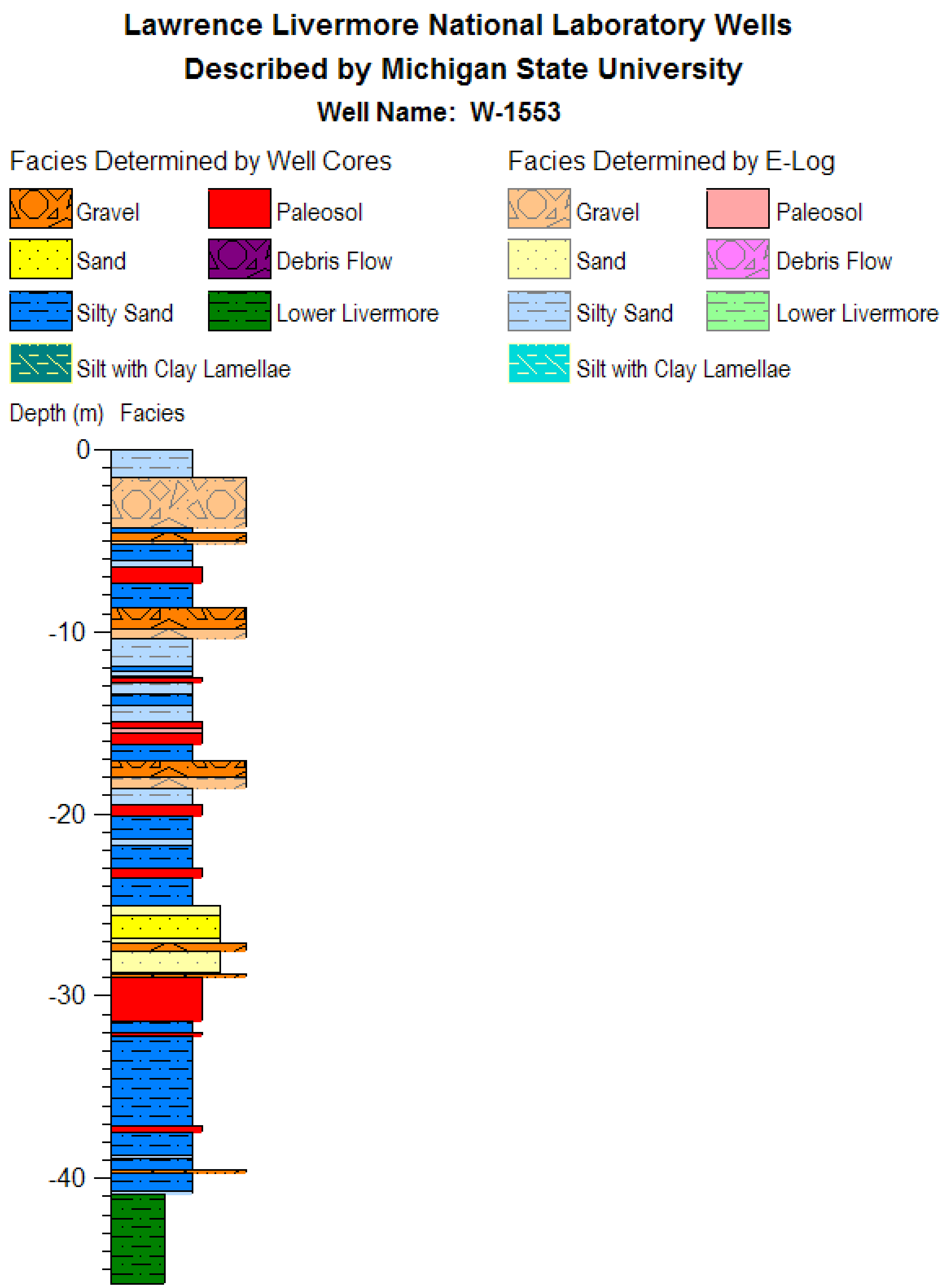

Figure 191. W-1553 stratigraphic column.

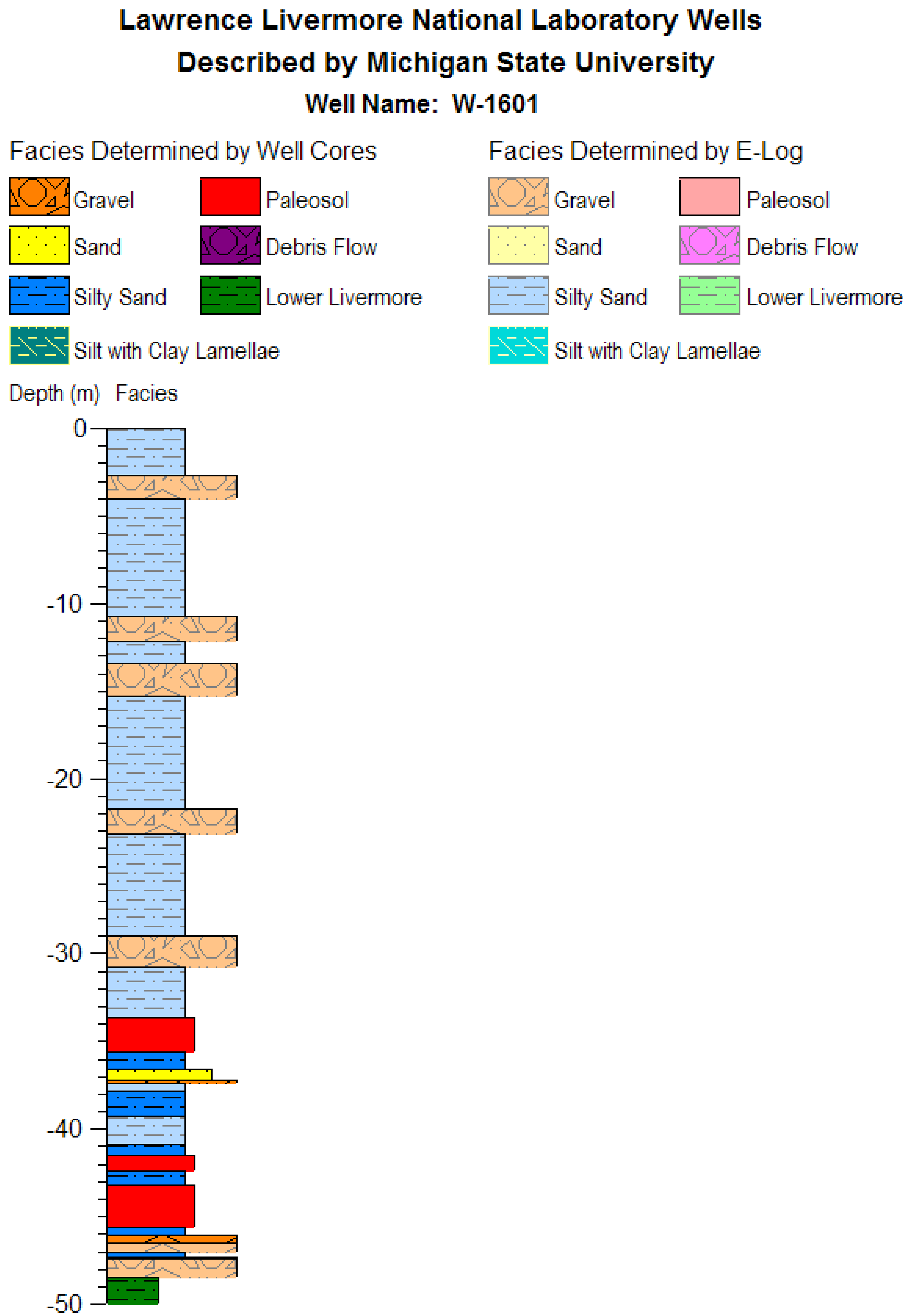

Figure 192. W-1601 stratigraphic column.

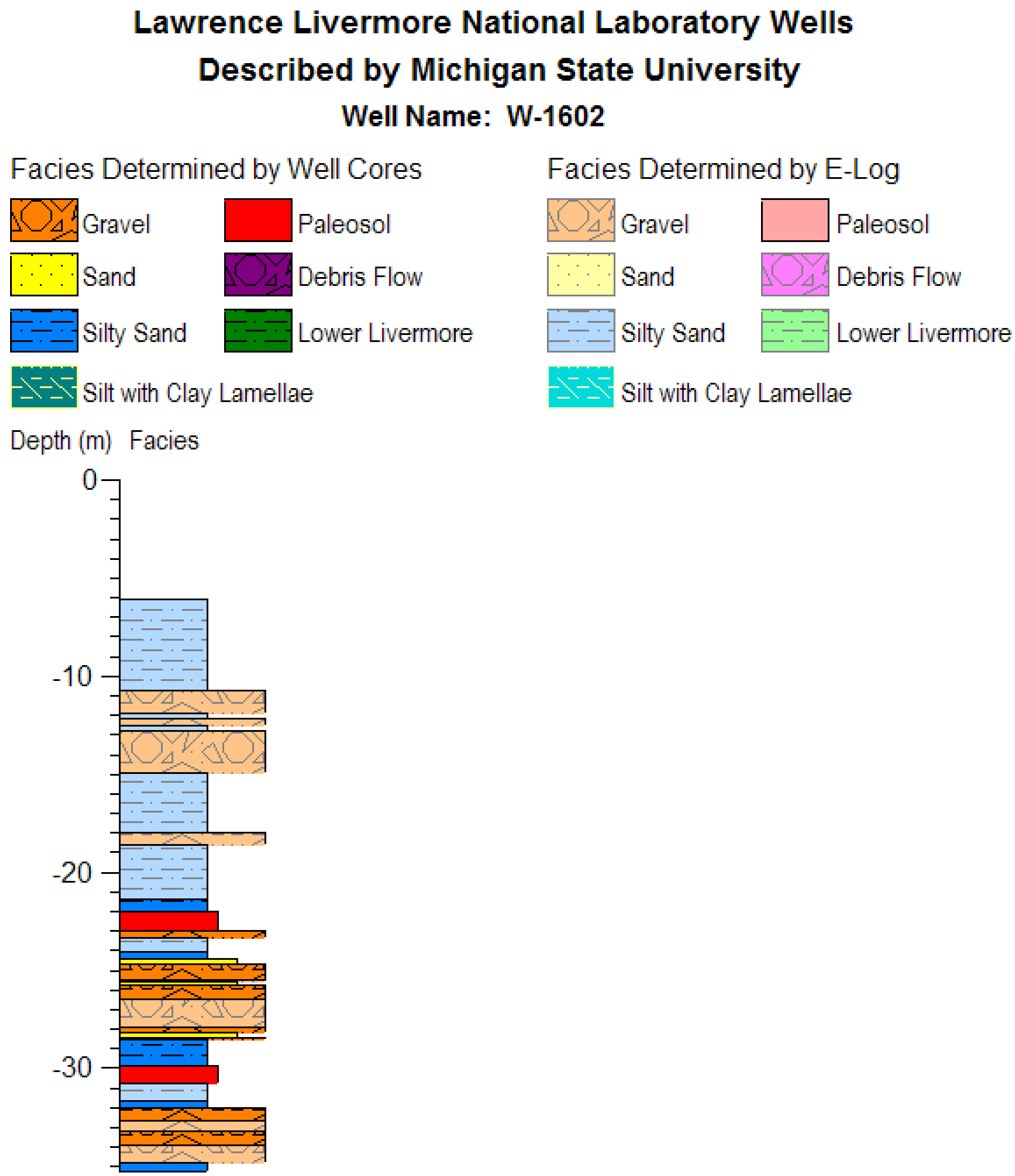

Figure 193. W-1602 stratigraphic column.

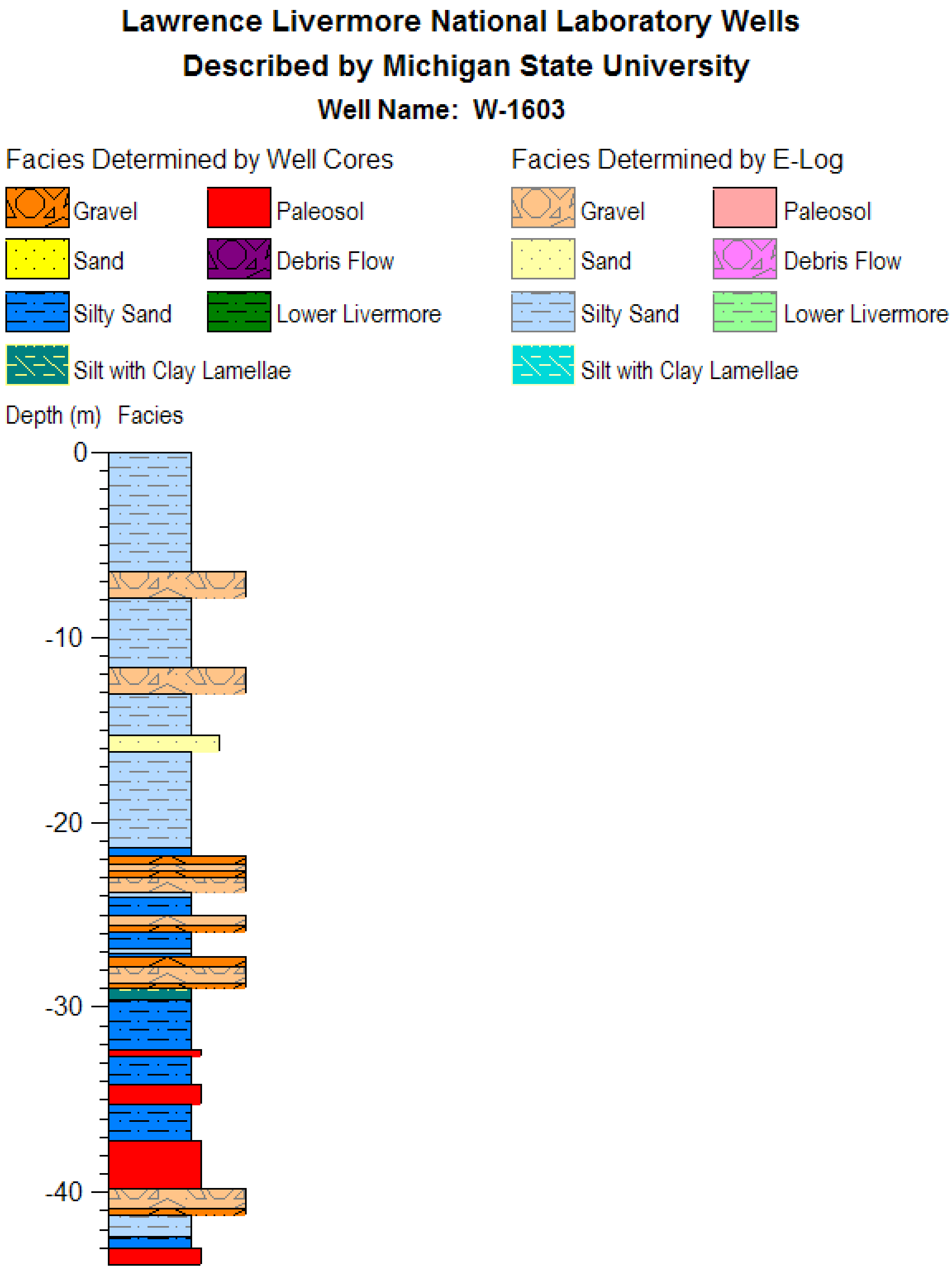

Figure 194. W-1603 stratigraphic column.

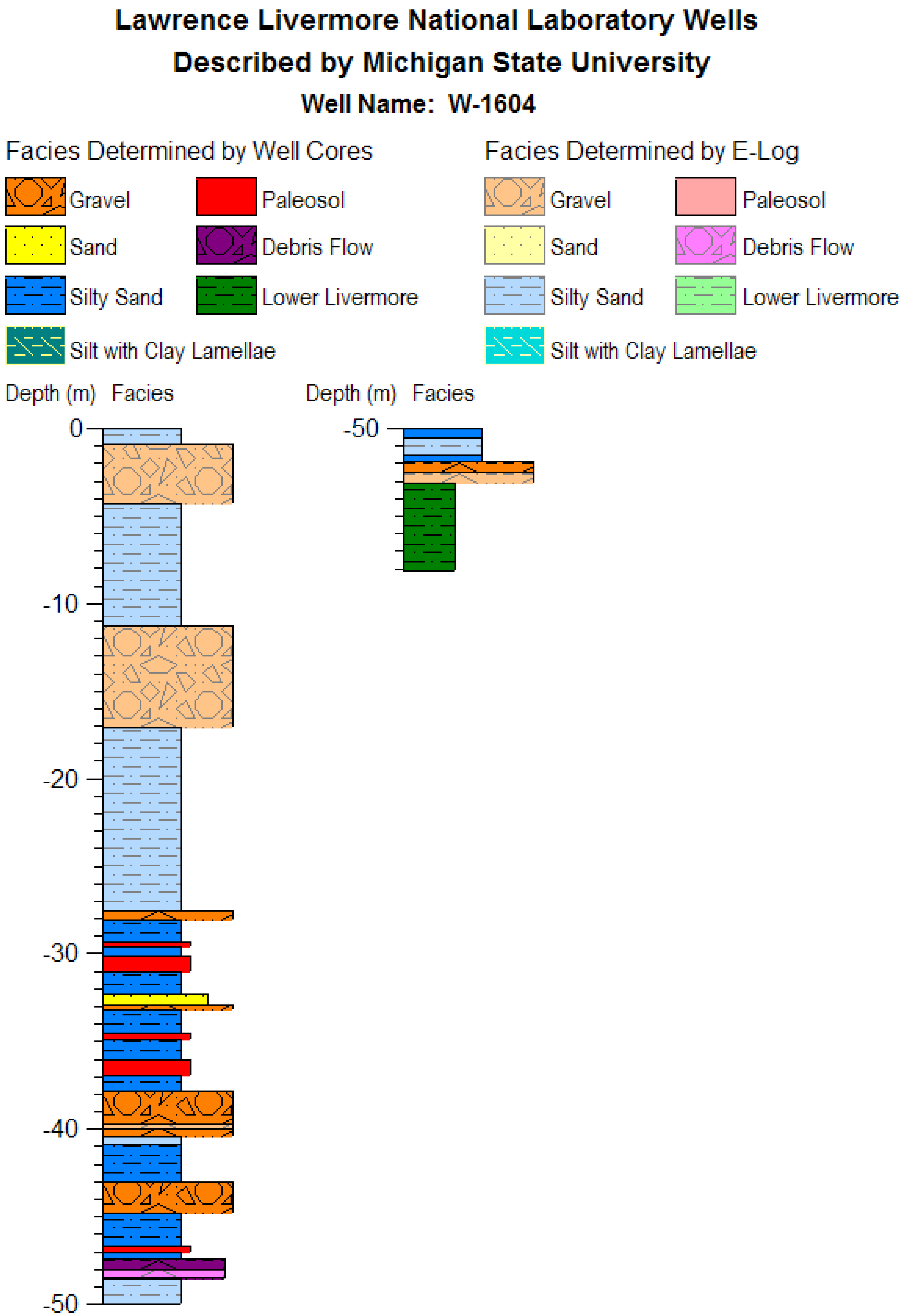

Figure 195. W-1604 stratigraphic column.

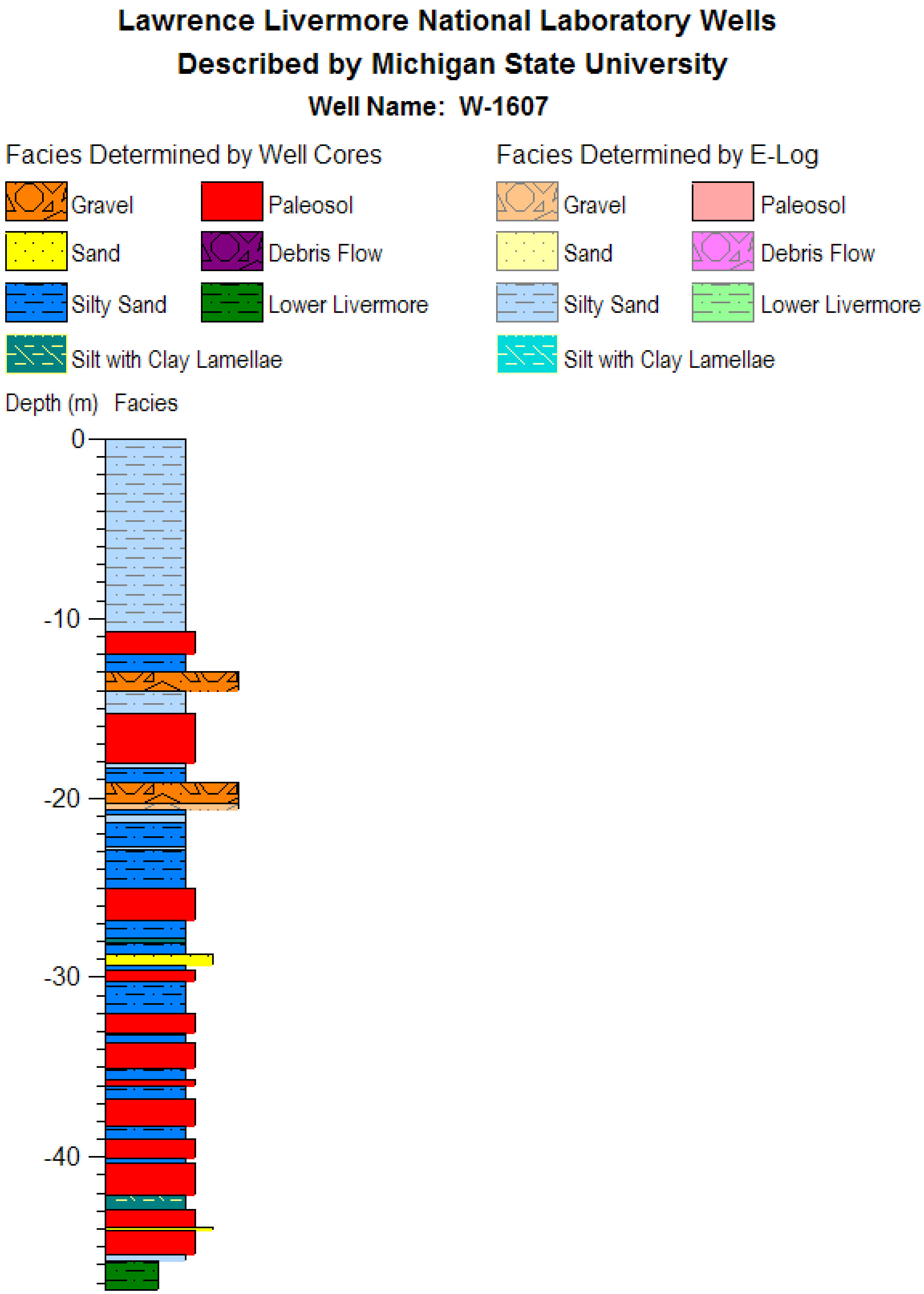

Figure 196. W-1607 stratigraphic column.

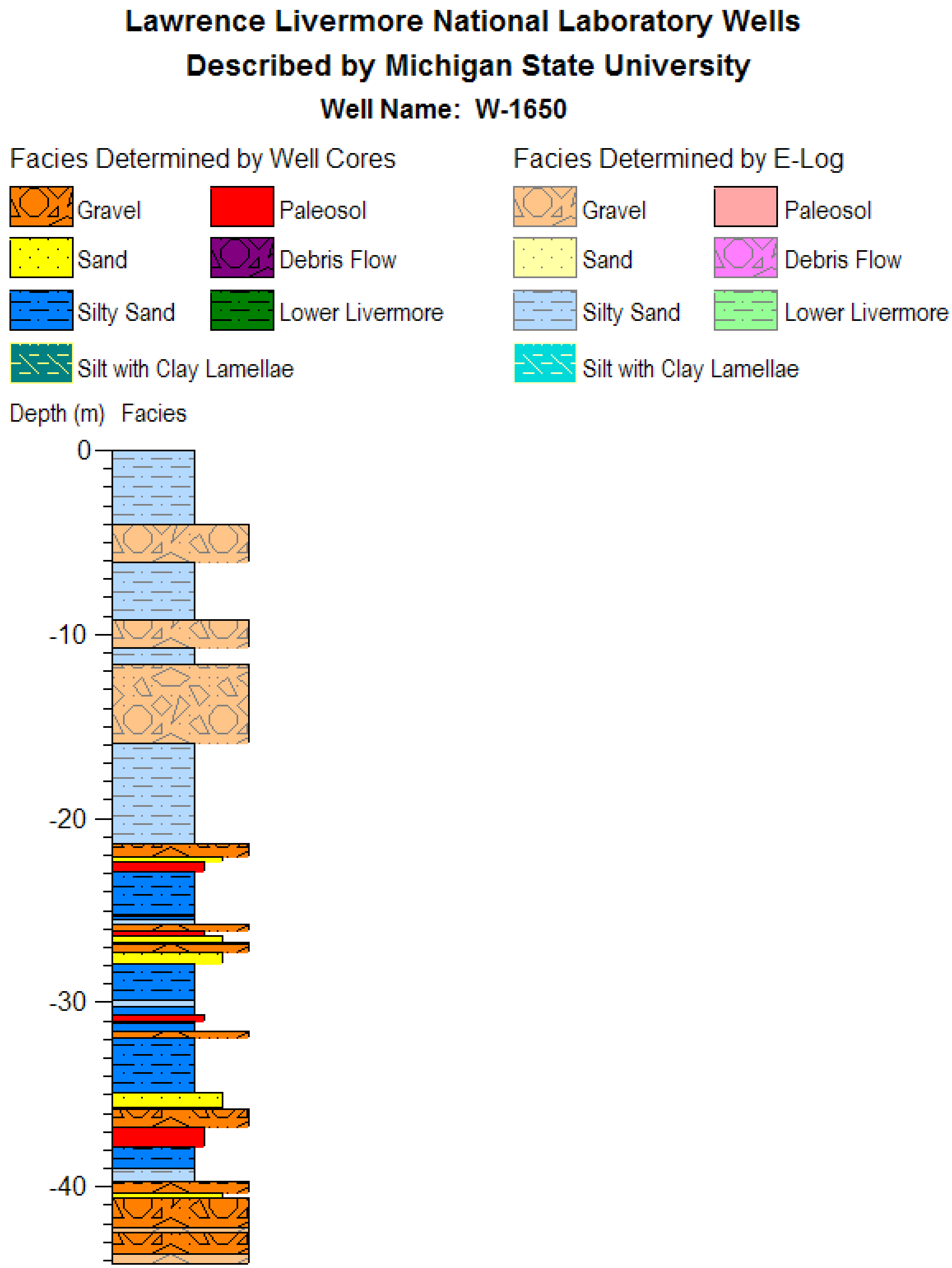

Figure 197. W-1650 stratigraphic column.

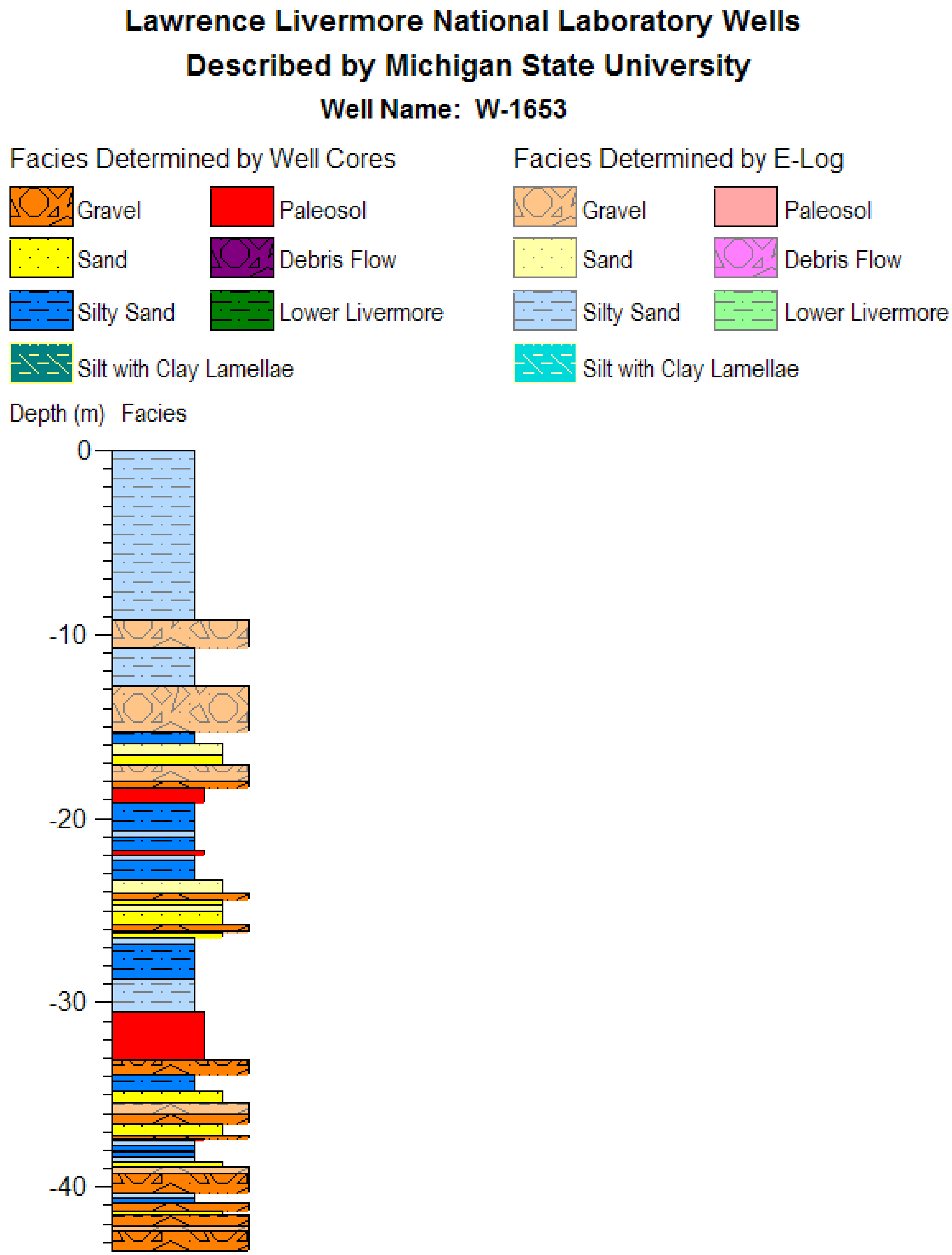

Figure 198. W-1653 stratigraphic column.

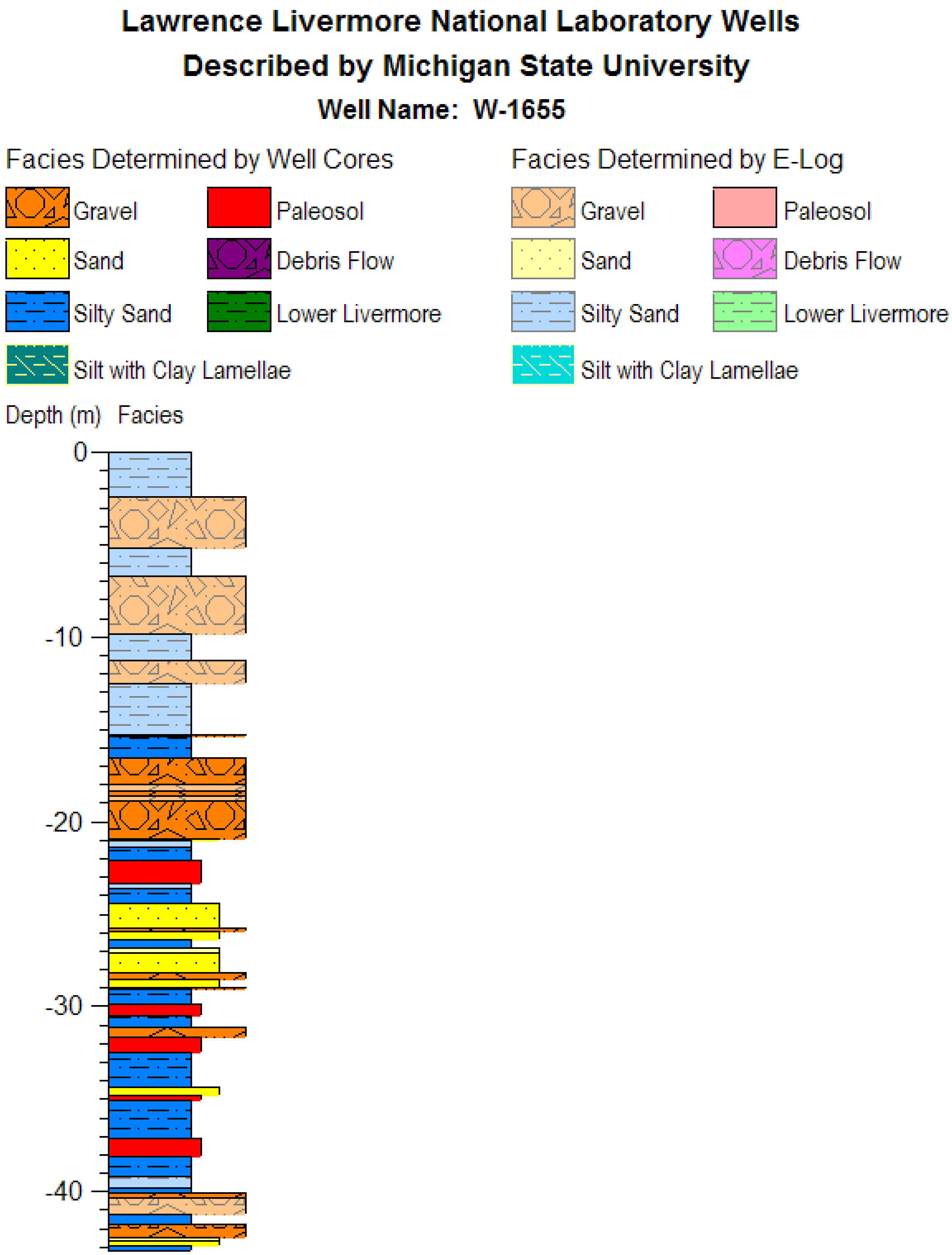

Figure 199. W-1655 stratigraphic column.

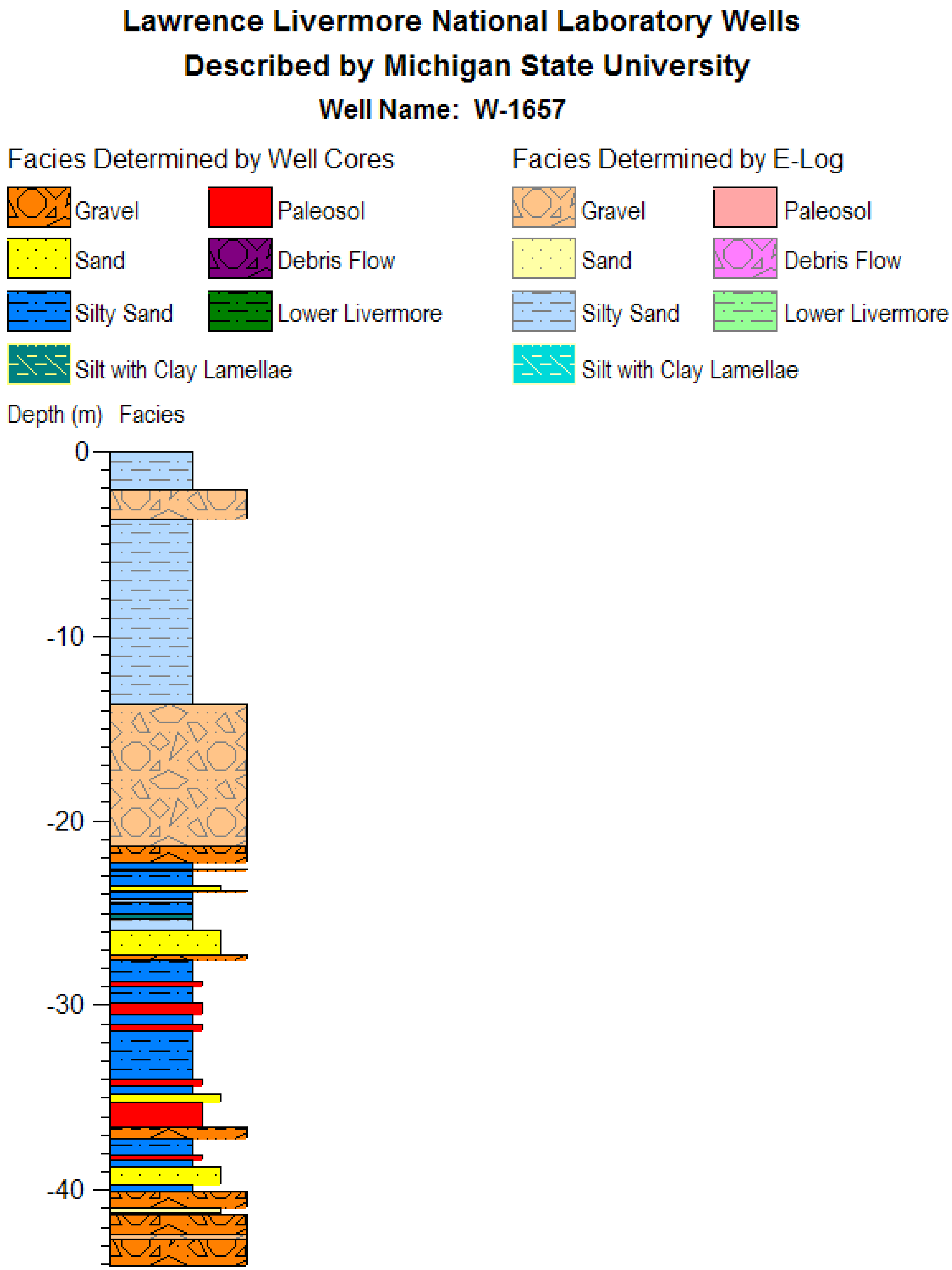

Figure 200. W-1657 stratigraphic column.

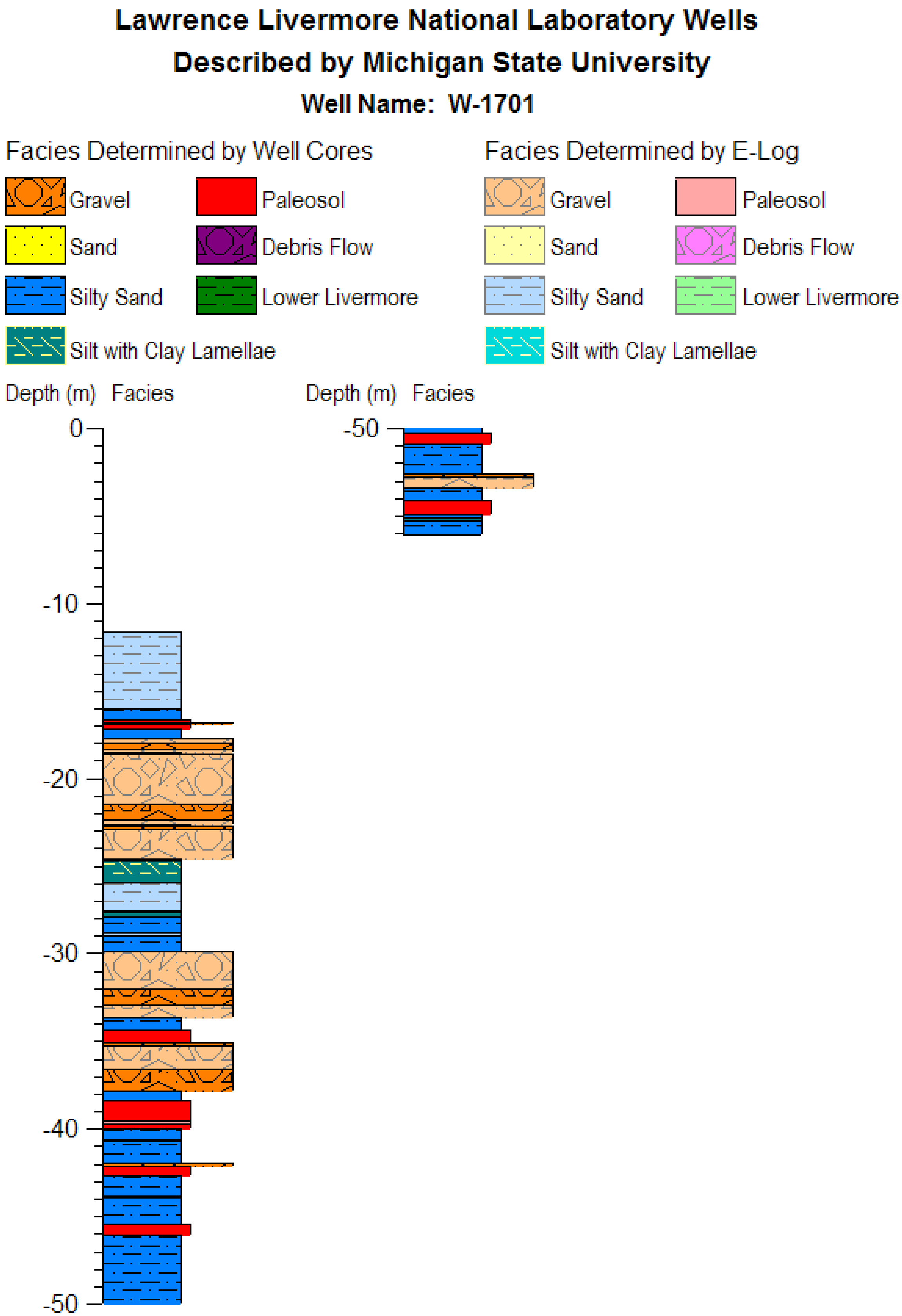

Figure 201. W-1701 stratigraphic column.

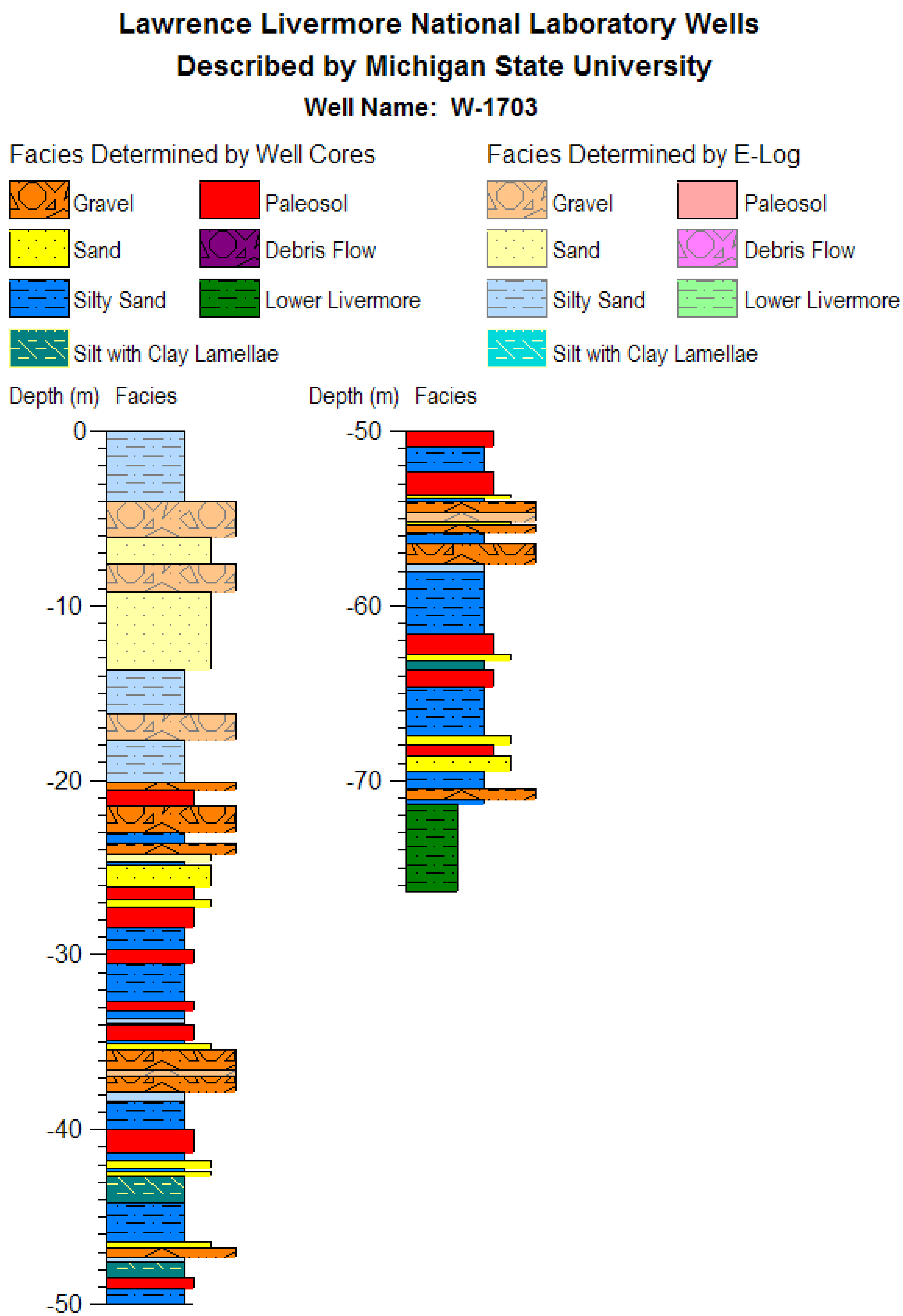

Figure 202. W-1703 stratigraphic column.

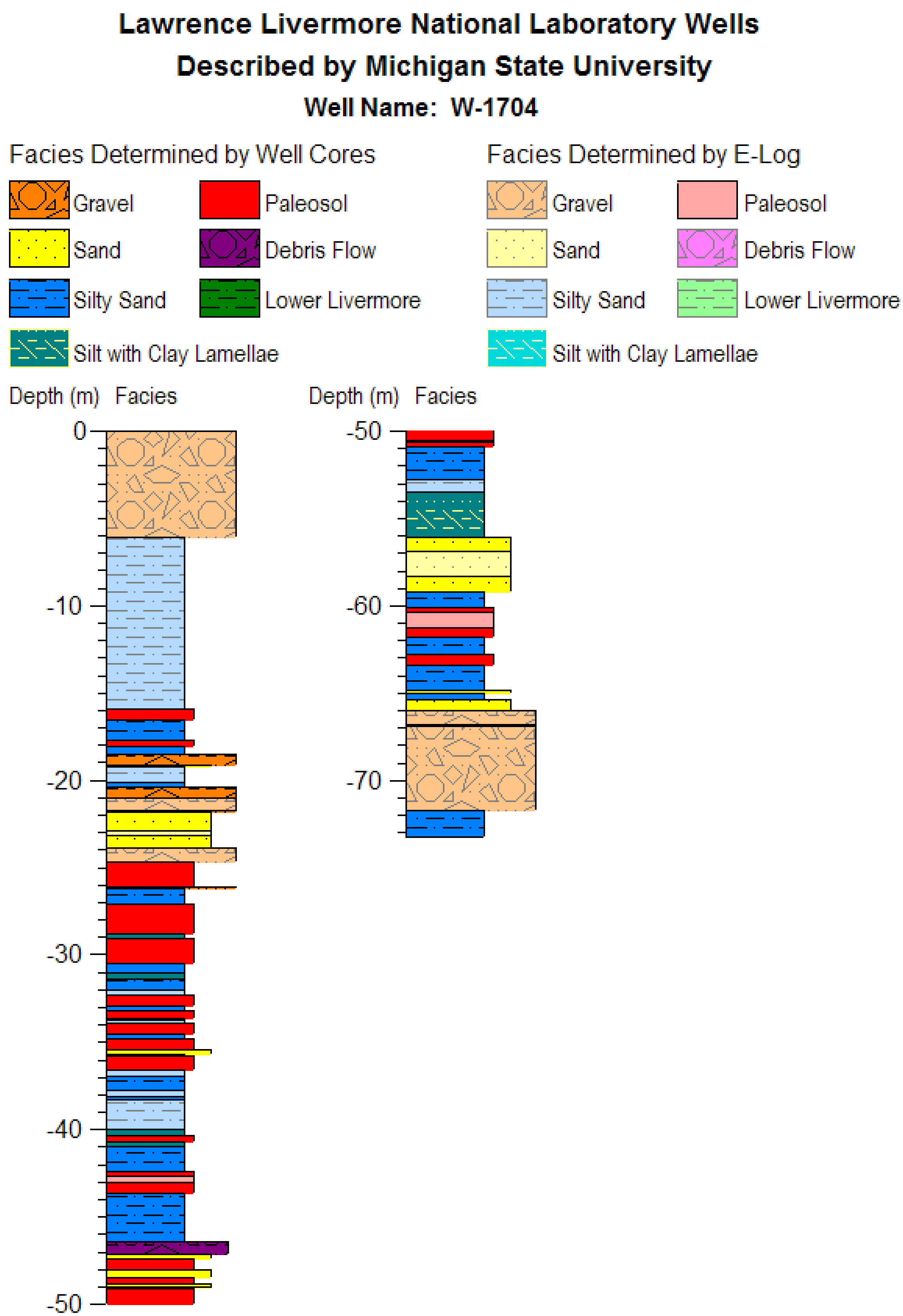

Figure 203. W-1704 stratigraphic column.

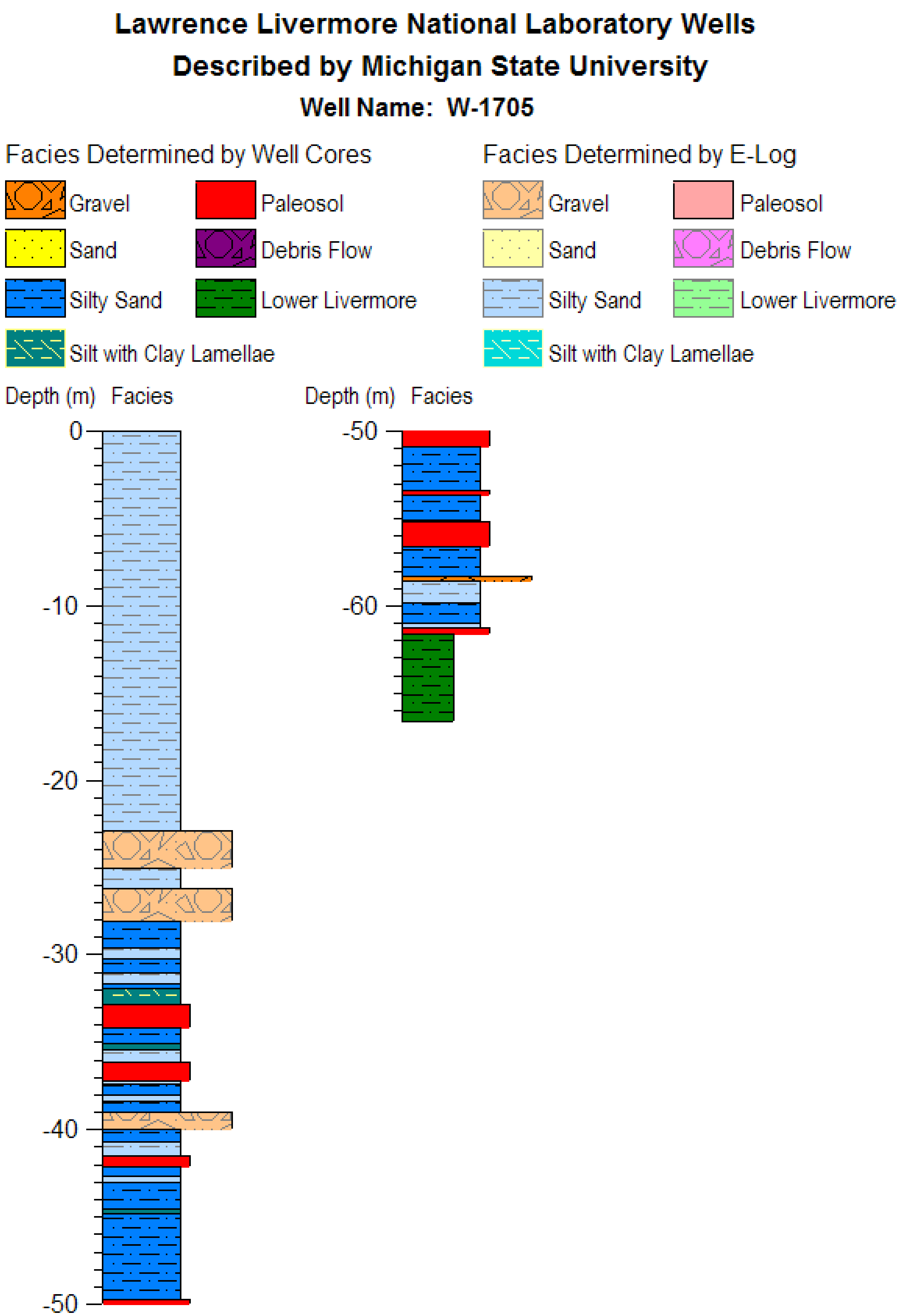

Figure 204. W-1705 stratigraphic column.

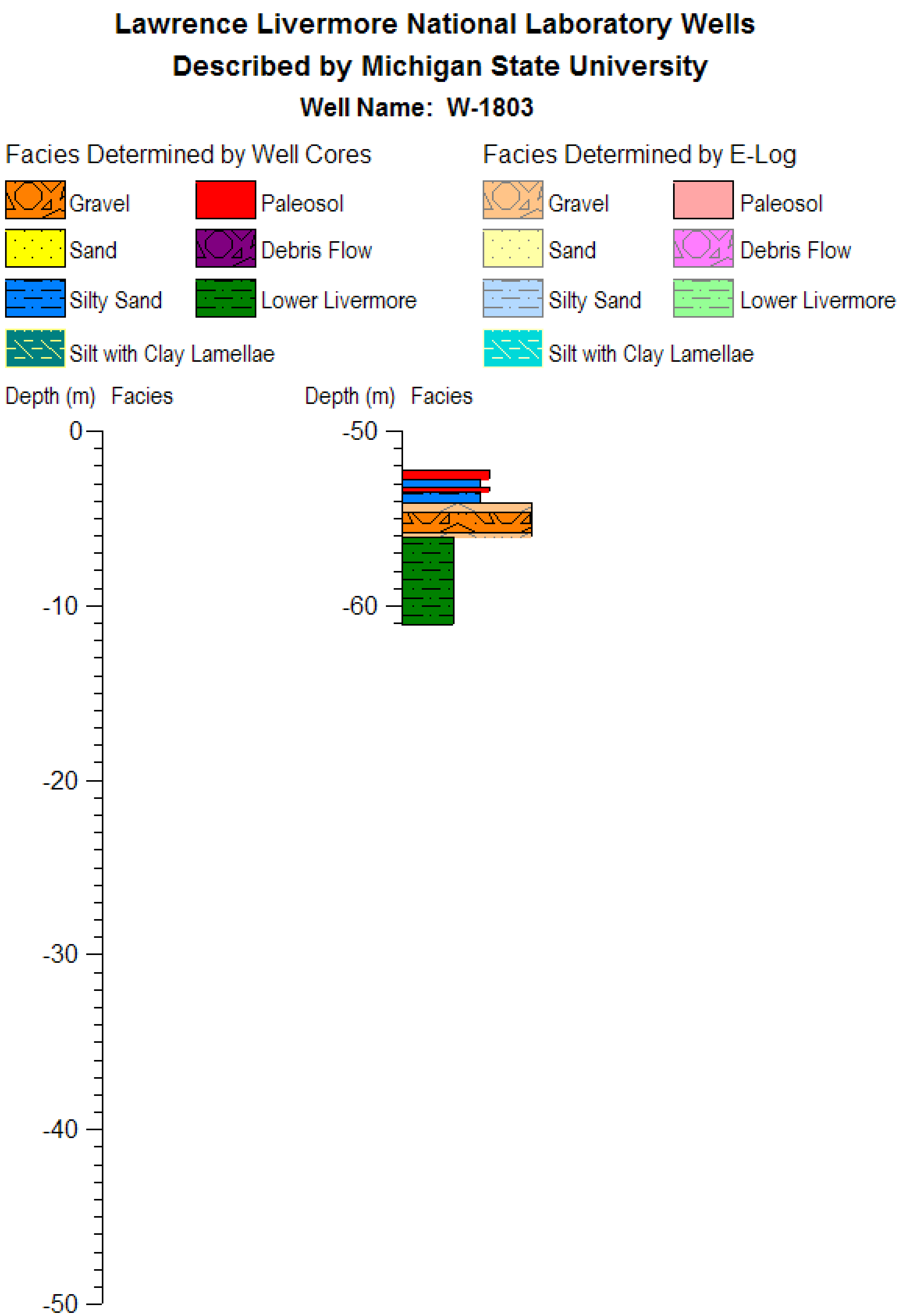

Figure 205. W-1803 stratigraphic column.

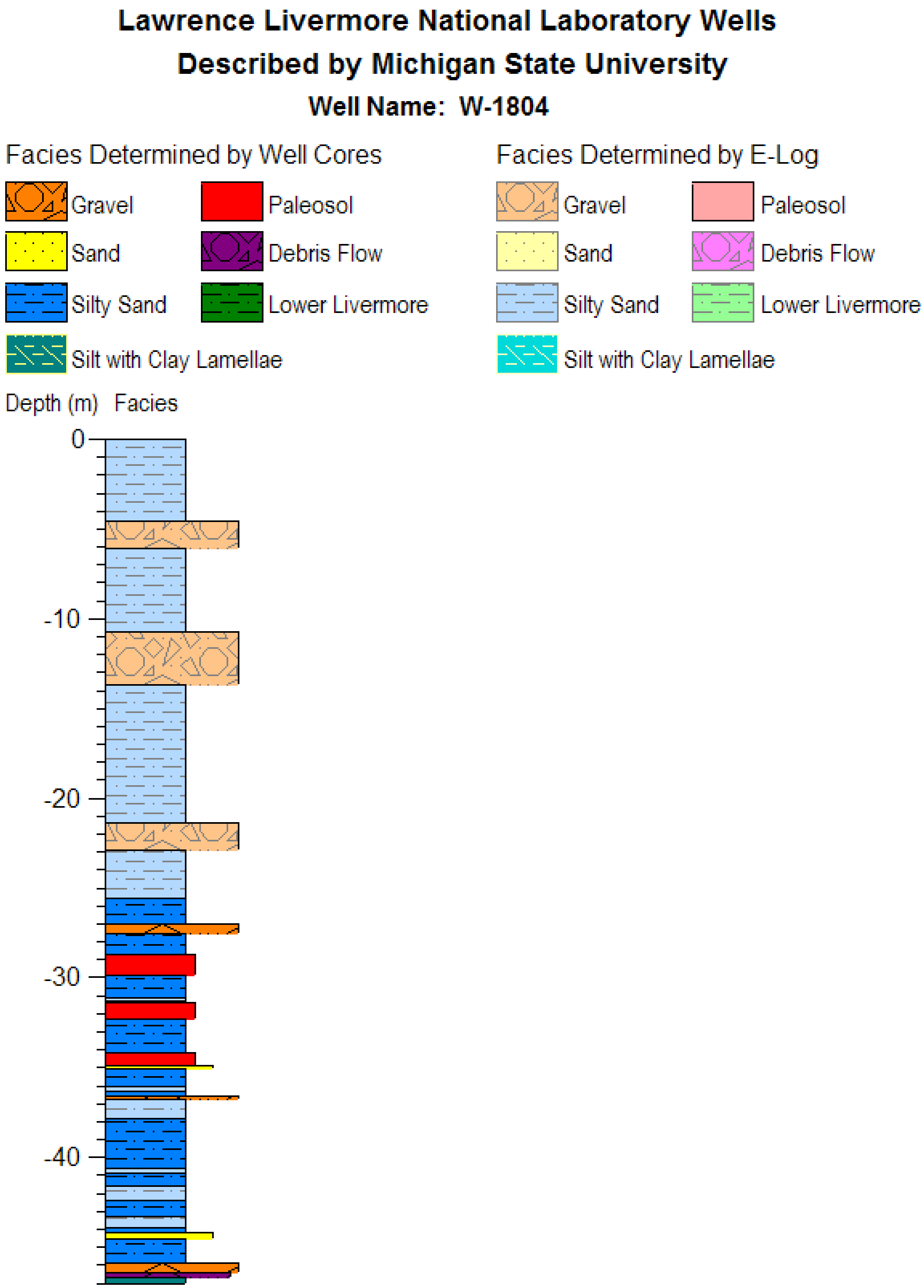

Figure 206. W-1804 stratigraphic column.

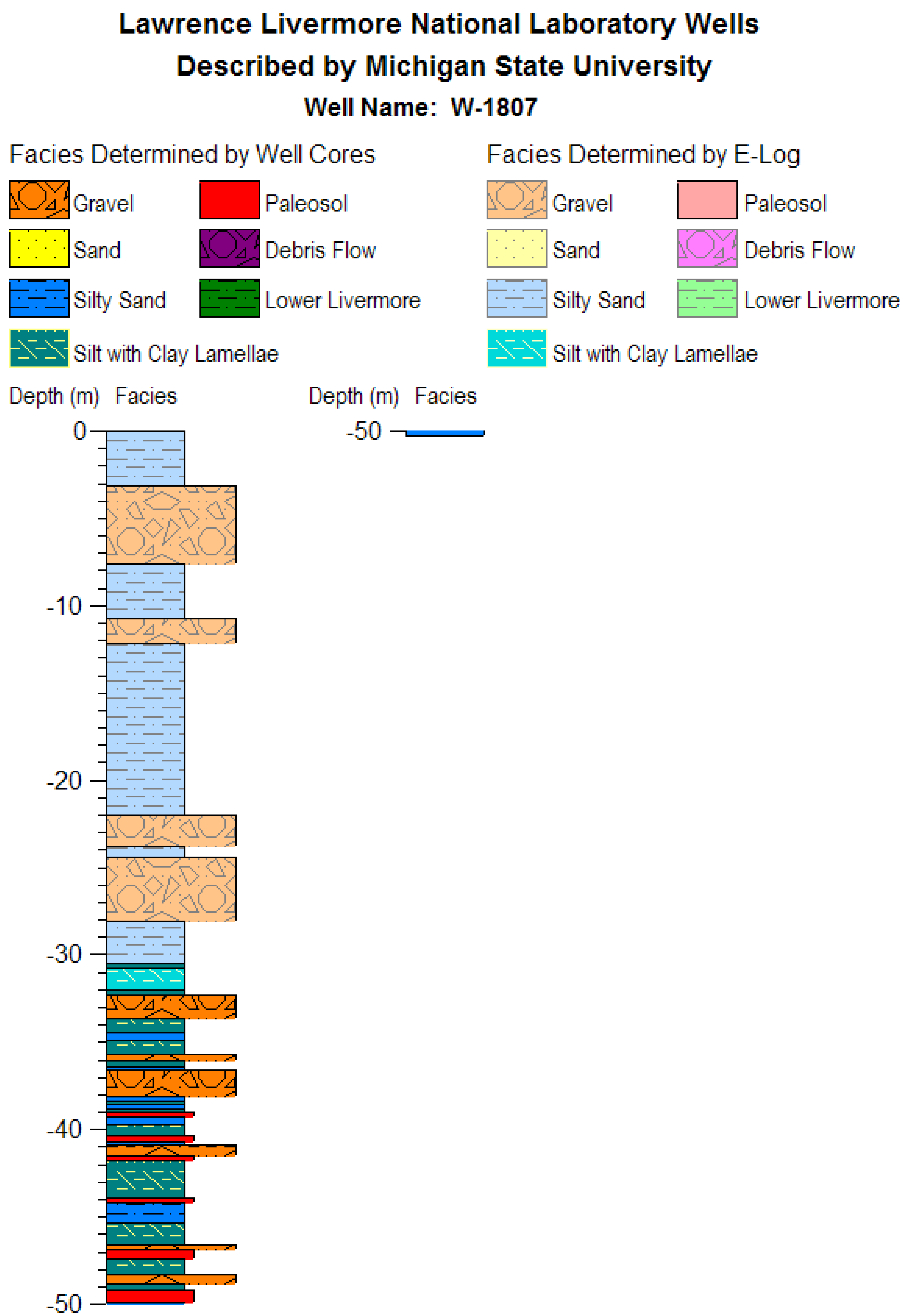

Figure 207. W-1807 stratigraphic column.

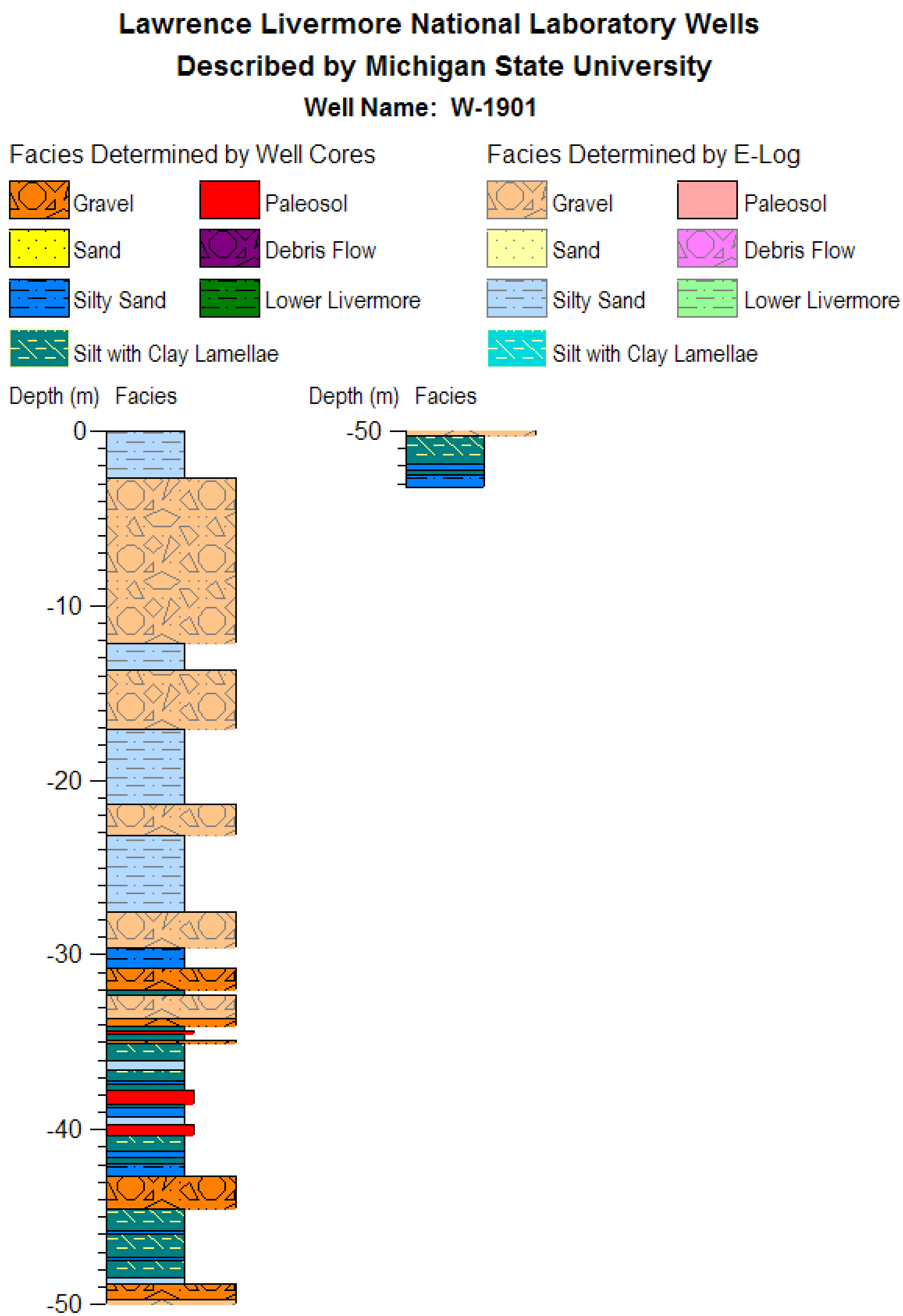

Figure 208. W-1901 stratigraphic column.

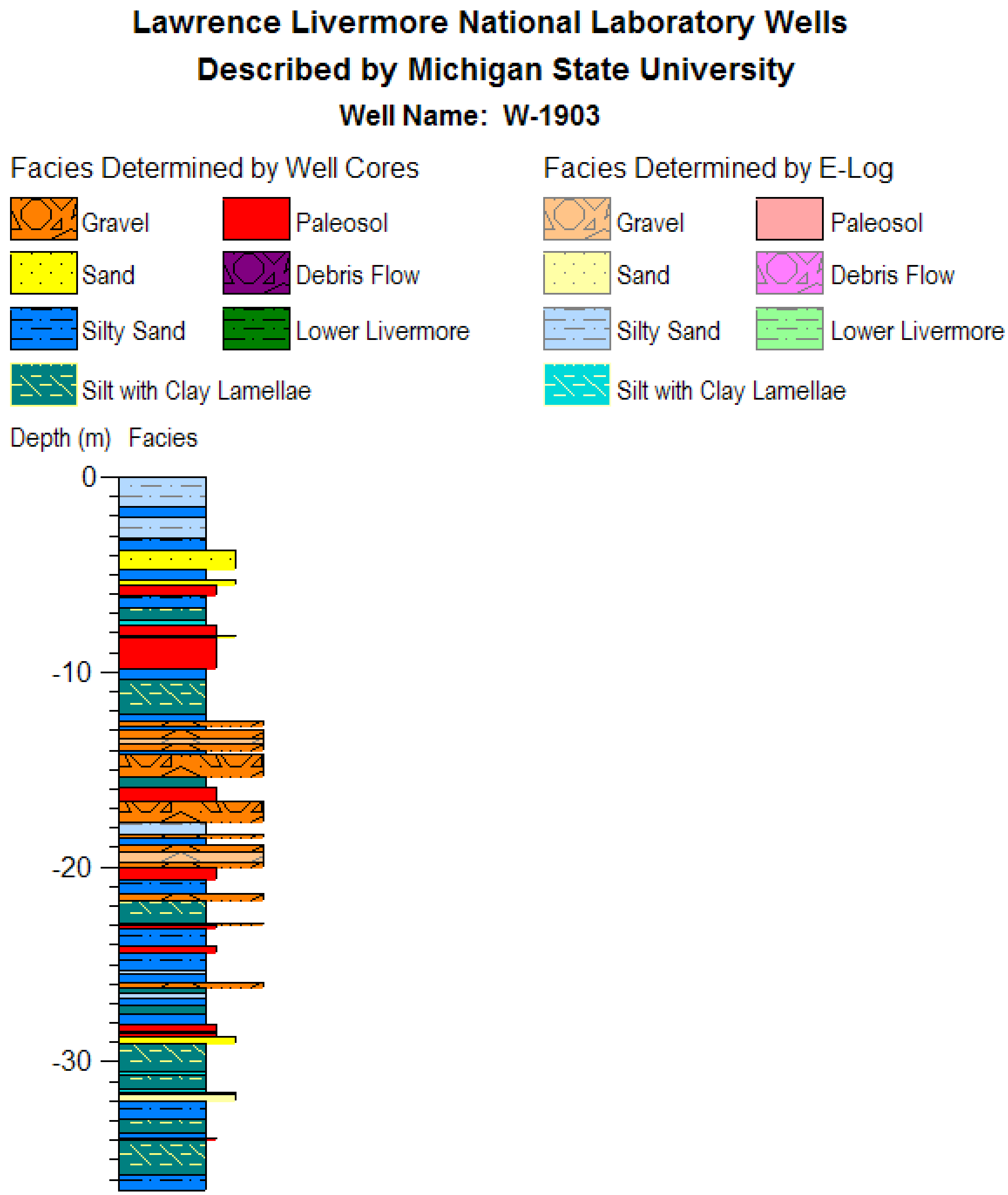

Figure 209. W-1903 stratigraphic column.

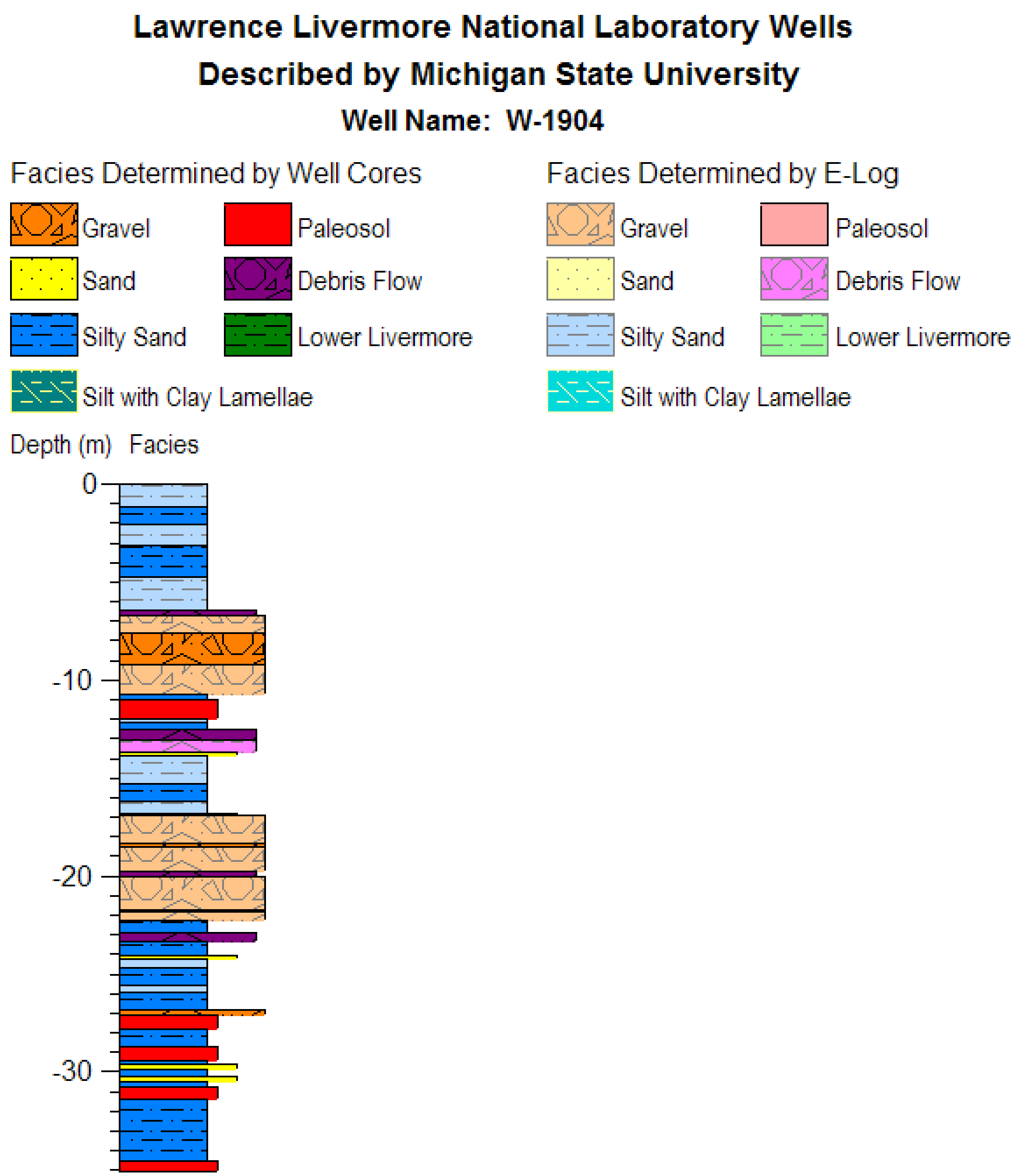

Figure 210. W-1904 stratigraphic column.

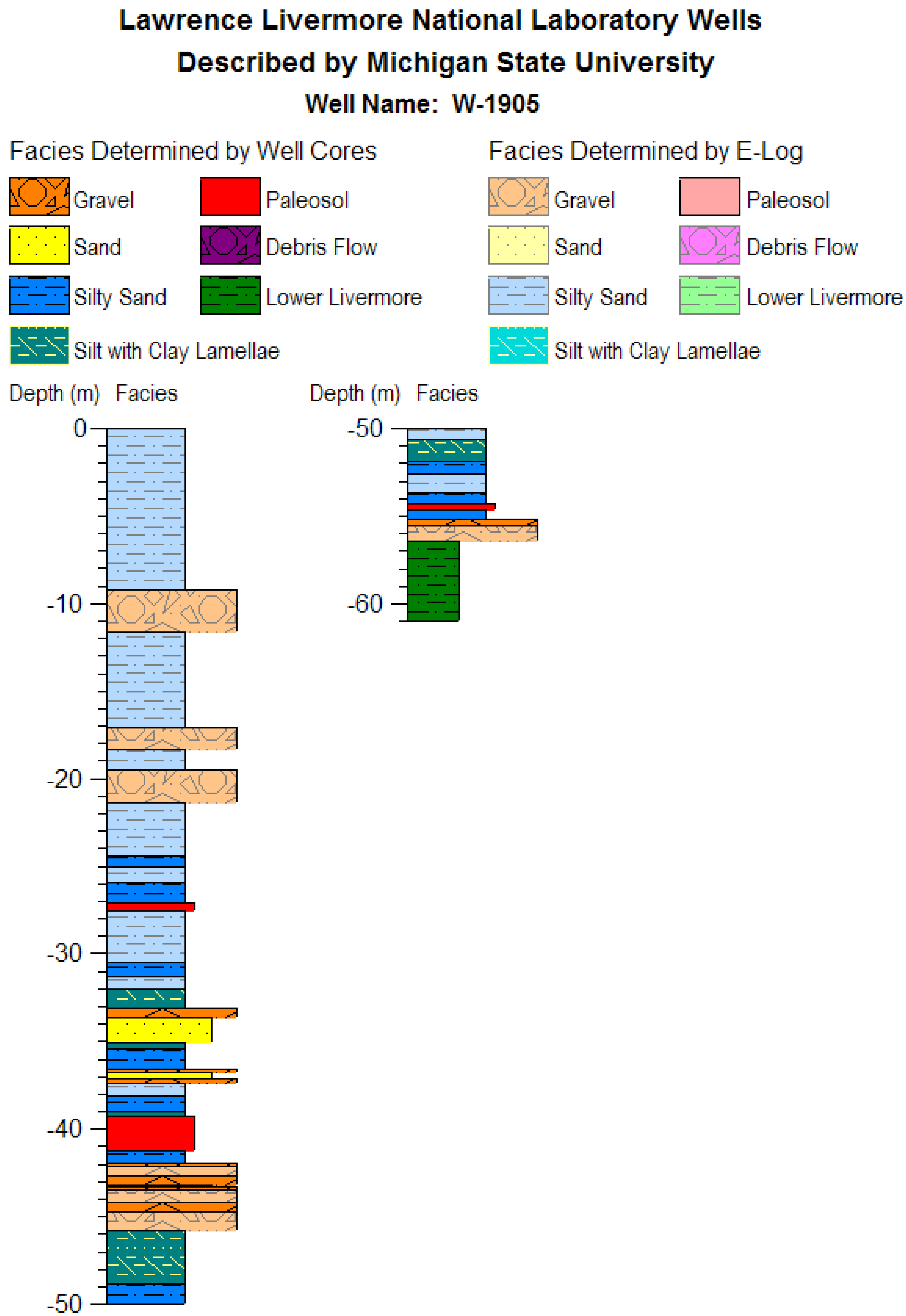

Figure 211. W-1905 stratigraphic column.

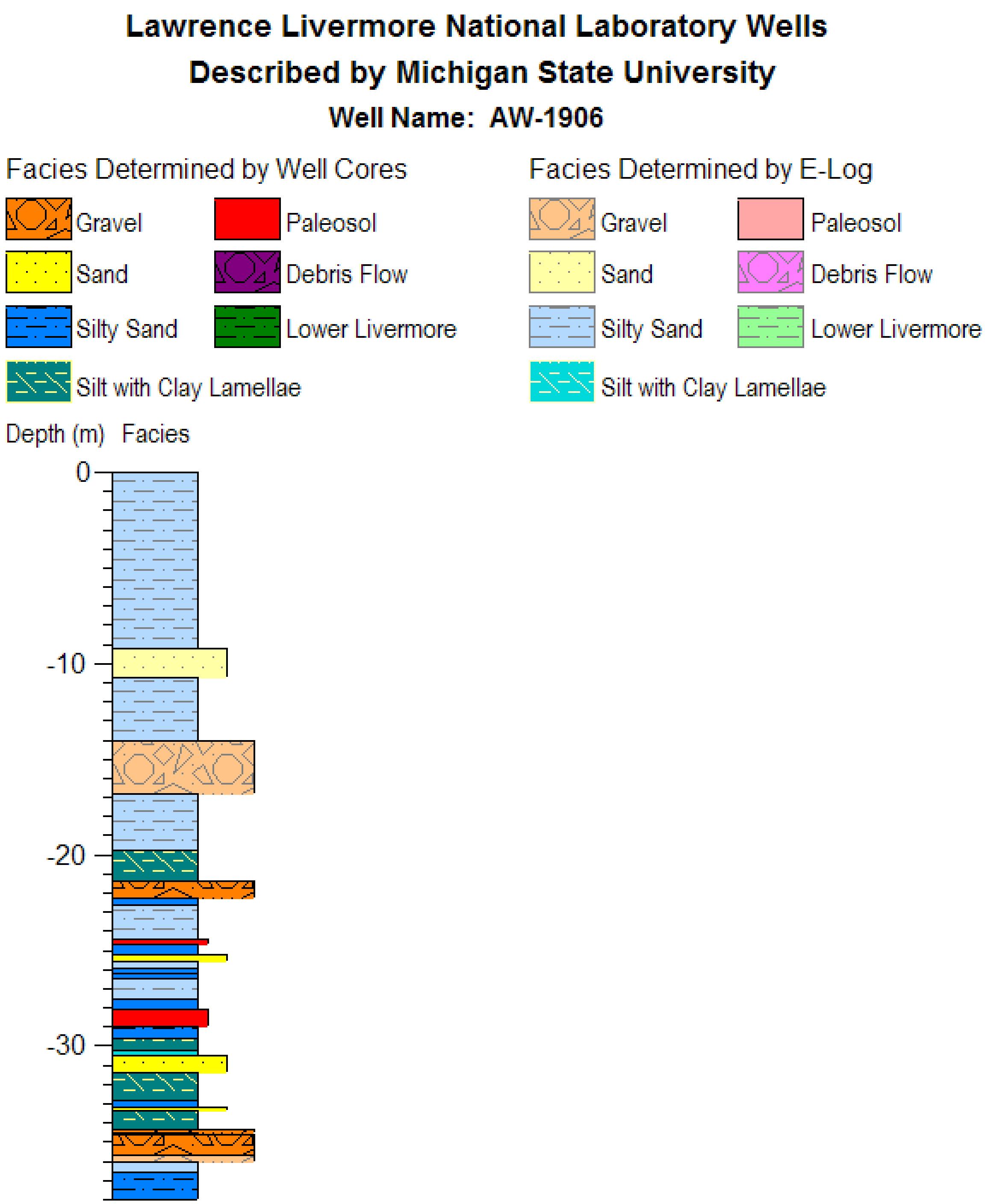

Figure 212. AW-1906 stratigraphic column.

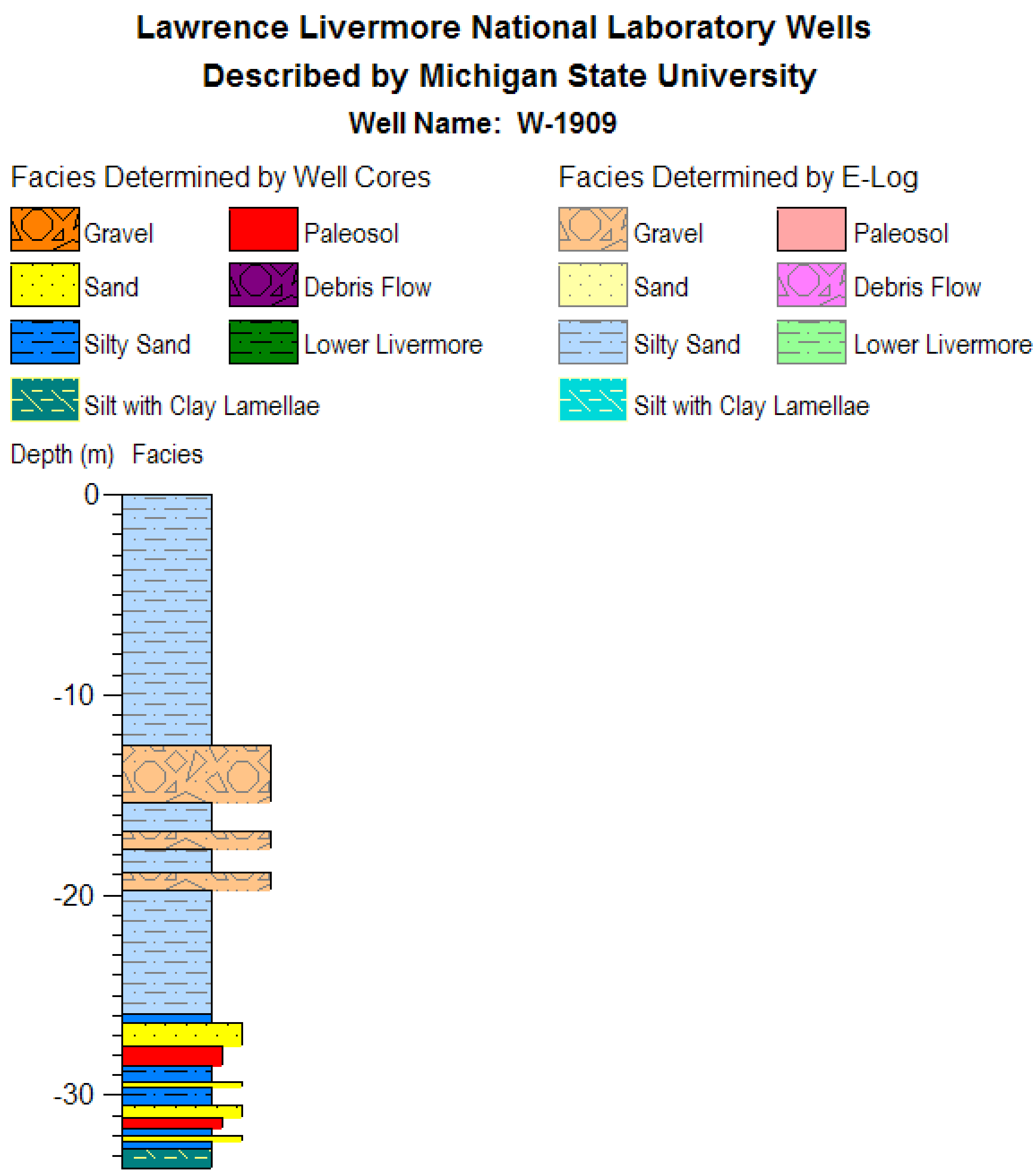

Figure 213. W-1909 stratigraphic column.

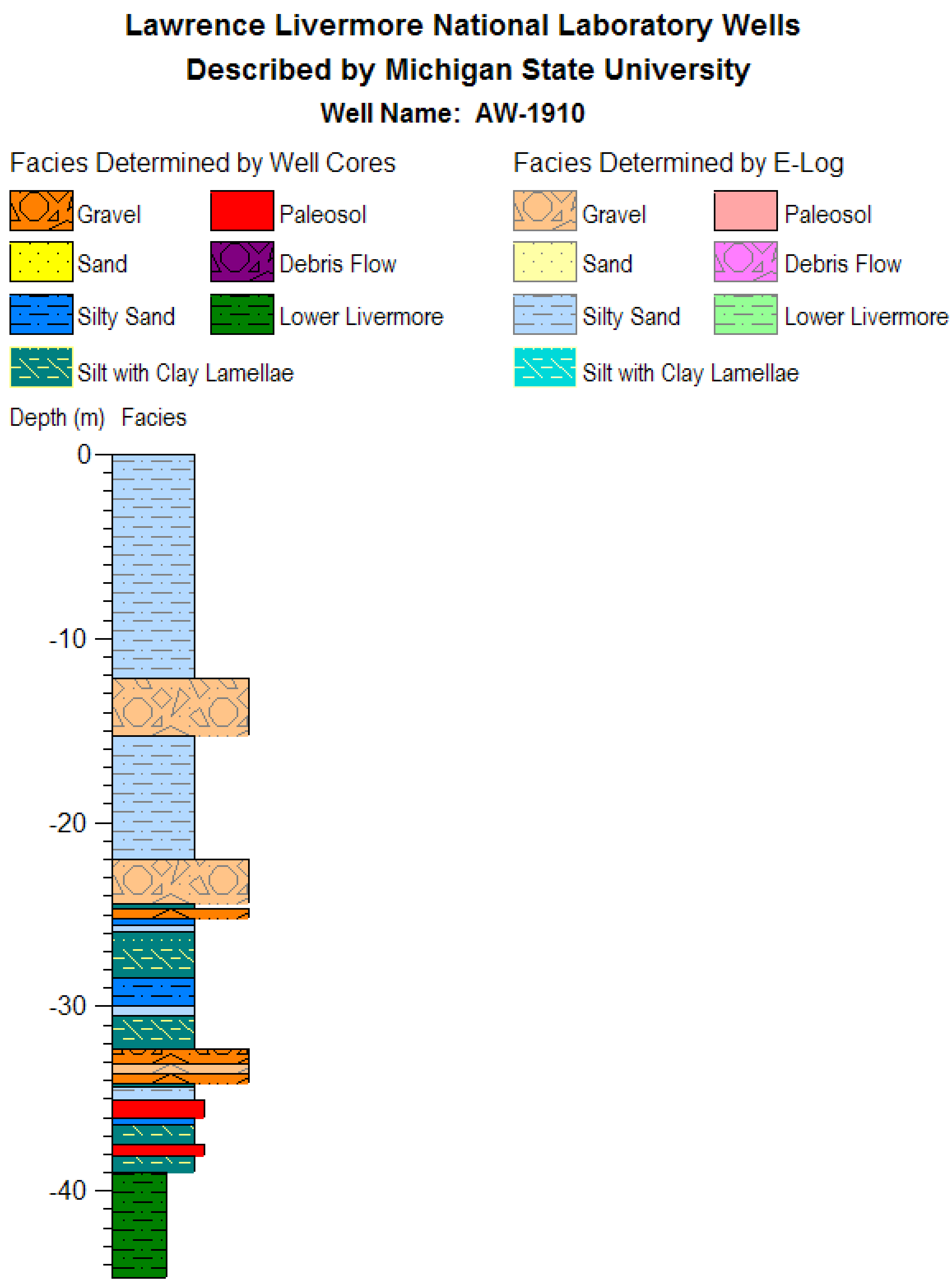

Figure 214. AW-1910 stratigraphic column.

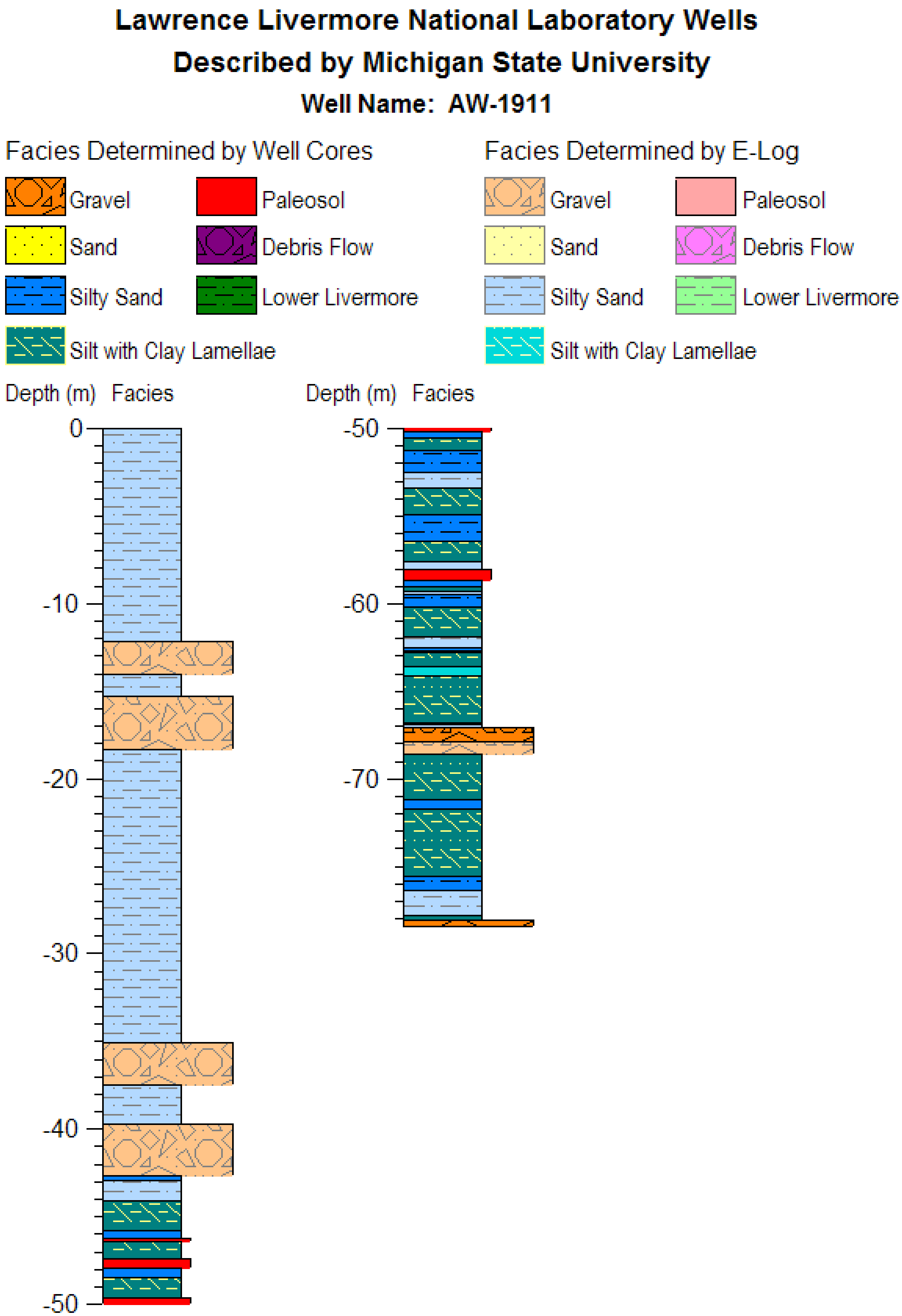

Figure 215. AW-1911 stratigraphic column.

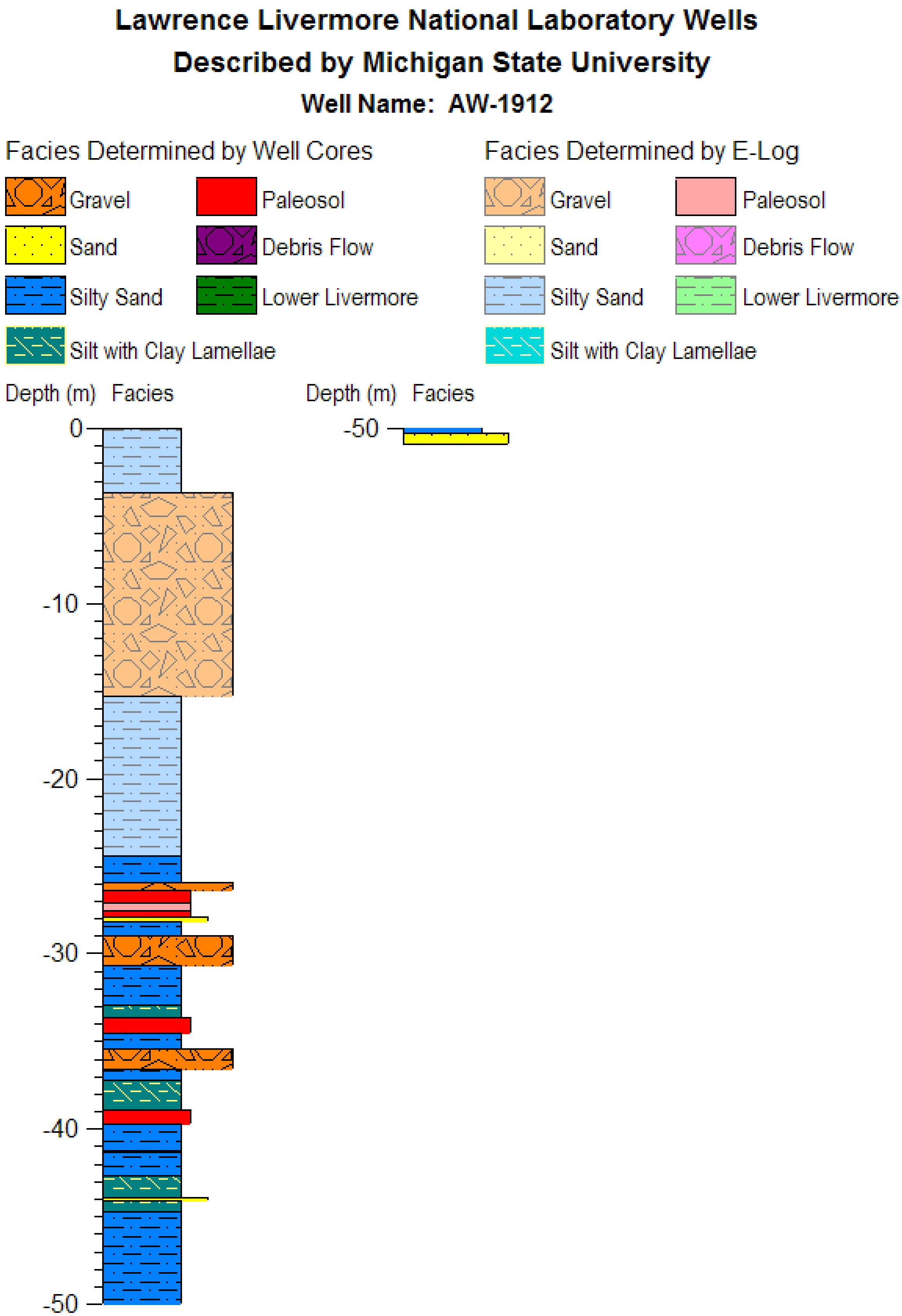

Figure 216. AW-1912 stratigraphic column.

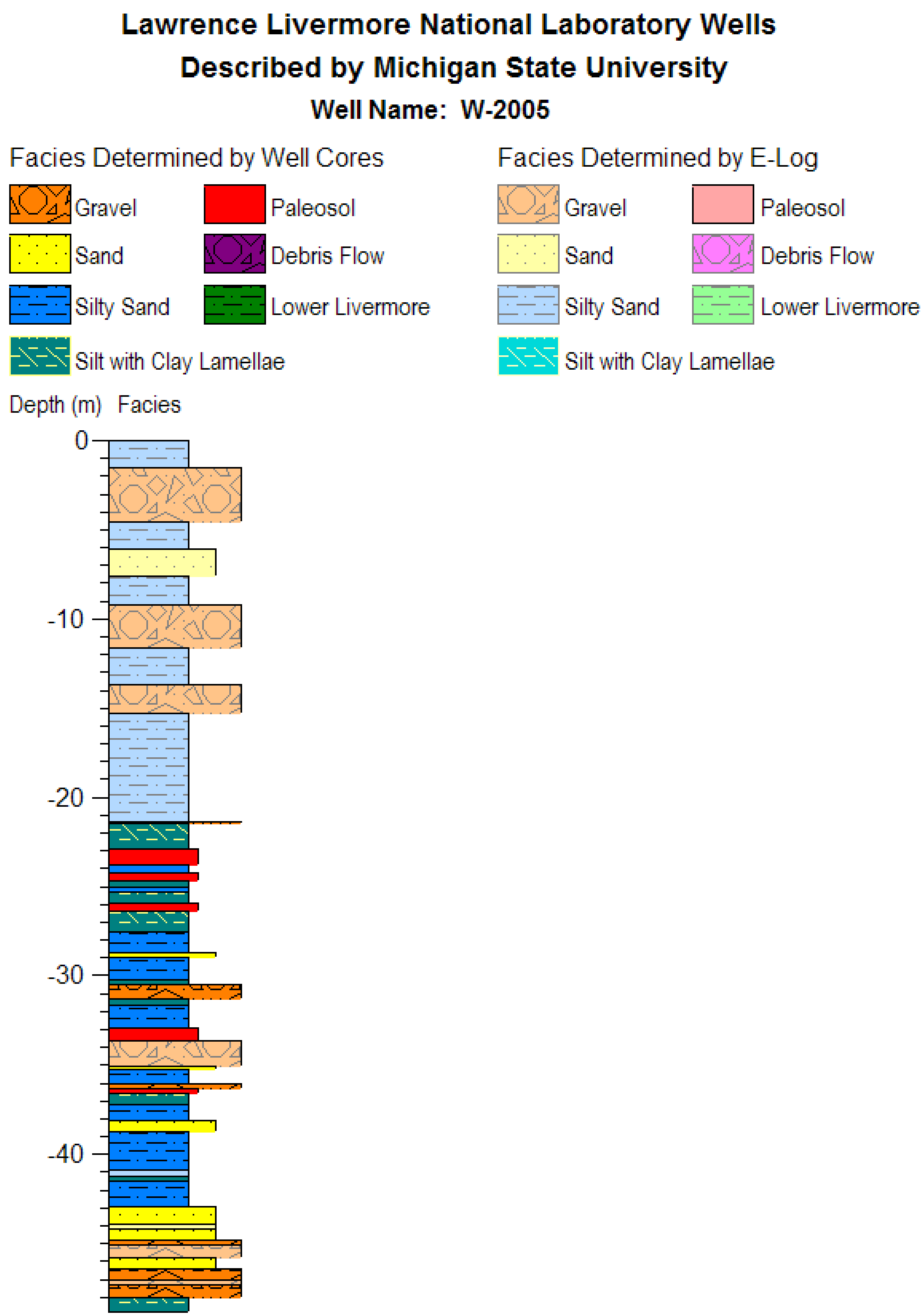

Figure 217. W-2005 stratigraphic column.

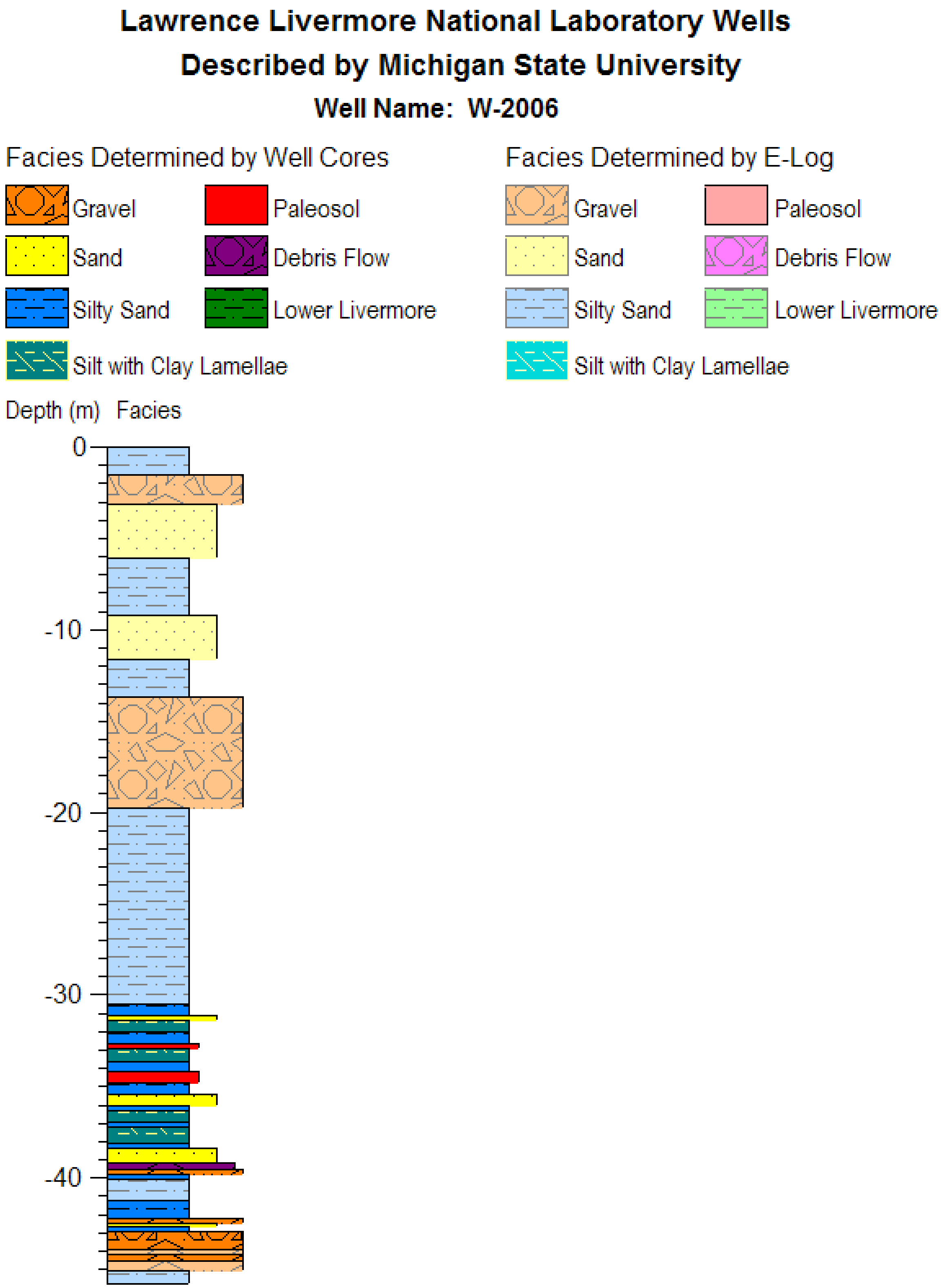

Figure 218. W-2006 stratigraphic column.

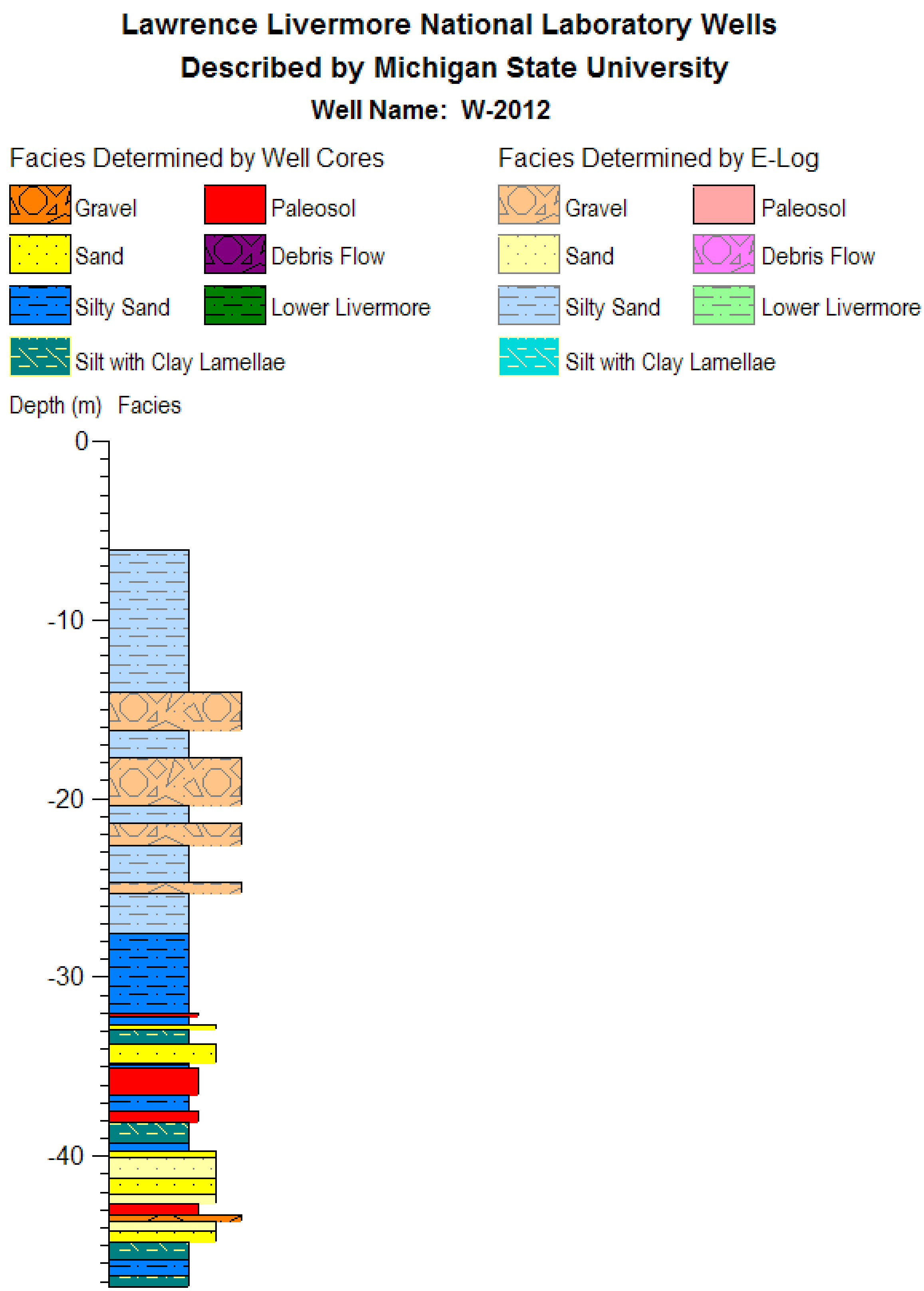

Figure 219. W-2012 stratigraphic column.

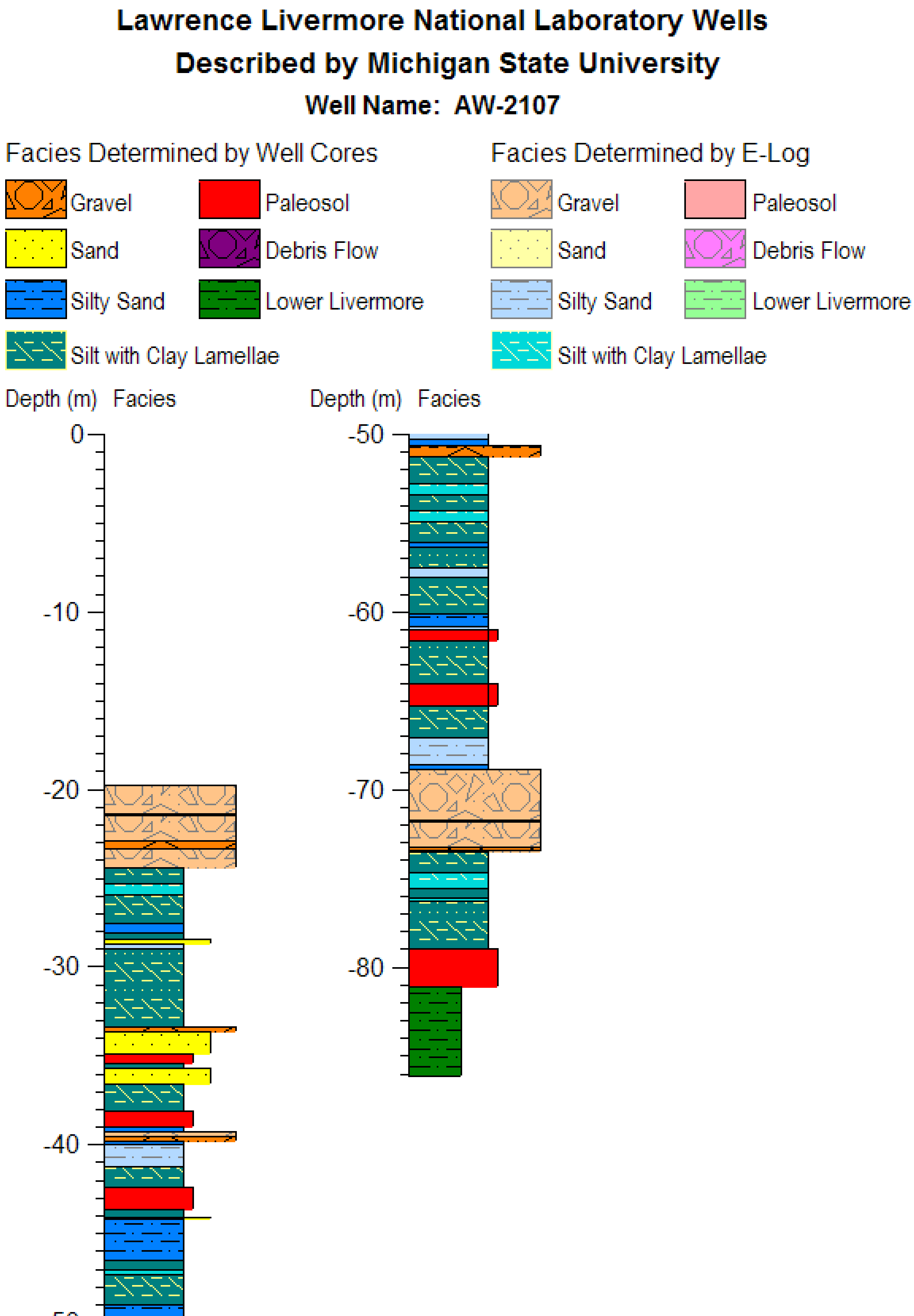

Figure 220. AW-2107 stratigraphic column.

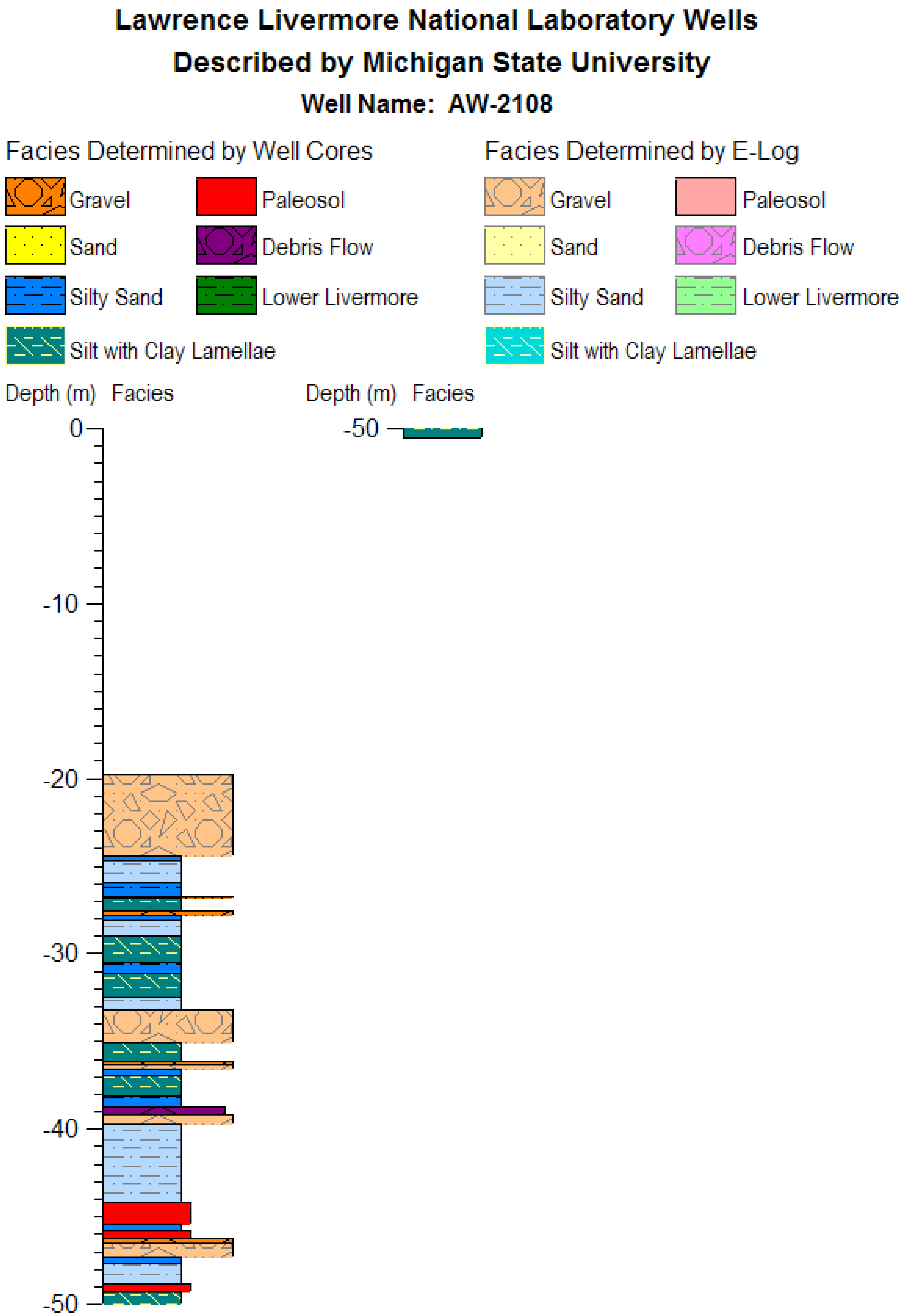

Figure 221. AW-2108 stratigraphic column.

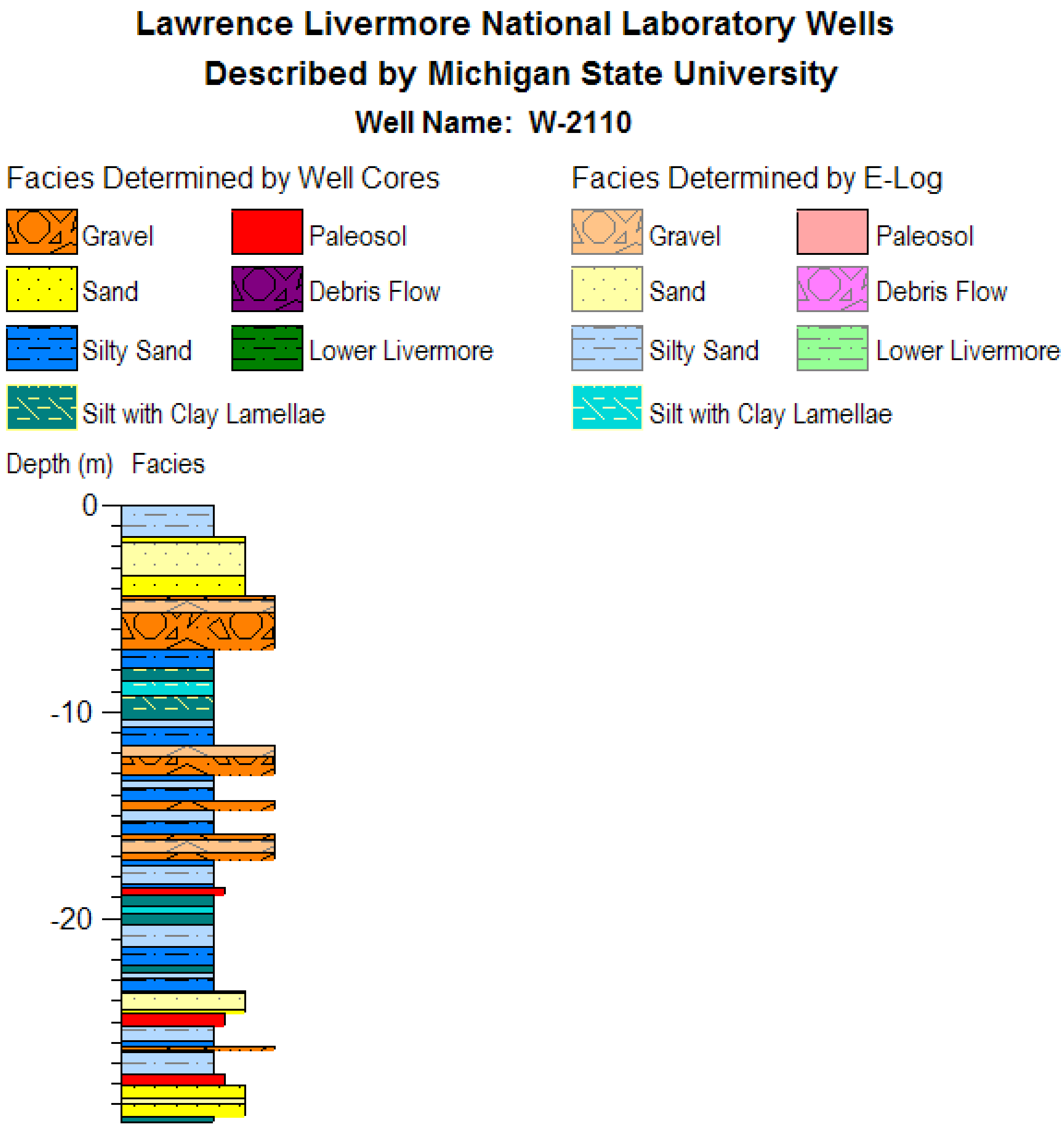

Figure 222. W-2110 stratigraphic column.

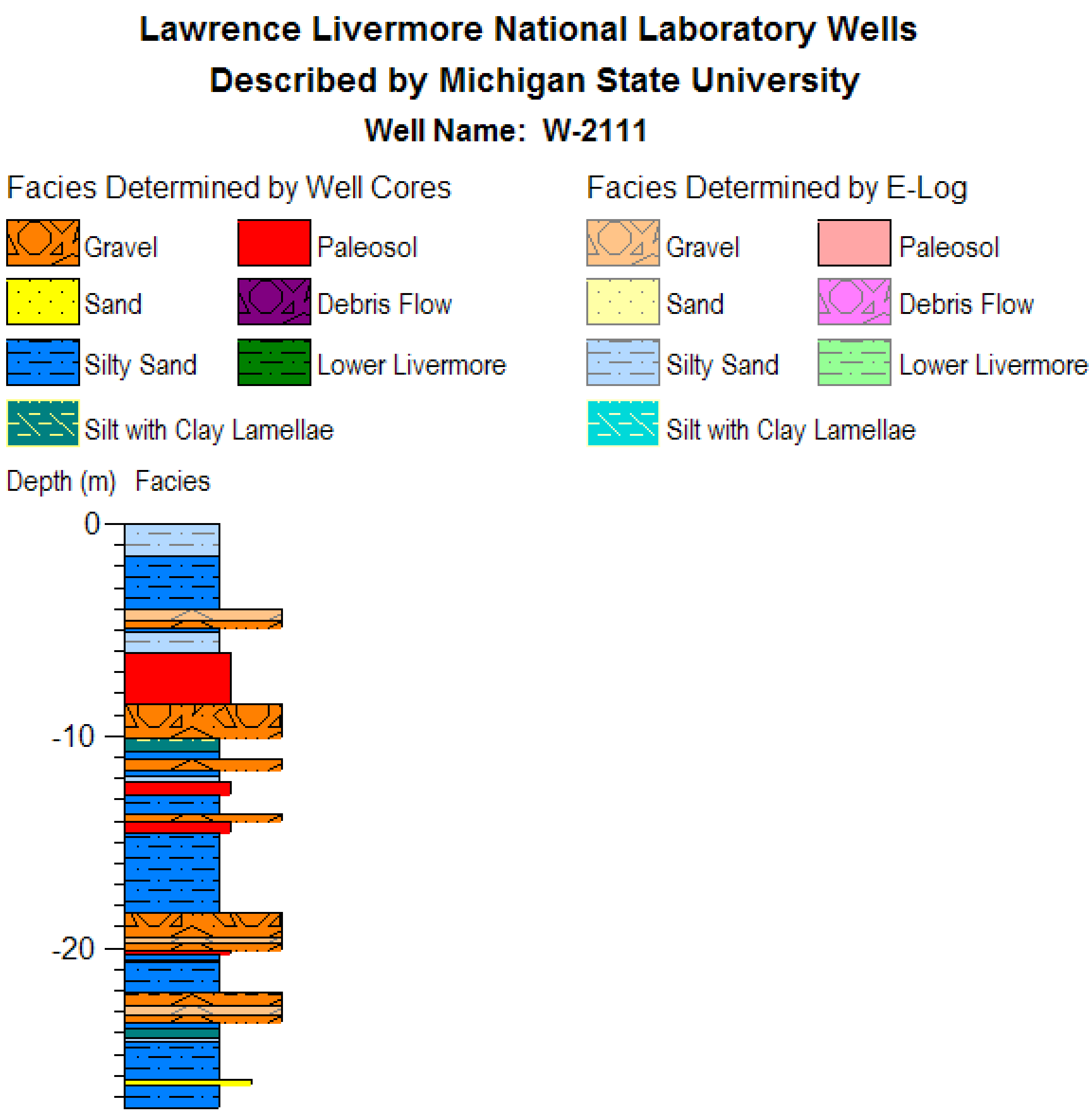

Figure 223. W-2111 stratigraphic column.

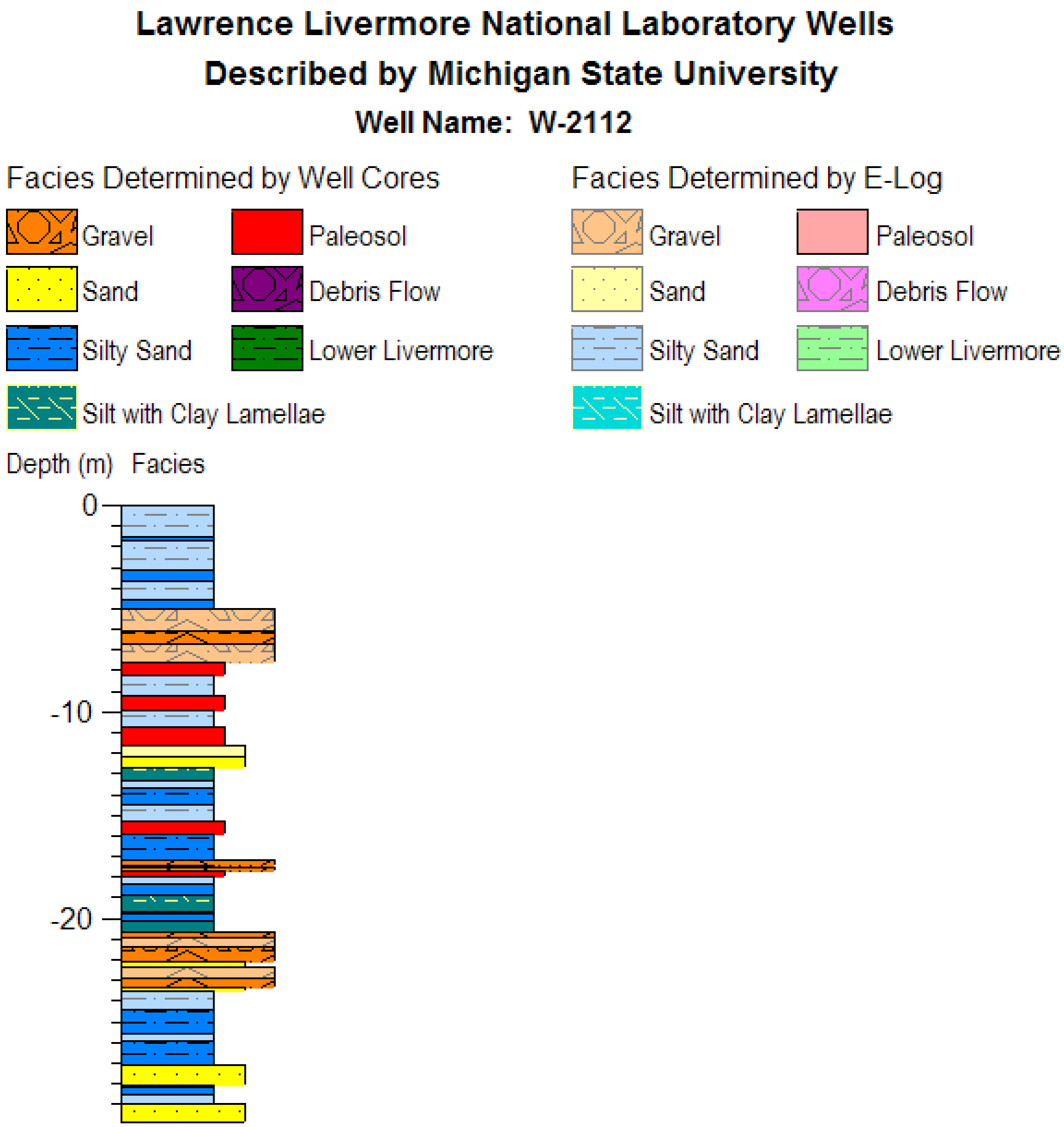

Figure 224. W-2112 stratigraphic column

BIBLIOGRAPHY

Chapter 2

Bibliography

Alonso-Zarza, A.M., Alfonso, S., Sánchez-Moya, Y., 1999. Contrasting palaeosol development in two different tectonic settings: The Upper Buntsandstein of the Western Iberian Ranges, Central Spain. Terra Nova 11, 23-29.

Badía, D., Martí, C., Palacio, E., Sancho, C., Poch, R.M., 2009. Soil evolution over the Quaternary perios in a semiarid climate (Segre river terraces, northeast Spain). Catena 77, 165-174.

Chorover, J. Amistadi, M.K., Chadwick, O.A., 2004. Surface charge evolution of mineral-organic complexes during pedogenesis in Hawaiian basalt. Geochimica et Cosmochimica Acta 68 (23), 4859-4876.

Gile, L.H., Peterson, F.F., Grossman, R.B., 1966. Morphological and genetic sequences of carbonate accumulation in desert soils. Soil Science 101, 347-360.

Harden, J.W., Taylor, E.M., Hill, C., Mark, R.K., McFadden, L.D., Reheis, M.C., Sowers, J.M., Wells, S.G., 1991. Rates of soil development from four soil chronosequences in the southern Great Basin. Quaternary Research 35, 383-399.

Harrell, J., 1984. A visual comparator of degrees of sorting in thin and plane sections. Journal of Sedimentary Petrology 54, p. 646-450

Jiang, J., Renkou, X., Anzhen, Z., 2011. Surface chemical properties and pedogenesis of topical soils derived from basalts with different ages in Hainan, China. Catena 87 (3), 334-340.

Munsell Color, 1998. Munesll soil color charts. GretagMacbeth, New Windsor, New York.

Powers, M.C., 1953. A new roundness scale for sedimentary particles. Journal of Sedimentary Petrology 23, 117-119.

Reading, H.G. (Ed.), 1996. Sedimentary Environments: Processes, Facies and Stratigraphy 3rd Edition. Blackwell Science, Cambridge, Massachusetts, 688 pp.

Retallack, G.J., 1988. Field recognition of paleosols. In: Reinhardt, J., Sigleo, W.R. (Eds.), Paleosols and Weathering through Geologic Time; Principles and Applications, vol. 216. Geological Society of America Special Paper, Boulder, Colorado, p. 1-20.

RockWare, 2002. LogPlot v. 2003. Golden, Colorado. 238 pp.

Rust, G.L., 2006. Geologically-Based Modeling of Complex Goundwater Flow Patterns at Lawrence Livermore National Laboratory: A Combined Application of Geostatistical Methods and Multiple Geologic Scenarios for Capturing Subsurface Realities. MS Thesis, University of New Mexico, Albuquerque, New Mexico, 216 pp.

Sauer, D., 2010. Approaches to quantify progressive soil development with time in Mediterranean climate – I. Use of field criteria. Journal of Plant Nutrition and Soil Science 173, 822-842.

Schaetzl, R.J., Anderson, S., 2005. Soils: Genesis and Geomorphology. Cambridge University Press, New York. 817 pp.

Shlemon, R.J., 1985. Application of soil-stratigraphic techniques to engineering geology. Bulletin of the Association of Engineering Geologists 22 (2), 129-142.

Soil Survey Staff. 1975. Soil taxonomy. U.S. Department of Agriculture Handbook Number 436, Washington, D.C., United States Government Printing Office. 754 pp.

Soil Survey Staff, 1999. Soil Taxonomy. US Department of Agriculture Handbook number 436. Washington, D.C., United States Government Printing Office.

Trahan, R.S., 2003. Evaluating Geologically-Constrained Models with Pumping Tests in a Heterogeneous Alluvial Aquifer Helipad Site at Lawrence Livermore National Laboratory, California. MS Thesis, Michigan State University, East Lansing, Michigan, 264 pp.

Weissmann, G.S., 2001. Geologic characterization of the Helipad Site (TFD), Lawrence Livermore National Laboratory, California. Report for subcontract number B503482, Michigan State University, East Lansing, Michigan, 65 pp.

Weissmann, G.S., Mount, J.F., Fogg, G.E., 2002. Glacially driven cycles in accumulation space and sequence stratigraphy of a stream-dominated alluvial fan, San Joaquin Valley, California, USA. Journal of Sedimentary Research 72, 270-281.

Wentworth, C.K., 1922. A scale of grade and class terms for clastic sediments. Journal of Geology 30, 377-392.

Wigginton, W.B., Carey, D., 1982. Age dating of Holocene deposits within the Livermore and San Ramon valleys. In: Hart, E.W., Hirschfeld, S.E., Schulz, S.S. (Eds.), Conference of Earthquake Hazards in the Eastern San Francisco Bay Area, Special Publican 62. California Department of Conservation, Division of Mines and Geology, Sacramento, CA, p. 207-216.

Wright, V.P., 1990. Estimating rates of calcrete formation and sediment accretion in ancient alluvial deposits. Geology Magazine 127 (3), 273-276.

CHAPTER 3

Stream Capture and Piracy Recorded by Provenance in Fluvial Fan Strata

By

Leslie R. Mikesell, Gary S. Weissmann, and John A. Karachewski

Geomorphology 115 (2010) 267 – 277

doi:10.1016/j.geomorph.2009.04.025

Abstract

Stream capture and piracy in tectonically active regions have been described in geomorphic systems worldwide; however, few studies show the influence stream capture has on the rock record. We present an analysis of fluvial fan stratigraphy that developed as a result of multiple stream capture events, building a complex stratigraphic succession beneath the Lawrence Livermore National Laboratory (LLNL), California. The LLNL site is located in the southeast portion of the tectonically active Livermore Basin, a transpressional basin in the California Coast Ranges. Geomorphic evidence for this stream capture include: (1) the Arroyo Seco enters the basin from the south through an uplifted fault block, (2) south of this fault block lies an abandoned Arroyo Seco fluvial fan, (3) north of the fault block, in the Livermore Basin, Arroyo Seco built a 7-km^2 fluvial fan, apparently forcing the Arroyo Las Positas, a smaller stream that enters the basin from the east, northward around the Arroyo Seco fan, and (4) a knickpoint exists near the point of capture on Arroyo Seco. Stratigraphic evidence reflecting this shift in the Arroyo Seco position into the Livermore Basin was evaluated through a provenance study of 215 gravel units from 34 boreholes spaced evenly over the 2.6 km^2 LLNL site. The Arroyo Seco derives its sediment from both the Jurassic-Cretaceous Franciscan Assemblage and the Altamont Hills (which are comprised of Mesozoic Great Valley Group and Tertiary continental sediments). The Arroyo Las Positas drains only the Altamont Hills and thus lacks the Franciscan Assemblage-derived clasts. The origin of the individual gravel units was determined by the percentage of Franciscan Assemblage indicator pebbles (red chert, green chert and blueschist) in the samples. Through this analysis, we determined that high-percentage Franciscan Assemblage-derived clasts were present below a depth of approximately 35 m below the surface, low-percentage Franciscan Assemblage-derived clasts were present at depths

between 35 m and 18 m, and high-percentage Franciscan Assemblage-derived clasts were present from depths of approximately 18 m to the surface of the fluvial fan. These results indicate that the Arroyo Seco flowed north and deposited sediments at the LLNL site, then was later absent from the basin at which time it formed a fan south of the fault block. During this absence of the Arroyo Seco, the Arroyo Las Positas, a westerly flowing stream, dominated the sediment supply at the LLNL site. The Arroyo Seco was then captured by a gully headward eroding through the uplifted fault block, redirecting the Arroyo Seco into the basin once again. This history of multiple stream captures created three stratigraphic units with alternating overall channel and paleoflow orientations.

1. Introduction

Stream capture and piracy is relatively common around the world and well documented. While most studies cite geomorphic expressions as evidence of this process (e.g. Bishop, 1995; Calvache and Viseras, 1997; Wenzens and Wenzens, 1997; Trudgill, 2002; Stokes and Mather, 2003), stratigraphic evidence for extrabasinal stream capture and piracy is rarely cited in the geologic literature (e.g., Silva et al., 1999; Zaprowski et al., 2002; Clift et al., 2006). Stream capture occurs when a headward-eroding stream actively incises into an uplifted surface, intersects a less active stream, and ultimately re-routes the second stream (Stokes and Mather, 2003; Twidale, 2004). With stream capture, the watershed boundaries are changed (Mather, 2000; Zaprowski et al., 2002; Maher et al., 2007). This shifting of watershed and sometimes even drainage basin boundaries alters the catchment size and shape of the two systems (Mather, 1993; Calvache et al., 1997; Maher et al., 2007). Stream capture, or stream piracy, has been identified from most major regions around the world, including Spain (Harvey and Wells, 1987;

Calvache and Viseras, 1997; Wenzens and Wenzens, 1997; Stokes and Mather, 2003; Maher et al., 2007), Israel (Ben-David et al., 2002), Mexico (Montgomery and Lopez-Blanco, 2003), and the American West (Smith, 1994; Zaprowski et al., 2001; Trudgill, 2002). Because stream capture is relatively common, the alluvial stratigraphic record should contain evidence for stream capture if deposition occurred in a sedimentary basin, particularly those in close proximity to tectonically active regions.

Recognition of extrabasinal stream capture and resulting fan sediments in the rock record may be important for petroleum reservoir or aquifer characterization, paleotectonic analysis, paleogeographic reconstructions, and paleoclimatic evaluations. When a new river shifts into a sedimentary basin due to upstream capture, facies orientations and geometries may change to align with this new influx of sediment and water. Identification of stratigraphic change due to stream capture can allow one to develop a predictive model of facies orientation for fluid flow modeling if paleostream directions are known, or, at a minimum, this type of stratigraphic change could alert the researchers of possible change in facies orientations. Additionally, since stream capture is related to specific types of tectonic activity, extrabasinal history may be interpreted from the sedimentary rock record.

Studies of modern fluvial fan deposits that reflect extrabasinal stream capture can provide an analog for ancient fluvial successions from similar basins worldwide, serving as a template for recognition of extrabasinal stream capture and piracy in the rock record. We use the term fluvial fan to indicate fans that are dominated by fluvial processes in order to distinguish these fan-shaped deposits from alluvial fans which are dominated by debris-flow or sheet-flood (Weissmann et al., 2005). This study documents a stream capture event where evidence of this capture is preserved in fluvial fan sediments beneath the Lawrence Livermore National

Laboratory (LLNL), located approximately 65 km east of San Francisco, California in the southeast corner of the Livermore Basin. This basin is situated in the Coast Range Province (Figure 225). The climate at this study site is Mediterranean with an average annual rainfall of 37.6 cm and January being the wettest month averaging 7.6 cm of precipitation (Thorpe et al., 1990).

LLNL is an ideal site for a fluvial fan study. LLNL was constructed on a relatively small fluvial fan (approximately 7 km^2) near the margins of a tectonically active basin. Since the early 1980's, over 15,000 meters of continuous well core and associated high quality geophysical well logs have been collected from over 700 boreholes distributed relatively evenly over the 2.6 km^2 site. These boreholes were drilled, logged, and collected by LLNL staff to facilitate a groundwater remediation project, thus providing a superb data set from which to asses the complex fluvial fan stratigraphy.

At this site, geomorphic evidence for stream capture led to evaluation of subsurface lithology in order to determine whether stream capture was evident in the basin sedimentary record. A provenance study of 215 gravel units from 34 boreholes distributed evenly across LLNL allowed recognition of three stacked fluvial fan successions at this site.

2. Background

Stream capture occurs when a headward-eroding stream actively incises into an uplifted surface, intersects a less active stream, and ultimately re-routes the second stream (Bishop, 1995; Stokes and Mather, 2003; Twidale, 2004). With stream capture, the watershed boundaries are changed resulting in a reduction in the size of one watershed, leading to a significant loss of sediment and discharge (Mather, 2000; Zaprowski et al., 2002; Maher et al., 2007), and an

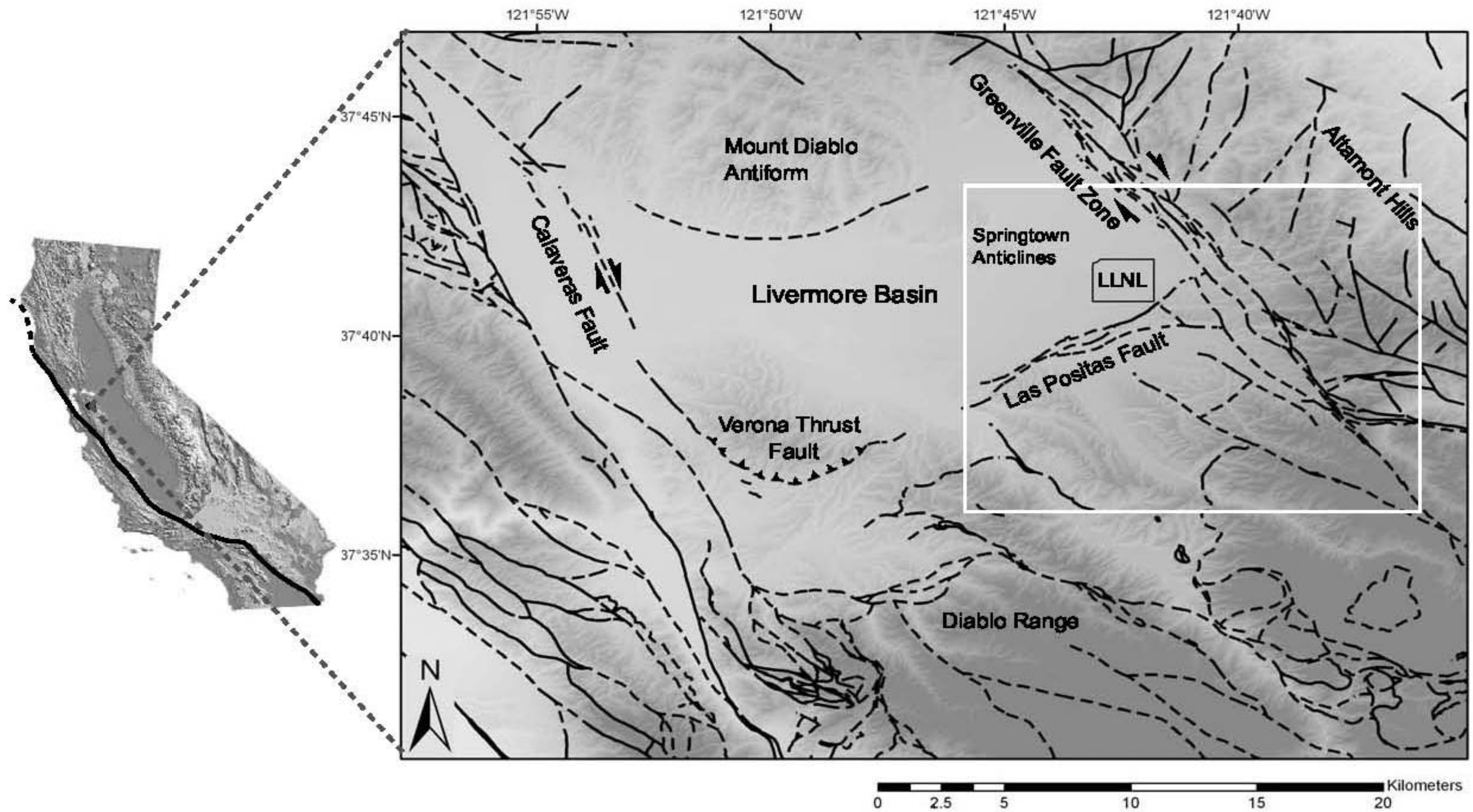

Figure 225. The Livermore Basin including the structural bounding features. The Lawrence Livermore National Laboratory (LLNL) is located in the southeast section of the basin. The light-colored box indicates the location of Figure 226. The DEM is from the Shuttle Radar Topographic Mission (SRTM) 1 arcsec coverage.

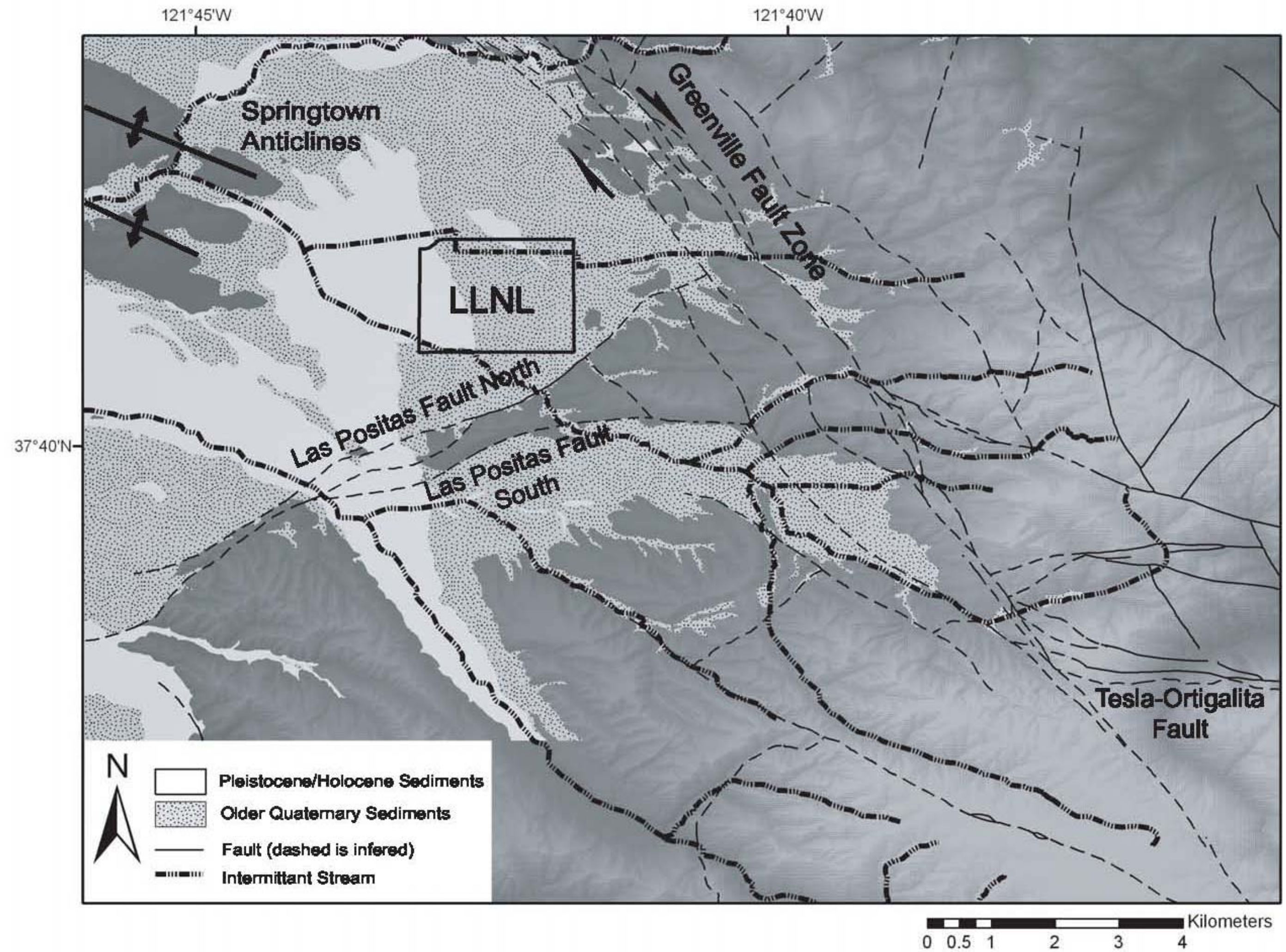

Figure 226. The southeastern portion of the Livermore Basin and associated features. The shading indicates Quaternary sediments as delineated from Helley and Graymer (1997). The light shading indicates Pleistocene/Holocene sediments and the stippled shading indicates older Quaternary sediments. The darker gray is the topography uplands from the SRTM 1 arcsec coverage.

enlargement of the capturing stream's watershed (Schumm, 1972; Mather, 2000; Stokes and Mather, 2003; Maher et al., 2007). This shifting of watershed, and sometimes even basinal, boundaries ultimately alters the geomorphology of the two systems (Mather, 1993, 2000; Calvache et al., 1997).

Evidence for stream capture includes: knickpoints in a stream profile, streams flowing through a topographic barrier, and changes in fluvial fan shapes and sizes within the basin. Not apparent at LLNL, but features that can also indicate stream capture include a distinct bend in the stream, known as an "elbow of capture" at a confluence (Zaprowski et al., 2002), fluvialgaps or windgaps, which are breaks in the topography where a stream once flowed but is now dry due to the stream being pirated further upstream (Trudgill, 2002), or a floodplain that is much larger than the current discharge of the river would dictate due to its river being captured resulting in a decrease of discharge (Zaprowski et al., 2002).

2.1 Mechanisms of Capture

The two primary mechanisms that control stream capture are tectonics and climate change (e.g., Bull, 1991; Mather, 2000; Zaprowski et al., 2002; Stokes and Mather, 2003). Tectonic uplift, faulting, and folding change the topography of the surface by raising or lowering landmasses in relation to one another, and this increase in gradient increases stream power (Ethridge et al,, 1998; Mather, 2000; Zaprowski et al., 2001; Stokes and Mather, 2003). Therefore, the most likely response to differential regional uplift is for a stream to incise a valley and begin to erode headward (Schumm, 1972; Mater, 2000; Stokes and Mather, 2003; Twidale, 2004). The intersection of such headward-eroding streams with other drainage systems results in stream capture.

Stream capture in tectonically active areas is also affected by climate change. Climate change can accelerate erosion and weathering by increasing a stream's power due to increased discharge (Blair, 1999), and it may lead to stream bank instability by decreasing vegetation (Bull, 1991). On an alluvial fan in the tectonically active northern California, Koltermann and Gorelick (1992) did establish a link between sediment architecture and paleoclimate, but they also noted strong influence by faulting and base-level change. It is more likely that an increased regional gradient associated with uplift would encourage aggressive headward erosion of a stream than would a climatic change (Harvey and Wells, 1987; Mather, 2000).

In contrast to fluvial fans in tectonically active regions, on surfaces that are not undergoing active tectonic uplift (such as passive mountain fronts or on larger alluvial fans, and during times of tectonic quiescence), captures are due to stream avulsion in the gently sloping surfaces (Field, 2001; Harvey et al., 2003). However, closely spaced streams flowing in a meandering pattern that happen to intersect each other is not true stream capture, but rather a stream system reworking sediments (Field, 2001).

One additional means of stream capture that involves neither active tectonics nor climate change is ultimately the result of bedload size (Foley, 1980). Foley (1980) describes stream capture in a piedmont. Small streams in the region adjust their gradient to the fine-grained sediment through which they are flowing and this gradient is often gentler than larger rivers in the region. The larger rivers, which are transporting coarse bedload from the mountains and thus have an armored bed, develop a steeper channel gradient. Due to this condition, the smaller stream is able to cut more easily into its bed and headward erode, intersecting the larger river and capturing its discharge.

3. Site Description

3.1 Tectonic Setting

The LLNL study area lies in the Livermore Basin within the central Coast Range. The rocks in the Livermore Basin and surrounding areas have formed in a complex and evolving tectonic setting. The Jurassic-Cretaceous Franciscan Assemblage south of the site consists of oceanic and continental rocks that formed in a subduction zone as the Farallon Plate slid beneath the North American Plate, whereas the Cretaceous Great Valley Group to the east of the site was deposited in a forearc basin. About 10 Ma, as the Mendocino triple junction passed offshore and to the north, this area was converted into a pull-apart basin controlled by strike-slip faulting and localized uplift (Nilsen and Clarke, 1987). More recently, the central Coast Range experienced a compressive stress regime that began 3.5 Ma and was affected by another tectonic pulse approximately 400 ka (Page et al., 1998; Unruh et al., 2007). The surrounding mountains are presently rising at a rate of 1 and 2 mm/yr due to thickening in the middle crust caused by this horizontal contraction (Page et al., 1998). The neotectonics of the central Coast Ranges is mainly transpressional strike-slip faulting as seen by earthquake focal mechanisms with components of both right-lateral strike-slip and thrust motions (Page et al., 1998; Hauksson et al., 2004). The northwest-trending San Andreas Fault with a maximum of 25 mm of right-lateral slip per year (Titus et al., 2005) is the major fault from a regional perspective; however, the Hayward, Calaveras, and Greenville faults are present east of San Francisco Bay (Page et al., 1998).

The Livermore Basin is an east-west topographical and structural depression within the northwest-trending central Coast Range (Figure 225). The Livermore Basin is about 25 km long, 11 km wide, and is underlain by up to 1200 m of mainly continental Tertiary and Quaternary deposits (Carpenter et al., 1980, 1984). Overall, the basin slopes from 220 m elevation on the eastern side to 92 m elevation in the southwest corner. The Livermore Basin separates the Mount Diablo antiform to the north from the Diablo Range to the south. It is bordered on the east by the Greenville Fault, which is located at the western base of the Altamont Hills, and to the west by the Calaveras Fault, both of which are right-lateral, northwest-trending transpressional faults (Herd, 1977; Dibblee, 1980a, 1980b; Barlock, 1989; Andersen et al., 1995; Graymer et al., 1996) (Figure 225). The Livermore Basin is bordered to the southeast by the Las Positas Fault (LPF), a left- lateral, northeast-trending fault. The LPF consists of two splays, a northern and a southern branch, that terminate to the east at the Greenville Fault (Herd, 1977; Bonilla et al., 1980; Dibblee, 1980b; Graymer et al., 1996) (Figures 225 and 226). Vertical movement along the LPF created a horst between the fault branches (Thorpe et al., 1990) that plays a critical role in our stream capture hypothesis. The southwestern border of the basin is the Verona Thrust Fault (Unruh and Sawyer, 1997) (Figure 225).

The Livermore Basin is currently undergoing basin inversion. Basin inversion occurs when a basin switches from subsidence in an extensional regime to uplift in a compressional regime (Followill and Mills, 1982; Stokes, 2008 and references therein). This inversion can be seen in the surficial features as well as in the sub-surface geology. The Mount Diablo antiform to the north of the basin is a result of late Tertiary uplift and crustal shortening (Unruh and Sawyer, 1997). This region also shows late Quaternary vertical deformation (Sawyer, 1999). To the south of the basin, between the Greenville and Calaveras faults, the Diablo Range block is rotating clockwise relative to the Coast Ranges (Prescott et al., 1981; Followill and Mills, 1982), causing a relative northward motion against the Livermore Basin block (Followill and Mills, 1982).

In order to accommodate the southwest-northeast shortening, the Livermore Basin block is undergoing compressional deformation as shown by thrust faults and fold features. The LPF horst, Springtown Anticlines northwest of LLNL, and the Verona thrust fault are a direct result of this crustal deformation (Unruh and Sawyer, 1997; Sawyer, 1999) (Figures 225 and 226). This basin inversion and compressional regime is also reflected by deformation of late Pliocene to Quaternary sediments (Followill and Mills, 1982; Unruh and Sawyer, 1997). Though basin inversion is occurring, the presence of recent sediments in the stratigraphic succession, as shown by Pleistocene mammoth fossil (14 ka) (Kielusiak, 1998) recovered from the shallow depths (15 - 25 m, Pers. Comm. Zafer Demir, 2008) beneath the LLNL site indicates that subsidence is still occurring in portions of the Livermore Basin.

3.2 Drainage Basin Geology

South and east of LLNL are two distinct lithologic provinces – the Diablo Range with Jurassic-Cretaceous Franciscan Assemblage rocks and the Altamont Hills with Mesozoic Great Valley Group overlain by Tertiary rocks respectively (Figure 227). These tectonically and lithologically distinct units were juxtaposed by the Coast Range Thrust, which placed the Great Valley Group structurally over the Franciscan Assemblage (Bailey et al., 1970; Raymond, 1973; Dibblee, 1980b). The northwest-trending Tesla-Ortigalita Fault represents the tectonic contact between these two complexes near LLNL (Vickery, 1924; Huey, 1948; Raymond, 1973) (Figures 226 and 227).

The Franciscan Assemblage is an accretionary prism that formed in an east-dipping subduction zone off the coast of North America during the Mesozoic and Tertiary (e.g. Lawson, 1895; Hamilton, 1969; Ernst, 1970, 1993; Hsu, 1971; Seiders, 1988; Unruh et al., 2007). The

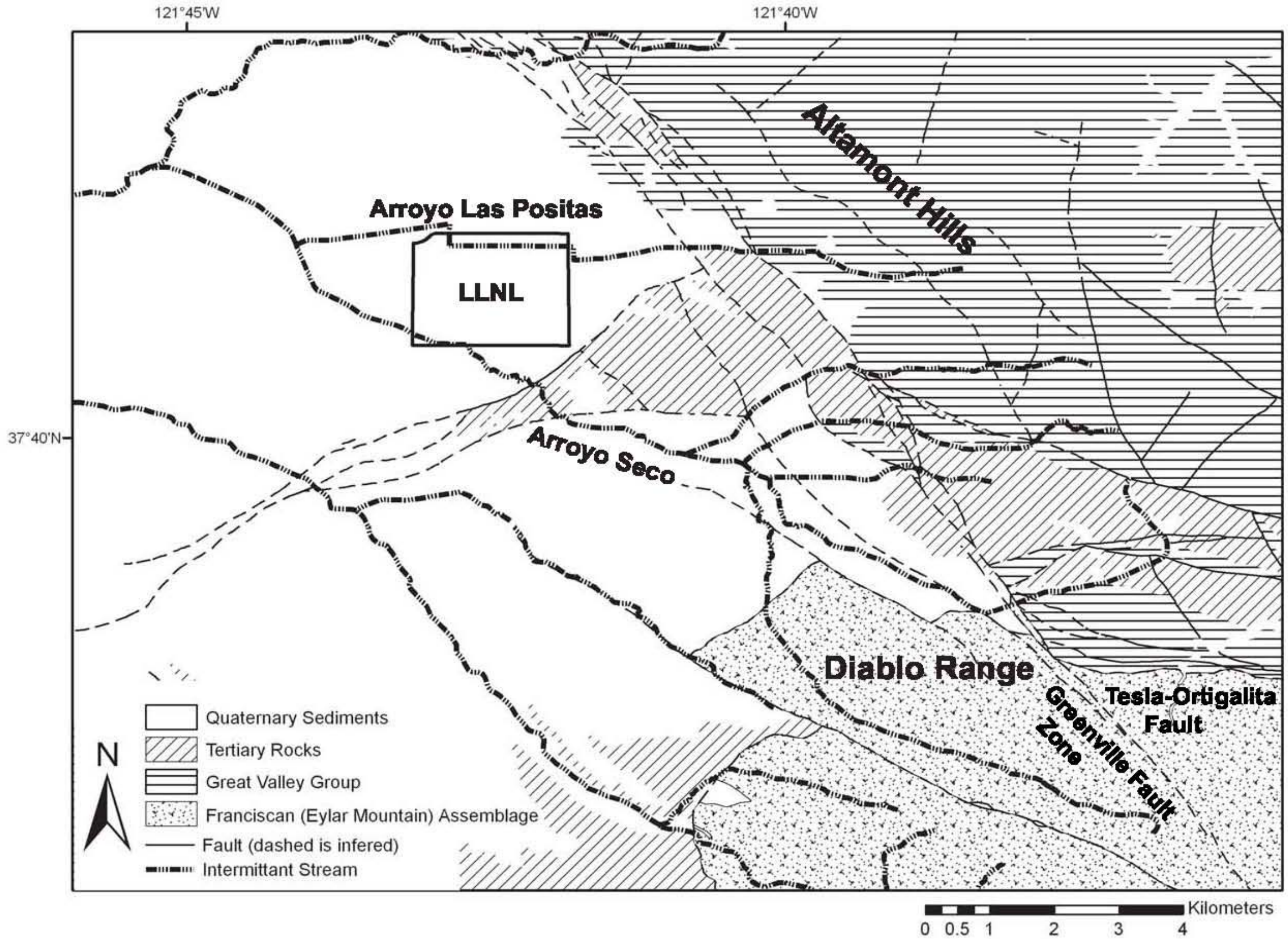

Figure 227. Simplified geologic map of the southeastern portion of the Livermore Basin showing intermittent streams, as well as the Great Valley Group, Franciscan Assemblage and their contact, along with Tertiary rocks and Quaternary sediments that influenced the gravel composition of the fluvial fan deposits in the area (modified from Graymer et al., 1996).

Franciscan Assemblage consists of graywacke, metagraywacke, shale, greenstone, chert, limestone, serpentine, mafic and ultramafic igneous rocks, and blueschist (e.g. Huey, 1948; Dibblee, 1980b; Barlock, 1989; Ernst, 1993; Schemmann et al., 2008). Near LLNL, the most distinctive Franciscan lithologies are derived from the Late Jurassic and/or Early Cretaceous Eylar Mountain Terrane (Figure 227), which consists of metabasalt, red chert, green chert, and blueschist (Sweeney and Springer, 1981; Springer, 1983; Carpenter et al., 1984; Thorpe et al., 1990; Graymer et al., 1996). Quaternary sediments exposed south of LLNL in a roadcut through the LPF horst contain red chert, green chert, and blueschist clasts which were derived from the Eylar Mountain Terrane.

The Altamont Hills are comprised of the Mesozoic Great Valley Group and overlying Tertiary rocks. The Great Valley Group consists of marine sedimentary rocks that were deposited in a Late Mesozoic forearc basin west of an Andean-type arc in the Sierras (Bailey et al., 1964; Ingersoll, 1978, 1979; Dickinson and Seely, 1979; Dickinson, 1995; Unruh et al., 2007). These relatively undeformed Cretaceous units consist of variably cemented, stratified sedimentary rocks, including conglomerates, massive bedded arkosic to lithic arenites, and graywackes (Ingersoll, 1978; Mansfield, 1979; Suchecki, 1984; Seiders, 1988; Barlock, 1989; Williams, 1993; Graymer et al., 1996). The Great Valley Group is overlain by Tertiary sedimentary rocks, including the Neroly Sandstone and the Cierbo Sandstone (Graymer et al., 1996). These primarily continental deposits consist of recycled sedimentary rocks and consist of gravels, conglomerates, sandstones, silts, clays, and coal (Huey, 1948; Carpenter et al., 1980, 1984; Graymer et al., 1996).

3.3 Current Fluvial Geomorphology

The Arroyo Seco (AS) is an intermittent stream that drains the Diablo Range and the Altamont Hills and enters the Livermore Basin from the southeast following the Tesla-Ortigalita Fault (Figure 227). The catchment geology for the AS consists of the Great Valley Group on the north side of the stream and the Franciscan Assemblage on the south side of the stream (Figure 227). The catchment size is approximately 36.40 km^2. This stream is unique in the area in that its catchment includes both complexes of rock. The AS passes through the LPF horst and runs northwest across the southwest corner of LLNL. LLNL is located primarily on the modern AS fluvial fan, a fan that is roughly 7 km^2 in area (Figure 228). At present, AS is confined to a concrete channel for flood control. Past shifts of the AS channel near LLNL are the focus of this study, and characteristic lithologies of the Franciscan Assemblage found in this drainage basin aids in determining these shifts.

Arroyo Las Positas (ALP) enters the Livermore Basin east of LLNL and crosses the northeast corner of the study site. The ALP drains only rocks of the Great Valley Group and Tertiary deposits of the Altamont Hills (Figure 227). Its catchment size is approximately 7.66 km^2. This stream originally entered LLNL from the east and drained the northern section of the site, but in 1965 it was redirected and channelized to the north and west as part of an erosion-control program (Carpenter et al., 1984). West of LLNL, ALP now flows through the northwest-southeast trending Springtown Anticlines, reflecting relatively recent channel adjustment to the late Quaternary uplift (Sawyer, 1999).

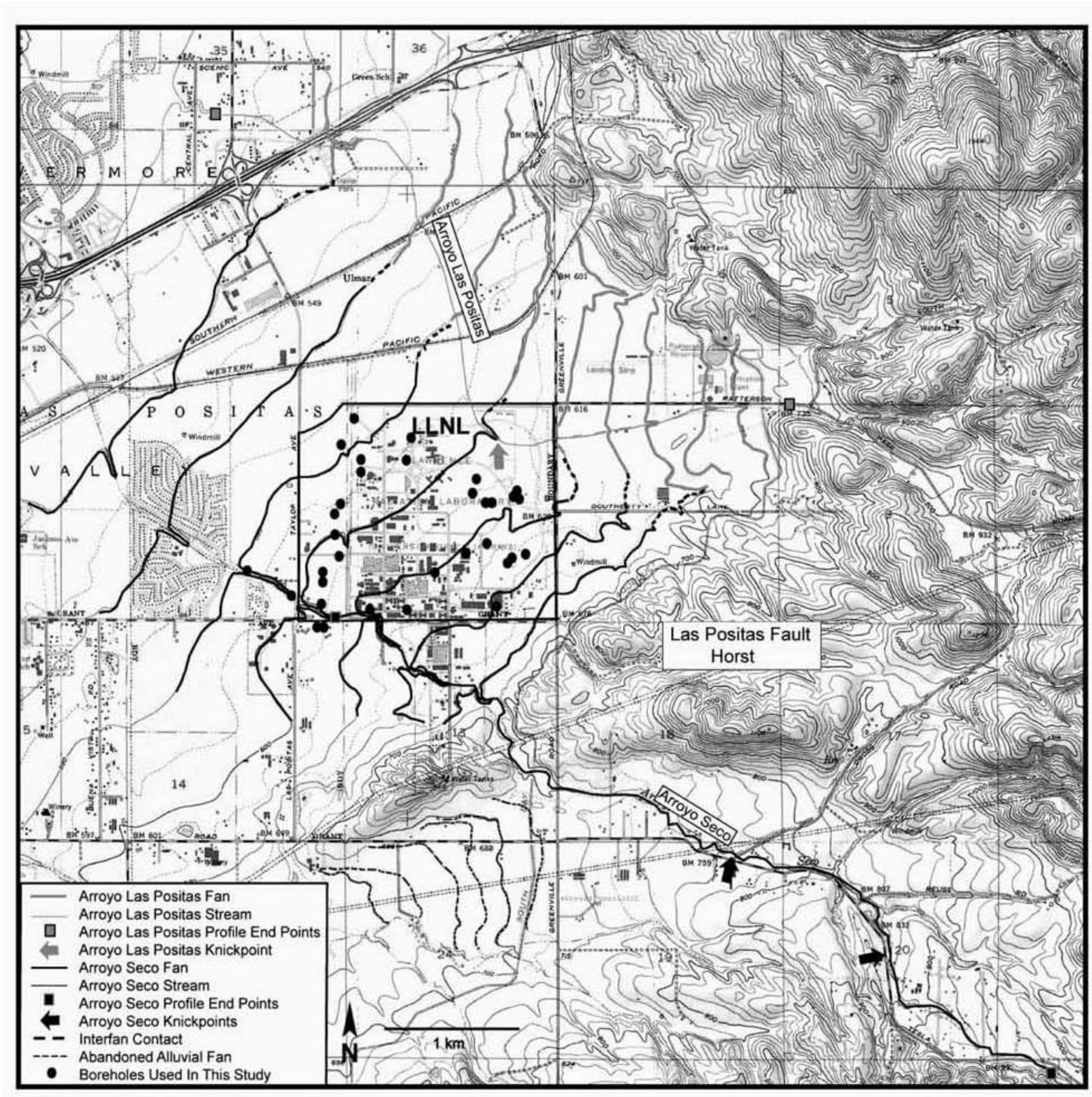

Figure 228. Topographic map with the AS fan, the ALP fan and the abandoned alluvial fan highlighted (base map is USGS, 1985). The overall topography slopes down to the northwest. Arrows indicate the knickpoints of both the AS and the ALP. The sites of the borehole cores used in this study are indicated with a dot.

4. Evidence for Stream Capture of Arroyo Seco

4.1 Geomorphic Evidence

Both geomorphic and subsurface geologic evidence suggests that the AS is a captured stream that was relatively recently rerouted into the Livermore Basin. The first line of evidence for AS stream capture is the existence of an abandoned fluvial fan south of the LPF horst (Figures 226 and 228). Several studies have been conducted in various basins with fluvial fans to assess the impact of stream loss on a basin (Mather, 1993, 2000; Wenzens and Wenzens, 1997). The reduction in and eventual cessation of deposition due to the loss of sediment will cause the fluvial fan to maintain its size (Wenzens and Wenzens, 1997; Mather, 2000). As the sediment supply diminishes, minor incisions may occur on the established fan (Mather, 1993). Eventually, a fan-shaped deposit will be left with no stream feeding it. The abandoned fan, or "alluvial fan relict" (Ben-David et al., 2002), is evidence that a stream was captured and diverted from the basin (Zaprowski et al., 2002). The abandoned fan south of the LPF horst marks the flow path of AS before it was captured and diverted through the horst. At the apex of this fan is an abandoned valley that Carpenter et al. (1984) surmise was the ancestral course of the AS. The age of these surficial deposits is older than the current AS fan surface (Helley and Graymer 1997) (Figure 226). The abandoned fan, or "alluvial fan relict" (Ben-David et al., 2002), is evidence that a stream was captured and diverted from the basin (Zaprowski et al., 2002).

Age dating of these geomorphic surfaces was outside the original scope of the project so data was not collected. However, Helley and Graymer (1997) report the abandoned fan south of the LPF horst is Pleistocene in age, whereas the fluvial fan at LLNL is reported as Pleistocene to Holocene in age The basis of this relative age assessment was based on terrace positions, and it is consistent with soil development indicated on surveys of the area (USDA, 1966).

Upgradient from LLNL, AS displays two knickpoints along its profile (Figure 229A). The first knickpoint is located approximately 3.9 km southeast of where AS crosses the LLNL border, and 1.2 km southeast of the abandoned AS fan head (Figure 228). The second knickpoint is located approximately 1.8 km up the drainage basin from the first knickpoint and marks where the channel goes from alluvium to bedrock. Similar knickpoints have been noted in captured streams and are due to differing original slopes between the capturing and captured streams (Bank, 1998; Zaprowski et al., 2001; Ben-David et al., 2002; Trudgill, 2002; Montgomery and Lopez-Blanco, 2003). The profile of the capturing stream may get steeper until a new profile can be achieved to accommodate the new sediment supply and discharge (Calvache et al., 1997). Until the profile has adjusted, some streams have knickpoints where the slope above such point is different than the slope below such point (Bank, 1998; Zaprowski et al., 2001; Ben-David et al., 2002; Trudgill, 2002; Montgomery and Lopez-Blanco, 2003). Knickpoints are not always indicators of capture, so they must be viewed along with other evidence.

Another line of evidence is that the AS currently flows northwesterly into the Livermore Basin through the LPF horst. The local tectonics and faulting uplifted the LPF horst and allowed a minor stream at LLNL to erode in a headward or southeasterly direction and ultimately to capture the larger AS, which then entered the basin through a topographic barrier (Figure 226). Streams that crosscut older drainage patterns and topographic barriers are frequently cited as evidence that a capture has occurred (Trudgill, 2002; Stokes and Mather, 2003). This crosscutting relationship is due to tectonics and faulting which uplift blocks and disrupts the old drainage pattern and allows for stream capture (Trudgill, 2002).

A

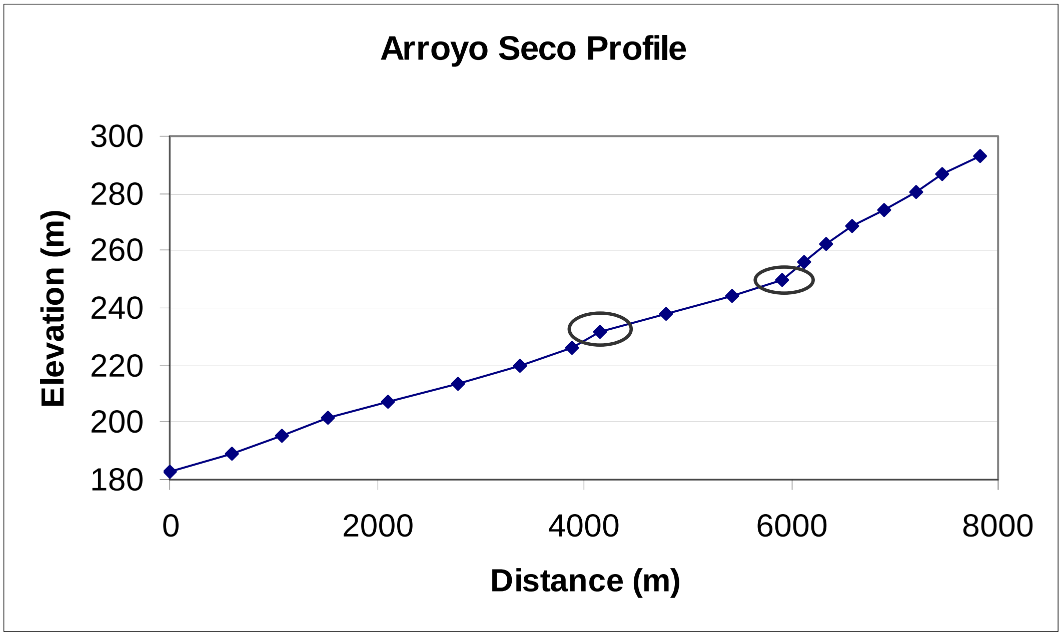

B

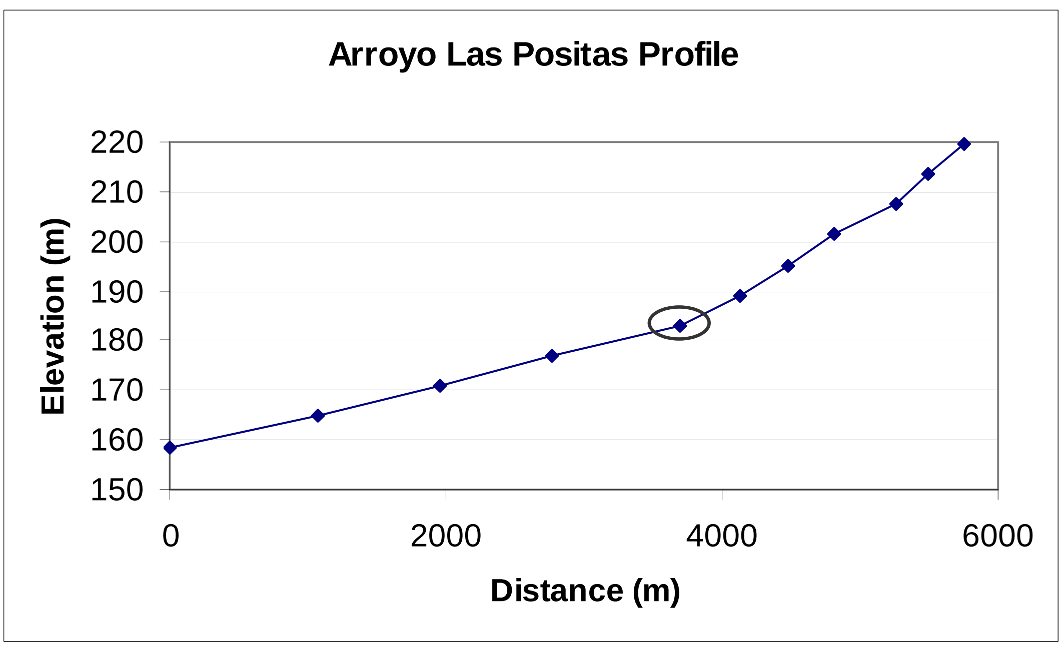

Figure 229. A. The stream profile of AS from 183.0 m to 292.8 m with its two knickpoints indicated by circles. The first knickpoint is close to its capture point, and its second knickpoint is where the stream transitions from alluvium to bedrock. B. The stream profile of ALP from 158.6 m to 219.6 m with its knickpoint indicated by a circle. The knickpoint is where the stream gradient changes and it turns to the north (see figure 228 for map locations of knickpoints and profiles).

A fluvial fan which receives an increased sediment supply and discharge due to a stream augmentation usually grows rapidly and becomes larger than other fans in the basin (Calvache et al., 1997; Mather, 2000). The AS deposited a fluvial fan (7 km^2) that coalesced with the smaller, ALP fan (3 km^2) to the north and east (Figure 228). The morphology of the smaller ALP fan suggests a northerly migration of deposition due to the growth and local elevated topography created by the larger AS fan. Based on evaluation of historic topographic maps, it was noted that the old ALP channel (prior to being redirected for erosion-control purposes) turned distinctly to the north around the AS fan at a point in the northeastern section of LLNL (Figure 228). At that same point, the gradient of the stream decreases, consistent with a stream that is forced across a longer path after being blocked by the growing AS fan (Figure 229B). The new flowpath of the ALP caused it to erode through the concurrently uplifting Springtown Anticlines northwest of LLNL (Unruh and Sawyer, 1997; Sawyer, 1999) (Figures 226 and 228).

4.2 Geologic Evidence

The AS and ALP sedimentary deposits should have distinctive character because each drainage basin crosses a different lithologic province. Provenance change is the primary stratigraphic evidence preserved in the rock record from an upgradient stream capture because the augmented stream receives a sudden influx of new sediment, occasionally with a different provenance, and stream discharge (Cat, 1988; Foster and Beaumont, 1992; Trudgill, 2002; Zaprowski et al., 2002). With this understanding, gravel samples were collected from the modern stream beds to determine if the modern gravels were distinguishable in hand sample. It was found that the modern AS gravel samples contained red chert, green chert, and blueschist from the Franciscan Assemblage, while the modern ALP lacked these clasts. Thus, we focused on assessing the lithology of clasts from gravel units beneath LLNL to determine whether we can distinguish AS from ALP deposits.

4.2.1 Methodology

For this study, 215 gravel samples from 34 boreholes were chosen from across the site (Figure 228). The gravel samples were soaked in water and disaggregated. The slurry was then passed through a 2 mm (-1.0 Φ) sieve to obtain the gravel size fraction. Granule and pebble sized clasts (2 – 16 mm) were analyzed. If the sample size was large, a sample splitter was used to reduce the sample size before analysis. Three hundred grains were selected at random from each sample, and lithology for each grain was identified. The quantity of 300 grains per sample was chosen because of the high confidence limit it provides while keeping the sample size manageable (Van der Plas and Tobi, 1965). The grains were classified as red chert, green chert, blueschist or "other". The distinctive lithologies of the Eylar Mountain Terrane of the Franciscan Assemblage are easily identified in hand samples. A percentage of indicator clasts from the Franciscan Assemblage was calculated for each sample.

4.2.2 Results

Since the AS is the only stream whose catchment includes the Franciscan Assemblage, AS sediments would have more indicator pebbles. These percentage values were plotted versus depth below ground surface (Figure 230). We assume that the ground surface had a similar slope in the past and that surfaces of equal depth can serve as approximate chronostratigraphic surfaces at this site; thus we are able to use depth to correlate these data across the site. Three clusters emerge from these data. One cluster extends from the ground surface to a depth of 18 m depth

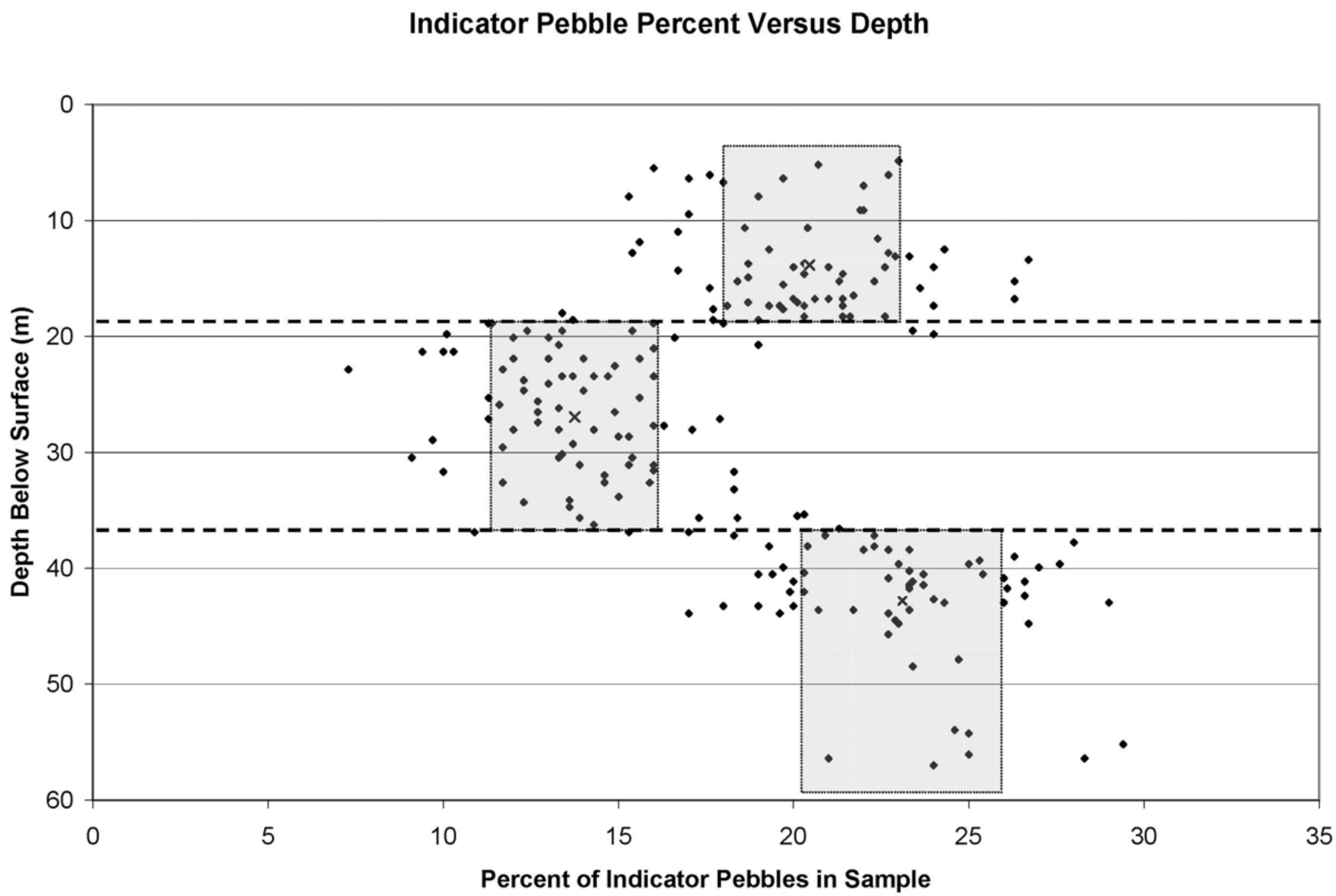

Figure 230. Plot of percent Franciscan Assemblage indicator pebbles versus depth below the ground surface. The shaded boxes encompass one standard deviation in the percent of Franciscan Assemblage-derived indicator pebbles, with the mean of the sample indicated by an 'X'. Dashed horizontal lines approximate the bounding surfaces between the successions.

and has a mean value of indicator pebbles of 20.46 percent. A second cluster lies at a depth between 18 m and 35 m and is centered on an indicator pebbles value of 13.75 percent. The third cluster lies below 35 m and is centered on an indicator pebbles value of 23.11 percent.

4.2.3 Interpretation of Geology

The uppermost and lowermost clusters display higher proportions of indicator clasts, indicating those sediments are Franciscan Assemblage-derived and were most likely deposited by AS. The middle cluster with the lower percent value indicates fewer Franciscan Assemblage indicator pebbles and thus suggests this section was primarily deposited by ALP. However, the middle cluster is not completely devoid of Franciscan Assemblage indicator pebbles due to limited additions of Franciscan Assemblage-derived sediments from the LPF horst to the south. This topographic high is comprised of Franciscan Assemblage-derived fluvial sediments and could have contributed minor indicator pebbles to the LLNL fan due to gully wash even when the AS was diverted to the south of the LPF horst.

These results indicate that there are three stacked fluvial fan successions beneath LLNL. Below a depth of 35 m are deposits dominated by a paleo-AS, between 18 m and 35 m are deposits that indicate lack of AS and dominance by ALP, and above 18 m is the current AS-dominated fan with the current ALP deposition forced further to the north.

Carpenter et al. (1984) did not find distinctive stratigraphic marker horizons in the sediments beneath LLNL. They felt that the fan was characterized by rapid lateral and vertical facies changes which hindered correlation of subsurface units. However, while rapid facies changes in fluvial fans create problems for correlating individual units; our work demonstrates that correlating large-scale fan successions is possible by using distinctive gravel units and understanding their provenance.

From the stacked fluvial fan successions, we are able to interpret the history of the LLNL site (Figure 231). During the earliest stage, the AS flowed north into the basin from the Diablo Range and deposited its sediment, including the Franciscan Assemblage-derived red chert, green chert, and blueschist, beneath what is now LLNL (Figure 231, Block 1). Later AS was absent from the Livermore Basin during which time it flowed south of the ALP horst and deposited an alluvial fan (Figure 231, Block 2). Two hypotheses for the AS absence are 1) possible uplift of the LPF horst which diverted the AS flowpath, but the timing of the uplift is not constrained, or 2) avulsion of AS. In the absence of AS, ALP was the main contributor of sediment to the LLNL site. Although minor Franciscan Assemblage indicator pebbles are found in the ALP deposits, they were probably derived from somewhat older sediments exposed on the LPF horst. During the Pleistocene AS was captured, most likely by a headward-eroding gully exploiting the weaker lithology of the original AS fan and flowpath. The gully cut through the LPF horst captured the AS and redirected it back onto the LLNL site causing it to abandon its former fan to the south of the horst (Figure 231, Block 3). The timing of these events was inferred by the relative surface ages of the abandoned and modern fans (Helley and Graymer, 1997) (Figure 226). The newly captured AS, with its larger catchment area, discharge, and sediment supply deposited a fan that resulted in northward migration of the smaller ALP fan. This northerly migration of the ALP fan occurred concurrently with the growth of the Springtown Anticlines (Figure 226). Due to the dynamic tectonic setting continuing subsidence near the LLNL site resulted in the development of accommodation space for the AS sediments and in effect, created a base-level difference that enhanced the potential for stream capture.

Legend for Figure 231
1 – Arroyo Seco
2 – Arroyo Las Positas
3 – Greenville Fault Zone
4 – Las Positas Fault Horst
5 – Abandoned Alluvial Fan

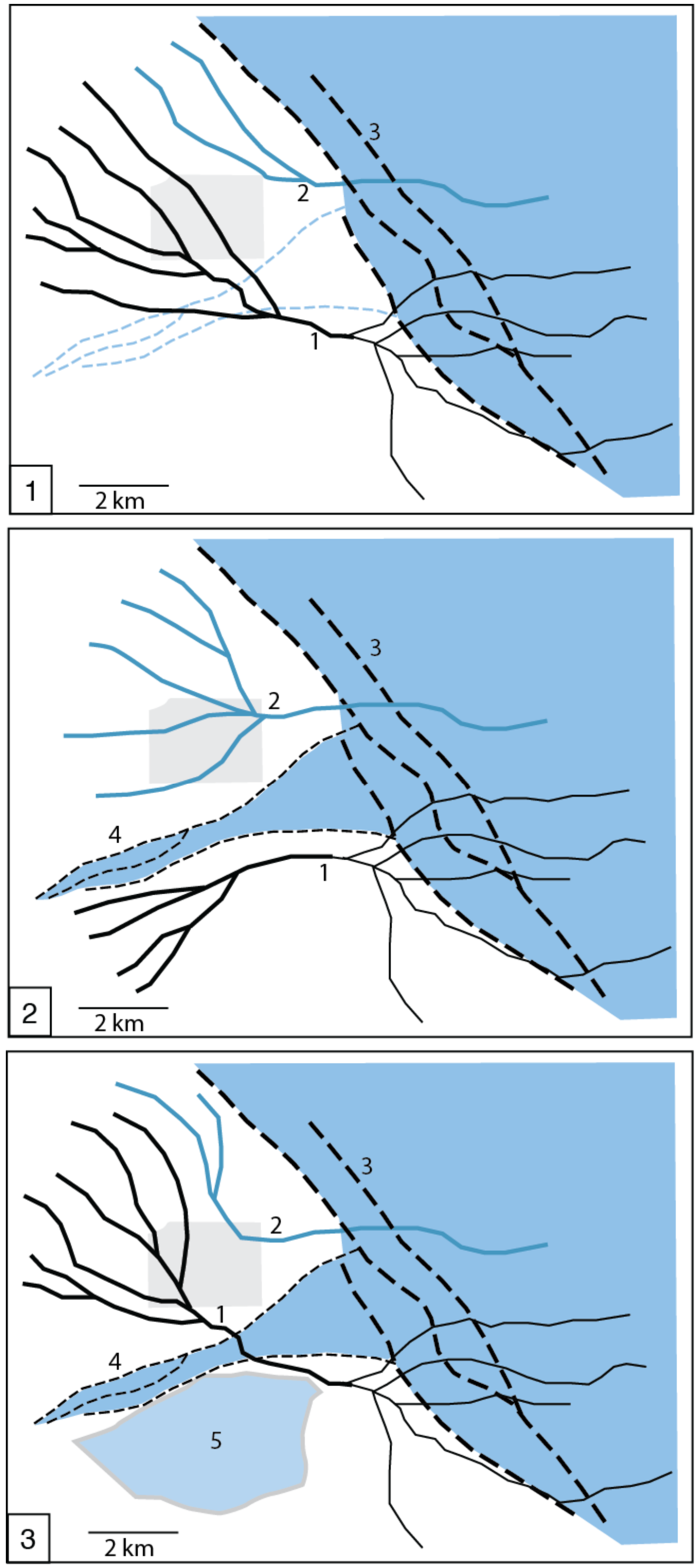

Figure 231. Interpreted schematic diagrams of the geological history of the LLNL site. The LLNL property is shaded in light gray. Dark blue indicates the topographic

Figure 231 (continued). highlands. Block 1 shows the streams in the region at the earliest time step. The LPF is indicated by dashed lines because relief around the horst is uncertain. Block 2 shows the flowpath of the AS while it was absent from the Livermore Basin and depositing a fluvial fan south of the horst. During this time, the ALP was depositing its fan at the LLNL site. Block 3 shows the current condition in the region. The AS is the dominant source of sediment for the LLNL site. This new location resulted in an abandoned alluvial fan south of the horst. Due to its smaller watershed and discharge, the ALP has been forced northward by the AS fan.

5. Implications for Sedimentology and Stratigraphy Studies

An understanding of the AS fan successions is important for assessing the anisotropy of channel orientations in the subsurface deposits. AS channels radiate outward into the basin from an apex located south or southeast of the LLNL site, thus channel deposits are expected to be generally oriented in a north-south or northwest-southeast direction (Figure 231). In contrast, ALP channels form a radial pattern away from an apex located east of the site, so ALP channel deposits are expected to be generally oriented in an east-west direction. Since these successions are stacked, channel orientation will vary with depth (Figure 231).

In the case of LLNL, this predicted orientation can be used to constrain conceptual geologic models for characterizing groundwater flow. For example, Carle et al. (1998) assumed that the entire stratigraphic section at LLNL was oriented relative to the AS apex and thus aligned the Markov chain models to this direction. The resulting simulations of aquifer heterogeneity resulted in modeled facies that retained this orientation, and simulated pumping tests using these models reasonably matched observed data at the site (Fogg et al., 2000). Trahan (2003) evaluated a pumping test from a very limited area of the LLNL site. These facies orientations provided a valuable framework that allowed Trahan (2003) to reasonably match observed pumping test results in many of his simulations. Rust (2006) used channel orientations from this provenance study to help constrain aquifer stratigraphic models at another study area at the LLNL site. Thus, knowledge of channel orientations and distribution of facies based on understanding variability caused by extrabasinal stream capture can lead to improved characterization of aquifer heterogeneity and more realistic numerical models.

In addition to channel orientation, sediment texture may also vary with depth. The units deposited by AS should have coarser-grained sediment in the southern portion of LLNL, closer to the apex of its fan, with finer-grained sediment to the north (Figure 231). In contrast, the ALP units should have coarser-grained sediment to the east and finer-grained sediment to the west (Figure 231). We are currently continuing our research to test this hypothesis. Understanding variation in channel orientations and sediment texture with depth in basins where stream capture is common will aid in determining preferential pathways for fluid flow in aquifers and petroleum reservoirs.

Finally, the record of Earth's past is held in deposits of sedimentary basins and recognition of extrabasinal events reflected in the rock record can aid in paleogeographic reconstruction, paleotectonic interpretation, and paleoclimatic analysis. In this case, we observed an abrupt change in gravel provenance as a response to extrabasinal stream capture. This provenance shift, along with an expected abrupt change in overall channel sandbody orientation, can provide evidence of stream capture in similar ancient basins.

6. Conclusions

We were able to show that the AS is a captured stream based on geomorphic evidence such as the AS flow path through a horst, an abandoned fluvial fan south of this horst, a knickpoint in the AS near the point of capture, and the northern migration of ALP. Evaluation of gravel provenance provides additional supporting evidence that three distinct lithologic successions exist in the fan stratigraphy, indicating multiple events of capture in the past. By this evidence we determined that the paleo-AS once flowed north into the Livermore Basin until it shifted to the south possibly due to faulting and uplift of the LPF horst. During this time, AS deposited a fluvial fan south of the horst and only minor Franciscan Assemblage sediments derived from the uplifted topographic high was deposited at the LLNL site. The ALP built its fan with sediment eroded from the Great Valley Group and Tertiary deposits of the Altamont Hills. Finally, during the Pleistocene, a headward-eroding gully captured the AS and redirected it back onto the LLNL site leaving an abandoned fan south of the horst. The re-introduction of the AS and its fan with its larger catchment, discharge, and sediment supply forced the smaller ALP fan to migrate towards the north.

The stratigraphic successions of the fluvial fan beneath the LLNL site recorded a provenance change of the sediments. Provenance changes, along with geomorphic evidence, indicate multiple stream captures along this tectonically active basin margin. We would expect to find similar stratigraphic signatures of other succession in fluvial fans located in tectonically active basins where stream capture occurs.

Acknowledgements

This material is based upon work supported by the National Science Foundation under Grant No. EAR-0617992 and EAR-0133666. Any opinions, findings, and conclusions or recommendations expressed in this material are those of the authors and do not necessarily reflect the views of the National Science Foundation. The authors would like to thank those from the Environmental Restoration Division at LLNL who provided immense help and support to this project, including Fred Hoffman, Charlie Noyes, Zafer Demir, Ben Johnson, Paul Anderson, and Jon Ulrech. We also thank students from MSU who provided lab and field support, including Beth Apple, Sara Auer, Kent Dankenbring, Aimee Kniesel, Karen Strickling, Luke Zoet, and Sarah Holmstrom. This manuscript benefited greatly from review by Adrian Harvey, Martin Stokes and two anonymous reviewers. We appreciate their edits and comments.

BIBLIOGRAPHY

Chapter 3

Bibliography

Andersen, D. W., Isaacson, K. A., Barlock, V. E., 1995. Neogene evolution of the Livermore basin within the California Coast Ranges. In: Fritsche, A.E. (Ed.), Cenozoic Paleogeography of the Western United States – II. SEPM Pacific Section, Book 75, pp. 151-161.

Bailey, E. H., Irwin, W. P., Jones, D. L., 1964. Franciscan and related rocks, and their significance in the geology of western California. California Division of Mines and Geology, Bulletin 183, 177pp.

Bailey, E. H., Blake, M. C., Jr., Jones, D. L., 1970. On-land Mesozoic oceanic crust in the California Coast Ranges. United States Geological Survey Professional Paper 700-C, C70-C81.

Bank, G. C., 1998. Headward advance of the James River basin by the capture of St. Marys River from the Shenandoah River basin, Virginia. Geological Society of America Abstracts with Programs 1998, A-140.

Barlock, V. E., 1989. Sedimentology of the Livermore gravels (Miocene-Pleistocene), southern Livermore Valley, California. United States Geological Survey, Open-File Report 89-31.

Ben-David, R., Eyal, Y., Zilberman, E., Bowman, D., 2002. Fluvial systems response to rift margin tectonics: Makhtesh Ramon area, southern Israel. Geomorphology 45, 147-163.

Bishop, P., 1995. Drainage rearrangement by river capture, beheading and diversion. Progress in Physical Geography 19 (4), 449-473.

Blair, T. C., 1999. Cause of dominance by sheetflood vs. debris-flow processes on two adjoining alluvial fans, Death Valley, California. Sedimentology 46, 1015-1028.

Bonilla, M. G., Lienkaemper, J. J., Tinsley, J. C., 1980. Surface faulting near Livermore, California associated with the January 1980 earthquakes. United States Geological Survey, Open-File Report 80-523.

Bull, W. B., 1991. Geomorphic Response to Climatic Change. New York, Oxford University Press, 326 pp.

Calvache, M. L., Viseras C., 1997. Long-term control mechanisms of stream piracy processes in southeast Spain. Earth Surface Processes and Landforms 22, 93-105.

Calvache, M. L., Viseras, C., Fernandez, J., 1997. Controls on fan development – evidence from fan morphometry and sedimentology; Sierra Nevada, SE Spain. Geomorphology 21, 69-84.

Carle, S.F., LaBolle, E.M., Weissmann, G.S., Van Brocklin, D., Fogg, G.E., 1998. Conditional simulation of hydrofacies architecture: a transition probability / Markov approach. In: Fraser, G.S., Davis, J.M. (Eds.), Hydrogeologic Models of Sedimentary Aquifers, pp. 147-170.

Carpenter, D. W., Puchlik, K. P., Ramirez, A. L., Wagoner, J. L., Knauss, K. G., Kasameyer, P. W., 1980. Status report on the geology of the Lawrence Livermore National Laboratory site and adjacent areas, Volume 1: Text and appendices A-E. Livermore, California, Lawrence Livermore National Laboratory (UCRL-53065 Vol. 1), 97 pp.

Carpenter, D. W., Sweeney, J. J., Kasameyer, P. W., Burkhard, N. R., Knauss, K. G., Shlemon, R. J., 1984. Geology of the Lawrence Livermore National Laboratory site and adjacent areas. Livermore, California, Lawrence Livermore National Laboratory (UCRL-53316), 188 pp.

Cat, J. A., 1988. Quaternary Geology for Scientists and Engineers. New York, John Wiley & Sons, 340 pp.

Clift, P. D., Blusztajn, J., Duc, N. A., 2006. Large-scale drainage capture and surface uplift in eastern Tibet-SW China before 24 Ma inferred from sediments of the Hanoi Basin, Vietnam. Geophysical Research Letters 33 (19), L19403.

Dibblee, T. W., 1980a. Preliminary geologic map of the Livermore Quadrangle, Alameda and Contra Costa Counties, California. United States Geological Survey, Open-File Report 80-533B.

Dibblee, T. W., 1980b. Preliminary geologic map of the Altamont Quadrangle, Alameda County, California. United States Geological Survey, Open-File Report 80-538.

Dickinson, W.R., 1995. Forearc basins. In: Busby, C.J., Ingersoll, R.V. (Eds.), Tectonics of Sedimentary Basins. Cambridge, Blackwell, pp. 221-261.

Dickinson, W. R., Seely, D. R., 1979. Structure and stratigraphy of forearc regions. American Association of Petroleum Geologists Bulletin 63 (1), 2-31.

Ernst, W. G., 1970. Tectonic contact between the Franciscan Melange and the Great Valley Sequence – crustal expression of a Late Mesozoic Benioff Zone. Journal of Geophysical Research 75, 886-901.

Ernst, W.G., 1993. Metamorphism of Franciscan tectonostratigraphic assemblage, Pacheco Pass area, east-central Diablo range, California Coast Ranges. Geological Society of America Bulletin 105, 618-636.

Ethridge, F. G., Wood, L. J., and Schumm, S. A., 1998. Cyclic variables controlling fluvial sequence development: Problems and perspectives. In: Stanley, K. W., McCabe, P. J., (Eds.), Relative Role of Eustasy, Climate, and Tectonism in Continental Rocks. Society for Sedimentary Geology Special Publication 59, 17-29.

Field, J., 2001. Channel avulsion on alluvial fans in southern Arizona. Geomorphology 37, 93-104.

Fogg, G. E., Carle, S. F., Green, C., 2000. Connected-network paradigm for the alluvial aquifer system. In: Zhang, D., Winter, C. L., (Eds.), Theory, Modeling, and Field Investigation in Hydrogeology: A Special Volume in Honor of Shlomo P. Neuman's 60^{th} Birthday. Boulder, Colorado, Geological Society of America Special Paper 348, 25-42.

Foley, M. G., 1980. Quaternary diversion and incision, Dearborn River, Montana. Geological Society of America Bulletin 91, part 2, 2152-2188.

Followill, F. E., Mills, J. M., 1982. Locations and focal mechanisms of recent microearthquakes and tectonics of Livermore Valley, California. Bulletin of the Seismological Society of America 72 (3), 821-840.

Foster, N. H., Beaumont, E. A., (Eds.), 1992. Photogeology and Photogeomorphology. Tulsa, American Association of Petroleum Geologists Treatise of Petroleum Geology Reprint Series No. 18, 555 pp.

Graymer, R. W., Jones, D. L., Barbb, E. E., 1996. Preliminary geologic map emphasizing bedrock formations in Alameda County, California: Derived from the digital database. United States Geological Survey, Open-File Report 96-252.

Hamilton, W., 1969. Mesozoic California and the underflow of the Pacific mantle. Geological Society of America Bulletin 80, 2409-2430.

Harvey, A. M., Wells, S. G., 1987. Response of Quaternary fluvial systems to differential epeirogenic uplift: Aguas and Feos River systems, south-east Spain. Geology 15, 689-693.

Harvey, A. M., Foster, G., Hannam, J., Mather, A. E., 2003. The Tabernas alluvial fan and lake system, southeast Spain: applications of mineral magnetic and pedogenic iron oxide analyses towards clarifying the Quaternary sediment sequences. Geomorphology 50, 151-171.

Hauksson, E., Oppenheimer, D., Brocher, T. M., 2004. Imaging the source region of the 2003 San Simeon earthquake within the weak Franciscan subduction complex, central California. Geophysical Research Letters 31, L20607.

Helley, E.J., Graymer, R.W., 1997. Quaternary geology of Alameda County and parts of Contra Costa, Santa Clara, San Mateo, San Francisco, Stanislaus, and San Joaquin counties, California. A Digital Database, United States Geological Survey, Open-File Report 97-97.

Herd, D. G., 1977. Geologic map of the Las Positas, Greenville, and Verona Faults, eastern Alameda County, California. United States Geological Survey, Open-File Report 77-689.

Hsu, K. J., 1971. Franciscan Melange as a model for eugeosynclinal sedimentation and underthrusting tectonics. Journal of Geophysical Research 76, 1162-1170.

Huey, A. S., 1948. Geology of the Tesla Quadrangle, California. California Division of Mines, San Francisco, CA, Bulletin 140, 75.

Ingersoll, R.V., 1978. Petrofacies and petrologic evolution of the late Cretaceous forearc basin, northern and central California. Journal of Geology 86, 335-352.

Ingersoll, R. V., 1979. Evolution of the Late Cretaceous forearc basin, northern and central California. Geological Society of America Bulletin, Part I 90, 813-826.

Kielusiak, C., 1998. Evacuation of mammoth bones at the NIF construction site. Lawrence Livermore National Laboratory (UCRL-JC-132153 Abs).

Koltermann, C. E., Gorelick, S. M., 1992. Paleoclimatic signature in terrestrial flood deposits. Science 256, 1775-1782.

Lawson, A. C., 1895. Sketch of the geology of the San Francisco Peninsula, California. United States Geological Survey, 15th Anniversary Report, 349-476.

Maher, E., Harvey, A.M., France, D., 2007. The impact of a major Quaternary river capture on the alluvial sediments of a beheaded river system, the Rio Alias SE Spain. Geomorphology 84, 344-356.

Mansfield, C. F., 1979. Upper Mesozoic subsea fan deposits in the southern Diablo Range, California: record of the Sierra Nevada magmatic arc. Geological Society of America Bulletin 90, Part I, 1025-1046.

Mather, A. E., 1993. Basin inversion: some consequences for drainage evolution and alluvial architecture. Sedimentology 40, 1069-1089.

Mather, A. E., 2000. Impact of headwater river capture on alluvial system development: an example from the Plio-Pleistocene of the Sorbas Basin, SE Spain. Journal of the Geological Society, London 157, 957-966.

Montgomery, D. R., Lopez-Blanco, J., 2003. Post-Oligocene river incision, southern Sierra Madre Occidental, Mexico. Geomorphology 55, 235-247.

Nilsen, T. H., Clarke, Jr., S. H., 1987. Geological evolution of the late Cenozoic basins of northern California. In: Schymiczek, H., Suchsland, R., (Eds.), Tectonics, Sedimentation and Evolution of the Eel River and Associated Coastal Basins of Northern California; proceedings of a symposium, Bakersfield, CA, San Joaquin Geological Society, pp. 15-29.

Page, B. M., Thompson, G. A., Coleman, R. G., 1998. Late Cenozoic tectonics of the central and southern Coast Ranges of California. Geological Society of America Bulletin 110 (7), 846–876.

Prescott, W. H., Lisowski, M., Savage, J. C., 1981. Geodetic measurement of crustal deformation on the San Andreas, Hayward and Calaveras faults near San Francisco, California. Journal of Geophysical Research 86 (B11), 10853-10869.

Raymond, L.A., 1973. Tesla-Ortigalita Fault, Coast Range Thrust Fault, and Franciscan metamorphism, northeastern Diablo Range, California. Geological Society of America Bulletin 84, 3547-3562.

Rust, G.L., 2006. Geologically-based modeling of complex groundwater flow patterns at Lawrence Livermore National Laboratory: A combined application of geostatistical methods and multiple geologic scenarios for capturing subsurface realities. unpublished MS Thesis, University of New Mexico, 216 pp.

Sawyer, T. L., 1999. Assessment of contractional deformation rates of the Mt. Diablo fold and thrust belt, eastern San Francisco Bay region, northern California: Final technical report. United States Geological Survey, Department of the Interior, National Earthquake Hazards Reduction Program, Award Number 98-HQ-GR-1006, 38 pp.

Schemmann, K., Unruh, J. R., Moores, E. M., 2008. Kinematics of Franciscan Complex exhumation: new insights from the geology of Mount Diablo, California. Geological Society of America Bulletin 120 (5/6), 543–555.

Schumm, S. A., (Ed.), 1972. River Morphology: Stroudsburg, Pennsylvania, Dowden, Hutchinson & Ross, Inc., 429 pp.

Seiders, V. M., 1988. Origin of conglomerate stratigraphy in the Franciscan assemblage and Great Valley sequence, northern California. Geology 16, 783-787.

Silva, P. G., Palomares, M., Rubio, F., Goy, J. L., Hoyos, M., Marin-Serrano, A., Zazo, C., and Alberdi, M. T., 1999. Geomorphology, stratigraphy, paleontology and provenance of Quaternary arkoses from the Prados-Guaten Depression; southwestern Madrid. Cuaternario y Geomorfologia 13 (1-2), 79-94.

Smith, G. A., 1994. Climatic influences on continental deposition during late-stage filling of an extensional basin, southeastern Arizona. Geological Society of American Bulletin 106, 1212-1228.

Springer, J. E., 1983. Structural analysis of the southeastern Livermore Basin, California. Livermore, California, Lawrence Livermore National Laboratory (UCID-19805).

Stokes, M., 2008. Plio-Pleistocene drainage development in an inverted sedimentary basin: Vera basin, Betic Cordillera, SE Spain. Geomorphology (doi: 10.1016/j.geomorph.2007.10.026).

Stokes, M., Mather, A. E., 2003. Tectonic origin and evolution of a transverse drainage: The Rio Almanzora, Betic Cordillera, southeast Spain. Geomorphology 50, 59-81.

Suchecki, R. K., 1984. Facies history of the Upper Jurassic-Lower Cretaceous Great Valley Sequence; response to structural development of an outer-arc basin. Journal of Sedimentary Petrology 54 (1), 170-191.

Sweeney, J. J., Springer, J. E., 1981. Geology of the southeastern Livermore Valley, Alameda County, California. Lawrence Livermore National Laboratory (UCRL-53200), Rev. 1, 54 pp.

Thorpe, R. K., Isherwood, W. S., Dresn, M. D., Webster-Scholten, C. P., 1990. Remedial investigations report for the LLNL Livermore Site. Livermore, California, Lawrence Livermore National Laboratory (UCAR-10299).

Titus, S. J., DeMets, C., Tikoff, B., 2005. New slip rate estimates for the creeping segment of the San Andreas fault, California. Geology 33 (3), 205-208.

Trahan, R. S., 2003. Evaluating geologically-constrained models with pumping tests in a heterogeneous alluvial aquifer, Helipad Site at Lawrence Livermore National Laboratory, California. unpublished M.S. Thesis, Michigan State University, 264 pp.

Trudgill, B. D., 2002. Structural controls on drainage development in the Canyonlands grabens of southeast Utah. American Association Petroleum Geologists Bulletin 86 (6), 1095-1112.

Twidale, C. R., 2004. River patterns and their meaning. Earth-Science Reviews 67, 159-218.

Unruh, J. R., Sawyer, T. L., 1997. Assessment of blind seismogenic sources, Livermore valley, eastern San Francisco Bay region: Final technical report. United States Geological Survey, Department of the Interior, National Earthquake Hazards Reduction Program, Award Number 1434-95-G-2611, 88 pp.

Unruh, J. R. Dumitru, T. A., Sawyer, T. L., 2007. Coupling of early Tertiary extension in the Great Valley forearc basin with blueschist exhumation in the underlying Franciscan accretionary wedge at Mount Diablo, California. Geological Society America Bulletin 119 (11/12), 1347–1367.

USDA, Soil Conservation Service, 1966. Soil Survey Alameda Area, California. US Department of Agriculture Soil conservation Service, Series 1961, No. 41, 95 pp.

Van der Plas, L., Tobi, A. C., 1965. A chart for judging the reliability of point counting results. American Journal of Science 263, 87-90.

Vickery, F. P., 1924. Structural dynamics of the Livermore region. unpublished Ph.D. Thesis, Stanford University, 70 pp.

Weissmann, G. S., Bennett, G. L., Lansdale, A. L., 2005. Factors controlling sequence development on Quaternary fluvial fans, San Joaquin Basin, California, USA. In: Harvey, A. M., Mather, A. E., Stokes, M. (Eds.), Alluvial Fans: Geomorphology, Sedimentology, Dynamics. Geological Society, London, Special Publications 251, 169–186.

Wenzens, E., Wenzens, G., 1997. The influence of tectonics, sea-level fluctuations and river capture on the Quaternary morphogenesis of the semi-arid Pulpi Basin (southeast Spain). Catena 30, 283-293.

Williams, T.A., 1993. Current views on the deposition and sequence stratigraphy of the Great Valley Group, Sacramento Basin. In: Graham, S.A., Lowe, D.R. (Eds.), Advances in the Sedimentary Geology of the Great Valley Group, Sacramento Valley, California. Pacific Section, Society of Economic Petrologists and Mineralogists Book 73, pp. 5-17.

Zaprowski, B. J., Evenson, E. B., Pazzaglia, F. J., Epstein, J. B., 2001. Knickzone propagation in the Black Hills and northern High Plains: a different perspective on the late Cenozoic exhumation of the Laramide Rocky Mountains. Geology 29 (6), 547-550.

Zaprowski, B. J., Evenson, E. B., Epstein, J. B., 2002. Stream piracy in the Black Hills: a geomorphology lab exercise. Journal of Geoscience Education 50 (4), 380-388.

CHAPTER 4

Lawrence Livermore National Laboratory

Geochemical Data Analysis and Results

1. Introduction

Geochemical data have long been a useful tool in geological studies as an indicator of magma source (Butler and Woronow, 1986; Mertz et al., 2001), alteration and/or weathering of material (Vogt, 1927; Ruxton, 1968; Parker, 1970; Vogel, 1975; Nesbitt, 1979; Nesbitt and Young, 1982; Velbel, 1985; Harnois, 1988; Chittleborough, 1991; Velbel et al., 2009), provenance of detrital material (Larue and Sampayo, 1990; Linn et al., 1991; Linn and DePaolo, 1993; Cullers, 1994; Reheis et al., 2002; Kimoto et al., 2006; Mitchell and Sheldon, 2010), soil-forming processes, or pedogenesis, (Feakes and Retallack, 1988; Maynard, 1992; Panahi et al., 2000; Oze et al., 2004; Laveuf et al., 2008; Laveuf and Cornu, 2009; Sheldon and Tabor, 2009; Mitchell and Sheldon, 2010) and paleo-environment during pedogenesis (Maynard, 1992; Garcia-Ruiz, 1998; Compton et al., 2003; Gruau et al., 2004; Sheldon and Tabor, 2009; Mitchell and Sheldon, 2010; Li et al., 2011). Researchers rely on the well-known behaviors of elements in the environment in order to interpret the history of a sample. Some elements are considered immobile during alteration of parent material [e.g., zirconium (Zr) (e.g., Harden, 1987; Maynard, 1992), aluminum (Al) (e.g., Vogt, 1927; Ruxton, 1968; Vogel, 1975; Nesbitt and Young, 1982; Harnois, 1988), yttrium (Y) (e.g., Pearce and Cann, 1973; Winchester and Floyd, 1977), titanium (Ti) (e.g., Maynard, 1992; Taylor and Blum, 1995), niobium (Nb) (e.g., Maynard, 1992; Hill et al., 2000; Panahi et al., 2000)], while other elements are mobile in that same environment [e.g., sodium (Na), potassium (K), magnesium (Mg), and calcium (Ca)] and can be leached from the system (e.g., Parker, 1970; Nesbitt and Young, 1982; Panahi et al., 2000). Some elements are mobile under some conditions and immobile under others. For example, iron (Fe) is mobile in its reduced state which allows for translocation and possible leaching, but is considered immobile in its oxidized state (Price and Velbel, 2000; Price and Velbel, 2003; Velbel and

Barker, 2008). Although Al is generally considered immobile, it can become mobile after all the alkalis are leached (Maynard, 1992), and may also be mobile during early stages of weathering (Velbel et al., 2009). With the understanding of elemental behaviors, geochemical analyses provide a very useful tool in interpreting the history (i.e., formation location, transport mechanisms, depositional environment, and alteration) of a sediment sample.

The goal of this study is to better understand the sedimentology and stratigraphy at LLNL. The stratigraphic character at LLNL is complex due to the previously discussed local tectonics which control the underlying structure as well as the variable sediment sources creating stacked fluvial fan successions beneath the site. The complexity of the stratigraphy at LLNL necessitated the attempt to use of geochemistry as a tool in understanding the site.

2. Methods

At the LLNL site, six well cores were selected for sampling. Five of these wells were located at what was known as the Helipad Site, and one well was located to the southwest of the Helipad Site by approximately 140 m (Figure 232). The Helipad Site is approximately 1600 m^2 with a well spacing of approximately 6 m to 8 m. Samples were taken from clay-rich, silty, and silty-sand units. This size fraction was chosen because previous studies have shown that geochemistry varies with grain size (e.g., Cullers et al., 1987, 1988; Cullers, 1988, 1994; Nyakairu and Koeberl, 2002; Whitmore et al., 2004). Cullers (1988, 1994) found that REE patterns and mineralogy of the clay and silt size fraction most closely mimicked the source rock while sand size fraction had the most variable composition when compared to source rocks. Retrieval of LLNL core was not 100%, so material was collected within desired units with an

Map of Michigan State University Described Well Cores

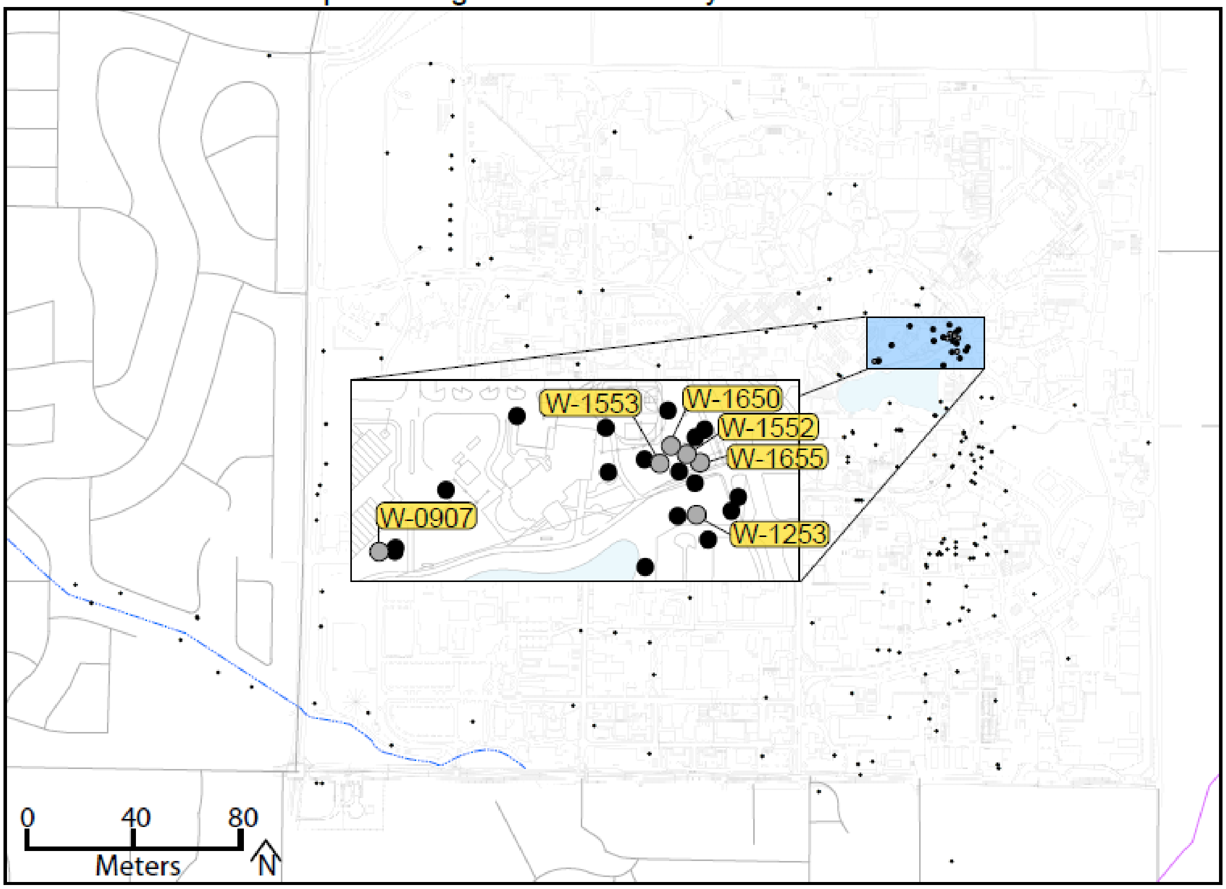

Figure 232. Blow up of Helipad Site with wells labeled that were sampled for geochemical analyses. Scale bar indicates distances within the enlarged box.

approximate spacing of every 10 cm where core was available. A total of 149 samples were collected for geochemical analysis.

The samples were analyzed at Michigan State University to determine abundance of major elements using the X-ray fluorescence (XRF) spectrometer, and minor and trace elements using the laser ablation inductively coupled plasma-mass spectrometer (LA-ICP-MS). In the laboratory, each sample was disaggregated by light grinding with a mortar and pestle. Then secondary carbonate was removed by boiling the sample in a leach solution of sodium acetate, glacial acetic acid and distilled water, after which the sample was rinsed three times with distilled water over a vacuum pump to facilitate elimination of water. Secondary carbonates forming as a result of the environmental conditions do not reflect the original composition of the parent material; therefore, removal of these carbonates was necessary to ensure a more accurate depiction of the parent material. The samples were then prepared for analysis by the staff at the XRF laboratory at Michigan Sate University. Each sample was ground and 3 g of rock powder was mixed with a flux of 9 g of lithium tetraborate and 0.5 g of ammonium nitrate to facilitate melting. The low dilution fusion (LDF) was used for the LLNL samples because both the XRF and LA-ICP-MS analyses were performed on the same sample. The rock and flux mixture was melted and allowed to cool in molds producing a one-phase glass disk. The disks were then analyzed at the XRF laboratory on the Rigaku S-Max and at the LA-ICP-MS laboratory on the Micromass Hex. These instruments provided elemental abundances for 10 major elements reported as oxides [i.e., silicon (Si), aluminum (Al), titanium (Ti), manganese (Mn), iron (Fe), sodium (Na), magnesium (Mg), potassium (K), calcium (Ca), phosphorous (P)] (Appendix C: Figures 269 – 278 and Table 4) and 26 minor and trace elements reported in parts per million (ppm) [i.e., vanadium (V), chromium (Cr), rubidium (Rb), strontium (Sr), yttrium (Y), zirconium (Zr), niobium (Nb), barium (Ba), lanthanum (La), cerium (Ce), praseodymium (Pr), neodymium (Nd), samarium (Sm), europium (Eu), gadolinium (Gd), terbium (Tb), dysprosium (Dy), holmium (Ho), erbium (Er), ytterbium (Yb), lutetium (Lu), hafnium (Hf), tantalum (Ta), lead (Pb), thorium (Th), uranium (U)] from each sample (Appendix C: Figures 279 – 304 and Table 5). For all plots of geochemical data in this study the colored bars correspond to the appropriate well and indicate where core was recovered. The yellow lines within the colored bars indicate gravel units that were not sampled for geochemical analysis. The black dots indicate the Lower Livermore unit which was not included in this study and therefore not sampled.

3. Geochemical Data

3.1 Correlation at LLNL Using Geochemical Data

As discussed in Chapter 2, paleosol units at LLNL had limited utility as stratigraphic markers in facies correlation due to their discontinuous nature and apparent offsets from faulting. However, stratigraphic correlation remained a goal of this study. Therefore, geochemical data were employed as a possible tool to facilitate correlation across LLNL. Individual paleosols might exhibit a unique geochemical signature which they acquired during soil development, that would persist after burial, and that could be measured through sample analyses (Yaalon, 1971). If a unique signature exists for one or more paleosols, it could be traced across LLNL and thus that unit could be correlated. Since, as previously mentioned, the stratigraphy at the Helipad Site is known, that site was chosen as a test case to determine if geochemical data would correlate with known stratigraphy and be useful as a facies correlation tool. The expected outcome for this exercise would be for the known correlatable paleosol units from the Helipad Site to exhibit distinct and unique geochemical signatures. These signatures could include elemental enrichments or depletions with respect to the unaltered parent material in the well core. A specific geochemical signature could then be correlatable from well to well within the Helipad Site and possibly across the LLNL site. Geochemical data were plotted from five wells at the Helipad Site and one additional well southeast of the Helipad Site (Figure 232 and Appendix C: Figures 233 – 268).

3.1.1 Chemical Reactions During Pedogenesis

The first attempt to use geochemistry data as a correlation tool was intended to assign a unique or distinct value to each of the paleosols which would identify it for potential use as a stratigraphic marker. Analyses were conducted based on the four main chemical reactions that occur in the soil-forming process: hydrolysis or incongruent dissolution, oxidation, hydration, and congruent dissolution (Retallack, 1990). The reverse of these reactions (alkalization, reduction, dehydration, and precipitation respectively) also occur in the soil as well as within the paleosol during burial (Retallack, 1990). These reactions occur during pedogenesis and leave observable effects that can be measured in paleosols (Retallack, 1990). For this study, these analyses were not performed to determine the environmental conditions during pedogenesis, but to determine whether, based on those conditions, a unique value existed within each paleosol. Retallack (1990 p.62-75, and references therein) is the source for the following descriptions of these chemical reactions and their measurement techniques. Measuring the consequence of these chemical reactions is made much easier by the fact that they mainly involve the 8 elements that make up 98% (both by weight and volume) of the Earth's crust and soils: oxygen (O), silica (Si), aluminum (Al), iron (Fe), magnesium (Mg), calcium (Ca), sodium, (Na), and potassium (K). With the knowledge that these chemical reactions occur to varying degrees during soil formation, it was thought likely that the values obtained from elemental ratios shown by previous workers to distinguish chemical reactions will also vary from paleosol to paleosol. A positive result could include anomalously high or low ratio values that would occur in correlatable paleosol units. Distinct values for each paleosol will be used to correlate each paleosol unit from well to well.

3.1.1.1 Hydrolysis or Incongruent Dissolution

The first category of reactions is hydrolysis, also known as incongruent dissolution, which produces clay as well as ions and molecules when acidic ground water interacts with cation-rich minerals resulting in the destruction of silicate minerals. In modern soils, pH is a measure that is used to determine the prevalence of hydrolysis. pH is known to change after burial, so direct measurement of pH in paleosols is not a good indicator of the soil-forming process. In order to determine the extent of hydrolysis that occurred during soil formation, several elemental ratios are used in the paleosols. The ratio of base cations / alumina ($(CaO+MgO+K_2O+NaO)/Al_2O_3$) allows the researcher to determine if the soil was alkaline or acidic. Values close to zero indicate a very acidic soil environment in which hydrolysis liberates base cations from weatherable minerals allowing them to be leached from the system. A larger number indicates an alkaline environment. In the case of an acidic soil, the silica / alumina (SiO_2/Al_2O_3) ratio is a better weathering ratio to use. At low pH values (below 4.5), alumina-rich clays will dissolve but quartz is resistant. Marbut (1935) calculated a value of 138 for an E horizon in an acidic soil and a value of 53 for a comparable horizon in a more neutral soil. Values of between 7 and 16 can be expected for alkaline soils. Another weathering ratio that is used to indicate hydrolysis is barium (Ba) / strontium (Sr). With strontium being the more soluble of these two trace elements, the values for this ratio range from near 10 in acidic soils to near 2 in most rocks and their soils. For this study, the values of base / alumina (Figure 233), silica / alumina (Figure 234), and barium / strontium (Figure 235) were calculated for each sample and plotted.

Hydrolysis Proxy

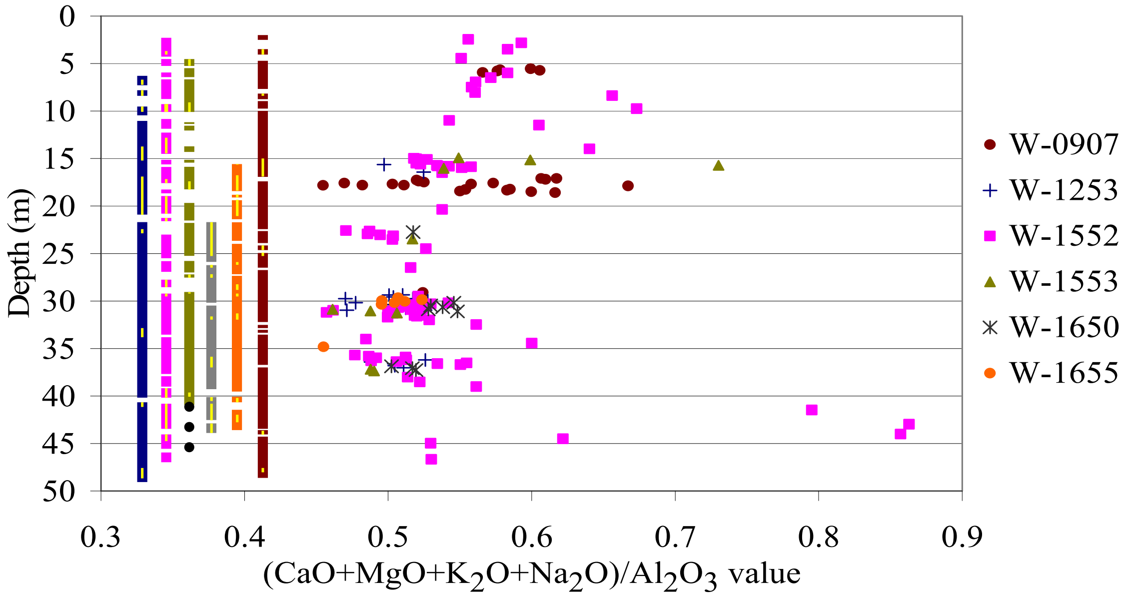

Figure 233. Base / alumina ratio to proxy hydrolysis or incongruent dissolution in pedogenesis.

Hydrolysis Proxy

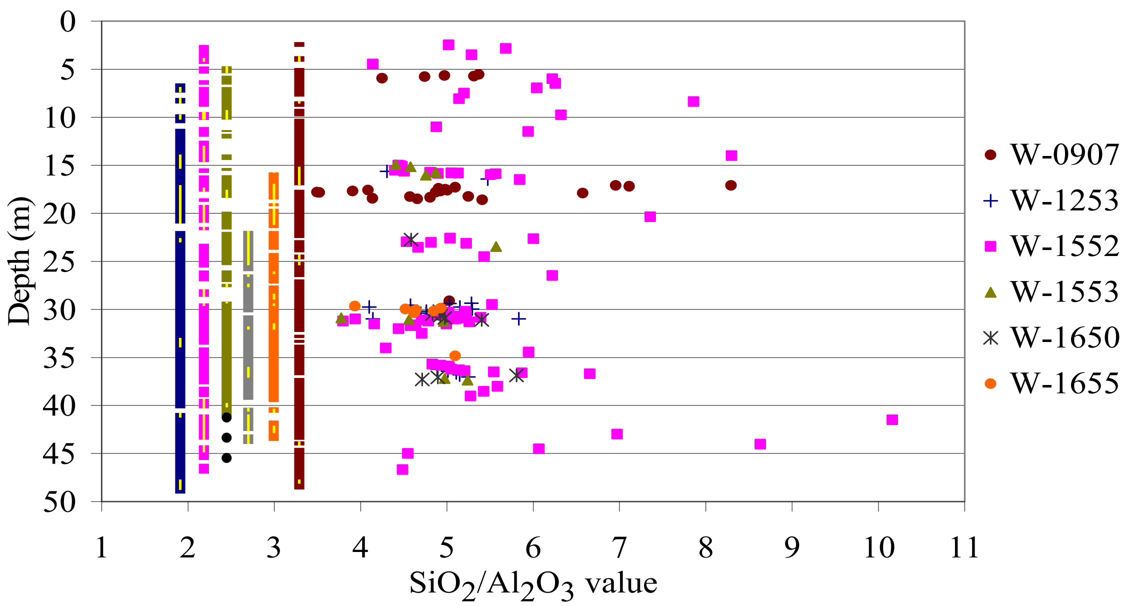

Figure 234. Silica / alumina ratio to proxy hydrolysis or incongruent dissolution in pedogenesis.

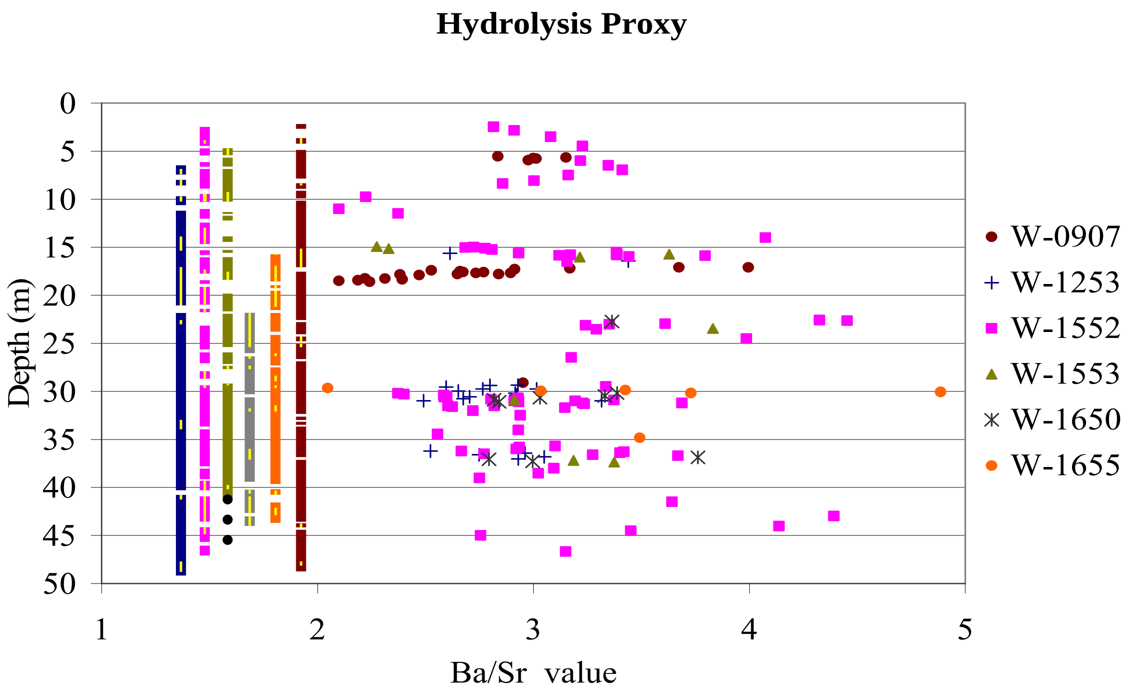

Figure 235. Barium / strontium ratio to proxy hydrolysis or incongruent dissolution in pedogenesis.

3.1.1.2 Oxidation

Oxidation is when an element loses an electron while forming a compound. The reverse reaction, in which an element gains an electron, is known as reduction. Eh is the measure of this reaction. In soils, a low negative value indicates a reducing environment while a high positive value suggests an oxidizing environment. As with the pH, the soil formation Eh values change upon burial. There are two ways to determine the formation redox state. The first is a simple observation of the color of the soil material. Ferrous iron (Fe^{2+}) is a reduced state, usually found in water-logged environments, and gives the soil material an overall bluish-green to gray color. Ferric iron (Fe^{3+}) is oxidized, usually found in well-drained soils, and gives the soil material a reddish-orange to brown color. When the redox state fluctuates between reducing and oxidizing both gray and orange colors are present in distinct zones known as mottles.

The second way to determine the formation redox state is by using weathering ratios that determine if regolith has undergone oxidation or reduction. Fe^{3+} / Fe^{2+} is the best ratio to use when determining redox state because Fe^{2+} is soluble in water and is leached from the soil, while Fe^{3+} accumulates in the soil. This ratio provides a more complete picture when it is compared to unaltered parent material. However, the two species of iron are seldom differentiated when elemental analyses are performed on soil. A weight percent value for total Fe is provided in most methods of bulk chemical analysis. An additional method is needed to distinguish one of the oxidation states from the other, after which, the abundance of the other oxidized state can be estimated by molar difference (Retallack, 2001). In the absence of these additional analyses, the weathering ratio of total Fe / alumina can be used to indicate if pedogenesis has occurred and ions have been leached from the system. Additionally, (total Fe+Mg) / alumina may also indicate pedogenesis. When calculating this pedogenic indicator, the value for magnesium may be added to the total iron value because these elements behave similarly in soils. These ratios are based on the assumption that aluminum is immobile in these conditions. The ratios using total iron have values that range from less than 0.4 in most North American soils to 1.2 in spodic horizons, and even reach 1.9 in very deeply weathered horizons (Marbut, 1935). For this study, the values of Fe / alumina (Figure 236) and (total Fe+Mg) / alumina (Figure 237) were calculated for each sample and plotted.

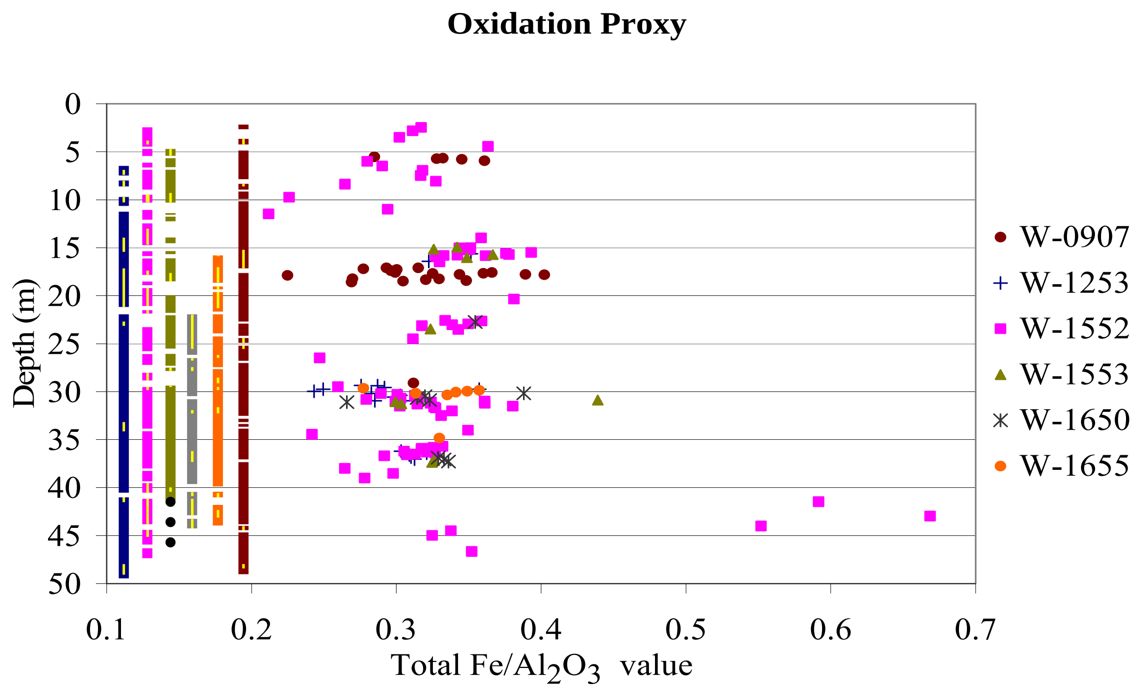

Figure 236. Fe / alumina ratio to proxy oxidation in pedogenesis.

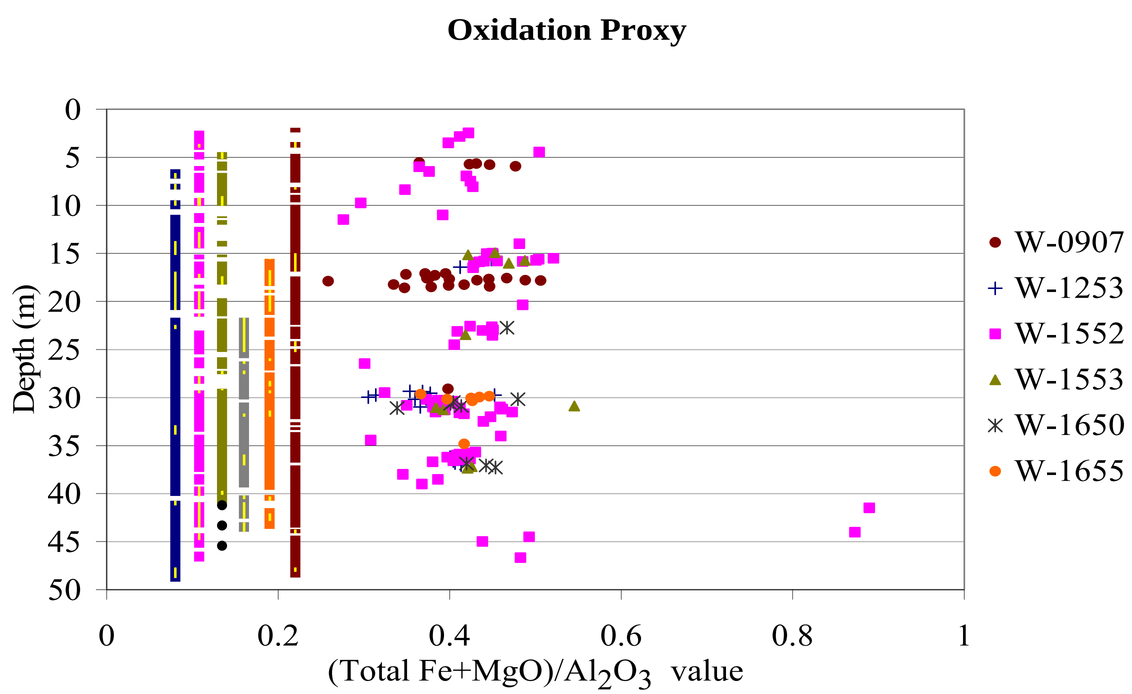

Figure 237. (Total Fe+Mg) / alumina ratio to proxy oxidation in pedogenesis.

3.1.1.3 Hydration

Hydration and dehydration are reactions by which minerals are altered by the addition of structural water or the loss of structural water respectively. The ratio of silica to sesquioxides ($SiO_2/Al_2O_3+Fe_2O_3$) is not an exact proxy for the hydration state of the soil during formation, but it can be used as a guide. Paleosols with high ratio values are quartz-rich with few hydrated minerals. Paleosols with low ratio values indicate the original soils may have been clayey with a large amount of iron oxyhydrates and hydrated clays. For this study, the value of silica / sesquioxides (Figure 238) was calculated for each sample and plotted.

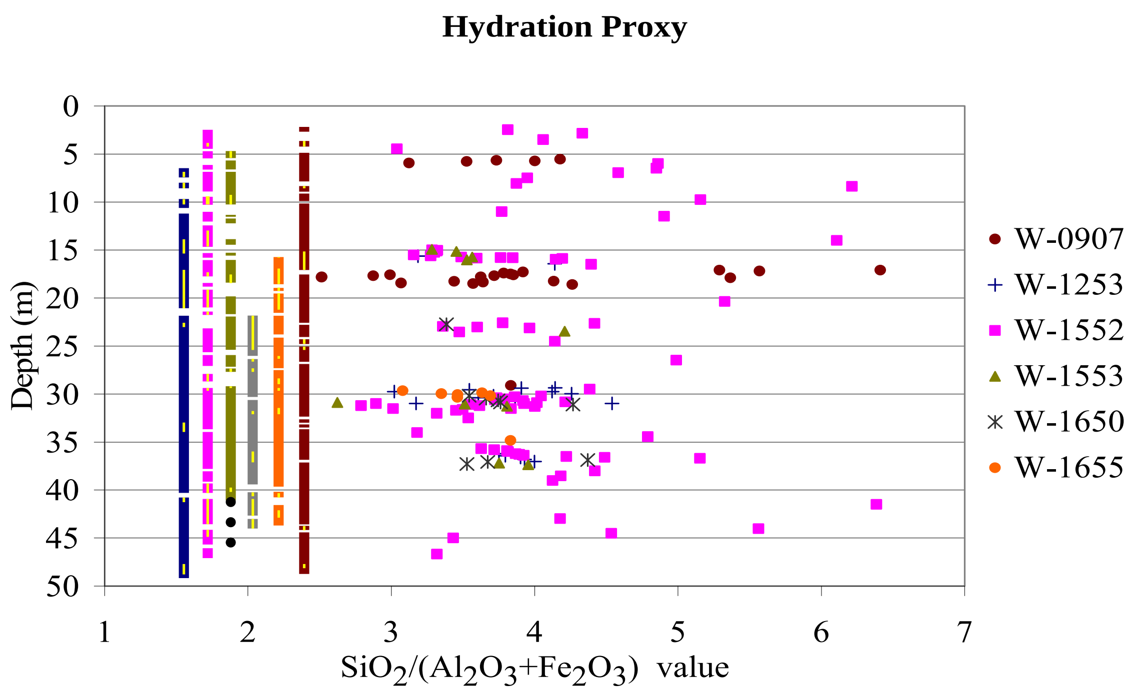

Figure 238. Silica / sesquioxides to proxy hydration in pedogenesis.

3.1.1.4 Congruent Dissolution

The last of the four chemical reactions that occur during soil-formation is congruent dissolution with its reverse reaction precipitation. Congruent dissolution is the reaction by which minerals and compounds disaggregate into their constituent ions in water. This is similar to hydrolysis, or incongruent dissolution; however, in hydrolysis new insoluble minerals are formed as part of the reaction while that is not the case in congruent dissolution. Congruent dissolution can be directly observed through the presents of etch features on mineral surfaces. It can be indirectly measured through the degree of salinization, or the saturation conductivity of the soil pore water, which is the concentration of salts. Since paleosols do not contain the original pore fluids that were present during soil formation, this measurement is not possible; however, weathering ratios may again serve to approximate that environment. Highly alkaline environments that are conducive to evaporative mineral formation promote quartz dissolution. The ratios of alkalis / alumina (K_2O+Na_2O/Al_2O_3), soda / potash (Na_2O/K_2O), and soda / alumina (Na_2O/Al_2O_3) all serve this purpose. Like the weathering ratios used to approximate the hydrolysis reactions, these ratios work because the alkalis are soluble (with sodium being more soluble than potassium) and alumina is assumed to be insoluble. For this study, the values of alkalis / alumina (Figure 239), soda / potash (Figure 240), and soda / alumina (Figure 241) were calculated for each sample and plotted.

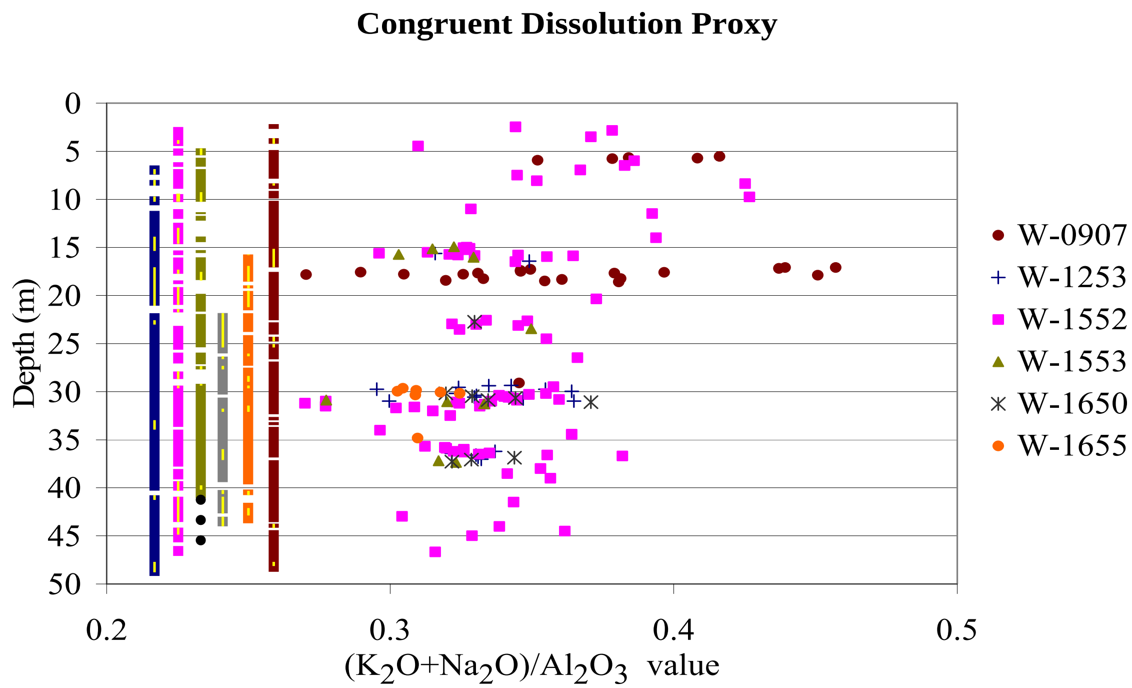

Figure 239. Alkalis / alumina ratio to proxy congruent dissolution in pedogenesis.

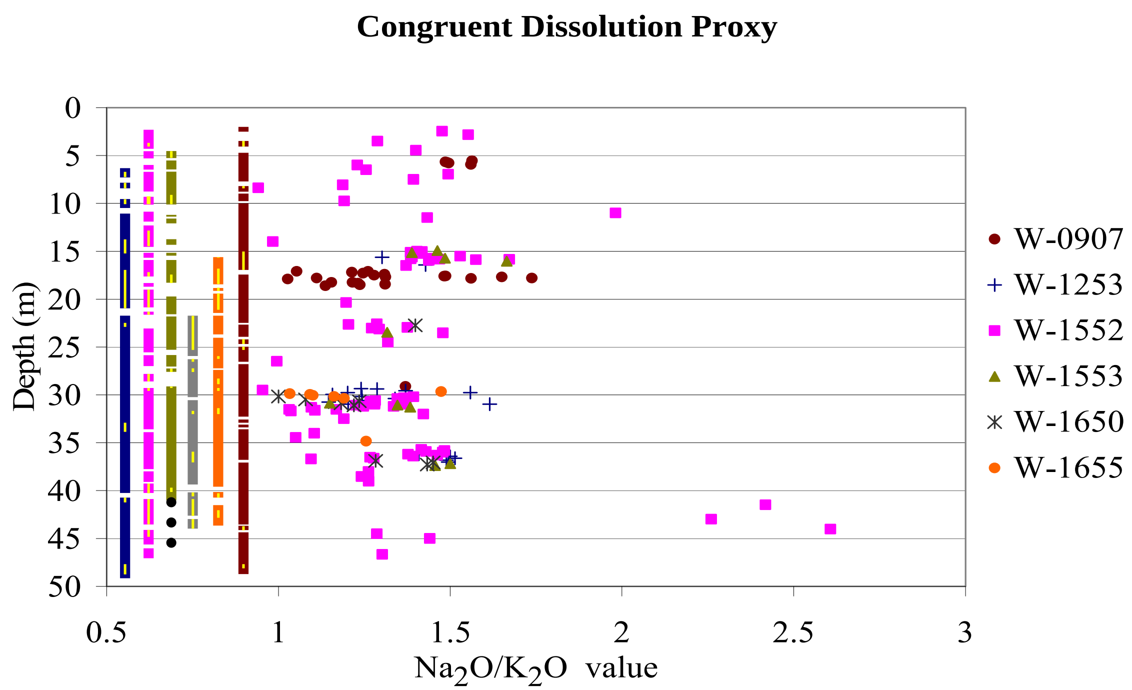

Figure 240. Soda / potash ratio to proxy congruent dissolution in pedogenesis.

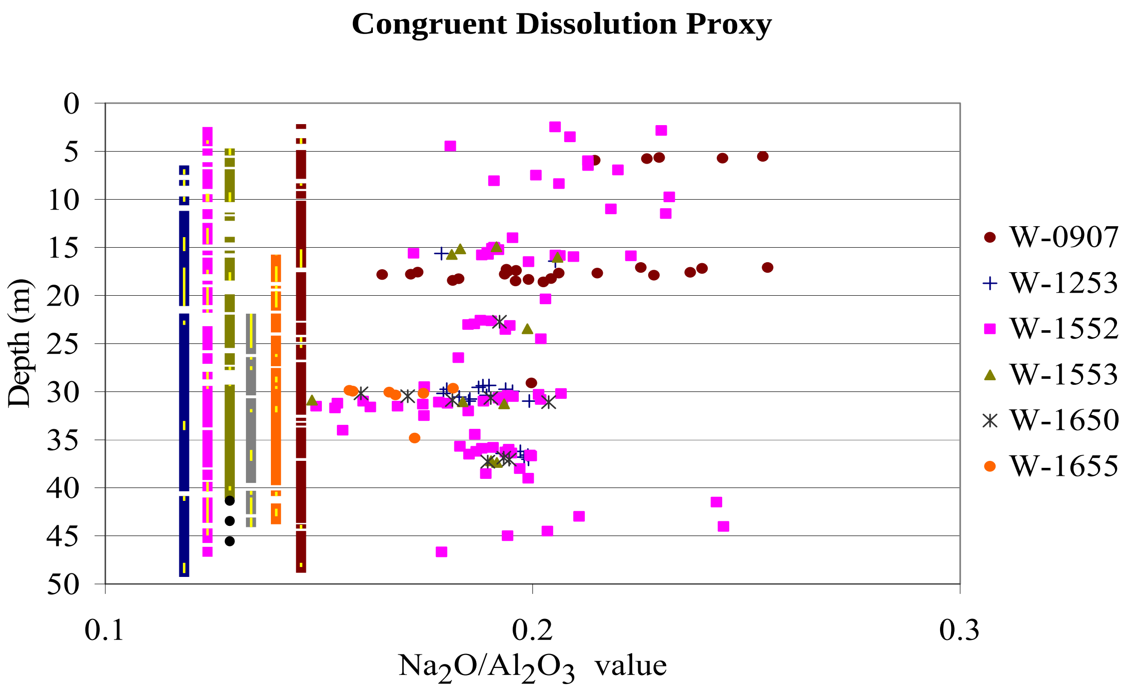

Figure 241. Soda / alumina ratio to proxy congruent dissolution in pedogenesis.

3.1.2 Elemental Ratios

Many researchers have used elemental ratios to determine degree of weathering (e.g., Harden, 1988; Maynard, 1992; Jun et al., 1999; McCarthy et al., 1999; Young, 1999; Lianwen et al., 2001; Sreenivas et al., 2001; Grimley et al., 2003; Jun et al., 2003; Utsunomiya et al., 2003; Ufnar et al., 2004). These ratios can also show translocation of an element within a profile as seen by a lower value in the upper profile indicating depletion of an element, and higher value in the lower profile indicating an enrichment of that same element. Also, ratio values of mobile to immobile elements will decrease over time as the mobile elements are leached from the system. This intra-profile comparison is useful for studying the evolution of a soil, but does not aid with correlations between wells. However, calculating these ratios is beneficial if they yield a unique or distinct value for a paleosol which could aid in inter-core site-wide correlations. For this study, the elemental ratios were calculated for several mobile to immobile elements (i.e., Fe/Ti, Al/Fe, Ca+Na/Ti, P/Ti, Ca/Zr, Na/Zr, Fe/Zr) (Figures 242 – 248) and ratios of relatively inert geochemical indicators (i.e., Ti/Y, Ti/Zr, Zr/Y, Al/Ti) (Figures 249 – 252). Zr and Hf are confined to the same mineral, zircon. Therefore, Zr/Hf (Figure 253) is considered a precise tracer of parent material, and was also plotted (Maynard, 1992).

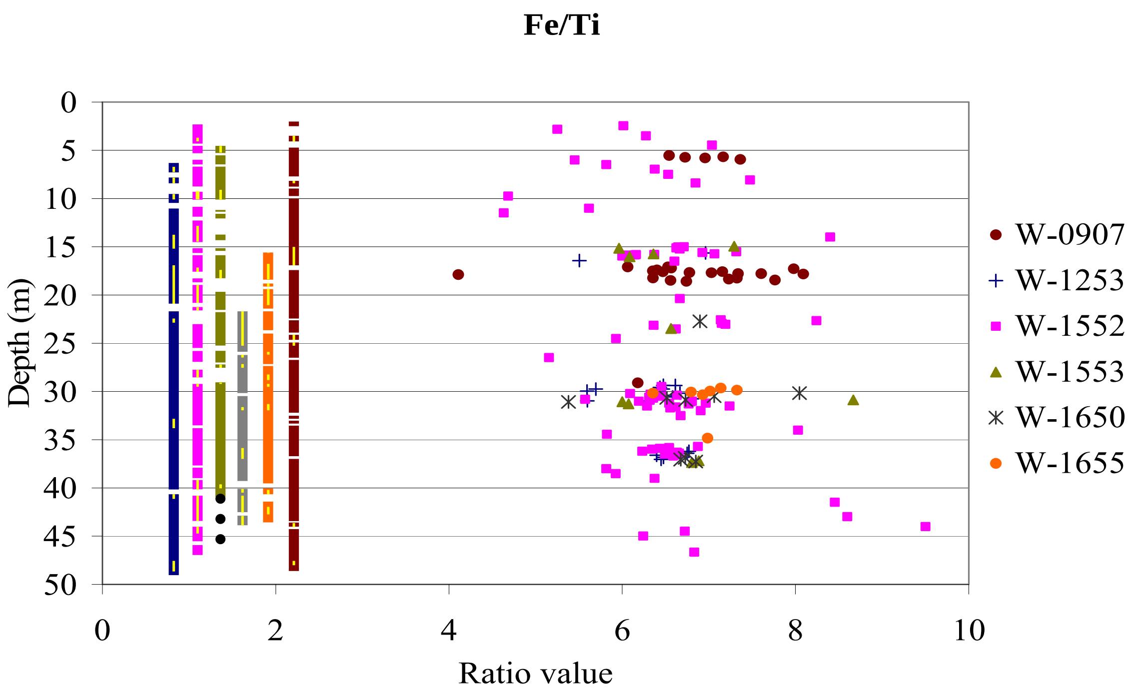

Figure 242. Mobile to immobile elemental ratio of Fe/Ti with depth.

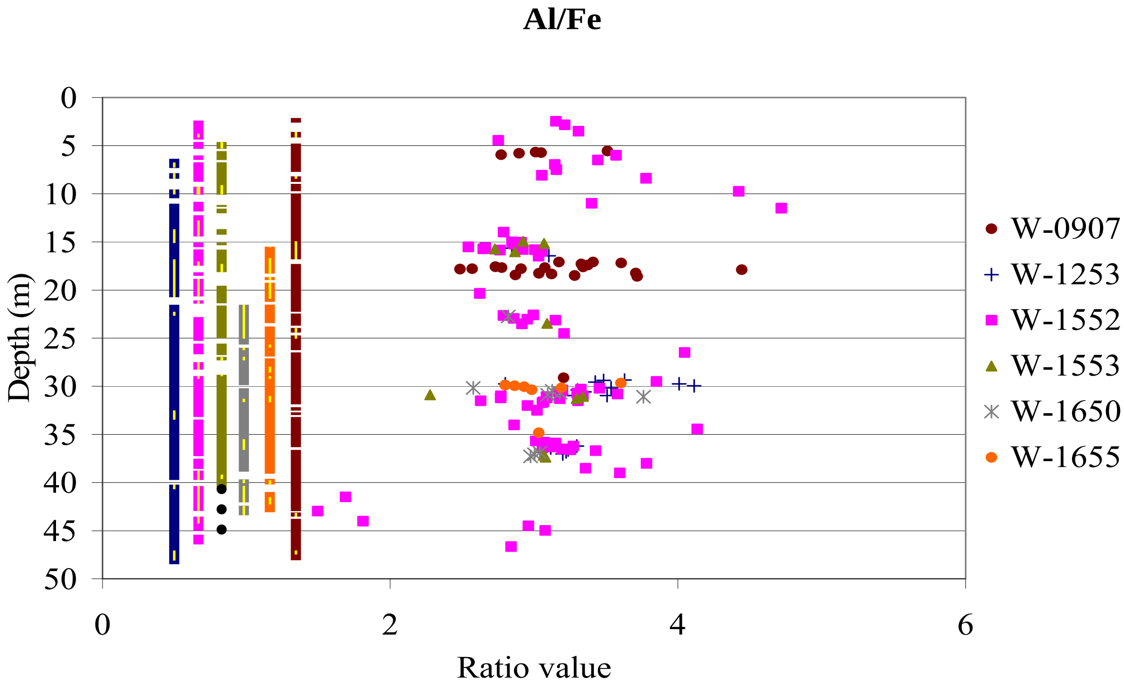

Figure 243. Mobile to immobile elemental ratio of Al/Fe with depth.

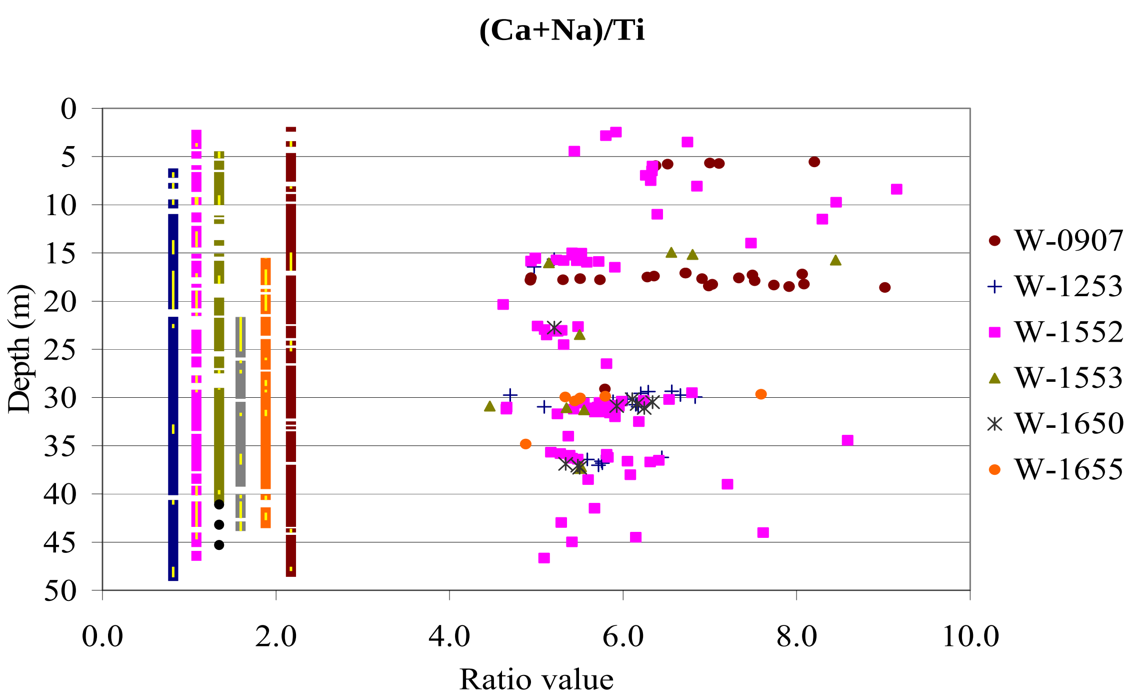

Figure 244. Mobile to immobile elemental ratio of Ca+Na/Ti with depth.

P/Ti

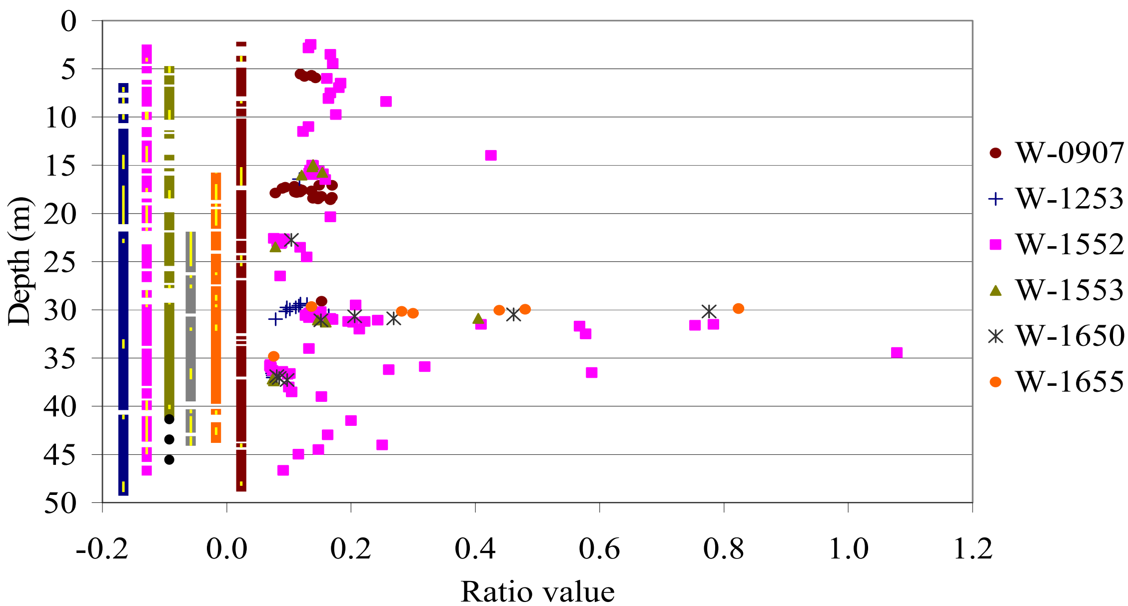

Figure 245. Mobile to immobile elemental ratio of P/Ti with depth.

Ca/Zr

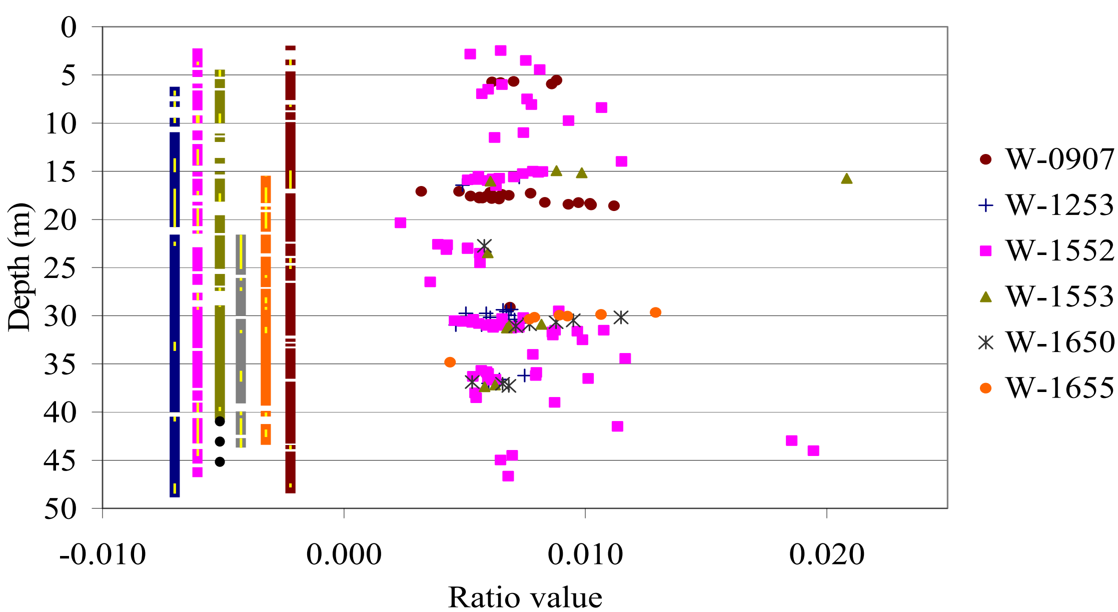

Figure 246. Mobile to immobile elemental ratio of Ca/Zr with depth.

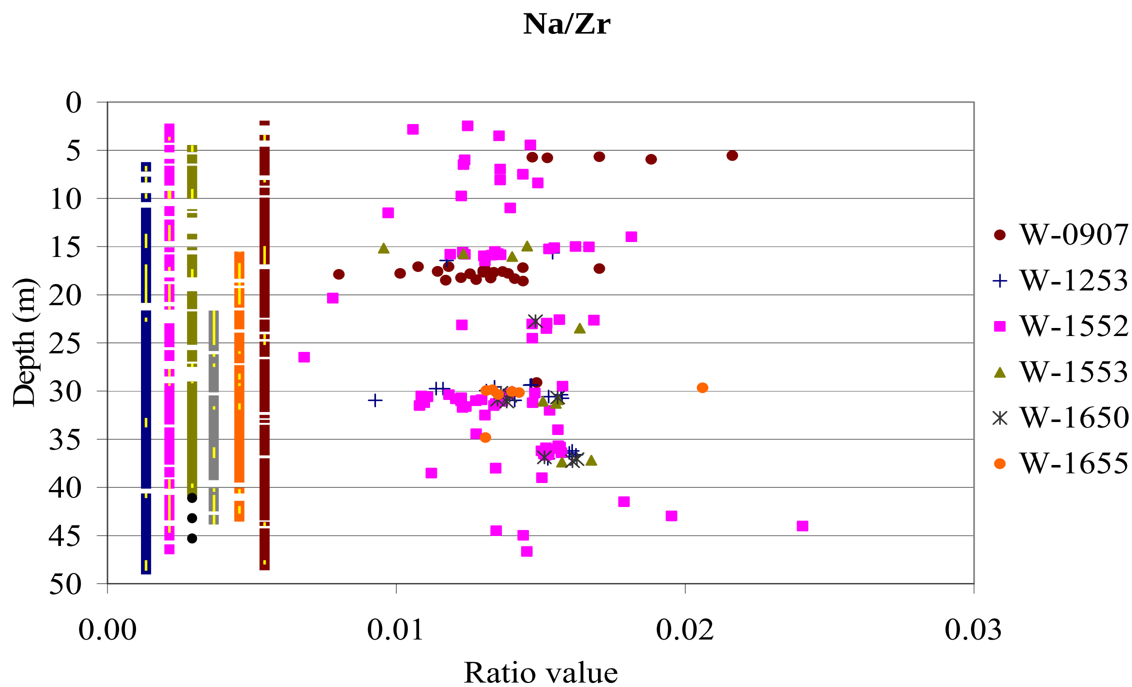

Figure 247. Mobile to immobile elemental ratio of Na/Zr with depth.

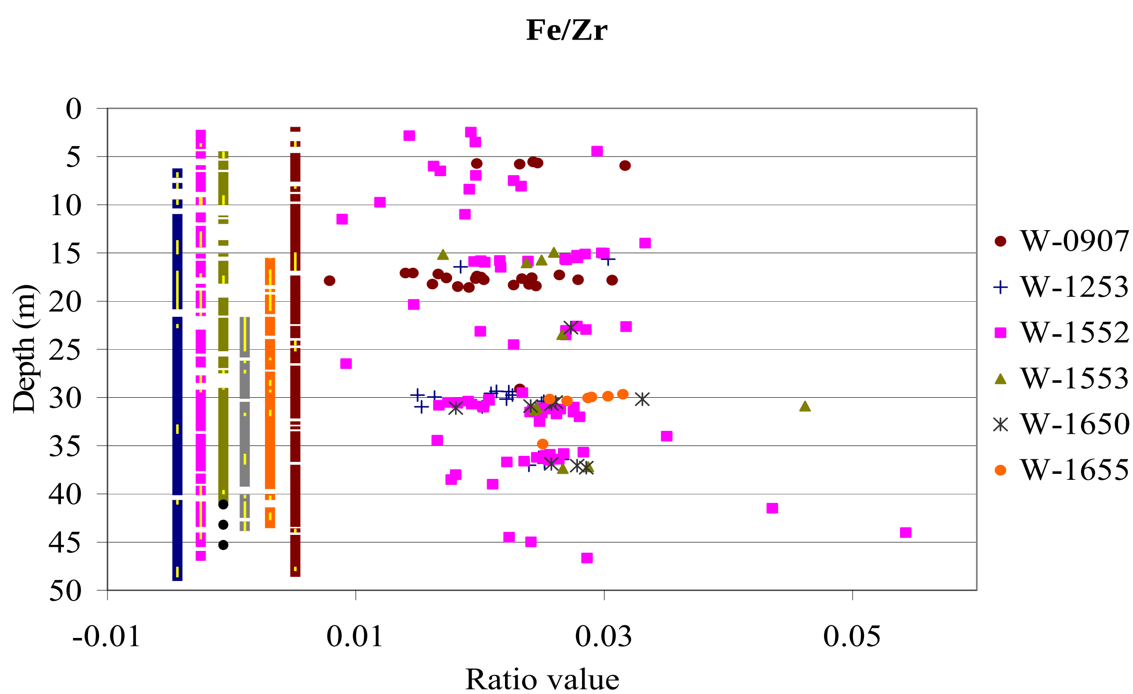

Figure 248. Mobile to immobile elemental ratio of Fe/Zr with depth.

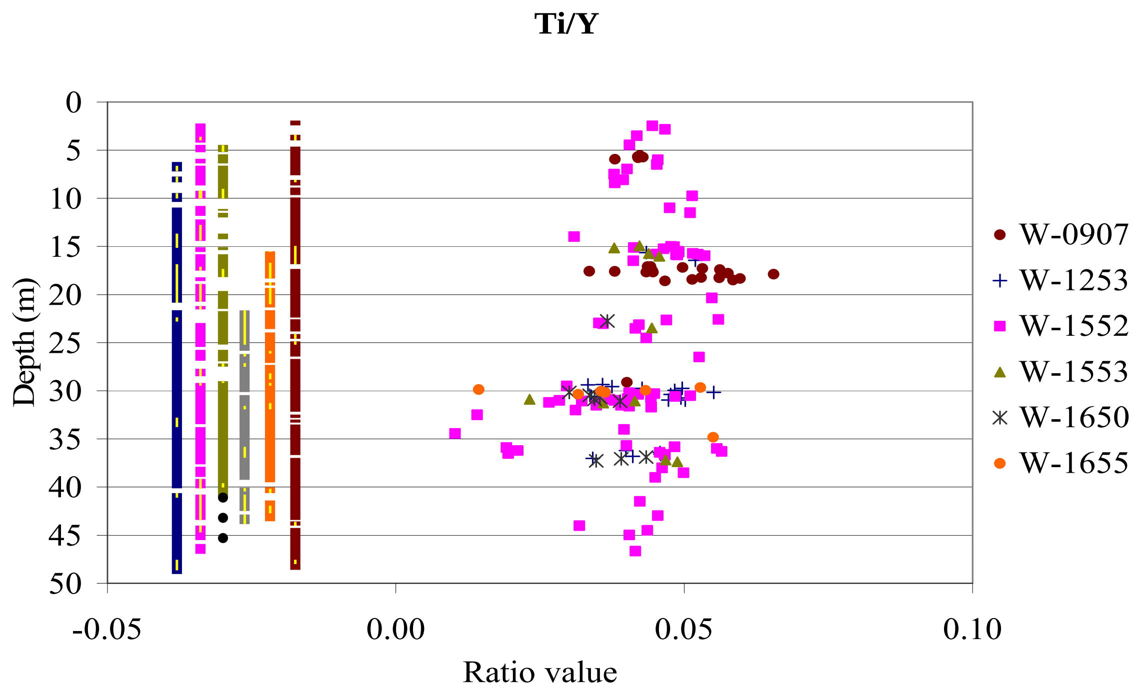

Figure 249. Relatively inert elemental ratio of Ti/Y with depth.

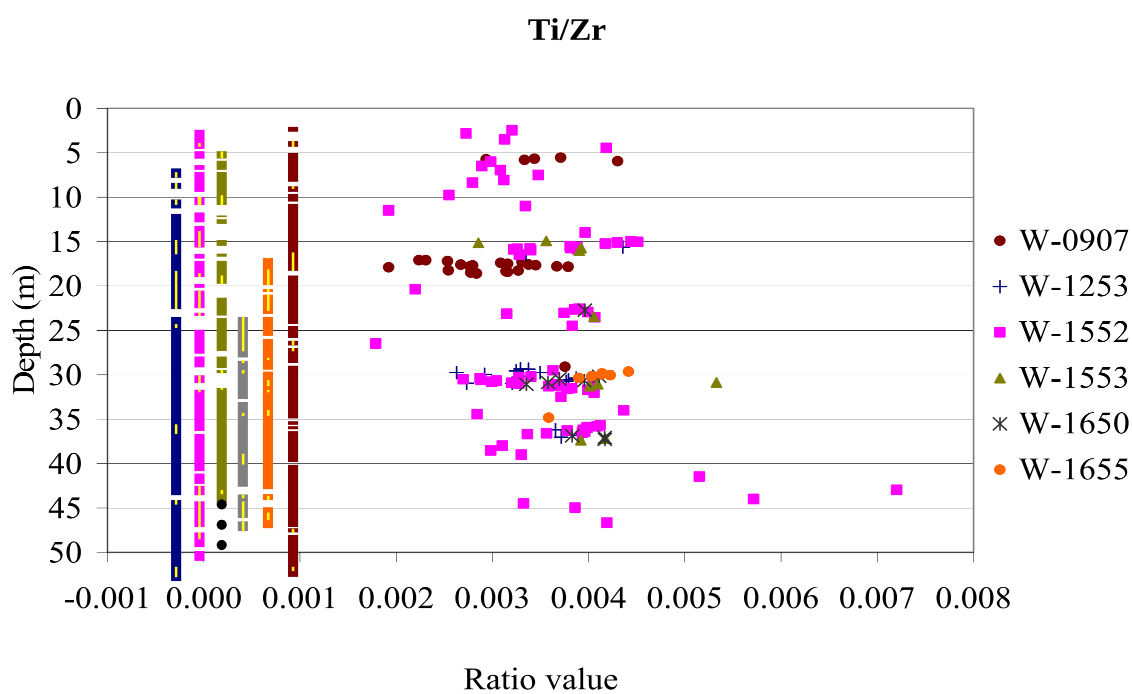

Figure 250. Relatively inert elemental ratio of Ti/Zr with depth.

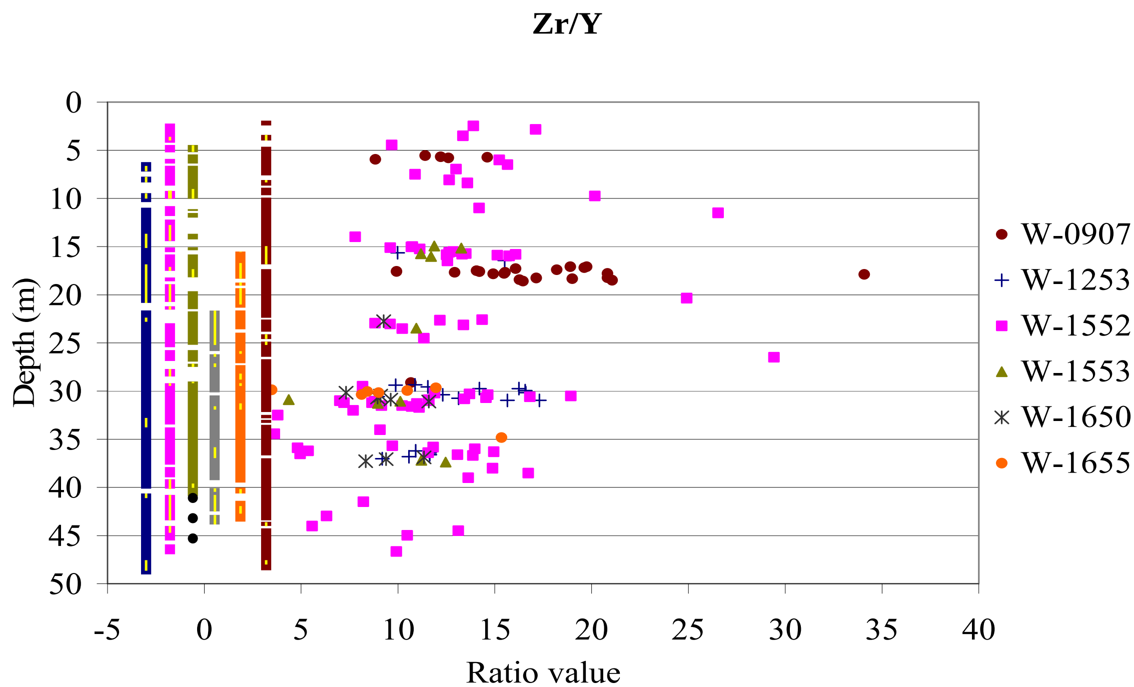

Figure 251. Relatively inert elemental ratio of Zr/Y with depth.

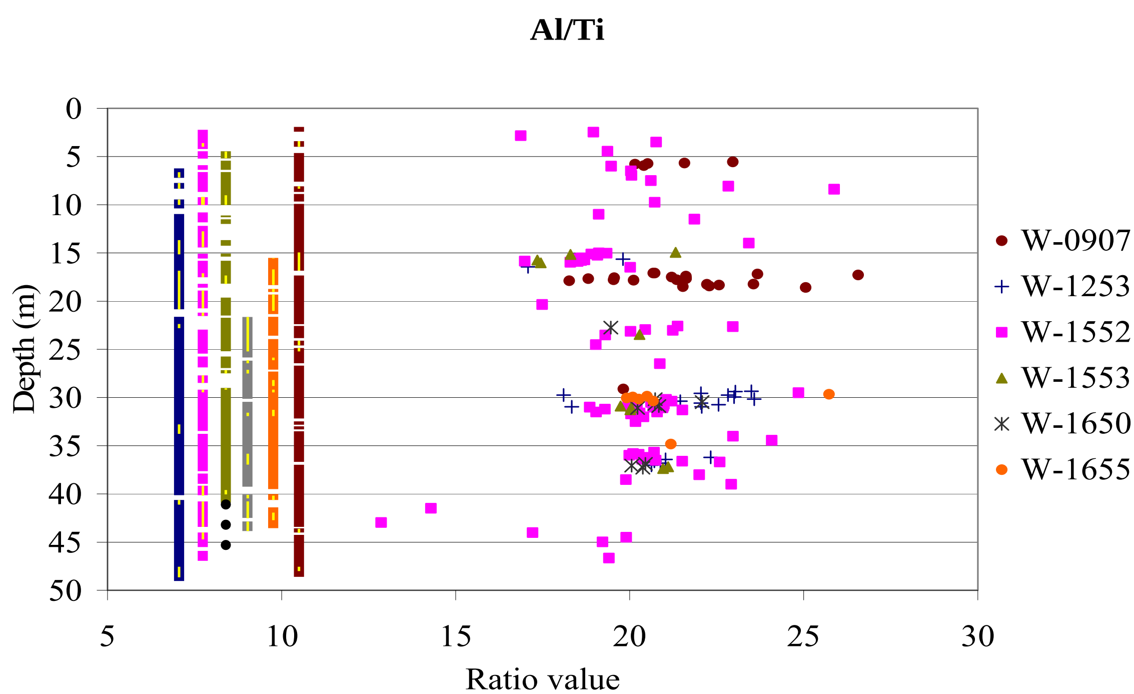

Figure 252. Relatively inert elemental ratio of Al/Ti with depth.

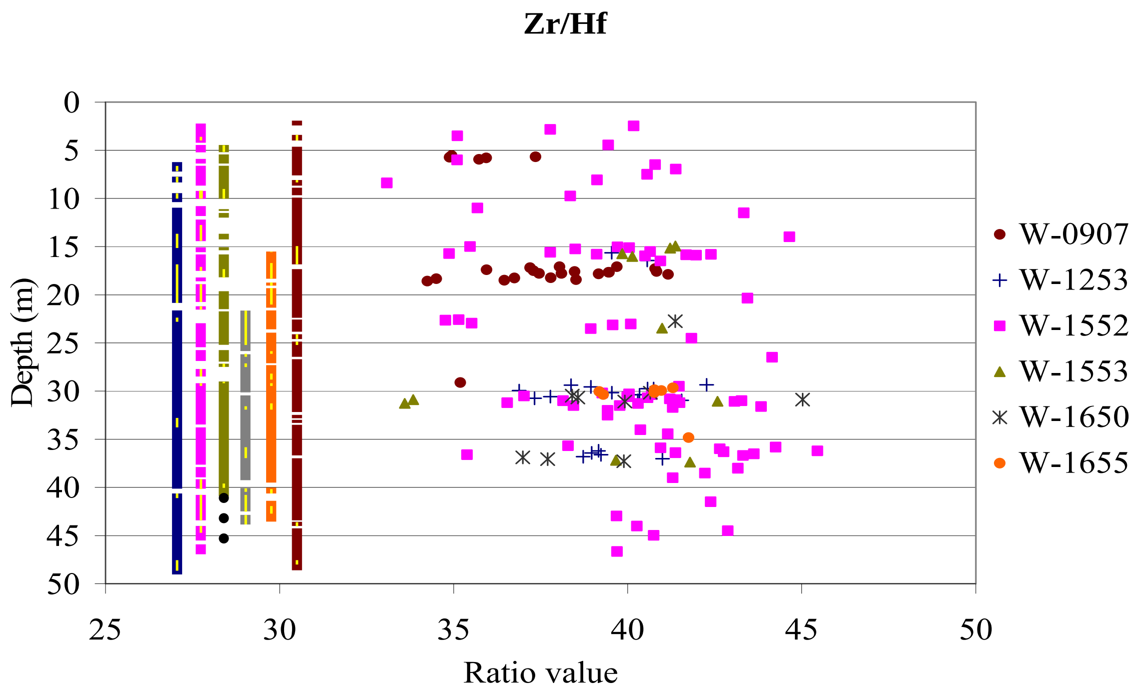

Figure 253. Parent material tracer elemental ratio of Zr/Hf with depth.

3.1.3 Weathering Indices

In addition to elemental ratios, weathering indices have been developed using elemental abundances to improve on the simple ratio of two elements by adding several elements together in both the numerator and denominator (Chittleborough, 1991 and references therein). These calculations take into consideration the mobility and activity of multiple mobile elements in order to obtain a more accurate depiction of mineral weathering in soils. These ratios include the Weathering Ratio as $WR=(CaO+MgO+Na_2O)/ZrO_2$ (Chittleborough, 1991), Chemical Index of Weathering as $CIW=[Al_2O_3/(Al_2O_3+CaO+Na_2O)]x100$ (Harnois, 1988), Chemical Index of Alteration as $CIA=[Al_2O_3/(Al_2O_3+CaO+Na_2O+K_2O)]x100$ (Nesbitt and Young, 1982), the Weathering Index as $WI=[(2Na_2O/0.35)+(MgO/0.9)+(2K_2O/0.25)+(CaO/0.7)]x100$ (Parker, 1970; Harnois, 1988), and the Vogt ratio as $V=(Al_2O_3+K_2O)/(MgO+CaO+Na_2O)$ (Vogt, 1927 in Chittleborough, 1991). Price and Velbel (2003) conducted a study in which they calculated several weathering indices in order to evaluate their potential application on in situ weathering profiles. They made note that weathering indices are widely used in modern and ancient in situ weathering profiles. However, even in their extensive literature review regarding application of weathering indices, no mention was made of studies utilizing weathering indices on transported parent material. Weathering indices are not often used in paleosols; more often, simple elemental ratios are used. However, neither weathering indices nor elemental ratios have been used as a tool when attempting to correlate strata. These five weathering indices were calculated for each sample, not to determine the degree of weathering, but as a tool to obtain a unique value to aid in correlating the units (Figures 254 – 258).

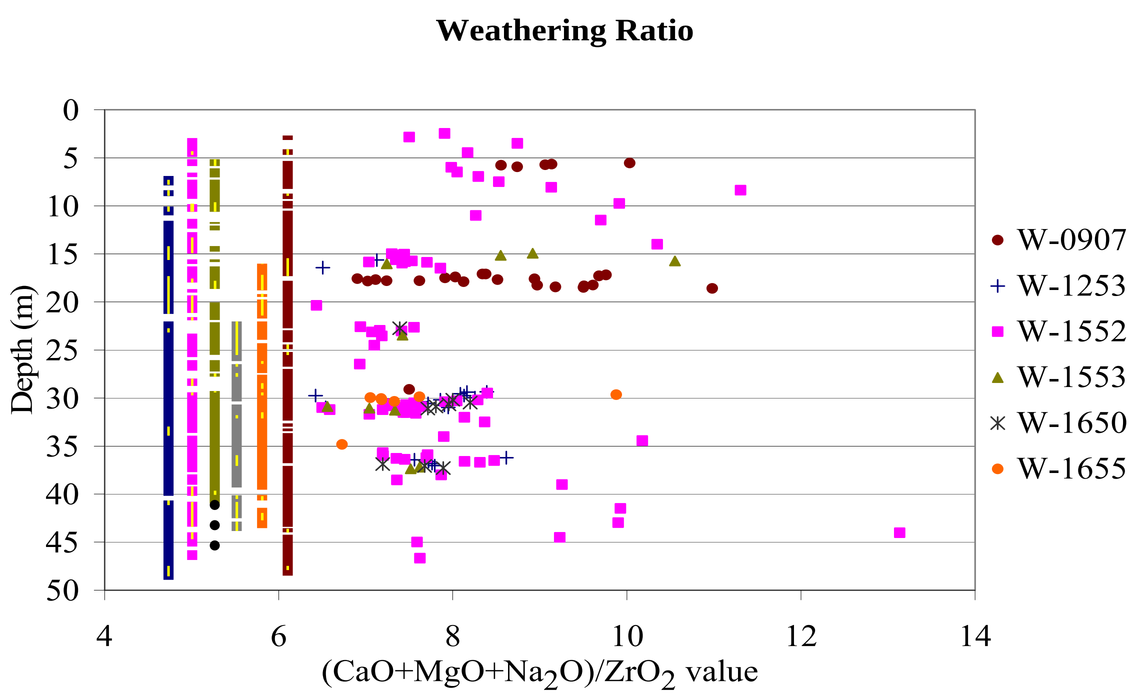

Figure 254. Weathering Ratio values with depth.

Chemical Index of Weathering

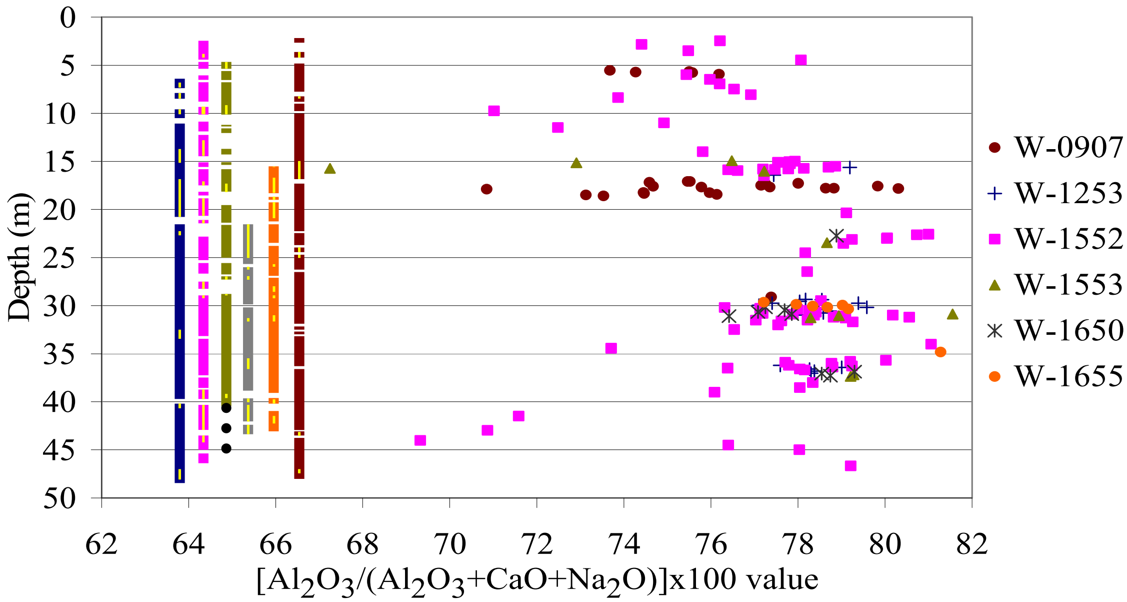

Figure 255. Chemical Index of Weathering values with depth.

Chemical Index of Alteration

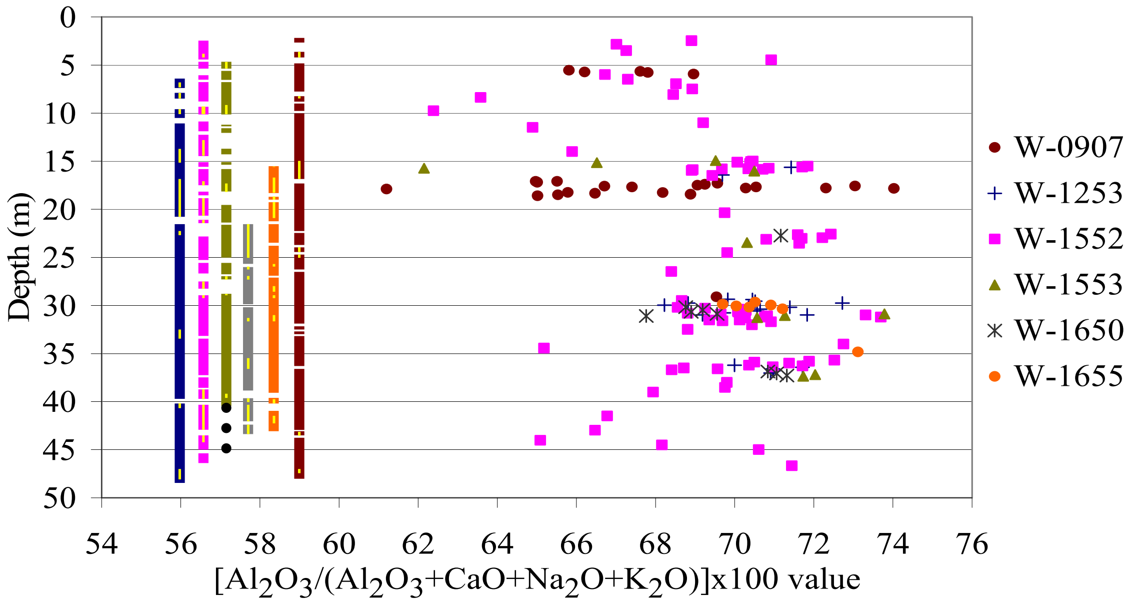

Figure 256. Chemical Index of Alteration values with depth.

Weathering Index of Parker

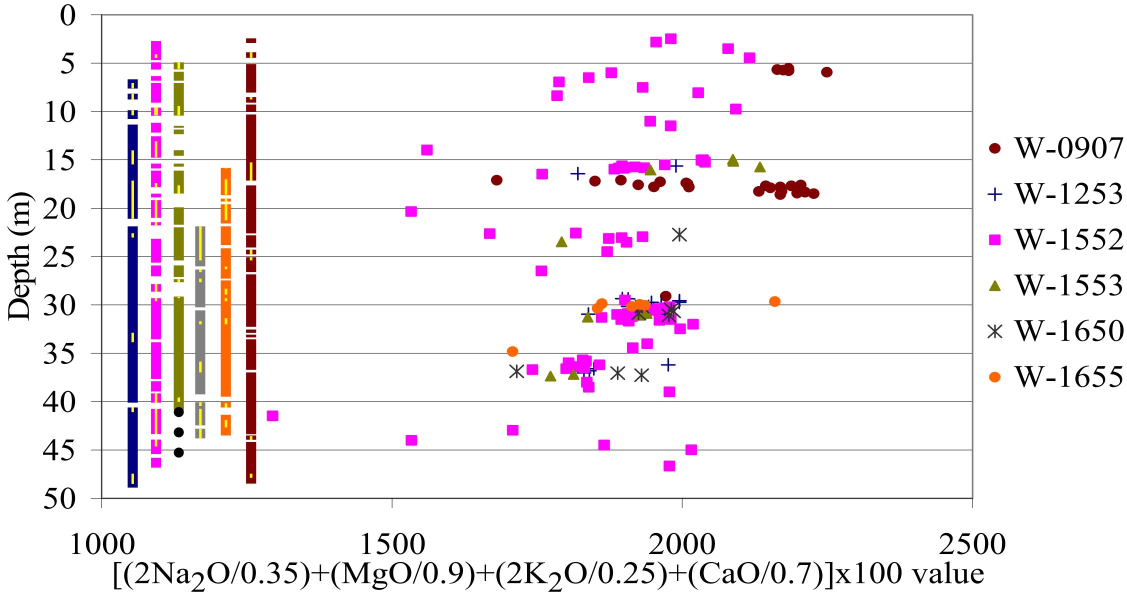

Figure 257. Weathering Index of Parker values with depth.

Vogt Ratio

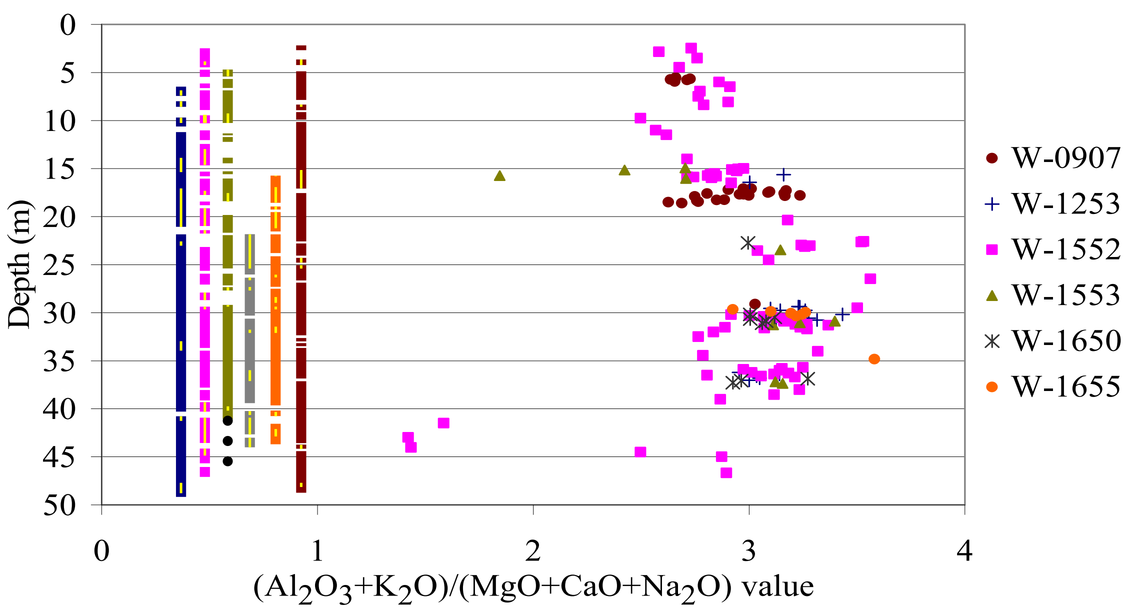

Figure 258. Vogt Ratio values with depth.

3.1.4 Interpretation of Geochemical Data

Upon visual inspection of the geochemical data plots, no discernable unique value was observed to indicate a paleosol. The data exhibit some scatter, but no repeating patterns were present. Within the scatter occasional linear patterns were observed seeming to indicate an enrichment up profile, while other linear patterns indicated a depletion up profile. These patterns could indicate a correlatable unit if they occurred in paleosol units located at similar depths in multiple wells. When attempting to correlate these patterns, some allowances were made for vertical location of such units from well to well due to paleo-topography at the time of soil development and possible post-burial faulting. However, these patterns appeared random and did not occur in multiple wells. Also, the data for some wells did not exhibit any such patterns.

The paleosols at LLNL have been identified as most likely being alluvial soils based on the accepted soil science definition (Schaetzl and Anderson, 2005). These soils typically form on floodplains in stratified parent material (i.e. fluvial sediments), exhibit little profile development, and contain some organic matter (Schaetzl and Anderson, 2005). Some soils were likely cumulic and developed syndepositionally with periodic additional sediment which was minor enough to be incorporated into the soil instead of burying it. The soils were likely in the order of Entisol, Inceptisol, or Mollisol. The most strongly developed paleosols, which were encountered in the northwest section of LLNL, exhibited thick B horizons with high clay and carbonate content and moderately well developed ped structures (Figure 12 in Chapter 2). These soils were most likely Alfisols with a representative horizon sequence of A/E/Bt/C or A/E/Bk/C (Schaetzl and Anderson, 2005). The lesser developed paleosols that exhibited thinner B horizons with moderate clay and carbonate content and weakly developed ped structures were most likely

Inceptisols with a representative horizon sequence of A/Bw/C (Schaetzl and Anderson, 2005). The weakest paleosols had the thinnest B horizons with little clay and carbonate content and little to no discernable ped structures. These soils were most likely Entisols with a representative horizon sequence of A/C, A/Bs/C, or A/Bw/C (Schaetzl and Anderson, 2005). Most of the paleosols at LLNL would be classified as Inseptisols or Entisols, of which neither order represents strongly developed soils.

Pedogenesis and mineral weathering are not synonymous; however, both progress and generally the more strongly developed soils also tend to have more strongly weathered minerals (Maynard, 1992; Mills and Allison, 1995). Therefore, the indices which indicate strongly weathered material could loosely correlate to strongly developed soils. This argument is strengthened by the geochemical data and weathering indices from this study. LLNL paleosols are not strongly developed which correlates to weathering indices which do not exhibit strong trends.

3.1.5 Geochemistry Data and Particle Size Distribution

Particle size distribution was determined for 94 samples from five of the six well cores used in the geochemical analyses (i.e., W-0907, W-1253, W-1552, W-1650, and W-1655) (Figure 232). The particle size distribution was determined for each of the samples at the Michigan State University Sedimentology / Stratigraphy Laboratory. To prepare for analysis, any visible driller's mud was removed by scraping from the exterior of the core that was to be analyzed. The sample was then disaggregated in a porcelain bowl taking care to not crush individual grains. The unconsolidated sample was placed in a drying oven for a minimum of four hours to drive off water. The sample was then passed through a series of U.S. standard sieve meshes making sure each sieve only caught solitary grains and not aggregates. If aggregates were observed, they were disaggregated and passed through again. The sample passed through U.S. standard sieve meshes of 5 (-2.0ϕ), 7 (-1.5 ϕ), 10 (-1.0 ϕ), 14 (-0.5 ϕ), 18 (0.0 ϕ), 25 (0.5 ϕ), 35 (1.0 ϕ), 45 (1.5 ϕ), 60 (2.0 ϕ), 80 (2.5 ϕ), 120 (3.0 ϕ), 170 (3.5 ϕ), and 230 (4.0 ϕ). The samples trapped by each sieve were weighed and normalized. The sample fraction that was smaller than mesh 230 (4.0 ϕ) was run through a Micromeretics 5000ET sedigraph to determine the fine grain distribution. The sedigraph yielded per cent of sample values for < 8.0 ϕ (i.e., the silt/clay break) which were converted to per cent of total sample values. The mean grain size was calculated for each sample and then plotted against Fe (Figures 259 – 263) and Al concentrations (Figures 264 – 268). A trend line was also added to each plot. The trend of each plot indicates there is a correlation between grain size and elemental abundance. The increase in Fe and Al with decreasing grain size indicates the variable elemental abundances are due to grain size. Fe and Al is taken up by neoformation of clay minerals and thus concentrated in the smaller size fraction. The geochemistry data showed no strong trends with depth but did correlate weakly with grain size. Therefore, it was concluded that the scatter observed in the geochemistry data is a result of grain size.

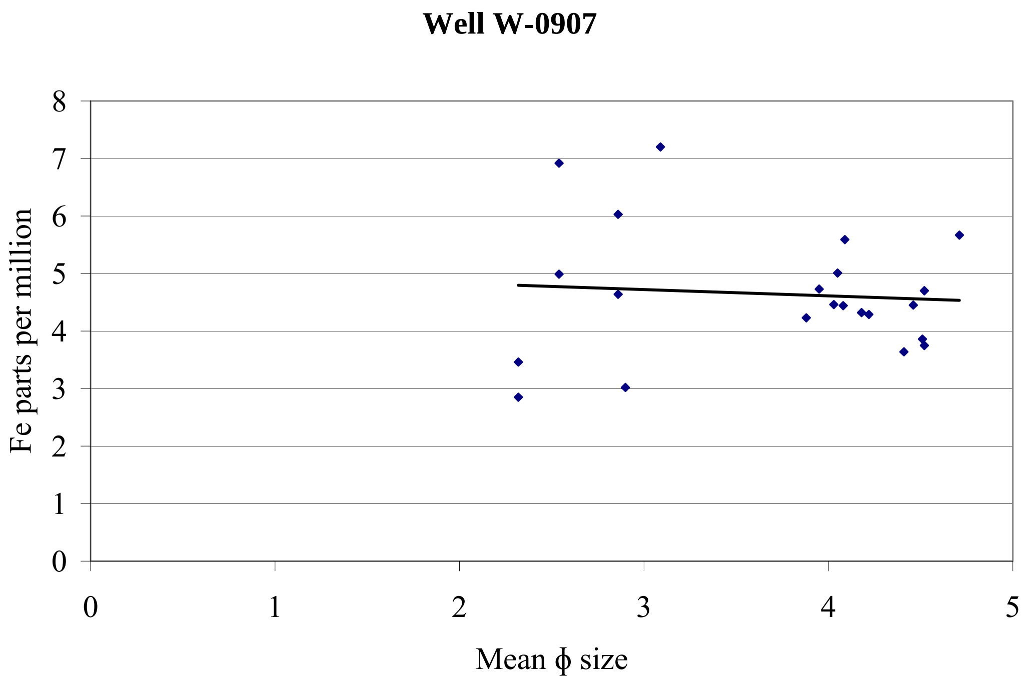

Figure 259. Well W-0907 mean ϕ size against Fe. The slope of the trend line is $y = -0.1083x + 5.0466$ with $r^2 = 0.0064$.

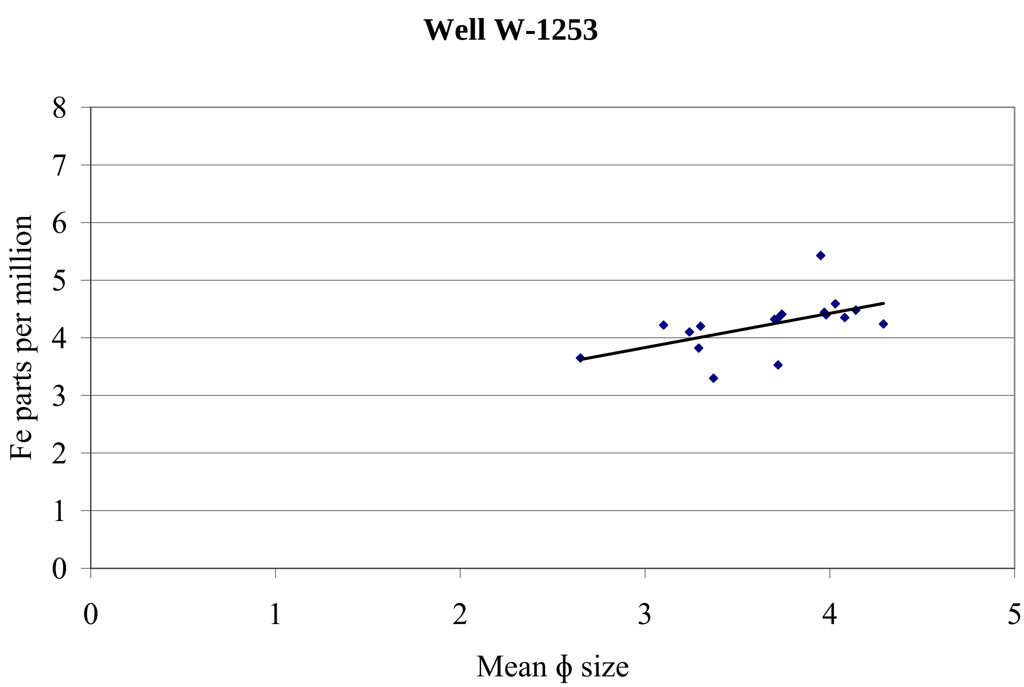

Figure 260. Well W-1253 mean ϕ size against Fe. The slope of the trend line is $y = 0.5933x + 2.0517$ with $r^2 = 0.2989$.

Well W-1552

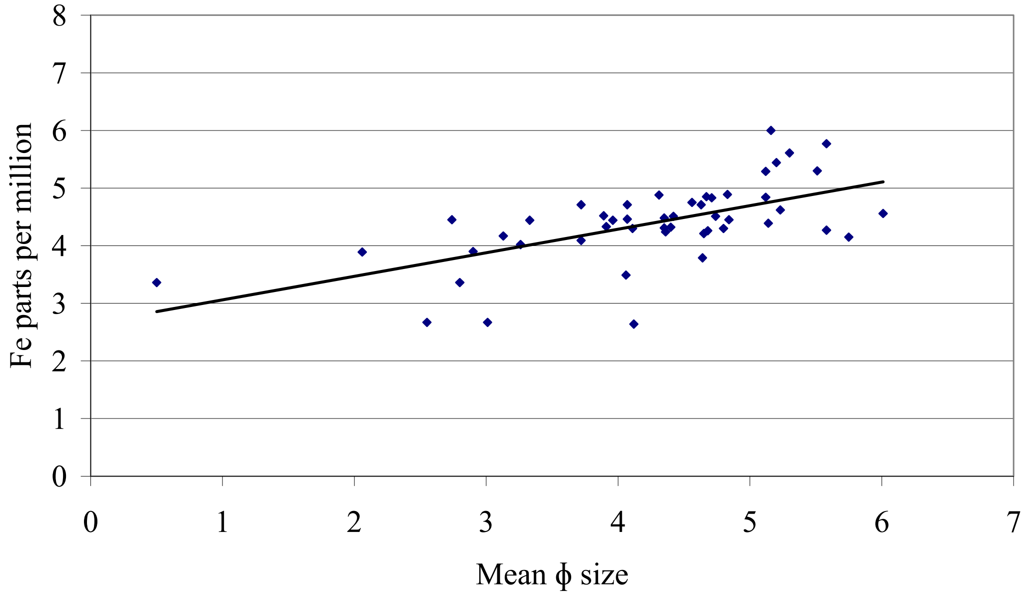

Figure 261. Well W-1552 mean ϕ size against Fe. The slope of the trend line is $y = 0.408x + 2.6543$ with $r^2 = 0.3707$.

Well W-1650

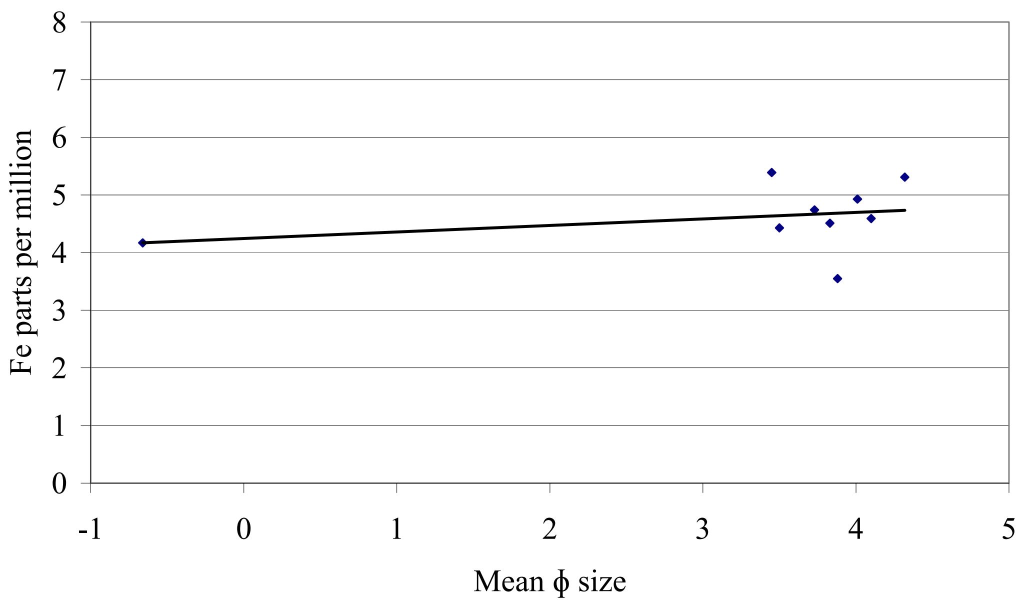

Figure 262. Well W-1650 mean ϕ size against Fe. The slope of the trend line is $y = 0.1139x + 4.2429$ with $r^2 = 0.0942$.

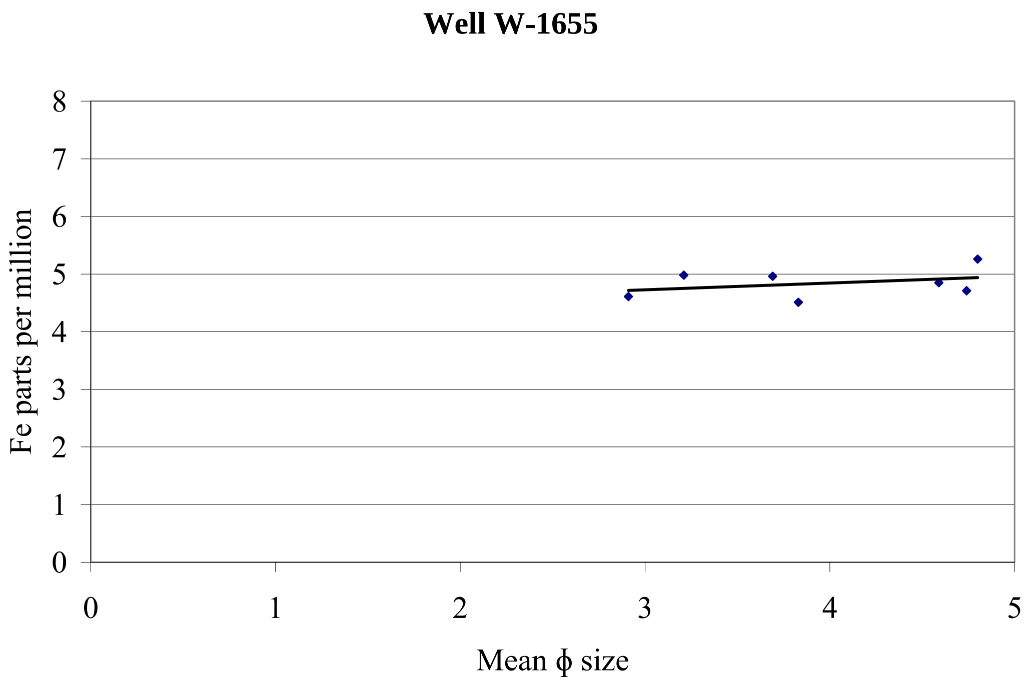

Figure 263. Well W-1655 mean ϕ size against Fe. The slope of the trend line is $y = 0.1168x + 4.3767$ with $r^2 = 0.1214$.

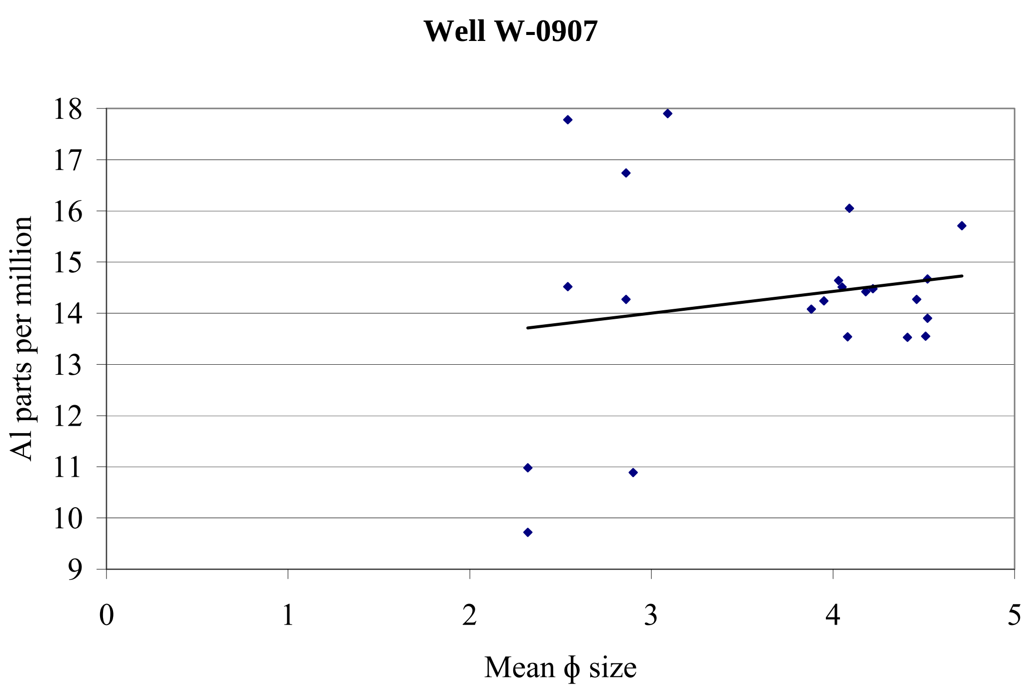

Figure 264. Well W-0907 mean ϕ size against Al. The slope of the trend line is $y = 0.4251x + 12.724$ with $r^2 = 0.0312$.

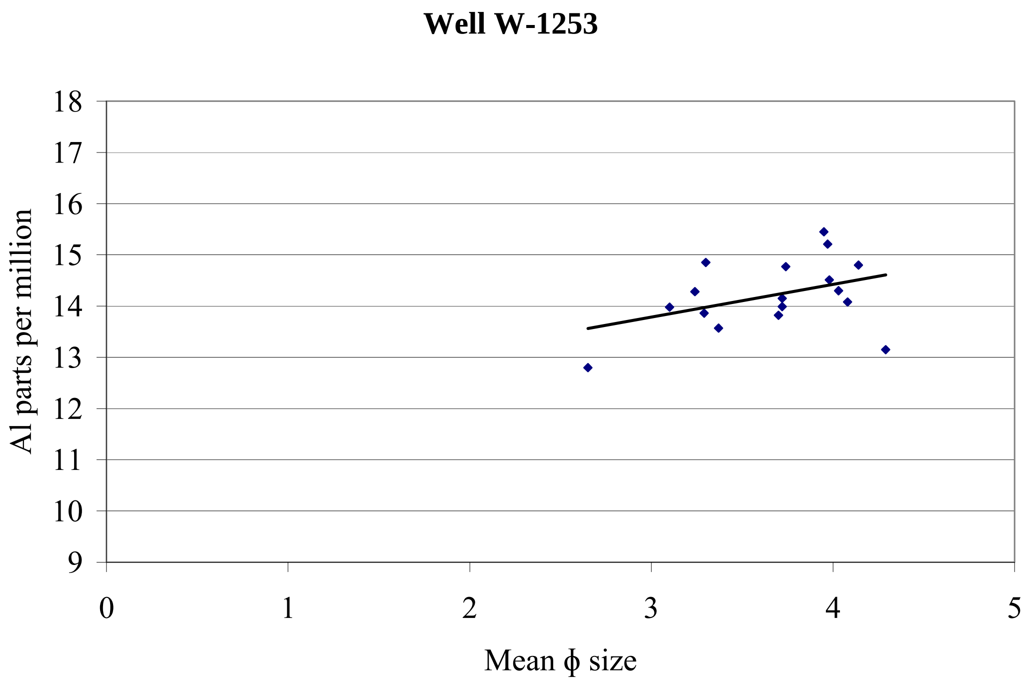

Figure 265. Well W-1253 mean ϕ size against Al. The slope of the trend line is $y = 0.639x + 11.869$ with $r^2 = 0.1659$.

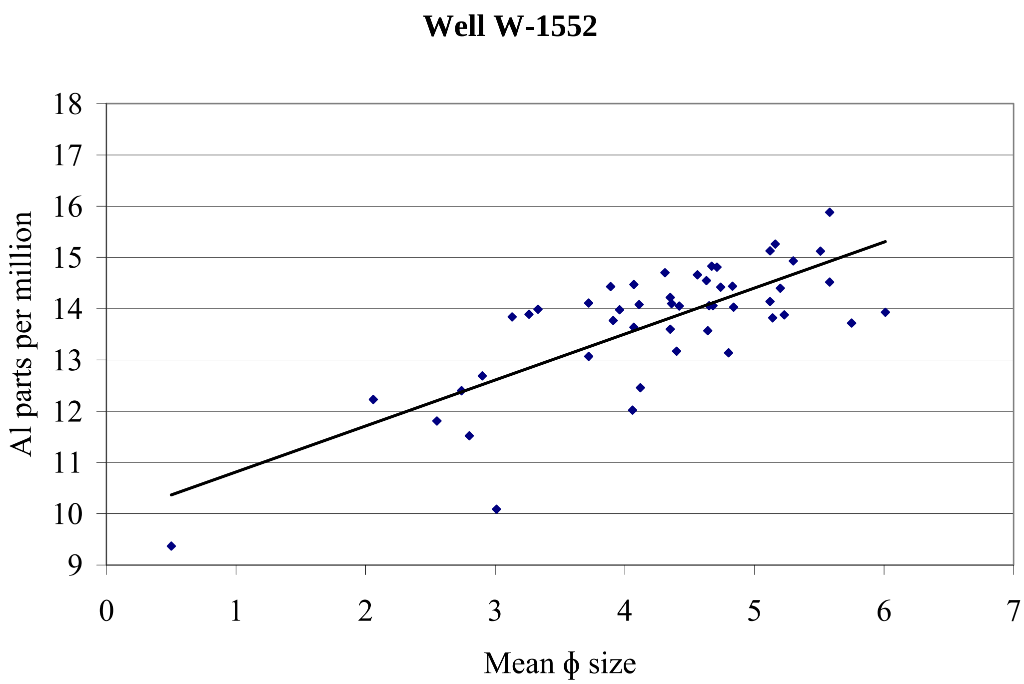

Figure 266. Well W-1552 mean ϕ size against Al. The slope of the trend line is $y = 0.8973x + 9.9156$ with $r^2 = 0.5778$.

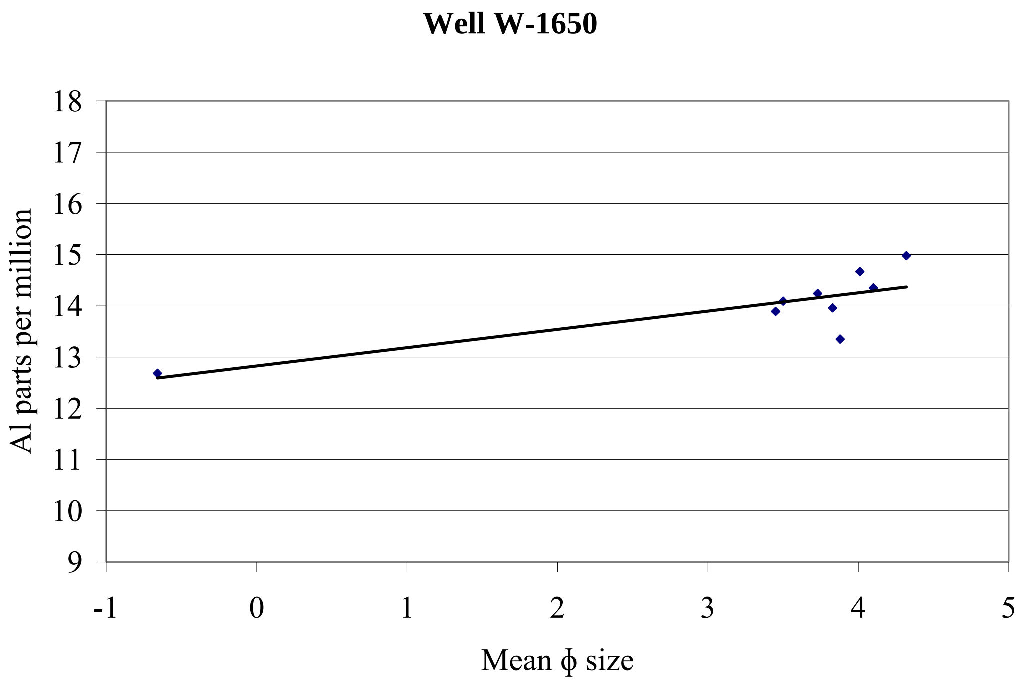

Figure 267. Well W-1650 mean ϕ size against Al. The slope of the trend line is $y = 0.357x + 12.827$ with $r^2 = 0.6322$.

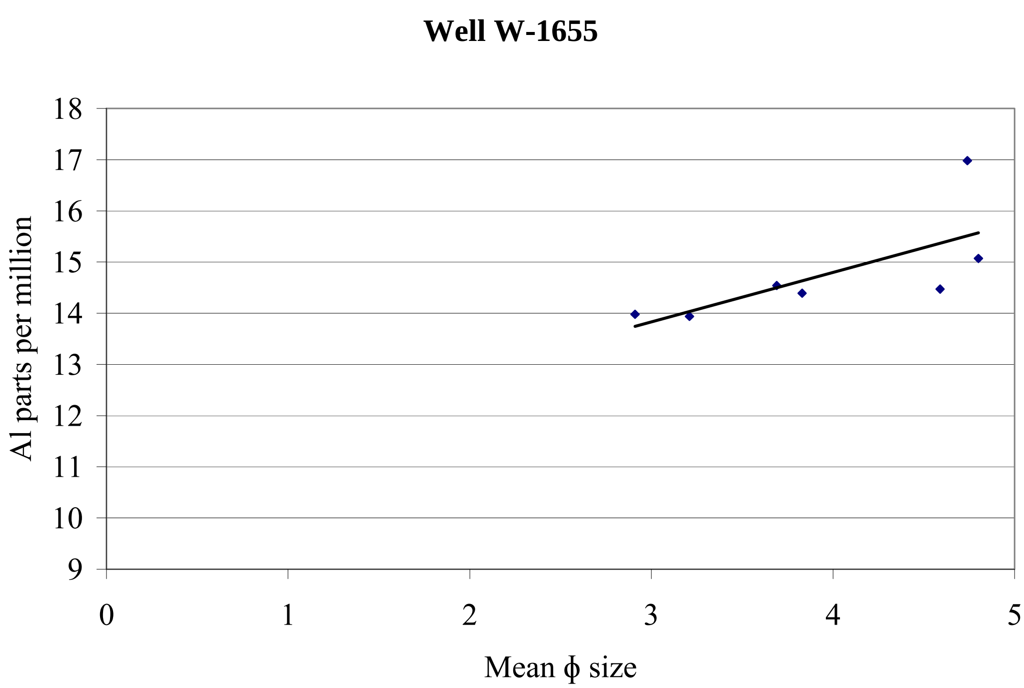

Figure 268. Well W-1655 mean ϕ size against Al. The slope of the trend line is $y = 0.9668x + 10.932$ with $r^2 = 0.4927$.

3.2 Paleosols as Stratigraphic Markers Conclusion

Geochemical data from well cores at LLNL Helipad Site did not provide a unique value for individual paleosols. Neither the data analyses designed to indicate pedogenesis, nor the analyses designed to indicate weathering were useful in distinguishing individual paleosols from the parent material. The Helipad Site was chosen for this geochemistry study because the stratigraphy is moderately well known (Weissmann, 2001; Trahan, 2003) and would allow any unique values to be matched with the corresponding paleosol. The intent was to match unique values to paleosols locally then correlate the Helipad Site paleosols with units further out and eventually LLNL-wide. However, since the geochemistry data did not distinguish correlatable individual paleosols at the Helipad Site it was determined that geochemistry data would not aid in localized nor site-wide facies correlation.

4. Provenance Determination Using Geochemical Data

Geochemical data has been used to determine provenance based on distinct chemical signatures from different source areas (e.g., Larue and Sampayo, 1990; Linn et al., 1991; Linn and DePaolo, 1993; Cullers, 1994; Reheis et al., 2002; Kimoto et al., 2006; Mitchell and Sheldon, 2010). Using major and trace elements, Linn et al. (1991) were able to determine the primary source of the sediments for the Upper Cretaceous Great Valley Group in California was the Sierra Nevada arc. Cullers (1994) looked at a variety of elemental ratios and was able to distinguish sediments derived from silicic sources versus those from basic sources. Mitchell and Sheldon (2010) were able to determine that the source for the paleosols in their study was homogeneous. With the historical success of geochemistry as a tool to determine provenance, a study was conducted at LLNL to determine the source of the sediments on site.

4.1 Provenance Study at LLNL

Mikesell et al. (2010) conducted a provenance study at the LLNL site (Chapter 3). They were able to map three fluvial fan successions beneath LLNL using easily recognizable clasts that were derived from one of the two source areas contributing sediment to the site. A synopsis of Mikesell et al. (2010) is presented here.

4.1.1 Geology and Source Area for LLNL Sediments

LLNL is bordered on the east by the Altamont Hills with Mesozoic Great Valley Group (GVG) overlain by Tertiary rocks, and to the south by the Diablo Range with Jurassic-Cretaceous Franciscan Assemblage (FA) rocks. These two lithologically distinct complexes were juxtaposed by the Coast Range thrust which placed the GVG structurally over the FA. The tectonic contact between these two complexes is the northwest-trending Tesla-Ortigalita fault to the southeast of LLNL.

The GVG consists of marine sedimentary rocks that were deposited in a Late Mesozoic forearc basin west of the Sierras. These variably cemented, stratified sedimentary rocks include conglomerates, massive bedded arkosic to lithic arenites and graywackes. The Tertiary sedimentary rocks that overlay the GVG locally include the Neroly Sandstone and the Cierbo Sandstone which are primarily continental deposits of conglomerates, sandstones, silts, clays, and coal. The Arroyo Las Positas (ALP) is an intermittent stream that drains the GVG of the Altamont Hills. ALP enters the Livermore Basin east of LLNL, and crosses the northeast corner of the study site.

The FA is a metamorphosed accretionary prism that formed in the subduction zone off the coast of North America during the Mesozoic and Tertiary. Locally, distinctive FA lithologies are derived from the Late Jurassic to Early Cretaceous Eylar Mountain Terrane which consists of metabasalt, red chert, green chert, and blueschist. Quaternary sediments exposed south of LLNL in a roadcut contain clasts of these distinct lithologies. The Arroyo Seco (AS) is an intermittent stream that drains the Altamont Hills and the Diablo Range following the Tesla-Ortigalita fault. AS enters the Livermore Basin through the Las Positas Fault pop up structure from the southeast and flows northwest across the southwest corner of LLNL. The catchment geology for AS consists of GVG on the north side of the stream and FA on the south side of the stream, including the distinctive red chert, green chert, and blueschist. This stream is unique in that its catchment includes both complexes of rock.

4.1.2 Stream Capture and Resulting Stacked Fluvial Fan Successions

Both geomorphic and subsurface geologic evidence suggest that AS is a captured stream. Geomorphic evidence includes: 1) AS currently flows northwesterly through a pop up which was up lifted by localized tectonic movement on the Las Positas Fault (Figure 228 in Chapter 3), 2) a fan-shaped deposit of sediment south of the Las Positas Fault pop up with no stream feeding it (Figure 228 in Chapter 3), and 3) knickpoints in AS upgradient from LLNL indicating differing original slopes between the capturing and captured stream (Figure 229 in Chapter 3). The geologic evidence for stream capture is the relative abundances of distinct FA indicator pebbles in the subsurface. Since AS is the only stream depositing sediment at LLNL whose catchment includes FA, AS sediments will contain more red chert, green chert, and blueschist than will ALP sediments. ALP sediments may not be devoid of all red chert, green chert, and blueschist due to possible reworking of older sediment and incorporation of those sediments into ALP deposits. Mikesell et al. (2010) chose 215 gravel samples from 34 boreholes from across the site. Three hundred granule and pebble sized clasts (2 – 16 mm) from each sample were randomly chosen and classified into four categories: red chert, green chert, blueschist, and "other." A percentage of indicator clasts from FA was calculated for each sample. The percentages were plotted against depth, and three clusters of data became evident (Figure 230 in Chapter 3). One cluster extends from the ground surface to a depth of 18 m and has a mean value of indicator pebbles of 20.46%. A second cluster of data lies at a depth between 18 m and 35 m and is centered on an indicator pebble value of 13.75%. The third cluster of data lies below 35 m and has a mean indicator value of 23.11%. The uppermost and lowermost clusters of data display higher proportions of indicator clasts, indicating those sediments are FA derived and were most likely deposited by AS. The middle cluster with the lower percentage value indicates fewer FA indicator pebbles and thus suggests this section was primarily deposited by ALP. Theses results indicate three stacked fluvial fan successions exist beneath LLNL. As stated earlier in this chapter, site-wide facies correlations based on paleosols were very limited; however, this provenance study based on pebble-sized clasts demonstrates that correlating large-scale successions is possible at LLNL.

4.2 Provenance Determination at LLNL Using Geochemical Data

Geochemical data did not prove to be a useful tool in facies correlations at LLNL. However, with the knowledge of three stacked fluvial fan successions beneath LLNL, the second application of the geochemistry data was as a possible tool for provenance determination. The same geochemistry plots that were created for possible paleosol identification were employed in this study (Figures 230 – 294). With the knowledge that there was a fan succession boundary at 18 m depth and another succession boundary at 35 m depth the data were examined within these zones between boundaries for evidence of clustering which would make that zone distinct from other zones. To be useful as a provenance indicator, the geochemistry data in the uppermost and lowermost zones, which were AS deposited sediments, would need to be similar yet both distinct from the middle zone which was ALP deposited sediments. No distinct clustering of data was observed in any of the plots of elemental data, ratio calculations or weathering indices.

5. LLNL Geochemical Data Interpretation and Conclusions

5.1 Paleosol Correlation Using Geochemistry

Geochemical data analysis proved to not be useful at LLNL as a correlation tool. The only linear trends observed in the geochemical data plots were not patterns indicating pedogenesis or degree of weathering, but were attributed to increased immobile element concentrations correlating to decreasing grain size. Despite plotting elemental abundances against depth, and calculating elemental ratios designed to be a proxy for determining soil-formation environmental conditions, and using elemental ratios and weathering indices designed to indicate degree of weathering, no unique or distinct geochemical signature was observed. Without such a signature for any paleosol unit a site-wide facies correlation could not be accomplished based on geochemistry.

5.2 Provenance Determination

Even the larger scale fluvial fan successions were not distinguishable using geochemistry data. Given that geochemistry has been used successfully for provenance determination in other settings (e.g., Linn et al., 1991; Linn and DePaolo, 1993; Cullers, 1994; Mitchell and Sheldon, 2010) by indicating differences in source area geochemistry and subsequent detritus, and yet was not successful at LLNL, then GVG and FA must be geochemically similar and possibly genetically linked. Dickinson et al. (1982) studied graywacke sandstones from FA and the coeval sandstones from GVG. By classification and comparison of detrital grains, they noticed significant and consistent overlap of FA and GVG grains in QFL (total quartz grains, total feldspar, total unstable aphanitic lithic fragments), QmFLt (monocrystalline quartz grains, total feldspar, total aphanitic lithic fragments of both unstable and quartzose), QpLvLs (polycrystalline quartzose, lithic fragments, sedimentary lithic fragments), QmPK (monocrystalline quartz grains, plagioclase grains, K-feldspar grains) triangular plots. The conclusions of their study state that the detrital modes of the sandstones are similar enough to suggest that most of the detritus in both terranes was derived from related sources with a common provenance, and that the differences in these two data sets are not great enough to suggest major differences in provenance.

The ancestral Sierran-Klamath arc and its extension to the south are the probable provenance for both GVG and FA based on regional geologic relations. GVG forearc basin receive sediment along the strike of the arc-trench system while FA sediment reached the subduction zone trench by way of submarine canyons which bypassed the sediment trap of GVG. In addition to ancestral Sierran-Klamath arc sediments, FA may have received recycled trench and slope sediments as well as oceanic sediments accounting for the mentioned dissimilarities between the two.

Two more studies were conducted on GVG and FA and both supported Dickinson et al. (1982) (Seiders, 1988; Seiders and Blome, 1988). Whereas Dickinson et al. (1982) focused on the sandstones, the other two studies focused on conglomerates. The differences in the mineralogy of the clasts of GVG and FA are due to FA being buried to a depth of 20 – 30 km

(Seiders, 1988) then returned to the surface. At this depth, FA accretionary prism was subjected to blueschist facies metamorphism (Moore and Liou, 1979) which is low temperature and high pressure. GVG was not metamorphosed and has a distinctly different rock assemblage than FA. In addition to the FA indicator clasts used in the previously mentioned provenance study (Mikesell et al., 2010), heavy minerals within FA are glaucophane, jadeite, pumpellyite, lawsonite, enstatite, tremolite, actinolite, and chromium spinel (Yancey and Lee, 1972). Heavy minerals from GVG include augite, hypersthene, hornblende (Yancey and Lee, 1972). Seiders (1988) and Seiders and Blome (1988) concluded that the differences in composition of GVG and FA is not due to an exotic FA terrane being tectonically juxtaposed to GVG on the North American margin, but rather due to metamorphism acting upon FA sediments while not affecting GVG sediments. While rock assemblages differ between GVG and FA allowing for a successful provenance determination of sediments at LLNL based on easily identifiable clasts, the two terranes are indistinguishable based on geochemical data due to GVG and FA both having the same sediment source which was the ancestral Sierran-Klamath arc.

6. Zone of Enrichment and Future Study

Plots of V, Rb, Nb, Ba, La, Ce, Pr, Nd, Sm, Eu, Gd, Tb, Dy, Ho, Er, Yb, Lu, Ta, Pb, Th, Mn, and P (Appendix C) elemental concentration with depth show a zone of enrichment in these elements between approximately 30 m and 35 m in five of the six wells analyzed for geochemistry (i.e. W-1253, W-1552, W-1553, W-1650, W-1655). The samples that are enriched in these elements were all collected from units identified as a paleosol. Three possible theories for this zone of enrichment include: 1) enrichment due to translocated elements during weathering or pedogenesis, 2) a marker of a lithologic discontinuity, or 3) anthropogenic sources.

The elements enriched at the 30 m zone (i.e., Ti, Mn, P, V, Rb, Nb, Ba, La, Ce, Pr, Nd, Sm, Eu, Gd, Tb, Dy, Ho, Er, Yb, Lu, Ta, Pb, Th) are considered immobile and not likely to translocate within sediment or soil (e.g., Ruxton, 1968; Harden, 1987; Maynard, 1992). Therefore this enrichment is not likely due to down-profile movement as a result of weathering or pedogenesis. REE (e.g., Ce, Pr, Nd, Sm, Eu, Gd, Tb, Dy, Ho, Er, Yb, Lu, Th) are known to adsorb onto clays and thus be enriched in clay-rich units such as paleosols (Dia et al., 2000; Compton et al., 2003; Willis and Johannesson, 2011). If this enrichment was a result of weathering and/or pedogenesis, each weathered unit or paleosol would exhibit enrichment in these elements. However, enrichment was not observed in other zones within the stratigraphic column. Due to the immobile nature of these elements and the enrichment occurring in only one zone, it is not likely that this is due to weathering and translocation of the elements.

As discussed earlier in section 5.2, the material in the two source areas of LLNL sediment is geochemically similar and apparently derived from the same ancestral Sierran-Klamath arc sediments. Any lithologic discontinuity present in LLNL sediments was not be distinguishable using geochemistry. Also, as discussed in section 4.1.2, the lower boundary between the stacked fan successions is located at 35 m below the surface. The zone of enrichment does not correspond with the known fan succession boundary, which is 5 m below or at the lower reach of the zone of enrichment. This enrichment is likely not a result of a lithologic discontinuity.

I hypothesize this zone of enrichment has anthropogenic origins. The zone of enrichment is approximately at the same depth as the water table during the 1940's and 50's when a landfill was present on LLNL, which is the likely contaminant source (Pers. Comm., Charles Noyes, 2011). Prior to land development for the city of Livermore, the land surrounding the LLNL site was agricultural with heavy ground water pumping for irrigation. The water table was, by some estimates, approximately 20 m deeper than its current depth of 25 m due to pumping (Pers. Comm., Charles Noyes, 2011). The land now occupied by LLNL was used as a Naval Air Base beginning in 1942, at the onset of World War II, through 1946. During that time, airplanes were serviced, repaired and cleaned on site. The resultant industrial chemical waste was disposed of in landfills on site. One such landfill site was located north of what is now ETC and east of the Helipad Site where our sampled well cores were recovered. Industrial chemicals and other waste products used by the military were placed in barrels and buried. The time the landfill was active coincides with the deeper water table. It is likely that contaminants leached out of the landfill and became entrained in the vadose zone above the water table. As urbanization encroached on LLNL during the 1970's, the farmland decreased lessening the need for irrigation and ground water pumping. Due to decreased pumping the water table rose to its current location. This upward migration of the water table brought water into contact with the contaminants held within the sediments and mobilized the contaminants in ground water flow. The general direction of flow is eastward and toward the Helipad Site and the wells that were sampled for this study. It should be noted that samples from W-0907 did not show elemental enrichment in this zone. W-0907 is approximately 180 m west of the Helipad Site and not included in the cluster of wells with the other five wells (Figure 232). I hypothesize the dispersal of these elements was not wide enough to reach W-0907 before they were adsorbed onto the clays within the paleosols. The barrels have subsequently been removed under the direction of LLNL and disposed of properly. It is likely that these barrels were one source of contaminants currently in the ground water at LLNL.

In addition to contaminants from the landfill site, underground gasoline storage containers leaked approximately 70,000 liters in the southeast section of the site (Aines et al., 1994). A former filling station occupied the site from 1952 to 1979 (Thorpe et al., 1990; Aines et al., 1994). LLNL personnel discovered a concentration zone of petroleum at approximately 32 m to 38 m under the ground surface. LLNL personnel hypothesize the gasoline infiltrated the sediment and floated on the water table surface because of its immiscibility with water. The gasoline adsorbed to the clay and silty sediment, and remained in place as the water table rose due to decreased pumping (Pers. Comm., Charles Noyes, 2011). This gasoline-enriched zone marks a previous water table depth and coincides with the zone of elemental enrichment observed in the geochemical data for this study. During the time of the spill, gasoline in the United States was leaded (USEPA, 1973); and as noted, Pb was also observed to be enriched at 30 m to 32 m depth in the helipad site.

Future research could determine the source of the enrichment zone at 30 m. LLNL is in possession of a list of barrels that were buried and later removed from the landfill site; however, the list is not exhaustive of what was uncovered during removal. The contents of the barrels were not detailed accurately, and the exact nature of the buried material is not fully known. It is likely that material containing the elements of interest was place in the barrels that leaked at the landfill. A researcher could obtain the existing list of the landfill contents from LLNL and investigate as to the likely contributors of the elemental enrichment at 30 m. Also, using Pb isotope data, a researcher would be able to determine if the Pb enrichment at 30 m was due to gasoline. The original samples would have to be retested to determine Pb isotopes because isotope data was beyond the scope of this study and not requested during analysis.

APPENDIX C

Lawrence Livermore National Laboratory

Geochemical Data

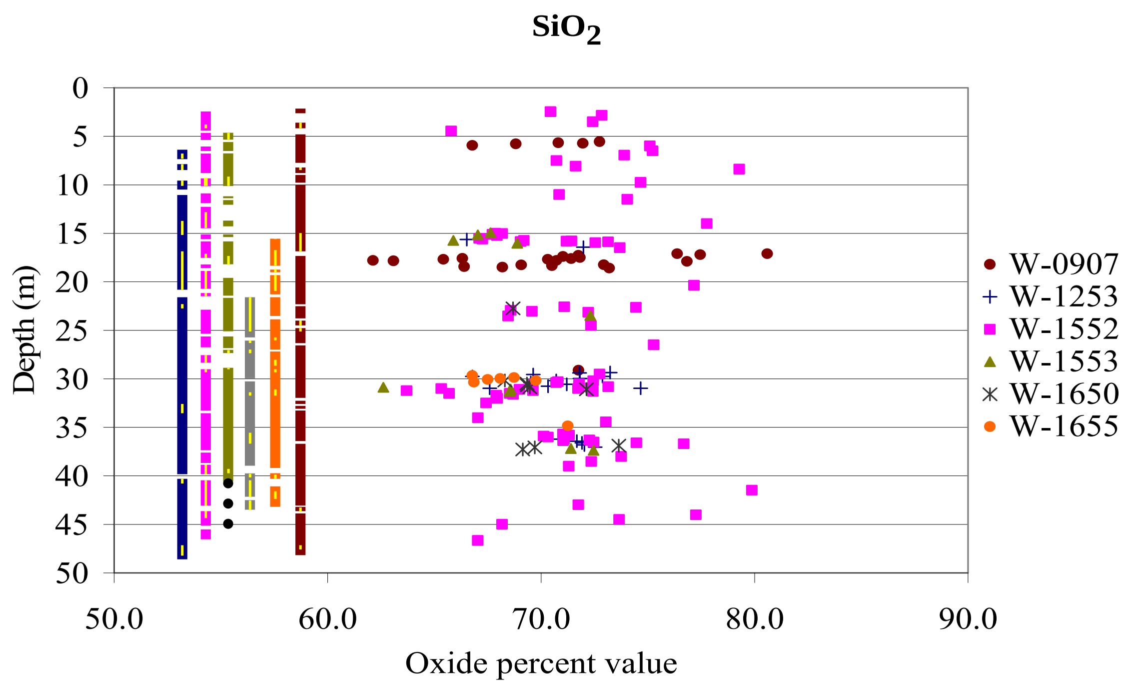

Figure 269. SiO_2 percent with depth.

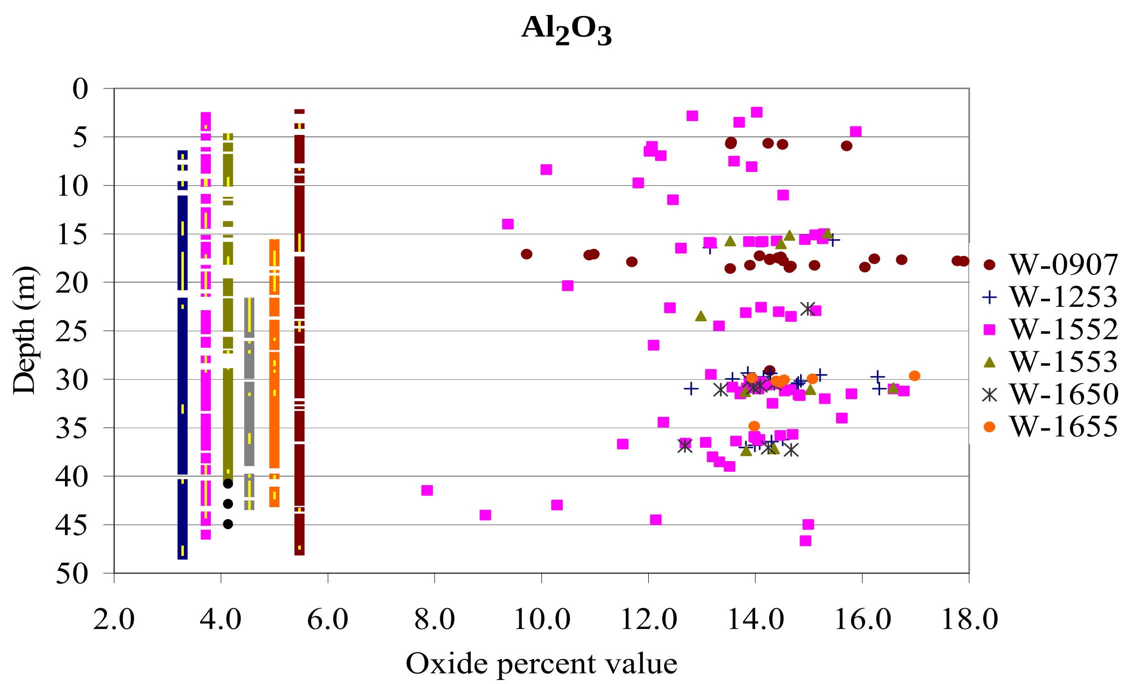

Figure 270. Al_2O_3 percent with depth.

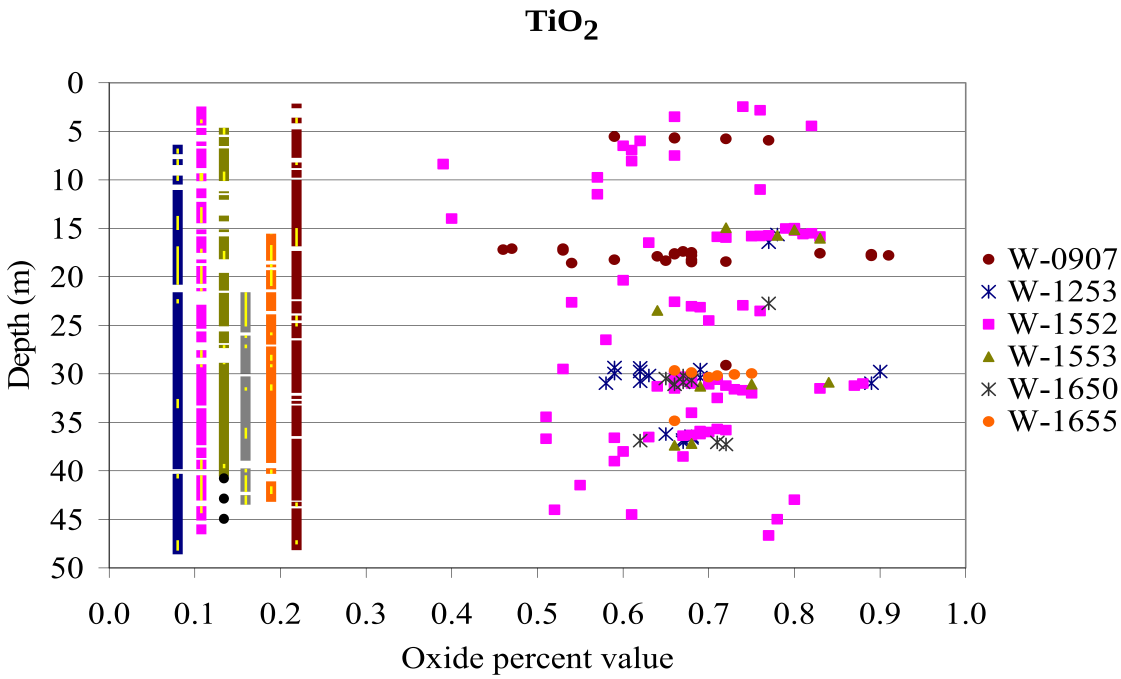

Figure 271. TiO$_2$ percent with depth.

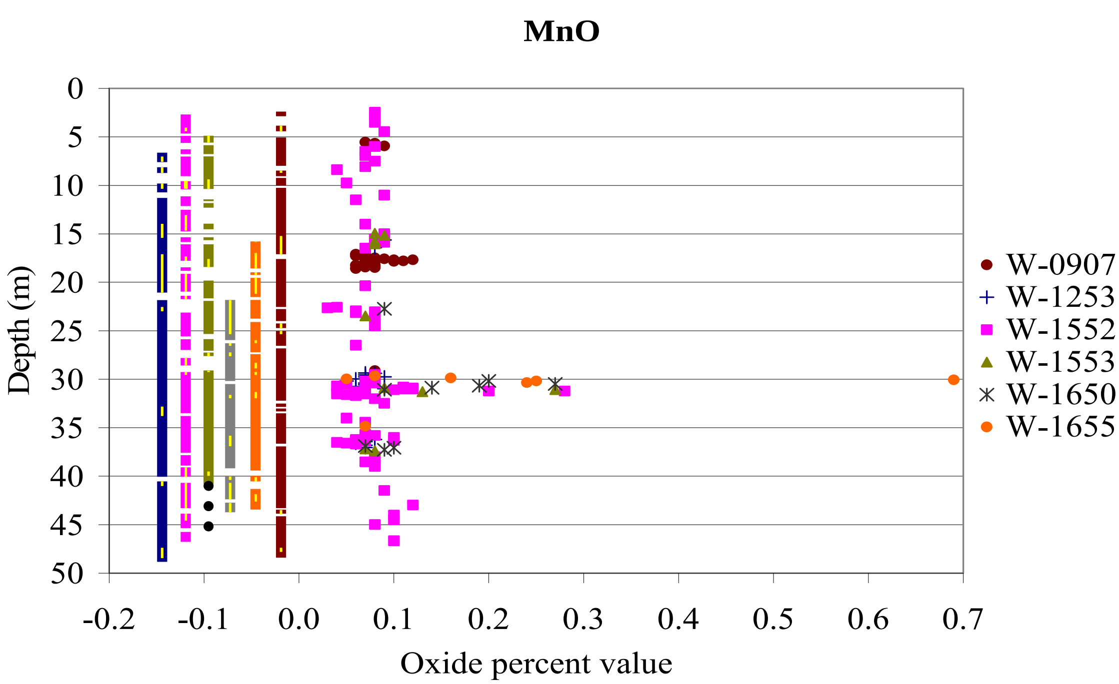

Figure 272. MnO percent with depth.

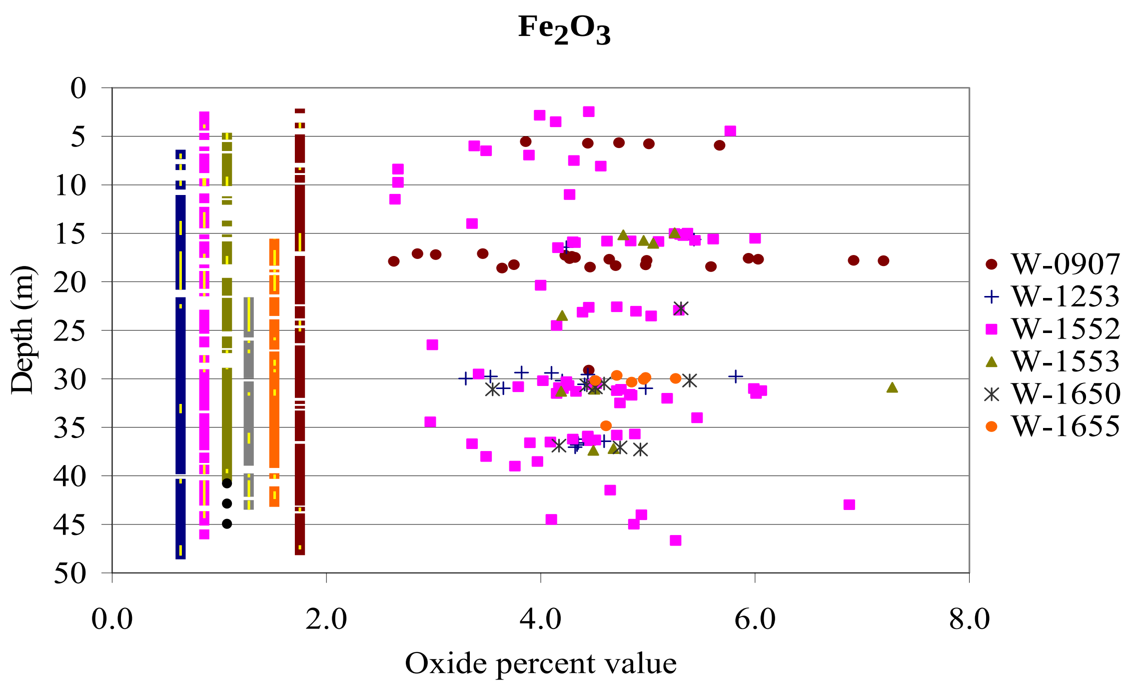

Figure 273. Fe_2O_3 percent with depth.

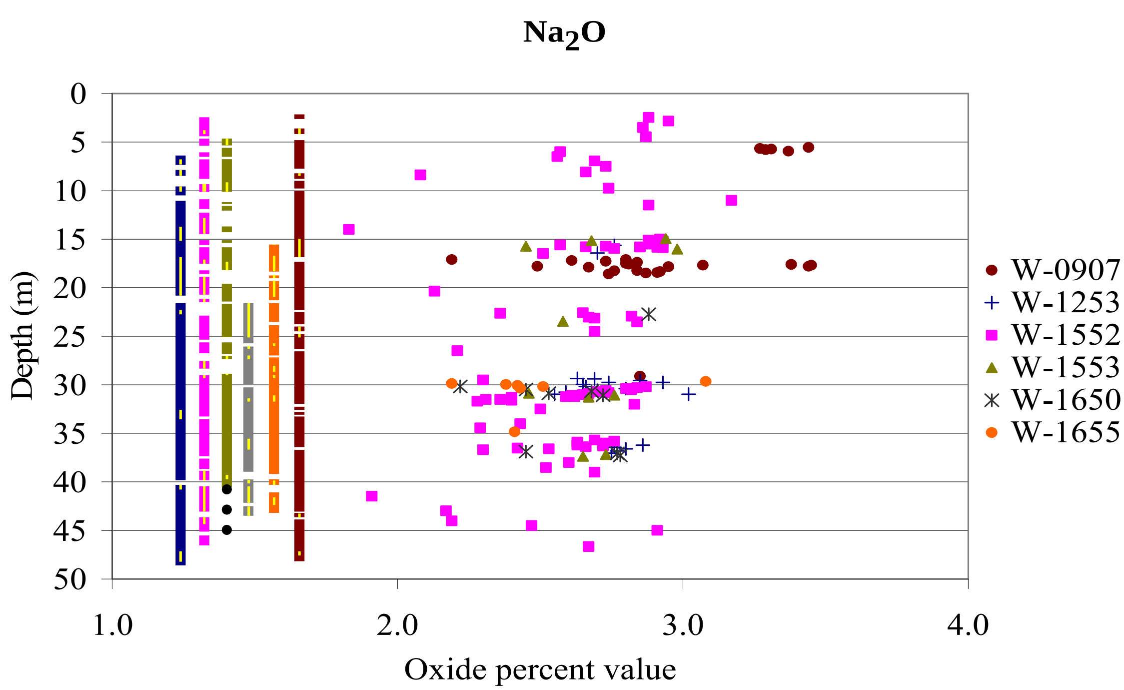

Figure 274. Na_2O percent with depth.

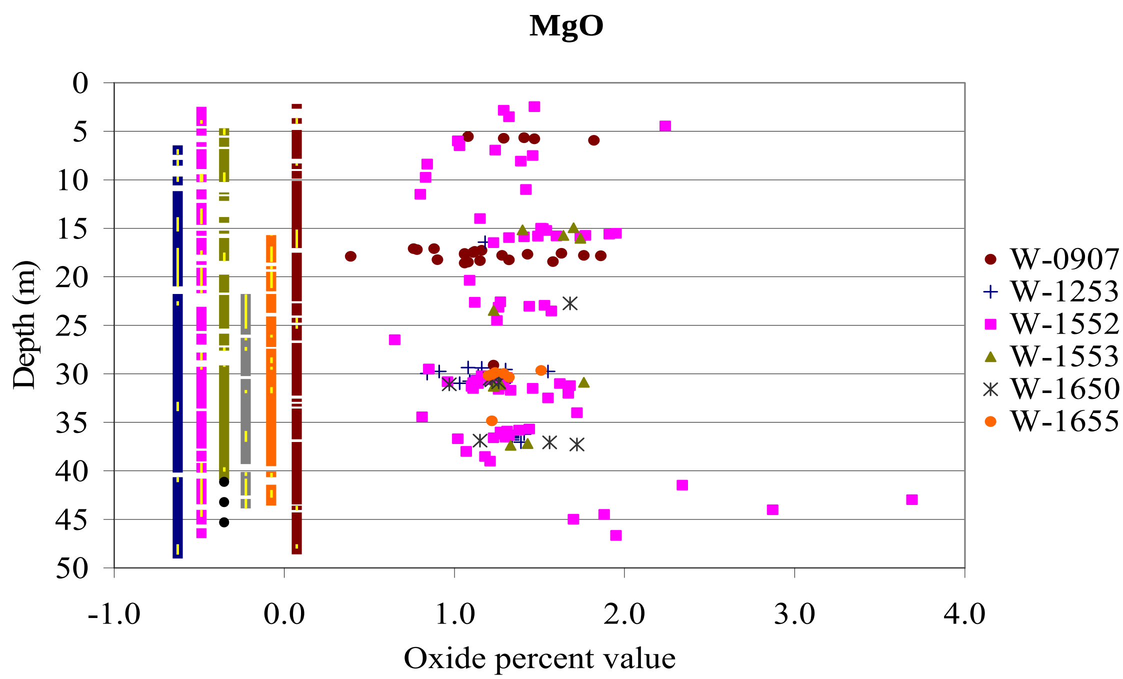

Figure 275. MgO percent with depth.

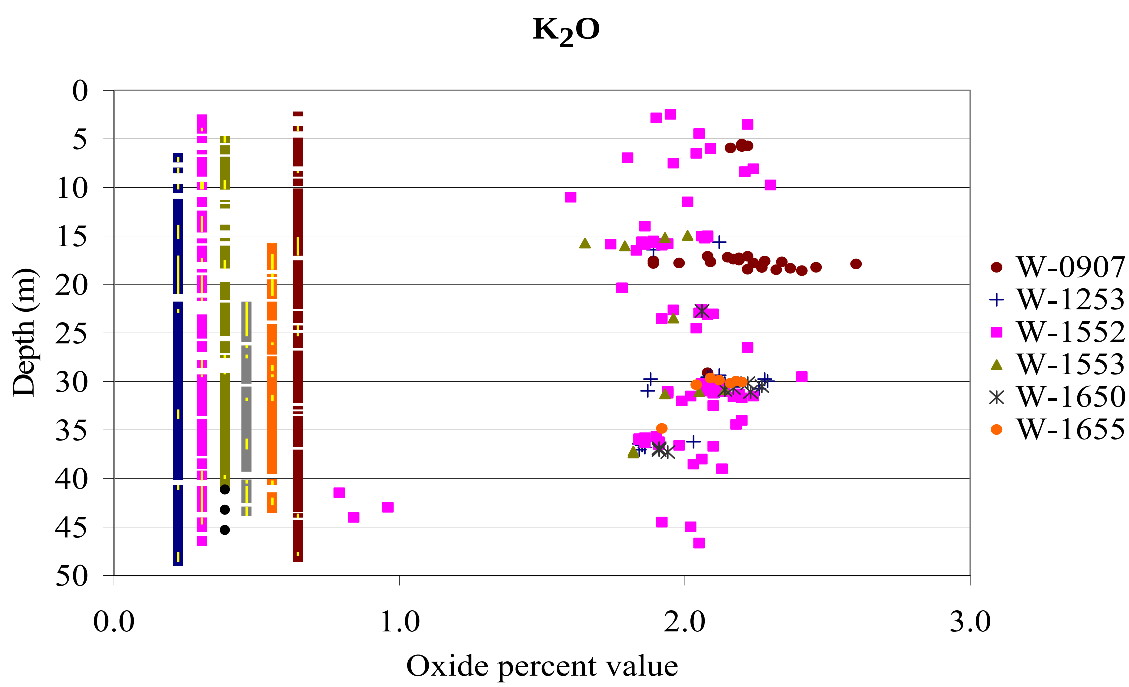

Figure 276. K_2O percent with depth.

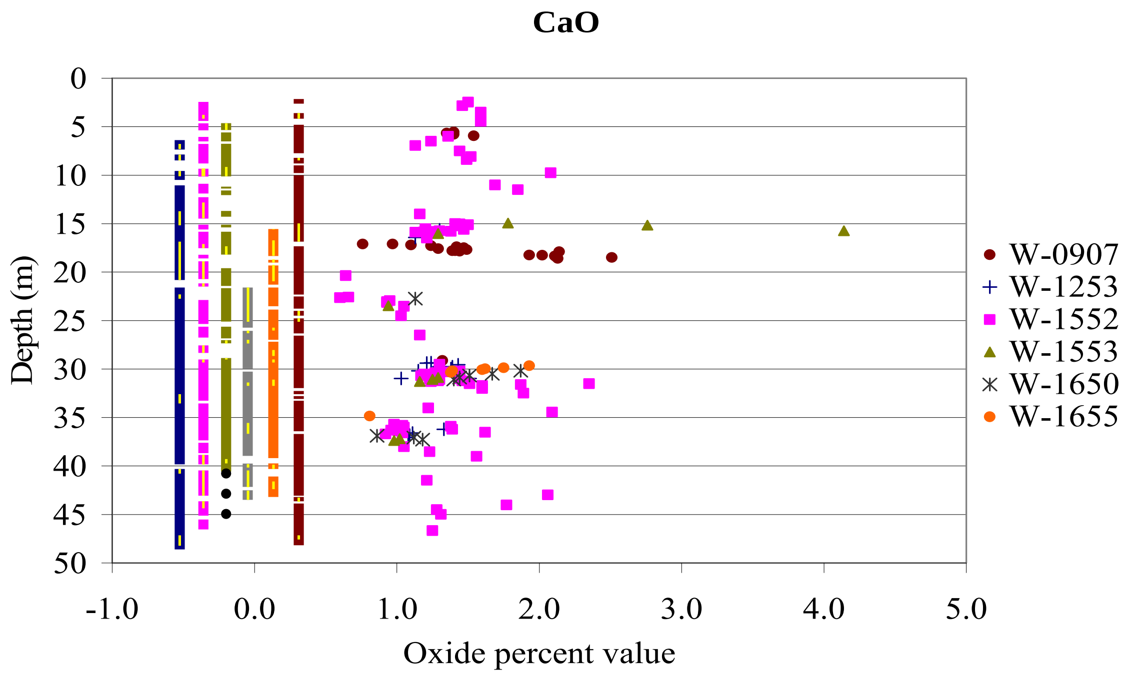

Figure 277. CaO percent with depth.

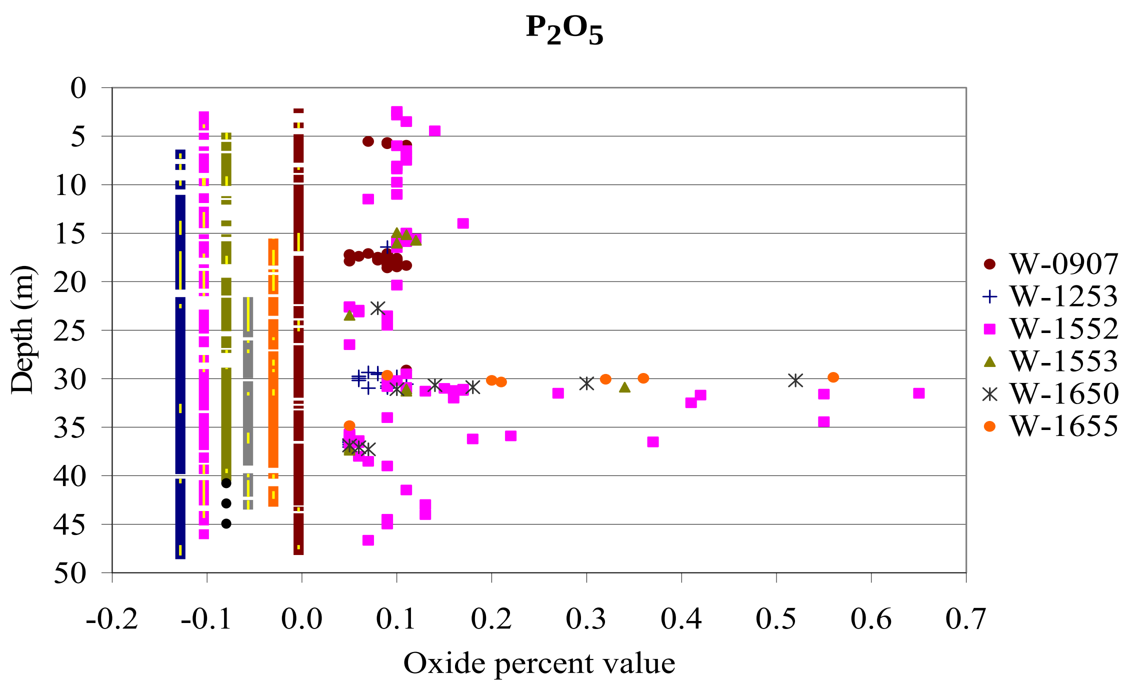

Figure 278. P_2O_5 percent with depth.

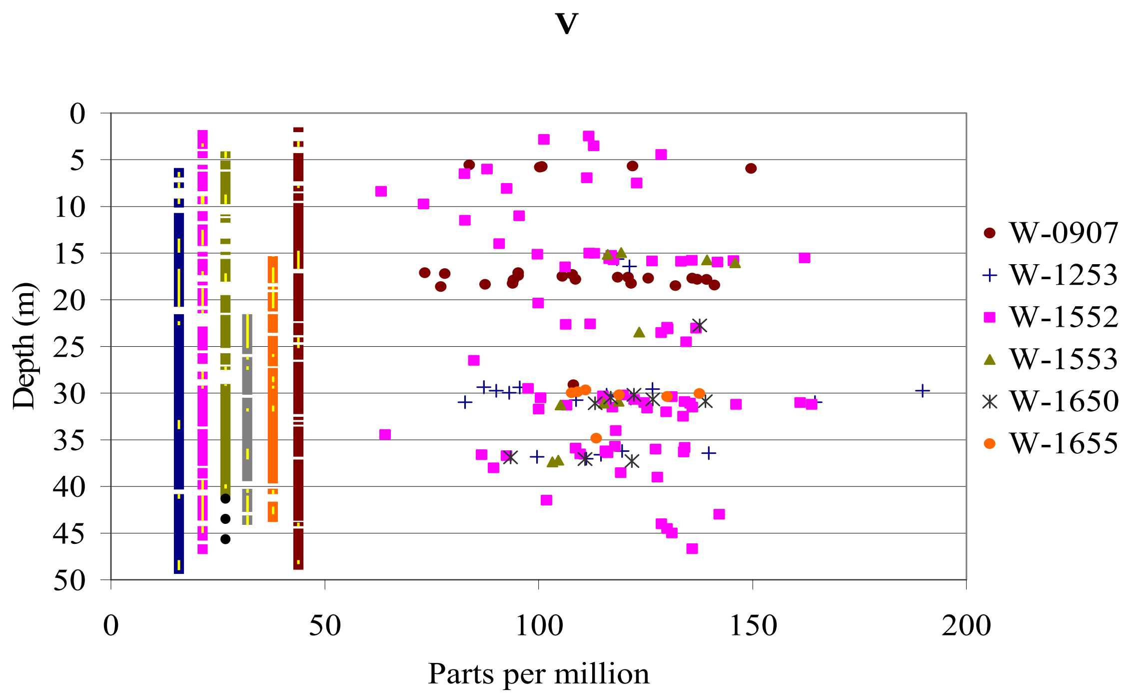

Figure 279. V parts per million with depth.

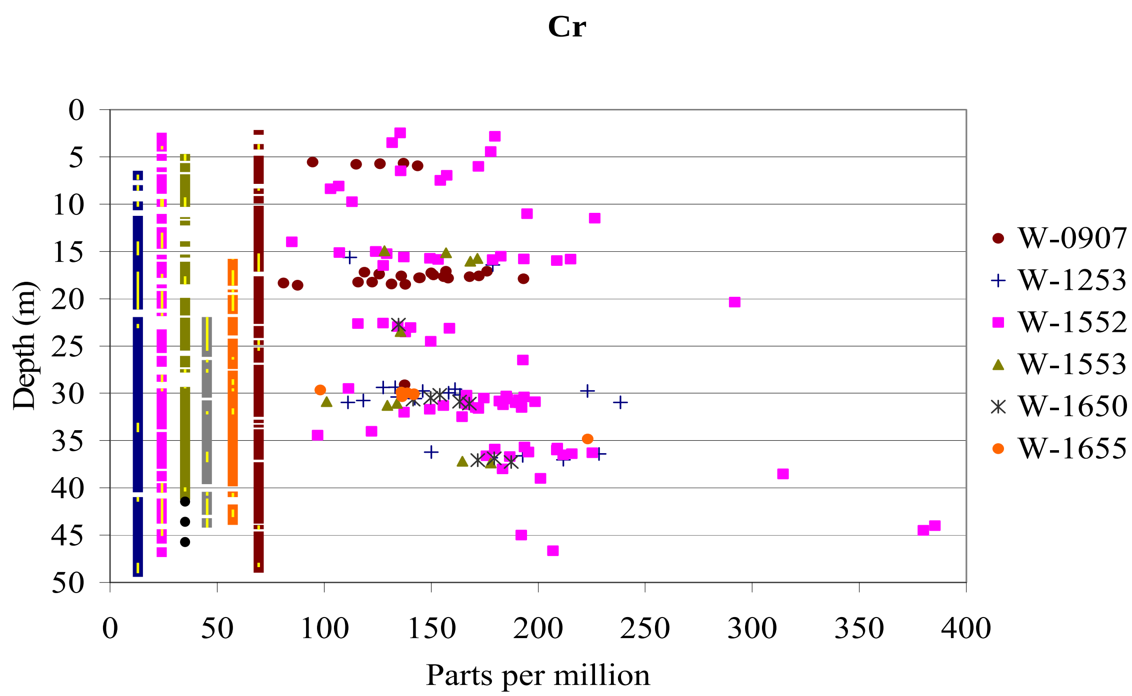

Figure 280. Cr parts per million with depth.

Rb

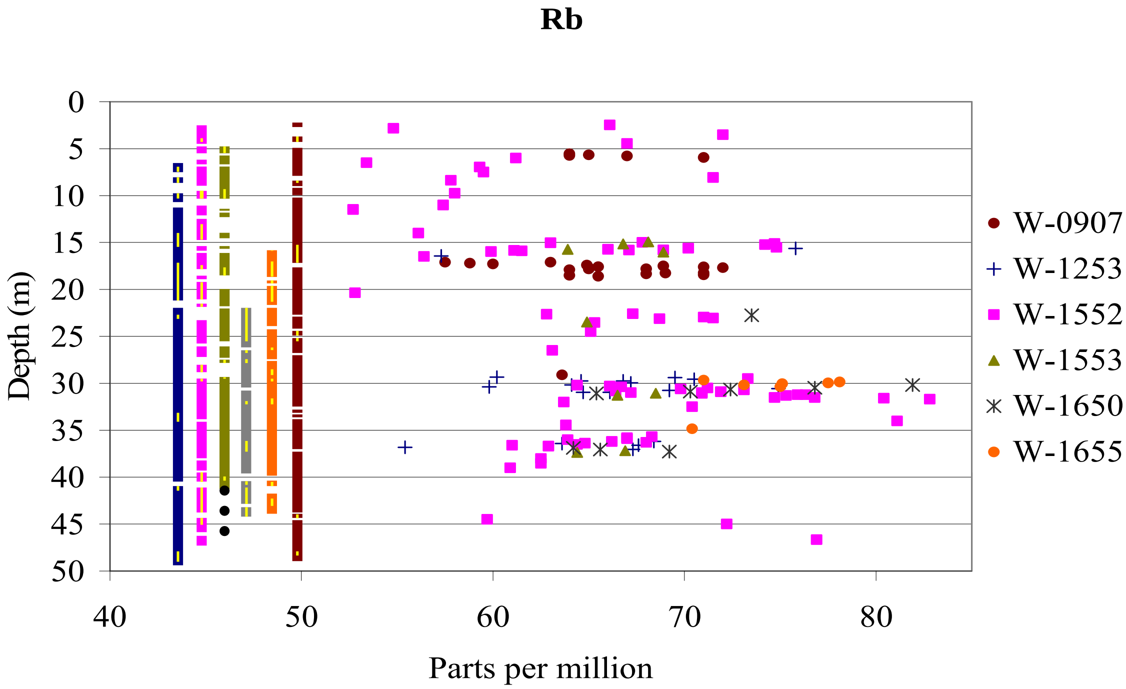

Figure 281. Rb parts per million with depth.

Sr

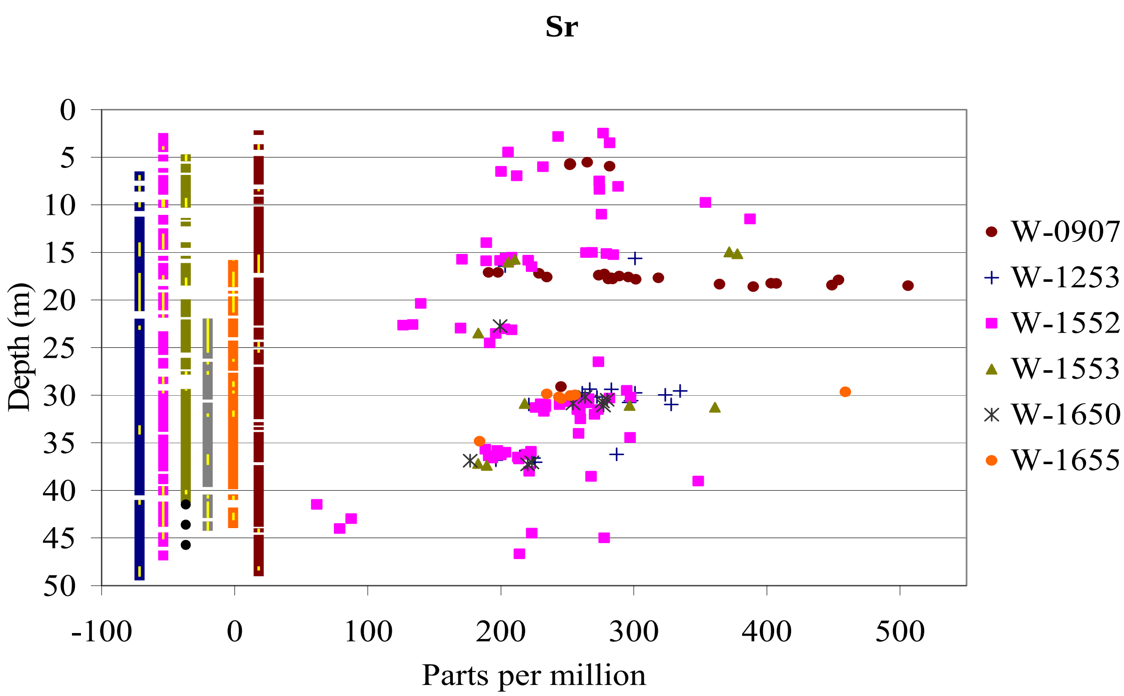

Figure 282. Sr parts per million with depth.

Y

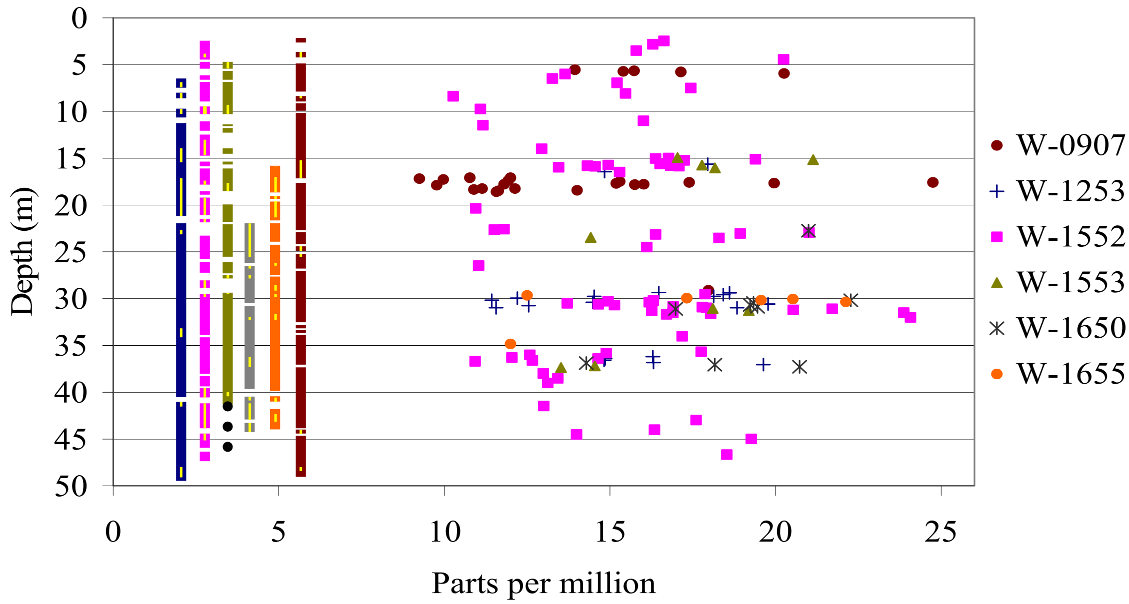

Figure 283. Y parts per million with depth.

Zr

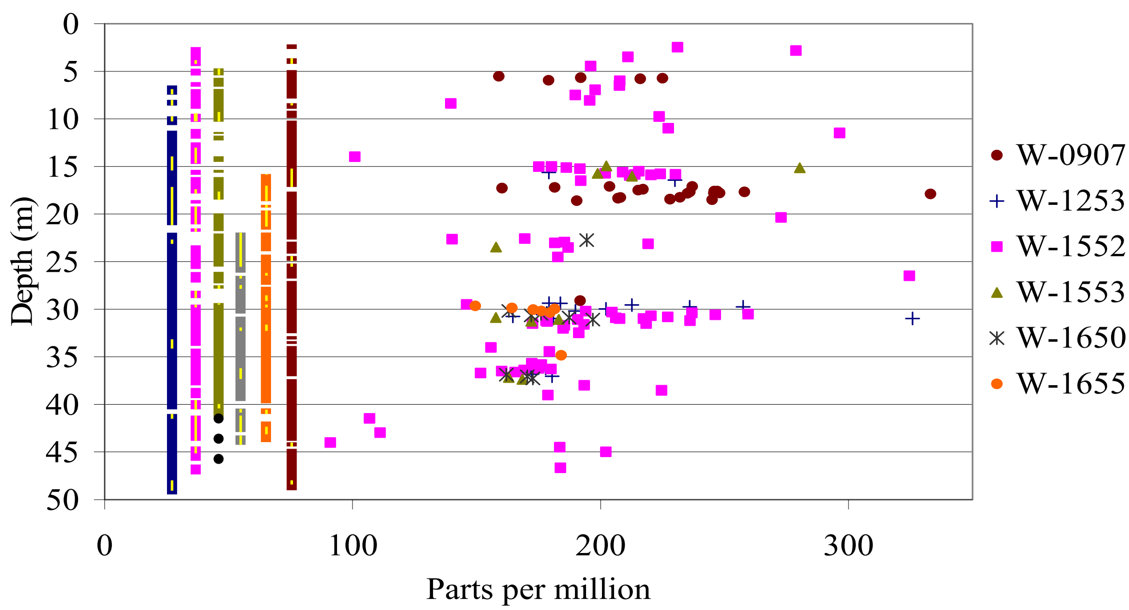

Figure 284. Zr parts per million with depth.

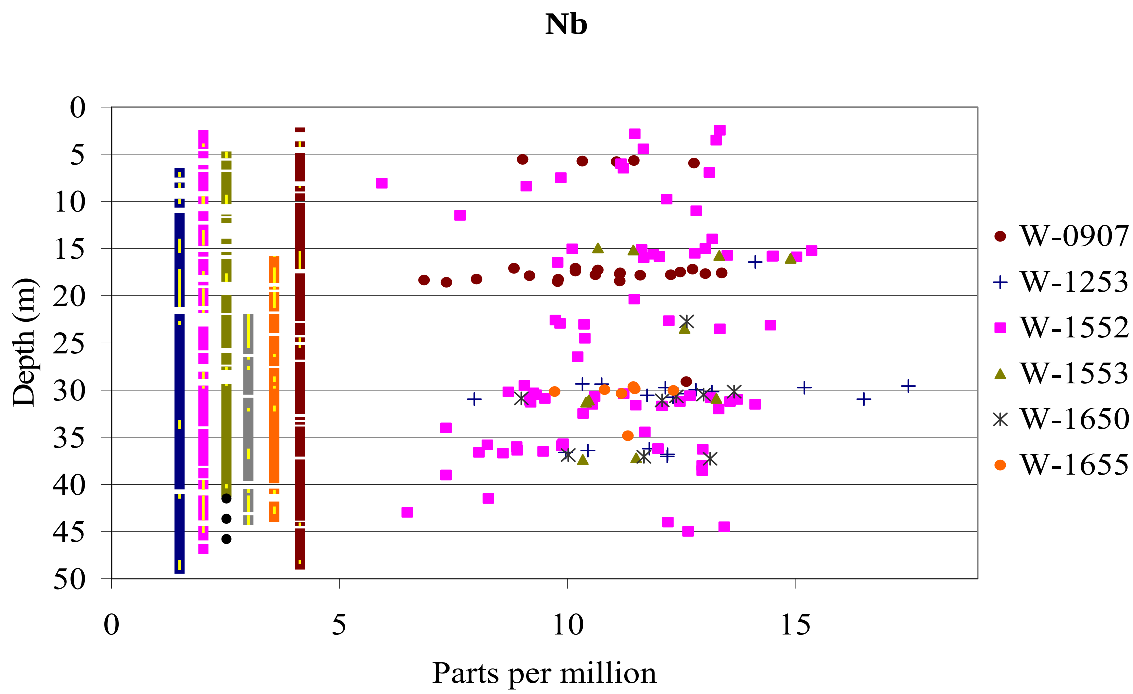

Figure 285. Nb parts per million with depth.

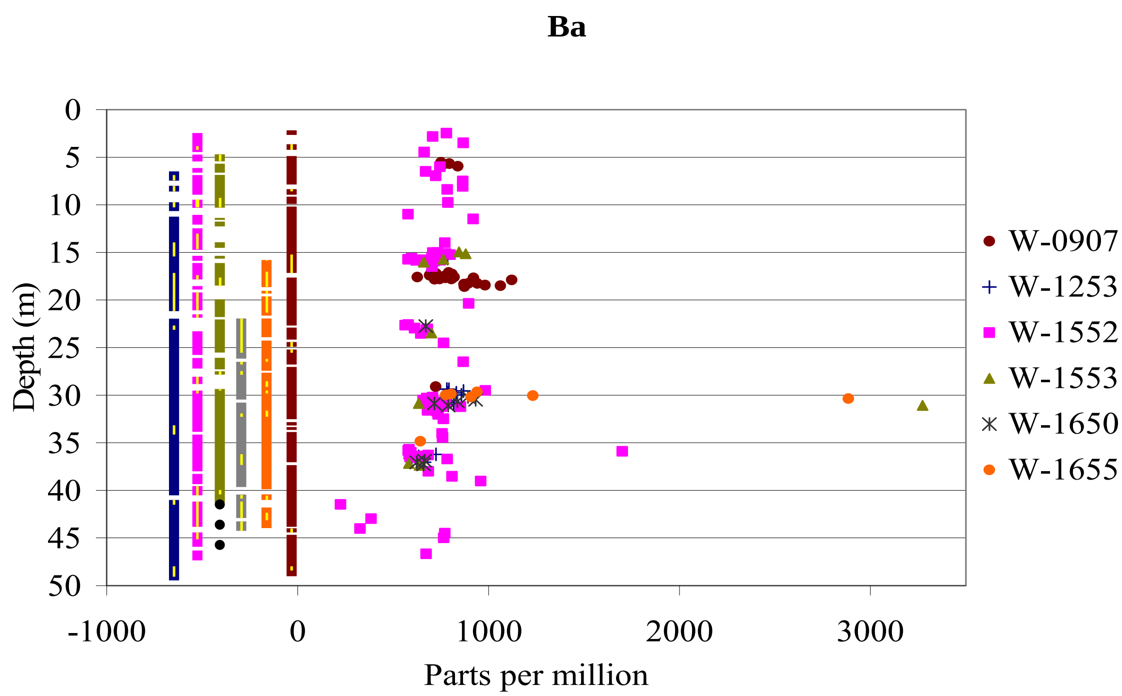

Figure 286. Ba parts per million with depth.

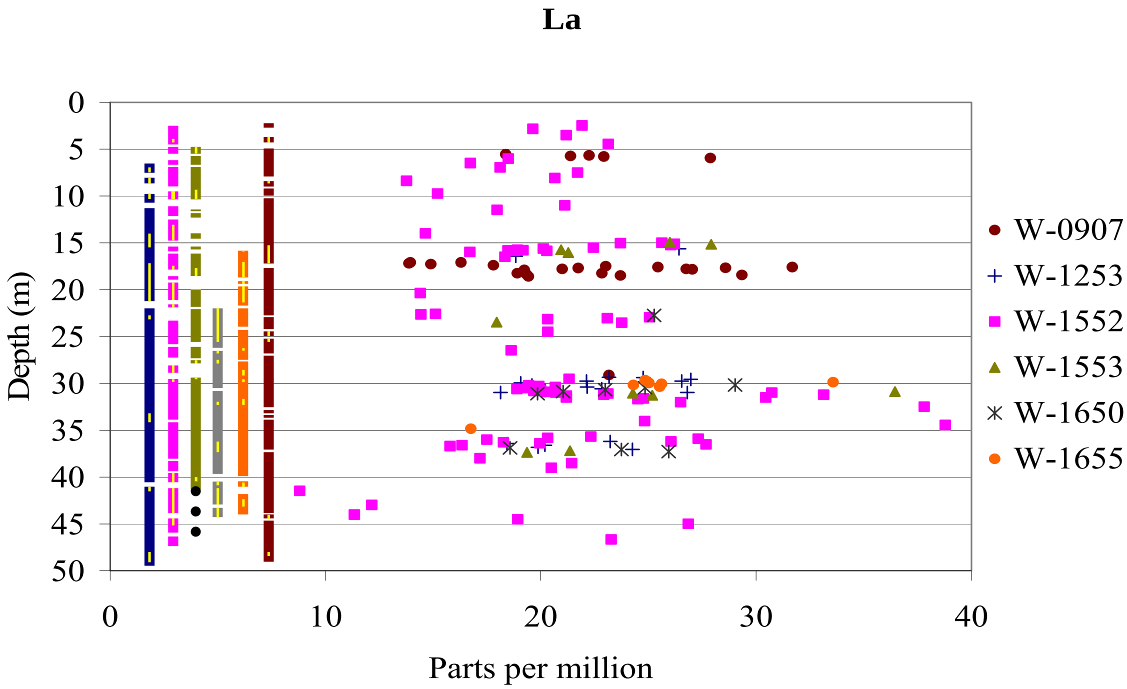

Figure 287. La parts per million with depth.

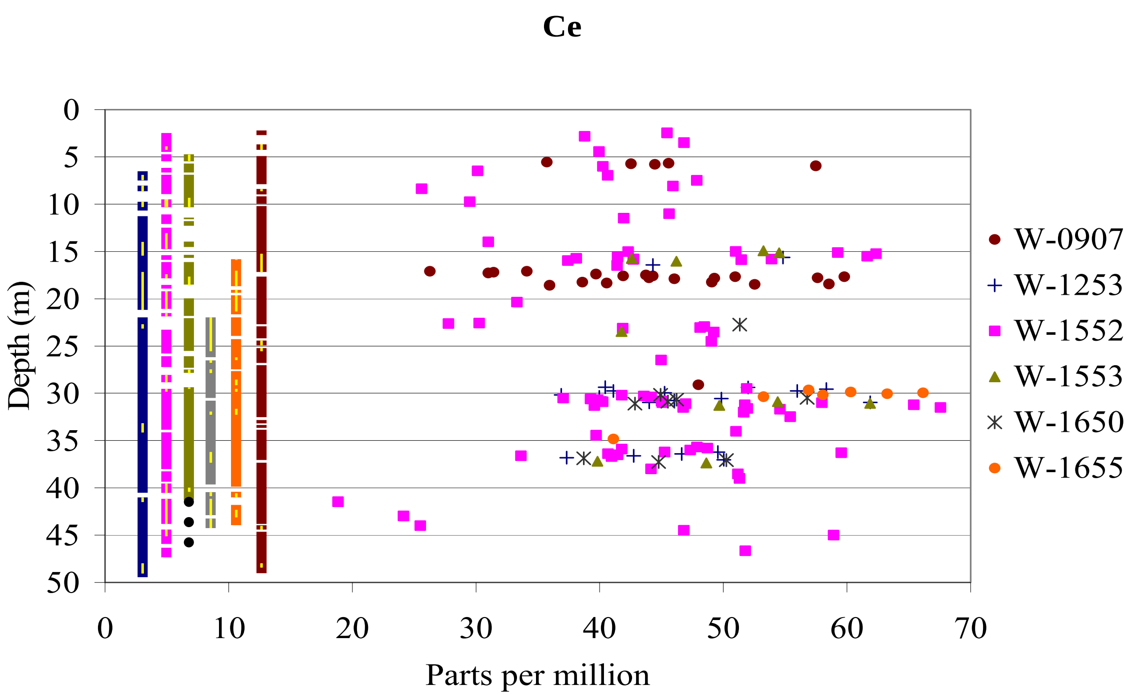

Figure 288. Ce parts per million with depth.

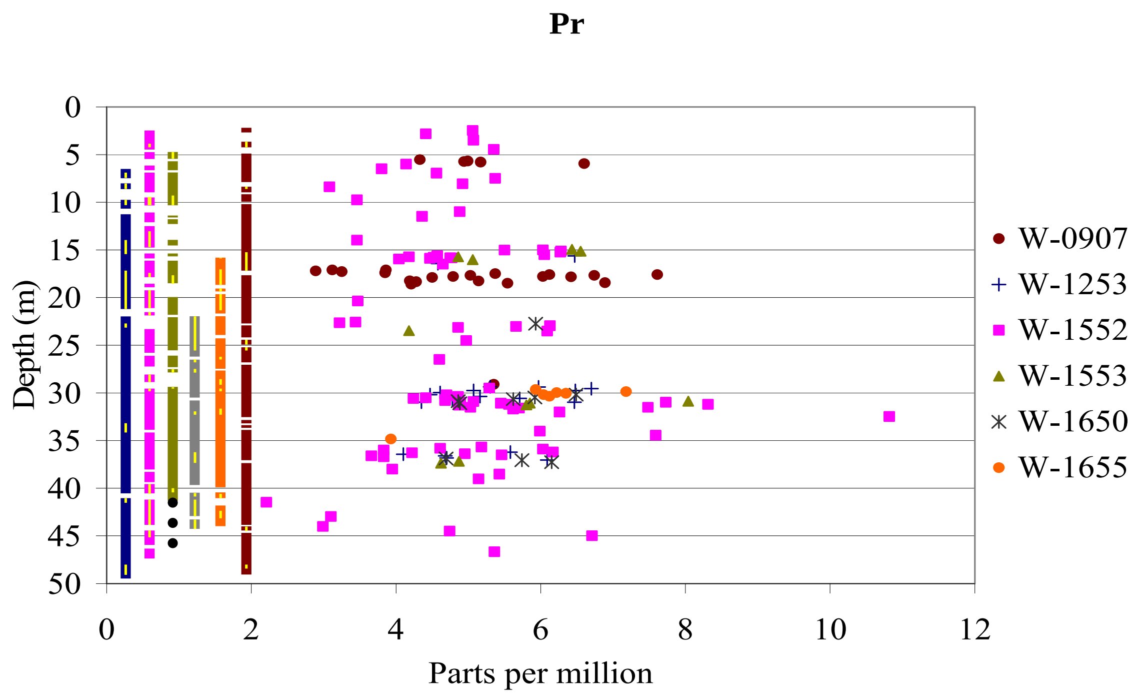

Figure 289. Pr parts per million with depth.

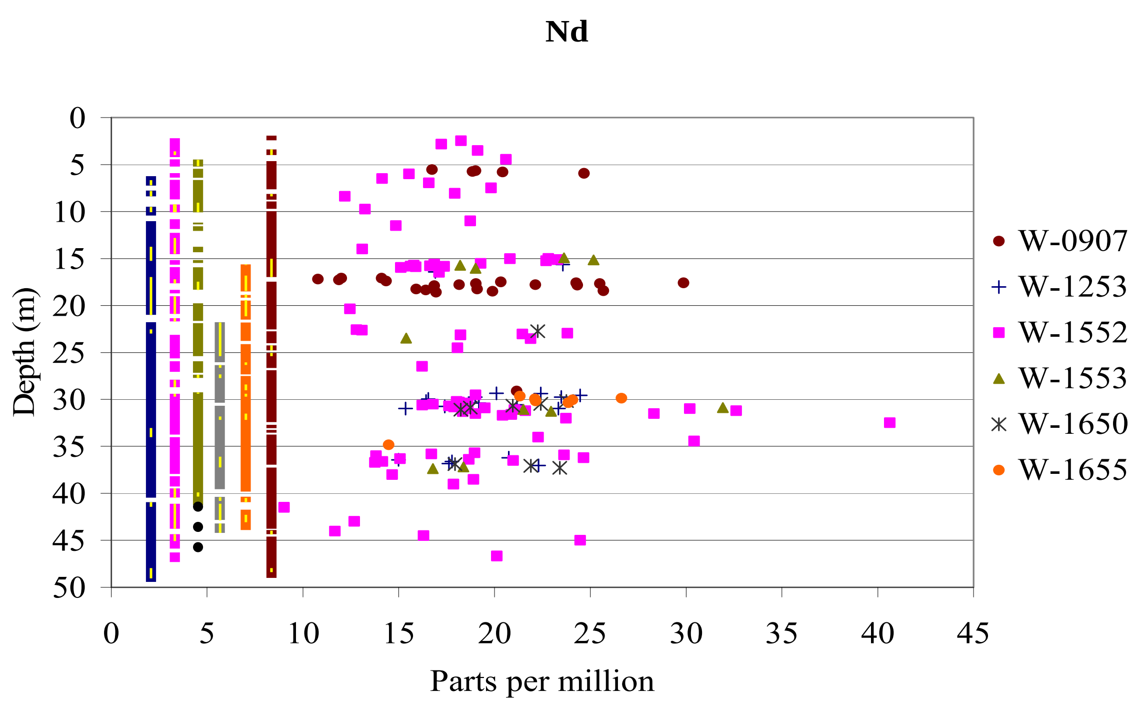

Figure 290. Nd parts per million with depth.

Sm

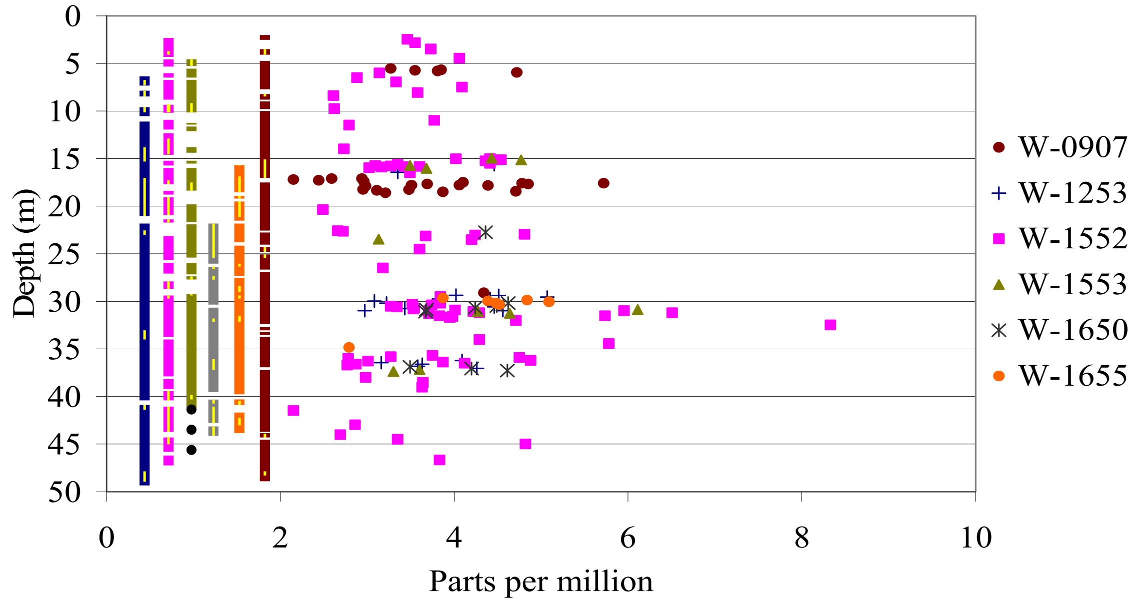

Figure 291. Sm parts per million with depth.

Eu

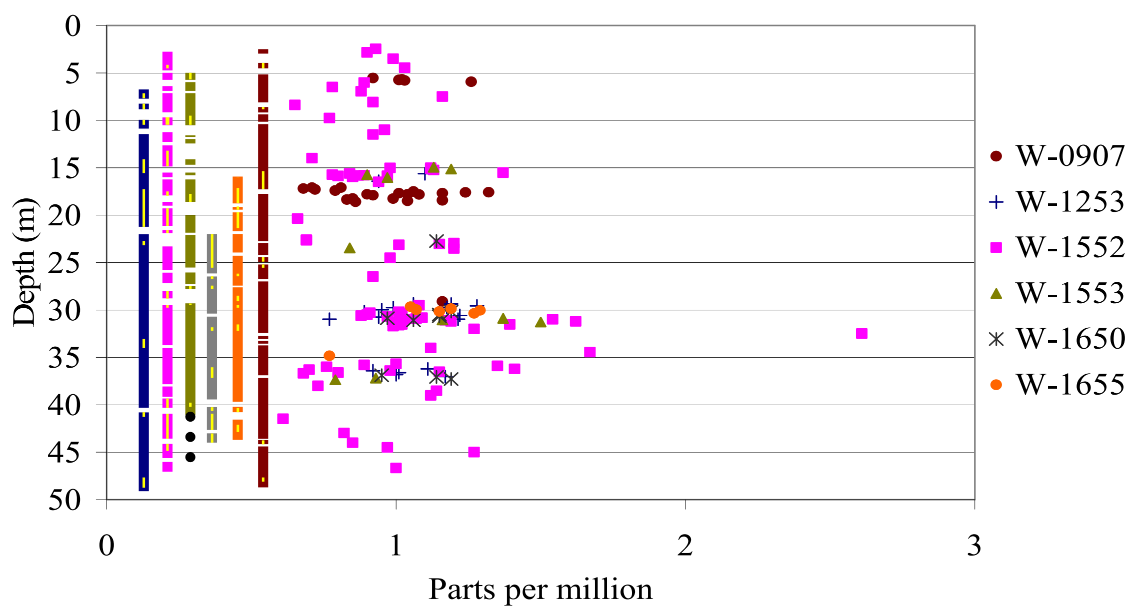

Figure 292. Eu parts per million with depth.

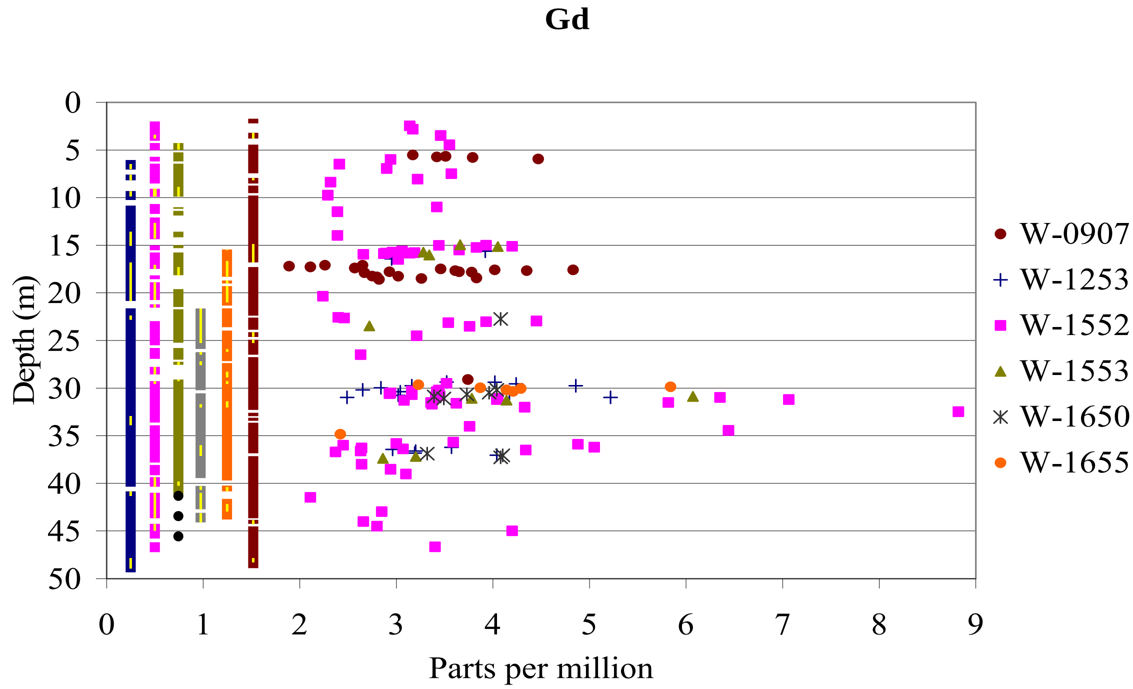

Figure 293. Gd parts per million with depth.

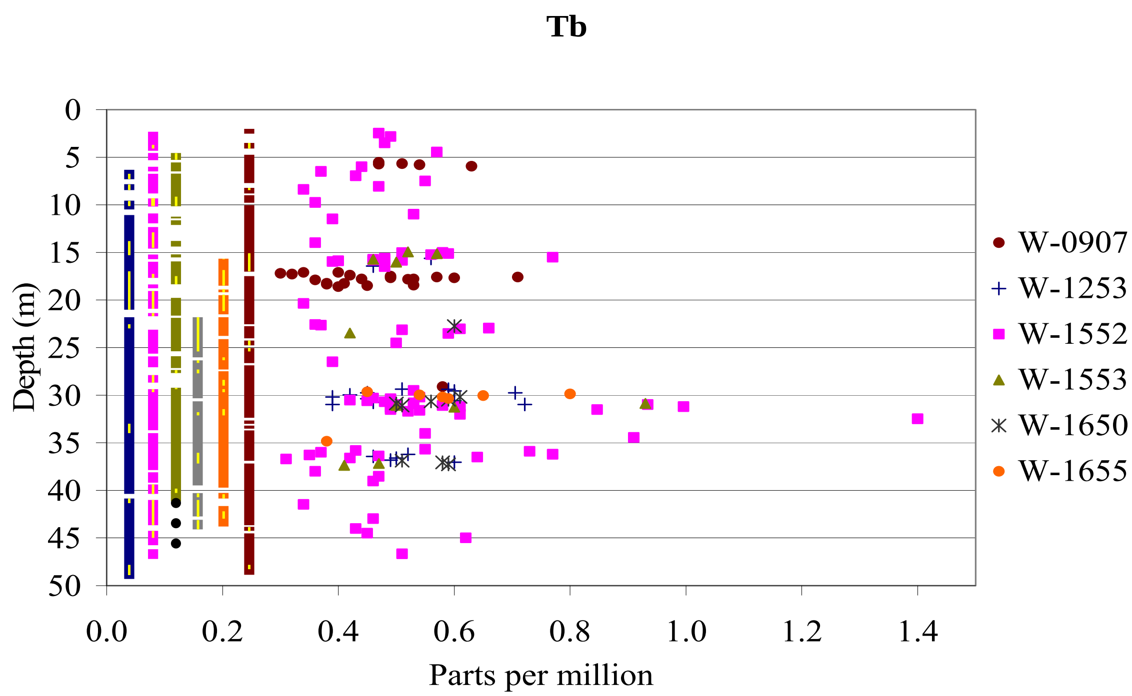

Figure 294. Tb parts per million with depth.

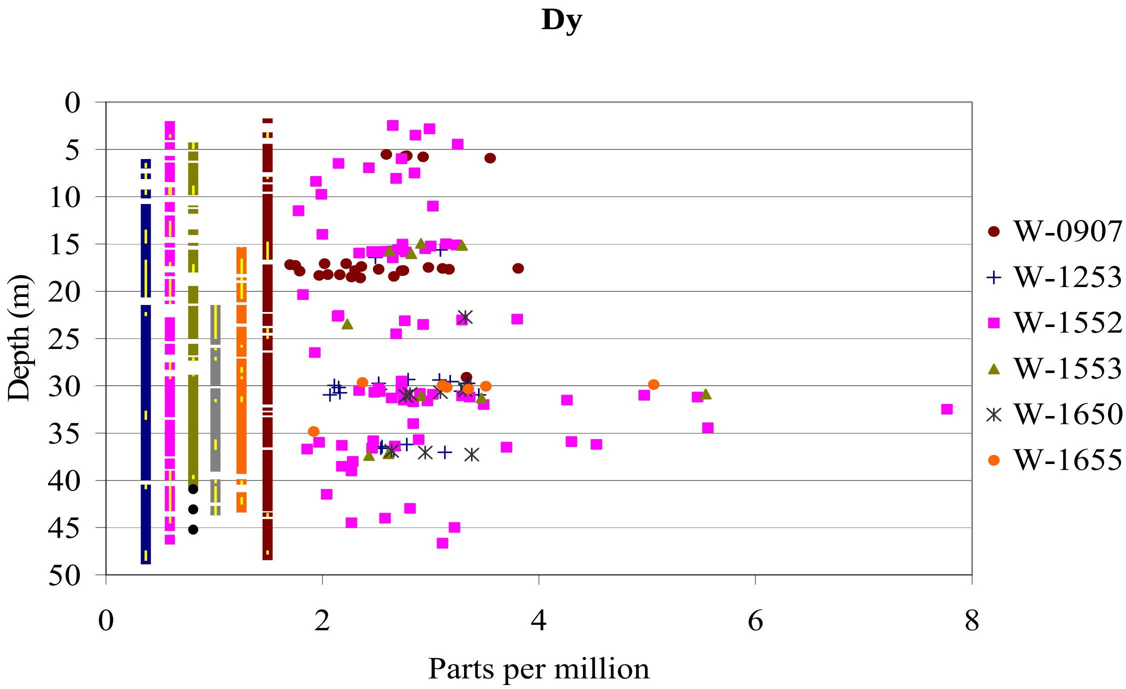

Figure 295. Dy parts per million with depth.

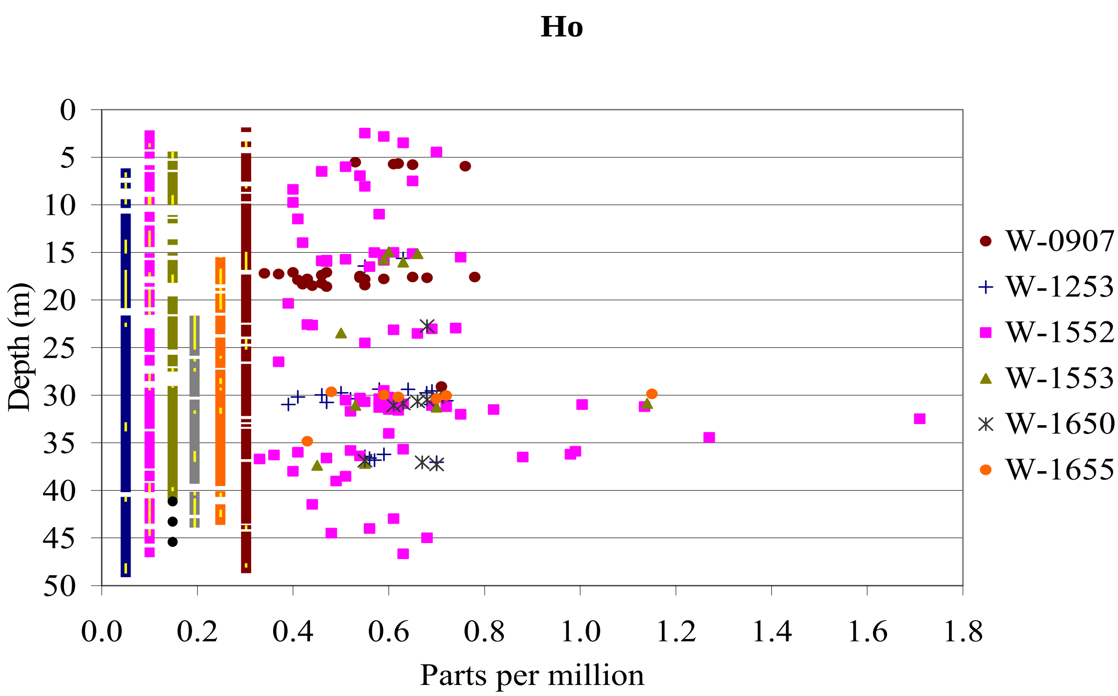

Figure 296. Ho parts per million with depth.

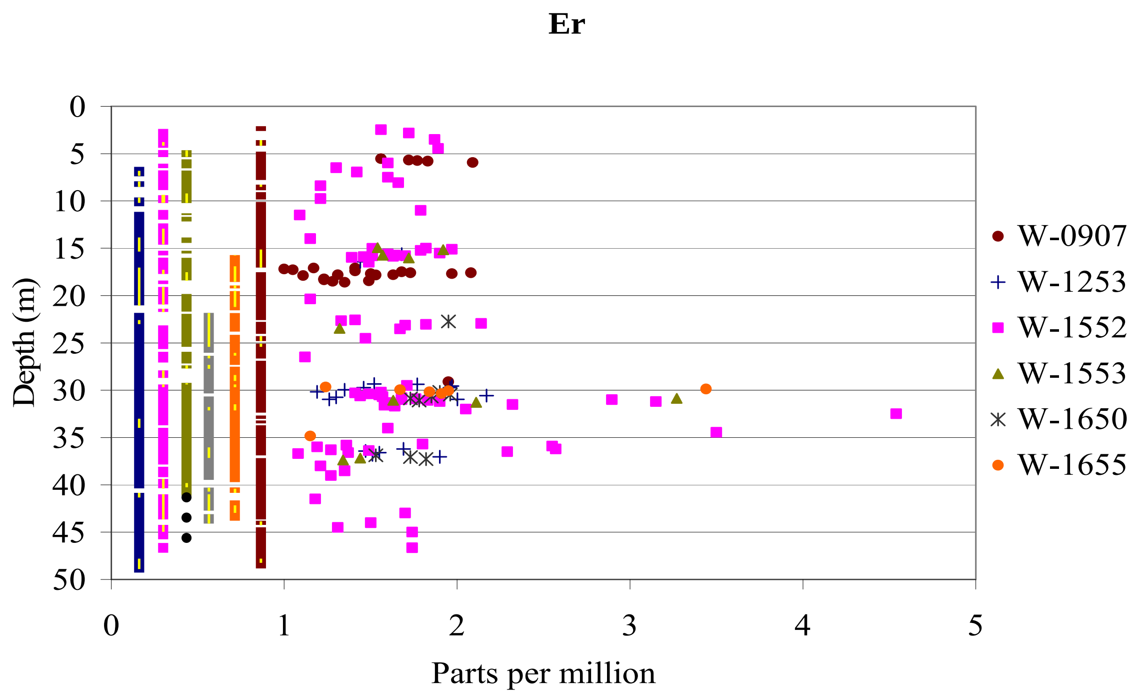

Figure 297. Er parts per million with depth.

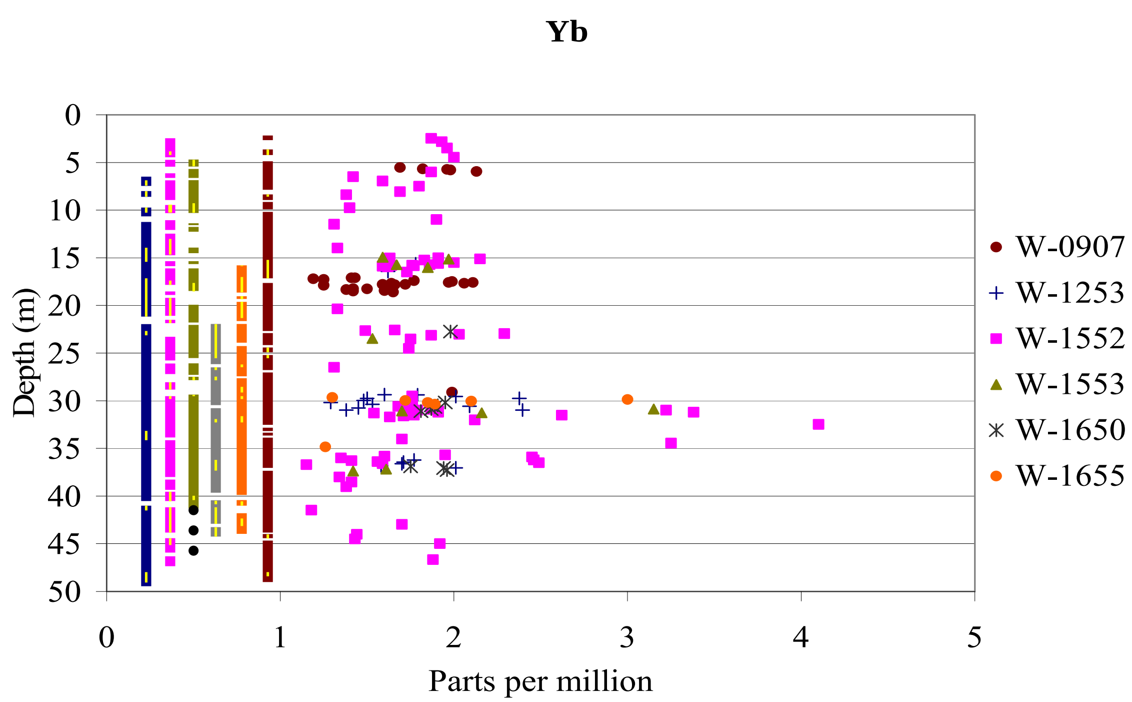

Figure 298. Yb parts per million with depth.

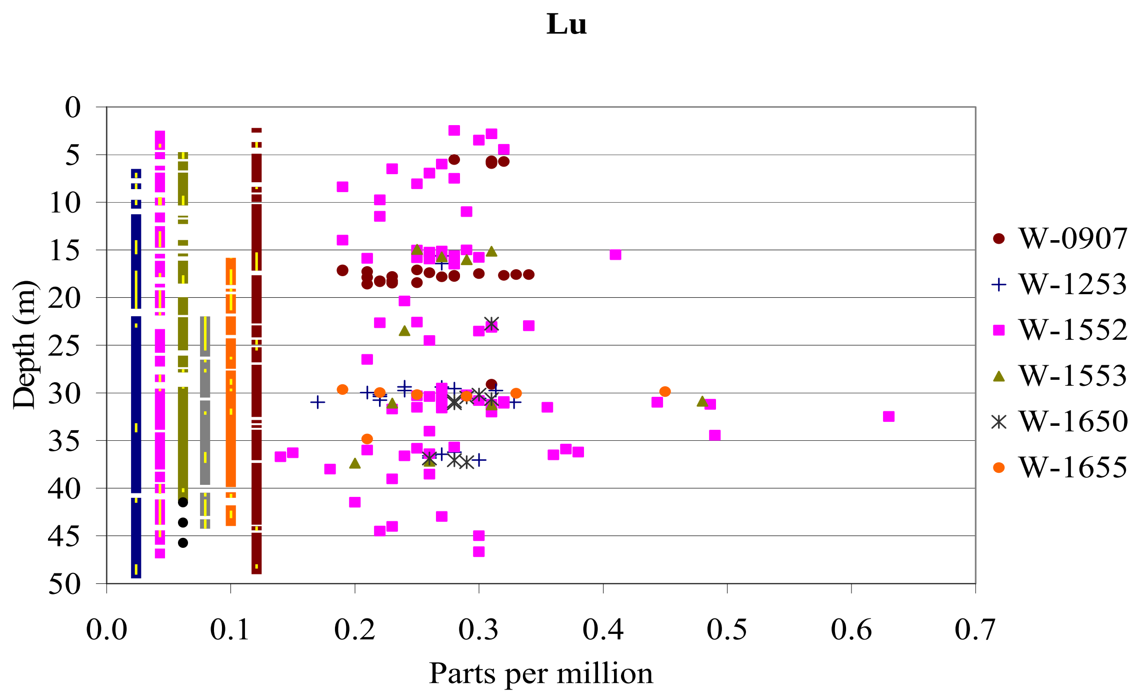

Figure 299. Lu parts per million with depth.

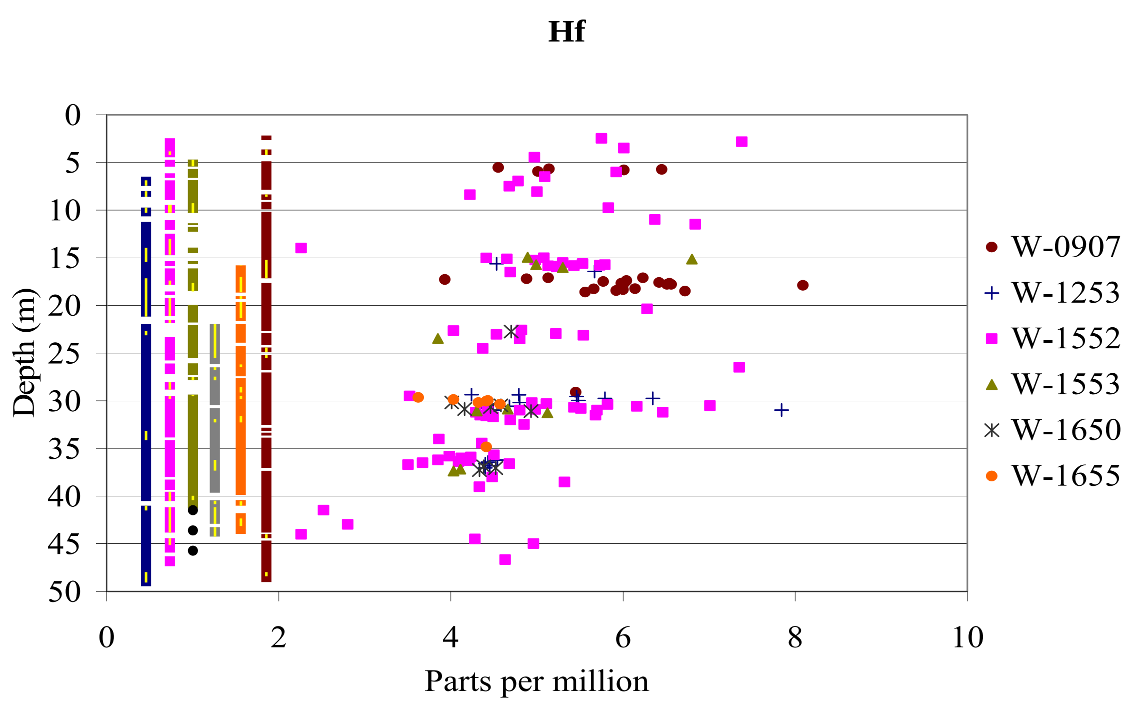

Figure 300. Hf parts per million with depth.

Ta

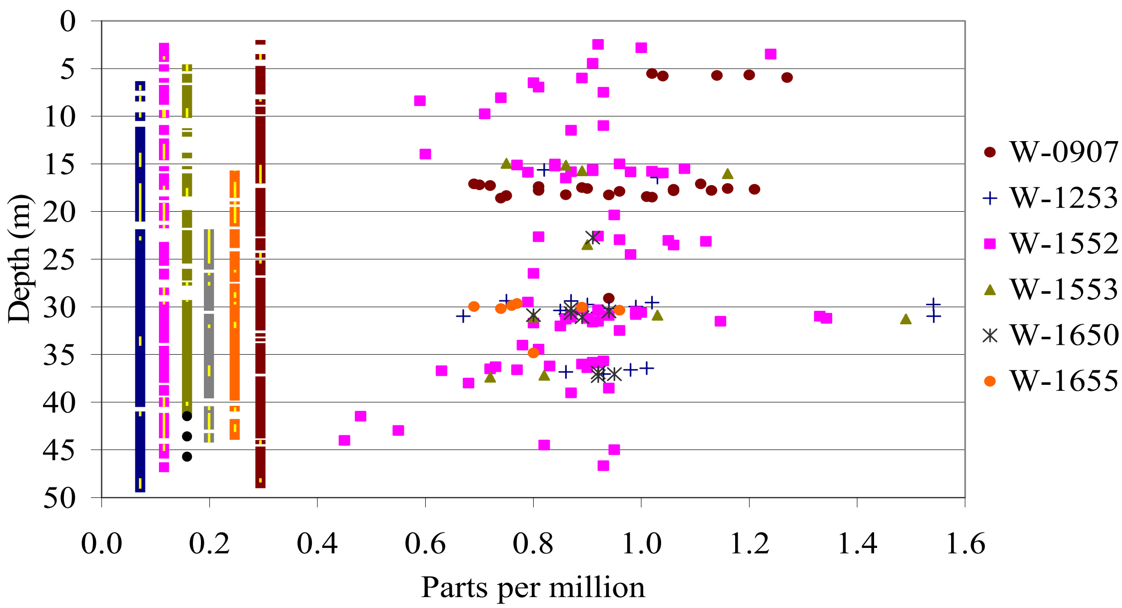

Figure 301. Ta parts per million with depth.

Pb

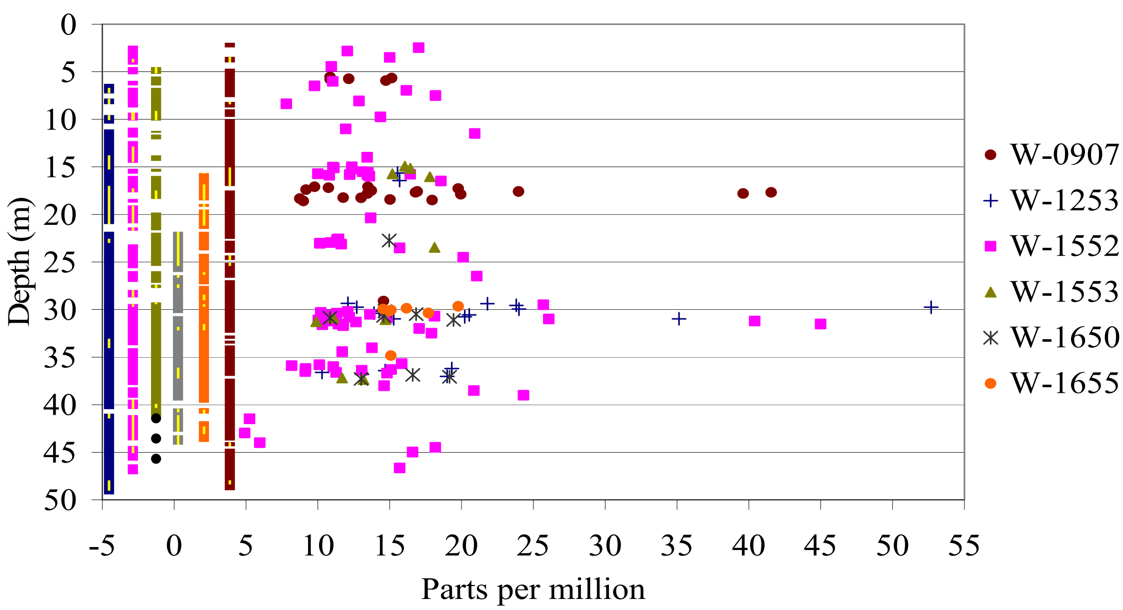

Figure 302. Pb parts per million with depth.

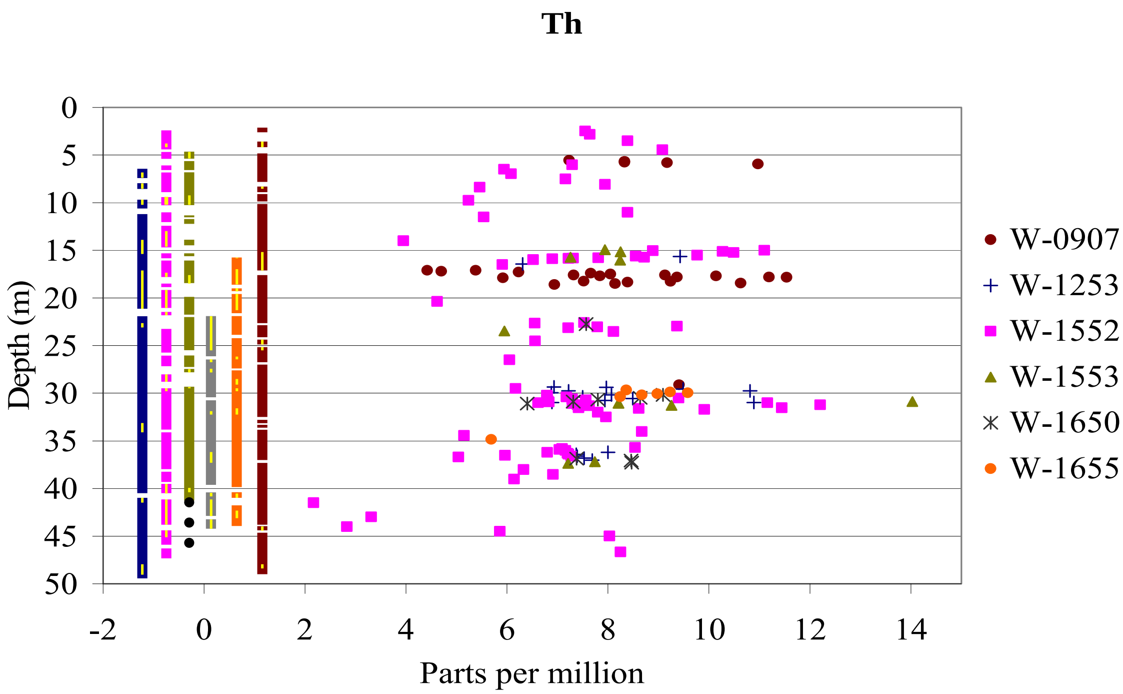

Figure 303. Th parts per million with depth.

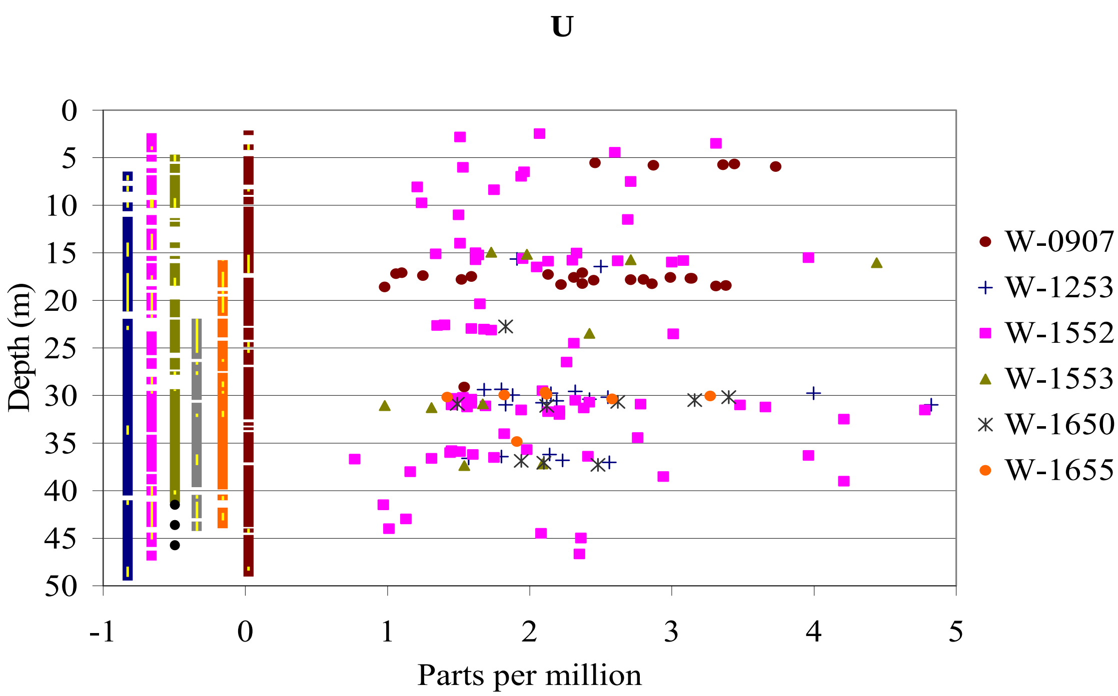

Figure 304. U parts per million with depth.

Table 4. Geochemical data of major elements from XRF analyses

Sample	Depth (m)	SiO_2	TiO_2	Al_2O_3	Fe_2O_3	MnO	MgO	CaO	Na_2O	K_2O	P_2O_5	Totals
1253-051.3	15.64	66.52	0.78	15.45	5.43	0.09	1.50	1.30	2.76	2.12	0.11	96.06
1253-053.9	16.43	71.98	0.77	13.15	4.24	0.08	1.18	1.13	2.70	1.89	0.09	97.21
1253-096.3	29.35	73.23	0.59	13.86	3.82	0.07	1.08	1.24	2.63	2.12	0.07	98.71
1253-096.4	29.38	71.80	0.62	14.28	4.10	0.08	1.16	1.21	2.69	2.09	0.08	98.11
1253-097.0	29.57	69.63	0.69	15.21	4.44	0.07	1.30	1.43	2.85	2.08	0.08	97.78
1253-097.6	29.75	72.87	0.62	14.15	3.53	0.07	0.91	1.39	2.74	2.28	0.06	98.62
1253-097.6 Fines	29.75	66.78	0.90	16.29	5.82	0.09	1.55	1.30	2.93	1.88	0.10	97.64
1253-098.3	29.96	71.82	0.59	13.57	3.30	0.06	0.84	1.38	2.65	2.29	0.06	96.56
1253-099.0	30.18	70.71	0.63	14.85	4.20	0.05	1.14	1.15	2.66	2.14	0.06	97.59
1253-099.7	30.39	69.52	0.69	14.80	4.48	0.07	1.21	1.26	2.80	2.09	0.09	97.01
1253-100.3	30.57	71.20	0.67	14.77	4.41	0.07	1.18	1.29	2.70	2.17	0.11	98.57
1253-100.9	30.75	70.32	0.62	13.98	4.22	0.06	1.09	1.22	2.59	2.26	0.09	96.45
1253-101.6	30.97	74.66	0.58	12.80	3.65	0.06	1.03	1.03	2.55	2.12	0.09	98.57
1253-101.6 Fines	30.97	67.59	0.89	16.32	4.98	0.09	1.29	1.51	3.02	1.87	0.07	97.63
1253-118.8	36.21	70.92	0.65	14.51	4.40	0.08	1.41	1.33	2.86	2.03	0.05	98.24
1253-119.5	36.42	71.68	0.68	14.30	4.59	0.07	1.34	1.04	2.76	1.84	0.05	98.35
1253-120.1	36.61	71.91	0.68	14.08	4.35	0.06	1.34	1.11	2.80	1.85	0.05	98.23
1253-120.8	36.82	72.03	0.67	13.99	4.34	0.07	1.34	1.09	2.77	1.86	0.05	98.21
1253-121.5	37.03	72.53	0.67	13.82	4.32	0.07	1.39	1.08	2.75	1.84	0.05	98.52
1552-008.1	2.47	70.45	0.74	14.03	4.45	0.08	1.47	1.50	2.88	1.95	0.10	97.65
1552-009.3	2.83	72.84	0.76	12.82	3.99	0.08	1.29	1.46	2.95	1.90	0.10	98.19
1552-011.5	3.51	72.42	0.66	13.70	4.14	0.08	1.32	1.59	2.86	2.22	0.11	99.10
1552-014.6	4.45	65.79	0.82	15.88	5.77	0.09	2.24	1.59	2.87	2.05	0.14	97.24

Table 4 (continued). Geochemical data of major elements from XRF analyses

Sample	Depth (m)	SiO_2	TiO_2	Al_2O_3	Fe_2O_3	MnO	MgO	CaO	Na_2O	K_2O	P_2O_5	Totals
1552-019.7	6.00	75.10	0.62	12.07	3.38	0.08	1.02	1.36	2.57	2.09	0.10	98.39
1552-021.3	6.49	75.22	0.60	12.02	3.49	0.07	1.03	1.24	2.56	2.04	0.11	98.38
1552-022.8	6.95	73.89	0.61	12.23	3.89	0.07	1.24	1.13	2.69	1.80	0.11	97.66
1552-024.6	7.50	70.72	0.66	13.60	4.31	0.08	1.46	1.44	2.73	1.96	0.11	97.07
1552-026.5	8.08	71.62	0.61	13.93	4.56	0.07	1.39	1.52	2.66	2.24	0.10	98.70
1552-027.5	8.38	79.28	0.39	10.09	2.67	0.04	0.84	1.49	2.08	2.21	0.10	99.19
1552-032.0	9.75	74.66	0.57	11.81	2.67	0.05	0.83	2.08	2.74	2.30	0.10	97.81
1552-036.1	11.00	70.84	0.76	14.52	4.27	0.09	1.42	1.69	3.17	1.60	0.10	98.46
1552-037.7	11.49	74.04	0.57	12.46	2.64	0.06	0.80	1.85	2.88	2.01	0.07	97.38
1552-045.9	13.99	77.76	0.40	9.37	3.36	0.07	1.15	1.16	1.83	1.86	0.17	97.13
1552-049.2	15.00	67.85	0.80	15.29	5.37	0.09	1.51	1.41	2.92	2.08	0.11	97.43
1552-049.3	15.03	68.18	0.79	15.28	5.25	0.09	1.52	1.44	2.92	2.06	0.11	97.64
1552-049.6	15.12	67.73	0.80	15.12	5.30	0.09	1.51	1.50	2.88	2.08	0.11	97.12
1552-050.0	15.24	67.93	0.80	15.26	5.33	0.09	1.54	1.42	2.93	2.07	0.11	97.48
1552-050.9	15.51	67.10	0.82	15.26	6.00	0.08	1.95	1.20	2.89	1.89	0.11	97.30
1552-051.2	15.61	67.25	0.81	14.93	5.61	0.09	1.91	1.47	2.57	1.85	0.12	96.61
1552-051.6	15.73	69.19	0.77	14.40	5.44	0.08	1.77	1.30	2.73	1.89	0.11	97.68
1552-051.8	15.79	71.42	0.76	14.14	4.84	0.08	1.60	1.38	2.66	1.92	0.11	98.91
1552-051.9	15.82	71.19	0.75	13.88	4.62	0.08	1.49	1.25	2.85	1.94	0.10	98.15
1552-052.0	15.85	69.04	0.83	14.10	5.10	0.08	1.74	1.19	2.91	1.74	0.11	96.84
1552-052.1	15.88	73.14	0.71	13.14	4.30	0.09	1.41	1.13	2.93	1.86	0.11	98.82
1552-052.4	15.97	72.54	0.72	13.17	4.32	0.08	1.32	1.26	2.76	1.92	0.10	98.19
1552-054.1	16.49	73.69	0.63	12.61	4.16	0.07	1.23	1.21	2.51	1.83	0.10	98.04

Table 4 (continued). Geochemical data of major elements from XRF analyses

Sample	Depth (m)	SiO_2	TiO_2	Al_2O_3	Fe_2O_3	MnO	MgO	CaO	Na_2O	K_2O	P_2O_5	Totals
1552-066.8	20.36	77.16	0.60	10.49	4.00	0.07	1.09	0.64	2.13	1.78	0.10	98.06
1552-074.1	22.59	71.09	0.66	14.11	4.71	0.04	1.27	0.66	2.65	2.06	0.05	97.30
1552-074.3 Psl	22.65	74.44	0.54	12.40	4.45	0.03	1.12	0.60	2.36	1.96	0.05	97.95
1552-075.3 Psl	22.95	68.58	0.74	15.13	5.29	0.06	1.53	0.95	2.82	2.05	0.06	97.21
1552-075.6	23.04	69.57	0.68	14.44	4.89	0.08	1.44	0.93	2.67	2.10	0.06	96.86
1552-075.9	23.13	72.21	0.69	13.82	4.39	0.06	1.26	0.93	2.69	2.08	0.06	98.19
1552-077.2	23.53	68.46	0.76	14.67	5.03	0.08	1.57	1.05	2.84	1.92	0.09	96.47
1552-080.4	24.51	72.34	0.70	13.32	4.15	0.08	1.25	1.03	2.69	2.04	0.09	97.69
1552-086.9	26.49	75.28	0.58	12.10	2.99	0.06	0.65	1.16	2.21	2.22	0.05	97.30
1552-096.8	29.50	72.74	0.53	13.17	3.42	0.08	0.85	1.30	2.30	2.41	0.11	96.91
1552-099.1	30.21	72.44	0.66	13.89	4.02	0.07	1.16	1.44	2.87	2.06	0.10	98.71
1552-099.4	30.30	70.79	0.67	14.10	4.24	0.08	1.21	1.34	2.84	2.08	0.09	97.44
1552-099.7	30.39	70.70	0.68	14.42	4.51	0.08	1.31	1.27	2.80	2.08	0.09	97.94
1552-100.1	30.51	71.78	0.70	14.43	4.52	0.05	1.28	1.19	2.82	2.09	0.09	98.95
1552-100.4	30.60	69.61	0.71	14.22	4.48	0.07	1.21	1.21	2.73	2.13	0.09	96.46
1552-100.7	30.69	71.77	0.67	14.06	4.26	0.04	1.13	1.17	2.70	2.13	0.09	98.02
1552-101.1	30.82	73.15	0.68	13.57	3.79	0.11	0.96	1.27	2.74	2.14	0.09	98.50
1552-101.4	30.91	72.33	0.66	13.84	4.17	0.12	1.11	1.26	2.67	2.10	0.11	98.37
1552-101.7	31.00	71.73	0.68	14.06	4.21	0.11	1.14	1.23	2.65	2.07	0.11	97.99
1552-101.7 Fines	31.00	65.33	0.88	16.59	5.99	0.12	1.62	1.44	2.66	1.94	0.15	96.72
1552-102.0	31.09	68.99	0.70	14.66	4.75	0.10	1.29	1.30	2.61	2.13	0.17	96.70
1552-102.4	31.21	69.62	0.72	14.55	4.71	0.20	1.27	1.29	2.62	2.10	0.16	97.24
1552-102.4 Fines	31.21	63.70	0.87	16.78	6.06	0.28	1.68	1.46	2.59	1.94	0.17	95.53

Table 4 (continued). Geochemical data of major elements from XRF analyses

Sample	Depth (m)	SiO_2	TiO_2	Al_2O_3	Fe_2O_3	MnO	MgO	CaO	Na_2O	K_2O	P_2O_5	Totals
1552-102.7	31.30	72.43	0.64	13.77	4.33	0.06	1.10	1.24	2.40	2.19	0.13	98.29
1552-103.4	31.52	68.53	0.66	13.72	4.15	0.07	1.11	1.51	2.31	2.24	0.27	94.57
1552-103.4 Fines	31.52	65.69	0.83	15.80	6.01	0.04	1.46	2.35	2.36	2.02	0.65	97.21
1552-103.7	31.61	68.69	0.73	14.81	4.83	0.05	1.26	1.87	2.40	2.17	0.55	97.36
1552-104.0	31.70	67.91	0.74	14.83	4.85	0.06	1.33	1.60	2.28	2.20	0.42	96.22
1552-105.0	32.00	67.94	0.75	15.30	5.18	0.08	1.67	1.60	2.83	1.99	0.16	97.50
1552-106.6	32.49	67.42	0.71	14.32	4.74	0.09	1.55	1.89	2.50	2.10	0.41	95.73
1552-111.6	34.02	67.04	0.68	15.62	5.46	0.05	1.72	1.22	2.43	2.20	0.09	96.51
1552-113.0	34.44	73.03	0.51	12.28	2.97	0.07	0.81	2.09	2.29	2.18	0.55	96.78
1552-117.1	35.69	71.02	0.71	14.70	4.88	0.07	1.44	0.98	2.69	1.90	0.05	98.44
1552-117.5	35.81	71.31	0.72	14.47	4.71	0.08	1.38	1.04	2.76	1.86	0.05	98.38
1552-117.8	35.91	70.12	0.69	13.98	4.44	0.07	1.31	1.38	2.63	1.84	0.22	96.68
1552-118.1	36.00	70.32	0.70	13.99	4.44	0.10	1.27	1.05	2.72	1.84	0.05	96.48
1552-118.8	36.21	71.08	0.69	14.08	4.30	0.06	1.29	1.39	2.63	1.91	0.18	97.61
1552-119.1	36.30	72.26	0.68	14.05	4.51	0.10	1.32	0.96	2.72	1.86	0.05	98.51
1552-119.4	36.39	71.03	0.67	13.64	4.46	0.07	1.32	1.01	2.66	1.91	0.06	96.83
1552-119.8	36.52	72.45	0.63	13.07	4.09	0.04	1.30	1.62	2.42	1.91	0.37	97.90
1552-120.1	36.61	74.46	0.59	12.69	3.90	0.05	1.23	1.04	2.53	1.98	0.06	98.53
1552-120.4	36.70	76.68	0.51	11.52	3.36	0.06	1.02	0.92	2.30	2.10	0.05	98.52
1552-124.7	38.01	73.75	0.60	13.20	3.49	0.08	1.07	1.05	2.60	2.06	0.06	97.96
1552-126.4	38.53	72.35	0.67	13.33	3.97	0.07	1.18	1.23	2.52	2.03	0.07	97.42
1552-128.0	39.01	71.30	0.59	13.52	3.76	0.08	1.21	1.56	2.69	2.13	0.09	96.93
1552-136.1	41.48	79.87	0.55	7.86	4.65	0.09	2.34	1.21	1.91	0.79	0.11	99.38

Table 4 (continued). Geochemical data of major elements from XRF analyses

Sample	Depth (m)	SiO_2	TiO_2	Al_2O_3	Fe_2O_3	MnO	MgO	CaO	Na_2O	K_2O	P_2O_5	Totals
1552-141.0	42.98	71.74	0.80	10.29	6.88	0.12	3.69	2.06	2.17	0.96	0.13	98.84
1552-144.4	44.01	77.25	0.52	8.95	4.94	0.10	2.87	1.77	2.19	0.84	0.13	99.56
1552-146.0	44.50	73.66	0.61	12.14	4.10	0.10	1.88	1.28	2.47	1.92	0.09	98.25
1552-147.6	44.99	68.17	0.78	14.99	4.87	0.08	1.70	1.31	2.91	2.02	0.09	96.92
1552-153.1	46.66	67.03	0.77	14.94	5.26	0.10	1.95	1.25	2.67	2.05	0.07	96.09
1553-049.0	14.94	67.63	0.72	15.35	5.25	0.08	1.70	1.78	2.94	2.01	0.10	97.56
1553-049.7	15.15	67.03	0.80	14.64	4.77	0.09	1.40	2.76	2.68	1.93	0.11	96.21
1553-051.6	15.73	65.89	0.78	13.53	4.96	0.08	1.64	4.14	2.45	1.65	0.12	95.24
1553-052.6	16.03	68.88	0.83	14.48	5.05	0.08	1.74	1.29	2.98	1.79	0.10	97.22
1553-077.0	23.47	72.30	0.64	12.98	4.20	0.07	1.23	0.94	2.58	1.96	0.05	96.95
1553-101.3	30.88	62.61	0.84	16.58	7.28	0.09	1.76	1.29	2.46	2.14	0.34	95.39
1553-101.9	31.06	68.57	0.75	15.03	4.50	0.27	1.27	1.25	2.76	2.05	0.11	96.56
1553-102.6	31.27	68.52	0.69	13.81	4.19	0.13	1.23	1.16	2.67	1.93	0.11	94.44
1553-122.0	37.19	71.39	0.68	14.35	4.68	0.07	1.43	1.02	2.73	1.82	0.05	98.22
1553-122.6	37.37	72.45	0.66	13.83	4.49	0.08	1.33	0.98	2.65	1.82	0.05	98.34
1650-074.6	22.74	68.68	0.77	14.98	5.31	0.09	1.68	1.13	2.88	2.06	0.08	97.66
1650-099.0	30.18	68.30	0.67	13.89	5.39	0.20	1.27	1.87	2.22	2.22	0.52	96.55
1650-100.0	30.48	69.34	0.65	14.35	4.59	0.27	1.21	1.67	2.45	2.27	0.30	97.10
1650-100.6	30.66	69.36	0.68	14.09	4.43	0.19	1.22	1.51	2.68	2.17	0.14	96.47
1650-101.3	30.88	69.47	0.67	13.96	4.51	0.14	1.26	1.44	2.53	2.14	0.18	96.30
1650-102.0	31.09	72.12	0.66	13.35	3.55	0.09	0.97	1.40	2.72	2.23	0.10	97.19
1650-121.0	36.88	73.64	0.62	12.68	4.17	0.07	1.15	0.86	2.45	1.91	0.05	97.60
1650-121.6	37.06	69.71	0.71	14.24	4.74	0.10	1.56	1.12	2.77	1.91	0.06	96.92

Table 4 (continued). Geochemical data of major elements from XRF analyses

Sample	Depth (m)	SiO_2	TiO_2	Al_2O_3	Fe_2O_3	MnO	MgO	CaO	Na_2O	K_2O	P_2O_5	Totals
1650-122.3	37.28	69.14	0.72	14.67	4.93	0.09	1.72	1.18	2.78	1.94	0.07	97.24
1655-097.3	29.66	66.78	0.66	16.98	4.71	0.08	1.51	1.93	3.08	2.09	0.09	97.91
1655-098.0	29.87	68.73	0.68	13.94	4.98	0.16	1.24	1.75	2.19	2.12	0.56	96.35
1655-098.3	29.96	68.09	0.75	15.07	5.26	0.05	1.29	1.62	2.38	2.18	0.36	97.05
1655-098.6	30.05	67.50	0.73	14.54	4.96	0.69	1.22	1.60	2.42	2.20	0.32	96.18
1655-099.0	30.18	69.75	0.71	14.39	4.51	0.25	1.20	1.39	2.51	2.16	0.20	97.07
1655-099.6	30.36	66.85	0.70	14.47	4.85	0.24	1.32	1.38	2.43	2.04	0.21	94.49
1655-114.3	34.84	71.25	0.66	13.98	4.61	0.07	1.22	0.81	2.41	1.92	0.05	96.98
907-018.2	5.55	72.74	0.59	13.55	3.86	0.07	1.08	1.40	3.44	2.20	0.07	99.00
907-018.6 Psl	5.67	70.81	0.66	14.24	4.73	0.08	1.41	1.35	3.27	2.20	0.09	98.84
907-018.8	5.73	71.95	0.66	13.54	4.44	0.08	1.29	1.38	3.31	2.22	0.09	98.96
907-019.0	5.79	68.82	0.72	14.51	5.01	0.08	1.47	1.40	3.29	2.20	0.09	97.59
907-019.5 Psl	5.94	66.78	0.77	15.71	5.67	0.09	1.82	1.54	3.37	2.16	0.11	98.02
907-056.1a	17.10	80.59	0.47	9.72	2.85	0.06	0.76	0.97	2.19	2.08	0.07	99.76
907-056.1b	17.10	76.38	0.53	10.98	3.46	0.07	0.88	0.76	2.80	2.22	0.09	98.17
907-056.43	17.20	77.46	0.46	10.89	3.02	0.06	0.78	1.10	2.61	2.15	0.05	98.58
907-056.7	17.28	71.74	0.53	14.08	4.23	0.06	1.16	1.24	2.73	2.19	0.05	98.01
907-057.09	17.40	71.02	0.67	14.48	4.29	0.07	1.12	1.42	2.84	2.17	0.06	98.14
907-057.41	17.50	71.82	0.68	14.42	4.32	0.08	1.11	1.47	2.80	2.19	0.08	98.97
907-057.7 Fines	17.59	66.31	0.83	16.23	5.94	0.09	1.63	1.29	2.81	1.89	0.10	97.12
907-057.74	17.60	71.41	0.66	14.27	4.27	0.07	1.06	1.46	3.38	2.28	0.08	98.94
907-058.01	17.68	65.42	0.89	16.74	6.03	0.12	1.43	1.45	3.45	2.09	0.10	97.72
907-058.02	17.68	70.31	0.66	14.27	4.64	0.10	1.06	1.49	3.07	2.34	0.09	98.03

Table 4 (continued). Geochemical data of major elements from XRF analyses

Sample	Depth (m)	SiO_2	TiO_2	Al_2O_3	Fe_2O_3	MnO	MgO	CaO	Na_2O	K_2O	P_2O_5	Totals
907-058.4	17.80	70.72	0.68	14.52	4.99	0.07	1.28	1.41	2.49	2.24	0.08	98.48
907-058.4	17.80	62.13	0.91	17.78	6.92	0.11	1.76	1.39	3.44	1.98	0.10	96.52
907-058.5	17.83	63.08	0.89	17.90	7.20	0.10	1.86	1.44	2.95	1.89	0.10	97.41
907-058.71	17.89	76.83	0.64	11.69	2.63	0.08	0.39	2.14	2.67	2.60	0.05	99.72
907-059.86	18.25	72.94	0.59	13.90	3.75	0.06	0.90	1.93	2.84	2.46	0.09	99.46
907-059.9	18.26	69.07	0.68	15.11	4.98	0.08	1.32	2.02	2.76	2.27	0.10	98.39
907-060.19	18.35	70.51	0.65	14.67	4.70	0.08	1.15	2.11	2.92	2.37	0.11	99.27
907-060.5	18.44	66.40	0.72	16.05	5.59	0.07	1.58	2.12	2.91	2.22	0.10	97.76
907-060.68	18.50	68.19	0.68	14.64	4.46	0.08	1.08	2.51	2.87	2.32	0.10	96.93
907-061.0	18.59	73.19	0.54	13.53	3.64	0.06	1.06	2.13	2.74	2.41	0.09	99.39
907-095.5	29.11	71.75	0.72	14.27	4.45	0.08	1.23	1.32	2.85	2.08	0.11	98.86

Table 5. Geochemical data of minor and trace elements from LA-ICP-MS analyses

Sample	Depth (m)	Rb	Sr	Zr	V	Cr	Nb	Y	Ba	La	Ce	Pr
1253-051.3	15.64	75.80	300.90	179.10	118.28	111.98	11.67	17.95	786.26	26.42	54.83	6.47
1253-053.9	16.43	57.30	203.30	230.00	121.22	178.80	14.12	14.83	699.25	18.83	44.31	4.58
1253-096.3	29.35	60.20	266.82	179.20	87.21	133.20	10.33	16.47	781.13	23.17	40.45	5.30
1253-096.4	29.38	69.50	283.00	183.80	95.56	127.58	10.75	18.61	792.07	24.76	52.00	5.97
1253-097.0	29.57	70.50	334.80	212.60	126.60	161.07	17.48	18.42	868.81	26.96	58.33	6.70
1253-097.6	29.75	66.80	300.83	235.90	90.05	146.06	12.15	14.52	831.63	22.12	41.11	5.07
1253-097.6 Fines	29.75	64.60	261.20	257.50	189.76	223.04	15.20	18.13	787.60	26.54	55.98	6.48
1253-098.3	29.96	67.20	323.50	202.10	93.11	158.19	12.82	12.20	857.85	19.07	45.25	4.61
1253-099.0	30.18	64.10	272.31	189.80	115.88	163.50	13.17	11.43	793.94	19.59	36.89	4.47
1253-099.7	30.39	59.80	260.72	178.30	115.96	134.37	12.42	14.48	761.64	22.15	39.97	5.16
1253-100.3	30.57	74.90	297.80	176.80	121.54	142.36	11.75	19.77	805.20	22.83	49.83	5.71
1253-100.9	30.75	69.20	296.40	164.60	108.73	118.28	12.32	12.54	792.75	20.20	46.04	4.78
1253-101.6	30.97	66.10	221.10	180.90	82.81	111.13	7.96	11.56	733.15	18.13	44.01	4.35
1253-101.6 Fines	30.97	64.70	328.10	325.80	164.61	238.46	16.50	18.83	817.26	26.81	61.88	6.46
1253-118.8	36.21	68.40	287.00	177.80	119.46	150.07	11.80	16.29	724.10	23.22	49.55	5.58
1253-119.5	36.42	63.60	214.30	172.60	139.75	228.38	10.45	14.85	634.52	18.43	46.63	4.10
1253-120.1	36.61	67.60	224.60	172.60	114.57	192.73	9.96	14.82	617.23	20.19	42.75	4.68
1253-120.8	36.82	55.40	196.28	172.30	99.63	177.79	12.20	16.31	598.51	19.87	37.34	4.70
1253-121.5	37.03	67.30	225.70	180.40	111.11	211.81	12.19	19.63	661.29	24.26	50.03	6.09
1552-008.1	2.47	66.10	276.90	231.00	111.71	135.58	12.51	16.63	779.60	21.92	45.45	5.06
1552-009.3	2.83	54.80	243.07	278.80	101.24	179.83	13.35	16.29	707.63	19.63	38.79	4.41
1552-011.5	3.51	72.00	281.80	211.00	112.88	131.77	11.48	15.79	867.88	21.18	46.83	5.07
1552-014.6	4.45	67.00	205.52	196.00	128.63	177.84	13.27	20.24	663.12	23.14	39.95	5.35

Table 5 (continued). Geochemical data of minor and trace elements from LA-ICP-MS analyses

Sample	Depth (m)	Rb	Sr	Zr	V	Cr	Nb	Y	Ba	La	Ce	Pr
1552-019.7	6.00	61.20	231.72	207.80	87.96	172.07	11.67	13.64	745.42	18.50	40.27	4.14
1552-021.3	6.49	53.40	200.16	207.60	82.63	135.75	11.18	13.26	669.85	16.73	30.13	3.80
1552-022.8	6.95	59.30	212.00	197.80	111.24	157.29	11.23	15.21	723.28	18.11	40.65	4.56
1552-024.6	7.50	59.50	273.90	189.80	122.94	154.25	13.12	17.44	865.74	21.71	47.85	5.37
1552-026.5	8.08	71.50	288.30	195.60	92.52	106.79	9.86	15.47	865.63	20.66	45.93	4.92
1552-027.5	8.38	57.80	274.10	139.60	63.19	103.06	5.93	10.27	783.28	13.77	25.60	3.08
1552-032.0	9.75	58.00	353.78	223.60	73.09	113.08	9.10	11.09	786.62	15.21	29.49	3.46
1552-036.1	11.00	57.40	275.61	227.30	95.46	194.83	12.18	16.01	578.42	21.12	45.62	4.88
1552-037.7	11.49	52.70	387.40	296.40	82.79	226.44	12.83	11.17	919.51	17.97	41.95	4.36
1552-045.9	13.99	56.10	189.10	100.90	90.77	84.91	7.65	12.94	770.56	14.64	31.00	3.46
1552-049.2	15.00	67.80	268.56	180.20	111.84	124.15	13.18	16.77	731.48	25.63	51.00	6.03
1552-049.3	15.03	63.00	264.13	175.10	113.02	124.21	13.03	16.38	708.96	23.70	42.30	5.50
1552-049.6	15.12	74.70	279.45	186.20	99.73	107.16	10.11	19.39	775.53	26.20	59.26	6.28
1552-050.0	15.24	74.20	284.52	191.70	116.98	129.23	11.63	17.24	798.84	26.03	62.36	6.27
1552-050.9	15.51	74.80	208.07	215.40	162.19	182.55	15.36	16.77	704.40	22.44	61.64	6.05
1552-051.2	15.61	70.20	203.50	208.90	116.48	137.24	12.80	16.51	596.64	20.12	41.46	4.57
1552-051.6	15.73	66.00	170.94	201.90	117.49	149.50	11.89	14.95	578.60	18.92	38.11	4.18
1552-051.8	15.79	68.90	207.10	224.10	135.82	193.34	13.51	16.83	656.65	19.17	42.75	4.52
1552-051.9	15.82	67.10	220.59	230.20	145.51	215.17	14.52	14.32	747.15	18.48	53.89	4.75
1552-052.0	15.85	61.10	199.40	213.80	126.52	153.26	14.50	17.08	621.95	20.28	42.72	4.77
1552-052.1	15.88	61.50	189.02	220.30	133.28	178.74	12.02	14.55	717.41	18.79	51.45	4.47
1552-052.4	15.97	59.90	205.25	211.80	141.82	208.70	15.03	13.45	706.43	16.71	37.43	4.04
1552-054.1	16.49	56.40	223.10	192.00	106.18	127.62	11.68	15.29	704.07	18.34	41.40	4.65

Table 5 (continued). Geochemical data of minor and trace elements from LA-ICP-MS analyses

Sample	Depth (m)	Rb	Sr	Zr	V	Cr	Nb	Y	Ba	La	Ce	Pr
1552-066.8	20.36	52.80	139.80	272.80	99.89	291.82	9.79	10.95	896.17	14.41	33.31	3.47
1552-074.1	22.59	67.30	133.86	169.40	112.08	127.55	11.47	11.80	578.92	15.11	30.26	3.44
1552-074.3 Psl	22.65	62.80	126.59	140.10	106.35	115.77	9.74	11.51	563.64	14.44	27.77	3.22
1552-075.3 Psl	22.95	71.00	169.77	185.40	130.01	134.41	12.23	21.01	612.87	25.06	48.46	6.13
1552-075.6	23.04	71.50	203.00	181.60	136.80	140.37	9.84	18.93	680.29	23.09	48.14	5.66
1552-075.9	23.13	68.70	208.20	219.20	130.15	158.56	10.37	16.38	674.76	20.32	41.86	4.86
1552-077.2	23.53	65.30	196.20	186.90	128.64	137.92	14.46	18.29	645.76	23.76	49.23	6.09
1552-080.4	24.51	65.10	191.70	182.80	134.46	149.89	13.35	16.11	764.21	20.33	49.04	4.97
1552-086.9	26.49	63.10	273.30	324.50	84.89	192.86	10.39	11.03	867.71	18.63	44.97	4.60
1552-096.8	29.50	73.30	294.60	146.00	97.55	111.35	10.23	17.87	982.62	21.32	51.90	5.29
1552-099.1	30.21	64.40	297.50	194.00	119.76	166.56	9.06	16.31	705.82	19.44	41.78	4.70
1552-099.4	30.30	66.10	281.70	204.60	115.04	185.15	8.71	14.94	676.11	19.92	43.56	4.70
1552-099.7	30.39	66.70	266.10	236.80	131.17	193.42	9.26	16.18	687.90	20.68	44.17	4.86
1552-100.1	30.51	71.20	253.30	259.50	100.48	174.58	11.24	13.71	657.99	19.39	37.05	4.41
1552-100.4	30.60	69.80	255.70	246.30	115.05	185.60	9.32	14.65	661.42	18.89	39.27	4.24
1552-100.7	30.69	73.10	249.10	220.30	122.31	190.99	12.69	15.14	729.54	19.99	39.85	4.68
1552-101.1	30.82	66.40	264.60	227.10	115.55	181.87	10.60	16.91	741.78	19.68	45.00	4.68
1552-101.4	30.91	71.90	230.02	206.10	134.07	198.56	13.14	17.79	775.83	20.27	40.25	5.07
1552-101.7	31.00	67.20	244.20	207.70	124.68	189.45	9.51	17.92	710.90	20.70	45.06	4.89
1552-101.7 Fines	31.00	70.90	233.50	217.30	161.14	191.21	13.73	31.03	745.50	30.73	57.98	7.73
1552-102.0	31.09	70.90	232.70	190.80	135.40	166.26	9.18	21.71	682.12	23.12	46.96	5.45
1552-102.4	31.21	75.90	233.50	178.00	146.13	167.37	9.18	20.53	753.71	22.93	51.74	5.56
1552-102.4 Fines	31.21	76.30	231.60	236.10	163.83	183.57	13.57	32.75	854.05	33.14	65.40	8.31

Table 5 (continued). Geochemical data of minor and trace elements from LA-ICP-MS analyses

Sample	Depth (m)	Rb	Sr	Zr	V	Cr	Nb	Y	Ba	La	Ce	Pr
1552-102.7	31.30	75.30	226.29	178.50	106.52	155.73	12.47	16.26	732.08	21.19	39.57	4.87
1552-103.4	31.52	74.70	257.50	172.60	117.25	170.80	9.20	16.90	725.83	21.19	46.76	5.03
1552-103.4 Fines	31.52	76.80	273.10	218.40	135.95	192.29	14.12	23.87	711.02	30.45	67.56	7.48
1552-103.7	31.61	80.40	259.50	193.30	125.34	172.11	10.55	18.04	681.04	24.77	51.95	5.70
1552-104.0	31.70	82.80	232.40	185.40	100.00	149.35	11.50	16.71	730.95	24.51	54.58	5.62
1552-105.0	32.00	63.70	270.50	184.90	129.78	137.39	12.08	24.07	735.83	26.49	51.66	6.26
1552-106.6	32.49	70.40	259.80	191.20	133.78	164.46	13.32	50.39	763.47	37.81	55.42	10.82
1552-111.6	34.02	81.10	258.50	155.80	118.02	122.16	10.35	17.18	757.34	24.82	51.03	5.99
1552-113.0	34.44	63.80	297.20	179.40	64.11	96.96	7.34	49.68	759.63	38.79	39.72	7.59
1552-117.1	35.69	68.30	188.30	172.30	117.83	193.66	11.70	17.75	583.70	22.33	47.88	5.18
1552-117.5	35.81	67.00	197.50	176.10	134.12	208.93	9.91	14.89	579.51	20.32	48.71	4.61
1552-117.8	35.91	67.00	222.70	173.20	108.67	179.69	8.25	35.94	1700.37	27.31	41.79	6.03
1552-118.1	36.00	63.90	203.50	175.70	127.32	208.76	9.88	12.58	594.21	17.50	47.33	3.83
1552-118.8	36.21	66.20	219.20	175.00	115.59	195.49	8.89	32.63	584.45	26.05	45.26	6.17
1552-119.1	36.30	68.00	200.09	180.00	133.89	225.30	11.99	12.04	684.14	18.27	59.54	4.22
1552-119.4	36.39	64.80	190.91	169.20	116.10	215.72	12.97	14.64	649.26	19.95	40.67	4.95
1552-119.8	36.52	64.40	212.80	160.10	109.72	211.71	8.90	32.34	589.84	27.68	41.46	5.46
1552-120.1	36.61	61.00	193.69	165.60	86.68	175.87	9.47	12.66	634.28	16.34	33.63	3.66
1552-120.4	36.70	62.90	213.58	151.60	92.49	186.69	8.06	10.93	783.64	15.79	40.96	3.83
1552-124.7	38.01	62.50	221.37	193.40	89.47	183.41	8.59	12.99	685.12	17.18	44.15	3.95
1552-126.4	38.53	62.50	267.80	224.60	119.19	314.48	12.96	13.43	809.35	21.44	51.18	5.43
1552-128.0	39.01	60.90	348.50	178.80	127.74	201.07	12.96	13.12	958.22	20.49	51.31	5.14
1552-136.1	41.48	27.00	61.70	106.80	101.85	1127.91	7.34	13.00	224.70	8.81	18.83	2.21

Table 5 (continued). Geochemical data of minor and trace elements from LA-ICP-MS analyses

Sample	Depth (m)	Rb	Sr	Zr	V	Cr	Nb	Y	Ba	La	Ce	Pr
1552-141.0	42.98	31.40	87.60	111.10	142.24	501.47	8.27	17.60	384.67	12.15	24.14	3.10
1552-144.4	44.01	24.20	78.90	91.00	128.68	385.33	6.49	16.34	326.42	11.34	25.50	2.99
1552-146.0	44.50	59.70	223.30	183.50	130.03	379.96	12.21	13.99	770.52	18.93	46.81	4.74
1552-147.6	44.99	72.20	277.70	202.10	131.16	192.09	13.44	19.27	765.31	26.85	58.92	6.71
1552-153.1	46.66	76.90	214.00	183.80	135.88	206.94	12.65	18.53	673.94	23.27	51.79	5.36
1553-049.0	14.94	68.10	371.70	202.30	119.31	128.16	10.67	17.04	845.35	26.00	53.24	6.43
1553-049.7	15.15	66.80	377.80	280.30	116.11	156.91	11.45	21.13	879.95	27.91	54.51	6.55
1553-051.6	15.73	63.90	210.50	198.80	139.34	171.61	13.33	17.78	763.91	20.94	42.59	4.86
1553-052.6	16.03	68.90	205.50	212.70	145.90	168.29	14.90	18.17	660.55	21.28	46.21	5.06
1553-077.0	23.47	64.90	183.10	157.80	123.50	135.70	12.57	14.42	701.48	17.95	41.77	4.18
1553-101.3	30.88	91.10	217.90	157.70	118.68	101.15	13.27	36.23	634.59	36.45	54.41	8.04
1553-101.9	31.06	68.50	296.78	183.10	115.24	134.07	10.47	18.10	3272.88	24.28	61.87	5.85
1553-102.6	31.27	66.50	360.94	172.00	105.11	129.50	10.41	19.19	13294.65	25.18	49.67	5.80
1553-122.0	37.19	66.90	182.85	163.00	104.60	164.62	11.51	14.54	582.44	21.35	39.82	4.87
1553-122.6	37.37	64.40	189.39	168.40	103.21	177.82	10.34	13.52	638.92	19.36	48.62	4.62
1650-074.6	22.74	73.50	199.50	194.40	137.62	134.71	12.62	20.99	670.98	25.26	51.33	5.93
1650-099.0	30.18	81.90	263.31	163.00	122.28	154.03	13.66	22.27	891.77	29.02	44.93	6.49
1650-100.0	30.48	76.80	279.88	175.90	116.85	149.77	12.99	19.33	932.29	24.84	56.78	5.92
1650-100.6	30.66	72.40	276.24	172.00	126.65	141.57	12.39	19.23	837.09	22.99	46.22	5.62
1650-101.3	30.88	70.30	254.20	187.30	138.96	163.28	8.99	19.45	716.16	21.03	45.51	4.86
1650-102.0	31.09	65.40	277.20	196.80	113.19	167.84	12.08	16.98	787.53	19.85	42.85	4.88
1650-121.0	36.88	64.20	176.90	162.00	93.42	179.48	10.02	14.28	665.36	18.57	38.71	4.69
1650-121.6	37.06	65.60	223.30	170.40	110.82	171.76	11.68	18.16	623.87	23.74	50.24	5.74

Table 5 (continued). Geochemical data of minor and trace elements from LA-ICP-MS analyses

Sample	Depth (m)	Rb	Sr	Zr	V	Cr	Nb	Y	Ba	La	Ce	Pr
1650-122.3	37.28	69.20	220.18	172.70	121.78	187.39	13.13	20.72	659.74	25.94	44.77	6.15
1655-097.3	29.66	71.00	458.90	149.50	110.99	98.20	11.45	12.50	939.45	24.85	56.91	5.93
1655-098.0	29.87	78.10	234.58	164.30	109.08	136.05	11.48	47.28	803.50	33.58	60.31	7.18
1655-098.3	29.96	77.50	255.86	181.50	107.70	138.91	10.82	17.32	776.39	25.03	66.16	6.22
1655-098.6	30.05	75.10	252.17	172.80	137.61	142.04	12.33	20.52	1232.11	25.61	63.25	6.35
1655-099.0	30.18	73.10	243.74	176.10	118.82	141.82	9.72	19.56	908.77	24.30	58.06	6.04
1655-099.6	30.36	75.00	245.50	179.60	130.01	136.45	11.19	22.12	2884.51	25.53	53.26	6.12
1655-114.3	34.84	70.40	184.10	184.10	113.47	223.07	11.33	12.00	642.80	16.76	41.12	3.93
907-018.2	5.55	64.00	264.92	159.00	83.79	94.65	9.02	13.94	751.19	18.37	35.73	4.33
907-018.6 Psl	5.67	65.00	252.10	192.00	121.93	137.11	11.46	15.73	794.22	22.25	45.58	4.99
907-018.8	5.73	64.00	252.43	225.00	100.77	126.16	10.33	15.40	756.94	21.38	42.54	4.94
907-019.0	5.79	67.00	251.96	216.00	100.30	114.93	11.08	17.14	759.05	22.93	44.47	5.17
907-019.5 Psl	5.94	71.00	281.81	179.00	149.65	143.72	12.78	20.26	838.58	27.88	57.48	6.60
907-056.1a	17.10	57.50	190.82	203.60	73.36	156.91	8.83	10.77	700.97	13.95	26.27	3.12
907-056.1b	17.10	63.00	197.98	237.00	95.21	176.15	10.18	12.00	790.87	16.30	34.10	3.86
907-056.43	17.20	58.80	228.58	181.50	78.07	118.87	12.75	9.25	724.28	13.88	31.42	2.89
907-056.7	17.28	60.00	277.88	160.30	107.83	149.99	10.67	9.97	809.31	14.90	31.00	3.25
907-057.09	17.40	64.90	273.66	217.10	95.21	125.72	10.18	11.93	691.46	17.80	39.70	3.85
907-057.41	17.50	68.90	289.05	215.20	105.51	151.07	12.48	15.30	768.99	23.02	43.74	5.37
907-057.7 Fines	17.59	65.50	234.57	245.80	120.88	136.01	13.39	24.75	627.33	31.68	41.90	7.61
907-057.74	17.60	71.00	295.78	247.00	118.47	172.33	11.16	17.39	819.25	25.44	44.31	6.12
907-058.01	17.68	72.00	283.10	258.00	135.87	155.91	13.03	19.96	774.11	28.58	59.79	6.74
907-058.02	17.68	65.00	318.50	236.00	125.61	168.02	11.15	15.19	921.76	21.74	50.96	5.03

Table 5 (continued). Geochemical data of minor and trace elements from LA-ICP-MS analyses

Sample	Depth (m)	Rb	Sr	Zr	V	Cr	Nb	Y	Ba	La	Ce	Pr
907-058.4	17.80	65.00	283.99	245.70	108.60	144.40	10.62	11.80	806.33	21.00	44.00	4.79
907-058.4	17.80	68.00	280.83	248.00	137.08	144.88	12.27	16.02	743.55	26.76	57.62	6.03
907-058.5	17.83	65.00	301.50	235.00	139.22	157.94	11.60	15.75	718.23	27.04	49.28	6.42
907-058.71	17.89	64.00	453.84	333.00	94.07	193.18	9.17	9.77	1121.42	19.24	46.04	4.50
907-059.86	18.25	71.00	403.09	232.00	93.92	122.42	8.01	11.14	894.89	18.91	38.61	4.19
907-059.9	18.26	69.00	407.06	208.00	121.63	115.91	9.80	12.13	941.21	22.84	49.07	5.14
907-060.19	18.35	68.00	364.42	207.00	87.49	81.04	6.86	10.89	871.74	19.33	40.57	4.28
907-060.5	18.44	71.00	448.97	228.00	141.10	131.53	11.15	14.01	981.69	29.34	58.54	6.89
907-060.68	18.50	64.00	506.05	245.00	131.95	137.93	9.79	11.63	1062.09	23.70	52.53	5.54
907-061.0	18.59	65.50	389.83	190.40	77.12	87.68	7.35	11.57	873.67	19.43	35.95	4.21
907-095.5	29.11	63.60	245.23	191.80	108.15	137.63	12.61	17.97	723.66	23.17	47.98	5.35

Table 5 (continued). Geochemical data of minor and trace elements from LA-ICP-MS analyses

Sample	Depth (m)	Nd	Sm	Eu	Gd	Tb	Dy	Ho	Er	Yb	Lu	Hf
1253-051.3	15.64	23.56	4.46	1.10	3.92	0.56	3.09	0.63	1.68	1.78	0.27	4.53
1253-053.9	16.43	16.91	3.35	0.94	2.95	0.46	2.49	0.55	1.44	1.62	0.27	5.67
1253-096.3	29.35	20.10	4.02	1.06	3.52	0.51	2.79	0.58	1.52	1.60	0.24	4.24
1253-096.4	29.38	22.41	4.51	1.19	4.02	0.59	3.08	0.64	1.77	1.79	0.27	4.79
1253-097.0	29.57	24.47	5.07	1.28	4.24	0.60	3.18	0.69	1.97	2.01	0.28	5.46
1253-097.6	29.75	18.99	3.84	0.99	3.16	0.45	2.52	0.50	1.46	1.50	0.24	5.79
1253-097.6 Fines	29.75	23.48	4.41	1.18	4.86	0.71	3.34	0.68	1.96	2.38	0.31	6.35
1253-098.3	29.96	16.54	3.08	0.95	2.84	0.42	2.11	0.46	1.35	1.48	0.21	5.48
1253-099.0	30.18	16.42	3.22	0.89	2.65	0.39	2.15	0.41	1.19	1.29	0.22	4.80
1253-099.7	30.39	19.18	3.75	1.00	3.04	0.45	2.53	0.52	1.44	1.53	0.22	4.42
1253-100.3	30.57	21.16	4.46	1.22	4.17	0.60	3.28	0.72	2.17	2.09	0.30	4.68
1253-100.9	30.75	17.40	3.43	0.94	3.02	0.46	2.16	0.47	1.30	1.45	0.22	4.41
1253-101.6	30.97	15.36	2.97	0.77	2.49	0.39	2.07	0.39	1.26	1.38	0.17	4.49
1253-101.6 Fines	30.97	23.33	4.56	1.21	5.22	0.72	3.45	0.69	2.00	2.40	0.33	7.84
1253-118.8	36.21	20.74	4.09	1.11	3.57	0.52	2.78	0.59	1.69	1.77	0.28	4.54
1253-119.5	36.42	14.99	3.16	0.92	2.96	0.46	2.55	0.55	1.47	1.71	0.27	4.43
1253-120.1	36.61	17.77	3.63	1.01	3.20	0.50	2.54	0.56	1.55	1.70	0.26	4.40
1253-120.8	36.82	17.62	3.58	1.00	3.19	0.49	2.66	0.57	1.51	1.58	0.26	4.45
1253-121.5	37.03	22.29	4.26	1.17	4.04	0.60	3.13	0.70	1.90	2.01	0.30	4.40
1552-008.1	2.47	18.25	3.46	0.93	3.14	0.47	2.65	0.55	1.56	1.87	0.28	5.75
1552-009.3	2.83	17.22	3.55	0.90	3.17	0.49	2.99	0.59	1.72	1.93	0.31	7.38
1552-011.5	3.51	19.12	3.73	0.99	3.46	0.48	2.86	0.63	1.87	1.96	0.30	6.01
1552-014.6	4.45	20.59	4.06	1.03	3.55	0.57	3.25	0.70	1.89	2.00	0.32	4.97

Table 5 (continued). Geochemical data of minor and trace elements from LA-ICP-MS analyses

Sample	Depth (m)	Nd	Sm	Eu	Gd	Tb	Dy	Ho	Er	Yb	Lu	Hf
1552-019.7	6.00	15.53	3.14	0.89	2.94	0.44	2.73	0.51	1.60	1.87	0.27	5.92
1552-021.3	6.49	14.13	2.88	0.78	2.41	0.37	2.15	0.46	1.30	1.42	0.23	5.09
1552-022.8	6.95	16.57	3.33	0.88	2.90	0.43	2.43	0.54	1.42	1.59	0.26	4.78
1552-024.6	7.50	19.82	4.09	1.16	3.57	0.55	2.85	0.65	1.60	1.80	0.28	4.68
1552-026.5	8.08	17.92	3.58	0.92	3.22	0.47	2.68	0.55	1.66	1.69	0.25	5.00
1552-027.5	8.38	12.19	2.61	0.65	2.32	0.34	1.94	0.40	1.21	1.38	0.19	4.22
1552-032.0	9.75	13.24	2.62	0.77	2.29	0.36	1.99	0.40	1.21	1.40	0.22	5.83
1552-036.1	11.00	18.74	3.77	0.96	3.42	0.53	3.02	0.58	1.79	1.90	0.29	6.37
1552-037.7	11.49	14.85	2.79	0.92	2.39	0.39	1.78	0.41	1.09	1.31	0.22	6.84
1552-045.9	13.99	13.10	2.73	0.71	2.39	0.36	2.00	0.42	1.15	1.33	0.19	2.26
1552-049.2	15.00	22.81	4.41	1.12	3.93	0.58	3.14	0.61	1.82	1.91	0.29	5.08
1552-049.3	15.03	20.81	4.02	0.98	3.44	0.51	2.74	0.57	1.51	1.63	0.25	4.41
1552-049.6	15.12	23.29	4.54	1.12	4.20	0.59	3.24	0.65	1.97	2.15	0.27	4.65
1552-050.0	15.24	22.70	4.36	1.13	3.83	0.56	3.00	0.59	1.79	1.83	0.26	4.98
1552-050.9	15.51	19.27	4.41	1.37	3.65	0.77	2.95	0.75	1.90	2.00	0.41	5.30
1552-051.2	15.61	16.85	3.35	0.84	3.06	0.48	2.70	0.59	1.60	1.91	0.28	5.53
1552-051.6	15.73	15.79	3.09	0.78	2.96	0.46	2.65	0.51	1.64	1.86	0.27	5.79
1552-051.8	15.79	16.63	3.27	0.89	3.19	0.48	2.57	0.59	1.70	1.76	0.30	5.73
1552-051.9	15.82	15.62	3.60	0.87	2.89	0.46	2.46	0.47	1.51	1.64	0.25	5.43
1552-052.0	15.85	17.37	3.43	0.97	3.14	0.51	2.77	0.59	1.63	1.77	0.28	5.13
1552-052.1	15.88	15.88	3.16	0.80	2.87	0.40	2.51	0.46	1.46	1.59	0.21	5.25
1552-052.4	15.97	15.11	3.02	0.85	2.66	0.39	2.34	0.47	1.39	1.62	0.26	5.23
1552-054.1	16.49	17.11	3.49	0.94	3.02	0.48	2.65	0.56	1.49	1.73	0.28	4.69

Table 5 (continued). Geochemical data of minor and trace elements from LA-ICP-MS analyses

Sample	Depth (m)	Nd	Sm	Eu	Gd	Tb	Dy	Ho	Er	Yb	Lu	Hf
1552-066.8	20.36	12.45	2.49	0.66	2.24	0.34	1.82	0.39	1.15	1.33	0.24	6.28
1552-074.1	22.59	12.80	2.66	0.69	2.40	0.36	2.15	0.43	1.41	1.66	0.25	4.82
1552-074.3 Psl	22.65	13.09	2.72	0.69	2.46	0.37	2.14	0.44	1.33	1.49	0.22	4.03
1552-075.3 Psl	22.95	23.80	4.81	1.20	4.45	0.66	3.80	0.74	2.14	2.29	0.34	5.22
1552-075.6	23.04	21.46	4.24	1.15	3.93	0.61	3.29	0.69	1.82	2.03	0.31	4.53
1552-075.9	23.13	18.23	3.67	1.01	3.54	0.51	2.76	0.61	1.70	1.87	0.31	5.54
1552-077.2	23.53	21.88	4.20	1.20	3.76	0.59	2.93	0.66	1.67	1.75	0.30	4.80
1552-080.4	24.51	18.07	3.60	0.98	3.21	0.50	2.68	0.55	1.47	1.74	0.26	4.37
1552-086.9	26.49	16.22	3.18	0.92	2.63	0.39	1.93	0.37	1.12	1.31	0.21	7.35
1552-096.8	29.50	19.01	3.84	1.08	3.52	0.53	2.73	0.59	1.71	1.76	0.27	3.52
1552-099.1	30.21	18.03	3.84	1.01	3.44	0.54	2.73	0.60	1.56	1.76	0.29	4.94
1552-099.4	30.30	18.15	3.52	0.91	3.16	0.46	2.52	0.54	1.41	1.73	0.25	5.11
1552-099.7	30.39	18.61	3.74	1.02	3.42	0.49	2.73	0.58	1.49	1.76	0.26	5.82
1552-100.1	30.51	16.79	3.27	0.90	2.94	0.42	2.34	0.51	1.55	1.76	0.27	7.01
1552-100.4	30.60	16.23	3.34	0.88	2.93	0.45	2.53	0.54	1.44	1.68	0.27	6.16
1552-100.7	30.69	17.63	3.54	0.97	3.16	0.48	2.48	0.55	1.57	1.73	0.27	5.43
1552-101.1	30.82	17.89	3.53	1.09	3.45	0.53	2.90	0.60	1.68	1.89	0.30	5.51
1552-101.4	30.91	19.50	4.01	1.07	3.41	0.53	3.02	0.63	1.76	1.87	0.32	4.98
1552-101.7	31.00	18.51	3.71	1.03	3.41	0.50	2.78	0.61	1.68	1.79	0.27	4.80
1552-101.7 Fines	31.00	30.19	5.95	1.54	6.35	0.93	4.97	1.00	2.90	3.22	0.44	5.70
1552-102.0	31.09	21.04	4.22	1.17	4.05	0.58	3.29	0.69	1.83	1.91	0.32	4.43
1552-102.4	31.21	21.61	4.29	1.19	4.04	0.61	3.36	0.72	1.90	1.91	0.31	4.29
1552-102.4 Fines	31.21	32.61	6.51	1.62	7.06	1.00	5.47	1.13	3.15	3.38	0.49	6.46

Table 5 (continued). Geochemical data of minor and trace elements from LA-ICP-MS analyses

Sample	Depth (m)	Nd	Sm	Eu	Gd	Tb	Dy	Ho	Er	Yb	Lu	Hf
1552-102.7	31.30	18.34	3.71	0.99	3.08	0.49	2.64	0.58	1.61	1.54	0.27	4.43
1552-103.4	31.52	19.00	3.83	1.02	3.36	0.49	2.75	0.60	1.60	1.77	0.25	4.34
1552-103.4 Fines	31.52	28.32	5.74	1.39	5.82	0.85	4.26	0.82	2.32	2.62	0.36	5.68
1552-103.7	31.61	20.88	3.98	1.01	3.62	0.54	2.97	0.62	1.58	1.71	0.27	4.41
1552-104.0	31.70	20.42	3.95	0.99	3.37	0.52	2.84	0.52	1.64	1.63	0.23	4.49
1552-105.0	32.00	23.73	4.71	1.27	4.33	0.61	3.49	0.75	2.05	2.12	0.31	4.69
1552-106.6	32.49	40.63	8.33	2.61	8.82	1.40	7.77	1.71	4.54	4.10	0.63	4.85
1552-111.6	34.02	22.27	4.29	1.12	3.76	0.55	2.84	0.60	1.60	1.70	0.26	3.86
1552-113.0	34.44	30.42	5.78	1.67	6.44	0.91	5.56	1.27	3.50	3.25	0.49	4.36
1552-117.1	35.69	18.96	3.75	1.00	3.59	0.55	2.89	0.63	1.80	1.95	0.28	4.50
1552-117.5	35.81	16.71	3.27	0.89	3.00	0.43	2.47	0.52	1.36	1.60	0.25	3.98
1552-117.8	35.91	23.63	4.75	1.35	4.88	0.73	4.30	0.99	2.55	2.45	0.37	4.23
1552-118.1	36.00	13.81	2.78	0.76	2.45	0.37	1.97	0.41	1.19	1.35	0.21	4.12
1552-118.8	36.21	24.65	4.88	1.41	5.05	0.77	4.53	0.98	2.57	2.46	0.38	3.85
1552-119.1	36.30	15.07	3.01	0.70	2.64	0.35	2.18	0.36	1.27	1.41	0.15	4.21
1552-119.4	36.39	18.66	3.87	0.98	3.07	0.47	2.67	0.54	1.49	1.56	0.26	4.09
1552-119.8	36.52	20.97	4.12	1.15	4.34	0.64	3.70	0.88	2.29	2.49	0.36	3.67
1552-120.1	36.61	14.15	2.87	0.80	2.63	0.42	2.46	0.47	1.37	1.59	0.24	4.68
1552-120.4	36.70	13.76	2.77	0.68	2.37	0.31	1.86	0.33	1.08	1.15	0.14	3.50
1552-124.7	38.01	14.66	2.98	0.73	2.64	0.36	2.28	0.40	1.21	1.34	0.18	4.48
1552-126.4	38.53	18.90	3.64	1.14	2.94	0.47	2.18	0.51	1.35	1.41	0.26	5.32
1552-128.0	39.01	17.86	3.63	1.12	3.10	0.46	2.27	0.49	1.27	1.38	0.23	4.33
1552-136.1	41.48	9.02	2.15	0.61	2.11	0.34	2.04	0.44	1.18	1.18	0.20	2.52

Table 5 (continued). Geochemical data of minor and trace elements from LA-ICP-MS analyses

Sample	Depth (m)	Nd	Sm	Eu	Gd	Tb	Dy	Ho	Er	Yb	Lu	Hf
1552-141.0	42.98	12.68	2.86	0.82	2.85	0.46	2.81	0.61	1.70	1.70	0.27	2.80
1552-144.4	44.01	11.67	2.69	0.85	2.66	0.43	2.58	0.56	1.50	1.44	0.23	2.26
1552-146.0	44.50	16.30	3.35	0.97	2.80	0.45	2.27	0.48	1.31	1.43	0.22	4.28
1552-147.6	44.99	24.47	4.82	1.27	4.20	0.62	3.22	0.68	1.74	1.92	0.30	4.96
1552-153.1	46.66	20.12	3.83	1.00	3.40	0.51	3.11	0.63	1.74	1.88	0.30	4.63
1553-049.0	14.94	23.62	4.43	1.13	3.66	0.52	2.91	0.60	1.54	1.59	0.25	4.89
1553-049.7	15.15	25.17	4.77	1.19	4.05	0.57	3.29	0.66	1.92	1.97	0.31	6.80
1553-051.6	15.73	18.21	3.49	0.90	3.28	0.46	2.62	0.59	1.57	1.67	0.27	4.99
1553-052.6	16.03	19.01	3.68	0.97	3.34	0.50	2.82	0.63	1.72	1.85	0.29	5.30
1553-077.0	23.47	15.39	3.13	0.84	2.72	0.42	2.23	0.50	1.32	1.53	0.24	3.85
1553-101.3	30.88	31.91	6.11	1.37	6.07	0.93	5.54	1.14	3.27	3.15	0.48	4.66
1553-101.9	31.06	21.50	4.27	1.16	3.78	0.50	2.91	0.53	1.63	1.70	0.23	4.30
1553-102.6	31.27	22.95	4.64	1.50	4.14	0.60	3.47	0.70	2.11	2.16	0.31	5.12
1553-122.0	37.19	18.38	3.60	0.93	3.20	0.47	2.61	0.55	1.44	1.61	0.26	4.11
1553-122.6	37.37	16.78	3.30	0.79	2.86	0.41	2.43	0.45	1.34	1.42	0.20	4.03
1650-074.6	22.74	22.25	4.36	1.14	4.08	0.60	3.32	0.68	1.95	1.98	0.31	4.70
1650-099.0	30.18	23.75	4.62	1.19	4.04	0.61	3.31	0.70	1.90	1.95	0.30	4.01
1650-100.0	30.48	22.41	4.49	1.15	3.96	0.59	3.32	0.68	1.96	1.87	0.29	4.58
1650-100.6	30.66	20.95	4.24	1.15	3.73	0.56	3.09	0.66	1.85	1.89	0.31	4.46
1650-101.3	30.88	18.73	3.68	0.97	3.39	0.50	2.81	0.63	1.73	1.87	0.28	4.16
1650-102.0	31.09	18.24	3.67	1.06	3.49	0.51	2.77	0.61	1.78	1.81	0.28	4.93
1650-121.0	36.88	17.93	3.49	0.95	3.32	0.51	2.64	0.55	1.53	1.75	0.26	4.38
1650-121.6	37.06	21.89	4.20	1.14	4.10	0.58	2.95	0.67	1.73	1.94	0.28	4.52

Table 5 (continued). Geochemical data of minor and trace elements from LA-ICP-MS analyses

Sample	Depth (m)	Nd	Sm	Eu	Gd	Tb	Dy	Ho	Er	Yb	Lu	Hf
1650-122.3	37.28	23.40	4.61	1.19	4.08	0.59	3.38	0.70	1.82	1.96	0.29	4.33
1655-097.3	29.66	21.32	3.87	1.05	3.23	0.45	2.37	0.48	1.24	1.30	0.19	3.62
1655-098.0	29.87	26.62	4.84	1.19	5.84	0.80	5.06	1.15	3.44	3.00	0.45	4.03
1655-098.3	29.96	22.10	4.39	1.07	3.87	0.54	3.11	0.59	1.67	1.72	0.22	4.43
1655-098.6	30.05	24.07	5.09	1.29	4.29	0.65	3.51	0.72	1.95	2.10	0.33	4.41
1655-099.0	30.18	22.15	4.48	1.15	4.14	0.58	3.15	0.62	1.84	1.85	0.25	4.32
1655-099.6	30.36	23.86	4.52	1.27	4.21	0.59	3.35	0.70	1.91	1.89	0.29	4.57
1655-114.3	34.84	14.48	2.79	0.77	2.42	0.38	1.92	0.43	1.15	1.26	0.21	4.41
907-018.2	5.55	16.74	3.27	0.92	3.17	0.47	2.59	0.53	1.56	1.69	0.28	4.55
907-018.6 Psl	5.67	19.01	3.85	1.02	3.51	0.51	2.78	0.62	1.72	1.82	0.31	5.14
907-018.8	5.73	18.85	3.55	1.01	3.42	0.47	2.76	0.61	1.77	1.96	0.32	6.45
907-019.0	5.79	20.42	3.81	1.03	3.79	0.54	2.93	0.65	1.83	1.98	0.31	6.01
907-019.5 Psl	5.94	24.67	4.72	1.26	4.47	0.63	3.55	0.76	2.09	2.13	0.31	5.01
907-056.1a	17.10	12.01	2.59	0.71	2.26	0.34	2.02	0.40	1.17	1.41	0.19	5.13
907-056.1b	17.10	14.11	2.94	0.81	2.65	0.40	2.22	0.47	1.41	1.43	0.25	6.23
907-056.43	17.20	10.78	2.15	0.68	1.89	0.30	1.70	0.34	1.00	1.19	0.19	4.88
907-056.7	17.28	11.88	2.44	0.72	2.11	0.32	1.75	0.37	1.05	1.25	0.21	3.93
907-057.09	17.40	14.34	2.96	0.79	2.57	0.42	2.36	0.46	1.41	1.77	0.26	6.04
907-057.41	17.50	20.33	4.10	1.06	3.46	0.49	2.98	0.54	1.68	1.99	0.30	5.77
907-057.7 Fines	17.59	29.87	5.72	1.32	4.83	0.71	3.81	0.78	2.08	2.11	0.33	6.02
907-057.74	17.60	24.26	4.78	1.24	4.02	0.57	3.11	0.65	1.73	1.97	0.34	6.42
907-058.01	17.68	25.49	4.85	1.16	4.35	0.60	3.17	0.68	1.97	2.06	0.32	6.54
907-058.02	17.68	19.03	3.69	1.01	3.61	0.49	2.52	0.54	1.50	1.64	0.28	5.98

Table 5 (continued). Geochemical data of minor and trace elements from LA-ICP-MS analyses

Sample	Depth (m)	Nd	Sm	Eu	Gd	Tb	Dy	Ho	Er	Yb	Lu	Hf
907-058.4	17.80	18.15	3.51	0.90	2.93	0.44	2.30	0.43	1.31	1.59	0.23	6.56
907-058.4	17.80	22.14	4.06	1.04	3.65	0.53	2.75	0.59	1.63	1.72	0.28	6.51
907-058.5	17.83	24.32	4.39	1.08	3.78	0.52	2.73	0.55	1.53	1.66	0.27	6.00
907-058.71	17.89	16.85	2.98	0.92	2.67	0.36	1.79	0.41	1.11	1.25	0.21	8.09
907-059.86	18.25	15.91	2.95	0.85	2.75	0.38	2.05	0.42	1.23	1.42	0.22	6.14
907-059.9	18.26	19.09	3.48	0.99	3.02	0.41	2.16	0.46	1.23	1.50	0.23	5.66
907-060.19	18.35	16.41	3.11	0.83	2.80	0.38	1.97	0.42	1.23	1.38	0.22	6.00
907-060.5	18.44	25.68	4.71	1.16	3.83	0.53	2.66	0.55	1.49	1.60	0.25	5.92
907-060.68	18.50	19.90	3.87	1.04	3.26	0.45	2.27	0.44	1.28	1.42	0.23	6.72
907-061.0	18.59	16.95	3.21	0.86	2.82	0.40	2.35	0.47	1.35	1.65	0.21	5.56
907-095.5	29.11	21.15	4.34	1.16	3.74	0.58	3.33	0.71	1.95	1.99	0.31	5.45

Table 5 (continued). Geochemical data of minor and trace elements from LA-ICP-MS analyses

Sample	Depth (m)	Ta	Pb	Th	U
1253-051.3	15.64	0.82	15.55	9.43	1.91
1253-053.9	16.43	1.03	15.69	6.31	2.50
1253-096.3	29.35	0.75	12.10	6.93	1.80
1253-096.4	29.38	0.87	21.80	7.97	1.68
1253-097.0	29.57	1.02	23.81	9.49	2.32
1253-097.6	29.75	0.90	12.70	7.22	2.15
1253-097.6 Fines	29.75	1.54	52.68	10.81	4.00
1253-098.3	29.96	0.99	24.00	6.88	1.88
1253-099.0	30.18	0.94	14.28	8.07	2.55
1253-099.7	30.39	0.85	13.91	7.50	2.42
1253-100.3	30.57	0.92	20.54	8.49	2.19
1253-100.9	30.75	0.86	20.23	7.94	2.09
1253-101.6	30.97	0.67	15.28	6.89	1.83
1253-101.6 Fines	30.97	1.54	35.14	10.89	4.82
1253-118.8	36.21	0.92	19.33	8.00	2.14
1253-119.5	36.42	1.01	14.69	7.37	1.80
1253-120.1	36.61	0.98	10.29	7.39	1.57
1253-120.8	36.82	0.86	13.07	7.53	2.23
1253-121.5	37.03	0.93	19.00	7.69	2.56
1552-008.1	2.47	0.92	17.03	7.55	2.07
1552-009.3	2.83	1.00	12.06	7.64	1.51
1552-011.5	3.51	1.24	15.01	8.39	3.31
1552-014.6	4.45	0.91	10.95	9.08	2.60

Table 5 (continued). Geochemical data of minor and trace elements from LA-ICP-MS analyses

Sample	Depth (m)	Ta	Pb	Th	U
1552-019.7	6.00	0.89	11.04	7.29	1.53
1552-021.3	6.49	0.80	9.78	5.94	1.96
1552-022.8	6.95	0.81	16.17	6.08	1.94
1552-024.6	7.50	0.93	18.20	7.16	2.71
1552-026.5	8.08	0.74	12.88	7.94	1.21
1552-027.5	8.38	0.59	7.81	5.46	1.75
1552-032.0	9.75	0.71	14.37	5.24	1.24
1552-036.1	11.00	0.93	11.95	8.39	1.50
1552-037.7	11.49	0.87	20.93	5.54	2.69
1552-045.9	13.99	0.60	13.44	3.95	1.51
1552-049.2	15.00	0.96	12.37	11.10	1.62
1552-049.3	15.03	0.84	11.06	8.89	2.33
1552-049.6	15.12	0.77	11.13	10.27	1.34
1552-050.0	15.24	0.84	12.36	10.49	1.64
1552-050.9	15.51	1.08	13.13	9.77	3.96
1552-051.2	15.61	0.91	13.49	8.55	1.95
1552-051.6	15.73	0.91	10.01	8.72	1.62
1552-051.8	15.79	1.02	16.44	7.81	2.30
1552-051.9	15.82	0.87	12.22	7.31	3.08
1552-052.0	15.85	0.98	13.46	7.22	2.62
1552-052.1	15.88	0.79	10.80	6.90	2.13
1552-052.4	15.97	1.04	13.59	6.52	3.00
1552-054.1	16.49	0.86	18.58	5.91	2.05

Table 5 (continued). Geochemical data of minor and trace elements from LA-ICP-MS analyses

Sample	Depth (m)	Ta	Pb	Th	U
1552-066.8	20.36	0.95	13.69	4.62	1.65
1552-074.1	22.59	0.92	11.45	7.53	1.40
1552-074.3 Psl	22.65	0.81	11.34	6.55	1.35
1552-075.3 Psl	22.95	0.96	10.88	9.37	1.59
1552-075.6	23.04	1.05	10.14	7.79	1.68
1552-075.9	23.13	1.12	11.64	7.21	1.73
1552-077.2	23.53	1.06	15.71	8.11	3.01
1552-080.4	24.51	0.98	20.13	6.56	2.31
1552-086.9	26.49	0.80	21.07	6.05	2.26
1552-096.8	29.50	0.79	25.70	6.17	2.09
1552-099.1	30.21	0.89	12.09	6.79	1.53
1552-099.4	30.30	0.92	10.21	6.80	1.46
1552-099.7	30.39	0.92	11.31	7.18	1.59
1552-100.1	30.51	0.99	13.63	9.40	2.32
1552-100.4	30.60	1.00	10.55	7.29	1.47
1552-100.7	30.69	0.99	18.12	7.56	2.42
1552-101.1	30.82	0.99	12.20	6.81	1.59
1552-101.4	30.91	0.94	14.82	6.83	2.78
1552-101.7	31.00	0.87	10.59	6.62	1.45
1552-101.7 Fines	31.00	1.33	26.08	11.16	3.48
1552-102.0	31.09	0.87	10.04	7.30	1.69
1552-102.4	31.21	0.90	11.03	7.40	1.56
1552-102.4 Fines	31.21	1.34	40.41	12.21	3.66

Table 5 (continued). Geochemical data of minor and trace elements from LA-ICP-MS analyses

Sample	Depth (m)	Ta	Pb	Th	U
1552-102.7	31.30	0.86	12.66	7.63	2.38
1552-103.4	31.52	0.92	11.43	7.42	1.94
1552-103.4 Fines	31.52	1.15	45.01	11.44	4.78
1552-103.7	31.61	0.91	10.33	8.61	2.21
1552-104.0	31.70	0.80	11.77	9.91	2.13
1552-105.0	32.00	0.85	17.06	7.80	2.21
1552-106.6	32.49	0.96	17.91	7.96	4.21
1552-111.6	34.02	0.78	13.77	8.67	1.82
1552-113.0	34.44	0.81	11.70	5.15	2.76
1552-117.1	35.69	0.93	15.84	8.54	1.98
1552-117.5	35.81	0.91	10.11	7.09	1.45
1552-117.8	35.91	0.92	8.18	7.04	1.51
1552-118.1	36.00	0.89	11.09	7.16	1.44
1552-118.8	36.21	0.83	9.16	6.80	1.60
1552-119.1	36.30	0.73	15.11	7.20	3.96
1552-119.4	36.39	0.90	13.05	7.22	2.41
1552-119.8	36.52	0.72	9.13	5.96	1.75
1552-120.1	36.61	0.77	11.28	7.27	1.31
1552-120.4	36.70	0.63	14.81	5.04	0.77
1552-124.7	38.01	0.68	14.62	6.33	1.16
1552-126.4	38.53	0.94	20.87	6.91	2.94
1552-128.0	39.01	0.87	24.33	6.14	4.21
1552-136.1	41.48	0.48	5.25	2.17	0.97

Table 5 (continued). Geochemical data of minor and trace elements from LA-ICP-MS analyses

Sample	Depth (m)	Ta	Pb	Th	U
1552-141.0	42.98	0.55	4.92	3.31	1.13
1552-144.4	44.01	0.45	5.97	2.83	1.01
1552-146.0	44.50	0.82	18.18	5.86	2.08
1552-147.6	44.99	0.95	16.61	8.03	2.36
1552-153.1	46.66	0.93	15.71	8.25	2.35
1553-049.0	14.94	0.75	16.06	7.94	1.73
1553-049.7	15.15	0.86	16.44	8.25	1.98
1553-051.6	15.73	0.89	15.20	7.26	2.71
1553-052.6	16.03	1.16	17.80	8.24	4.44
1553-077.0	23.47	0.90	18.13	5.95	2.42
1553-101.3	30.88	1.03	11.10	14.03	1.67
1553-101.9	31.06	0.80	14.70	8.21	0.98
1553-102.6	31.27	1.49	9.89	9.26	1.31
1553-122.0	37.19	0.82	11.69	7.74	2.09
1553-122.6	37.37	0.72	13.19	7.21	1.54
1650-074.6	22.74	0.91	14.97	7.57	1.83
1650-099.0	30.18	0.87	14.68	9.09	3.40
1650-100.0	30.48	0.94	16.85	8.64	3.16
1650-100.6	30.66	0.87	14.58	7.80	2.62
1650-101.3	30.88	0.80	10.85	7.31	1.49
1650-102.0	31.09	0.89	19.45	6.40	2.12
1650-121.0	36.88	0.92	16.60	7.38	1.94
1650-121.6	37.06	0.95	19.17	8.46	2.10

Table 5 (continued). Geochemical data of minor and trace elements from LA-ICP-MS analyses

Sample	Depth (m)	Ta	Pb	Th	U
1650-122.3	37.28	0.92	13.02	8.47	2.48
1655-097.3	29.66	0.77	19.77	8.36	2.11
1655-098.0	29.87	0.76	16.18	9.23	2.12
1655-098.3	29.96	0.69	14.55	9.58	1.82
1655-098.6	30.05	0.89	15.10	8.98	3.27
1655-099.0	30.18	0.74	15.00	8.67	1.42
1655-099.6	30.36	0.96	17.71	8.24	2.58
1655-114.3	34.84	0.80	15.08	5.69	1.91
907-018.2	5.55	1.02	10.86	7.23	2.46
907-018.6 Psl	5.67	1.20	15.14	8.33	3.44
907-018.8	5.73	1.14	12.15	8.33	3.36
907-019.0	5.79	1.04	10.88	9.17	2.87
907-019.5 Psl	5.94	1.27	14.75	10.97	3.73
907-056.1a	17.10	0.69	9.78	4.42	1.10
907-056.1b	17.10	1.11	13.49	5.38	2.37
907-056.43	17.20	0.70	10.74	4.70	1.06
907-056.7	17.28	0.72	19.77	6.23	2.13
907-057.09	17.40	0.81	9.19	7.66	1.25
907-057.41	17.50	0.89	13.73	8.05	1.59
907-057.7 Fines	17.59	0.90	23.97	9.13	2.31
907-057.74	17.60	1.16	16.93	7.32	2.99
907-058.01	17.68	1.21	41.56	10.14	3.13
907-058.02	17.68	1.06	16.80	7.84	3.14

Table 5 (continued). Geochemical data of minor and trace elements from LA-ICP-MS analyses

Sample	Depth (m)	Ta	Pb	Th	U
907-058.4	17.80	0.81	13.46	9.37	1.52
907-058.4	17.80	1.13	39.61	11.19	2.80
907-058.5	17.83	1.06	84.51	11.54	2.71
907-058.71	17.89	0.96	19.96	5.92	2.45
907-059.86	18.25	0.86	11.78	7.52	2.37
907-059.9	18.26	0.94	13.02	9.24	2.86
907-060.19	18.35	0.75	8.74	8.39	2.22
907-060.5	18.44	1.01	15.03	10.63	3.38
907-060.68	18.50	1.02	17.96	8.14	3.31
907-061.0	18.59	0.74	9.00	6.94	0.98
907-095.5	29.11	0.94	14.58	9.41	1.54

BIBLIOGRAPHY

Chapter 4

Bibliography

Aines, R., Newmark, R., Ziagos, J., Copeland, A., Udell, K., 1994. Cleaning up underground contaminants. Energy and Technology Review (LLNL UCRL-52000-94-5), 11-21.

Buter, J.C., Woronow, A., 1986. Discrimination among tectonic settings using trace element abundances of basalts. Journal of Geophysical Research 91 (B10), 10,289-10,300.

Chittleborough, D.J., 1991. Indices of weathering for soils and palaeosols formed on silicate rocks. Australian Journal of Earth Sciences 38, 115-120.

Compton, J.S., White, R.A., Smith, M., 2003. Rare earth element behavior in soils and salt pan sediments of a semi-arid granitic terrain in the Western Cape, South Africa. Chemical Geology 201, 239-255.

Culler, R.L., 1988. Mineralogical and chemical changes of soil and stream sediment formed by intense weathering of the Danburg granite, Georgia, USA. Lithos 21, 301-314.

Cullers, R.L., 1994. The chemical signature of source rocks in size fractions of Holocene stream sediment derived from metamorphic rocks in the Wet Mountains region, Colorado, USA. Chemical Geology 113, 327-343.

Culler, R.L., Basu, A., Suttner, L., 1988. Geochemical signature of provenance in sand-size material in soils and stream sediments near the Tobacco Root batholith, Montana, USA. Chemical Geology 70, 335-348.

Culler, R.L., Barret, T., Carlson, R., Robinson, B., 1987. Rare-earth and mineralogic changes in Holocene soil and stream sediment: A case study in the Wet Mountains, USA. Chemical Geology 63, 275-297.

Dia, A., Gruau, G., Olivié-Lauquet, G., Riou, C., Molénat, J., Curmi, P., 2000. The distribution of rare earth elements in groundwaters: Assessing the role of source-rock composition, redox change and colloidal particles. Geochimica et Cosmochimica Acta 64 (24), 4131-4151.

Dickinson, W.R., Ingersoll, R.V., Cowan, D.S., Helmold, K.P., Suczek, C.A., 1982. Provenance of Franciscan graywackes in coastal California. Geological Society of America Bulletin 93, 95-107.

Feakes, C.R., Retallack, G.J., 1988. Recognition and chemical characterization of fossil soils developed on alluvium; A Late Ordovician example. In: Reinhardt, J., Sigleo, W.R. (Eds.), Paleosols and Weathering through Geologic Time; Principles and Applications, vol. 216. Geological Society of America Special Paper, Boulder, Colorado, p. 35-48.

Garcia-Ruiz, J.M., 1998. Carbonate precipitation into alkaline silica-rich environments. Geology 26 (9), 843-846.

Grimley, D.A., Follmer, L.R., Hughes, R.E., Solheid, P.A., 2003. Modern, Sangamon and Yarmouth soil development in loess of unglaciated southwestern Illinois. Quaternary Science Reviews 22 (2-4), 225-244.

Gruau, G., Dia, A., Olivié-Lauquet, G., Davranche, M., Pinay, G., 2004. Controls on the distribution of rare earth elements in shallow groundwaters. Water Research 38, 3576-3586.

Harden, J.W., 1987. Soils developed in granitic alluvium near Merced, California. United States Geological Survey Bulletin 1590-A, A1-A65.

Harden, J.W., 1988. Genetic interpretations of elemental and chemical differences in a soil chronosequences, California. Geoderma 43, 179-193.

Harnois, L., 1988. The CIW index: A new chemical index of weathering. Sedimentary Geology 55, 319-322.

Hill, I.G., Worden, R.H., Meighan, I.G., 2000. Yttrium: The immobility-mobility transition during basaltic weathering. Geology 28 (10), 923-926.

Jun, C., Nianwen, L., Yang, C., Junfeng, J., Huayu, L., 2003. Variation of Zr/Rb ratios in the Chinese loess sequences during the last 130kyr and its implication for changes in winter monsoon strength. Congress of the International Union for Quaternary Research 16, 216.

Jun, C., Zhisheng, A., Yonghin, W., Junfeng, J., Yang, C., Hau, L., 1999. Distribution of Rb and Sr in the Luochuan loess-paleosol sequence of China during the last 800ka: Implications for paleomonsoon variations. Science in China Series D, Earth Science 42 (3), 225-232.

Kimoto, A., Nearing, M.A., Zhang, X.C., Powell, D.M., 2006. Applicability of rare earth element oxides as a sediment tracer for coarse-textured soils. Catena 65, 214-221.

Larue, D.K., Sampayo, M.M., 1990. Lithic-volcanic sandstones derived from oceanic crust in the Franciscan complex of California: 'Sedimental memories' of source rock geochemistry. Sedimentology 37, 879-889.

Laveuf, C., Cornu, S., 2009. A review on the potentiality of rare earth elements to trace pedogenetic processes. Geoderma 154, 1-12.

Laveuf, C., Cornu, S., Juillot, F., 2008. Rare earth elements as tracers of pedogenetic processes. Comptes Rendus Geoscience 340, 523-532.

Li, M., Zhu, L., Wang, J., Wang, L., Yi, C., Galy, A., 2011. Multiple implications of rare earth elements for Holocene environmental changes in Nam Co, Tibet. Quaternary International 236, 96-106.

Lianwen, L., Jun, C., Hongtao, W., Yang, C., 2001. A chemical index of weathering without effect of wind sorting: Fe/Mg ratios in the acid-insoluble phases of loess deposits. Chinese Science Bulletin 46 (16), 1384-1387.

Linn, A.M., DePaolo, D.J., 1993. Provenance controls on the Nd-Sr-O isotopic composition of sandstones: Examples from late Mesozoic Great Valley forearc basin, California. In: Johnsson, M.J., Basu, A. (Eds.), Processes Controlling the Composition of Clastic Sediments, vol. 284. Geological Society of America Special Paper, Boulder, Colorado, pp. 121-133.

Linn, A.M., DePaolo, D.J., Ingersoll, R.V., 1991. Nd-Sr isotopic provenance analysis of upper Cretaceous Great Valley fore-arc sandstones. Geology 19, 803-806.

Marbut, C.F., 1935. Atlas of American agriculture. Part III. Soils of the United States. Government Printer, Washington, D.C.

Maynard, J.B., 1992. Chemistry of modern soils as a guide to interpreting Precambrian paleosols. The Journal of Geology 100, 279-189.

McCarthy, P.J., Faccini, U.F., Plint, A.G., 1999. Evolution of an ancient coastal plain: Paleosols, interfluves and alluvial architecture in a sequence stratigraphic framework, Cenomanian Dunvegan formation, NE British Columbia, Canada. Sedimentology 46, 861-891.

Mertz, D.F., Weinrich, A.J., Sharp, W.D., Renne, P.R., 2001. Alkaline intrusions in a near-trench setting, Franciscan complex, California: Constraints from geochemistry, petrology, and $^{40}AR/^{39}AR$ chronology. American Journal of Science 301, 877-911.

Mikesell, L.R., Weissmann, G.S., Karachewski, J.A., 2010. Stream capture and piracy recorded by provenance in fluvial fan strata. In: Wilford, D., Giles, P., Nichols, G. (Eds.), Alluvial Fan Research and Management: From Reconstructing Past Environments to Identifying contemporary hazards, vol. 115 (3-4). Geomorphology, Exeter, UK, pp. 267-277.

Mills, H.H., Allison, J.B., 1995. Weathering and soil development on fan surfaces as a function of height above moern drainageways, Roan Mountain, North Carolina. Geomorphology 14, 1-17.

Mitchell, R.L., Sheldon, N.D., 2010. The ~1100 Ma Sturgeon Falls paleosol revisited: Implications for Mesoproterozoic weathering environments and atmospheric CO_2 levels. Precambrian Research 183, 738-748.

Moore, D.E., Liou, J.G., 1979. Mineral chemistry of some Franciscan blueschist facies metasedimentary rocks from the Diablo Range, California: Summary. Geological Society of America Bulletin Part I 90, 1089-1091.

Nesbitt, H.W., 1979. Mobility and fractionation of rare earth elements during weathering of a granodiorite. Nature 279, 206-210.

Nesbitt, H.W., Young, G.M., 1982. Early Proterozoic climates and plate motions inferred from major element chemistry of lutites. Nature 299 (5885), 715-717.

Nyakairu, G.W.A., Koeberl, C., 2002. Variation of mineral, chemical, and rare earth element composition of size fractions of clay-rich sediments from the Kajjansi and Ntawo Clay deposits, central Uganda. Chemie der Erde Geochemistry 62, 73-86.

Oze, C., Fendorf, S., Bird, D.K., Coleman, R.G., 2004. Chromium geochemistry in serpentinized ultramafic rocks and serpentine soils from the Franciscan complex of California. American Journal of Science 304, 67-101.

Panahi, A., Young, G.M., Rainbird, R.H., 2000. Behavior of major and trace elements (including REE) during Paleoproterozoic pedogenesis and diagenetic alteration of an Archean granite near Ville Marie, Québec, Canada. Geochimcia et Cosmochimica Acta 64 (13), 2199-2220.

Parker, A., 1970. An index of weathering for silicate rocks. Geological Magazine 107, 501-504.

Pearce, J.A., Cann, J.R., 1973. Tectonic setting of basic volcanic rocks determined using trace element analyses. Earth and Planetary Science Letters 19, 290-300.

Price, J.R., Velbel, M.A., 2000. Weathering of the Eaton Sandstone (Pennsylvanian), Grand Ledge, Michigan: Geochemical mass-balance and implications for reservoir properties beneath unconformities. Journal of Sedimentary Research 70 (5), 1118-1128.

Price, J.R., Velbel, M.A., 2003. Chemical weathering indices applied to weathering profiles developed on heterogeneous felsic metamorphic parent rock. Chemical Geology 202, 397-416.

Reheis, M.C., Budahn, J.R., Lamothe, P.J., 2002. Geochemical evidence for diversity of dust sources in the southwestern United States. Geochimica et Cosmochimica Acta 66 (9), 1569-1587.

Retallack, G.J., 1990. Soils of the Past: An Introduction to Paleopedology. Unwin Hynman, Inc., Winchester, Massachusetts. 520 pp.

Retallack, G.J., 2001. Soils of the Past: An Introduction to Paleopedology. Blackwell Science Ltd., Malden, Massachusetts. 404 pp.

Ruxton, B.P., 1968. Measures of the degree of chemical weathering of rocks. Journal of Geology 76, 518-527.

Schaetzl, R.J., Anderson, S., 2005. Soils: Genesis and Geomorphology. Cambridge University Press, New York. 817 pp.

Seiders, V.M., 1988. Origin of conglomerate stratigraphy in the Franciscan assemblage and Great Valley sequence, northern California. Geology 16, 783-787.

Seiders, V.M., Blome, C.D., 1988. Implications of upper Mesozoic conglomerate for suspect terrane in western California and adjacent areas. Geological Society of America Bulletin 100, 374-391.

Sheldon, N.D., Tabor, N.J., 2009. Quantitative paleoenvironmental and paleoclimatic reconstruction using paleosols. Earth-Science Reviews 95, 1-52.

Sreenivas, B., Roy, A.B., Srinivasan, R., 2001. Geochemistry of sericite deposits at the base of the Paleoproterozoic Aravalli supergroup, Rajasthan, India: Evidence for metamorphosed and metasomatised Precambrian paleosol. Procedures of the Indian Academy of Science: Earth and Planetary Science 110 (1), 39-61.

Taylor, A., Blum, J.D., 1995. Relation between soil age and silicate weathering rates determined from the chemical evolution of a glacial chronosequence. Geology 23, 979-982.

Thorpe, R.K., Isherwood, W.S., Dresen, M.D., Webster-Scholten, C.P., 1990. Remedial investigations report for the LLNL Livermore Site. Lawrence Livermore National Laboratory Report UCRL-AR-10299.

Trahan, R.S., 2003. Evaluating Geologically-Constrained Models with Pumping Tests in a Heterogeneous Alluvial Aquifer Helipad Site at Lawrence Livermore National Laboratory, California. MS Thesis, Michigan State University, East Lansing, Michigan, 264 pp.

Ufnar, D.F., Ludvigson, G.A., Gonzalez, L.A., Brenner, R.L., Witzke, B.J., 2004. High latitude meteoric delta ^{18}O compositions; Paleosol siderite in the middle Cretaceous Nanushuk formation, North Slope, Alaska. Geological Society of America Bulletin 116 (3-4), 463-473.

United States of America Environmental Protection Agency (USEPA), 1973. Fuel Regulations: Control of Lead Additives in Gasoline. Federal Regulation 38 (234), 33734 pp.

Utsunomiya, S., Murakami T., Nakada M., Kasama, T., 2003. Iron oxidation state of a 2.45-Byr-old paleosol developed on mafic volcanics. Geochimica et Cosmochimica Acta 67 (2), 213-221.

Velbel, MA., 1985. Geochemical mass balances and weathering rates in forested watersheds of the southern Blue Ridge. American Journal of Science 285, 904-930.

Velbel, M.A., Barker, W.W., 2008. Pyroxene weathering to smectite: Conventional and cryo-field emission scanning electron microscopy, Koua Bocca ultramafic complex, Ivory Coast. Clays and Clay Mineralogy 56, 111-126.

Velbel, M.A., Donatelle, A.R., Formolo, M.J., 2009. Reactant-product textures, volume relations, and implications from major-element mobility during natural weathering of hornblende, Tallulah Falls formation, Georgia Blue Ridge, USA. American Journal of Science 309, 661-688.

Vogel, D.E., 1975. Precambrian weathering in acid metavolcanic rocks from the Superior Province, Villebon Township, south-central Quebec. Canadian Journal of Earth Sciences 12, 2080-2085.

Vogt, T., 1927. Sulitjelmafeltets geologi og petrografi. Norges Geologiske Undersokelse 121, 1-560 as seen in Chittleborough, D.J., 1991. Indices of weathering for soils and palaeosols formed on silicate rocks. Australian Journal of Earth Science 38, 115-120.

Weissmann, G.S., 2001. Geologic characterization of the Helipad Site (TFD), Lawrence Livermore National Laboratory, California. Report for subcontract number B503482, Michigan State University, East Lansing, Michigan, 65 pp.

Whitmore, G.P., Crook, K.A.W., Johnson, D.P., 2004. Grain size control of mineralogy and geochemistry in modern river sediment, New Guinea collision, Papua New Guinea. Sedimentary Geology 171, 129-157.

Willis, S.S., Johannesson, K.H., 2011. Controls on the geochemistry of rare earth elements in sediments and groundwaters of the Aquia aquifer, Maryland, USA. Chemical Geology 285, 32-49.

Winchester, J.A., Floyd, P.A., 1977. Geochemical discrimination of different magma series and their differentiation products using immobile elements. Chemical Geology 20 (4), 325-343.

Yaalon, D.H., 1971. Soil-forming processes in time and space. In: Yaalon, D. H (Ed.), Paleopedology: Origin, Nature and Dating of Paleosols, Jerusalem, Israel, 27-39.

Yancey, T.E., Lee, J.W., 1972. Major heavy mineral assemblages and heavy mineral provinces of the central California coast region. Geological Society of America Bulletin 83, 2099-2104.

Young, G.M., 1999. A geochemical investigation of paleosols developed on Lewisian rocks beneath the Torridonian Applecross formation, NW Scotland. Scottish Journal of Geology 35 (2), 107-118.

CHAPTER 5

Development and Application of an Index to Assess the Development of Buried Paleosols Above the Springtown Anticlines in the Livermore Basin, California

1. Introduction

Quantification has long been practiced to provide summary numeric values for physical phenomena, allowing for comparisons among them. Many disciplines of science have found indices and scales to be valuable tools. Geologists use quantification techniques in the study of mineral weathering (e.g., Parker, 1970; Nesbitt and Young, 1982; Harnois, 1988; Chittleborough, 1991), sandstone maturity (Hubert, 1962), volcano explosivity (Newhall and Self, 1982), and bituminous coal development (Bonnett et al., 1991). Even cosmologists use an index when studying solar flare strength (Sawyer, 1967). The commonality of these tools is that they are all based on mathematical formulae that allow calculations to be made from semi-quantified (or ordinally classified) descriptions of an array of characteristics. The calculated values, i.e., the indices derived from these data, may then be rigorously compared.

In soil science, numerical indices have also been developed to compare soils, and their degrees of development, to each other. For example, pedological features such as strength of podzolization (Schaetzl and Mokma, 1988), a soil's natural drainage characteristics (Schaetzl et al., 2009), rubification (Markovic et al., 2009), color development (Buntley, 1965), color to represent wetness and aeration (Evans and Franzmeier, 1988), soil quality (Jimenez et al. 2002; Chaer et al., 2009), soil shrink-swell potential (Thomas et al., 2000), and textures associated with chemical weathering (Torrent and Nettleton, 1979) have all been indexed. Pedogenic data, when combined into indexes such as these, are also useful for estimating the age of the soils or surfaces that the soils have formed in (e.g., Harden and Taylor, 1983; Harden, 1990; Tsai et al., 2007; Lewis et al., 2009). To date, these indices have been developed for, and applied to, surface soils. That is, such quantification techniques do not yet exist for the rigorous comparison of buried paleosols and paleosol characteristics. The purpose of this paper is to present a new index of paleosol development based on paleopedological features, which will facilitate comparisons among buried paleosols. Particularly, this index can be applied to paleosols that are observable only in cores, i.e., for which full exposure does not exist. I intend to demonstrate its application by comparing buried paleosols of varying degrees of development and relating that variability to structural features in a tectonically active California basin.

2. Study Area

The Lawrence Livermore National Laboratory (LLNL) provides an excellent setting in which to study paleosol development in a tectonically-active basin which exhibits variable subsidence rates. The Lawrence Livermore National Laboratory is a 2.6 km^2 site located in the southeastern portion of the Livermore Basin, 65 km east of San Francisco, CA (Figure 305). The basin is an east-west topographical and structural depression within the northwest-trending central Coast Range. It is about 25 km long, 11 km wide, and is underlain by up to 1200 m of mainly continental Tertiary and Quaternary deposits (Carpenter et al., 1980, 1984). It is bordered on the east by the Greenville Fault, which is located at the western base of the Altamont Hills, and to the west by the Calaveras Fault, both of which are right-lateral, northwest-trending transpressional faults (Herd, 1977; Dibblee, 1980a, 1980b; Barlock, 1989; Andersen et al., 1995; Graymer et al., 1996). On the north, the basin is bordered by the Mount Diablo antiform, on the southwest by the Verona Thrust Fault (Unruh and Sawyer, 1997), and on the southeast by the Las Positas Fault, a left-lateral, northeast-trending fault. The Las Positas Fault consists of two splays, a northern and a southern branch, that terminate to the east at the Greenville Fault (Herd, 1977; Dibblee, 1980b; Graymer et al., 1996). The Livermore Basin is currently undergoing

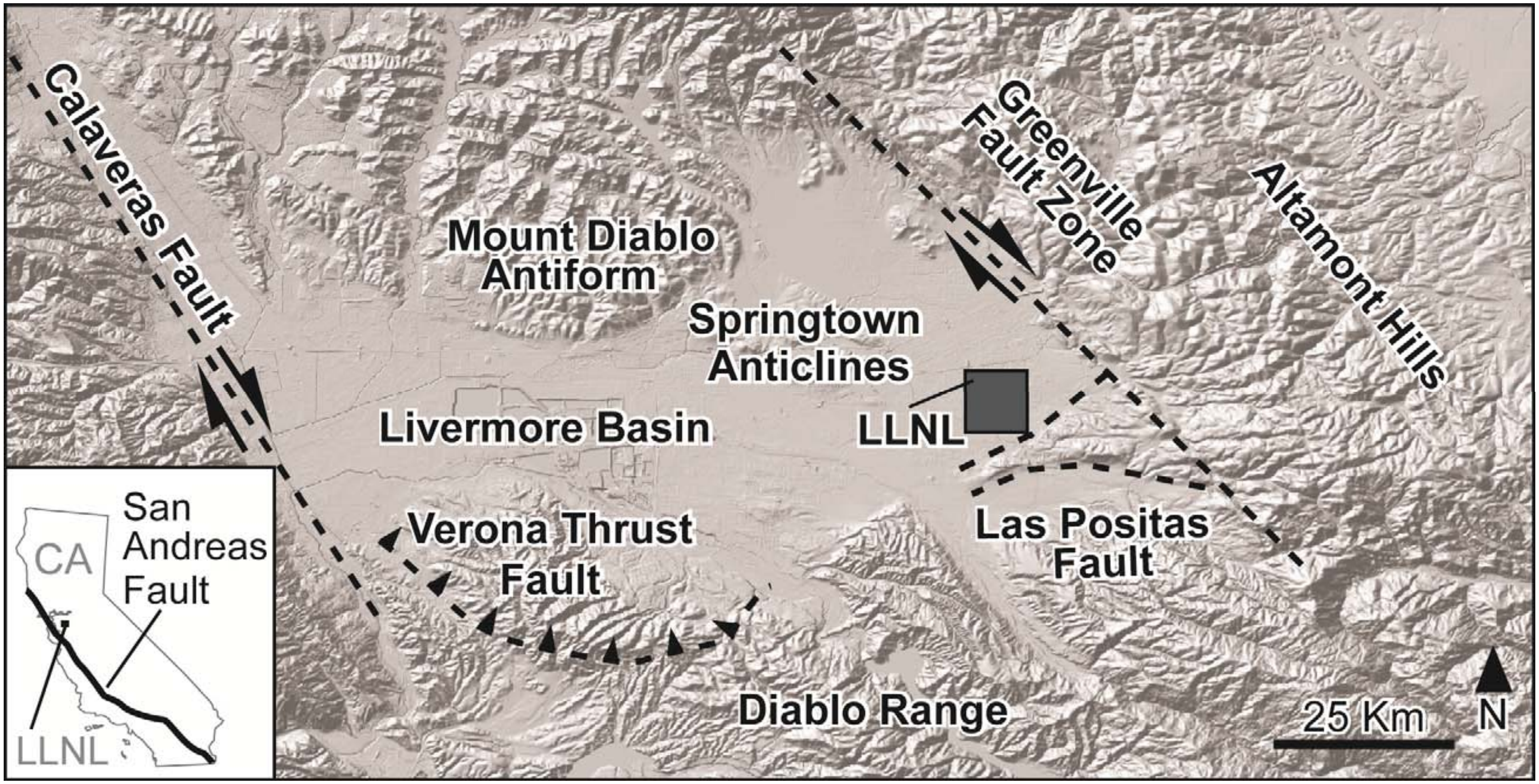

Figure 305. A 10 m DEM hillshade of Livermore Basin with bounding features labeled. The location of Lawrence Livermore National Laboratory is indicated by the dark square.

basin inversion that is changing from an extensional regime with subsidence to localized uplift due to compression (Followill and Mills, 1982; Stokes, 2008 and references therein). In order to accommodate the regional northeast-southwest shortening, the Livermore Basin block is undergoing compressional deformation as shown by thrust faults and fold features (Followill and Mills, 1982; Unruh and Sawyer, 1997). This deformation can be seen in surficial features such as the Springtown anticlines northwest of LLNL and the Las Positas Fault uplift south of LLNL.

The Livermore Basin is an aggrading landscape due to the overall net subsidence in the basin. However, the subsidence rate varies within the basin due to structures that are deforming to accommodate compressional tectonic stresses (Unruh and Sawyer, 1997). For example, the Springtown anticlines are a local structural feature accommodating those stresses (Unruh and Sawyer, 1997). These anticlines are southeast-plunging Quaternary folds (Sawyer, 1999) that are expressed as a pair of low-amplitude hills located three km northwest of LLNL (Unruh and Sawyer, 1997; Sawyer, 1999). Because the anticlines plunge to the southeast, they have no surficial topographic expression at LLNL. However, their deformation allows for varied subsidence rates locally at LLNL. Subsidence rates are greater over the syncline as opposed to over the anticlines, even though both regions are subsiding overall. As a result, the stratigraphic relations are expected to be different over the anticline versus the syncline. Analysis of core data from LLNL shows that the greater subsidence over they syncline has resulted in coarser-grained and thicker sedimentary units than in cores recovered from areas above the anticline.

LLNL is located on a 7 km^2 Quaternary-aged fluvial fan that was deposited by two intermittent streams (Figure 306). The Arroyo Seco - one of the two streams - drains the Altamont Hills to the southeast of LLNL. It enters the Livermore Basin from the southeast and

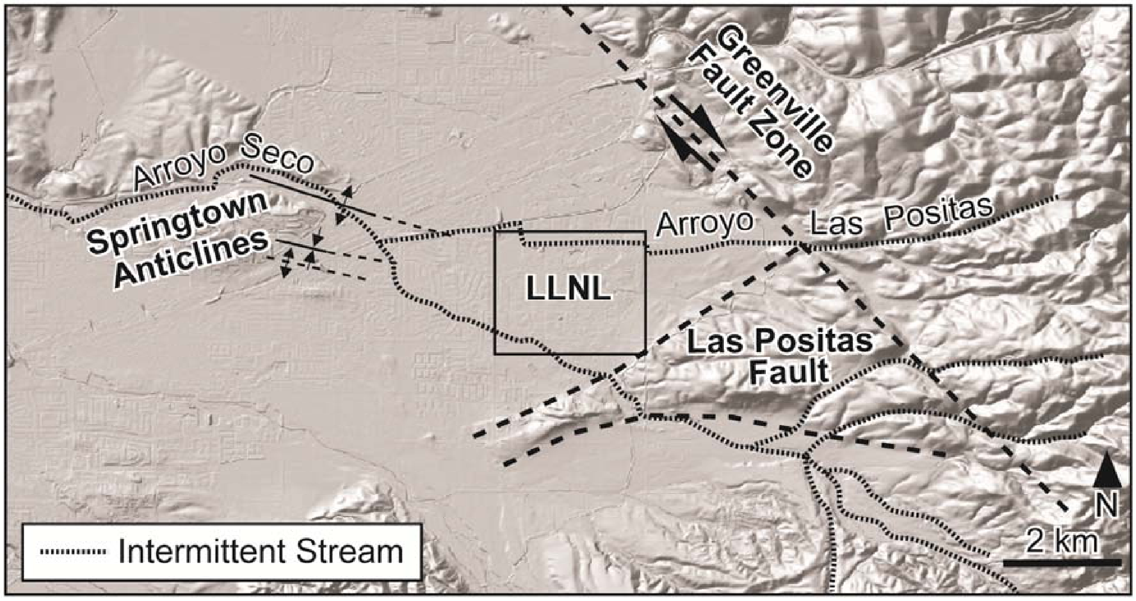

Figure 306. A 1/9 arcsec DEM of the southeastern portion of the Livermore Basin with the locations of LLNL, Arroyo Seco, and Arroyo Las Positas indicated. The Springtown anticlines are indicated with solid lines where they are mapped, and dashed lines where the plunging structures are inferred (Unruh and Sawyer, 1997).

flows to the northwest across the southwestern portion of LLNL. The second stream is the westerly-flowing Arroyo Las Positas, which enters the basin east of LLNL. The Arroyo Las Positas once flowed across the northeastern portion of LLNL, but is currently not free-flowing and has been directed around the northern side of LLNL. These two streams deposited at least 60 m of fluvial fan and alluvial sediments beneath LLNL (Mikesell et al., 2010) since the late Pliocene (Herd, 1977).

3. Soils and Paleosols

3.1 Soil Development

Soils can form when a natural body of unconsolidated mineral and organic matter is altered by environmental factors of parent material, climate, organic additions, and topography over time (Schaetzl and Anderson, 2005). Other factors such as, but not limited to, eolian dust, acid rain, and fire will also affect the development of a soil locally (Schaetzl and Anderson, 2005). Soils form best and most rapidly on stable land surfaces, and when sufficient time is provided for the soil-forming factors to interact and act on sediment. Due to the interactions of the five soil-forming factors and the varying stabilities of land surfaces, soils vary in degree of development across the landscape, and therefore reflect their developmental environment. A well-developed soil is one that has had sufficient time and surface stability for its features to develop and be strongly expressed.

Knowing that soil development varies on surfaces of different geomorphic stabilities, differential soil development can also be linked to the development of structural features in a tectonic basin, as it is associated with relative subsidence rates within that basin (Alonso-Zarza et al., 1999). Soils on geomorphically stable surfaces will generally be better developed than soils on an unstable surface. Anticline surfaces may be stable, unless erosional processes can strip the uplifted surface of sediment and possibly eroded some of the soils there. However, if an anticline is forming syndepositionally and keeping pace with sediment accumulation, surficial erosion on the anticline may be minimal (Bridge and Leeder, 1979), and may not be reflected in soil development.

It is possible for structures to form at the same rate as subsidence. A syncline forming at the same rate as subsidence could increase the rate of local subsidence creating sediment accumulation space (Table 6) and affect the overlying stratigraphy and soil development by affecting the flow paths for streams (Bridge and Leeder, 1979). An anticline forming at the same rate as subsidence could place the crest of the anticline at the same position relative to the land surface for the duration of formation. When this happens, the rate of sediment accumulation is slow and the geomorphic surface is relatively stable allowing for long periods of soil

Table 6. Subsidence rate and the formation of structural features

Structural Feature	Structure Development with Rapid Subsidence	Structure Development with Slow Subsidence
Anticlines	Anticlines will: • not reach land surface • will remain buried • accommodation space will be created even with uplifting anticline	Anticlines will: • be positive relief Anticline development may keep pace with subsidence • crest will stay in relative position to land surface • stable land surface
Synclines	Synclines will: • topographic low • fill but not completely • accommodation space will be created rapidly	Synclines will: • topographic low • may fill completely • sedimentation may keep pace with accommodation space creation

development (Table 6). At LLNL, such an anticline does exist. Here the buried feature is not expressed on the surface but it exists in the subsurface.

Soil development varies across anticlinal and synclinal surfaces largely because of the varying amounts of surface stability they create (Table 7). Generally, on aggrading surfaces, surface soils commonly get buried before they can attain strong development, whereas on eroding surfaces soils often get eroded, reducing the likelihood of their burial and preservation as paleosols. Geomorphic instability represents periods of either increased deposition or erosion, when soil development is inhibited. Instability as a result of increased deposition is due to high sedimentation rates on the geomorphic surface that out-pace pedogenic processes, which transform the new sediment into soil, and bury any preexisting soils. Instability as a result of erosion results in a loss of soil due to removal of material and also inhibits soil development.

Table 7. Comparative soil development on geologic structural features

Soil Development on a Rapidly-Forming Structure	Soil Development on a Slowly-Forming Structure
Rapidly-forming anticlines: • uplifted surfaces • increased erosion • relatively unstable • pedogenesis is inhibited, and thus, soils are either minimally developed or lost due to erosion • few buried soils	Slowly-forming anticlines: • uplifted surfaces • some erosion • relatively stable • pedogenesis may keep pace with erosion, allowing for longer periods of pedogenesis and better-developed soils • buried paleosols can occur
Rapidly-forming synclines: • downwarping surfaces • rapid sedimentation • pedogenesis is inhibited and soils get buried • many buried paleosols	Slowly-forming synclines result: • downwarping surfaces • intermittent periods of sedimentation • pedogenesis may keep pace with sedimentation, resulting in moderately-well developed soils • few buried paleosols

3.2 Soil Development Index

Perhaps the most widely accepted and used index in soil science is the Profile Development Index (PDI), of Harden (1982). She developed this quantitative index to compare the degree of soil profile development in a chronosequence of soils in central California. The PDI was designed to convert soil property data, as described in the field, into an index that could be used to evaluate the development of a soil profile relative to its parent material. It provides a numeric value for degree soil development, thereby facilitating quantitative comparisons between soil profiles. The PDI assumes that soil properties get increasingly strong as they develop, i.e., as time passes.

Harden (1982) evaluated eight soil properties for the index: 1) clay morphology, 2) texture plus wet consistence, 3) rubification (color and hue), 4) structure, 5) dry consistence, 6) moist consistence, 7) color value, and 8) pH. Other properties can be added to this index, if desired. And not every property need be used to calculate the index.

Every horizon, as well as the parent material, is assessed and given a value for each of the eight (or more, or less, at the discretion of the user) soil properties. Given that soil properties change as the soil develops, the assessed values are assigned to each property within the horizon based on the amount of change from the parent material that has occurred. The data are then normalized to ensure that the value of any one property will represent a similar degree of soil development to any other property and the resulting index will not place undue emphasis on any one property. Normalization is done by dividing the assessed value by the maximum value allowed for that property. After the property values for each horizon are normalized, a Horizon Index (HI) value is calculated for each horizon by summing all the normalized property values, and then dividing this sum by the number of properties evaluated. Dividing the sum by the number of evaluated properties ensures that any missing (or deliberately excluded) data will not affect the overall HI value. The HI for each horizon is then multiplied by the horizon thickness in centimeters to provide an index-cm of development. The final step in calculating the PDI involves summing the index-cm of all horizons in the profile to arrive at a total value for the profile. This final value is the PDI, which provides a quantitative value of development for the entire profile, taking into consideration multiple properties.

3.3 Paleosol Development

A paleosol is a soil that formed on a landscape in the geologic past (Ruhe, 1965), and is usually buried (Johnson, 1998). Retallack (2001) augmented Ruhe's traditional definition to include the statement that a paleosol is the remains of an ancient soil that has been buried, and is no longer forming in the same way as it once did. The study of paleosols is called paleopedology, the theory and applications of which can provide valuable tools to help with interpreting paleoenvironments. Paleosols in the sedimentologic record indicate times when the surface they formed on was stable and subaerial for a period of time long enough for a soil to have formed (Ruhe et al., 1971; Schaetzl and Anderson, 2005). Areas of non-soil, or depositional sequences between paleosols, represent times of geomorphic instability. At such times, surface soils could have been buried or eroded, depending on the local site conditions; both situations imply instability on the landscape (Schaetzl and Anderson, 2005).

Structures in a basin will affect the surface stability and hence, soil development. In a basin undergoing net aggradation, buried soils can be expected as a result. Paleosol distribution within a basin will be affected by forming structures (Table 8) just as structures affect soil development (Table 6) (Alonso-Zarza et al., 1999). Paleosols will be more numerous in regions of the basin that are relatively more stable for longer periods of time, thus allowing soils to develop. Paleosols will be less numerous in regions of the basin where soils are unable to form either due to high sedimentation rates or high erosion rates.

Table 8. Theoretical matrix showing paleosol distribution affected by development on geomorphically stable or unstable regions

Degree of Paleosol Development	Many Buried Paleosols	Few Buried Paleosols
Well-Developed Paleosols	Indicate: • relatively stable region • occasional sedimentation events • sufficient time for soil development between sedimentation events	Indicate: • relatively stable region • few sedimentation events • sufficient time to become well-developed before being buried Alternatively: • an unstable region experiencing erosion • soil development keeps pace with erosion producing well-developed soils
Poorly-Developed Paleosols	Indicate: • relatively unstable region • frequent sedimentation events • insufficient time for soil development between sedimentation events	Indicate: • an unstable region experiencing erosion • erosion removes material, not allowing soils to become well-developed

3.4 Well Core Descriptions at Lawrence Livermore National Laboratory

As part of an ongoing groundwater remediation project, LLNL personnel have collected over 12 km of core from over 500 wells from LLNL and the immediate vicinity. For this study, 6.7 km of core, either three or five inches in diameter, from 202 of those wells, were described in detail. The cores were split length-wise to expose a fresh surface for visual inspection and description. Seven basic facies were described within the LLNL well cores: paleosol, silty sand, silty sand with lamellae, sand, clast-supported gravel, matrix-supported gravel, and the clay-rich aquitard, locally named the “Lower Livermore” (Table 9).

Table 9. Facies described in LLNL well cores with interpreted depositional environments

Facies	Description	Interpretation
Paleosol	Moderate- to well-sorted, silt- to medium-grained sand, exhibiting pedogenic characteristics (e.g., root traces, burrows, argillans, carbonate accumulations, soil structural units, manganese oxide concentrations)	Soils that were at one time on the landscape surface, but have since been buried
Silty sand	Poorly-sorted, silt- to fine-grained sand, angular to subangular grains, massive, no discernable structural soil units	Floodplain deposits
Silty sand with clay lamellae	Silty sand facies interbedded with darker, clay-rich lamellae	Crevasse splay and floodplain deposits
Sand	Well- to moderately well-sorted, medium- to coarse-grained sand, subangular to subrounded grains, units were often friable	Sand bar and point bar deposits
Clast-Supported Gravel	Very poorly-sorted, sand to coarse gravel, angular to rounded, clast-supported with fine-grained matrix	Channel deposits
Matrix-supported gravel	Very poorly-sorted, angular to rounded, matrix-supported with clay-rich matrix	Apex of fan, result of mass movement or hyperconcentrated flow
"Lower Livermore" (local nomenclature)	Below the fluvial fan and the lower boundary of fan system, clay-rich aquitard with dense bluish-green to blue-black clay beds, often exhibited very thick carbonate accumulations	Playa lake with reducing conditions resulting in the bluish color due to reduced iron

3.5 Lawrence Livermore National Laboratory Paleosols

A paleosol classification system was developed for this study based on the presence of a combination of pedogenic features (Table 10). The features described from the LLNL site well cores were ordinally categorized and ranked by degree of expression. Root traces were noted and the rare animal burrow was measured and documented. The relative degree of clay translocation was determined by examining argillans with a hand lens and determining their morphology (i.e., thin, thin to moderate, moderate, moderate to thick, thick, and very thick). This distinction is important because argillans thicken with soil development (Holliday, 1988).

Table 10. Criteria used for paleosol determination

Paleosol Characteristic	Description of Variability
Biogenic Features	• Root traces • Animal burrows
Clay Argillans	• Thin • Thin to Moderate • Moderate • Moderate to Thick • Thick • Very Thick
Carbonate Accumulation	• Stage I - diffuse to few thin filaments • Stage I+ - many filaments • Stage II - many filaments and small nodules • Stage II+ - large nodules and filled root traces • Stage III - core-diameter nodules to cemented core
Soil Structural Units	• Massive • Prismatic – slight/weak or prominent • Subangular – slight/weak or prominent • Blocky – slight/weak or prominent • Platy – slight/weak or prominent
Manganese Oxide Concentrations	• Small Concentrations • Large Concentrations • Root-Filling • Ped-Coating

The amount of carbonate accumulation was recorded using the classification scheme, or Stages, of Gile et al. (1966). Carbonate coatings, like argillans, increase as soils develop (Machette, 1985). Soil structural units, or peds, when present, were noted as slight/weak or prominent. If no structures were noted, the core was described as massive. When present and clearly observable, the type of ped shape was also noted (i.e., prismatic, subangular, blocky, or platy).

Soil structural units do not necessarily progress from one form to another with soil development. The form of the ped is dictated more by the arrangement of the material present, particle size, and/or the moisture regime than by duration of soil development (Birkeland, 1999; Schaetzl and Anderson, 2005). Manganese oxide concentrations in LLNL well cores were noticeably larger and more common in paleosol sequences than in other core material, and thus, were assumed to be indicative of a paleosol. They were noted as small or large concentrations, root-fillings, and ped-coatings.

Assessing paleosol development is difficult when using well core material because a well core provides only a three-inch diameter cylinder of soil or sediment. As a result, without the benefit of a fully-exposed soil pit, critical information may be missed that would aid in fully assessing the degree of paleosol development. Nonetheless, some degree of assessment of paleosol development is possible, even with this limited amount of material.

The drilling process that collects the well cores may also result in the physical loss of core material. At LLNL, some intervals of cored stratigraphic sections were not available to us because some of the unconsolidated material fell from the core barrel. When working with paleosols, particularly ones from well cores, the material preserved provides all the data available for assessment and some evidence may be missed.

Several qualifiers must be considered when studying paleosol development, particularly for paleosols studied from well cores. Determining horizonation within the paleosol is sometimes difficult, depending on the type of soil. Cumulic paleosols generally possess no distinct horizons, making development based on soil properties within horizons difficult to assess. In addition to their often indistinguishable horizons, the paleosols are often not entirely preserved. It is common for the paleosol to have been truncated, having lost the upper portion of the profile (where soil features are most strongly-expressed) prior to burial; these situations result in incomplete data.

While describing well cores at LLNL, workers noticed that paleosols over the plunging Springtown anticlines were more numerous and more strongly-developed than those over the adjacent plunging syncline. Knowing that soils develop on stable land surfaces, it seemed both possible and likely that surface soils, and hence the paleosols below, would be stronger above the relatively stable anticlines, as opposed to the downwarping and more rapidly subsiding syncline with its enhanced production of accommodation space and consequent greater rates of sediment aggradation (Table 6). The syncline would have been the preferred pathway for the Arroyo Seco to cross the southern portion of the Livermore Basin, and thus a more constant supply of alluvium would have been directed through the syncline (Potter, 1978; Bridge and Leeder, 1979). Alluviation above the syncline would have introduced new sediment at a rate that would have inhibited surface soil development and buried the soils there. As a result, that region would have fewer and more poorly-developed paleosols with thicker layers of intervening sediment than in the region above the anticline (Table 8). I assumed that an index of paleosol development could help determine whether a difference in paleosol development – and hence, landscape stability - existed between the region above the anticlines and the region above the syncline. As a result, I developed the Index of Paleosol Development (IPD).

4. Development of the Index of Paleosol Development (IPD)

Most soil development indices are based on the premise that soil properties vary not only among horizons, but also from the parent material. The paleosols at LLNL were likely accumulative hydromorphic soils. These soils form in alluvium and are immature, lacking distinct horizons due to aggradational sedimentation (Reading, 1996). Because the paleosols observed at LLNL did not exhibit distinguishable horizons that could be individually described, calculating Harden's (1982) PDI was difficult, if not impossible.

In order to calculate the PDI, soil horizon data are compared to the unaltered parent material. However, at the LLNL site, parent material below the paleosols may also have been altered after burial due to diagenesis. Also, the paleosols may have formed in a parent unlike that of the sediment below, and from core data only, this would have been difficult to determine.

Until now, all soil development indices were derived for use on fully described surface soils, or at the very least, soils that are intact, i.e., not eroded. Even paleosols that have distinguishable horizons – for which a PDI can be determined - may have been truncated due to erosion prior to burial. As a result, use of the PDI in its traditional form may provide skewed results due to the loss of important portions of the profile. Due to the differences between paleosols and soils (e.g., discernable horizons, complete profiles, and parent material), which affect the outcome of the PDI calculation, a new index, one developed specifically for paleosols in well cores, was deemed necessary.

The primary consideration in developing a paleosol development index was choosing the correct pedogenic features to evaluate that would provide results that accurately reflect the degree of soil development for the paleosols at LLNL. In order to accurately evaluate the LLNL paleosols and their development, pedogenic conditions of the Livermore Basin need to be studied, including present soils and environmental conditions.

4.1 Livermore Basin Climate

The Livermore Basin has a typical Mediterranean climate, with cool, wet winters and warm-hot, but dry, summers. The annual average temperature for the City of Livermore ranges between 13 – 16.5ºC with the mean maximum temperature of 30ºC occurring in July and the mean low temperature of 4ºC occurring in January (Soil Survey Staff, 1966). Livermore is a semi-arid region having an average annual precipitation of 370 mm, with the rain mainly occurring during the winter months and very little to no precipitation during the summer (Soil Survey Staff, 1966). The winter rain saturates the soil to the bottom of the root zone; however, summer warmth and drought exhaust the stored moisture (Soil Survey Staff, 1966).

4.2 Livermore Basin Soils

Mediterranean climate soils typically have low organic matter content and tend to be reddish in color (Sauer, 2010). Carbonate-rich soils tend to occupy eroded positions on the landscape in drier areas within the climate regime (Sauer, 2010). Most soil groups within the Mediterranean climate are characterized by clay translocation (Sauer, 2010).

The soils in and around LLNL are dominated by the Yolo – Pleasanton and Positas – Perkins soil associations on terraces, alluvial fans, and floodplains. (Soil Survey Staff, 1966). A full description of the soil series in the associations is provided in Appendix D. The associations are typified by Entisols, Inceptisols, and Alfisols, forming in a xeric soil moisture regime, and are fine-silty and fine-loamy particle size families. In line with other reported Mediterranean climate soils (Sauer, 2010), the soils in the Yolo – Pleasanton and Positas – Perkins associations are carbonate- and clay-rich.

4.3 Choosing Soil Properties for Evaluation

Four features that normally increase in soils as they develop, and which are commonly associated with soil development in the region (Table 10), were chosen for the Index of Paleosol Development (IPD): 1) thickness of argillans, 2) degree of carbonate accumulation, 3) manganese oxide content, along with 4) presence of soil structural units. Argillans and carbonate accumulations were chosen because the modern soils in and around LLNL contain both illuvial carbonates and clay (Soil Survey Staff, 1966). It is assumed that the soils of the recent past were similar in development to the present soils, and therefore should have developed the same general types of pedogenic features. Additionally, argillans and carbonates are relatively persistent after burial (Yaalon, 1971). Although some soil features are easily altered upon burial of a soil (e.g., mottles, spodic horizons, mollic horizons), argillic (i.e., clay-rich) and calcic horizons are relatively persistent (Yaalon, 1971). Yaalon (1971) defined relatively persistent features as those features that are slowly adjusting, generally requiring more than 1,000 years to reach steady state with respect to new conditions, and are metastable after burial. He explained that semi-arid soils act as sinks for these materials, and thus, these kinds of accumulations rank among the best indicators of pedogenic processes. Most importantly, after argillic and calcic horizons develop, they will generally persist in buried paleosols.

The other two features chosen for this index (soil structural units and manganese oxide concentrations) are also clearly observable in the core paleosols. Soil structure becomes more pronounced with soil development and can generally be used to indicate degree of soil development. The prominence of strong ped development and soil structure indicates a strongly developed paleosol. The size of manganese oxide concentrations was observed to generally increase proportionally with increasing argillan thickness, and therefore also probably correlate to strength of development. Neither soil structures nor manganese oxide concentrations are considered persistent features by Yaalon (1971), and as a result, I placed more emphasis on argillan thicknesses and carbonate accumulations in the development of the CIPD. Nonetheless, in this dry, xeric environment, these types of features may persist in buried paleosols.

5. Calculation of the Index of Paleosol Development

The Index of Paleosol Development (IPD) was designed to provide a numeric value that reflects the overall degree of paleosol development, as observable within a well core. Like all soil development indices, it provides data that can be used to compare and contrast paleosol development. The index is based on assessing the strength of development for each individual paleosol within a well core The process involves calculating a value for each paleosol within a well core based on the degree of expression of paleosol properties. The IPD values from each individual paleosol within a well core are then used to calculate the Core Index of Paleosol Development (CIPD), which is a value representative of the average strength of paleosol development with the entire core. The CIPD values may then be compared to one another to determine relative degree of paleosol development among cores from a region.

5.1 Calculation of the Index of Paleosol Development (IPD)

Calculating the IPD is accomplished by first assigning an allowable minimum and maximum value for each of the four assessed soil properties based on the maximum number of subcategories represented in each feature's development. After the minimum and maximum allowed values are set, the range is divided by the number of developmental stages represented within LLNL paleosols (Table 11). A numerical, but ordinal, value is then assigned to each assessed feature within each paleosol unit. Because individual horizons were not observed in the LLNL paleosols, each paleosol is treated as a single unit and assessed as such.

Table 11. Values assigned to each qualitatively assessed feature found in buried paleosols from LLNL

A = Argillan thickness

Qualitative Assessment	Value Assigned	Maximum Value
Thin	1	3.5
Thin to moderate	1.5	
Moderate	2	
Moderate to thick	2.5	
Thick	3	
Very thick	3.5	

C = Carbonate accumulation

Qualitative Assessment	Value Assigned	Maximum Value
Stage I	1	3
Stage I+	1.5	
Stage II	2	
Stage II+	2.5	
Stage III	3	

S = Soil structural units or ped

Qualitative Assessment	Value Assigned	Maximum Value
None observed	0	1
Weak or slight	0.5	
Structure present	1	

M = Manganese oxide concentration

Qualitative Assessment	Value Assigned	Maximum Value
Small concentrations	1	2
Large concentrations	1.5	
Filling root traces	1.5	
Coating soil structure faces	2	

The IPD is then calculated for each paleosol within the well core using the following formula:

$IPD = (A + C + S + M) * T$

A = (assessed argillan thickness value / maximum argillan value) * 2

C = (assessed carbonate accumulation value / maximum carbonate value) * 1.5

S = assessed soil structural unit value / maximum soil structural unit value

M = assessed manganese oxide concentration value / maximum manganese value

T = thickness of paleosol unit in centimeters

Dividing the feature's assessed value by the maximum value normalizes the value with regards to the other features being evaluated. Like in Harden's (1982) PDI, normalization also provides a number between 0 and 1, which equates to a percentage of the most strongly developed feature. Argillan and carbonate calculations include multipliers (2.0 and 1.5, respectively) that placed more emphasis on these features as defining features of the paleosols at LLNL. These weighting values are a departure from the PDI formula (Harden, 1982), and reflect the feature's importance in paleosol recognition because of their persistence and value as indicators of preexisting soil development (Yaalon, 1971). At LLNL, IPD values range from 49 to 2427 with an average value of 495.

5.2 Calculation of the Core Index of Paleosol Development (CIPD)

After an IPD is calculated for each paleosol, the Core Index of Paleosol Development (CIPD) is determined for each well core, using the following formula:

$$CIPD = (\sum IPD / L) * 100$$

L = total length of described well core in centimeters

By dividing the sum of IPD values by the total length of described well core, the CIPD provides a value that presents a weighted average of the amount of paleosol material in the core based on the strength of development of the individual paleosols. The 100 value is used as a multiplier, to make the final CIPD a whole number. At LLNL CIPD values ranged from 4 to 188 with and average value of 55. The CIPD provided each well core with a numeric value, representative of the amount of paleosol material in a core and their average strength of development throughout the whole well core. These data could be compared to other well cores in the region.

5.3 Interpreting the IPD and CIPD values

IPD and CIPD data provide a means by which the paleosols in the well cores could be compared. A schematic representation of the interpretation of IPD and CIPD values is presented in figure 307. A high IPD value indicates a strongly-developed paleosol and a low IPD value indicates a weaker paleosol. Well cores containing at least one strongly-developed paleosol will have a high maximum IPD value, whereas a low maximum IPD value indicates that the core contains only poorly-developed paleosols. High CIPD values indicate well cores with a high

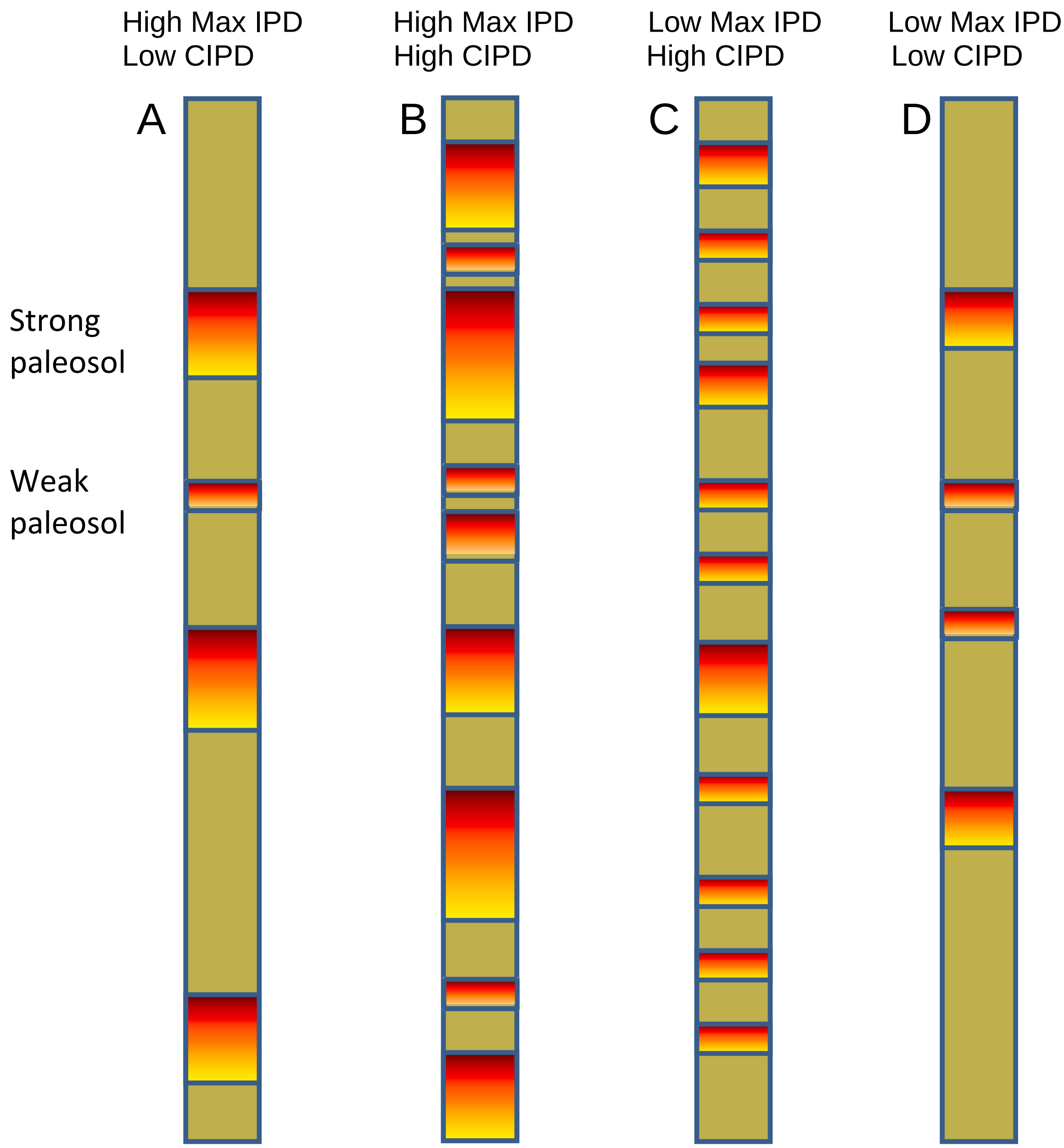

Figure 307. A schematic representation of the interpretation of IPD and CIPD values.

percentage of paleosol material. Cores with high CIPD values can contain many paleosols (Figure 307, Column C) or perhaps less paleosols, but of generally stronger development (Figure 307, Column B). Low CIPD values indicate well cores with a lower percentage of paleosol material. Wells with low CIPD can consist of either a few well-developed paleosols (Figure 307, Column A) or few weakly developed paleosols (Figure 307, Column D), although the latter will generally have lower CIPD values. The highest CIPD values are from well cores with the combination of a high percentage of paleosol material and in which, the paleosols are strongly-developed (Figure 307, Column B). The lowest CIPD values are from well cores with the combination of a low percentage of paleosol material, in which the paleosols are often weakly-developed (Figure 307, Column D).

Several factors affect pedogenesis and in turn affect the IPD and CIPD values (Table 12). Sufficient time and a stable surface are needed for soil development; and structures affect the stability of a land surface.

Table 12. Interpretation of IPD and CIPD values.

Index	High Value	Low Value
IPD	High IPD values indicate: • well-developed soils High IPD values would be found on relatively stable surfaces	Low IPD values indicate: • poorly-developed soils Low IPD values would be found on relatively unstable surfaces
CIPD	High CIPD values: • wells may contain many weak to moderately well-developed soils (Figure 307, Column C) • wells may contain very well-developed soils (Figure 307, Column B) • result from higher IPD values High CIPD values would be found on: • relatively stable surfaces • e.g., the region above anticlines experiencing slow differential deformation and subsidence relative to adjacent synclines	Low CIPD values indicate: • wells may contain weakly-developed (Figure 307, Column D) • wells may contain few moderately-well developed (Figure 307, Column A) • result from predominately low to very low IPD Low CIPD values would be found on: • relatively unstable surfaces • e.g., the region above synclines, and downwarped or sloped surfaces

6. GIS Analysis

Kriging is a geostatistical modeling tool (Matheron, 1963; Isaaks and Srivastava, 1989). Four different kriged maps were created using the geostatistical wizard module of ArcGIS (ESRI, 2010). The minimum number of neighbors used in this modeling was 12 and the maximum number of neighbors was 15. The isolines were clipped to the approximate extent of the well spacing so that the presented kriged model did not extrapolate isoline data beyond the extent of the well study area. The kriged maps were then paired to a digital elevation model (DEM) of the southeastern portion of the Livermore Basin. Kriged maps were made for maximum IPD (or strongest paleosol in each well) and CIPD data. In addition to mapping the maximum IPD and CIPD values, maps were developed to show the percentage of each well core that was categorized as paleosol, and the percentage that was categorized as gravel. On all of the kriged maps, the warmer-colored isolines indicate higher values and the cooler-colored isolines indicate lower values.

7. Results

Kriged maps of IPD and CIPD data for the study area suggest that paleosols are more strongly developed and more numerous in the northwestern portion of LLNL (Figure 308). The maximum IPD values for each well are higher in the northwestern region, with lower values in the central western region (Figure 308). The well cores in the southwestern region exhibit a slightly higher maximum IPD than those just to the north in the central western region. These data suggest that the most strongly developed paleosols are in the northwestern parts of the study area. However, the isolines in the farthest northwestern region and central western region project into regions of no data; this fact should be kept in mind when interpreting the isoline data in

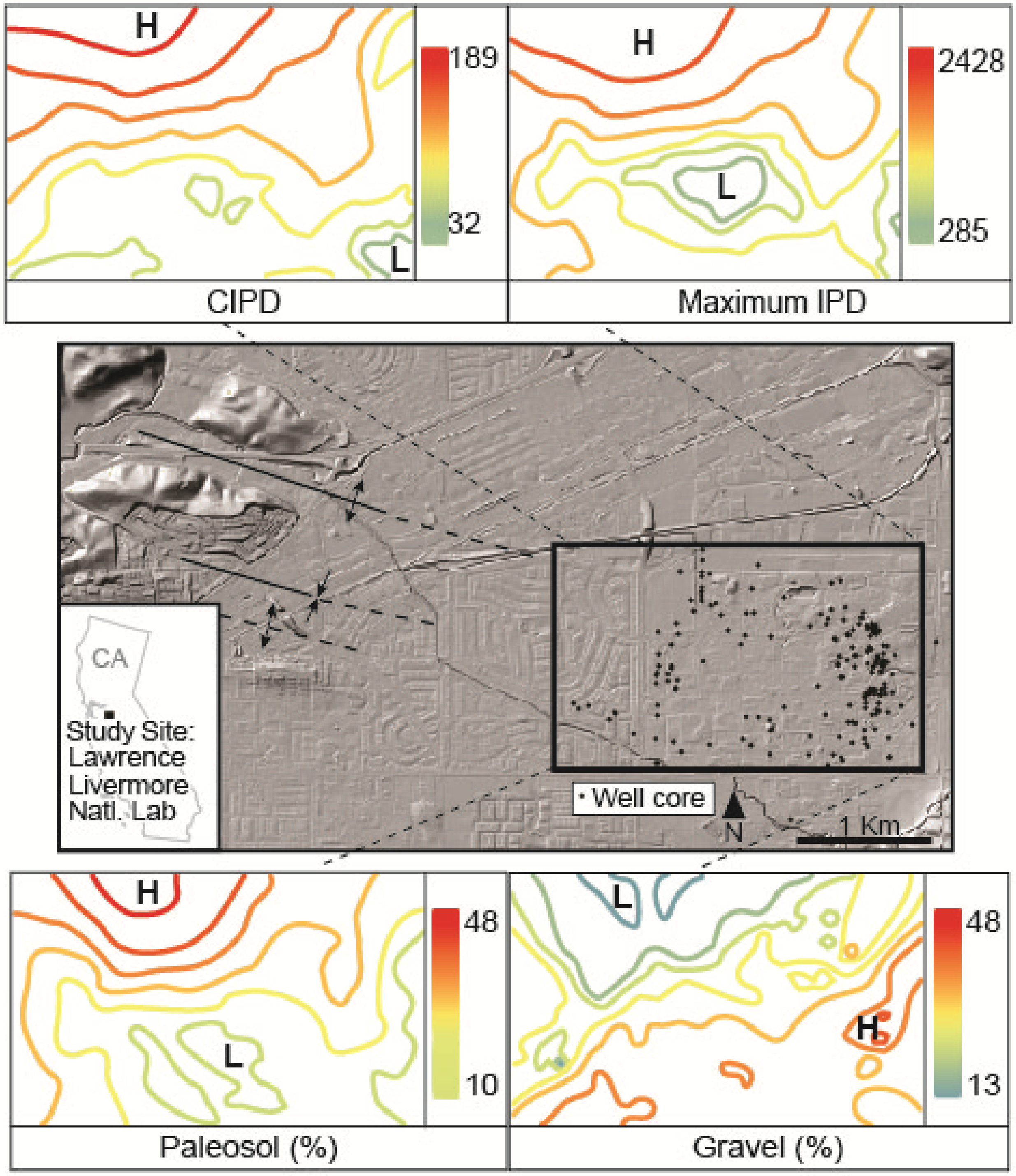

Figure 308. Kriged maps of CIPD values, maximum IPD values, percentage of well core material that is paleosol, and percentage of well core material that is gravel, for the LLNL study area. The location of the LLNL study site is indicated on the DEM by the black box. The plunging anticlines and syncline are indicated on the western side of the DEM. The solid lines indicate the mapped structural features and the dashed line indicate the proposed subsurface extension of the features (Unruh and Sawyer, 1997).

those regions. The lowest maximum IPD values are found in central LLNL where sampling was sparse due to inaccessibility for drilling. The lack of samples may have impacted the kriging routine, resulting in the low kriged values in that region.

Not only are the IPD values higher in the northwest, but the CIPD values are also highest in that region. The CIPD was designed to provide a numeric value for each well core, indicating the amount and strength of paleosol development throughout the core for purposes of comparison. The kriged map of CIPD values (Figure 308) shows that higher values exist in the northwestern portion of the study area, whereas the wells in the central western and southwestern portion of LLNL have lower CIPD values. The lowest CIPD values are found in the southeastern portion of LLNL.

The kriged map of the percentage of well core material that was paleosol is similar to the CIPD value map with the highest percentages in the northwestern region. Like the maximum IPD value map, the lowest percentages were found in central LLNL where sampling was sparse.

In addition to more strongly developed paleosols in the northwest, those wells also contain the highest percentage of core material classified as paleosol, with lesser amounts in the central western and southwestern regions (Figure 308). It was also observed that there was a loosely inversely proportional relationship between the percentage of the well core that was paleosol and the percentage of the well core that was gravel in each core. As the amount of gravel in the well core decreased, the amount of paleosol material increased, resulting in the northwestern region having a lower percentage of gravel than the central western and southwestern regions (Figure 308).

8. Discussion

The IPD and CIPD values both provide information regarding paleosol strength and abundance. High maximum IPD values indicate at least one strongly-developed paleosol in the well core, possibly because soils had been developing on a relatively stable surface with sufficient time to be strongly expressed. Low maximum IPD values indicate only poorly-developed paleosols in the well core. The CIPD provides a value of overall paleosol development for well cores, based on the degree of development of individual soil features. The CIPD is calculated from the sum of the IPD in each well core and can indicate several possibilities about the soil development in a region. High CIPD values indicate a high percentage of paleosol material in a well core, whether it be from a few well-developed paleosols or many weaker paleosols. Low CIPD values indicate less paleosol material in the well core and generally poorly-developed paleosols. The degree of paleosol development and amount of paleosol material in each well core can then in turn provide insight into the paleoenvironment of soil formation (Table 12).

Two other data sets provide additional information about soil development the study area. The number of paleosols in a well core reflects the stability of the geomorphic surface in the past. Well core collection methods at LLNL created problems for determining the number of paleosols that were present in each core. Missing intervals of core occurred because they were sampled by LLNL personnel before descriptions were made for this study, or poor recovery due to core spilling form the core barrel. Determining the actual number of paleosols per well core was impossible due to the unknown nature of the missing core material; paleosol material may have been missing. The CIPD was designed to account for the missing data by multiplying the assigned value for each soil property by the length of core classified as paleosol, then dividing the cumulative IPD sum by the total amount of core that was actually described/recovered. Because the amount of paleosol material per well core could not be reported as simply the number of paleosols per core, the amount of paleosol material is given in percentage of total available core material that was classified as paleosol - the best estimate of the number of paleosols present in each well core (Figure 308).

Another possible indicator of surface stability and amount of aggradation is the amount of gravel per well core (Figure 308). Gravel units at LLNL were interpreted as channel deposits and thus reflect areas of geomorphic aggradation and surface instability. These regions would have been experiencing alternating periods of erosion due to the stream incising into the landscape and removing material, and periods of aggradation due to sediment deposition, both of which would be prohibitive to pedogenesis. The wells with a low percentage of gravel are found in the northwestern portion of LLNL where the CIPD and maximum IPD values are highest. The low percentage of gravel material in the northwestern part of the study area supports the argument that the surface here has been comparatively more stable over time. The well cores with the highest percentage of gravel are found in the southeastern portion of LLNL - proximal to the apex of the fluvial fan. The apex of the fan is where the stream gradient lessens and the coarsest sediments are deposited due to lessening water velocity resulting in gravel deposition.

The loosely inverse proportionality between the percentage of well core that is paleosol and the percentage of well core that is gravel would be expected, and agrees with general concepts of geomorphic stability for this region. The northern region is relatively stable as indicated by well cores with high CIPD and maximum IPD values, and wells with a high percentage of paleosol material (Figure 308). Maximum IPD, CIPD, and percent paleosol values for the central western well cores are lower than those seen in the northern region, and the percentage of gravel in the cores is also higher. These co-associations in the central region suggest that the increased amount proportion of gravel – that were interpreted as channel deposits – points to stream channels being frequently located in the region. Fluvial activity here could have inhibited soil development. In the northern region, where well cores contain comparatively less gravel and more paleosol material, fluvial activity was less common, likely allowing soils to become well-developed.

At LLNL, high CIPD values are due to high maximum IPD values in addition to a high percentage of the core material was classified as paleosol within the wells. The region where CIPD values are the highest at LLNL is the northwestern region, which aligns with the mapped off-site anticline that is plunging to the southeast beneath LLNL (Figures 306 and 308).

Lower CIPD values at LLNL are located in the central western region where the well cores also have lower maximum IPD values and less paleosol material within each well core. The regions of the low CIPD values, lowest maximum IPD, lowest percent of core classified as paleosol within the well, and high percent of core classified as gravel align with the mapped off-site syncline that is plunging beneath LLNL (Figures 306 and 308).

Even though the CIPD values in the southwestern region are low, the maximum IPD values for that region are higher than the values for the central western well cores (Figure 308). This higher maximum IPD region in the southern region aligns with the southern plunging anticline and could be a consequence of that deformation. The southern anticline is more proximal to the apex of the fan and therefore more susceptible to deposition of coarser sediment, i.e., gravels, than is the northern anticline. The geomorphic surface above the southern anticline is likely relatively stable on which soils may become moderately well-developed but the proximity to the apex of the fan produces episodic burial by coarse sediment.

The Springtown anticlines plunge beneath LLNL with no surficial expression on site (Unruh and Sawyer, 1997). However, their effects are observed in the development of the paleosols and sediments above them. Due to its presumed lower subsidence rates, the northern anticline provided a more stable surface for soils to develop between occasional burial events by fluvial fan aggradation. Although the southern anticline is indicated by slightly higher maximum IPD values than in the central western region, a high percentage of the core material here is classified as gravel. This pattern indicates the landscape was frequently overwhelmed by alluvium such that the number of soils that could form (per unit length of core) above the southern anticline was low, resulting in a lower CIPD than above the northern anticline.

Due to increased instability caused by higher subsidence rates, the soils above the syncline did not develop as strongly, as indicated by lower maximum IPD and lower CIPD values. The well cores in this region also contain more gravel material than the cores from the northwestern region (Figure 308). The gravel units were interpreted to be channel deposits, indicating frequent stream deposition. This region was more frequently buried than the northern region so that soils were not able to develop as strongly as those in the north. Soils here did not have enough time to develop into strong soils before being overwhelmed by sedimentation and becoming buried. The rate of sedimentation was high enough to keep the landscape unstable and not allow for as many strongly-developed soils to form.

Deformation of the anticlines and synclines is likely syndepositional, as seen by the pattern of CIPD. The deposition of sediments in the central western and southwestern regions out-paced pedogenesis and did not allow strong soils to develop. This sedimentation rate is likely linked to the preferred flow path of the Arroyo Seco, as facilitated by the downwarping of the syncline and the area's proximity to the fan apex. The northwestern region exhibits stronger paleosols development due to the stability of the surface above the anticline.

9. Conclusions

This study presents a new index of paleosol development. This index was deemed necessary to study the Springtown anticlines at LLNL in order to relate the paleosol development to the underlying structural features. Although the Springtown anticlines plunge beneath LLNL, with no surficial expression on site, their subsurface location can be inferred through study of the overlying stratigraphy. Well core descriptions from across LLNL reveal patterns in paleosol development and location that suggest differential subsidence rates associated with the location of the plunging anticlines and syncline.

The IPD allows paleopedogenic features to be assigned a value that can be combined and manipulated to provide a number that represents the strength of paleosol development for each paleosol within a well core. The IPD values are then combined to provide the CIPD, a number that is representative of the amount of paleosol material in a core and their average strength of development throughout the whole well core.

Kriged maps of maximum IPD, CIPD, percent of well core that was paleosol, and percent of the well core that was gravel all show some trends that point to the locations of the plunging anticlines and syncline. Map data indicate that the northwestern region of LLNL has high maximum IPD values, high CIPD values, high percentages of material in the well cores described as paleosol, and low percentages of material in the well cores being composed of gravel units; this area corresponds to the plunging northern anticline. Likewise, the same maps show the central western and southwestern regions at LLNL have low maximum IPD values and low CIPD values, low percentages of material in well cores described as paleosol, and high percentages of material in well cores being composed of gravel units: this area corresponds to the plunging syncline. Higher maximum IPD values in the southern region indicate the location of the southern anticline. I conclude that although the Springtown anticlines and intervening syncline are not exhibited geomorphically on site, the examination of well core data provides a clear indication of their location below the surface based on paleosol development.

This study presents a new index of paleosol development that was developed in order to quantify the strength of paleosol development using paleosol features. This new index is a tool that provides a means to compare paleosol development and understand the larger environment.

APPENDIX D

Descriptions of Soil Series in and Around

Lawrence Livermore National Laboratory,

Livermore Basin, California

<u>Yolo – Pleasanton Soil Association Soil Series Descriptions</u> (Soil Survey Staff, 1966)

<u>Yolo Soil Series</u> Makes up 30 percent of the association. (NRCS, 2012)

Taxonomic Class: Fine-silty, mixed, superactive, nonacid, thermic Mollic Xerofluvents

Typical Pedon: Yolo silt loam - cultivated (Colors are for dry soil unless otherwise noted.)

Ap1--0 to 2 inches; Grayish brown (2.5Y 5/2) silt loam, very dark grayish brown (10YR 3/2) moist; moderate thick platy structure; hard, friable, slightly sticky, plastic; many very fine roots; many very fine interstitial and tubular pores; neutral (pH 6.7); abrupt wavy boundary.

Ap2--2 to 8 inches; Grayish brown (2.5Y 5/2) silt loam, dark brown (10YR 3/3) moist; massive; hard, friable, sticky, plastic; many very fine roots; common very fine tubular pores; neutral (pH 7.1); clear wavy boundary.

A1--8 to 19 inches; Grayish brown (2.5Y 5/2) silt loam, dark brown (10YR 3/3) rubbed, very dark grayish brown (10YR 3/2) coatings moist; weak coarse subangular blocky structure; hard, friable, slightly sticky, plastic; common very fine roots; many very fine tubular and clusters of interstitial pores associated with worm casts; few thin clay films on peds and continuous thin clay films in pores; neutral (pH 7.2); clear wavy boundary.

A2--19 to 26 inches; Grayish brown (2.5Y 5/2) silt loam, very dark grayish brown (10YR 3/2) moist; massive; slightly hard, friable, slightly sticky, plastic; many very fine and few fine roots; many very fine tubular pores; neutral (pH 7.3); clear irregular boundary.

C1--26 to 33 inches; Brown (10YR 5/3) silt loam, olive brown (2.5Y 4/4) moist; massive; slightly hard, friable, slightly sticky, plastic; common very fine roots; common very fine tubular and clusters of interstitial pores associated with worm casts; mildly alkaline (pH 7.4); clear irregular boundary.

C2--33 to 41 inches; Pale brown (10YR 6/3) silt loam, olive brown (2.5Y 4/4) moist, dark grayish brown (2.5Y 4/2) stains in root channels moist; massive; soft, very friable, slightly sticky, slightly plastic; few very fine roots; common very fine tubular and many very fine interstitial pores; mildly alkaline (pH 7.4); abrupt wavy boundary.

Ab--41 to 58 inches; Grayish brown (2.5Y 5/2) silty clay loam, very dark grayish brown (2.5Y 3/2) moist; massive; slightly hard, friable, very sticky, plastic; few very fine roots; common very fine tubular pores; mildly alkaline (pH 7.4); clear wavy boundary.

C3--58 to 65 inches; Pale brown (10YR 6/3) silt loam, mottled olive brown (2.5Y 4/4) and olive (5Y 4/3) moist; massive; slightly hard, very friable, slightly sticky, slightly plastic; few very fine roots; many very fine tubular and interstitial pores; mildly alkaline (pH 7.5).

<u>Pleasanton Soil Series</u> Makes up 20 percent of the association. (NRCS, 2012)

Taxonomic Class: Fine-loamy, mixed, superactive, thermic Mollic Haploxeralfs

Typical Pedon: Pleasanton gravelly fine sandy loam - cultivated. (Colors are for dry soil unless otherwise noted.)

Ap--0 to 9 inches; grayish brown (10YR 5/2) gravelly fine sandy loam, very dark grayish brown (10YR 3/2) moist; massive; hard, friable, slightly sticky, slightly plastic; many very fine, common fine and medium roots; common very fine and fine interstitial pores; slightly acid (pH 6.3); abrupt smooth boundary.

A1--9 to 21 inches; grayish brown (10YR 5/2) gravelly fine sandy loam, very dark grayish brown (10YR 3/2) moist; massive; hard, friable, slightly sticky, slightly plastic; many very fine, common fine and medium roots; common very fine and fine interstitial pores; neutral (pH 6.8); clear smooth boundary.

B2t--21 to 48 inches; brown (10YR 4/3) gravelly sandy clay loam, dark brown (10YR 3/3) moist; moderate medium subangular blocky structure; very hard, friable, sticky, plastic; common very fine and fine roots; many very fine and fine, few medium tubular pores; common moderately thick clay films on peds and in pores; neutral (pH 7.3); gradual wavy boundary.

B3--48 to 64 inches; brown (10YR 4/3) gravelly loam; dark brown (10YR 3/3) moist; weak medium subangular blocky structure; very hard, friable, sticky, plastic; few very fine roots; many very fine, common fine pores; few thick and few thin clay films on peds and in pores; neutral (pH 7.3); gradual wavy boundary.

C1--64 to 72 inches; yellowish brown (10YR 5/4) gravelly fine sandy loam near gravelly loam, dark yellowish brown (10YR 4/4) moist; weak blocky structure; hard, friable, sticky, slightly plastic; many very fine, common fine, few medium pores; few thin clay films on peds and in pores; slightly alkaline (pH 7.4).

<u>Sycamore Soil Series</u> Makes up 20 percent of the association. (NRCS, 2012)

Taxonomic Class: Fine-silty, mixed, superactive, nonacid, thermic Mollic Endoaquepts

Typical Pedon: Sycamore silty clay loam - cultivated (Colors are for dry soil unless otherwise noted.)

Ap--0 to 14 inches; grayish brown (2.5Y 5/2) silty clay loamy very dark grayish brown (2.5Y 3/2) moist; massive; hard, friable, sticky, plastic; many very fine roots; many very fine pores; moderately low organic matter contest; few mica flakes; slightly acid; clear smooth boundary.

Bg1--14 to 26 inches; grayish brown (2.5Y 5/2) silt loam, dark grayish brown (2.5Y 4/2) moist; few fine distinct mottles of yellowish brown or strong brown (lOYR 5/6 or 7.5YR 5/6); massive;

slightly hard, friable, slightly sticky, slightly plastic; many very fine roots; many very fine, common fine pores; few mica flakes; mildly alkaline; gradual smooth boundary.

Bg2--26 to 42 inches; light brownish gray (2.5Y 6/2) silt loam, dark grayish brown (2.5Y 4/2) moist; common fine distinct mottles of yellowish brown and strong brown (lOYR 5/6 and 7.5YR 5/6); massive; slightly hard, friable, slightly sticky, slightly plastic; few roots; many very fine, common fine pores; slightly calcareous, lime mainly disseminated; moderately alkaline; gradual smooth boundary.

C--42 to 60 inches; stratified light brownish gray (lOYR 6/2) and pale brown (lOYR 6/3) loam, fine sandy loam, and loamy fine sand with some silty lenses, dark grayish brown and dark brown (lOYR 4/2 and 4/3) moist; many fine distinct yellowish brown and strong brown mottles; massive; slightly hard, friable; common very fine and fine pores; slightly calcareous, lime mainly disseminated; water table may fluctuate in this horizon depending on the level of the water in the river; moderately alkaline.

Livermore Soil Series Makes up 20 percent of the association. (NRCS, 2012)

Taxonomic Class: Loamy-skeletal, mixed, superactive, thermic Typic Haploxerolls

Typical Pedon: Livermore very gravelly coarse sandy loam.
(Colors given are for dry conditions unless otherwise stated.)

Ap1--0 to 4 inches; brown (10YR 5/3) very gravelly coarse sandy loam, dark brown (10YR 3/3) moist; single grained; loose, friable; very porous; slightly acid (pH 6.4); diffuse smooth boundary.

Ap2--4 to 12 inches; dark grayish brown (10YR 4/2) very gravelly coarse sandy loam, very dark grayish brown (10YR 3/2) moist; massive; slightly hard, friable, slightly sticky; porous, many fine and very fine roots; many fine and very fine pores; few cobbles; neutral (pH 6.7); diffuse smooth boundary.

A--12 to 21 inches; dark grayish brown (10YR 4/2) very gravelly coarse sandy loam, very dark grayish brown (10YR 3/2) moist; massive; slightly hard, friable, slightly sticky; abundant fine and very fine roots and pores; few thin discontinuous clay films in pores; few cobbles and stones; neutral (pH 6.8); diffuse smooth boundary.

Bw1--21 to 28 inches; brown (10YR 5/3) very gravelly coarse sandy loam, dark brown (10YR 3/3) moist; massive; slightly hard, friable, slightly sticky; few fine roots; many fine and very fine pores; few thin clay films in pores; few cobbles and stones; neutral (pH 7.0); diffuse, smooth boundary.

Bw2--28 to 34 inches; brown (10YR 5/3) very gravelly coarse sandy loam, dark brown (10YR 4/3) moist; massive; slightly hard, friable, slightly sticky; few fine roots; many fine and very fine pores; very thin nearly continuous clay films in pores; few cobbles and stones; neutral (pH 7.1); diffuse smooth boundary.

C--34 to 60 inches; brown (10YR 5/3) very gravelly coarse sand, dark brown (10YR 4/3) moist; massive; slightly hard, friable; few fine roots; many fine and very fine pores; a small amount of colloid in bridges between sand grains and as stains on sand and gravels; neutral (pH 7.1).

<u>Zamora Soil Series</u> Makes up minor amounts of the association. (NRCS, 2012)

Taxonomic Class: Fine-silty, mixed, superactive, thermic Mollic Haploxeralfs

Typical Pedon: Zamora silt loam - cultivated (Colors are for dry soil unless otherwise noted.)

Ap--0 to 10 inches; Grayish brown (2.5Y 5/2) silt loam, very dark grayish brown (10YR 3/2) moist; massive; hard, friable, slightly sticky, slightly plastic; many fine roots; common very fine pores; slightly acid (pH 6.3); clear wavy boundary.

B21t--10 to 24 inches; Brown (10YR 5/3) silty clay loam, dark brown (10YR 3/3) moist; weak coarse angular blocky structure; hard, friable, sticky, plastic; many fine roots; common very fine pores; few thin clay films on faces of peds and lining pores; neutral (pH 7.0); gradual wavy boundary.

B22t--24 to 40 inches; Brown (10YR 5/3) silty clay loam, dark brown (10YR 4/3) moist; weak coarse angular blocky structure; hard, friable, sticky, plastic; common fine roots; common very fine pores; continuous moderately thick clay films on faces of peds and lining pores; neutral (pH 7.0); gradual wavy boundary.

C1--40 to 51 inches; Yellowish brown (10YR 5/4) silt loam, dark yellowish brown (10YR 4/4) moist; massive; slightly hard, friable, slightly sticky, slightly plastic; common fine roots; common very fine pores; few thin clay films line pores; neutral (pH 7.0); clear wavy boundary.

C2--51 to 60 inches; Yellowish brown (10YR 5/4) gravelly loam, dark yellowish brown (10YR 4/4) moist; massive; slightly hard, friable, slightly sticky, slightly plastic; few fine roots; common very fine pores; slightly effervescent; lime segregated in concretions; slightly alkaline (pH 7.5).

<u>Positas – Perkins Soil Association Soil Series Descriptions</u> (Soil Survey Staff, 1966)

<u>Positas Soil Series</u> Makes up 70 percent of the association. (NRCS, 2012)

Taxonomic Class: Fine, smectitic, thermic Mollic Palexeralfs

Typical Pedon: Positas gravelly loam, annual grass pasture. (Colors are for dry soil unless otherwise noted.)

Ap--0 to 8 inches; brown (10YR 5/3) gravelly loam, dark brown (7.5YR 3/3) moist; massive with weak horizontal partings in the top few inches; hard, friable, nonsticky and nonplastic; many very fine roots; many very fine pores; medium acid (pH 6.0); abrupt smooth boundary.

A--8 to 11 inches; similar to above in all respects except color values are nearly 1/2 chip higher; abrupt smooth boundary.

Bt1--11 to 20 inches; reddish brown (5YR 4/3) clay, dark reddish brown (5YR 3/3) moist; strong coarse prismatic structure; extremely hard, extremely firm, sticky and very plastic; few very fine roots along structure faces; few very fine tubular pores; thick continuous dark reddish gray (5YR 4/2) clay films on faces of peds and nearly filling pores; common slickensides; slightly acid (pH 6.5); gradual smooth boundary.

Bt2--20 to 29 inches; reddish brown (5YR 4/4) dry and moist, clay; strong coarse prismatic structure; extremely hard, extremely firm, sticky and very plastic; few very fine roots along structure faces, few very fine tubular pores; thick continuous clay films on faces of peds and nearly filling pores; common slickensides; moderately alkaline (pH 8.0); abrupt smooth boundary.

Bt3--29 to 39 inches; brown (7.5YR 5/5) clay loam, brown (7.5YR 4/4) and yellowish red (5YR 4/6) moist, strong medium angular blocky structure; very hard, firm, sticky and plastic; few very fine roots; few very fine tubular pores; moderately thick continuous yellowish red (5YR 5/5) clay films on faces of peds and lining pores; common fine (1 to 2 mm) black stains on faces of peds; very weakly calcareous moderately alkaline (pH 8.0); gradual smooth boundary.

Bt4--39 to 54 inches; light yellowish brown (10YR 6/5) clay loam, brown (10YR 5/3) and yellowish red (5YR 4/6) moist; strong medium angular blocky structure; very hard, firm, sticky and slightly plastic; few very fine roots; few very fine tubular pores; moderately thick continuous yellowish red (5YR 4/6) clay films on peds and lining pores; common fine black stains on faces of peds; very weakly calcareous; moderately alkaline (pH 8.0); gradual smooth boundary.

2C--54 to 60 inches; light yellowish brown (10YR 6/5) very gravelly sandy clay loam, yellowish brown (10YR 5/4) moist; few yellowish red (5YR 4/6) dry and moist coatings; massive; slightly hard, friable, nonsticky and nonplastic; moderately alkaline (pH 8.0).

<u>Shedd Soil Series</u> Makes up 10 percent of the association. (NRCS, 2012)

Taxonomic Class: Fine-silty, mixed, superactive, calcareous, thermic Typic Xerorthents

Typical Pedon: Shedd silty clay loam - annual grass range. (Colors are for dry soil unless otherwise stated.)

A11--0 to 5 inches; gray (5Y 6/1) silty clay loam, dark grayish brown (2.5Y 4/2) moist; moderate medium angular blocky structure; hard, very friable, sticky, plastic; common very fine roots; common very fine interstitial and common very fine tubular pores; strongly effervescent with disseminated lime; moderately alkaline (pH 8.0); clear smooth boundary.

A12--5 to 12 inches; gray (5Y 6/1) silty clay loam, very dark grayish brown (2.5Y 3/2) moist; strong medium subangular blocky structure; slightly hard, very friable, slightly sticky, slightly plastic; common very fine roots; many very fine interstitial, common very fine, fine and medium tubular pores; strongly effervescent with disseminated lime; moderately alkaline (pH 8.0); gradual smooth boundary.

A13--12 to 23 inches; gray (5Y 6/1) silty clay loam, very dark grayish brown (2.5Y 3/2) moist; strong medium subangular blocky structure; slightly hard, very friable, sticky, plastic; few very fine roots; many very fine interstitial and common very fine, fine and medium tubular pores; violently effervescent with disseminated lime; moderately alkaline (pH 8.0); abrupt wavy boundary.

C1ca--23 to 30 inches; light gray (2.5Y 7/2) silty clay loam, very dark grayish brown (2.5Y 3/2) moist; moderate medium subangular blocky structure; slightly hard, very friable, sticky, plastic; few very fine roots; many very fine interstitial and few fine and medium tubular pores; violently effervescent with disseminated lime; moderately alkaline (pH 8.0); gradual smooth boundary.

C2--30 to 36 inches; light gray (5Y 7/2) soft calcareous shale.

<u>Diablo Soil Series</u> Makes up 10 percent of the association. (NRCS, 2012)

Taxonomic Class: Fine, smectitic, thermic Aridic Haploxererts

Typical Pedon: Diablo silty clay, grain field. (Colors are for dry soil unless otherwise noted.)

Ap--0 to 6 inches; dark gray (5Y 4/1) silty clay, very dark gray (5Y 3/1) moist; the immediate very thin surface crust dries light gray and gray (5Y 6/1, 7/1); the surface 1 to 3 inches has string medium granular structure, the remainder has strong coarse and medium blocky structure; very hard, very firm, sticky, very plastic; common fine roots mainly along faces of peds; few very fine tubular pores; neutral; clear wavy boundary.

A--6 to 15 inches; dark gray (5Y 4/1) silty clay, very dark gray (5Y 3/1) moist; moderate coarse prismatic and moderate coarse blocky structure; very hard, very firm, sticky, very plastic;few fine roots mainly along faces of peds; noneffervescent except for an occasional small white lime nodule; mildly alkaline; clear smooth boundary**.**

Bkss1--15 to 26 inches; finely mixed gray and olive gray (5Y 5/1 and 5/2) silty clay, dark gray and olive gray (5Y 4/1 and 4/2) moist; moderate coarse prismatic and medium blocky structure; very hard, very firm, sticky, very plastic; few fine roots along faces of peds; few fine and very fine tubular pores; numerous slickensides; slightly effervescent in matrix, strongly effervescent few white lime nodules; moderately alkaline; clear wavy boundary.

Bkss2--26 to 32 inches; finely mixed gray and olive gray (5Y 5/1 and 5/2) silty clay, dark gray and olive gray (5Y 4/1 and 4/2) moist); weak coarse prismatic and weak medium blocky structure; very hard, very firm, sticky, very plastic; few fine roots mainly along faces of peds, roots distinctly flattened in appearance; few fine and very fine tubular pores; numerous slickensides; slightly effervescent matrix, strongly effervescent few small hard white lime nodules; diffuse smooth boundary.

Bck--32 to 42 inches; light olive gray (5Y 6/2) silty clay, olive gray (5Y 5/2) moist; weak medium subangular blocky structure; very hard, very firm, slightly sticky, plastic; few fine roots; few fine and very fine tubular pores; many white lime films and soft segregations; moderately alkaline; clear wavy boundary.

C--42 to 50 inches; fine and medium mottled appearing olive gray and light olive gray (5Y 5/2, 6/2) silty clay loam, olive gray (5Y 5/2, 4/2) moist; weak fine and medium subangular blocky structure; very hard, very firm, slightly sticky, plastic; few fine roots; few fine and very fine tubular pores; many shale fragments; strongly effervescent soft white filaments; soft and hard lime nodules; moderately alkaline; clear smooth boundary.

Cr--50 to 60 inches; light olive gray (5Y 6/2) slightly effervescent shale and fine grained sandstone with white films on facings.

Perkins Soil Series Makes up 5 percent of the association. (NRCS, 2012)

Taxonomic Class: Fine-loamy, mixed, superactive, thermic Mollic Haploxeralfs

Typical Pedon: Perkins loam - on a west facing slope of 1 percent under annual grasses at an elevation of 142 feet. (Colors are for dry soil unless otherwise stated. When described on June 14, l984, the soil was slightly moist below 20 inches.)

A--0 to 5 inches; brown (7.5YR 5/4) loam, dark brown (7.5YR 3/4) moist; massive; very hard, friable, slightly sticky and slightly plastic; common very fine roots; common very fine interstitial and tubular pores; 2 percent pebbles; neutral (pH 7.0); clear smooth boundary.

Bt1--5 to 13 inches; strong brown (7.5YR 5/6) clay loam, dark brown (7.5YR 3/4) moist; weak coarse subangular blocky structure; very hard, friable, slightly sticky and slightly plastic;

common very fine roots; common very fine, fine and medium tubular pores; common thin clay films lining pores; 5 percent pebbles; neutral (pH 7.0); clear smooth boundary.

Bt2--13 to 23 inches; yellowish red (5YR 5/6) clay loam, dark reddish brown (5YR 3/4) moist; moderate coarse subangular blocky structure; very hard, friable, slightly sticky and slightly plastic; common very fine roots; common very fine and fine and many medium tubular pores; common thin clay films on ped faces and lining pores; 5 percent pebbles; neutral (pH 7.0); gradual smooth boundary.

Bt3--23 to 35 inches; yellowish red (5YR 5/6) loam, reddish brown (5YR 4/4) moist; weak coarse subangular blocky structure; very hard, friable, slightly sticky and slightly plastic; few very fine roots; common very fine, fine and medium and few coarse tubular pores; common thin clay films on ped faces and lining pores; 5 percent pebbles; neutral (pH 6.8); gradual smooth boundary.

Bt4--35 to 47 inches; yellowish red (5YR 5/6) loam, reddish brown (5YR 4/4) moist; weak coarse subangular blocky structure; very hard, friable, sticky and plastic; few very fine roots; common very fine and fine and few medium tubular pores; common thin clay films on ped faces; 5 percent pebbles; neutral (pH 7.0); gradual smooth boundary.

Bt5--47 to 58 inches; yellowish red (5YR 5/6) loam; yellowish red (5YR 4/6) moist; massive; hard, friable, slightly sticky and slightly plastic; few very fine roots; common very fine and fine and few medium tubular pores; common thin clay films lining pores; 5 percent pebbles; neutral (pH 7.0); clear smooth boundary.

BC--58 to 66 inches; yellowish red (5YR 5/6) sandy loam, yellowish red (5YR 4/6) moist; massive; slightly hard, very friable, slightly sticky and nonplastic; few very fine roots; common very fine and fine pores; 5 percent pebbles; neutral (pH 7.0); clear smooth boundary.

2C--66 to 72 inches; yellowish red (5YR 4/6) very gravelly sandy loam, dark reddish brown (5YR 3/4) moist; massive; slightly hard, very friable, nonsticky and nonplastic; few very fine pores; 35 percent cobbles; 20 percent pebbles; neutral (pH 7.2).

Azule Soil Series Makes up 5 percent of association. (NRCS, 2012)

Taxonomic Class: Fine, smectitic, thermic Mollic Haploxeralfs

Typical Pedon: Azule clay loam, rangeland. (Colors are for dry soil unless otherwise noted).

A--0 to 6 inches; grayish brown (10YR 5/2) clay loam, very dark grayish brown (2.5Y 3/2) moist; massive; hard, firm, sticky and plastic; many fine and very fine roots; many very fine, common fine and few medium tubular pores; slightly acid (pH 6.5); clear smooth boundary.

Bt1--6 to 12 inches; grayish brown (10YR 5/2) clay, very dark grayish brown (2.5Y 3/2) moist; moderate coarse prismatic parting to strong medium angular blocky structure very hard, very firm, slightly sticky and slightly plastic; many fine and common very fine roots; many very fine and fine tubular pores; common thin clay films on faces of peds and lining pores; slightly acid (pH 6.5); diffuse smooth boundary.

Bt2--12 to 21 inches; dark grayish brown (2.5Y 4/2) clay, very dark grayish brown (2.5Y 3/2) moist; moderate coarse prismatic parting to moderate medium angular blocky structure; very hard, very firm, sticky and very plastic; many fine and very fine roots; many very fine and fine, few medium pores; common moderately thick clay films on faces of peds and lining pores; slightly acid (pH 6.5); gradual irregular boundary.

Bt3-21 to 25 inches; grayish brown (2.5Y 5/2) and light yellowish brown (2.5Y 6/4) clay which has a mottled appearance, very dark grayish brown (2.5Y 3/2) and light olive brown (2.5 5/4) moist; moderate coarse subangular blocky structure; very hard, very firm, sticky and very plastic; few very fine roots; many very fine and fine tubular pores; common thin clay films on faces of peds and lining pores; slightly acid (pH 6.5); clear smooth boundary.

Cr--25 to 40 inches; light yellowish brown (2.5Y 6/4) consolidated sediments, light olive brown (2.5Y 5/4) moist; massive; very hard, firm, sticky and plastic; few thin clay films in pores.

BIBLIOGRAPHY

Chapter 5

Bibliography

Alonso-Zarza, A.M., Alfonso, S., Sánchez-Moya, Y., 1999. Contrasting palaeosol development in two different tectonic settings: The Upper Buntsandstein of the Western Iberian Ranges, Central Spain. Terra Nova 11, 23-29.

Andersen, D. W., Isaacson, K. A., Barlock, V. E., 1995. Neogene evolution of the Livermore basin within the California Coast Ranges. In: Fritsche, A.E. (Ed.), Cenozoic Paleogeography of the Western United States – II. SEPM Pacific Section, Book 75, pp. 151-161.

Barlock, V. E., 1989. Sedimentology of the Livermore gravels (Miocene-Pleistocene), southern Livermore Valley, California. United States Geological Survey, Open-File Report 89-131.

Birkland, P.W., 1999. Soils and Geomorphology. Oxford University Press, New York, New York, 430 pp.

Bonnett, R., Czechowski, F, Hughes, P., 1991. Porphyrin analysis and coal rank; porphyrin index of coalification for bituminous coals. Chemical Geology 91 (2), 193-206.

Bridge, J.S., Leeder, M.R., 1979. A simulation model of alluvial stratigraphy. Sedimentology 26, 617-644.

Buntley, G.J., Westin, F.C., 1965. A comparative study of developmental color in a Chestnut-Chernozem-Brunizem soil climosequence. Soil Society of America Proceedings 29, 579-582.

Carpenter, D. W., Puchlik, K. P., Ramirez, A. L., Wagoner, J. L., Knauss, K. G., Kasameyer, P. W., 1980. Status report on the geology of the Lawrence Livermore National Laboratory site and adjacent areas, Volume 1: Text and appendices A-E. Livermore, California, Lawrence Livermore National Laboratory (UCRL-53065 Vol. 1), 97 pp.

Carpenter, D. W., Sweeney, J. J., Kasameyer, P. W., Burkhard, N. R., Knauss, K. G., Shlemon, R. J., 1984. Geology of the Lawrence Livermore National Laboratory site and adjacent areas. Livermore, California, Lawrence Livermore National Laboratory (UCRL-53316), 188 pp.

Chaer, G.M., Myrold, D.D., Bottomley, P.J., 2009. A soil quality index based on the equilibrium between soil organic matter and biochemical properties of undisturbed coniferous forest soils of the Pacific Northwest. Soil Biology and Biochemistry 41, 822-830.

Chittleborough, D.J., 1991. Indices of weathering for soils and palaeosols formed on silicate rocks. Australian Journal of Earth Sciences 38, 115-120.

Dibblee, T. W., 1980a. Preliminary geologic map of the Livermore Quadrangle, Alameda and Contra Costa Counties, California. United States Geological Survey, Open-File Report 80-533B.

Dibblee, T. W., 1980b. Preliminary geologic map of the Altamont Quadrangle, Alameda County, California. United States Geological Survey, Open-File Report 80-538.

Evans, C.V., Franzmeier, D.P., 1988. Color index values to represent wetness and aeration in some Indiana soils. Geoderma 41, 353-368.

Followill, F. E., Mills, J. M., 1982. Locations and focal mechanisms of recent microearthquakes and tectonics of Livermore Valley, California. Bulletin of the Seismological Society of America 72 (3), 821-840.

Gile, L.H., Peterson, F.F., Grossman, R.B., 1966. Morphological and genetic sequences of carbonate accumulation in desert soils. Soil Science 101, 347-360.

Graymer, R. W., Jones, D. L., Barbb, E. E., 1996. Preliminary geologic map emphasizing bedrock formations in Alameda County, California: Derived from the digital database. United States Geological Survey, Open-File Report 96-252.

Harden, J.W., 1982. A quantitative index of soil development for field descriptions: Examples from a chronosequence in central California. Geoderma 28, 1-28.

Harden, J.W., 1990. Soil development on a stable landform and implications for landscape studies. Geomorphology 3, 391-398.

Harden, J.W., Taylor, E.M., 1983. A quantitative comparison of soil development in four climatic regimes. Quaternary Research 20, 342-359.

Harnois, L., 1988. The CIW index: A new chemical index of weathering. Sedimentary Geology 55, 319-322.

Herd, D. G., 1977. Geologic map of the Las Positas, Greenville, and Verona Faults, eastern Alameda County, California. United States Geological Survey, Open-File Report 77-689.

Holliday, V.T., 1988. Genesis of late-Holocene soil chronosequence at the Lubbock Lake Archeological Site, Texas. Annals of the Association of American Geographers 78 (4), 594-610.

Hubert, J.F., 1962. A zircon-tourmaline-rutile maturity index and the interdependence of the composition of heavy mineral assemblages with the gross composition and texture of sandstones. Journal of Sedimentary Petrology 32 (3), 440-450.

Isaaks, E.H., Srivastava, R.M., 1989. An Introduction to Applied Geostatistics. Oxford University Press, New York, New York, 561 pp.

Jimenez, M. de la P., de la Horra, A.M., Pruzzo, L., Palma, R.M., 2002. Soil quality: A new index based on microbiological and biochemical parameters. Biology and Fertility of Soils 35 (4), 302-306.

Johnson, D.L. 1998. Paleosols are buried soils. Quaternary International 51/52, 7.

Lewis, C.J., McDonald, E.V., Sancho, C.S., Pena, J.L., Rhodes, E.J., 2009. Climatic implications of correlated upper Pleistocene glacial and fluvial deposits on the Cinca and Gallego Rivers (NE Spain) based on OSL dating and soil stratigraphy. Global and Planetary Change 67, 141-152.

Machette, M.N., 1985. Calcic soils of the southwestern United States. Geological Society of America Special Paper 203, 1- 21.

Markovic, S.B., Hambach, U., Catto, N., Jovanovic, M., Buggle, B., Machalett, B., Zoller, L., Glaser, B., Frechen, M.., 2009. Middle and late Pleistocene loess sequences at Batajnica, Vojvodina, Seria. Quaternary International 198, 255-266.

Matheron, G., 1963. Principles of geostatistics. Economic Geology 58, 1246-1266.

Mikesell, L.R., Weissmann, G.S., Karachewski, J.A., 2010. Stream capture and piracy recorded by provenance in fluvial fan strata. In: Wilford, D., Giles, P., Nichols, G. (Eds.), Alluvial Fan Research and Management: From Reconstructing Past Environments to Identifying contemporary hazards, vol. 115 (3-4). Geomorphology, Exeter, UK, pp. 267-277.

Natural Resources Conservation Service (NRCS). 2012. Soil data mart. http://soildatamart.nrcs.usda.gov/ (last accessed June 2012).

Nesbitt, H.W., Young, G.M., 1982. Early Proterozoic climates and plate motions inferred from major element chemistry of lutites. Nature 299 (5885), 715-717.

Newhall, C.G., Self, S., 1982. The volcanic explosivity index (VEI) an estimate of explosive magnitude for historical volcanism. Journal of Geophysical Rseearch 87 (C2), 1231-238.

Parker, A., 1970. An index of weathering for silicate rocks. Geological Magazine 107, 501-504.

Potter, P.E., 1978. Significance and origin of big rivers. Journal of Geology 86, 13-33.

Reading, H.G. (Ed.), 1996. Sedimentary Environments: Processes, Facies and Stratigraphy 3rd Edition. Blackwell Science, Cambridge, Massachusetts, 688 pp.

Retallack, G.J., 2001. Soils of the Past: An Introduction to Paleopedology. Blackwell Science Ltd., Malden, Massachusetts. 404 pp.

Ruhe, R.V., 1965. Quaternary paleopedology. In: Wright, H.E., Frey, D.G. (Eds.), The Quaternary of the United States. Princeton University Press, Princeton, New Jersey, p. 755-764.

Ruhe, R.V., Miller, G.A., Vreeken, W.J., 1971. Paleosols, loess sedimentation and soil stratigraphy. In: Yaalon, D.H. (Ed.), Paloepedology: Origin, Nature and Dating of Paleosols. Israel Univ. Press, Jerusalem. p. 41-60

Sauer, D., 2010. Approaches to quantify progressive soil development with time in Mediterranean climate – I. Use of field criteria. Journal of Plant Nutrition and Soil Science 173, 822-842.

Sawyer C.B., 1967. A daily index of solar flare activity. Journal of Geophysical Research 72 (1), 385-391.

Sawyer, T. L., 1999. Assessment of contractional deformation rates of the Mt. Diablo fold and thrust belt, eastern San Francisco Bay region, northern California: Final technical report. United States Geological Survey, Department of the Interior, National Earthquake Hazards Reduction Program, Award Number 98-HQ-GR-1006, 38 pp.

Schaetzl, R.J., Mokma, D.L., 1988. A numerical index of podzol and podzolic soil development. Physical Geography 9 (3), 232-246.

Schaetzl, R.J., Anderson, S., 2005. Soils: Genesis and Geomorphology. Cambridge University Press, New York. 817 pp.

Schaetzl, R.J., Krist, F.J., Stanley, K., Hupy, C.M., 2009. The natural soil drainage index: An ordinal estimate of long-term soil wetness. Physical Geography 30 (5), 383-409.

Soil Survey Staff, 1966. Soil Survey Alameda Area, California. US Department of Agriculture Soil conservation Service, Series 1961, No. 41, 95 pp.

Stokes, M., 2008. Plio-Pleistocene drainage development in an inverted sedimentary basin: Vera basin, Betic Cordillera, SE Spain. Geomorphology (doi: 10.1016/j.geomorph.2007.10.026).

Thomas, P.J., Baker, J.C., Zelazny, L.W., 2000. An expansive soil index for predicting shrink-swell potential. Soil Science Society of America Journal 64 (1), 268-274.

Torrent, J., Nettleton, W.D., 1979. A simple textural index for assessing chemical weathering in soils. Soil Society of America Journal 43 (2), 373-377.

Tsai, H., Huang, W., Hseu, Z., 2007. Pedogenic correlation of lateritic river terraces in central Taiwan. Geomorphology 88, 201-213.

Unruh, J. R., Sawyer, T. L., 1997. Assessment of blind seismogenic sources, Livermore valley, eastern San Francisco Bay region: Final technical report. United States Geological Survey, Department of the Interior, National Earthquake Hazards Reduction Program, Award Number 1434-95-G-2611, 88 pp.

Yaalon, D.H., 1971. Soil-forming processes in time and space. In: Yaalon, D. H (Ed.), Paleopedology: Origin, Nature and Dating of Paleosols, Jerusalem, Israel, 27-39.

CHAPTER 6

Summary and Conclusions

1. Sedimentology and Stratigraphy

Two hundred and two well cores collected from LLNL were described in detail resulting in recognition of seven facies: 1) clast-supported gravel, interpreted to be channel deposits, 2) matrix-supported gravel, interpreted to be debris flow deposits, 3) sand, interpreted to be channel bar deposits, 4) silty sand, interpreted to be floodplain deposits, 5) silty sand with clay lamellae, interpreted to be floodplain and crevasse splay deposits, 6) paleosol, interpreted to be buried soil, and the locally named 7) "Lower Livermore" (LL), interpreted to be clay-rich playa lake deposits which lie beneath the fluvial fan defining the lower boundary of the fan system and serves locally as an aquitard. The facies present in the lithostratigraphic units above the LL form a typical fluvial fan system.

Attempts at lithostratigraphic correlations at LLNL were unsuccessful. Soils generally form on the geomorphic surface, and therefore, buried soils generally are laterally continuous and serve as marker units for stratigraphic correlations; however, the paleosols at LLNL did not serve as marker units. Individual sedimentary deposits, including the paleosols, on this fluvial fan are not laterally continuous, limited to several meters of lateral extent and are occasionally offset vertically by the underlying tectonic structures. Even at the Helipad Site on LLNL with a relatively close well spacing of 9 m to 20 m, the accuracy of correlation scenarios was suspect. At LLNL, the optimal well spacing for good stratigraphic correlation appears to be 3 m to 6 m.

Working from the hypothesis that different paleosols would exhibit different geochemical signatures, geochemical analyses were performed on samples of paleosols from the Helipad Site well cores for the purpose of providing a possible tool for stratigraphic correlation. The geochemical data were used to calculate weathering indices and elemental ratios widely used in determining weathering and soil development. The calculated values and elemental abundances were plotted against depth, and then the plots were inspected for geochemical patterns that would indicate distinct stratigraphic units. However, no distinct geochemical patterns were observed rendering the geochemical data not useful as a tool for stratigraphic correlation. Although no distinct patterns were observed, slight overall trends were noticed within the plots. Fe and Al concentrations were weakly correlated with grain size and exhibited a slight increase in concentration with decreasing grain size. This trend suggests Fe and Al are taken up by neoformation of clay minerals, and thus, concentrated in the fine-grained size fraction. Variability in elemental concentrations was controlled by grain size and not lithostratigraphic units.

2. Stream Capture and Piracy

A stream capture and piracy event is recorded in the sediments beneath LLNL. Two intermittent streams deposited the sediments at LLNL creating a fluvial fan with stacked fluvial successions. The Arroyo Las Positas is a westerly flowing intermittent stream that drains the Great Valley Group rocks of the Altamont Hills. The Arroyo Seco is a northwesterly flowing intermittent stream whose catchment includes both the Great Valley Group and the Franciscan Assemblage of the Altamont Hills. Several lines of evidence show that the Arroyo Seco is a captured stream. Evidence for the capture includes the Arroyo Seco's flow path through the Las Positas Fault uplift, an abandoned fluvial fan south of that uplift, and a knickpoint in the stream's profile near the point of capture. After capture, redirecting the Arroyo Seco into the Livermore Basin also affected the Arroyo Las Positas as seen in the northern migration of the Arroyo Las Positas. A gravel provenance study of the LLNL sediments provided additional supporting evidence for the stream capture. Three distinct lithologic fan successions exist in the fan stratigraphy, indicating events of capture in the past. The lowest lithologic succession is enriched in Franciscan Assemblage indicator pebbles as compared to the other lithologically distinct successions. The middle succession is depleted in Franciscan Assemblage indicator pebbles as compared to the other successions. The uppermost succession is moderately enriched in Franciscan Assemblage indicator pebbles as compared to the other successions. All the evidence indicates that the paleo-Arroyo Seco once flowed north into the Livermore Basin depositing Franciscan Assemblage-rich sediments until it shifted to the south possibly because of the uplift due to transpression on the Las Positas Fault. During this time, the paleo-Arroyo Seco deposited a fluvial fan south of the Las Positas Fault uplift. While the Arroyo Seco was absent from the Livermore Basin, the paleo-Arroyo Las Positas built its fan depleted of Franciscan Assemblage indicator pebbles on top of the older Arroyo Seco sediment. Finally, a headward-eroding gully captured the Arroyo Seco, redirecting it back onto the LLNL site with Franciscan Assemblage sediments and leaving an abandoned fan south of the Las Positas Fault uplift. The re-introduction of the Arroyo Seco and its fan with its larger catchment, discharge, and sediment supply forced the smaller Arroyo Las Positas fan to migrate towards the north. The three distinct fan successions beneath LLNL correspond to times during which the Arroyo Seco was either flowing into the Livermore Basin or was absent from the basin.

2.1 Geochemical Evidence of Stream Capture and Piracy

A gravel provenance study at LLNL resulted in recognizing three distinct lithologic successions based on the relative abundances of Franciscan Assemblage indicator pebbles. Although the geochemical data was not a useful tool for stratigraphic correlation, the geochemical data plots were examined with the knowledge of three distinct fan successions beneath LLNL. It was hypothesized that the lithologic differences would be evident in the geochemical signatures from the three fan successions. However, the geochemical depth plots did not show any differences between the three fan successions. The uniform geochemical data is likely due to the common source area for both the Great Valley Group and the Franciscan Assemblage being the ancestral Sierran-Klamath arc. The Franciscan Assemblage was metamorphosed more or less isochemically creating the lithological differences between it and the Great Valley Group, yet the geochemical signatures of these two units, and of clastic sediment derived from them, remained similar.

3. Springtown Anticlines and the Index of Paleosol Development

The Springtown anticlines are a pair of low-amplitude, southeast-plunging Quaternary folds that plunge beneath LLNL and produce locally variable subsidence rates. Although the Springtown anticlines plunge beneath LLNL with no surficial expression on site, soil data show that the structural features beneath the site are detectable based on features preserved in the strata. Paleosols above the anticlines and syncline exhibit differential development. The well cores from above the anticlines contained a higher percentage of paleosol material and more strongly developed paleosols than did the cores from above the syncline.

In order to quantify the differences between the regions, a new index was developed. The Index of Paleosol Development (IPD) was developed to assess the strength of paleosol development with well cores. The IPD is calculated for individual paleosols from values assigned to paleosol features (i.e., argillan thicknesses, carbonate accumulations, soil structural units, and manganese oxide concentrations) based on how strongly each feature is expressed. High IPD values indicate well-developed paleosols and low IPD values indicate poorly-developed paleosols. The IPD values within a core are used to calculate the Core Index of Paleosol Development (CIPD), which was designed to numerically assess the amount of paleosol material and average strength of paleosol development within each well core for purposes of comparing one well to another. High CIPD values indicate well cores that contain well-developed paleosols or many poorly-developed paleosols. Low CIPD values indicate well cores that contain poorly-developed paleosols or very few paleosols. Kriged maps were then created from the maximum IPD value for each well and for the CIPD values. Each map showed the highest values for both the IPD and CIPD above the anticline and the lowest values above the syncline. The results indicate the region above the anticline is stable allowing soils to develop and become strongly-expressed soils. Both maps also indicate the region above the syncline did not allow for strong soil development, likely due to a less stable and aggrading surface.

In addition to calculating the IPD and CIPD, percentages were calculated for the amount of material in each well core that was paleosol and the amount of material in each well core that was gravel. Kriged maps were created from the paleosol percentages and gravel percentages. The well cores from the region above the northern anticline contained a high percentage of paleosol material and a low percentage of gravel material. These results agreed with conclusions drawn from IPD and CIPD kriged maps indicating stable geomorphic surfaces above the anticline. The well cores from the region above the syncline contained a low percentage of paleosol material and a high percentage of gravel material indicating less stable geomorphic surfaces, also in agreement with IPD and CIPD data. The clast-supported gravel facies were interpreted as channel deposits at LLNL. The abundance of gravel in the well cores above the syncline suggests that region was likely a preferred flow path for the streams that crossed the site, thus inhibiting soil development. Although the Springtown anticlines are not expressed geomorphically on site, the examination of well cores provided a clear indication of their extension beneath the surface.

4. Conclusions

The Livermore Basin proved to be an excellent area to study basin architecture in a tectonically active region experiencing variable syndepositional subsidence rates. At LLNL, the success of lithostratigraphic correlation varies with spatial scale. Small-scale features such as facies and sedimentary units were not laterally extensive and exhibited limited correlatability. Even though paleosols serve as marker beds and correlate over large areas as seen in the Kings River fan, such was not the case at LLNL. ERD's hydrostratigraphic units demonstrated hydraulic connectivity within distinct units across LLNL; however, the interconnectedness of hydrofacies, as determined by pumping tests, was not constrained by lithostratigraphic boundaries. Although paleosols, and other facies, at LLNL were not laterally continuous, and therefore limited in their usefulness in stratigraphic correlations in this research, knowledge about LLNL stratigraphy may provide insight into the stratigraphy of other similar regions. Such knowledge may aid future researchers when planning sampling schemes in similar environmental settings to LLNL.

Even though stratigraphic correlation at LLNL was not successful, large-scale phenomena did correlate. The ~20 meter-thick stacked fluvial fan succession were distinguishable beneath LLNL. A provenance study, along with geomorphic evidence, provided an understanding of sedimentological signatures in the stratigraphic record for episodes of stream capture and piracy.

Paleosol development and lithostratigraphic variability were correlated to the large-scale feature of the plunging Springtown anticlines. The more strongly-developed paleosols were linked to the relatively stable surface above the plunging anticlines while poorly-developed paleosols were located above the plunging syncline and a relatively less stable surface. A new Index of Paleosol Development was created as a part of this study that can be used by other researchers to compare strength of paleosol development among wells in a region. In addition to paleosol development varying by region, the lithostratigraphy also varied by region with more gravel in the well cores above the syncline than in those above the anticlines.

Paleosols provided marker units in a study of the Kings River alluvial fan and allowed for correlation of hydrostratigraphic units. The average paleosol averaged 1.85 m in thickness and were correlated between wells across an area in excess of 100 km^2. It was hypothesized that the paleosols would also serve as marker units in correlation attempts at LLNL. However, this study of the lithostratigraphy resulted in observing paleosols with a lateral extent of less than 6 m to 9 m. Although smaller-scale features (i.e., paleosols, other facies and sedimentary units) did not correlate at LLNL, large-scale phenomena (i.e., stacked fluvial fan successions and the plunging Springtown anticlines) did correlate. The likely cause for the difference in stratigraphic correlatability between the Kings River fan and the fan beneath LLNL is the size difference between the two fans (Kings River is approximately 3150 km^2 and the fan beneath LLNL is approximately 7 km^2) and the variable subsidence rate caused by local tectonic activity in the Livermore Basin.

I conclude that the variability observed in the lithostratigraphy at LLNL varies with spatial scale and is due to local tectonic activity. Even though correlatability of facies was poor, this study provides insight into Livermore Basin architecture at LLNL where small-scale features do not correlate but large-scale features do correlate.